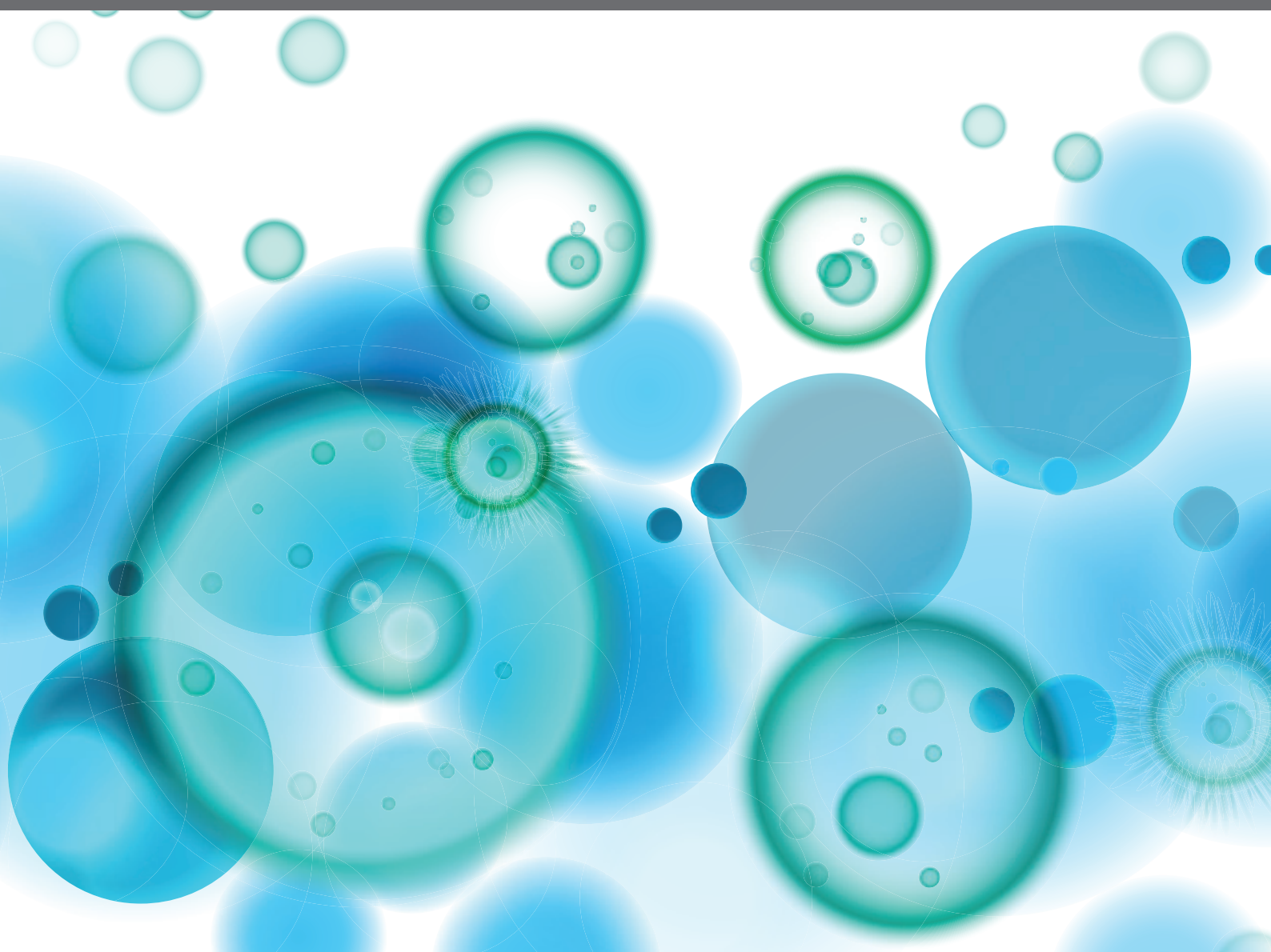


IMMUNOMODULATION OF INNATE IMMUNE CELLS

EDITED BY: Catarina R. Almeida, Barbara Bottazzi, Kate E. Lawlor and
Dominic De Nardo
PUBLISHED IN: *Frontiers in Immunology*





frontiers

Frontiers eBook Copyright Statement

The copyright in the text of individual articles in this eBook is the property of their respective authors or their respective institutions or funders. The copyright in graphics and images within each article may be subject to copyright of other parties. In both cases this is subject to a license granted to Frontiers.

The compilation of articles constituting this eBook is the property of Frontiers.

Each article within this eBook, and the eBook itself, are published under the most recent version of the Creative Commons CC-BY licence.

The version current at the date of publication of this eBook is CC-BY 4.0. If the CC-BY licence is updated, the licence granted by Frontiers is automatically updated to the new version.

When exercising any right under the CC-BY licence, Frontiers must be attributed as the original publisher of the article or eBook, as applicable.

Authors have the responsibility of ensuring that any graphics or other materials which are the property of others may be included in the CC-BY licence, but this should be checked before relying on the CC-BY licence to reproduce those materials. Any copyright notices relating to those materials must be complied with.

Copyright and source acknowledgement notices may not be removed and must be displayed in any copy, derivative work or partial copy which includes the elements in question.

All copyright, and all rights therein, are protected by national and international copyright laws. The above represents a summary only. For further information please read Frontiers' Conditions for Website Use and Copyright Statement, and the applicable CC-BY licence.

ISSN 1664-8714

ISBN 978-2-88963-574-0

DOI 10.3389/978-2-88963-574-0

About Frontiers

Frontiers is more than just an open-access publisher of scholarly articles: it is a pioneering approach to the world of academia, radically improving the way scholarly research is managed. The grand vision of Frontiers is a world where all people have an equal opportunity to seek, share and generate knowledge. Frontiers provides immediate and permanent online open access to all its publications, but this alone is not enough to realize our grand goals.

Frontiers Journal Series

The Frontiers Journal Series is a multi-tier and interdisciplinary set of open-access, online journals, promising a paradigm shift from the current review, selection and dissemination processes in academic publishing. All Frontiers journals are driven by researchers for researchers; therefore, they constitute a service to the scholarly community. At the same time, the Frontiers Journal Series operates on a revolutionary invention, the tiered publishing system, initially addressing specific communities of scholars, and gradually climbing up to broader public understanding, thus serving the interests of the lay society, too.

Dedication to Quality

Each Frontiers article is a landmark of the highest quality, thanks to genuinely collaborative interactions between authors and review editors, who include some of the world's best academicians. Research must be certified by peers before entering a stream of knowledge that may eventually reach the public - and shape society; therefore, Frontiers only applies the most rigorous and unbiased reviews.

Frontiers revolutionizes research publishing by freely delivering the most outstanding research, evaluated with no bias from both the academic and social point of view. By applying the most advanced information technologies, Frontiers is catapulting scholarly publishing into a new generation.

What are Frontiers Research Topics?

Frontiers Research Topics are very popular trademarks of the Frontiers Journals Series: they are collections of at least ten articles, all centered on a particular subject. With their unique mix of varied contributions from Original Research to Review Articles, Frontiers Research Topics unify the most influential researchers, the latest key findings and historical advances in a hot research area! Find out more on how to host your own Frontiers Research Topic or contribute to one as an author by contacting the Frontiers Editorial Office: researchtopics@frontiersin.org

IMMUNOMODULATION OF INNATE IMMUNE CELLS

Topic Editors:

Catarina R. Almeida, University of Aveiro, Portugal

Barbara Bottazzi, Milan University, Italy

Kate E. Lawlor, Hudson Institute of Medical Research, Australia

Dominic De Nardo, Monash University, Australia

Citation: Almeida, C. R., Bottazzi, B., Lawlor, K. E., De Nardo, D., eds. (2020). Immunomodulation of Innate Immune Cells. Lausanne: Frontiers Media SA. doi: 10.3389/978-2-88963-574-0

Table of Contents

- 05 Editorial: Immunomodulation of Innate Immune Cells**
Catarina R. Almeida, Barbara Bottazzi, Dominic De Nardo and Kate E. Lawlor
- 08 Advances in Research on Immunoregulation of Macrophages by Plant Polysaccharides**
Miao Yin, Ying Zhang and Hua Li
- 17 Super-Low Dose Lipopolysaccharide Dysregulates Neutrophil Migratory Decision-Making**
Brittany P. Boribong, Mark J. Lenzi, Liwu Li and Caroline N. Jones
- 29 DNA Sensor IFI204 Contributes to Host Defense Against Staphylococcus aureus Infection in Mice**
Wei Chen, Shui-Xing Yu, Feng-Hua Zhou, Xiao-Jing Zhang, Wen-Ying Gao, Kun-Yu Li, Zhen-Zhen Liu, Wen-Yu Han and Yong-Jun Yang
- 44 TonEBP Suppresses the HO-1 Gene by Blocking Recruitment of Nrf2 to its Promoter**
Eun Jin Yoo, Hwan Hee Lee, Byeong Jin Ye, Jun Ho Lee, Chae Young Lee, Hyun Je Kang, Gyu Won Jeong, Hyun Park, Sun Woo Lim, Whaseon Lee-Kwon, Hyug Moo Kwon and Soo Youn Choi
- 59 Dendritic Cell-Derived TSLP Negatively Regulates HIF-1 α and IL-1 β During Dectin-1 Signaling**
Matthew J. Elder, Steve J. Webster, Timothy J. Fitzmaurice, Aran S. D. Shaunak, Martin Steinmetz, Ronnie Chee, Ziad Mallat, E. Suzanne Cohen, David L. Williams, J. S. Hill Gaston and Jane C. Goodall
- 71 Regulation of Innate Immune Responses by Platelets**
Lucas Secchim Ribeiro, Laura Migliari Branco and Bernardo S. Franklin
- 80 Macrophages Down-Regulate Gene Expression of Intervertebral Disc Degenerative Markers Under a Pro-inflammatory Microenvironment**
Ana J. Silva, Joana R. Ferreira, Carla Cunha, João V. Corte-Real, Mafalda Bessa-Gonçalves, Mario A. Barbosa, Susana G. Santos and Raquel M. Gonçalves
- 90 Comparative Structure and Function Analysis of the RIG-I-Like Receptors: RIG-I and MDA5**
Morgan Brisse and Hinh Ly
- 117 Host Cell Death Responses to Non-typhoidal Salmonella Infection**
Madeleine A. Wemyss and Jaclyn S. Pearson
- 127 Pellino-1 Regulates Immune Responses to Haemophilus influenzae in Models of Inflammatory Lung Disease**
Bethany M. Hughes, Charlotte S. Burton, Abigail Reese, Maisha F. Jabeen, Carl Wright, Jessica Willis, Nika Khoshaein, Elizabeth K. Marsh, Peter Peachell, Shao C. Sun, David H. Dockrell, Helen M. Marriott, Ian Sabroe, Alison M. Condliffe and Lynne R. Prince
- 139 Exclusive Temporal Stimulation of IL-10 Expression in LPS-Stimulated Mouse Macrophages by cAMP Inducers and Type I Interferons**
Orna Ernst, Yifat Glucksam-Galnoy, Bibek Bhatta, Muhammad Athamna, Iris Ben-Dror, Yair Glick, Doron Gerber and Tsaffir Zor

- 155** *The Two Faces of Tumor-Associated Macrophages and Their Clinical Significance in Colorectal Cancer*
Marta L. Pinto, Elisabete Rios, Cecília Durães, Ricardo Ribeiro, José C. Machado, Alberto Mantovani, Mário A. Barbosa, Fatima Carneiro and Maria J. Oliveira
- 167** *Glycolysis is Required for LPS-Induced Activation and Adhesion of Human CD14⁺CD16⁻ Monocytes*
Man K. S. Lee, Annas Al-Sharea, Waled A. Shihata, Camilla Bertuzzo Veiga, Olivia D. Cooney, Andrew J. Fleetwood, Michelle C. Flynn, Ellen Claeson, Clovis S. Palmer, Graeme I. Lancaster, Darren C. Henstridge, John A. Hamilton and Andrew J. Murphy
- 177** *HECT E3 Ubiquitin Ligase-Regulated Txnip Degradation Facilitates TLR2-Mediated Inflammation During Group A Streptococcal Infection*
Po-Chun Tseng, Chih-Feng Kuo, Miao-Huei Cheng, Shu-Wen Wan, Chiou-Feng Lin, Chih-Peng Chang, Yee-Shin Lin, Jiunn-Jong Wu, Chi-Chen Huang and Chia-Ling Chen
- 190** *Profile of Histone H3 Lysine 4 Trimethylation and the Effect of Lipopolysaccharide/Immune Complex-Activated Macrophages on Endotoxemia*
Vichaya Ruenjaiman, Patcharavadee Butta, Yu-Wei Leu, Monnat Pongpanich, Asada Leelahavanichkul, Patipark Kueanjinda and Tanapat Palaga



Editorial: Immunomodulation of Innate Immune Cells

Catarina R. Almeida^{1*}, Barbara Bottazzi^{2*}, Dominic De Nardo^{3*} and Kate E. Lawlor^{4,5*}

¹ Department of Medical Sciences, Institute of Biomedicine - iBiMED, University of Aveiro, Aveiro, Portugal, ² Humanitas Clinical and Research Center, Rozzano, Italy, ³ Department of Anatomy and Developmental Biology, Monash Biomedicine Discovery Institute, Monash University, Melbourne, VIC, Australia, ⁴ Centre for Innate Immunity and Infectious Diseases, Hudson Institute of Medical Research, Melbourne, VIC, Australia, ⁵ Department of Molecular and Translational Science, Monash University, Melbourne, VIC, Australia

Keywords: innate immunity, PRRs, immunomodulation, pattern recognition, macrophage polarization

Editorial on the Research Topic

Immunomodulation of Innate Immune Cells

We are delighted to present this Research Topic for *Frontiers in Immunology*, focusing on “Immunomodulation of Innate Immune Cells”. This collective comprises both primary research articles and reviews of the current literature by experts in the field. Papers included in this collection highlight recent advances in our understanding of the fundamental mechanisms controlling activation and regulation of innate immune cells, as well as examine new strategies to study and manipulate their immunomodulation.

The innate immune system is the host's primary defense mechanism recognizing external and inherent danger signals, which range from pathogen-derived molecules to mislocalized or modified host factors. Physiologically, activation of innate immune cells protects the host from life-threatening infections and acute tissue damage, however, chronic and unwarranted activation can lead to numerous disease pathologies. Families of highly conserved germ-line sensor proteins, known as Pattern Recognition Receptors (PRRs) react to specific danger signals. Downstream of PRR activation intracellular signaling molecules co-ordinate the production of inflammatory mediators, such as cytokines, chemokines, and interferons, via the activity of specific transcriptional programmes or through proteolytic cleavage events. Inflammatory mediators then act to mobilize recruitment of an army of additional immune cells and facilitates acute inflammatory processes. In addition to production of inflammatory factors, PRR activation can also elicit other important cellular responses, including autophagy, metabolic reprogramming, and forms of programmed cell death.

Sensing of both microbial and host derived nucleic acids by PRRs is a critical function of the innate immune system. In their comprehensive review, Brisse and Ly. describe and contrast the RNA sensing retinoic-acid-inducible gene I (RIG-I)-like receptors (RLRs), RIG-I and MDA-5, including their evolution, structure, mechanism of activation, signaling, and modulation. Meanwhile, Ribeiro et al., examine the emerging concept of modulation of immune cells by platelets. Platelets are generally considered non-immune cells that circulate in the blood stream to primarily initiate clotting and prevent excessive blood loss. In this mini-review the authors detail the current immunomodulatory mechanisms employed by platelets—ranging from clustering of microbes to direct contact with monocytes to modulate inflammatory cytokine production. These specialized events have not only been associated with inflammation but also with altered cell survival signals and the production of Neutrophil extracellular traps (NETs). Overall, the fact platelets can induce immunomodulatory events to drive inflammatory disease highlights the exciting potential to target platelets as an alternative therapeutic approach.

OPEN ACCESS

Edited and reviewed by:

Francesca Granucci,
University of Milano Bicocca, Italy

*Correspondence:

Catarina R. Almeida
cra@ua.pt
Barbara Bottazzi
Barbara.Bottazzi@humanitasresearch.it
Dominic De Nardo
dominic.denardo@monash.edu
Kate E. Lawlor
kate.lawlor@hudson.org.au

Specialty section:

This article was submitted to
Molecular Innate Immunity,
a section of the journal
Frontiers in Immunology

Received: 08 January 2020

Accepted: 15 January 2020

Published: 11 February 2020

Citation:

Almeida CR, Bottazzi B, De Nardo D
and Lawlor KE (2020) Editorial:
Immunomodulation of Innate Immune
Cells. *Front. Immunol.* 11:101.
doi: 10.3389/fimmu.2020.00101

Dectin-1 is a transmembrane C-type lectin receptor (CLR) that recognizes β -glucan carbohydrate on the surface of fungi to elicit an anti-fungal immune response. Thymic stromal lymphopoietin (TSLP) is a pleiotropic cytokine important in immune regulation mainly produced by epithelial cells to activate DCs. In their original research article, Elder et al. demonstrate that DCs are in fact able to produce large amounts of TSLP that can down modulate dectin-1-induced immune cytokine responses. The authors uncover a regulatory mechanism whereby TSLPR signaling dampens phosphorylation of the tyrosine protein kinase, SYK and subsequently reduces HIF-1 α -driven IL-1 β expression. These findings implicate dysregulation of TSLP production in chronic fungal infections.

Pathogen modulation of the host immune response is widely recognized to facilitate bacterial and viral replication and dissemination. The mini-review by Wemyss and Pearson highlights how non-typhoidal *Salmonella* evades the host innate immune response via temporal and spatial translocation of specific type III secretion system effectors that modulate inflammatory responses and limit or induce programmed cell death pathways, including apoptosis, necroptosis, and pyroptosis. In a similar vein, the original research articles by Tseng et al. and Hughes et al. detail novel regulatory proteins and post-translational modification events mediated by pathogen-induced Toll-like receptor (TLR) signaling to increase infectious burden and cause excessive inflammation. Thioredoxin-interacting protein (Txnip) primarily functions as an inhibitor of the antioxidant Thioredoxin system that regulates a variety of biological processes, including activation of NF- κ B. Tseng et al. detail how Group A *Streptococcus* (GAS) engagement of TLR2 induces NOX2-dependent proteasomal degradation of Txnip via HECT E3 ubiquitin ligase and AMP kinase activity, and promotes inflammation via excessive cytokine and nitrite production. Similarly, Hughes et al. document TLR4-driven upregulation of the E3 ubiquitin ligase, Pellino-1, in response to LPS and Non-typeable *Haemophilus influenza* (NTHi) infection. Pellino-1 plays a critical role in regulating TLR signaling, where it can trigger degradative (K48-linked ubiquitylation) or activating signals (K63-linked ubiquitylation). The authors subsequently show that Pellino-1-deficient mice exhibit increased levels of the neutrophil Keratinocyte chemoattractant (KC) that is associated with increased neutrophil infiltrate and reduced NTHi burden in the lung. Together these two studies highlight how pathogens modulate molecular events to drive inflammation and infection, and that targeting the stability of these E3 ubiquitin ligases may be harnessed therapeutically.

Using single cell analysis, Boribong et al. demonstrates that pre-exposure to very low doses of LPS can pre-condition neutrophils, altering their preferential recruitment toward an endogenous inflammatory stimulus as opposed to a stimulus mimicking a bacterial infection. Neutrophils can thus adopt different profiles, altering their migratory decision making, which is dependent on the microenvironment and pathogens they encounter through their lifetime.

The cytosolic DNA sensor, interferon-inducible protein (IFI204) (p204, human homolog IFI6), is a well-known sensor of DNA viruses and intracellular bacteria. The original

research article by Chen et al. delves into whether extracellular *Staphylococcus aureus* infection is also recognized by IFI204. The authors report that IFI204 is indeed required for inflammatory STING-TBK1-NF- κ B signaling responses and host defense against *Staphylococcus* infection, including the promotion of extracellular traps.

The role of metabolism in modulating innate immune cells is undeniable. Monocyte activation and adhesion to the endothelium are crucial events in inflammation. Lee et al. studied the metabolic changes upon activation of CD14+CD16– (classical) monocytes, which are recruited to sites of injury during acute inflammation, where they adhere to vessels. LPS stimulation of these cells led to an increase in mTOR regulated glycolysis, essential for monocyte activation and adhesion. This increase in glycolysis is similar to the glycolytic profile found in M1-like macrophages, but an accompanying decrease in OXPHOS or mitochondrial activity was not observed. A better understanding of the dynamics of metabolic changes in different immune cells will be essential for the development of therapies that focus on metabolic reprogramming.

Many immune cells, with macrophages being the most prominent example, can polarize into different phenotypes, and assume an anti-inflammatory through to a pro-inflammatory profile, and include subsets more specialized toward fighting infection or tumors, inducing tissue remodeling. In this special issue, the review paper by Yin et al. lists major immunoregulatory plant polysaccharides and discusses the molecular mechanisms behind their effect in macrophages. Meanwhile, Yoo et al. describes how TonEBP, a transcriptional activator in M1-like macrophages, controls macrophage polarization. TonEBP suppresses expression of heme oxygenase-1 (HO-1) in M1-primed macrophages by reducing Nrf2 recruitment to the HO-1 promoter, which leads to a reduction in HO-1 expression. This mechanism then promotes induction of the M1 profile while suppressing the M2-like profile. Simultaneously, epigenetic regulation of macrophage plasticity has been investigated by Ruenjaiman et al. comparing classical macrophages that are capable of producing high amount of proinflammatory cytokines, with non-classical macrophages, that instead produce high levels of the key anti-inflammatory cytokine IL-10. In this study the authors show that active histone H3 Lysine 4 Trimethylation (H3K4me3) marks were increased to a greater extent in non-classical than classical macrophages. Moreover, adoptive transfer of non-classical macrophages dampens the production of proinflammatory cytokines in a mouse sepsis model, suggesting the potential therapeutic use of these cells. Ernst et al. have focused their work on murine IL-10 promoter elements mediating synergistic induction by cAMP. Transcription of IL-10 can be achieved via synergism between cAMP inducers and LPS signaling, providing a mechanism that can contribute to limit inflammation at its onset in specific contexts.

Macrophages are essential players in different pathological conditions. Silva et al. examined a widespread health issue represented by low back pain associated with intervertebral disc (IVD) degeneration. Silva et al. set up a co-culture system able to provide a simple *in vitro* model to investigate the interaction

between macrophages and IVD. This interesting model may be used to investigate the mechanisms by which macrophages and IVD cells interact during IVD aging and degeneration, and to test possible therapeutic tools. Furthermore, Pinto et al. presented their investigation of tumor-associated macrophages (TAM) in colorectal cancer (CRC). TAMs are the most abundant host cells that infiltrate tumors, where they acquire a non-classical polarization exerting essentially pro-tumoral functions. By performing immunohistochemical analysis on a series of CRC patients, Pinto et al., discovered that CD163+ non-classical macrophages are mostly localized in the invasive front of the tumor, whereas CD80+ classical macrophages are located in the normal adjacent mucosa. The results presented in this paper contribute to an increasing understanding of macrophage polarization within tumors, which is essential for the development of novel therapeutic strategies to reprogram macrophages toward a pro-inflammatory anti-tumor phenotype.

Together, the papers in this collection add new knowledge on the complex molecular map controlling innate activation, while also suggesting potential novel therapeutic strategies to modulate innate immune cells and treat diverse immunopathologies. We would like to take this opportunity to thank all the reviewers for their time and input, as well as the authors for their valuable contributions to this Research Topic.

AUTHOR CONTRIBUTIONS

All authors listed have made a substantial, direct and intellectual contribution to the work, and approved it for publication.

FUNDING

The activities in CRA laboratory are supported by the projects UIDB/04501/2020, PTDC/BIA-CEL/28791/2017 and POCI-01-0145-FEDER-028791, POCI-01-0145-FEDER-030882 and PTDC/BIA-MOL/30882/2017, through COMPETE2020 - Programa Operacional Competitividade e Internacionalização (POCI), and by national funds (OE), through FCT/MCTES. The activities in BB laboratory are made possible by funding from the European Research Council (ERC-No. 669415) and the Italian Association for Cancer Research [AIRC-IG and 5x1000 (contract 21147)]. DD was supported by a Monash University FMNHS Senior Postdoctoral Fellowship. KL was supported by an Australian Research Council Future Fellowship (FT190100266, Canberra, Australia), National Health and Medical Research Council Grants (1145788, 1162765, and 1181089, Canberra Australia) and operational infrastructure grants through the Australian Government IRIS and the Victorian State Government OIS.

Conflict of Interest: The authors declare that the research was conducted in the absence of any commercial or financial relationships that could be construed as a potential conflict of interest.

Copyright © 2020 Almeida, Bottazzi, De Nardo and Lawlor. This is an open-access article distributed under the terms of the Creative Commons Attribution License (CC BY). The use, distribution or reproduction in other forums is permitted, provided the original author(s) and the copyright owner(s) are credited and that the original publication in this journal is cited, in accordance with accepted academic practice. No use, distribution or reproduction is permitted which does not comply with these terms.



Advances in Research on Immunoregulation of Macrophages by Plant Polysaccharides

Miao Yin, Ying Zhang and Hua Li*

Shandong Provincial Key Laboratory of Animal Resistance Biology, College of Life Sciences, Shandong Normal University, Jinan, China

OPEN ACCESS

Edited by:

Catarina R. Almeida,
University of Aveiro, Portugal

Reviewed by:

Victor Ermilo Arana-Argáez,
Universidad Autónoma de Yucatán,
Mexico
Marit Inngjerdengen,
Oslo University Hospital, Norway

*Correspondence:

Hua Li
lihua@sdsu.edu.cn

Specialty section:

This article was submitted to
Molecular Innate Immunity,
a section of the journal
Frontiers in Immunology

Received: 14 November 2018

Accepted: 17 January 2019

Published: 05 February 2019

Citation:

Yin M, Zhang Y and Li H (2019)
Advances in Research on
Immunoregulation of Macrophages by
Plant Polysaccharides.
Front. Immunol. 10:145.
doi: 10.3389/fimmu.2019.00145

Polysaccharides are among the most important members of the biopolymer family. They are natural macromolecules composed of monosaccharides. To date, more than 300 kinds of natural polysaccharide compounds have been identified. They are present in plants, animals, and microorganisms, and they engage in a variety of physiological functions. In the 1950s, due to the discovery of their immunoregulatory and anti-tumor activities, polysaccharides became a popular topic of research in pharmacology, especially in immunopharmacology. Plants are an important source of natural polysaccharides. Pharmacological and clinical studies have shown that plant polysaccharides have many functions, such as immune regulation, anti-tumor activity, anti-inflammatory activity, anti-viral functions, anti-radiation functions, and a hypoglycaemic effect. The immunomodulatory effects of plant polysaccharides have received much attention. Polysaccharides with these effects are also referred to as biological response modifiers (BRMs), and research on them is one of the most active areas of polysaccharide research. Thus, we summarize immunomodulatory effects of botanical polysaccharides isolated from different species of plants on the macrophage. The primary effect of botanical polysaccharides is to enhance and/or activate macrophage immune responses, including increasing reactive oxygen species (ROS) production, and enhancing secretion of cytokines and chemokines. Therefore, it is believed that botanical polysaccharides have significant therapeutic potential, and represent a new method for discovery and development of novel immunomodulatory medicine.

Keywords: polysaccharide, immunoregulation, macrophage, receptors, plant

INTRODUCTION

A variety of polysaccharides have been discovered in different species of plants, and information about the structures and functional activities of some polysaccharides has been elucidated. It was found that the vast majority of plant polysaccharides are relatively non-toxic and do not cause significant side effects. Side effects are indeed an unsolved problem for the clinical application of immunomodulating polysaccharides derived from microorganisms and chemical synthesis. Plant polysaccharides thus represent an ideal alternative for immune modulation.

Most recent studies of plant polysaccharides have focused on separation and purification, analysis of the monosaccharide composition, structural analysis (including primary and advanced

structures), and the relationship between structure and function (1–5). **Table 1** shows the structures and biological activities of some plant polysaccharides. The range of the molecular weights of the polysaccharides is relatively large. The molecular weight of polysaccharide PAC-I is 10,000 kDa (6), and the molecular weight of FPS-1 is 14 kDa (8). Some polysaccharides are composed of complex sets of monosaccharides, whereas others have only one monosaccharide component. For example, *Cistanche deserticola* is made of glucose (9), and the monosaccharide component of PSPP is dextran (12), whereas CPE is made of arabinose, galactose, glucose, mannose, rhamnose, and xylose (10). The chemical structures and physiological activities of polysaccharides are related. Most polysaccharides with α - β -helix structure have strong biological functions. The glycosidic bonds of plant polysaccharides are mainly α -(1 \rightarrow 6)-D, α -(1 \rightarrow 4)-D, and β -(1 \rightarrow 4)-D. It has been found that even the polysaccharides derived from the same plant may be of different types. For example, the polysaccharides PAC-I, PAC-II, and PAC-III, which have different molecular weights, are extracted from *Aloe vera* L., and their monosaccharide compositions also differ (24).

The activities of plant polysaccharides include immune regulation, anti-tumor, anti-radiation, and anti-viral effects (21, 25–27), and the structures of polysaccharides are directly related to their functional activities (28). Kralovec et al. reported that a polysaccharide/glycoprotein complex with a molecular weight >100 kDa and consisting mainly of galactose, rhamnose, and arabinose has high biological activity (29). Lo et al. proposed that arabinose, mannose, xylose, and galactose are the four most important monosaccharide components contributing to macrophage stimulating activity, whereas glucose, as the most common monosaccharide component, showed no clear role in the immunoactivity of polysaccharides (30).

IMMUNOMODULATORY EFFECTS OF PLANT POLYSACCHARIDES

Numerous studies have shown that plant polysaccharides can regulate the immune system in multiple ways and at multiple levels. They not only activate immune cells, including T cells, B lymphocytes, macrophages, and natural killer cells, but they also activate complements and promote the production of cytokines, thus showing regulatory effects on the immune system in multiple ways (25, 31–34). Innate immune regulation has an important impact on the host's ability to respond rapidly to pathogens. As important members of the immune defense system of the host, macrophages can collaborate with other types of cells (such as neutrophils) to resist external adverse factors (35–40). The immunomodulatory effects of plant polysaccharides on macrophages are mainly achieved through the generation of reactive oxygen species (ROS), the secretion of cytokines, cell proliferation, and the phagocytic activity of macrophages (38).

Effect of Plant Polysaccharides on NO Production by Macrophages

NO is an important biologically active substance. In addition to being an important signal transducer in the central nervous

system, it is widely involved in the physiological and pathological processes of multiple systems, including immune responses, and inflammatory reactions (26, 32, 41–43). In the immune system, when macrophages are stimulated and activated, a large amount of nitric oxide (NO) is released, which can kill microorganisms, parasites, and tumor cells; it can also induce inflammatory reactions and protect the body from external adverse factors (38).

Park reported that the acidic polysaccharide component BRP-4, extracted from *Basella rebr* L., can promote NO production in macrophages RAW264.7 at a dose of 10–100 μ g/ml (44). A study by Luo et al. also showed that KMCP, a polysaccharide component extracted from *Ixeris polycephala*, can enhance macrophage-mediated non-specific immune responses by increasing NO production in macrophages (11). Polysaccharides extracted from *Pterospartum tridentatum* (L.) Willk. can also promote NO production in an *in vitro* culture of macrophages (45).

Similarly, the polysaccharides ASP (46), KMCP (11), SF1, SF2 (47), SPS (48), SBF (49), PG (50), and SHE (51) can stimulate NO release in mouse peritoneal macrophages and/or macrophage RAW264.7, in which SBF inhibits the release of NO in LPS-activated macrophages as well as the release of cytokines and activity mediators (49). Polysaccharides GG, SGG, and BPs inhibit the release of NO in LPS-activated macrophages RAW264.7, which suggests that these polysaccharides have similar immunomodulatory activity (36, 45).

Effect of Plant Polysaccharides on Cytokine Secretion by Macrophages

Cytokines play an important role in the regulation of cell-cell interactions, cell growth, and cell differentiation. Cytokines can be classified based on function as interleukins (IL), tumor necrosis factors (TNF), interferons (IFN), and colony stimulating factors (CSF). They play important roles in the regulation of inflammatory responses and immune responses, and they have regulatory effects on both innate immunity and adaptive immunity (36).

The *Citrus unshiu* polysaccharide component CPE-II can significantly increase the production of the pro-inflammatory cytokines TNF- α and IL-6 and the anti-inflammatory cytokine IL-12 in macrophage RAW264.7 (52). Thus, plant polysaccharides can simultaneously regulate the expression of pro- and anti-inflammatory cytokines (IL-12 acts as a negative feedback factor to prevent the over-activation of macrophages in the hyper-inflammatory response), which suggests that the body has a self-regulatory mechanism to maintain an equilibrium state (53). Kouakou et al. found that the polysaccharide component AP-AU-1, which is extracted from *Alchornea cordifolia*, downregulates the expression of cytokines such as IL-1 β , IL-6, IL-10, TNF- α , and GM-CSF in *in vitro* cultures of human and mouse macrophages (25). When LPS-activated macrophages were treated with BPs, the release of cytokines in the macrophages was inhibited, and the inhibition rates of TNF- α , IL-1 β , and IL-6 were 50, 89, and 97, respectively (36). Similarly, polysaccharides such as DIP and MSE can promote the release of cytokines in macrophages (26, 54).

TABLE 1 | The information of botanical polysaccharides.

Botany	Polysaccharides	Molecular weight	Ingredient	Glucosidic bond	Activity
<i>Aloe vera</i> L. (6)	PAC-I	10,000 kDa	90% Mannose, galactose, glucose, arabinose	β -(1 \rightarrow 4)-D- mannose	Anti-tumor, stimulate T and B cell proliferation, promote the production of IL-1 β , TNF- α , IL-2, IL-6, and IFN- γ
<i>Angelica sinensis</i> (7)	PAC-II	1,300 kDa	90% Mannose, galactose, glucose arabinose	β -(1 \rightarrow 4)-D- mannose	Radioprotection effect (ASP3)
	PAC-III	470 kDa	54% Mannose, 33% galactose, 13% arabinose		
	ASP1		Glucose, galactose, arabinose		
<i>Aconitum cammichaeli</i> (8)	ASP2	34 kDa (ASP3)	Galacturonic acid, rhamnose, galactose, arabinose	α -(1 \rightarrow 6)-D- glucan α -(1 \rightarrow 6)-D- glucan	Stimulate lymphocyte proliferation in mice
	FPS-1	14 kDa	Glucose		
	CPE	33 kDa	18.69% Arabinose, 14% galactose, 50.67% glucose, 12.97% mannose, 2.73% rhamnose, 0.94% xylose		
<i>Ilex polycephala</i> (11)	KMCP	1,950 kDa	Arabinogalactan	α -(1 \rightarrow 6)-D- glucan	Stimulate the synthesis of NO in macrophage
<i>Ipomoea batatas</i> (12)	PSPP	53.2 kDa	Glucan		
<i>Juniperus scopolorum</i> (13)	J-I- J-V	30-680 kDa	Arabogalactan		
<i>Phyllanthus niruri</i> (14)			Rhamnose, arabinose, xylose, galactose, glucose	α -(1 \rightarrow 4)-D- glucan	Stimulates lymphocyte proliferation, activate macrophages and NKcells J-I, J-II, J-III activate macrophages Stimulates the production of superoxide enzymes Antioxidant activity Activate macrophages
<i>Cucurbita moschata</i> (15)	sFTS		Glucose, glucuronic acid, galactose arabinose		
<i>Spondias cytherea</i> (16)			Rhamnose, arabinose, galactose, galacturonic acid		
<i>Vernonia kotschyana</i> (17, 18)	Vk100A2a	20 kDa	Rhamnose, arabinose, galactose	α -(1 \rightarrow 6)-D- glucan α -(1 \rightarrow 6)-D- glucan α -(1 \rightarrow 4)-D- glucan	Complement binding activity, promote B cell proliferation Induce chemotaxis of macrophages, Nk cells and Tcells Complement binding activity Inhibition reverse transcriptase activity of HIV-1
<i>Panax notoginseng</i> (19)	Vk100A2b	115 kDa			
	P1-a	1,140 kDa	Polygalacturonic acid, rhamnose, galactan		
	SMP 1	150 kDa			
<i>Rosa rugosa</i> (20)	SMP 0.5	1,390 kDa			
<i>Salvia miltiorrhiza</i> (21)	RR1	403 kDa	Glucan		Activate macrophages
<i>Tinospora cordifolia</i> (22)	Ths-2		Glucan		Ths-2, Ths-5, and thamnolan stimulate the proliferation of mouse spleen cells; Ths-4 and Ths-5 activate mouse peritoneal macrophages;
<i>Thamnia vermicularis</i> (23)	Ths-4, Ths-5 thamnolan		Furan galactose Furan galactose		Ths-2, Ths-4, and Ths-5 stimulated IL-10 release in spleen cells of mice

The synergistic effect of cytokines and plant polysaccharides on macrophages can also activate the immune response of macrophages. Im et al. found that the synergistic effect of polysaccharides SHP and IFN- γ could stimulate macrophages to release a large number of cytokines such as TNF- α , IL-1 β , and NO. The transcript levels of cytokines TNF- α and IL-1 were also significantly increased. In addition, the synergistic effect caused changes in the differentiation antigens CD11b, CD18, and CD24, which are expressed by macrophages (55).

MECHANISM OF IMMUNOREGULATION BY PLANT POLYSACCHARIDES

The study of mechanisms of immunoregulation by plant polysaccharides has reached the molecule and receptor level. Most research has shown that plant polysaccharides activate macrophages by recognizing and binding to specific receptors on the surfaces of macrophages, which initiates the immune response and exerts an immunomodulatory effect. These macrophage receptors are called pattern recognition molecules. Macrophages can bind to plant-derived polysaccharides and/or glycoproteins by Toll-like receptor 4 (TLR4), CD14, complement receptor 3 (CR3), scavenger receptor (SR), mannose receptor (MR), and Dectin-1. The activation of macrophage receptors can initiate a series of intracellular signaling cascades, leading to the transcriptional activation and production of inflammation-related cytokines (56–60), as shown in the **Figure 1** (35).

TLR4 Mediates the Activation of Macrophages by Plant Polysaccharides

TLR4 is a very important class of membrane receptors that are expressed on the surfaces of macrophages and mediate the activation of macrophages by converting extracellular signals (61–64). The binding of TLR4 to the ligand results in the formation of a complex between the TLR cytoplasmic domain, the adaptor protein myeloid differentiation primary response gene 88 (MyD88), and the interleukin-1 receptor-associated kinase (IRAK), which in turn activates tumor necrosis factor receptor-associated factor 6 (TRAF6) and finally initiates the mitogen-activated protein kinase (MAPK) signaling pathway (65–67). Polysaccharide CPE-II acts on RAW264.7 via TLR4 and TLR2, and it influences the level of IL-6 and NO by regulating MAPKs and nuclear factor- κ B (NF- κ B) (52). Similarly, the effect of G1-4A on macrophage RAW264.7 is related to TLR4. An experiment showed that macrophage activity could be decreased after blocking TLR4 activity using siRNA and antibodies, which suggests that G1-4A activates macrophages via a TLR4-MyD88-dependent pathway (22, 68).

Studies have shown that polysaccharide PG can activate macrophages through TLR4 (37, 69). Because activator protein 1 (AP-1) and MAPK are important downstream signaling molecules that mediate the activation of macrophages and the expression of inflammatory genes, T. Yeo Dae Yoon et al. investigated the effect of PG on AP-1 and MAPK activity in the macrophage RAW264.7. The electrophoretic mobility shift assay (EMSA) results showed that PG significantly increases the DNA binding activity of AP-1, and further experiments

demonstrated that PG activates three subgroups of MAPK (ERK1/2, SAPK/JNK, and p38 MAPK) (37, 66). When the induction effect of PG was detected after pretreatment of macrophages with specific inhibitors of these three kinases, PG did not show an activation effect, and the DNA binding activity of AP-1 was inhibited by the MAPK inhibitors. This indicates that PG activates macrophages through the TLR4 signaling pathway and that MAPK and AP-1 are involved. Wang's research showed that HRWP-A could recover the body condition and activated macrophage in Cyclophosphamide (CTX)-induced immunosuppressed mice which may depended on mouse peritoneal macrophages. qPCR and western blot revealed that HRWP-A upregulated the expression of TLR4 mRNA *in vitro*, and that process was accompanied by a clear increase in MyD88 expression and p-I κ B- α , but these effects were largely abrogated by pretreatment with anti-TLR4 antibodies (37). HRWP-A failed to induce the production of NO, IL-1 β , and IL-6 in peritoneal macrophages prepared from C3H/HeJ mice which have a point mutation in the Tlr4 gene, suggesting the involvement of the TLR4 molecule in HRWP-A-mediated macrophage activation (70).

CD14 and CR3 Mediate the Activation of Macrophages by Plant Polysaccharides

Studies have shown that many different receptors work together through pairing and cooperation. For example, TLR4 and CD14, Dectin-1 and TLR2, and CD14 and CR3 form complexes for signal transduction (71). CD14 is known to be a high-affinity receptor for LPS-activated macrophages. CR3 is a receptor for complement protein and β -glucan. Both are involved in the immune response to plant polysaccharides. CD14 antibody and CR3 antibody significantly reduced the amounts of NO released in PG-induced macrophages, suggesting that the surfaces of these two types of molecules may have binding sites for plant polysaccharides (72). Plant polysaccharides also affect the expression of receptors on the macrophage surface. For example, *Panax ginseng* polysaccharide significantly upregulates the expression of CD14 in mouse peritoneal macrophages and downregulates the expression of CR3 at the same time (73).

SR-Mediated Activation of Macrophages by Plant Polysaccharides

Scavenger receptors have multiple ligands, so these receptors play important roles in pathogen clearance, host defense, and the signal transduction of macrophages (74). Studies have shown that SR and CR3 activate phospholipase C (PLC) after binding to their ligands and that the product of PLC enzymolysis activates protein kinase C (PKC) and phosphatidylinositol 3-kinase (PI3K), resulting in the activation of MAPK, extracellular signal-regulated kinase (ERK), and NF- κ B, eventually triggering gene transcription events (75). PKC is a protein kinase that is commonly expressed in mammals. PKC signaling and MAPK signaling play important roles in the innate immune response of monocyte-macrophages (76).

Nakamura et al. found that the polysaccharide fucoidan, which has anticoagulant and anticancer activity, activates macrophages through SR to release NO (77). In the peritoneal macrophages of wild-type mice, fucoidan stimulates the release

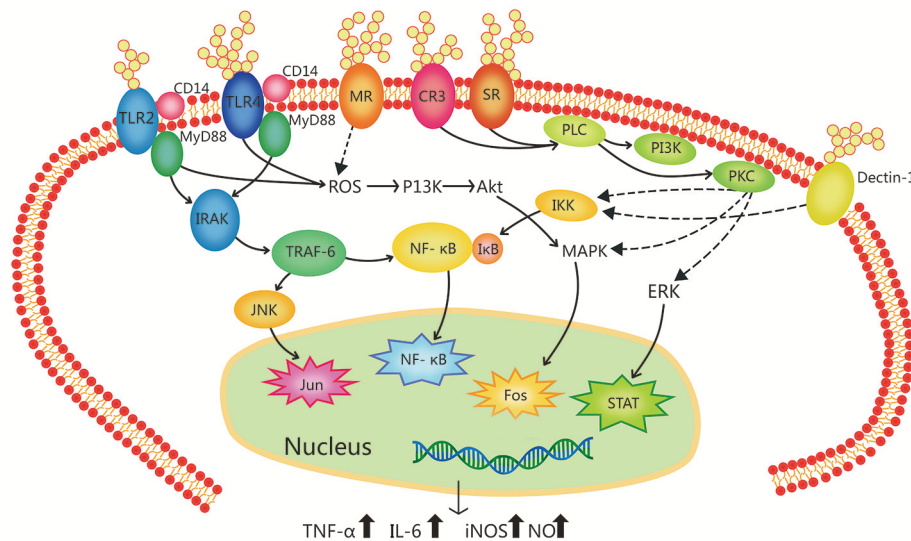


FIGURE 1 | Signal transduction pathway related to the immune-regulation of botanical polysaccharides in macrophage activation. Botanical polysaccharides can activate macrophages via different kinds of receptors, such as Toll-like receptor 4 (TLR4), Toll-like receptor 2 (TLR2), complement receptor 3 (CR3), mannose receptor (MR), scavenger receptor (SR), and Dectin-1. These receptors can work separately, and some different receptor types can cooperate with each other forming clusters of signaling complexes. (e.g., TLR4-CD14, TLR2-CD14, etc.) TLR4 and TLR2 ligation leads to the activation of IL-1R associated kinase (IRAK) via an adaptor myeloid differentiation protein 88 (MyD88), with subsequent activation of TNF receptor-associated factor 6 (TRAF-6), MAP kinases (e.g., p38 and JNK) and NF- κ B. It can also activate phosphoinositide-3-kinase (PI3K)-Akt pathway via reactive oxygen species (ROS), then leading to activation of the mitogen-activated protein kinase (MAPK). SR- and CR3-activated signaling pathways lead to phospholipase C (PLC) activating, whose products activate protein kinase C (PKC) and PI3K, leading to activation of the MAPK, extracellular signal regulated kinase (ERK). Activated PKC can make IKK to be phosphorylated, IKK complex phosphorylates I- κ B which leading the I- κ B ubiquitinated and degraded. In the end, nuclear factor- κ B (NF- κ B) liberated. Ultimately, these activating factors enter the nucleus cause induction of gene transcription. Activation of these transcription pathways induce expression of pro-inflammatory cytokines (TNF- α , IL-6, etc.) and inducible nitric oxide synthase (iNOS).

of NO in a dose-dependent manner, but it does not induce the production of NO in the peritoneal macrophages of SR knockout mice (SR^{-/-}), indicating that fucoidan activates macrophages via the SR pathway (74, 78). Furthermore, inhibition experiments using different signal molecules showed that fucoidan increases iNOS activity in macrophages through p38 MAPK signaling and NF- κ B signaling, thereby increasing the release of NO. p38 MAPK can activate multiple transcription factors, including cAMP-response element binding protein (CREB) and AP-1, and it participates in multiple processes of post-transcriptional gene regulation. Therefore, fucoidan and NF- κ B may have a synergistic effect on the activation of macrophages by the p38 MAPK pathway (79).

MR Mediates the Activation of Macrophages by Plant Polysaccharides

The mannose receptor is an important member of the C-type lectin-like receptor family. It can recognize glycosylated molecules that contain a mannose residue, a trehalose group, or an N-acetyl glucose residue (80). Many mannose receptors are expressed on the surfaces of alveolar macrophages, peritoneal macrophages, and mononuclear macrophages in blood, and they play an important role in the early immune response. After binding to plant polysaccharide ligands, mannose receptors can increase the phagocytic activity of macrophages, produce ROS, activate the transcription factor NF- κ B, and induce the secretion of cytokines (81).

Dectin-1 Mediates the Activation of Macrophages by Plant Polysaccharides

Dectin-1 is a surface receptor that is expressed in immune cells to defend against fungal pathogens. It is a type II membrane protein with a molecular weight of 28 kDa. Sequencing analysis showed that the extracellular domain of Dectin-1 is a C-type lectin-like receptor that binds β -glucan (82, 83). Dectin-1 recognizes glucans linked by β -1,3 and β -1,6 glycosidic bonds, which are derived from yeast, other fungi, plants, and bacteria, and it mediates phagocytosis and the immune response of macrophages to glucan while promoting the release of inflammatory mediators in macrophages (82, 83). Dectin-1 can also form a signaling complex with TLR2 to transmit the stimulatory signals of macrophages. During the signal transduction, the expression of Dectin-1 in the activated macrophages is significantly increased compared with that found in cells in a resting state (83).

Other Pathways to Activate Macrophages by Plant Polysaccharides

In addition to interacting with receptors to activate macrophages, plant polysaccharides can reach the interior of macrophages via phagocytosis. Unlike starch and glycogen, the phagocytosed plant polysaccharide molecules are not easily digested completely; therefore, the incompletely degraded polysaccharides can activate macrophages as a co-stimulatory signal (84).

Although multiple signaling pathways are involved in the activation of macrophages, almost all such signals are ultimately attributed to the expression of inflammation-related cytokines

and inducible nitric oxide synthase (iNOS). NF- κ B is a group of pleiotropic transcription factors that are known to be activated by more than 400 stimuli, and the number of stimuli is still increasing. NF- κ B is an important transcription factor regulating the immune response and inflammatory response. It mainly plays a role in regulating cell proliferation and apoptosis and immune and inflammatory responses, and it regulates the transcription of a variety of pro-inflammatory genes. iNOS is an important inflammatory gene regulated by NF- κ B. Studies have shown that a variety of polysaccharides, such as APS, AP-AU, CPE, and KMCP, can enhance the transcriptional activity of iNOS by activating NF- κ B, thus promoting the generation of NO in macrophages (11, 25, 52, 85).

PERSPECTIVE

The developments in mass spectrometry, GC-MS, X-ray fiber diffraction, nuclear magnetic resonance, electron diffraction, and other analytical techniques have made it possible to obtain structural information about plant polysaccharides and their mechanisms. However, there are still many unresolved issues. First, the relationship between the structure and function of plant polysaccharides is still not fully understood. The activities of polysaccharides originating from the same plant are also very different, suggesting that the structures of polysaccharides are directly related to the biological activities (59). However, due to the complex structure and wide variety of polysaccharides, the isolation, purification, and structure determination of polysaccharides are very difficult. Therefore, the structural characteristics of most of the reported active polysaccharides remain unclear.

Second, a large number of inflammatory mediators released in macrophages after activation by plant polysaccharides may cause excessive inflammation in the body. The appropriate amount of NO released by macrophages can exert beneficial functions and protect the body from adverse factors. If the macrophages receive continuous stimulation and release excessive NO, this may lead to sepsis and local or systemic inflammatory disorders. In particular, excessive inflammation is seriously harmful to human health. A large amount of experimental and clinical evidence indicates that long-term inflammation can increase the risk of cancer because a variety of inflammatory mediators can directly regulate the expression of oncogenes. In addition, key inflammation-related enzymes such as iNOS and COX-2 are associated with cancer induced by long-term inflammation (86, 87). Therefore, it is important to continue studying whether the pro- and anti-inflammatory factors induced by plant polysaccharides can maintain equilibrium in the body without causing harm due to excessive activation. The impact of this factor should be considered in clinical applications.

REFERENCES

1. Zhou JC, Fu TT, Sui N, Guo JR, Feng G, Fan JL, Song J. The role of salinity in seed maturation of the euhalophyte *Suaeda salsa*. *Plant Biosyst.* (2016) 150:83–90. doi: 10.1080/11263504.2014.976294

Third, the problem of endotoxin contamination in active plant polysaccharides needs to be excluded. Because polymyxin B can inhibit the activity of LPS, it is often used to indirectly detect the contamination of LPS. However, studies have shown that polymyxin B has different levels of impact on iNOS expression and cytokine production in addition to inhibiting LPS activity (88). Therefore, this detection method is also controversial. Finding safer and more effective methods for the detection of endotoxin contamination is another urgent problem to be solved.

Fourth, plant polysaccharides and microorganism-derived polysaccharides can bind to the same receptors on the surfaces of macrophages and induce similar immune responses, suggesting that polysaccharides from different sources may be highly conserved throughout evolutionary history. Therefore, we speculate that the response of macrophages to plant polysaccharides may mimic their natural immune responses to microbial pathogens. Although plant polysaccharides can bind to different receptors on the surfaces of macrophages, they activate similar signaling pathways. Does this mean that there is coordination or crosstalk between the signals transmitted by different receptors? These problems need to be further investigated.

With the rapid development of biology and medicine, the study of plant polysaccharides is receiving more extensive attention. Although there are still many unsolved puzzles in the field, the clinical value and broad application prospects of plant polysaccharides make them an important direction for the development of new drugs. A variety of plant polysaccharides have been used as drugs or as adjuvants to enhance drug efficacy or reduce side effects. As research progresses, the immunomodulatory mechanisms of active plant polysaccharides will be explained more clearly, and more active plant polysaccharides will be developed and utilized.

AUTHOR CONTRIBUTIONS

All authors listed have made a substantial, direct and intellectual contribution to the work, and approved it for publication. MY and HL wrote the manuscript together. YZ edited the manuscript.

ACKNOWLEDGMENTS

This work was supported by grants from the Shandong Provincial Natural Science Foundation of China (ZR2017BC073 and ZR2011HZ004) and the Project of Shandong Province Higher Educational Science and Technology Program (J16LE07 and J10LC21).

2. Zhang J, He C, Wu K, Teixeira da Silva JA, Zeng S, Zhang X, et al. Transcriptome analysis of *dendrobium officinale* and its application to the identification of genes associated with polysaccharide synthesis. *Front Plant Sci.* (2016) 7:5. doi: 10.3389/fpls.2016.00005

3. Zhao X, Leavitt SD, Zhao ZT, Zhang LL, Arup U, Grube M, et al. Towards a revised generic classification of lecanoroid lichens (*Lecanoraceae*, *Ascomycota*) based on molecular, morphological and chemical evidence. *Fungal Diversity* (2016) 78:293–304. doi: 10.1007/s13225-015-0354-5
4. Zha Z, Wang SY, Chu W, Lv Y, Kan H, Chen Q, et al. Isolation, purification, structural characterization and immunostimulatory activity of water-soluble polysaccharides from *Lepidium meyenii*. *Phytochemistry* (2018) 147:184–193. doi: 10.1016/j.phytochem.2018.01.006
5. Kong LA, Xie Y, Hu L, Si JS, Wang ZS. Excessive nitrogen application dampens antioxidant capacity and grain filling in wheat as revealed by metabolic and physiological analyses. *Sci Rep.* (2017) 7:43363. doi: 10.1038/srep43363
6. Leung MY, Liu C, Zhu LF, Hui YZ, Yu B, Fung KP. Chemical and biological characterization of a polysaccharide biological response modifier from *Aloe vera* L. var. *chinensis* (Haw.) Berg. *Glycobiology* (2004) 14:501–10. doi: 10.1093/glycob/cwh050
7. Sun Y, Tang J, Gu X, Li D. Water-soluble polysaccharides from *Angelica sinensis* (Oliv.) Diels: preparation, characterization and bioactivity. *Int J Biol Macromol.* (2005) 36:283–9. doi: 10.1016/j.ijbiomac.2005.07.005
8. Zhao C, Li M, Luo Y, Wu W. Isolation and structural characterization of an immunostimulating polysaccharide from fuzi, *Aconitum carmichaeli*. *Carbohydr Res.* (2006) 341:485–491. doi: 10.1016/j.carres.2005.11.032
9. Wu XM, Tu PF. Isolation and characterization of alpha-(1→6)-glucans from *Cistanche deserticola*. *J Asian Nat Prod Res.* (2005) 7:823–8. doi: 10.1080/10286020410001721087
10. Kim AJ, Kim YO, Shim JS, Hwang JK. Immunostimulating activity of crude polysaccharide extract isolated from *Curcuma xanthorrhiza* Roxb. *Biosci Biotechnol Biochem.* (2007) 71:1428–38. doi: 10.1271/bbb.60241
11. Luo B, Dong LM, Xu QL, Zhang Q, Liu WB, Wei XY, et al. Characterization and immunological activity of polysaccharides from *Ixeris polycephala*. *Int J Biol Macromol.* (2018) 113:804–12. doi: 10.1016/j.ijbiomac.2018.02.165
12. Zhao G, Kan J, Li Z, Chen Z. Characterization and immunostimulatory activity of an (1→6)-a-D-glucan from the root of *Ipomoea batatas*. *Int Immunopharmacol.* (2005) 5:1436–45. doi: 10.1016/j.intimp.2005.03.012
13. Schepetkin IA, Faulkner CL, Nelson-Overton LK, Wiley JA, Quinn MT. Macrophage immunomodulatory activity of polysaccharides isolated from *Juniperus scopulorum*. *Int Immunopharmacol.* (2005) 5:1783–99. doi: 10.1016/j.intimp.2005.05.009
14. Mellinger CG, Carbonero ER, Noletto GR, Cipriani TR, Oliveira MB, Gorin PA, et al. Chemical and biological properties of an arabinogalactan from *Phyllanthus niruri*. *J Nat Prod.* (2005) 68:1479–83. doi: 10.1021/np050129s
15. Yang X, Zhao Y, Lv Y. Chemical composition and antioxidant activity of an acidic polysaccharide extracted from *Cucurbita moschata* Duchesne ex Poiret. *J Agric Food Chem.* (2007) 55:4684–90. doi: 10.1021/jf070241r
16. Iacomini M, Serrato RV, Sasaki GL, Lopes L, Buchi DF, Gorin PA. Isolation and partial characterization of a pectic polysaccharide from the fruit pulp of *Spondias cytherea* and its effect on peritoneal macrophage activation. *Fitoterapia* (2005) 76:676–83. doi: 10.1016/j.fitote.2005.08.017
17. Nergard CS, Matsumoto T, Inngjerdengen M, Inngjerdengen K, Hokputsa S, Harding SE, et al. Structural and immunological studies of a pectin and a pectic arabinogalactan from *Vernonia kotschyana* Sch. Bip. ex Walp. (Asteraceae). *Carbohydr Res.* (2005) 340:115–30. doi: 10.1016/j.carres.2004.10.023
18. Nergard CS, Kiyohara H, Reynolds JC, Thomas-Oates JE, Matsumoto T, Yamada H, et al. Structure-immunomodulating activity relationships of a pectic arabinogalactan from *Vernonia kotschyana* Sch. Bip. ex Walp. *Carbohydr Res.* (2005) 340:1789–801. doi: 10.1016/j.carres.2005.05.012
19. Zhu Y, Pettolino F, Mau SL, Shen YC, Chen CF, Kuo YC, et al. Immunoactive polysaccharide-rich fractions from *Panax notoginseng*. *Planta Med.* (2006) 72:1193–9. doi: 10.1055/s-2006-947222
20. Fu M, Ng TB, Jiang Y, Pi ZF, Liu ZK, Li L, et al. Compounds from rose (*Rosa rugosa*) flowers with human immunodeficiency virus type 1 reverse transcriptase inhibitory activity. *J Pharm Pharmacol.* (2006) 58:1275–80. doi: 10.1211/jpp.58.9.0015
21. Wang X, Gao A, Jiao Y, Zhao Y, Yang X. Antitumor effect and molecular mechanism of antioxidant polysaccharides from *Salvia miltiorrhiza* Bunge in human colorectal carcinoma LoVo cells. *Int J Biol Macromol.* (2018) 108:625–34. doi: 10.1016/j.ijbiomac.2017.12.006
22. Gupta PK, Rajan MGR, Kulkarni S. Activation of murine macrophages by G1-4A, a polysaccharide from *Tinospora cordifolia*, in TLR4/MyD88 dependent manner. *Int Immunopharmacol.* (2017) 50:168–77. doi: 10.1016/j.intimp.2017.06.025
23. Omarsdottir S, Freysdottir J, Olafsdottir ES. Immunomodulating polysaccharides from the lichen *Thamnolia vermicularis* var. *subuliformis*. *Phytomedicine* (2007) 14:179–84. doi: 10.1016/j.phymed.2006.11.012
24. Liu C, Leung MY, Koon JC, Zhu LF, Hui YZ, Yu B, et al. Macrophage activation by polysaccharide biological response modifier isolated from *Aloe vera* L. var. *chinensis* (Haw.) Berg. *Int Immunopharmacol.* (2006) 6:1634–41. doi: 10.1016/j.intimp.2006.04.013
25. Kouakou K, Schepetkin IA, Yapi A, Kirpotina LN, Jutila MA, Quinn MT. Immunomodulatory activity of polysaccharides isolated from *Alchornea cordifolia*. *J Ethnopharmacol.* (2013) 146:232–42. doi: 10.1016/j.jep.2012.12.037
26. Jaja-Chimedza A, Graf BL, Simmler C, Kim Y, Kuhn P, Pauli GF, et al. Biochemical characterization and anti-inflammatory properties of an isothiocyanate-enriched moringa (*Moringa oleifera*) seed extract. *PLoS ONE* (2017) 12:e0182658. doi: 10.1371/journal.pone.0182658
27. Chen L, Huang G. Antitumor activity of polysaccharides: an overview. *Curr Drug Targets* (2018) 19:89–96. doi: 10.2174/1389450118666170704143018
28. Zhao X, Li J, Liu Y, Wu D, Cai P, Pan Y. Structural characterization and immunomodulatory activity of a water soluble polysaccharide isolated from *Botrychium ternatum*. *Carbohydr Polym.* (2017) 171:136–42. doi: 10.1016/j.carbpol.2017.05.014
29. Kralovec JA, Mettera KL, Kumar JR, Watson LV, Girouard GS, Guan Y, et al. Immunostimulatory principles from *Chlorella pyrenoidosa*—part 1: isolation and biological assessment *in vitro*. *Phytomedicine* (2007) 14:57–64. doi: 10.1016/j.phymed.2005.09.002
30. Lo TC, Kang MW, Wang BC, Chang CA. Glycosyl linkage characteristics and classifications of exo-polysaccharides of some regionally different strains of *Lentinula edodes* by amplified fragment length polymorphism assay and cluster analysis. *Anal Chim Acta* (2007) 592:146–53. doi: 10.1016/j.aca.2007.04.021
31. Sun YL, Li F, Su N, Sun XL, Zhao SJ, Meng QW. The increase in unsaturation of fatty acids of phosphatidylglycerol in thylakoid membrane enhanced salt tolerance in tomato. *Photosynthetica* (2010) 48:400–8. doi: 10.1007/s11099-010-0052-1
32. Deng YQ, Feng ZT, Yuan F, Guo JR, Suo SS, Wang BS. Identification and functional analysis of the autofluorescent substance in *Limonium bicolor* salt glands. *Plant Physiol Biochem.* (2015) 97:20–7. doi: 10.1016/j.plaphy.2015.09.007
33. Teng L, Fu H, Deng C, Chen J, Chen J. Modulating the SDF-1/CXCL12-induced cancer cell growth and adhesion by sulfated K5 polysaccharides *in vitro*. *Biomed Pharmacother.* (2015) 73:29–34. doi: 10.1016/j.biopha.2015.05.009
34. Cao SN, He JF, Zhang F, Tian HM, Liu CP, Wang HY, et al. *Baeomyces lotiformis* sp. nov. from China. *Mycotaxon* (2017) 132:831–7. doi: 10.5248/132.831
35. Schepetkin IA, Quinn MT. Botanical polysaccharides: macrophage immunomodulation and therapeutic potential. *Int Immunopharmacol.* (2006) 6:317–33. doi: 10.1016/j.intimp.2005.10.005
36. Cheng XQ, Li H, Yue XL, Xie JY, Zhang YY, Di HY, et al. Macrophage immunomodulatory activity of the polysaccharides from the roots of *Bupleurum smithii* var. *parvifolium*. *J Ethnopharmacol.* (2010) 130:363–8. doi: 10.1016/j.jep.2010.05.019
37. Shen XY, Wang ZL, Song XF, Xu JJ, Jiang CY, Zhao YX, et al. Transcriptomic profiling revealed an important role of cell wall remodeling and ethylene signaling pathway during salt acclimation in *Arabidopsis*. *Plant Mol Biol.* (2014) 86:303–17. doi: 10.1007/s11103-014-0230-9
38. Gong WP, Han R, Li HS, Song JM, Yan HF, Li GY, et al. Agronomic Traits and molecular marker identification of wheat-*Aegilops caudata* addition lines. *Front Plant Sci.* (2017) 8:1743. doi: 10.3389/fpls.2017.01743
39. Tong H, Mao D, Zhai M, Zhang Z, Sun G, Jiang G. Macrophage activation induced by the polysaccharides isolated from the roots of *Sanguisorba officinalis*. *Pharm Biol.* (2015) 53:1511–5. doi: 10.3109/13880209.2014.991834
40. Cao S, Du XH, Li LH, Liu YD, Zhang L, Pan X, et al. Overexpression of *Populus tomentosa* cytosolic ascorbate peroxidase enhances abiotic

- stress tolerance in tobacco plants. *Rus J Plant Physiol.* (2017) 64:224–34. doi: 10.1134/s1021443717020029
41. Chen TS, Yuan F, Song J, Wang BS. Nitric oxide participates in waterlogging tolerance through enhanced adventitious root formation in the *euhalophyte Suaeda salsa*. *Funct Plant Biol.* (2016) 43:244–53. doi: 10.1071/fp15120
 42. Kong XQ, Wang T, Li WJ, Tang W, Zhang DM, Dong HZ. Exogenous nitric oxide delays salt-induced leaf senescence in cotton (*Gossypium hirsutum* L.). *Acta Physiol Plantar.* (2016) 38:61. doi: 10.1007/s11738-016-2079-9
 43. Jiang CY, Tholen D, Xu JM, Xin CP, Zhang H, Zhu XG, et al. Increased expression of mitochondrial-localized carbonic anhydrase activity resulted in an increased biomass accumulation in *Arabidopsis thaliana*. *J Plant Biol.* (2014) 57:366–74. doi: 10.1007/s12374-014-0330-8
 44. Park HJ. Immune stimulatory activity of BRP-4, an acidic polysaccharide from an edible plant, *Basella rubra* L. *Asian Pac J Trop Med.* (2014) 7:849–53. doi: 10.1016/j.carbpol.2016.09.079
 45. Martins VM, Simoes J, Ferreira I, Cruz MT, Domingues MR, Coimbra MA. *In vitro* macrophage nitric oxide production by *Pterospartum tridentatum* (L.) Willk. inflorescence polysaccharides. *Carbohydr Polym.* (2017) 157:176–84. doi: 10.1016/j.carbpol.2016.09.079
 46. Liu SP, Dong WG, Wu DF, Luo HS, Yu JP. Protective effect of *angelica sinensis* polysaccharide on experimental immunological colon injury in rats. *World J Gastroenterol.* (2003) 9:2786–90. doi: 10.3748/wjg.v9.i12.2786
 47. DeSalvo SC, Liu Y, Choudhary GS, Ren D, Nangia S, Sureshkumar R. Signaling factor interactions with polysaccharide aggregates of bacterial biofilms. *Langmuir* (2015) 31:1958–66. doi: 10.1021/la504721b
 48. Na YS, Kim WJ, Kim SM, Park JK, Lee SM, Kim SO, et al. Purification, characterization and immunostimulating activity of water-soluble polysaccharide isolated from *Capsosiphon fulvescens*. *Int Immunopharmacol.* (2010) 10:364–70. doi: 10.1016/j.intimp.2009.12.011
 49. Wu MJ, Weng CY, Wang L, Lian TW. Immunomodulatory mechanism of the aqueous extract of sword brake fern (*Pteris ensiformis* Burm.). *J Ethnopharmacol.* (2005) 98:73–81. doi: 10.1016/j.jep.2004.12.031
 50. Zheng P, Fan W, Wang S, Hao P, Wang Y, Wan H, et al. Characterization of polysaccharides extracted from *Platycodon grandiflorus* (Jacq.) A.DC. affecting activation of chicken peritoneal macrophages. *Int J Biol Macromol.* (2017) 96:775–85. doi: 10.1016/j.ijbiomac.2016.12.077
 51. Im SA, Kim K, Lee CK. Immunomodulatory activity of polysaccharides isolated from *Salicornia herbacea*. *Int Immunopharmacol.* (2006) 6:1451–8. doi: 10.1016/j.intimp.2006.04.011
 52. Shin MS, Park SB, Shin KS. Molecular mechanisms of immunomodulatory activity by polysaccharide isolated from the peels of *Citrus unshiu*. *Int J Biol Macromol.* (2018) 112:576–83. doi: 10.1016/j.ijbiomac.2018.02.006
 53. Muzes G, Molnar B, Tulassay Z, Sipos F. Changes of the cytokine profile in inflammatory bowel diseases. *World J Gastroenterol.* (2012) 18:5848–61. doi: 10.3748/wjg.v18.i41.5848
 54. Deng C, Shang J, Fu H, Chen J, Liu H, Chen J. Mechanism of the immunostimulatory activity by a polysaccharide from *Dictyophora indusiata*. *Int J Biol Macromol.* (2016) 91:752–9. doi: 10.1016/j.ijbiomac.2016.06.024
 55. Im SA, Lee YR, Lee YH, Oh ST, Gerelchuluun T, Kim BH, et al. Synergistic activation of monocytes by polysaccharides isolated from *Salicornia herbacea* and interferon-gamma. *J Ethnopharmacol.* (2007) 111:365–70. doi: 10.1016/j.jep.2006.11.027
 56. Chen X, Yu G, Fan S, Bian M, Ma H, Lu J, et al. *Sargassum fusiforme* polysaccharide activates nuclear factor kappa-B (NF-kappaB) and induces cytokine production via Toll-like receptors. *Carbohydr Polym.* (2014) 105:113–20. doi: 10.1016/j.carbpol.2014.01.056
 57. Park CY, Yang YH, Kim SW, Lee SM, Kim HT, Jang BK, et al. Effect of La₂O₃ addition on interface chemistry between 4YSZ top layer and Ni based alloy bond coat in thermal barrier coating by EB PVD. *J Nanosci Nanotechnol.* (2014) 14:8659–64. doi: 10.1166/jnn.2014.10000
 58. Fang Q, Wang JF, Zha XQ, Cui SH, Cao L, Luo JP. Immunomodulatory activity on macrophage of a purified polysaccharide extracted from *Laminaria japonica*. *Carbohydr Polym.* (2015) 134:66–73. doi: 10.1016/j.carbpol.2015.07.070
 59. Liao W, Luo Z, Liu D, Ning Z, Yang J, Ren J. Structure characterization of a novel polysaccharide from *Dictyophora indusiata* and its macrophage immunomodulatory activities. *J Agric Food Chem.* (2015) 63:535–44. doi: 10.1021/jf504677r
 60. Sun W, Hu W, Meng K, Yang L, Zhang W, Song X, et al. Activation of macrophages by the ophiopogon polysaccharide liposome from the root tuber of *Ophiopogon japonicus*. *Int J Biol Macromol.* (2016) 91:918–25. doi: 10.1016/j.ijbiomac.2016.06.037
 61. Bi D, Zhou R, Cai N, Lai Q, Han Q, Peng Y, et al. Alginate enhances Toll-like receptor 4-mediated phagocytosis by murine RAW264.7 macrophages. *Int J Biol Macromol.* (2017) 105:1446–54. doi: 10.1016/j.ijbiomac.2017.07.129
 62. Wang Z, Liu Z, Zhou L, Long T, Zhou X, Bao Y. Immunomodulatory effect of APS and PSP is mediated by Ca²⁺-cAMP and TLR4/NF-kappaB signaling pathway in macrophage. *Int J Biol Macromol.* (2017) 94:283–9. doi: 10.1016/j.ijbiomac.2016.10.018
 63. Zhang XR, Qi CH, Cheng JP, Liu G, Huang LJ, Wang ZF, et al. *Lycium barbarum* polysaccharide LBP4-OL may be a new Toll-like receptor 4/MD2-MAPK signaling pathway activator and inducer. *Int Immunopharmacol.* (2014) 19:132–41. doi: 10.1016/j.intimp.2014.01.010
 64. Jia X, Liang Y, Zhang C, Wang K, Tu Y, Chen M, et al. Polysaccharide PRM3 from *Rhynchosia minima* root enhances immune function through TLR4-NF-kappaB pathway. *Biochim Biophys Acta* (2018) 1862:1751–9. doi: 10.1016/j.bbagen.2018.05.012
 65. Chen H, Zhang L, Long X, Li P, Chen S, Kuang W, Guo J. *Sargassum fusiforme* polysaccharides inhibit VEGF-A-related angiogenesis and proliferation of lung cancer *in vitro* and *in vivo*. *Biomed Pharmacother.* (2017) 85:22–7. doi: 10.1016/j.biopha.2016.11.131
 66. Shen T, Wang G, You L, Zhang L, Ren H, Hu W, et al. Polysaccharide from wheat bran induces cytokine expression via the toll-like receptor 4-mediated p38 MAPK signaling pathway and prevents cyclophosphamide-induced immunosuppression in mice. *Food Nutr Res.* (2017) 61:1344523. doi: 10.1080/16546628.2017.1344523
 67. Zhang HY, Zhang L, Gao B, Fan H, Jin JB, Botella MA, et al. Golgi apparatus-localized synaptotagmin 2 is required for unconventional secretion in arabidopsis. *PLoS ONE* (2011) 6:e26477. doi: 10.1371/journal.pone.0026477
 68. Liu XX, Fu C, Yang WW, Zhang Q, Fan H, Liu J. The involvement of TsFtsH8 in *Thellungiella salsuginea* tolerance to cold and high light stresses. *Acta Physiol Plantarum* (2016) 38:62. doi: 10.1007/s11738-016-2080-3
 69. Ueno M, Hiroki T, Takeshita S, Jiang Z, Kim D, Yamaguchi K, et al. Comparative study on antioxidative and macrophage-stimulating activities of polygluturonic acid (PG) and polymannuronic acid (PM) prepared from alginate. *Carbohydr Res.* (2012) 352:88–93. doi: 10.1016/j.carres.2012.02.005
 70. Wang H, Bi H, Gao T, Zhao B, Ni W, Liu J. A homogalacturonan from *Hippophae rhamnoides* L. Berries enhance immunomodulatory activity through TLR4/MyD88 pathway mediated activation of macrophages. *Int J Biol Macromol.* (2018) 107:1039–45. doi: 10.1016/j.ijbiomac.2017.09.083
 71. Wang CL, Lu CY, Pi CC, Zhuang YJ, Chu CL, Liu WH, et al. Extracellular polysaccharides produced by *Ganoderma formosanum* stimulate macrophage activation via multiple pattern-recognition receptors. *BMC Complement Altern Med.* (2012) 12:119. doi: 10.1186/1472-6882-12-119
 72. Yue GG, Chan BC, Han XQ, Cheng L, Wong EC, Leung PC, et al. Immunomodulatory activities of *Ganoderma sinense* polysaccharides in human immune cells. *Nutr Cancer* (2013) 65:765–74. doi: 10.1080/01635581.2013.788725
 73. Baravalle C, Dallard BE, Cadoche MC, Pereyra EA, Neder VE, Ortega HH, et al. Proinflammatory cytokines and CD14 expression in mammary tissue of cows following intramammary inoculation of Panax ginseng at drying off. *Vet Immunol Immunopathol.* (2011) 144:52–60. doi: 10.1016/j.vetimm.2011.07.003
 74. Do H, Pyo S, Sohn EH. Suppression of iNOS expression by fucoidan is mediated by regulation of p38 MAPK, JAK/STAT, AP-1 and IRF-1, and depends on up-regulation of scavenger receptor B1 expression in TNF-alpha- and IFN-gamma-stimulated C6 glioma cells. *J Nutr Biochem.* (2010) 21:671–9. doi: 10.1016/j.jnutbio.2009.03.013
 75. Murgas P, Cornejo FA, Merino G, von Bernhardt R. SR-A regulates the inflammatory activation of astrocytes. *Neurotox Res.* (2014) 25:68–80. doi: 10.1007/s12640-013-9432-1
 76. Li M, He P, Wu Y, Zhang Y, Xia H, Zheng Y, et al. Stimulatory effects of the degradation products from Mg-Ca-Sr alloy on the osteogenesis through regulating ERK signaling pathway. *Sci Rep.* (2016) 6:32323. doi: 10.1038/srep32323

77. Nakamura T, Suzuki H, Wada Y, Kodama T, Doi T. Fucoidan induces nitric oxide production via p38 mitogen-activated protein kinase and NF-kappaB-dependent signaling pathways through macrophage scavenger receptors. *Biochem Biophys Res Commun.* (2006) 343:286–94. doi: 10.1016/j.bbrc.2006.02.146
78. Teruya T, Tatemoto H, Konishi T, Tako M. Structural characteristics and *in vitro* macrophage activation of acetyl fucoidan from *Cladosiphon okamuranus*. *Glycoconj J* (2009) 26:1019–28. doi: 10.1007/s10719-008-9221-x
79. Che N, Ma Y, Xin Y. Protective Role of Fucoidan in Cerebral Ischemia-Reperfusion Injury through Inhibition of MAPK Signaling Pathway. *Biomol Ther (Seoul)* (2017) 25:272–8. doi: 10.4062/biomolther.2016.098
80. Li WJ, Tang XF, Shuai XX, Jiang CJ, Liu X, Wang LF, et al. Mannose Receptor mediates the immune response to ganoderma atrum polysaccharides in macrophages. *J Agric Food Chem.* (2017) 65:348–57. doi: 10.1021/acs.jafc.6b04888
81. Weiser JN, Roche AM, Hergott CB, LaRose MI, Connolly T, Jorgensen WL, et al. Macrophage migration inhibitory factor is detrimental in pneumococcal pneumonia and a target for therapeutic immunomodulation. *J Infect Dis.* (2015) 212:1677–82. doi: 10.1093/infdis/jiv262
82. Palma AS, Feizi T, Zhang Y, Stoll MS, Lawson AM, Diaz-Rodriguez E, et al. Ligands for the beta-glucan receptor, Dectin-1, assigned using “designer” microarrays of oligosaccharide probes (neoglycolipids) generated from glucan polysaccharides. *J Biol Chem.* (2006) 281:5771–9. doi: 10.1074/jbc.M511461200
83. Lee JB, Tanikawa T, Hayashi K, Asagi M, Kasahara Y, Hayashi T. Characterization and biological effects of two polysaccharides isolated from *Acanthopanax sciadophylloides*. *Carbohydr Polym.* (2015) 116:159–66. doi: 10.1016/j.carbpol.2014.04.013
84. Ueno M, Cho K, Hirata N, Yamashita K, Yamaguchi K, Kim D, et al. Macrophage-stimulating activities of newly isolated complex polysaccharides from *Parachlorella kessleri* strain KNK-A001. *Int J Biol Macromol.* (2017) 104:400–6. doi: 10.1016/j.ijbiomac.2017.06.014
85. Zhao Y, Zhao SS, Mao TL, Qu XL, Cao WH, Zhang L, et al. The plant-specific actin binding protein SCAB1 stabilizes actin filaments and regulates stomatal movement in arabidopsis. *Plant Cell* (2011) 23:2314–30. doi: 10.1105/tpc.111.086546
86. Decker ML, Grobusch MP, Ritz N. Influence of age and other factors on cytokine expression profiles in healthy children—a systematic review. *Front Pediatr.* (2017) 5:255. doi: 10.3389/fped.2017.00255
87. Kikete S, Luo L, Jia B, Wang L, Ondieki G, Bian Y. Plant-derived polysaccharides activate dendritic cell-based anti-cancer immunity. *Cytotechnology* (2018) 70:1097–110. doi: 10.1007/s10616-018-0202-z
88. Sibi G, Rabina S. Inhibition of pro-inflammatory mediators and cytokines by *chlorella vulgaris* extracts. *Pharmacognosy Res.* (2016) 8:118–22. doi: 10.4103/0974-8490.172660

Conflict of Interest Statement: The authors declare that the research was conducted in the absence of any commercial or financial relationships that could be construed as a potential conflict of interest.

Copyright © 2019 Yin, Zhang and Li. This is an open-access article distributed under the terms of the Creative Commons Attribution License (CC BY). The use, distribution or reproduction in other forums is permitted, provided the original author(s) and the copyright owner(s) are credited and that the original publication in this journal is cited, in accordance with accepted academic practice. No use, distribution or reproduction is permitted which does not comply with these terms.



Super-Low Dose Lipopolysaccharide Dysregulates Neutrophil Migratory Decision-Making

Brittany P. Boribong¹, Mark J. Lenzi², Liwu Li^{2*} and Caroline N. Jones^{2*}

¹ Genetics, Bioinformatics, and Computational Biology, Virginia Polytechnic Institute and State University, Blacksburg, VA, United States, ² Department of Biological Sciences, Virginia Polytechnic Institute and State University, Blacksburg, VA, United States

OPEN ACCESS

Edited by:

Catarina R. Almeida,
University of Aveiro, Portugal

Reviewed by:

Claudia Ida Brodskyn,
Gonçalo Moniz Institute (IGM), Brazil
Peter Monk,
University of Sheffield,
United Kingdom

*Correspondence:

Liwu Li
lwli@vt.edu
Caroline N. Jones
jonescn@vt.edu

Specialty section:

This article was submitted to
Molecular Innate Immunity,
a section of the journal
Frontiers in Immunology

Received: 21 November 2018

Accepted: 12 February 2019

Published: 12 March 2019

Citation:

Boribong BP, Lenzi MJ, Li L and
Jones CN (2019) Super-Low Dose
Lipopolysaccharide Dysregulates
Neutrophil Migratory Decision-Making.
Front. Immunol. 10:359.
doi: 10.3389/fimmu.2019.00359

Neutrophils are the first responders to infection and play a pivotal role in many inflammatory diseases, including sepsis. Recent studies have shown that lipopolysaccharide (LPS), a classical pattern recognition molecule, dynamically programs innate immune responses. In this study, we show that pre-treatment with super-low levels of LPS [1 ng/mL] significantly dysregulate neutrophil migratory phenotypes, including spontaneous migration and altering neutrophil decision-making. To quantify neutrophil migratory decision-making with single-cell resolution, we developed a novel microfluidic competitive chemotaxis-chip (μC^3) that exposes cells in a central channel to competing chemoattractant gradients. In this reductionist approach, we use two chemoattractants: a pro-resolution (N-Formyl-Met-Leu-Phe, fMLP) and pro-inflammatory (Leukotriene B₄, LTB₄) chemoattractant to model how a neutrophil makes a decision to move toward an end target chemoattractant (e.g., bacterial infection) vs. an intermediary chemoattractant (e.g., inflammatory signal). We demonstrate that naïve neutrophils migrate toward the primary end target signal in higher percentages than toward the secondary intermediary signal. As expected, we found that training with high dose LPS [100 ng/mL] influences a higher percentage of neutrophils to migrate toward the end target signal, while reducing the percentage of neutrophils that migrate toward the intermediary signal. Surprisingly, super-low dose LPS [1 ng/mL] significantly changes the ratios of migrating cells and an increased percentage of cells migrate toward the intermediary signal. Significantly, there was also an increase in the numbers of spontaneously migrating neutrophils after treatment with super-low dose LPS. These results shed light onto the directional migratory decision-making of neutrophils exposed to inflammatory training signals. Understanding these mechanisms may lead to the development of pro-resolution therapies that correct the neutrophil compass and reduce off-target organ damage.

Keywords: neutrophils, chemotaxis, gradients, sepsis, neutrophil memory, lipopolysaccharide, microfluidics

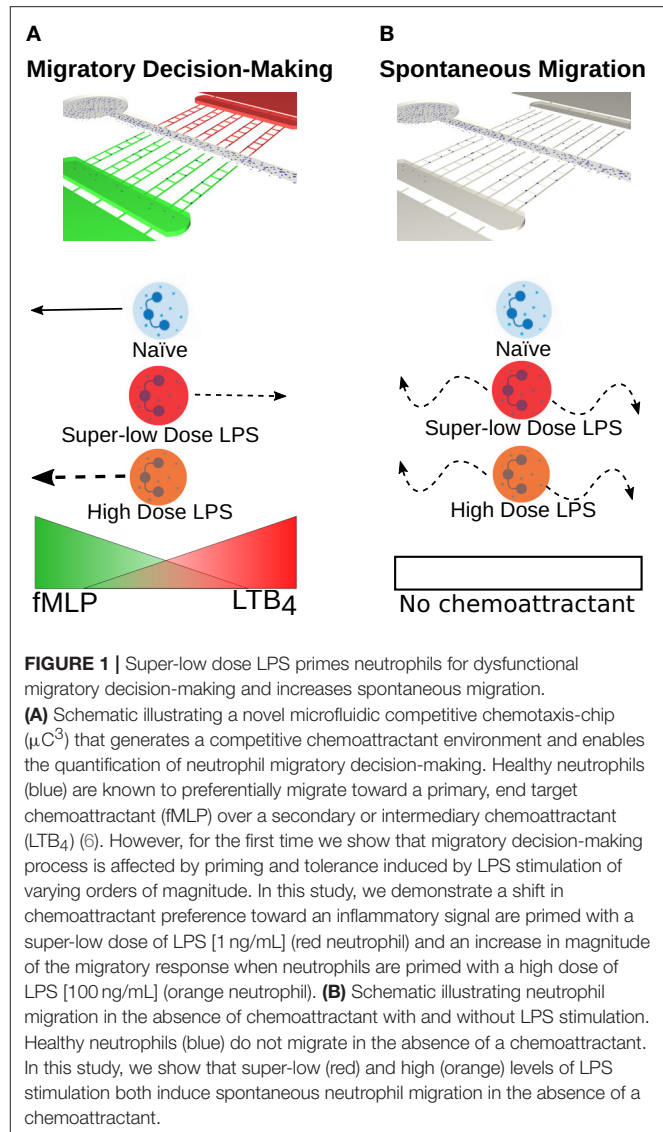
INTRODUCTION

Recent studies suggest that neutrophils are a key player in the development of sepsis, the current leading cause of death in hospitals (1–4). Neutrophils are the most abundant white blood cells (~60%) and are the first responders to infection and inflammation. Neutrophils can navigate effectively through complex tissue microenvironments toward pathogens and play a critical role in controlling infection under normal conditions (5). By necessity, in the setting of multiple

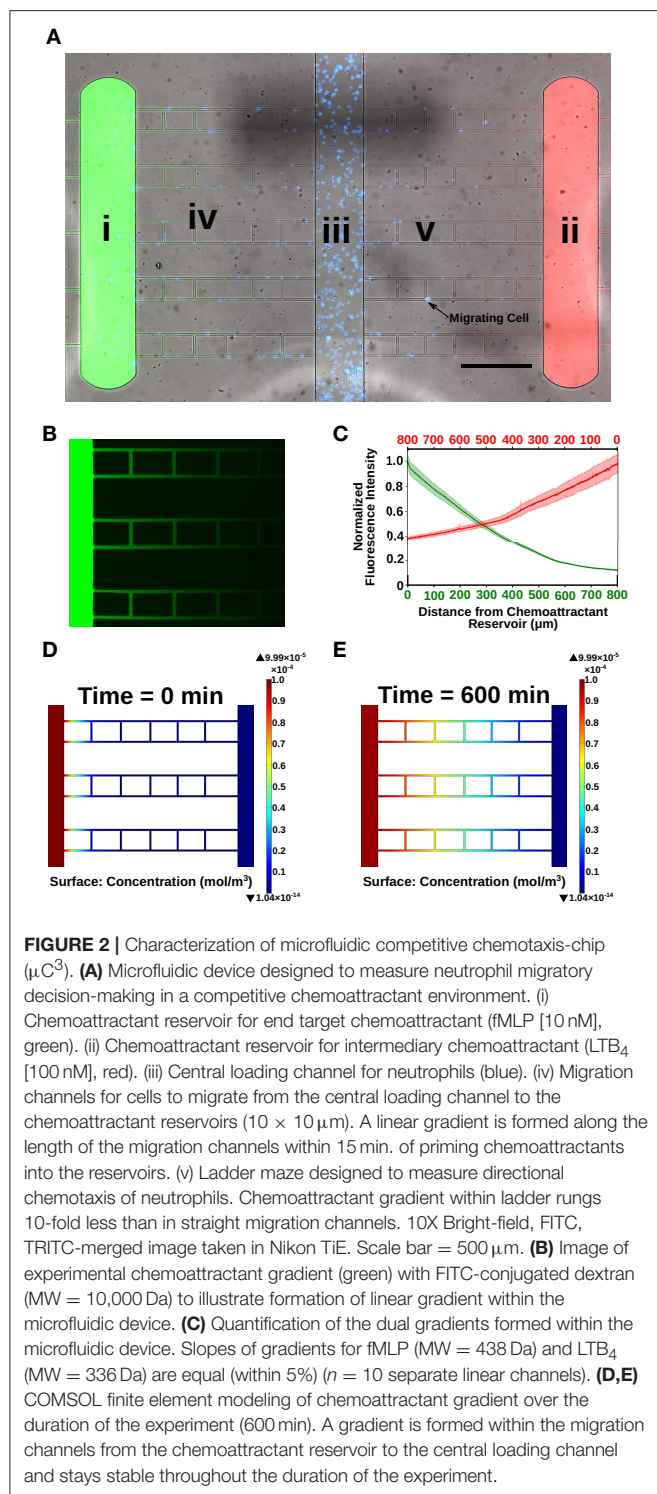
chemoattractants, neutrophils must prioritize, favoring end target chemoattractants (e.g., N-Formyl-Met-Leu-Phe, fMLP) emanating from the site of infection over intermediary endogenous chemoattractants [e.g., Leukotriene B₄ (LTB₄) and interleukin-8 (IL-8)] encountered en route to sites of infection (6). In septic patients, neutrophils migrate and accumulate in healthy organs instead of migrating toward the infection (2). However, lack of control of the tissue microenvironment and the complexity of tracking the trajectories of immune cells *in vivo* prohibits the study of cell migratory decision-making.

Previous work from us described a dysfunctional migration phenotype, including spontaneous migration, in neutrophils isolated from septic burn patients (7). Emerging studies suggest that dynamic programming of neutrophils may induce distinct memory states that influences cell phenotype (8, 9). Exposure to pro-inflammatory cytokines, chemokines, mitochondrial contents, and bacterial and viral products induces neutrophils to transition from a basal state into a primed one, which is currently defined as an enhanced response to activating stimuli (10). Phenotypic changes associated with priming also include activation of a subset of functions, including chemotaxis (3, 11–13). Recent studies from our group have suggested that neutrophil “priming or memory” may play a role in the dysfunction of neutrophils during sepsis. In chronic diseases, it has been shown that super-low levels of LPS prime monocytes, and most likely neutrophils (8, 14–17), for a dysfunctional and intense response to a secondary infection. It is unknown how this neutrophil memory affects cells migration. Previous studies on the hierarchies of chemoattractants show that neutrophils favor primary signals from pathogens over secondary inflammatory signals (18). This makes sense because the primary function of the immune system is to fight infectious invaders. However, these studies only studied the behavior of naïve neutrophils and failed to address the migratory decision-making of “pre-conditioned” memory neutrophils previously exposed to microbial/inflammatory signals. A previous study that examined migration phenotypes of stimulated neutrophils, found neutrophils to favor primary pro-resolution signals over a pro-inflammatory signals (19). However, this study focused on high-dose endotoxin priming [10 ng/mL]. Our study aims to understand the changes in migration patterns caused by neutrophil pre-conditioning with both super-low and high dose of LPS. To achieve this objective, we examined two neutrophil phenotypes: (1) migratory decision-making (**Figure 1A**); and (2) spontaneous migration (**Figure 1B**) following pre-conditioning with varying dosages of LPS. We quantified how super-low dose and high dose LPS pretreatment affects these phenotypes as compared to the “healthy,” untreated naïve cells (**Figure 1**). We hypothesized that the neutrophil migratory decision-making may be differentially affected by varying signal-strengths of LPS pre-conditioning.

To understand neutrophil function, it is important to recapitulate these complex gradients to more accurately depict *in vivo* migration responses in an *in vitro* experimental model. The gold standard to measure chemotaxis is the transwell assay or Boyden Chamber (20). This assay lacks



temporal resolution and measures only end-point neutrophil accumulation, and cannot measure individual cell velocity or directionality. To address these shortcomings, researchers have developed microfluidic assays to study cell chemotaxis in spatiotemporally controlled gradients (21–24). We report a novel microfluidic competitive chemotaxis-chip (μC^3) that enables the measurement of neutrophil migration in the presence of dual gradients (**Figures 1, 2A, Table 1**). The μC^3 allows us to define the competitive migratory behavior of neutrophils with high spatial and temporal resolution. This device is easy to use and does not require valves. Our device incorporates migration channels and mazes that we have recently reported, which will allow us to measure neutrophil directionality (1, 25). Neutrophil migration in confined channels is more directional, easier to quantify and more accurately models migration within the tissue compared to standard planar migration assays (26, 27). Using this device, we examined the migratory decision-making process of dHL-60 cells, a model neutrophil cell line, in the presence of two competing chemotaxis stimulants, LTB₄ and fMLP. fMLP is



a synthetic peptide that resembles bacterial byproducts and is a very powerful chemotactic factor. LTB₄ is a potent lipid mediator of allergic and inflammatory reactions, as well as a potent modulator of neutrophil chemotaxis (28). Furthermore, we use this system to examine the decision-making memory dynamics of dHL-60 neutrophil-like cells pre-challenged with super-low vs.

TABLE 1 | Migration Parameter definitions.

Migratory phenotype	Definition	Units
Percentage of cells migrated (chemoattractant reservoir or migration channels)	Number of Cells in the Chemoattractant Reservoir or Migration Channels at Each Time Point/Average Number of Cells in the Center Loading Channel Throughout Entire Experiment * 100	Percentage (%)
Rate of accumulation	Slope of the 1 h in which cells accumulated in the chemoattractant reservoir the greatest	% cells migrated/hour
dHL-60 Cell velocity	Distance Cell Traveled/ Time Elapsed	$\mu\text{m}/\text{min}$
Non-directional migration	dHL-60 cells that enter the cell mazes	Number of cells
Oscillatory migration	Cells that change directions in the x or y plane ≥ 3 times	Number of cells

high-dose of LPS (**Figure 1**). dHL-60 cells have been extensively characterized and are an accepted model for human peripheral blood neutrophils. Chemokinetic and chemotactic responses to chemotactic peptide are similar for dHL-60 cells and human peripheral blood neutrophils, and mean speed of migration, the fraction of migrated cells and the concentration of stimulus optimal for activation are similar (29–33). Furthermore, these cells have been utilized in previous microfluidic migration assays and work well in these platforms (26, 34, 35). Using dHL-60 cells in our studies enables us to prime cells with varying levels of LPS overnight without effecting the functionality of the cells, as would be the case with primary human peripheral blood neutrophils that have a short half-life (12 h) and lose functionality after being isolated from the blood microenvironment. Recent studies have shown that antioxidant preservatives can be used to extend the functionality of isolated human peripheral blood neutrophils and in future studies we could test LPS priming on primary human cells (36). We will also use primary neutrophils isolated from patients with varying levels of blood LPS (e.g., septic patients), however this will increase variability in samples and prohibit precise control of neutrophil priming conditions. For this proof-of-concept study, dHL-60 cells are an ideal model to allow precise control of cell priming with LPS and to reduce variability in cell decision-making in the presence of defined dual chemoattractant gradients. Our study provides novel insight toward neutrophil decision-making that may model dysregulated neutrophil behavior seen in sepsis.

RESULTS

Design and Optimization of Microfluidic Platform to Study Neutrophil Programming Dynamics by Super-Low Dose Endotoxin

We have designed a novel microfluidic competitive chemotaxis-chip (μC^3) that enables the formation of a dual, competitive chemoattractant gradient. Our μC^3 device is designed with two chemoattractant reservoirs (**Figure 2Ai,ii**) at opposite ends and

a center cell-loading channel (**Figure 2Aiii**). Connecting the cell-loading channel to the chemoattractant reservoirs are 10 linear migration channels on each side (**Figure 2Aiv**). Chemoattractant pipetted into the chemoattractant reservoirs diffuses down through the linear channels, creating a linear gradient from the cell-loading channel to the chemoattractant reservoirs (**Figure 2B**). Also included in the design are vertical cell mazes to test directionality of neutrophil chemotaxis (**Figure 2Av**). The cell mazes have a weaker chemoattractant signal than the linear channels, which enables us to classify the cells ability to follow the stronger gradient, as well as non-persistent chemotaxis. In our experiments, we primed one chemoattractant reservoir with fMLP (a model for an end target, or pro-resolution chemoattractant) and the second chemoattractant reservoir with LTB₄ (a model for an intermediary, pro-inflammatory chemoattractant). This allowed us to probe the decision-making dynamics of individual neutrophils. To evaluate the dynamics and stability of the chemoattractant gradients developed between the chemoattractant reservoirs and the cell-loading channel, we primed reservoir I with FITC-labeled dextran and reservoir II with TRITC-labeled dextran (both molecular mass, 10,000 Da) and measured the fluorescence levels over time. Linear gradients of chemoattractant are formed along the 900- μm -long, $10 \times 10 \mu\text{m}$ cross-section migration channels. The slopes of both gradients are similar ($\pm 5\%$) for both chemoattractants (**Figure 2C**). Biophysical modeling of chemoattractant diffusion in our device using the COMSOL simulation package shows that a chemoattractant gradient along the migration channel to the central cell-loading chamber are formed in <15 min for both chemoattractants and are still present at 5 hours after the start of the experiments (**Figures 2D,E**).

Priming With LPS Significantly Alters Neutrophil Migratory Decision-Making

We measured neutrophil chemotaxis in three different priming scenarios: unstimulated (**Supplementary Video 1**), stimulated with a super-low dose of LPS [1 ng/mL] overnight (**Supplementary Video 2**), stimulated with a high dose of LPS [100 ng/mL] overnight (**Supplementary Video 3**) (37). Cell counts were measured by automated counting of cells that fully migrated to the chemoattractant reservoir. Treatment with super-low dose (2% increase in cell viability compared to untreated control cells) and high dose LPS (no change compared to untreated control cells) had a negligible impact on cell viability (**Supplementary Figure 2**). In the unstimulated cells (**Figure 3A**) and the cells primed with a high dose of LPS (**Figure 3C**), a higher percentage of cells migrated toward fMLP over LTB₄. Treatment with a high-dose of LPS significantly amplified the percentage of dHL-60 cells migrating toward fMLP by ~ 2 -fold (19.4 ± 3.07 vs. $9.157 \pm 3.599\%$) ($p = 0.0199$), while simultaneously decreasing neutrophil migration to LTB₄ by 2-fold (1.894 ± 0.6725 vs. $4.811 \pm 3.822\%$) (**Figure 3D**). Importantly, super-low dose LPS significantly amplified the percentage of cells migrating toward LTB₄ by an order of magnitude (18.52 ± 6.944 vs. $4.811 \pm 3.822\%$) ($p = 0.0401$) and fMLP by ~ 2 -fold (16.06 ± 3.349 vs. $9.157 \pm 3.599\%$) (**Figures 3B,D**). Significantly, programming dHL-60 cells with super-low dose LPS switched cell-decision making priority from an end target chemoattractant (fMLP)

to an intermediary chemoattractant (LTB₄). The ratio of cells prioritizing migration toward a pro-resolution signal was altered in an opposite manner with high (10:1) vs. super-low dose (1:1) LPS-programming compared to untreated control (2:1) (**Figure 3E**). Additionally, stimulation with LPS affected the rate of accumulation of the dHL-60 cells into the chemoattractant reservoirs (**Figure 3F**). Rate of accumulation was measured by calculating the slope of the hour in which there was the highest accumulation of dHL-60 cells. Stimulation with a high-dose of LPS saw a significant increase in the rate of accumulation toward fMLP in comparison to the unstimulated dHL-60 cells ($14.56 \pm 1.388\%$ per hour vs. $4.604 \pm 2.869\%$ per hour) ($p = 0.0057$) (**Figure 3F**). Stimulation with a super-low dose of LPS also saw a ~ 2 -fold increase in the rate of accumulation toward fMLP in comparison to the unstimulated dHL-60 cells ($9.056 \pm 4.209\%$ per hour vs. $4.604 \pm 2.869\%$ per hour) (**Figure 3F**). Importantly, stimulation with super-low dose LPS significantly increases the rate of accumulation of dHL-60 cells toward LTB₄ in comparison to unstimulated dHL-60 cells ($10.73 \pm 0.3047\%$ per hour vs. $1.525 \pm 1.552\%$ per hours) ($p = 0.0005$) (**Figure 3F**). Stimulation with high-dose LPS sees a significant decrease in the rate of accumulation in comparison to the super-low dose LPS ($0.6950 \pm 0.6533\%$ per hour vs. $10.73 \pm 0.3047\%$ per hour) ($p < 0.0001$) (**Figure 3F**).

Single-Cell Analysis of Neutrophil Migratory Decision-Making

To further probe the differences in neutrophil migratory phenotypes caused by programming dHL-60 cells with high and super-low dose LPS, we measure the velocity of individual dHL-60 cells migrating toward both fMLP and LTB₄ chemoattractant gradients (**Table 2**). Interestingly, velocity of neutrophils migrating toward fMLP significantly decreased when neutrophils were stimulated with a super-low dose of LPS (**Figure 4A**) but increased toward LTB₄ (**Figure 4B**). The average dHL-60 velocity toward fMLP when stimulated with super-low dose LPS was $8.54 \mu\text{m}/\text{min}$ compared to $10.51 \mu\text{m}/\text{min}$ in the untreated control ($p < 0.0001$) (**Figure 4A**). Toward LTB₄ the opposite effect was observed, where stimulation with super-low dose LPS resulted in an average velocity of $9.58 \mu\text{m}/\text{min}$ compared to $9.45 \mu\text{m}/\text{min}$ in the untreated control (**Figure 4A**). High dose LPS significantly increased migratory velocity toward fMLP compared to the super-low LPS stimulated dHL-60 cells (10.23 vs. $8.54 \mu\text{m}/\text{min}$) ($p < 0.0001$) and significantly decreased velocity toward LTB₄ in comparison to the super-low dose LPS stimulated cells (8.66 vs. $9.58 \mu\text{m}/\text{min}$) ($p < 0.0001$) (**Figure 4B**). To better visualize the shifts in velocity caused by LPS programming, we binned velocities and graphed the number of cells migrating to each velocity range (**Figures 4C,D**). This clearly illustrates the shift in mid-range and high velocity dHL-60 cells toward fMLP after high dose LPS treatment compared to a shift in mid-range (**Figure 4C**) and high velocity dHL-60s toward LTB₄ after super-low dose LPS treatment (**Figure 4D**). Quantifying single-cell phenotypes will likely be important in the future when measuring primary patient neutrophils where there may be differentially primed sub-populations of neutrophils.

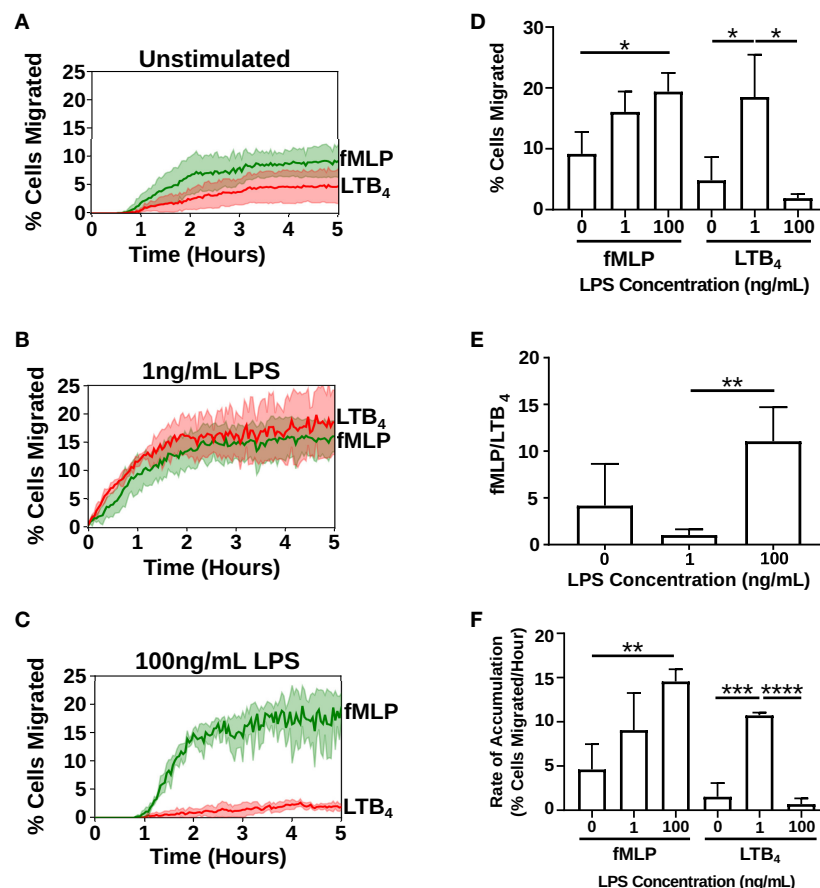


FIGURE 3 | Priming with super-low dose LPS alters neutrophil migratory decision-making. Neutrophil (dHL-60 cells) migration counts in the fMLP chemoattractant reservoir (green) and LTB₄ chemoattractant reservoir (red) over the duration of the experiment (5 h) ($n = 3$ separate experiments). **(A)** Unstimulated neutrophils preferentially migrate toward fMLP over LTB₄. **(B)** Neutrophils stimulated with a super-low dose of LPS [1 ng/mL] preferentially migrate toward LTB₄ over fMLP. **(C)** Neutrophils stimulated with a high dose of LPS [100 ng/mL] preferentially migrate toward fMLP over LTB₄. **(D)** Percentage of cells migrating toward fMLP and LTB₄ in the different treatment groups. dHL-60 cells show a significant increase in migration toward fMLP when stimulated with a high-dose of LPS. dHL-60 cells show a significant increase in migration toward LTB₄ when stimulated with a super-low dose of LPS compared to the unstimulated cells. dHL-60 cells showed a significant decrease in migration toward LTB₄ between the super-low dose and high-dose stimulation with LPS. **(E)** Ratio of cells migrating toward fMLP over LTB₄. Neutrophils significantly migrate toward fMLP over LTB₄ when stimulated with a high-dose of LPS vs. a super-low dose of LPS. **(F)** Calculated slope from the hour in which there was the highest accumulation of dHL-60 cells in the chemoattractant reservoirs. Data expressed as means and standard deviations. * $p < 0.5$, ** $p < 0.005$, *** $p < 0.0005$, **** $p < 0.0001$.

TABLE 2 | Migration variable summary/statistics.

	fMLP ($\mu\text{m}/\text{min}$)	LTB ₄ ($\mu\text{m}/\text{min}$)
Unstimulated	10.51 \pm 3.91	9.45 \pm 3.61
1 ng/mL LPS	8.54 \pm 2.87	9.58 \pm 3.36
100 ng/mL LPS	10.23 \pm 3.57	8.66 \pm 3.14

Super-Low Dose LPS Treatment Increases dHL-60 Cell Oscillatory Migration Patterns and Decreases Cell Directionality

We compared dHL-60 cells migration patterns after 0, 1, and 100 ng/mL LPS overnight treatment. Directional migration was defined as a cell that did not change direction in the x or y plane (Figures 5A,B and Supplementary Video 4). We

measured the number of cells that displayed non-directional migration, in which cells become “lost” and are unable to follow the stronger chemoattractant gradient and therefore enter the maze ladder rung (Figures 5A,B and Supplementary Video 5). We also measured the number of cells that displayed oscillatory migration, in which the cell changed directions in the x or y plane at least three time (Figure 5B and Supplementary Video 6). We showed that super-low dose LPS treatment cause a higher number of cells to become display non-directional migration. The number of cells that entered the ladder rung in the LTB₄ condition after super-low dose LPS treatment increased from 44 to 129 compared to the unprimed control (Figure 5C). A similar trend was also observed in the fMLP condition after super-low dose LPS treatment where cells entering the ladder rung increased from 61 to 178 (Figure 5C). Priming with high dose

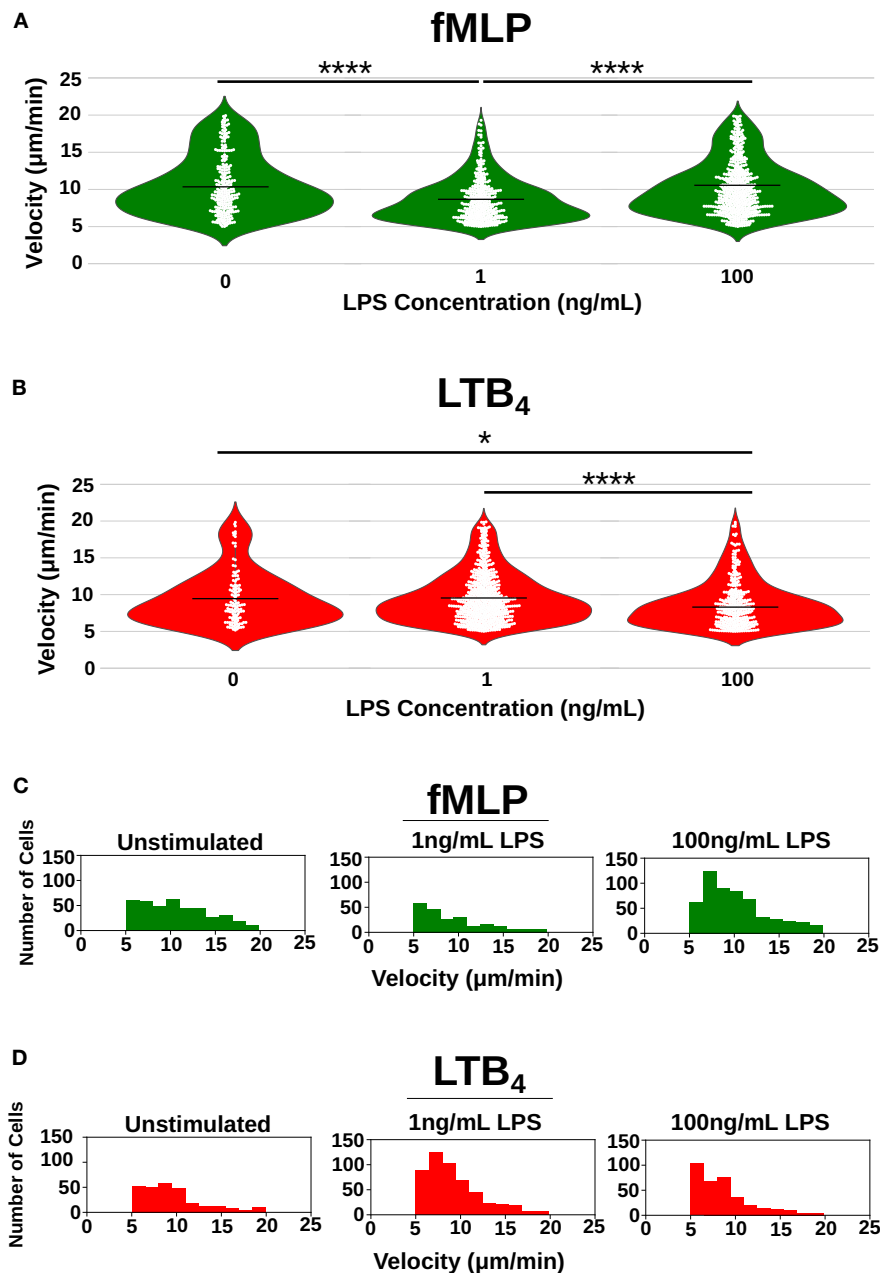


FIGURE 4 | Single-cell quantification of the effect of LPS priming on neutrophil velocity. Velocity [$\mu\text{m}/\text{min}$] of individual neutrophils as they migrate toward fMLP (green) and LTB₄ (red) recorded as a single circle on the plot. **(A)** Violin plots depicting distribution of single-cell velocities of neutrophils migrating toward fMLP in the unstimulated group ($n = 404$), super-low dose stimulated group ($n = 222$), and high-dose stimulated group ($n = 557$) where each white dot represents the velocity of a single-cell. High dose LPS [100 ng/mL] increases the mean velocity of dHL-60 cells migrating toward fMLP, whereas low dose LPS decreases the mean velocity of dHL-60 cells migrating toward fMLP. **(B)** Violin plots depicting distribution of single-cell velocities of neutrophils migrating toward LTB₄ in the unstimulated group ($n = 123$), super-low dose stimulated group ($n = 667$), and high-dose stimulated group ($n = 349$) where each white dot represents the velocity of a single-cell. Super-low dose LPS [1 ng/mL] increased the mean velocity of dHL-60 cells migrating toward LTB₄. **(C)** Histogram depicting distribution of velocities of neutrophils migrating toward fMLP in all three-treatment groups. Super-low dose LPS negatively shifts distribution of cell velocity, whereas high-dose LPS positively shifts distribution of cell velocities toward fMLP. **(D)** Histogram depicting distribution of velocities of neutrophils migrating toward LTB₄ in all three treatment groups. Super-low dose LPS positively shifts distribution of cell velocity, whereas high-dose LPS negatively shifts distribution of cell velocities toward fMLP. Data is representative of one experiment, however experiment was repeated at least 3 times. * $p < 0.05$, **** $p < 0.0001$.

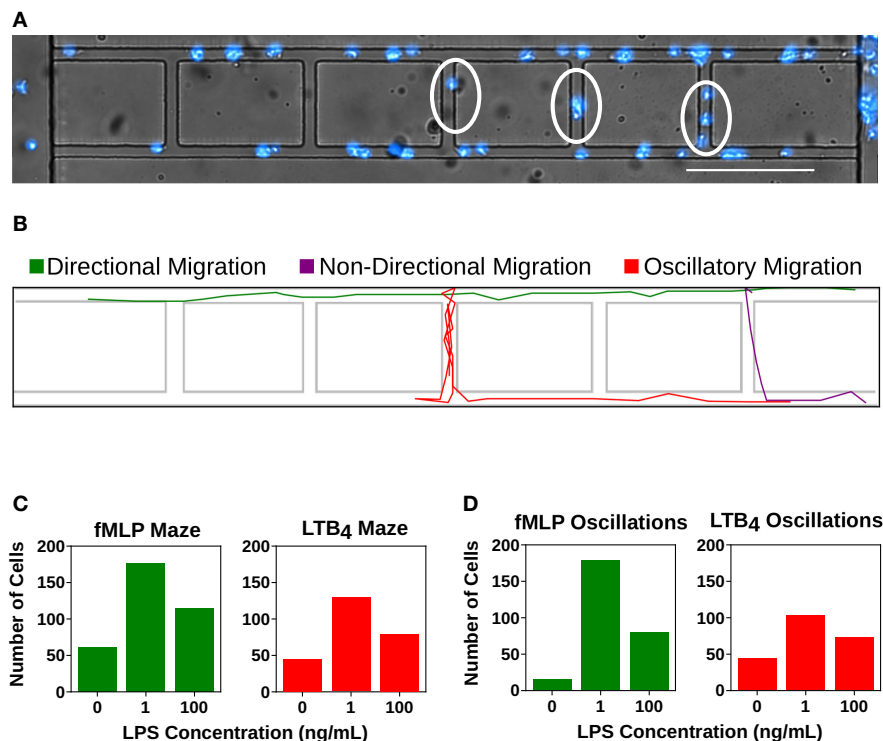


FIGURE 5 | Super-low dose LPS primes neutrophils for dysfunctional chemotaxis. Quantification of cells entering the mazes within the microfluidic device or displaying an oscillatory migration pattern. **(A)** dHL-60 cells (blue) migrating within the microfluidic device. Cells within the linear migration channel are migrating directionally toward the chemoattractant gradient. Circled cells are displaying non-directional migration as they are migrating within the mazes. Scale Bar = 150 μ m. **(B)** Computational recreation of cell migration tracks depicting directional migration (green), non-directional migration (purple), and oscillatory migration (red). **(C)** Number of “lost” cells that entered the maze while migrating toward fMLP (green) and LTB₄ (red) in the unstimulated group (fMLP: $n = 61$, LTB₄: 44), the group stimulated with super-low dose LPS (fMLP: $n = 177$, LTB₄ = 129), and the group stimulated with high-dose LPS (fMLP: $n = 114$, LTB₄: 79). Super-low dose LPS priming significantly increases the number of “lost” cells in both fMLP and LTB₄ conditions compared to both control and high dose LPS treatment groups. **(D)** Number of cells that displayed oscillatory migration patterns while migrating toward fMLP (green) and LTB₄ (red) in the unstimulated group (fMLP: $n = 14$, LTB₄: 43), the group stimulated with super-low dose LPS (fMLP: $n = 178$, LTB₄ = 102), and the group stimulated with high-dose LPS (fMLP: $n = 79$, LTB₄: 72). Super-low dose LPS priming significantly increases the number of oscillatory cells in both fMLP and LTB₄ conditions compared to both control and high dose LPS treatment groups. Data is representative of one experiment, however experiment was repeated at least 3 times.

LPS increased cell non-directionality compared to the unprimed control cells (114 vs. 61 toward fMLP and 79 vs. 44 toward LTB₄), but were only 75% as non-directional compared to the super-low dose treatment (114 vs. 177 toward fMLP and 79 vs. 129 toward LTB₄) (**Figure 5C**). We also observed an increase in oscillatory migration with super-low dose treatment of dHL-60s (**Figure 5D**). The number of cells that displayed oscillatory migration toward fMLP increased from 14 to 178 compared to the unprimed control (**Figure 5D**). Similarly, the number of cells that displayed oscillatory migration toward LTB₄ increased from 43 to 72 compared to the unprimed control (**Figure 5D**).

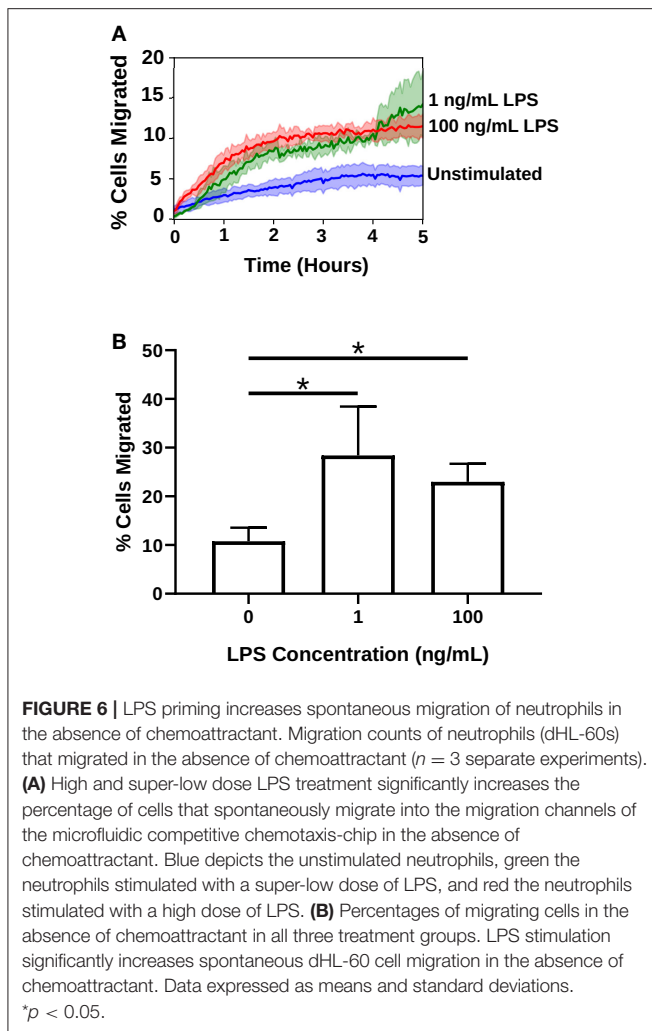
Priming With LPS Increases Spontaneous Migration in dHL-60s

We have previously developed a microfluidic device that identified a sepsis-specific spontaneous migration signature displayed by isolated neutrophils originating from septic patients (1). In order to probe whether programming dHL-60

cells with LPS could recapitulate this spontaneous migration phenotype, we compared cell migration in the absence of chemoattractant with and without pre-treatment with LPS [1 and 100 ng/mL]. In unstimulated cells, only ~10% of dHL-60s migrated in the absence of chemoattractant. After priming with super-low dose LPS [1 ng/mL], spontaneous migration significantly increased to ~30% of cells ($p = 0.0430$) (**Figure 6** and **Supplementary Video 7**). This finding illustrates that the “memory or training” of neutrophils considerably impact future migratory phenotypes.

DISCUSSION

In this study, we establish an effective microfluidic platform for the quantitative analysis of dHL-60 cells migration after LPS priming. For the first time, we demonstrate the significant effect that pre-treatment with super-low dose LPS has on neutrophil migratory decision-making. Super-low dose LPS pretreatment shifted dHL-60 cells to migrate preferentially



toward an intermediary, inflammatory chemoattractant (LTB₄) and increased spontaneous migration patterns. Furthermore, our results provide quantitative evidence, at the single-cell level, that neutrophil priming with varying levels of LPS influences subsequent migratory phenotype in opposing manners. Priming with high levels of LPS increases dHL-60 cells migration, whereas super-low dose LPS priming reverses the chemoattractant priorities of dHL-60 cells. Our data provide a range of quantitative characterizations of dHL-60 cell chemotaxis after LPS priming, including oscillatory migration patterns, directionality and cell velocity.

Although significant progress has been made in understanding the role of neutrophil activation in inflammation, dissecting the decision-making processes in different priming states is hampered by the complexity of *in vivo* conditions and the lack of detail of current *in vitro* assays. Microfluidics are emerging as an important tool for precisely quantifying neutrophil migratory phenotypes (1, 38–40). Compared to transwell (20), under-agarose, or Zigmond chamber assays, microfluidic systems provide extremely stable, linear gradients and allow direct observations and precise measurement of

individual neutrophils during their migration. The microfluidic competitive chemotaxis-chip (μC^3) presented in this study enables migratory decision-making of neutrophils to be observed simultaneously. The measurements enabled by the microfluidic device would not have been possible using traditional tools for observing cell migration. We are able to position a single neutrophil between two competitive signals and decipher how the neutrophil makes a decision which signal to follow. The intrinsic complexity of immune cell decision-making processes has been elusive for experimental immunologists despite expansive experimental studies with conventional reductionist cellular and molecular approaches. Engineering novel technologies to probe the competitive behavior of cells in precisely controlled environments is key to defining the diverse repertoires of cellular activation and differentiation states. A key feature of the assay is the ability to probe the effects of priming dHL-60 cells with varying levels of LPS. On the other hand, microfluidic cell analyses often requires specialized research facilities, such as microfabrication and live cell microscopy labs, as well as highly-skilled personnel to perform the experiments and analyze the data. We have adapted our design to be the first pump-free stand-alone microfluidic dual gradient device, which does not require external instrument controls, such as syringe pumps. The relatively simple and compact design of our microfluidic platform has the scaling potential to enable high-throughput screening of the priming effects of many different inflammatory mediators on a single chip by integrating multiple test units in parallel. In addition, we have developed an improved image analysis method to allow automated single cell tracking analysis, thus eliminate the need of lengthy and laborious post-experiment tracking analysis and permit instant result reporting.

This study confirms that the previous concept of LPS priming observed in monocytes and macrophages extends to neutrophil functional dynamics. Lower doses of LPS can induce a state of tolerance to subsequent toxic doses of LPS (37), but extremely low doses have an opposite effect, priming the immune system for an even more violent response to subsequent challenge. Microfluidic analysis of neutrophil chemotaxis has been recently demonstrated for successful diagnosis of sepsis (1, 4, 41). In sepsis, the immune response that is initiated by an invading pathogen fails to return to homeostasis, thus culminating in a pathological syndrome that is characterized paradoxically by sustained excessive inflammation and immune suppression (42). Correspondingly, pre-conditioning of experimental mice with super-low dose LPS exacerbate sepsis mortality (8). Our results show that pre-treating dHL-60 cells with super-low dose LPS can recapitulate many of the dysfunctional migration phenotypes observed in the septic, mouse model including elevated random migration and skewed migratory preference toward sterile inflammatory signals such as LTB₄. Our data collected with an innovative, reductionist approach microfluidic platform using well-controlled dHL-60 cells pre-conditioned with super-low dose LPS are consistent with the previous animal study that reported increased neutrophil infiltration in multi-organs such as liver and spleen from septic mice pre-conditioned

with super-low dose LPS *in vivo* (8). Recent studies further demonstrated that interruption or reversal of the impaired migration and antimicrobial function of neutrophils improves the outcome of sepsis in animal models (43). We also recently reported on oscillatory and spontaneous migration patterns in primary human peripheral blood neutrophils isolated from burn patients with sepsis (1). Spontaneous neutrophil migration is a unique phenotype, typical for patients with major burns during sepsis and often-observed one or two days before the diagnosis of sepsis is confirmed. The spontaneous neutrophil migration phenotype is rare in patients with major burns in the absence of sepsis, and is not encountered in healthy individuals. The recapitulation of this dysfunctional migratory phenotype in dHL-60 cells treated with super-low dose LPS is unprecedented and may shed light on the underlying preconditions that drive neutrophil dysfunction in sepsis. Further understanding the effects of super-low dose LPS on neutrophil function and decision-making will give insight into the effects of super-low level inflammation on future clinical outcomes. Furthermore, the device presented in this paper may be utilized to understand how programming neutrophils with pro-resolution mediators can restore the neutrophil migratory compass in inflammatory diseases, such as sepsis. One limitation of our study is that we fail to define the impact of neutrophil-neutrophil cross-talk. It is likely that dHL60 cells primed with LPS will produce an increase in pro-inflammatory mediators, including chemokines (LTB₄) that may affect neighboring neutrophil migratory behaviors (8, 44–48). In the future, it will be possible to integrate biosensors in the microfluidic platform to measure neutrophil phenotypes beyond migration, including cytokine secretion levels. Measurements of single-cells migratory trajectories will also enable us to statistically determine if neutrophils are more likely to follow a similar path as a preceding neutrophil. The type of microfluidic platform described in this study will also enable us to measure migratory decision-making of heterogeneous populations of primed and unprimed neutrophils to answer the complex question of whether primed neutrophils will influence the migration of unprimed cells. Furthermore, we can investigate heterogeneous populations of differing immune cells (e.g., neutrophils and TH17 cells or macrophages) (38, 49).

Advances in understanding of neutrophil behavior will come not only from molecular biology studies, but also from neutrophil phenotypic studies enabled by novel microfluidic platforms. In the future, we can engineer platforms with integrated biosensors (e.g., to quantify cytokine secretion) to measure other competitive behaviors of single immune cells, including differentiation or dynamic interaction with pathogens. In this study, we used a neutrophil-like differentiated human promyelocytic leukemia cell line (HL-60). In the future, we can use our platform to quantify neutrophil migratory decision-making from primary neutrophils isolated from mice models of sepsis or human septic patients. This study shows that super-low dose [1 ng/mL] LPS priming can significantly magnify spontaneous migration of neutrophils and redirect the neutrophil compass to favor pro-inflammatory chemoattractant signals. Further study of the effects of neutrophil priming

or memory on migratory decision-making is warranted. A deeper understanding of neutrophil priming mechanisms may ultimately provide the basis for intervention strategies that would enable appropriate infiltration of phagocytes into inflammatory sites while minimizing neutrophil-mediated tissue injury.

MATERIALS AND METHODS

Device Design and Fabrication

The microfluidic platform was designed with 2 opposing chemoattractant reservoirs and a central cell-loading channel (Figure 2A). The cell-loading chamber is connected to the chemoattractant reservoir by perpendicular cell migration ladders that enable precise measurements of cell directional migration and oscillatory migration. The master wafer was fabricated using standard photolithographic technologies with Mylar photomasks (FineLine Imaging, Colorado Springs, CO). Polydimethylsiloxane (PDMS) (Sylgard 184, Elsworth Adhesives, Wilmington, MA) microfluidic devices were made by replica molding from the master wafer. Briefly, PDMS and curing agent were combined at a 10:1 ratio, mixed thoroughly, and poured over the master wafer. PDMS was then degassed for 4 h and baked at 65°C overnight. The PDMS was then peeled from the master wafer, and channel inlets and outlets punched. The two outer chemoattractant loading chamber ports and central neutrophil loading ports were punched using a 1 mm puncher (Harris Uni-Core, Ted Pella Inc., Redding, CA). Each device was then cut out using an 8 mm puncher. Following oxygen plasma treatment (Nordson March, Concord, CA), devices and 6-well glass-bottom plates (MatTek Corp. Ashland, MA) were bonded at 80°C on a hotplate for 10 min.

Preparation of Microfluidic Migration Assay

To increase neutrophil adhesion to surface and to passivate device surface, 50 µL fibronectin (Sigma-Aldrich, St. Louis, MO) [11 µg/mL] was added to the top of the device. Fibronectin, a large glycoprotein, is one of the best-characterized cell adhesion-promoting extracellular matrix proteins (ECM) and is one of the most abundant proteins found in the human ECM (50). Fibronectin has been shown to increase the migration rate of neutrophils and has been used by us in previous microfluidic-based migration studies (1, 51). The device was then placed in a vacuum desiccator for 10 min and the fibronectin solution filled all of the channels as the air was displaced from the PDMS. The devices were then allowed to dry at room temperature for 30 min and the fibronectin absorbed to the glass and PDMS channel surfaces. The devices were then covered with complete media (4 mL). Chemoattractants were diluted using complete media. Ten microliters of each chemoattractant solution (N-Formylmethionine-leucyl-phenylalanine (fMLP, Sigma-Aldrich, St. Louis, MO) [10 nM] and Leukotriene B₄ (LTB₄, Cayman Chemical, Ann Arbor, MI) [100 nM] was then loaded into the chemoattractant reservoirs within the microfluidic device using a gel loading pipette tip. Optimal chemoattractant concentrations were chosen to induce maximal dHL-60 cell migration, are clinically relevant and

match those previously reported (**Supplementary Figure 1**) (1, 38, 52–55). Tetramethylrhodamine fluorescent dextran (10,000 Da MW, Thermo Fisher Scientific, Waltham, MA) and Fluorescein fluorescent dextran (10,000 Da MW, Thermo Fisher Scientific, Waltham, MA) were added for visualization of the chemoattractant gradients in the device. dHL-60 cells [500,000 cell/10 μ L] were loaded into the central cell-loading chamber within the microfluidic device using a gel loading pipette tips. The media surrounding the device was then removed and replaced with new complete media.

Neutrophil Preparation and Treatments

Human promyelocytic leukemia cells (HL-60 CCL-240, American Type Culture Collection ATCC, Manassas, VA) were cultured in complete media containing Iscove's Modified Dulbecco's Medium (IMDM, ATCC, Manassas, VA) supplemented with 10% fetal bovine serum (FBS, ATCC, Manassas, VA) at 37°C in 5% CO₂, according to ATCC instructions. HL-60 cells were differentiated to a neutrophil-like state by adding dimethyl sulfoxide (DMSO, Sigma-Aldrich, St. Louis, MO) (1.5% to 1.5 $\times 10^5$ cells mL⁻¹) for 5 days (26, 56) (denoted as dHL-60 cells). On the fourth day of differentiation, cells were stimulated with lipopolysaccharide (LPS, *Escherichia coli* 0111:B4, Sigma-Aldrich, St. Louis, MO) to a concentration of 1 ng/mL for super-low dose stimulation or 100 ng/mL for high dose stimulation and incubated overnight at 37°C in 5% CO₂. Cell viability was measured using a Trypan Blue exclusion test using an automated cell counter (Bio-Rad TC20™). Immediately prior to the migration experiment, dHL-60 cells were stained with Hoechst solution (Thermo Fisher Scientific, Waltham, MA) at a concentration of 20 mM for 10 min at 37°C in 5% CO₂. Before migration assays, dHL60s were spun down (130G, no break) at RT for 7 min and washed with PBS to remove any dead cells. Viability of dHL-60 cells primed into the neutrophil loading zone of the microfluidic platform were >99% viable, as confirmed by Hoechst stain and neutrophil polarized morphology (change from round to elongated shape) upon live-cell attachment to fibronectin.

Microscopy and Analysis

Time-lapse imaging experiments were performed at 37°C with 5% carbon dioxide on a fully-automated Nikon TiE microscope, using a Plan Fluor 10x Ph1 DLL (NA = 0.3) lens. Image capture was performed using NIS-elements (Nikon Inc., Melville, NY) and analysis performed using the ImageJ (TrackMate) (57). Images were recorded using fluorescent and bright-field channels at two and a half minute intervals for 5 h. dHL-60 cell migration was quantified as followed: (1) percentage of cells

migrating fully toward chemoattractant reservoirs, (2) velocity of migration, and (3) directionality of migration. Cell counts were conducted using ImageJ software (NIH). Cell tracking was performed automatically from DAPI images for the time-lapse sequences. All custom tracking and analysis algorithms are available for download at (<https://github.com/boribong/Single-Cell-Migration-Tracking>). Cell motility definitions are detailed in **Table 1**.

Statistical Analysis

All experiments were performed and replicated at least 3 times, unless otherwise stated. Statistical analysis was performed using Prism software (GraphPad Software, La Jolla, CA). Data expressed as means \pm standard deviations. To compare the parameters of dHL-60 cells migration between unstimulated, 1 ng/mL and 100 ng/mL overnight LPS treatment, we used a Student's *t*-test and differences were considered statistically significant for *p* < 0.05.

AUTHOR CONTRIBUTIONS

CJ and LL conceived the experiment(s). BB and CJ conducted the experiments and analyzed data. ML contributed to microfluidic device design. CJ, BB, and LL wrote the manuscript.

FUNDING

Research materials and equipment for this study were funded by the Department of Biological Sciences at Virginia Tech. BB was supported by the VT-Initiative for Maximizing Student Development (IMSD) (NIGMS 2R25GM072767-05A1). LL is supported by NIH R01 AI136386. This publication was supported in part by the Open Access Subvention Fund (OASF) at Virginia Tech.

ACKNOWLEDGMENTS

We would like to thank Amogh P. Jalihal for his assistance in developing scripts to automate the data analysis. We would also like to thank Lei Zhang for his assistance with the neutrophil illustrations.

SUPPLEMENTARY MATERIAL

The Supplementary Material for this article can be found online at: <https://www.frontiersin.org/articles/10.3389/fimmu.2019.00359/full#supplementary-material>

REFERENCES

- Jones CN, Moore M, Dimisko L, Alexander A, Ibrahim A, Hassell BA., et al. Spontaneous neutrophil migration patterns during sepsis after major burns. *PLoS ONE*. (2014) 9:e114509. doi: 10.1371/journal.pone.0114509
- Shen XF, Cao K, Jiang JP, Guan WX, Du JF. Neutrophil dysregulation during sepsis: an overview and update. *J Cell Mol Med*. (2017) 21:1687–97. doi: 10.1111/jcmm.13112
- Alves-Filho JC, Spiller F, Cunha FQ. Neutrophil paralysis in sepsis. *Shock*. (2010) 34(Suppl. 1):15–21. doi: 10.1097/SHK.0b013e3181e7e61b
- Ellett F, Jorgensen J, Marand AL, Liu YM, Martinez MM, Sein V, et al. Diagnosis of sepsis from a drop of blood by measurement of spontaneous neutrophil motility in a microfluidic assay. *Nat Biomed Eng*. (2018) 2:207–14. doi: 10.1038/s41551-018-0208-z
- Kolaczowska E, Kuberski P. Neutrophil recruitment and function in health and inflammation. *Nat Rev Immunol*. (2013) 13:159–75. doi: 10.1038/nri3399

6. Heit B, Tavener S, Raharjo E, Kubers P. An intracellular signaling hierarchy determines direction of migration in opposing chemotactic gradients. *J Cell Biol.* (2002) 159:91–102. doi: 10.1083/jcb.200202114
7. Demaret J, Venet F, Friggeri A, Cazalis MA, Plassais J, Jallades L, et al. Marked alterations of neutrophil functions during sepsis-induced immunosuppression. *J Leukoc Biol.* (2015) 98:1081–90. doi: 10.1189/jlb.4A0415-168RR
8. Chen K, Geng S, Yuan R, Diao N, Upchurch Z, Li L. Super-low dose endotoxin pre-conditioning exacerbates sepsis mortality. *EBioMedicine.* (2015) 2:324–33. doi: 10.1016/j.ebiom.2015.03.001
9. Pillay J, Ramakers BP, Kamp VM, Loi AL, Lam SW, Hietbrink F, et al. Functional heterogeneity and differential priming of circulating neutrophils in human experimental endotoxemia. *J Leukoc Biol.* (2010) 88:211–20. doi: 10.1189/jlb.1209793
10. Kim JW, Park JH, Kim DJ, Choi WH, Cheong JC, Kim JY. The delta neutrophil index is a prognostic factor for postoperative mortality in patients with sepsis caused by peritonitis. *PLoS ONE.* (2017) 12:e0182325. doi: 10.1371/journal.pone.0182325
11. Alves-Filho JC, Benjamin C, Tavares-Murta BM, Cunha FQ. Failure of neutrophil migration toward infectious focus in severe sepsis: a critical event for the outcome of this syndrome. *Mem Inst Oswaldo Cruz.* (2005) 100(Suppl. 1):223–6. doi: 10.1590/S0074-02762005000900038
12. Reddy RC, Standiford TJ. Effects of sepsis on neutrophil chemotaxis. *Curr Opin Hematol.* (2010) 17:18–24. doi: 10.1097/MOH.0b013e3283338f3
13. Raymond SL, Stortz JA, Mira JC, Larson SD, Wynn JL, Moldawer LL. Immunological defects in neonatal sepsis and potential therapeutic approaches. *Front Pediatr.* (2017) 5:14. doi: 10.3389/fped.2017.00014
14. Guo H, Diao N, Yuan R, Chen K, Geng S, Li M, et al. Subclinical-dose endotoxin sustains low-grade inflammation and exacerbates steatohepatitis in high-fat diet-fed mice. *J Immunol.* (2016) 196:2300–8. doi: 10.4049/jimmunol.1500130
15. Morris MC, Gilliam EA, Li L. Innate immune programming by endotoxin and its pathological consequences. *Front Immunol.* (2014) 5:680. doi: 10.3389/fimmu.2014.00680
16. Yuan R, Geng S, Chen K, Diao N, Chu HW, Li L. Low-grade inflammatory polarization of monocytes impairs wound healing. *J Pathol.* (2016) 238:571–83. doi: 10.1002/path.4680
17. Yuan R, Geng S, Li L. Molecular mechanisms that underlie the dynamic adaptation of innate monocyte memory to varying stimulant strength of TLR ligands. *Front Immunol.* (2016) 7:497. doi: 10.3389/fimmu.2016.00497
18. Lin F, Nguyen CM, Wang SJ, Saadi W, Gross SP, Jeon NL. Neutrophil migration in opposing chemoattractant gradients using microfluidic chemotaxis devices. *Ann Biomed Eng.* (2005) 33:475–82. doi: 10.1007/s10439-005-2503-6
19. Wang X, Qin W, Zhang Y, Zhang H, Sun B. Endotoxin promotes neutrophil hierarchical chemotaxis via the p38-membrane receptor pathway. *Oncotarget.* (2016) 7:74247–58. doi: 10.18632/oncotarget.12093
20. Boyden S. The chemotactic effect of mixtures of antibody and antigen on polymorphonuclear leucocytes. *J Exp Med.* (1962) 115:453–66. doi: 10.1084/jem.115.3.453
21. Yang K, Wu J, Xu G, Xie D, Peretz-Soroka H, Santos S, et al. A dual-docking microfluidic cell migration assay (D(2)-Chip) for testing neutrophil chemotaxis and the memory effect. *Integr Biol (Camb).* (2017) 9:303–12. doi: 10.1039/C7IB00037E
22. Cho H, Hamza B, Wong EA, Irimia D. On-demand, competing gradient arrays for neutrophil chemotaxis. *Lab Chip.* (2014) 14:972–8. doi: 10.1039/C3LC50959A
23. Moussavi-Harami SF, Pezzi HM, Huttenlocher A, Beebe DJ. Simple microfluidic device for studying chemotaxis in response to dual gradients. *Biomed Microdevices.* (2015) 17:9955. doi: 10.1007/s10544-015-9955-8
24. Nakajima A, Ishida M, Fujimori T, Wakamoto Y, Sawai S. The microfluidic lighthouse: an omnidirectional gradient generator. *Lab Chip.* (2016) 16:4382–94. doi: 10.1039/C6LC00898D
25. Ambravaneswaran V, Wong IY, Aranyosi AJ, Toner M, Irimia D. Directional decisions during neutrophil chemotaxis inside bifurcating channels. *Integr Biol.* (2010) 2(11–12): 639–47. doi: 10.1039/c0ib00011f
26. Boneschansker L, Yan J, Wong E, Briscoe DM, Irimia D. Microfluidic platform for the quantitative analysis of leukocyte migration signatures. *Nat Commun.* (2014) 5:4787. doi: 10.1038/ncomms5787
27. Lämmermann T, Germain RN. The multiple faces of leukocyte interstitial migration. *Semin Immunopathol.* (2014) 36:227–51. doi: 10.1007/s00281-014-0418-8
28. Lämmermann T, Afonso PV, Angermann BR, Wang JM, Kastenmüller W, Parent CA, et al. Neutrophil swarms require LTB4 and integrins at sites of cell death *in vivo*. *Nature.* (2013) 498:371–5. doi: 10.1038/nature12175
29. Hauert AB, Martinelli S, Marone C, Niggli V. Differentiated HL-60 cells are a valid model system for the analysis of human neutrophil migration and chemotaxis. *Int J Biochem Cell Biol.* (2002) 34:838–54. doi: 10.1016/S1357-2725(02)00010-9
30. Millius A, Weiner OD. Manipulation of neutrophil-like HL-60 cells for the study of directed cell migration. *Methods Mol Biol.* (2010) 591:147–58. doi: 10.1007/978-1-60761-404-3_9
31. Carrigan SO, Weppler AL, Issekutz AC, Stadnyk AW. Neutrophil differentiated HL-60 cells model Mac-1 (CD11b/CD18)-independent neutrophil transepithelial migration. *Immunology.* (2005) 115:108–17. doi: 10.1111/j.1365-2567.2005.02131.x
32. Liu X, Ma B, Malik AB, Tang H, Yang T, Sun B, et al. Bidirectional regulation of neutrophil migration by mitogen-activated protein kinases. *Nat Immunol.* (2012) 13:457–64. doi: 10.1038/ni.2258
33. Collins SJ, Ruscetti FW, Gallagher RE, Gallo RC. Normal functional characteristics of cultured human promyelocytic leukemia cells (HL-60) after induction of differentiation by dimethylsulfoxide. *J Exp Med.* (1979) 149:969–74. doi: 10.1084/jem.149.4.969
34. Liu Y, Sai J, Richmond A, Wikswo JP. Microfluidic switching system for analyzing chemotaxis responses of wortmannin-inhibited HL-60 cells. *Biomed Microdevices.* (2008) 10:499–507. doi: 10.1007/s10544-007-9158-z
35. Hamza B, Wong E, Patel S, Cho H, Martel J, Irimia D. Retrotaxis of human neutrophils during mechanical confinement inside microfluidic channels. *Integr Biol.* (2014) 6:175–83. doi: 10.1039/C3IB40175H
36. Sandlin RD, Wong KHK, Boneschansker L, Carey TR, Miller KL, Rose G, et al. Preservative solution that stabilizes erythrocyte morphology and leukocyte viability under ambient conditions. *Sci Rep.* (2017) 7:5658. doi: 10.1038/s41598-017-05978-7
37. Murray DA, Wilton JM. Lipopolysaccharide from the periodontal pathogen *Porphyromonas gingivalis* prevents apoptosis of HL60-derived neutrophils *in vitro*. *Infect Immun.* (2003) 71:7232–5. doi: 10.1128/IAI.71.12.7232-7235.2003
38. Jones CN, Dalli J, Dimisko L, Wong E, Serhan CN, Irimia D. Microfluidic chambers for monitoring leukocyte trafficking and humanized nanoporesolving medicines interactions. *Proc Natl Acad Sci USA.* (2012) 109:20560–5. doi: 10.1073/pnas.1210269109
39. Jones CN, Hoang AN, Martel JM, Dimisko L, Mikkola A, Inoue Y, et al. Microfluidic assay for precise measurements of mouse, rat, and human neutrophil chemotaxis in whole-blood droplets. *J Leukoc Biol.* (2016) 100:241–7. doi: 10.1189/jlb.5TA0715-310RR
40. Sackmann EK, Berthier E, Young EW, Shelef MA, Wernimont SA, Huttenlocher A, et al. Microfluidic kit-on-a-lid: a versatile platform for neutrophil chemotaxis assays. *Blood.* (2012) 120:e45–53. doi: 10.1182/blood-2012-03-416453
41. Raymond SL, Mathias BJ, Murphy TJ, Rincon JC, López MC, Ungaro R, et al. Neutrophil chemotaxis and transcriptomics in term and preterm neonates. *Transl Res.* (2017) 190:4–15. doi: 10.1016/j.trsl.2017.08.003
42. van der Poll T, van de Veerdonk FL, Scicluna BP, Netea MG. The immunopathology of sepsis and potential therapeutic targets. *Nat Rev Immunol.* (2017) 17:407–20. doi: 10.1038/nri.2017.36
43. Kurihara T, Jones CN, Yu YM, Fischman AJ, Watada S, Tompkins RG, et al. Resolvin D2 restores neutrophil directionality and improves survival after burns. *FASEB J.* (2013) 27:2270–81. doi: 10.1096/fj.12-219519
44. Doerfler ME, Danner RL, Shelhamer JH, Parrillo JE. Bacterial lipopolysaccharides prime human neutrophils for enhanced production of leukotriene B4. *J Clin Invest.* (1989) 83:970–7. doi: 10.1172/JCI113983
45. Fessler MB, Malcolm KC, Duncan MW, Worthen GS. A genomic and proteomic analysis of activation of the human neutrophil by lipopolysaccharide and its mediation by p38 mitogen-activated protein

- kinase. *J Biol Chem.* (2002) 277:31291–302. doi: 10.1074/jbc.M200755200
46. Akahoshi T, Sasahara T, Namai R, Matsui T, Watabe H, Kitasato H, et al. Production of macrophage inflammatory protein 3alpha (MIP-3alpha) (CCL20) and MIP-3beta (CCL19) by human peripheral blood neutrophils in response to microbial pathogens. *Infect Immun.* (2003) 71:524–6. doi: 10.1128/IAI.71.1.524-526.2003
 47. Naegelen I, Beaume N, Plançon S, Schenten V, Tschirhart EJ, Brécard S. Regulation of neutrophil degranulation and cytokine secretion: a novel model approach based on linear fitting. *J Immunol Res.* (2015) 2015:1–15. doi: 10.1155/2015/817038
 48. Zhang Y, Geng S, Prasad GL, Li L. Suppression of neutrophil antimicrobial functions by total particulate matter from cigarette smoke. *Front Immunol.* (2018) 9:2274. doi: 10.3389/fimmu.2018.02274
 49. Pelletier M, Maggi L, Micheletti A, Lazzeri E, Tamassia N, Costantini C, et al. Evidence for a cross-talk between human neutrophils and Th17 cells. *Blood.* (2010) 115:335–43. doi: 10.1182/blood-2009-04-216085
 50. Hsiao CT, Cheng HW, Huang CM, Li HR, Ou MH, Huang JR, et al. Fibronectin in cell adhesion and migration via N-glycosylation. *Oncotarget.* (2017) 8:70653–68. doi: 10.18632/oncotarget.19969
 51. Everitt EA, Malik AB, Hendey B. Fibronectin enhances the migration rate of human neutrophils *in vitro*. *J Leukoc Biol.* (1996) 60:199–206. doi: 10.1002/jlb.60.2.199
 52. McHugh D, Tanner C, Mechoulam R, Pertwee RG, Ross RA. Inhibition of human neutrophil chemotaxis by endogenous cannabinoids and phytocannabinoids: evidence for a site distinct from CB1 and CB2. *Mol Pharmacol.* (2008) 73:441–50. doi: 10.1124/mol.107.041863
 53. Hoffstein ST, Manzi RM, Razgaitis KA, Bender PE, Gleason J. Structural requirements for chemotactic activity of leukotriene B4 (LTB4). *Prostaglandins.* (1986) 31:205–15. doi: 10.1016/0090-6980(86)90047-X
 54. Elmgreen J, Ahnfelt-Rønne I, Nielsen OH. Inhibition of human neutrophils by auranofin: chemotaxis and metabolism of arachidonate via the 5-lipoxygenase pathway. *Ann Rheum Dis.* (1989) 48:134–8. doi: 10.1136/ard.48.2.134
 55. Nielsen OH, Elmgreen J. Activation of neutrophil chemotaxis by leukotriene B4 and 5-hydroxyeicosatetraenoic acid in chronic inflammatory bowel disease. *Scand J Clin Lab Invest.* (1987) 47:605–11. doi: 10.1080/00365518709168476
 56. Blair OC, Carbone R, Sartorelli AC. Differentiation of HL-60 promyelocytic leukemia cells: simultaneous determination of phagocytic activity and cell cycle distribution by flow cytometry. *Cytometry.* (1986) 7:171–7. doi: 10.1002/cyto.990070208
 57. Tinevez JY, Perry N, Schindelin J, Hoopes GM, Reynolds GD, Laplantine E, et al. TrackMate: an open and extensible platform for single-particle tracking. *Methods.* (2017) 115:80–90. doi: 10.1016/j.jymeth.2016.09.016

Conflict of Interest Statement: The authors declare that the research was conducted in the absence of any commercial or financial relationships that could be construed as a potential conflict of interest.

Copyright © 2019 Boribong, Lenzi, Li and Jones. This is an open-access article distributed under the terms of the Creative Commons Attribution License (CC BY). The use, distribution or reproduction in other forums is permitted, provided the original author(s) and the copyright owner(s) are credited and that the original publication in this journal is cited, in accordance with accepted academic practice. No use, distribution or reproduction is permitted which does not comply with these terms.



DNA Sensor IFI204 Contributes to Host Defense Against *Staphylococcus aureus* Infection in Mice

Wei Chen^{1†}, Shui-Xing Yu^{2†}, Feng-Hua Zhou¹, Xiao-Jing Zhang¹, Wen-Ying Gao³, Kun-Yu Li¹, Zhen-Zhen Liu¹, Wen-Yu Han^{1*} and Yong-Jun Yang^{1*}

¹ Key Laboratory of Zoonosis Research, Ministry of Education, College of Veterinary Medicine, Jilin University, Changchun, China, ² State Key Laboratory of Reproductive Regulation and Breeding of Grassland Livestock, School of Life Sciences, Inner Mongolia University, Hohhot, China, ³ Institute of Translational Medicine, The First Hospital, Jilin University, Changchun, China

OPEN ACCESS

Edited by:

Catarina R. Almeida,
University of Aveiro, Portugal

Reviewed by:

Xiaocui He,
La Jolla Institute for Immunology (LJI),
United States
Santo Landolfo,
University of Turin, Italy

*Correspondence:

Yong-Jun Yang
youngjune@jlu.edu.cn
Wen-Yu Han
hanwy@jlu.edu.cn

[†]These authors have contributed
equally to this work

Specialty section:

This article was submitted to
Molecular Innate Immunity,
a section of the journal
Frontiers in Immunology

Received: 31 December 2018

Accepted: 21 February 2019

Published: 18 March 2019

Citation:

Chen W, Yu S-X, Zhou F-H,
Zhang X-J, Gao W-Y, Li K-Y, Liu Z-Z,
Han W-Y and Yang Y-J (2019) DNA
Sensor IFI204 Contributes to Host
Defense Against *Staphylococcus
aureus* Infection in Mice.
Front. Immunol. 10:474.
doi: 10.3389/fimmu.2019.00474

Interferon-inducible protein (IFI204) (p204, the murine homolog of human IFI16) is known as a cytosolic DNA sensor to recognize DNA viruses and intracellular bacteria. However, little is known about its role during extracellular bacterial infection. Here we show that IFI204 is required for host defense against the infection of *Staphylococcus aureus*, an extracellular bacterial pathogen. IFI204 deficiency results in decreased survival, increased bacterial loads, severe organs damage, and decreased recruitment of neutrophils and macrophages. Production of several inflammatory cytokines/chemokines including IFN- β and KC is markedly decreased, as well as the related STING-IRF3 and NF- κ B pathways are impaired. However, exogenous administration of recombinant KC or IFN- β is unable to rescue the susceptibility of IFI204-deficient mice, suggesting that other mechanisms rather than KC and IFN- β account for IFI204-mediated host defense. IFI204 deficiency leads to a defect in extracellular bacterial killing in macrophages and neutrophils, although bacterial engulf, and intracellular killing activity are normal. Moreover, the defect of bactericidal activity is mediated by decreased extracellular trap formation in the absence of IFI204. Adoptively transferred WT bone marrow cells significantly protect WT and IFI204-deficient recipients against *Staphylococcus* infection compared with transferred IFI204-deficient bone marrow cells. Hence, this study suggests that IFI204 is essential for the host defense against *Staphylococcus* infection.

Keywords: *Staphylococcus aureus* (MRSA), IFI204, DNA sensor, STING, IFI16, innate immune, phagocytosis, extracellular trap

INTRODUCTION

The pathogen *Staphylococcus aureus* persistently colonizes a large proportion of the human population and is a frequent cause of skin and soft tissue infections, pneumonia, and sepsis. Despite intense research in understanding the pathogenesis and host-pathogen interaction, the mechanisms by which *Staphylococcus* is cleared from the host are largely unclarified, thereby impeding the development of novel strategies for control of this infection.

The innate immune system plays a key role in the early recognition and elimination of invading pathogens. Sensing bacteria through pattern recognition receptors (PRRs) enables innate immune cells to categorize microbial invaders and to initiate appropriate signaling cascades that mobilize

defense mechanisms (1). Characterized as a DNA sensor, interferon-inducible protein 204 (IFI204) (its human ortholog IFI16) is one member of PRRs that detects cytosolic DNA for the type I IFN response (2). In response to cytosolic DNA stimulation or virus infection, IFI204/IFI16 interacts with STING to induce TBK1-dependent IFN- β production. Several studies also reported that IFI204/IFI16 recognizes DNA viral genomes in the nucleus and activates the inflammasome pathway through ASC and caspase-1, leading to IL-1 β , and IL-18 production (3, 4).

IFI204/IFI16 is also implicated in sensing intracellular bacterial infection. Knockdown of IFI204/IFI16 by small interfering RNA significantly inhibited IFN- β release in response to intracellular bacterial infections such as *Francisella novicida* (5), *Listeria monocytogenes* (6), *Mycobacterium bovis* (7). Previously, we also showed that *Listeria monocytogenes*-derived genomic DNA triggered programmed cell death in human trophoblasts via IFI16 (8). Obviously, cytosolic bacteria-derived dsDNA is the stimulating ligand for IFI204/IFI16-mediated immune responses.

In contrast to the extensive studies of IFI204/IFI16-mediated response to viral and intracellular bacterial infections through gene knockdown *in vitro*, there is little knowledge regarding the role of IFI204/IFI16 in response to extracellular bacterial infection. Here, using IFI204-deficient mice we explored the action of IFI204 in host defense against *Staphylococcus*, which is generally spoken as an extracellular bacteria.

We find that IFI204 protects the host against *Staphylococcus* infection. IFI204-deficient mice exhibit higher mortality rates, more bacterial loads, and severer organs damage compared with control mice. Although IFI204 deficiency results in a defect of IFN- β and KC production through impairing STING-IRF3 and NF- κ B signaling, neither IFN- β nor KC accounts for IFI204-mediated host defense. IFI204 deficiency inhibits extracellular bacterial killing rather than engulf and intracellular killing activities. Interestingly, we find that the defect of bactericidal activity in the absence of IFI204 is mediated by decreased extracellular trap formation. Collectively, our results suggest that IFI204 is essential for the host defense against extracellular bacterial infection through enhancing bactericidal activity.

MATERIALS AND METHODS

Mice and Cells

IFI204-deficient mice were purchased from Nanjing Biomedical Research Institute of Nanjing University (Nanjing, China) and were subsequently backcrossed onto the C57BL/6J background for another eight generations. Heterozygous breeding pairs were used to generate wild-type (WT) mice. Bone marrow-derived macrophages (BMDMs) were isolated from mouse femurs of 8–10 week old mice and cultured in RPMI1640 medium containing 10% heat-inactivated FBS, 25% L929 cell-conditioned medium,

100 U/mL penicillin, and 100 U/mL streptomycin at 37°C in a humidified atmosphere containing 5% CO₂. Cells were harvested for assays at day 7 of differentiation. For isolation of elicited peritoneal macrophages (PMs), age- and sex-matched WT and IFI204-deficient mice were intraperitoneally (i.p.) injected with 1.0 mL of 3% sterile thioglycollate broth (Sigma-Aldrich). Four days after the injection, cells were harvested by i.p. lavage with ice-cold PBS and cultured in DMEM medium containing 10% heat-inactivated FBS.

Pulmonary and Systemic Infection

Staphylococcus USA300 strain was grown to exponential phase in Tryptic Soy Broth (TSB) at 37°C. Six to eight weeks old sex-matched mice were intranasally or intravenously infected with 1×10^8 or 2×10^8 colony-forming unit (CFU) *Staphylococcus* USA300 diluted in PBS in a total volume of 20 or 200 μ L. Bronchoalveolar lavage fluid (BALF) was obtained by lavaging the lung with 1 mL PBS containing 100 μ g/mL soybean trypsin inhibitor.

Bacterial Burden and Cytokine Measurements

Aseptically excised tissues were homogenized. Serial dilutions of tissue homogenates were plated on agar plates and bacterial loads (CFU/g) were determined by colony counting after overnight incubation. The tissues were homogenized mechanically in cold PBS (at a ratio of 6 mL per gram tissue) containing complete protease inhibitor cocktail and 1% Triton X-100. Tissue homogenates were then centrifuged at 12,000 rpm for 20 min. The supernatants were collected. Concentrations of various cytokines/chemokines in BALF, tissue homogenates or cell culture supernatants were determined by ELISA using antibody pairs from R&D according to manufacturer's manual.

Tissue Histology and Immunostaining

Tissue samples of lung and kidney were fixed in buffered formalin solution (4%) and embedded in paraffin. Tissue sections (5 μ m) were deparaffinized, rehydrated, and stained with hematoxylin-eosin. For immunohistochemistry, sections were subjected to an antigen retrieval step, followed by blocking for 1 h at room temperature, then stained with IFI204 (Lifespan), Ly-6G/Ly-6c (BioLegend), and F4/80 (BioLegend) antibodies. Subsequently, specific staining was detected using the UltraSensitive S-P Kit and DAB Detection Kit (Maixin-Bio) according to the manufacturer's directions. For immunofluorescence, cells were stained with phospho-IRF3 (Santa Cruz), IFI204 (Lifespan), STING (Proteintech) primary antibodies, and Alexa Fluor® 488-conjugated secondary antibodies (Invitrogen). Kidney cell apoptosis was analyzed by TUNEL staining using a commercial kit (KeyGEN Biotech). DAPI (1 μ g/mL) was used to stain nuclei.

Quantitative PCR

RNA was isolated using TRI reagent (Sigma-Aldrich) and converted into cDNA. Subsequently, Real-Time PCR assays were performed using SYBR Green (Roche) on ABI Prism 7500 sequence detection system (Applied Biosystems). Gene expression levels were calculated using the $2^{-\Delta C_t}$ method. The

Abbreviations: IFI204, interferon-inducible protein 204; IFI16, interferon gamma inducible protein 16; *Staphylococcus*, *Staphylococcus aureus*; MOI, multiplicity of infection; BMDM, bone marrow-derived macrophage; PMA, phorbol 12-myristate 13-acetate; PRR, pattern recognition receptor; TLR, toll-like receptor; STING, stimulator of interferon genes; CFU, colony-forming unit; H&E, hematoxylin and eosin; rIFN- β , recombinant IFN- β ; rKC, recombinant KC.

following primers were used: IFN- β sense 5'-ACT GCC TTT GCC ATC CAA GA-3', antisense 5'-CAC TGT CTG CTG GTG GAG TT-3'. KC sense 5'-ACC CTG AAG CTC CCT TGG TT-3', KC antisense 5'-AGA AGC CAG CGT TCA CCA GA-3'. IFI204 sense 5'-CAG GGA AAA TGG AAG TGG TG-3', IFI204 antisense 5'-CAG AGA GGT TCT CCC GAC TG-3'. GAPDH sense 5'-CAC CCC AGC AAG GAC ACT GAG CAA G-3', antisense 5'-GGG GGT CTG GGA TGG AAA TTG TGA G-3'.

Western Blotting

The cells or tissues were homogenized in lysis buffer solution (1% Triton X-100, 50 mM Tris-HCl, 150 mM NaCl, 0.1 mM Na₃VO₄) supplemented with complete protease inhibitor cocktail (Sigma-Aldrich). The lysates were separated by SDS-PAGE, and transferred onto PVDF membrane. The membranes were blotted with antibodies against IFI204 (Lifespan), phospho-IRF3 (Santa Cruz), phospho-I κ B α (Cell Signaling Technology), I κ B α (Cell Signaling), phospho-NF- κ B p65 (Cell Signaling), IRF3 (Abcam), IFI204 (Lifespan), STING (Proteintech), GAPDH (Proteintech), or β -Tubulin (Sungene Biotech).

Administration of Recombinant KC and IFN- β

IFI204^{-/-} mice were i.p. injected recombinant KC or IFN- β (MBL International) at a dose of 1.0 μ g per mouse in 100 μ L PBS on Day -1 and Day 0. The mice were infected intranasally with 1×10^8 CFU of *Staphylococcus* on Day 0. Aseptically excised tissues were homogenized at 24 hpi. Serial dilutions of tissue homogenates were plated on agar plates and bacterial loads (CFU/g) were determined by colony counting after overnight incubation.

In vivo Neutralization of IFNAR1

Mice were i.p. inoculated with 2.5 mg anti-mouse IFNAR1 neutralizing mAb (clone MAR1-5A3, BioXcell) or 2.5 mg IgG isotype control (Clone MOPC-21, BioXcell). Twenty-four hours later, the mice were anesthetized with pentobarbital sodium and i.v. challenged with 2×10^8 CFU of *Staphylococcus* suspended in 200 μ L PBS. Mortality was monitored.

Internalization Assay

To determine whether IFI204 impact the bacterial internalization of *Staphylococcus*, 2.5×10^9 CFU/mL live or heat-killed bacteria were incubated with 0.15 mg/mL fluorescein isothiocyanate (FITC) in the dark for 30 min at RT. The bacteria were washed 3 times with PBS to remove unbound FITC. WT or IFI204^{-/-} BMDM were treated with FITC-labeled live or killed bacteria (MOI = 5) for indicating times. The extracellular fluorescence was quenched using 0.2% trypan blue. The mean fluorescence intensity (MFI) of the FITC-positive cells were determined by flow cytometric analyses.

Intracellular and Extracellular Killing Assays

To determine whether IFI204 impact the intracellular bacterial killing capacity of macrophages, WT or IFI204^{-/-} BMDM were

incubated with *Staphylococcus* (MOI = 5) for 1 h, and then non-engulfed bacteria were killed with 100 μ g/mL gentamicin for 1 h. The cells were lysed with 0.1% Triton X-100 and intracellular bacterial were enumerated by serial dilution and plating on TSB agar plates. To determine whether IFI204 impact the extracellular bacterial killing capacity of macrophages or neutrophils, WT and IFI204^{-/-} BMDM or neutrophil were incubated with *Staphylococcus* (MOI = 5) for 6 h, the supernatant was collected and centrifuged at $600 \times g$ for 5 min. The pelleted bacteria were resuspended in PBS and plated on TSB agar plates to enumerate the extracellular bacteria.

ETs Formation Assays

Bone marrow macrophages or neutrophils were isolated from WT or IFI204^{-/-} mice. The cells were seeded on 12-mm 0.01% poly-L-lysine-coated coverslips in 24 well-plates and were challenged with bacteria (MOI = 50). Cells were fixed with 4% paraformaldehyde and then stained with SYTOX Orange (5 μ M) and Hoechst 33342 (2 μ M). ETs were visualized on a fluorescence microscope and images were taken. Macrophages were stimulated with bacteria (MOI = 50) and PMA (100 nM). SYTOX Orange was added after 6 h and fluorescence was measured by spectrofluorometry.

Adoptive Transfer of Bone Marrow Cells

Six-eight week old mice were lethally irradiated with 10 Gy of γ radiation at a rate of 1.5 Gy/min in a ¹³⁷Cs irradiator. Within 24 h of irradiation, mice received an intravenous injection of 8×10^6 bone marrow cells harvested from the femurs and tibias of WT or IFI204^{-/-} mice. Mice were allowed to recover at least 7 weeks before being used for experiments. Efficient reconstitution by donor bone marrow cells was confirmed by PCR for the IFI204 gene in splenocytes (Figure 8G).

MPO Assay

Lung tissues were homogenized in 0.5% cetyltrimethylammonium chloride (4 μ L/mg lung). The cleared supernatant was used for MPO assay to determine the infiltration of neutrophils. Briefly, samples in duplicate (75 μ L) were mixed with equal volumes of the substrate (3,3', 5,5'-tetramethyl-benzidine dihydrochloride, 3 mmol/L; resorcinol, 120 μ mol/L; and H₂O₂, 2.2 mmol/L) for 2 min. The reaction was stopped by adding 150 μ L of 2 mol/L H₂SO₄. The OD was measured at 450 nm.

Statistical Analysis

Data are represented as mean \pm SEM. Differences between mean values of normally distributed data were assessed with one-way ANOVA (Dunnett's *t*-test) and two-tailed Student's *t*-test. Log-rank test was used for statistical analysis of animal mortality. **p* < 0.05; ***p* < 0.01 compared with control group. Statistical analysis was performed using Prism (GraphPad Software, La Jolla, CA).

RESULTS

IFI204 Deficiency Attenuates Bacterial Clearance Following *Staphylococcus* Pulmonary Infection

Using *Staphylococcus* lung infection model, we initially explored the possible involvement of IFI204 in the host response to *Staphylococcus* infection. WT (wild-type) and IFI204^{-/-} (IFI204-deficient) mice were intranasally infected with 1×10^8 CFU (colony-forming units) of *Staphylococcus*. Bacterial burdens were assessed in BALF (bronchoalveolar lavage fluid), blood and various tissues at 16 hpi by CFU counting. Significantly more bacteria were detected in the lungs, BALF and blood of IFI204^{-/-} mice compared with WT mice (Figures 1A–F). In line with this, histopathological examination of lung tissues 48 h after *Staphylococcus* challenge showed that there were more severe injury in IFI204^{-/-} mice (Figure 1G). To further characterize the role of IFI204 in host defense against *Staphylococcus*, WT and IFI204^{-/-} mice were intranasally infected with 2×10^8 CFU of *Staphylococcus* and animal mortality was then monitored. IFI204^{-/-} mice demonstrated a slight lower survival rate than their WT counterparts within 48 hpi, but the difference was not significant (Figure 1H). Thus, these data suggest that IFI204 is involved in host defense against *Staphylococcus* pulmonary infection.

IFI204 Deficiency Decreased Inflammatory Cells Recruitment and Cytokines/Chemokines Production

To identify the potential mechanisms that contribute to higher bacterial loads in IFI204^{-/-} mice, we examined lung recruitment of neutrophil and macrophage because these cells are critical for the clearance of bacteria. Histological study showed less neutrophils and macrophages accumulation in the airways of IFI204^{-/-} mice at 24 hpi compared with WT mice (Figures 2A,B). In mice receiving the sham-operation, no significant cellular influx was observed in the lung of both genotype mice. To determine if the decreased inflammatory cells influx is dependent on inferior production of cytokines/chemokines following *Staphylococcus* infection, we measured the expression of cytokines (IL-6, IL-1 β , and IFN- β) and chemokines (KC/CXCL1, CXCL2, and CXCL10) in lung homogenates, BALF or blood at 24 h after *Staphylococcus* challenge (Figures 2C–N). Bacterial challenge dramatically induced the release of these cytokines/chemokines from WT mice. However, the production of these cytokines/chemokines in IFI204^{-/-} mice were attenuated compared with WT mice. Thus, IFI204 deficiency results in impaired immune responses to *Staphylococcus* pulmonary infection.

IFI204 Deficiency Attenuates Bacterial Clearance Following *Staphylococcus* Systemic Infection

To further characterize the role of IFI204 in pulmonary defense against *Staphylococcus*, the expression of IFI204 in the lung sections was investigated by immunohistochemical staining.

Our results showed that IFI204 staining was mainly detected in the recruited inflammatory cells of the infected lungs (Figure 3A). Next, we asked if IFI204 regulated host defense against *Staphylococcus* systemic infection. WT and IFI204^{-/-} mice were i.v. infected with 1×10^8 CFU of *Staphylococcus*. Animal mortality was then monitored for 10 d. IFI204^{-/-} mice demonstrated a significantly lower survival rate than their WT counterparts (Figure 3B). Kidney injury was more severe in IFI204^{-/-} mice compared with WT mice as determined by H&E and TUNEL histology (Figures 3C,D). To determine whether a defect in bacterial clearance contribute to the death of IFI204-deficient mice, bacterial numbers in blood, spleen, kidney, and liver were enumerated at 24 hpi. As compared with WT mice, IFI204-deficient mice had higher bacterial burdens in blood and kidney (Figures 3E–H), indicating that IFI204 deficiency facilitates bacterial growth and dissemination.

IFI204 Promotes Cytokines/Chemokines Production in Macrophages

Next, we set out to characterize the inflammatory response in WT and IFI204-deficient macrophages *in vitro*. Bone marrow-derived macrophages (BMDM) derived from WT mice were infected with *Staphylococcus* at a multiplicity of infection (MOI) of 1:50. IFI204 mRNA and protein levels were significantly up-regulated by bacteria challenge (Figures 4A,B). We further examined IFI204 expression by immunofluorescence. IFI204 was detected in the nuclear of WT cells and absent from IFI204-deficient cells (Figure 4C). We next asked if IFI204 deficiency impair cytokines production in macrophages. *Staphylococcus* dramatically induced IFN- β and KC mRNA and protein expression in WT cells (Figures 4D–G). However, the levels of IFN- β and KC were significantly reduced in IFI204-deficient macrophages. IFI204 is characterized as a DNA sensor. A similar effect of IFI204 on KC and IFN- β production triggered by *Staphylococcus*-derived genomic DNA was found (Figures 4H,I). Collectively, these results provided *in vitro* evidence that IFI204 mediates cytokine secretion, which was consistent with the *in vivo* data.

IFI204 Deficiency Suppresses STING-IRF3 and NF- κ B Signaling

To illustrate the signaling mechanism that results in cytokine decrease upon *Staphylococcus* infection in the absence of IFI204, IRF3 activation was assessed by Western blotting. The data showed that IRF3 was hypophosphorylated in IFI204-deficient BMDMs and peritoneal macrophages compared with the control cells (Figure 5A). To further dissect the pathway, we analyzed STING, which plays a pivotal role in DNA-triggered induction of IFN- β (9). A significant decreased induction of STING was seen in IFI204-deficient macrophages (Figure 5A). The defect activation of STING and IRF3 were confirmed by immunofluorescence assay (Figure 5B). IFI204 deficiency also inhibited bacterial genomic DNA-triggered STING and IRF3 activation (Figure 5C). Moreover, NF- κ B signaling was largely impaired in the absence of IFI204, showed by the reduced phosphorylation levels of p65 and I κ B α in the treated IFI204-deficient macrophages (Figure 5D). Consistently, the lung tissues

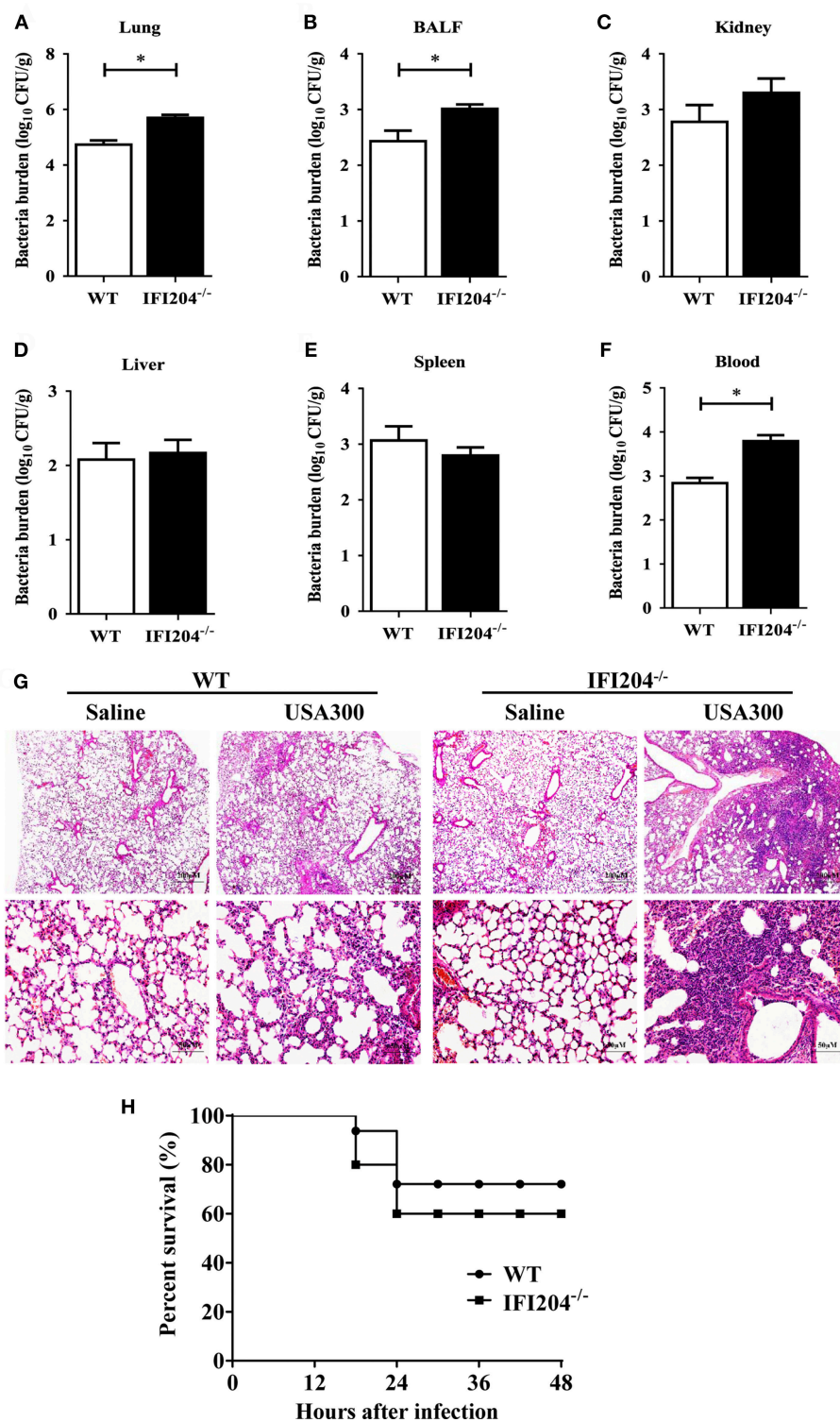


FIGURE 1 | Interferon-inducible protein 204 (IFI204)-deficient mice display increased susceptibility to *Staphylococcus* pulmonary infection. **(A–F)** Age- and sex-matched WT ($n = 8$) and IFI204^{-/-} ($n = 10$) mice were infected intranasally with 1×10^8 CFU of *Staphylococcus*. Homogenized tissues, BALF and blood were subjected to plating serial dilution for bacterial loads at 16 hpi. All data are shown as mean \pm SEM. Student's t -test was performed. * $p < 0.05$. **(G)** Hematoxylin-eosin staining of lung tissues collected from WT and IFI204^{-/-} ($n = 5$ each group) mice at 48 hpi. Magnification 40 \times or 200 \times . **(H)** WT and IFI204^{-/-} mice were inoculated intranasally with 2×10^8 CFU of *Staphylococcus* ($n = 15$) or PBS ($n = 13$). The animals were monitored every 6 h up to 48 h for survival.

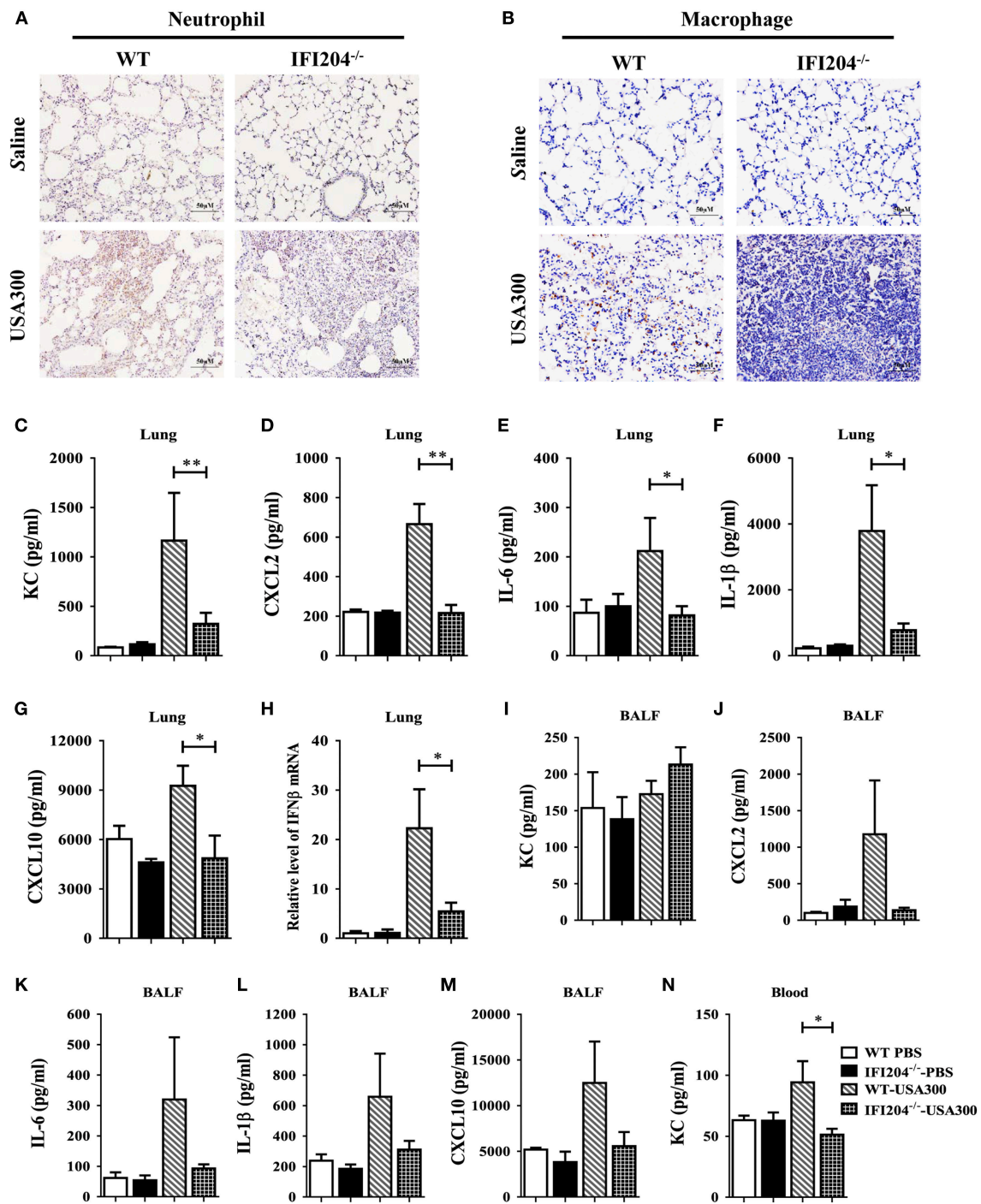


FIGURE 2 | IFI204 is required for elevated inflammatory cells recruitment and cytokines/chemokines production after *Staphylococcus* pulmonary infection. WT and IFI204^{-/-} mice ($n = 10$ each group) were infected intranasally with 1×10^8 CFU of *Staphylococcus* for 24 h. Representative immunohistochemical staining of (A) Gr-1 (a neutrophil marker) and (B) F4/80 (a macrophagocyte marker) were performed in the lung sections. (C–N) Levels of KC, CXCL2, IL-6, IL-1β, CXCL10, and IFN-β in lung, BALF or blood were determined. All data are shown as mean \pm SEM. Student's *t*-test was performed. * $p < 0.05$; ** $p < 0.01$.

of IFI204-deficient mice challenged with bacteria showed a similar trend in significantly reduced STING-IRF3 and NF-κB activation compared with the controls (Figure 5E). Collectively,

these results suggested that upon *Staphylococcus* challenge, IFI204 deficiency impaired the Sting-IRF3 and NF-κB pathways *in vitro* and *in vivo*.

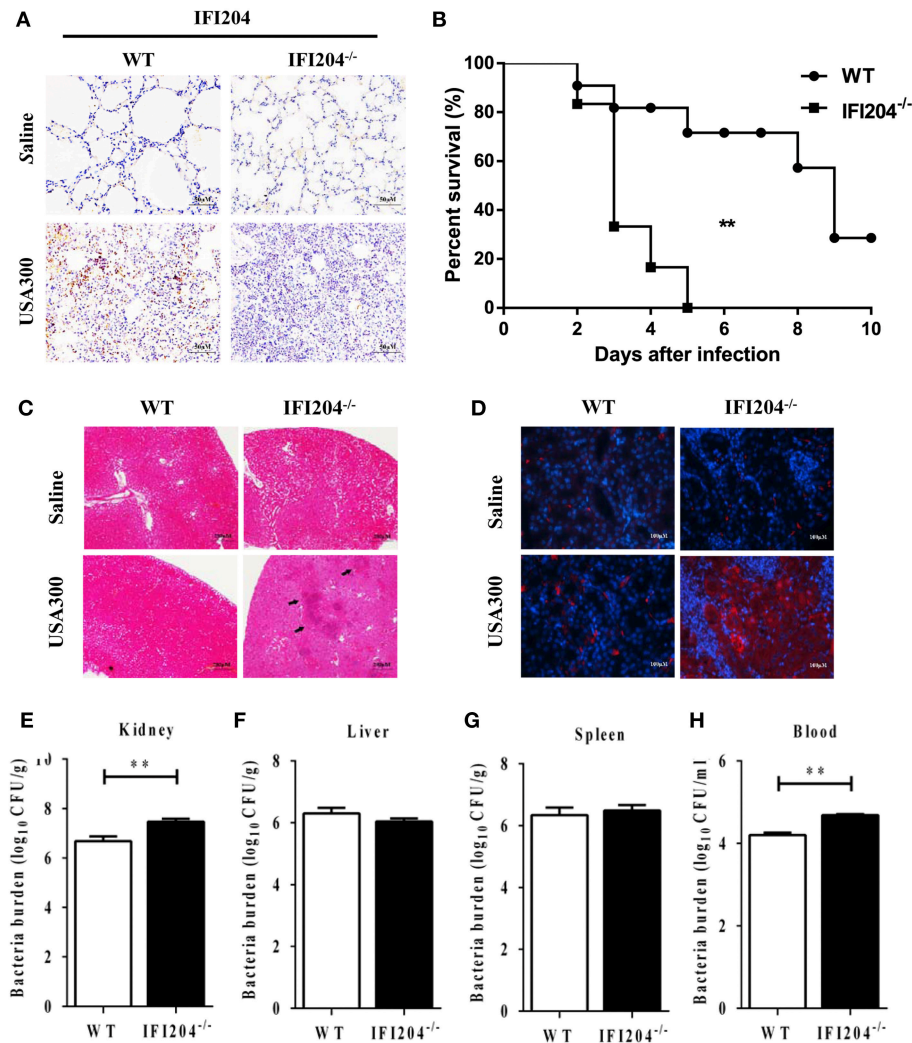


FIGURE 3 | IFI204-deficient mice displayed increased susceptibility to *Staphylococcus* systemic infection. **(A)** Lung sections were stained with anti-IFI204. **(B)** WT ($n = 15$) and IFI204^{-/-} ($n = 13$) mice were infected *i.v.* with 1×10^8 CFU of *Staphylococcus*. The animals were monitored daily up to 10 days for survival. The Kaplan-Meier and log-rank methods were used to analyze survival rates. **(C,D)** Kidney tissues were collected from WT and IFI204^{-/-} mice at 48 hpi ($n = 5$ each group). Kidney injury was assessed by hematoxylin-eosin staining **(C)** and terminal deoxynucleotidyl transferase dUTP nick end labeling (TUNEL) histology **(D)**. Representative results are depicted. **(E-H)** Bacterial loads in kidney, liver, spleen, and blood of WT ($n = 8$) and IFI204^{-/-} ($n = 10$) at 20 hpi were determined. All data are shown as mean \pm SEM. Student's *t*-test was performed. $^{**}p < 0.01$.

Neither KC Nor IFN- β Contributes to IFI204-Mediated Host Defense

Because cytokines generation and related proinflammatory signaling activation markedly attenuated in the absence of IFI204, we next examine whether exogenous administration of recombinant cytokines is able to rescue the susceptibility to infection in IFI204-deficient mice. IFI204-deficient mice were treated prophylactically (day -1 and day 0 of infection) with rKC or IFN- β and then infected with *Staphylococcus*. However, bacterial burdens in the lung tissue at 6 hpi were not inhibited by both recombinant proteins (**Figure 6A**). We further examined the effect of recombinant proteins at 24 hpi. A similar result was got (**Figures 6B,C**). Indeed, blockade of IFN signaling using

anti-IFNAR1 MAb significantly decreased the mortality induced by *Staphylococcus* systemic infection (**Figure 6D**). Therefore, KC and IFN- β was not necessary for the protective effects of IFI204 during bacterial infection.

IFI204 Deficiency Results in the Defect of Extracellular Trap-Mediated Bacteria Killing

Phagocytosis is a critical host defense mechanism used by macrophages. IFI204-deficient mice have elevated numbers of bacteria present in infected tissue, suggesting that these phagocytes are unable to effectively control bacterial multiplication in the absence of IFI204. We further evaluated

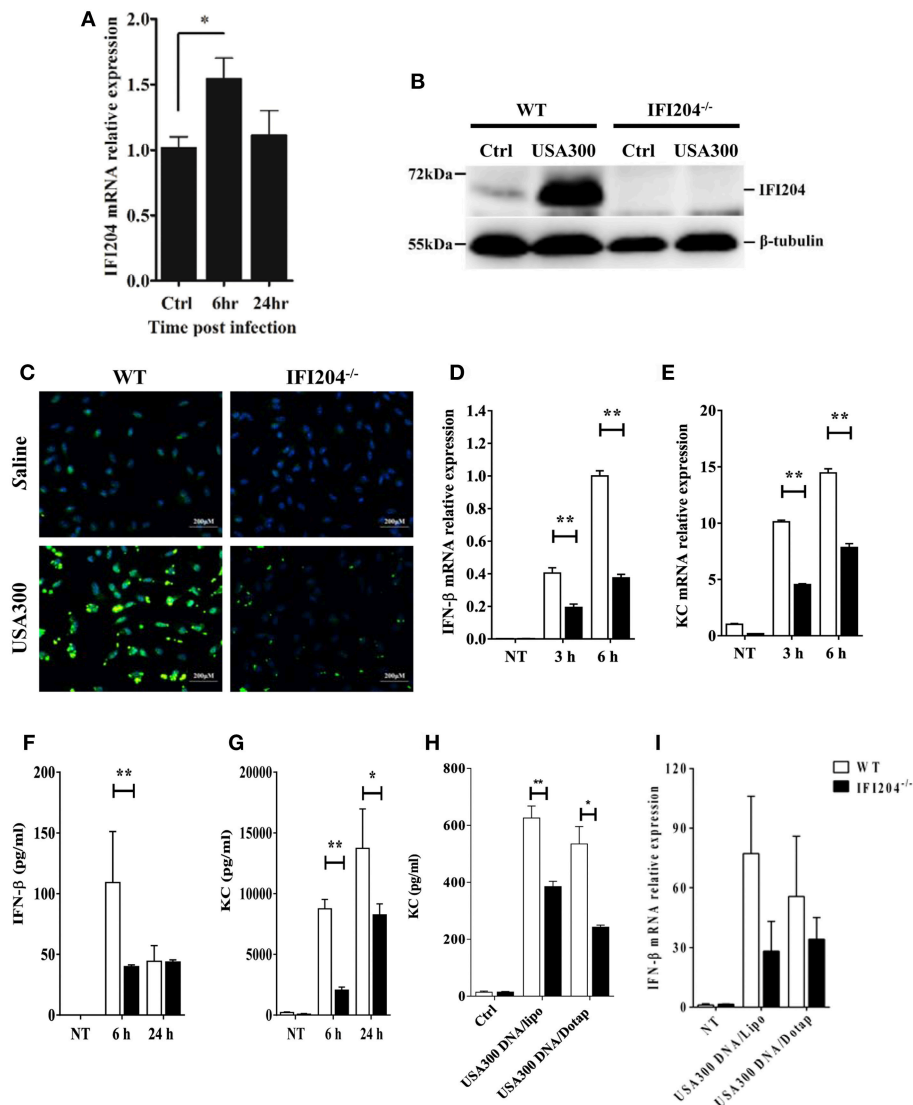


FIGURE 4 | IFI204 is upregulated and promotes proinflammatory cytokines production in BMDM following *Staphylococcus* challenge. WT and IFI204^{-/-} BMDM were untreated or exposed to *Staphylococcus* at a MOI of 1:50 for indicated time. **(A)** IFI204 mRNA levels were measured by qRT-PCR. IFI204 protein in cells at 24 hpi was measured by Western blotting **(B)** and immunofluorescence microscopy **(C)**. Shown are representative images from two independent experiments. **(D–G)** Protein and/or mRNA levels of IFN-β and KC in BMDM were examined at the indicated time after infection. **(H,I)** WT and IFI204^{-/-} BMDM were transfected with *Staphylococcus*-derived genomic DNA using Lipofectamine 2000 or DOTAP. KC and IFN-β levels were quantified by ELISA or qRT-PCR. Data shown is representative of at least three independent experiments. All data are shown as mean ± SEM. Student's *t*-test was performed. **p* < 0.05; ***p* < 0.01.

the bacterial killing capacity of IFI204-deficient macrophages *in vitro*. Our results showed that IFI204-deficient macrophages internalized similar numbers of FITC-labeled live or heat-killed bacteria compared with WT macrophage (**Figures 7A,B**). Moreover, the gentamicin protection assay showed that the number of recovered viable bacteria was comparable in macrophages from both genotypes, indicating IFI204 has no effect on intracellular bacterial killing (**Figure 7C**). Generally speaking, *Staphylococcus* are extracellular bacteria that are eventually killed by phagocytes via multiple mechanisms besides phagocytosis. We further examined whether IFI204 deficiency impair extracellular killing capacity by enumerating bacteria in

supernatants at 6 hpi. The results showed that IFI204 deficiency inhibited the extracellular killing capacity of macrophage (**Figure 7D**). Extracellular trap (ET) provides an extracellular site for microbial killing in the innate immune defense. To investigate the effect of IFI204 deficiency on ET formation, we stained macrophages with SYTOX Orange, a non-permeable dye that stains nucleic acid, a primary component of ET. Interestingly, MET formation was markedly decreased in IFI204-deficient macrophage vs. WT macrophages (**Figure 7E**). To quantify MET formation, we analyzed extracellular DNA content in the supernatants. A reduction of extracellular DNA was seen in IFI204-deficient macrophages compared with WT

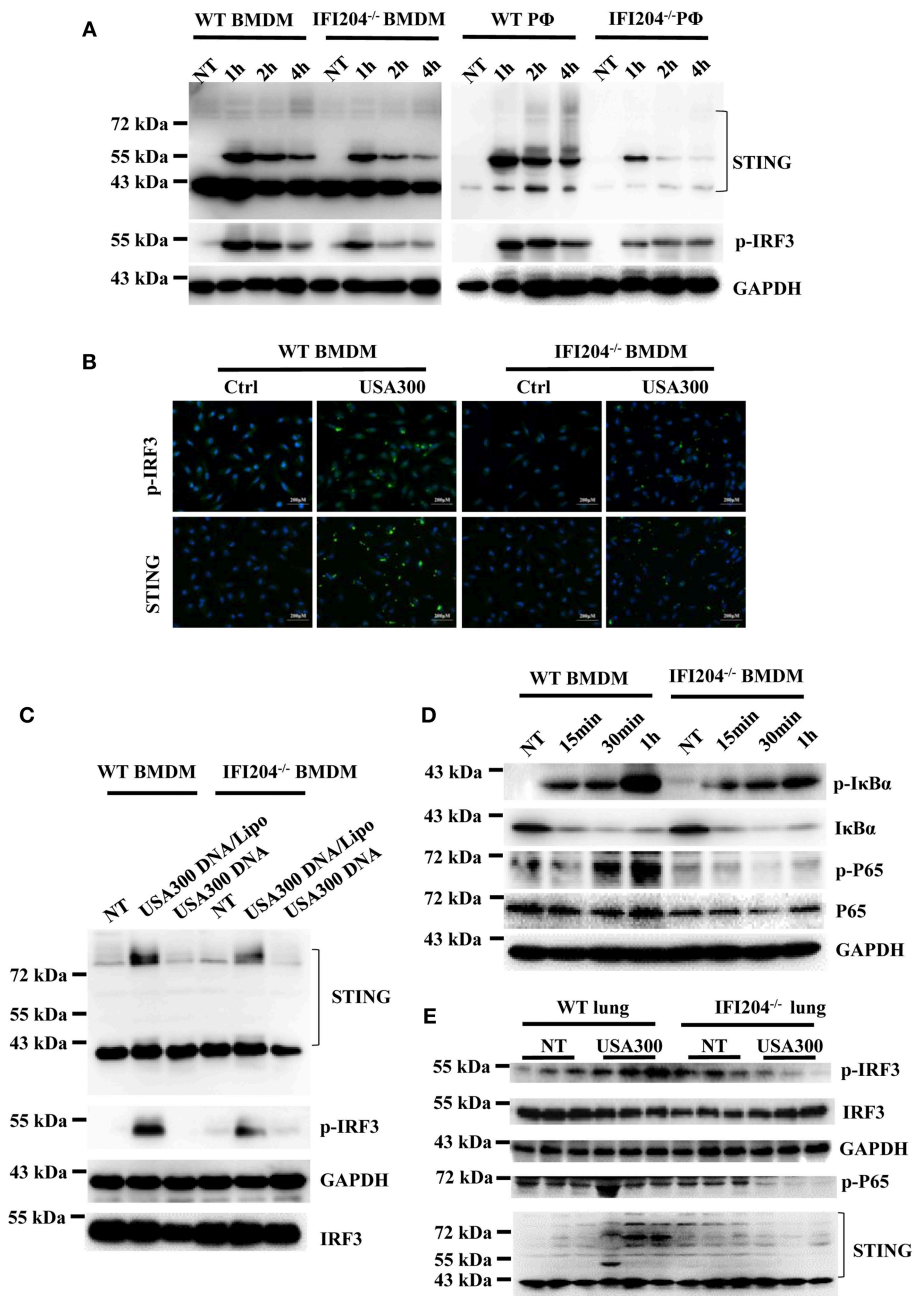


FIGURE 5 | IFI204 deficiency suppresses *Staphylococcus*-induced activation of STING-IRF3 and NF- κ B signaling. **(A)** WT and IFI204-deficient BMDM and peritoneal macrophages were untreated (NT) or exposed to *Staphylococcus* for the indicated times. The cell lysates were examined for expression levels of STING and phospho-IRF3 by Western blotting. The GAPDH served as a loading control. **(B)** WT and IFI204-deficient BMDM were exposed to *Staphylococcus* for 1 h. STING and phospho-IRF3 were analyzed by immunofluorescence. **(C)** WT and IFI204-deficient BMDM were incubated with USA300 DNA with or without Lipofectamine 2000 for 1 h. STING and phospho-IRF3 were examined by Western blotting. **(D)** WT and IFI204-deficient BMDM were exposed to *Staphylococcus* for the indicated times. Phospho-I κ B α , I κ B α , phospho-P65, P65, and GAPDH were examined by Western blotting. **(E)** WT and IFI204 $^{-/-}$ mice were infected intranasally with 1×10^8 CFU of *Staphylococcus*. Lung tissues were collected and homogenized at 24 h postinfection, and then immunoblotting for Sting and phospho-IRF3, IRF3, GAPDH, P65, and STING.

cells (**Figure 7F**). Moreover, IFI204 deficiency impaired PMA-induced extracellular DNA release. Because an initial description of ET appeared in neutrophil, another type of phagocyte that play important roles in host's defense against infection, we

further examined if there is a defect of ET formation in IFI204-deficient neutrophils. A similar defect of NET formation was observed in bacteria-infected IFI204-deficient neutrophils vs. WT neutrophils (**Figure 7G**). Correspondingly, IFI204-deficient

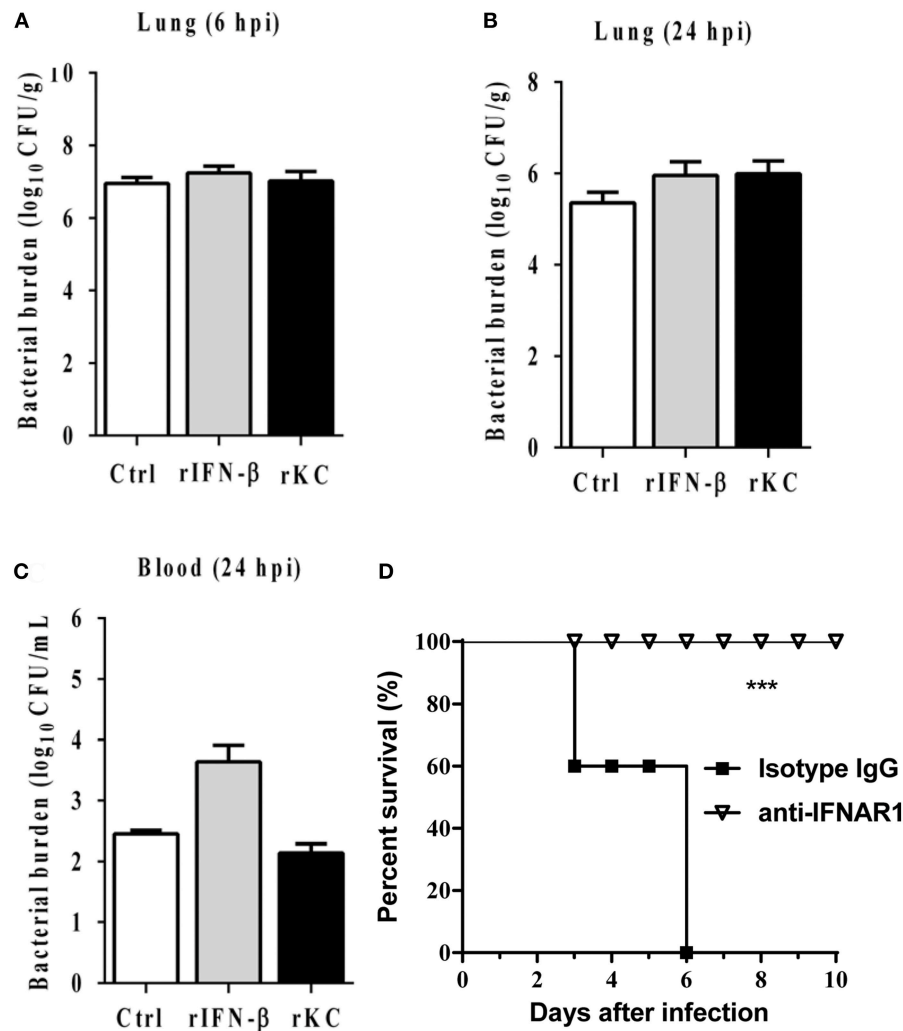


FIGURE 6 | IFN- β and KC are dispensable for IFI204-mediated host defense. IFI204^{-/-} mice were i.p. injected recombinant KC or IFN- β ($n = 10$ each group) at a dose of 1.0 μ g per mouse in 100 μ L PBS on Day -1 and Day 0. The mice were infected intranasally with 1×10^8 CFU of *Staphylococcus* on Day 0. **(A,B)** Homogenized lung tissues were subjected to plating serial dilution for bacterial loads at 6 hpi or 24 hpi. **(C)** Blood were subjected to plating serial dilution for bacterial loads at 24 hpi. All data are shown as mean \pm SEM. Student's t -test was performed. **(D)** The mice were i.p. injected with 2.5 mg anti-mouse IFNAR1 neutralizing mAb or 2.5 mg IgG isotype control ($n = 8$ each group), 24 h later, mice were i.v. challenged with 2×10^8 CFU of *Staphylococcus*. The animals were monitored daily for survival. *** $p < 0.005$.

neutrophils were incapable of killing extracellular bacteria compared with WT neutrophils (**Figure 7H**). Hence, these data suggested that IFI204 deficiency leads to a defect in extracellular bacterial killing by impairing ET formation in phagocytes.

Bone Marrow Transplantation Restore Bacteria Killing in IFI204-Deficient Mice

To further substantiate the pivotal role of IFI204 in enhancing extracellular bacteria killing, we further examined if transplantation of WT bone marrow (BM) rescue bacterial killing defect in IFI204-deficient mice. WT or IFI204-deficient recipient mice were lethally irradiated and injected with BM cells from WT or IFI204-deficient donors. Eight weeks after transplantation, those mice were inoculated with *Staphylococcus*, and bacterial

burdens in the lung and blood were determined. Similar to WT recipient mice that received WT BM, IFI204-deficient recipient mice that received WT BM had less bacterial burden (**Figures 8A,B**). Conversely, WT recipient mice that received IFI204-deficient BM had more bacterial burden in lung tissue, identical to that observed in IFI204-deficient recipient mice that received IFI204-deficient BM. The similar pattern was observed in the activity of MPO (**Figure 8C**), one granule enzyme which plays an important role in neutrophil antimicrobial responses and is required for neutrophil extracellular trap formation (10). The proinflammatory cytokines (KC and IL-1 β) in lung showed slight similar patterns (**Figures 8D-F**). Depletion of circulating cells and reconstitution with donor cells was confirmed (**Figure 8G**). Together, the results indicate that the protective effect of IFI204 against *Staphylococcus* infection

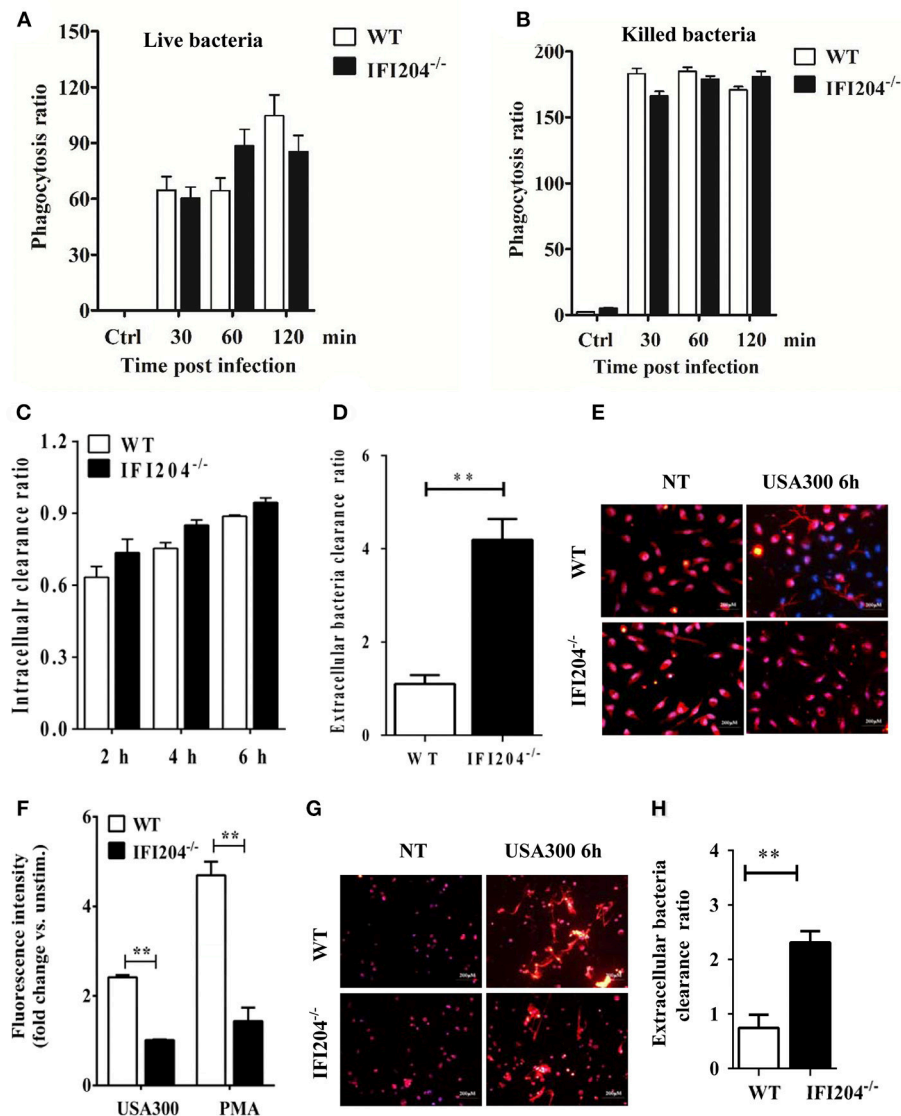


FIGURE 7 | IFI204 promotes extracellular trap-mediated bacteria killing in macrophages and neutrophils. Macrophages were treated with FITC-labeled live (A) or killed bacteria (B). The mean fluorescence intensity (MFI) of the FITC-positive cells were determined by flow cytometry. (C) Macrophages were infected with bacteria (MOI = 5) for 1 h. Non-engulfed bacteria were killed with gentamicin. The cells were lysed and intracellular bacterial were enumerated by plating on agar plates. (D) Extracellular bacterial killing capacity of macrophages were determined by assessing extracellular CFUs. (E) Macrophages were challenged with bacteria (MOI = 50) for 6 h. Representative microscopy pictures of NETs formation as indicated by SYTOX Orange. (F) Macrophages were stimulated with bacteria (MOI = 50) and PMA (100 nM). SYTOX Orange was added after 6 h and fluorescence was measured by spectrofluorometry. (G) Neutrophils were challenged with bacteria (MOI = 50) for 6 h. Representative microscopy pictures of NETs formation as indicated by SYTOX Orange. (H) Extracellular bacterial killing capacity of neutrophils were determined by assessing extracellular CFUs. All data are shown as mean \pm SEM. Student's *t*-test was performed. ***p* < 0.01.

is dependent on the ability of IFI204 enhancing phagocyte killing capacity.

DISCUSSION

Staphylococcus aureus infections are usually persistent and hard to eradicate. Development of new therapeutic strategies to combat *Staphylococcus* infections requires deeper understanding of molecular mechanisms underlying phagocyte functions in

antibacterial defense. Recently, several studies including ours showed that murine IFI204 or human ortholog IFI16 detects cytosolic bacterial DNA for the type I IFN response or cell death *in vitro* (5–8). Hence, IFI204/IFI16 is implicated in sensing intracellular bacterial infection. Generally speaking, *Staphylococcus* is extracellular bacteria. Using IFI204-deficient mice, we demonstrate that IFI204 promotes host survival and bacterial clearance during *Staphylococcus* pulmonary and systemic infection. Therefore, we defining a novel role for IFI204 in host defense against extracellular bacterial infection.

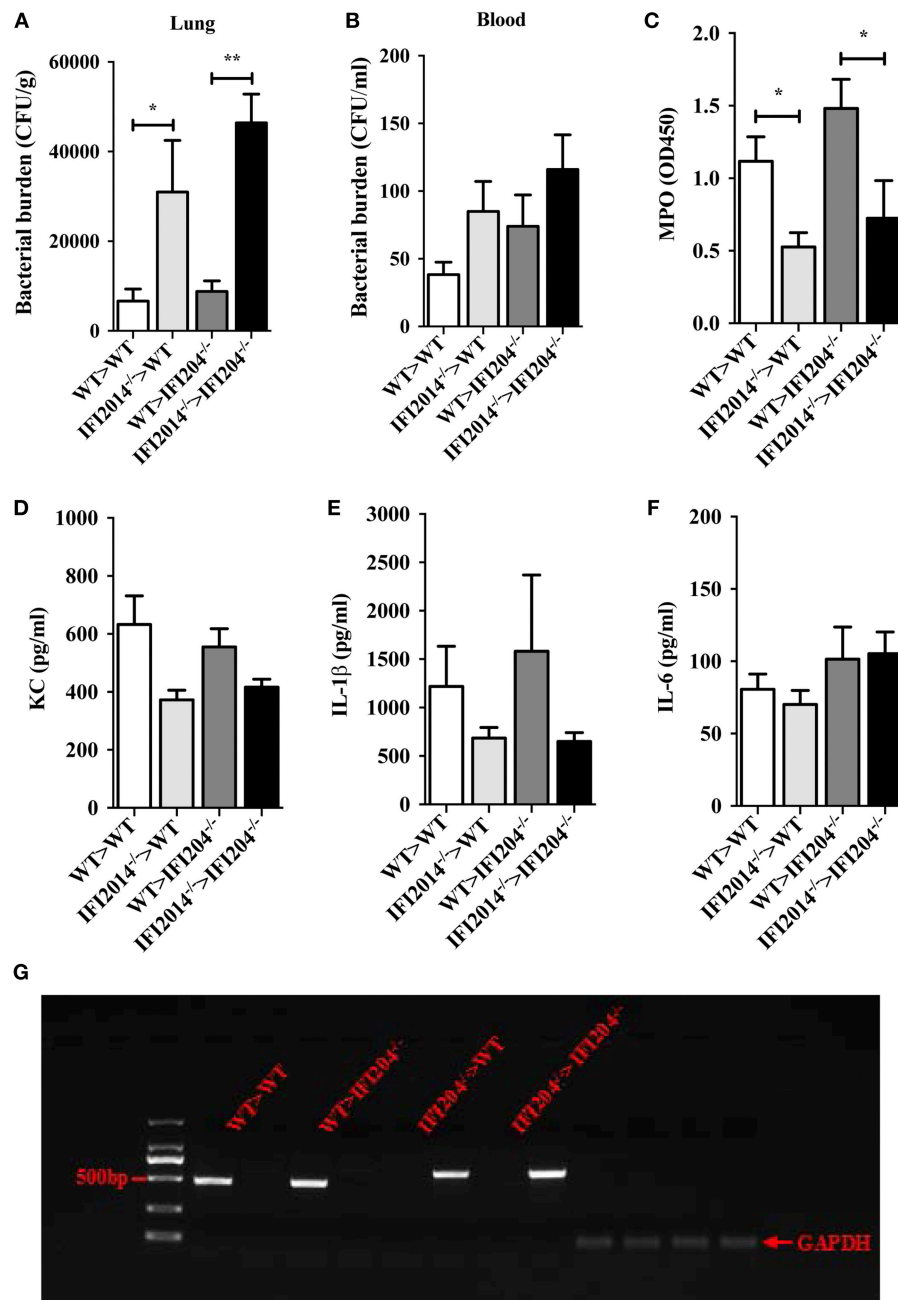


FIGURE 8 | Adoptive transfer of WT BM cells protects IFI204-deficient mice against *Staphylococcus* infection. Bone marrow cells isolated from WT or IFI204^{-/-} mice were adoptively transferred to irradiated IFI204^{-/-} or WT recipient mice. The recipient mice were then infected nasally with *Staphylococcus* (1×10^8 CFU, $n = 4-6$ each group) for 24 h. **(A,B)** Homogenized lung tissue and blood were subjected to plating serial dilution for bacterial loads. **(C)** Neutrophil activity in lung was determined by the amount of MPO. **(D-F)** The release of KC, IL-6, IL-1β in lung were determined by ELISA. **(G)** Efficient reconstitution by donor bone marrow cells was confirmed by PCR for the IFI204 gene in splenocytes. All data are shown as mean \pm SEM. Student's *t*-test was performed. * $p < 0.05$; ** $p < 0.01$.

To identify the potential mechanisms underlined IFI204-mediated defense, we set out to characterize the inflammatory response. IFI204 deficiency leads to an inferior production of cytokines/chemokines in the lung following *Staphylococcus* infection. Due to IFI204 mainly locating in the recruited inflammatory cells, bone marrow-derived macrophages were used for determine IFI204-mediated inflammatory response.

Consistent with *in vivo* data, IFI204 deficiency not only impairs cytokines production in macrophages, but also inhibits bacteria-induced STING-IRF3 and NF-κB activation. IFI204/IFI16 is extensively characterized as a DNA sensor, which detects cytosolic DNA derived from virus, bacteria, even host DNA (11). In the presence of intracellular DNA, IFI204/IFI16 interacts with STING to induce TBK1-dependent IFN-β responses. Using

Staphylococcus-derived genome DNA, we also showed that cytosolic DNA activates the STING-IRF3 pathway, and promotes IFN- β and KC productions. Hence, it is quite possible that IFI204 serve as DNA sensor to trigger inflammatory responses during *Staphylococcus* infection.

IFN- β is produced during viral infections and is responsible for defense against viruses. IFN- β also induced by *Staphylococcus*. However, the role of IFN- β during *Staphylococcus* infection varies. It can be both beneficial (12, 13) and detrimental (14–16) to the host, probably depending on the experimental design. We hypothesized that the defect of IFN- β production may leads to susceptibility to infection in the absence of IFI204. Unexpectedly, administration of recombinant IFN- β even promotes bacteria proliferation in IFI204-deficient mice. Moreover, blockade of IFN signaling significantly decreased the mortality induced by *Staphylococcus* systemic infection. Hence, it suggests that IFN- β was not only unnecessary for the protective effects of IFI204, but also detrimental to the host during *Staphylococcus* infection. Our data also showed that KC production is attenuated in IFI204-deficient mice and macrophages. KC has been shown to have a critical role in protective responses to *Staphylococcus* infection. However, administration of recombinant mouse KC is still unable to restrict *Staphylococcus* multiplication in IFI204-deficient mice.

Phagocytosis, a process by which myeloid cells such as macrophages and neutrophils internalize and kill microorganisms, is the critical host innate defense mechanism. Our results showed that IFI204-deficient macrophages internalized similar numbers of FITC-labeled live or heat-killed bacteria compared with WT macrophages. Moreover, WT and IFI204-deficient macrophages exhibit a comparable capacity for intracellular killing. Because bacterial phagocytosis in IFI204-deficient macrophages was not impaired, it is possible that IFI204 participates in the regulation of phagocytosis-independent bacterial killing such as the process mediated by extracellular trap. Extracellular trap was first described in neutrophils as the released of web-like structures after stimulation with Gram-positive or Gram-negative bacteria. Increased evidences showed that ET is not formed exclusively by neutrophils but also by other innate myeloid cells including macrophage (17), basophils (18), eosinophil (19), and mast cells (20) response to microbes. Activated innate myeloid cells release these structures composed of decondensed chromatin and antimicrobial proteins that trap and inhibit a broad range of microbes. Compared with control cells, both IFI204-deficient macrophages and neutrophils are incapable of killing extracellular bacteria, as well as reduce the release of extracellular DNA. Moreover, transplantation of WT bone marrow rescued bacterial killing defect in IFI204-deficient mice. Hence, our results indicate that the protective effect of IFI204 against *Staphylococcus* infection is dependent on the ability of IFI204 enhancing phagocyte killing capacity by promoting ET formation.

Some other pattern recognition receptor including TLR4 (21–23), TLR7/8 (24, 25), TLR2 (23, 26, 27), TLR6 (28),

TLR9 (29), lectin receptors Mincle and CLEC5A (30–32), Fc receptors Fc α RI and Fc γ RIIIb (33, 34) were implicated in neutrophil extracellular trap formation. TLR2/4 was found to modify NET formation in response to *Staphylococcus* infection but not to PMA stimulation (23). Interestingly, we observed that IFI204 impact both pathogen and PMA-induced extracellular DNA release. Several virulence factors of *Staphylococcus* were reported to elicit ET formation, including leukotoxin (35), leukocidins (36), phenol-soluble modulins (PSM α) (37), and protein A (38). Given the fact that IFI204 mediates PMA-induced extracellular DNA release, we speculate that IFI204 probably promotes extracellular bactericidal activity independent of DNA recognition. While understanding the underlying mechanism of IFI204 regulating ET awaits further investigation, this study extends our understanding the biological function of IFI204 in host innate immune response.

In summary, our studies demonstrate IFI204 is essential for host defense against *Staphylococcus* infection *in vivo*. IFI204 promotes bacteria eradication and inflammation response. However, inflammation response does not contribute to IFI204-mediated protection. Moreover, we provide evidence that IFI204 plays a role in extracellular bactericidal activity of phagocytes through enhancing extracellular trap formation. These observations document a novel and physiologically important role for IFI204 in host defense against extracellular bacterial infection.

DATA AVAILABILITY

All datasets generated for this study are included in the manuscript and/or the supplementary files.

ETHICS STATEMENT

All animal studies were conducted according to experimental practices and standards approved by the Animal Welfare and Research Ethics Committee at Jilin University (No. 20150601).

AUTHOR CONTRIBUTIONS

WC and Y-JY: designed experiments. WC, S-XY, F-HZ, and X-JZ: performed the experiments. WC and S-XY: analyzed the data. Y-JY: wrote the manuscript. W-YG, K-YL, Z-ZL, and W-YH: read the manuscript.

FUNDING

This work was supported by The National Key Research and Development Program of China [No. 2017YFD0501000], National Natural Science Foundation of China [No. 31872457, No. 31702211], Jilin Province Science and Technology Development Project [No. 20160101232JC].

REFERENCES

- Kaufmann SHE, Dorhoi A. Molecular determinants in phagocyte-bacteria interactions. *Immunity*. (2016) 44:476–91. doi: 10.1016/j.immuni.2016.02.014
- Unterholzner L, Keating SE, Baran M, Horan KA, Jensen SB, Sharma S, et al. IFI16 is an innate immune sensor for intracellular DNA. *Nat Immunol*. (2010) 11:997–1004. doi: 10.1038/ni.1932
- Monroe KM, Yang Z, Johnson JR, Geng X, Doitsh G, Krogan NJ, et al. IFI16 DNA sensor is required for death of lymphoid CD4 T cells abortively infected with HIV. *Science*. (2014) 343:428–32. doi: 10.1126/science.1243640
- Jakobsen MR, Bak RO, Andersen A, Berg RK, Jensen SB, Tengchuan J, et al. IFI16 senses DNA forms of the lentiviral replication cycle and controls HIV-1 replication. *Proc Natl Acad Sci USA*. (2013) 110:E4571–80. doi: 10.1073/pnas.1311669110
- Storek KM, Gertsvoelf NA, Ohlson MB, Monack DM. cGAS and Ifi204 cooperate to produce type I IFNs in response to Francisella infection. *J Immunol*. (2015) 194:3236–45. doi: 10.4049/jimmunol.1402764
- Hansen K, Prabakaran T, Laustsen A, Jorgensen SE, Rahbaek SH, Jensen SB, et al. *Listeria monocytogenes* induces IFN β expression through an IFI16-, cGAS- and STING-dependent pathway. *EMBO J*. (2014) 33:1654–66. doi: 10.15252/embj.201488029
- Chunfa L, Xin S, Qiang L, Sreevatsan S, Yang L, Zhao D, et al. The central role of IFI204 in IFN- β release and autophagy activation during *Mycobacterium bovis* infection. *Front Cell Infect Microbiol*. (2017) 7:169. doi: 10.3389/fcimb.2017.00169
- Chu X, Chen W, Li N, Hu XZ, Du CT, Yu SX, et al. Cytosolic double-stranded DNA induces non-necroptotic programmed cell death in trophoblasts via IFI16. *J Infect Dis*. (2014) 210:1476–86. doi: 10.1093/infdis/jiu272
- Barber GN. STING-dependent cytosolic DNA sensing pathways. *Trends Immunol*. (2014) 35:88–93. doi: 10.1016/j.it.2013.10.010
- Metzler KD, Fuchs TA, Nauseef WM, Reumaux D, Roesler J, Schulze I, et al. Myeloperoxidase is required for neutrophil extracellular trap formation: implications for innate immunity. *Blood*. (2011) 117:953–9. doi: 10.1182/blood-2010-06-290171
- Ma Z, Ni G, Damania B. Innate sensing of DNA virus genomes. *Annu Rev Virol*. (2018) 5:341–62. doi: 10.1146/annurev-virology-092917-043244
- Kaplan MJ, Kyme P, Wolf AJ, Becker CA, Tseng CW, Liu GY, et al. Failure to induce IFN- β production during *Staphylococcus aureus* infection contributes to pathogenicity. *J Immunol*. (2012) 189:4537–45. doi: 10.4049/jimmunol.1201111
- Kaplan A, Lee MW, Wolf AJ, Limon JJ, Becker CA, Ding M, et al. Direct antimicrobial activity of IFN- β . *J Immunol*. (2017) 198:4036–45. doi: 10.4049/jimmunol.1601226
- Martin FJ, Gomez MI, Wetzel DM, Memmi G, O'Seaghdha M, Soong G, et al. *Staphylococcus aureus* activates type I IFN signaling in mice and humans through the Xr repeated sequences of protein A. *J Clin Invest*. (2009) 119:1931–9. doi: 10.1172/JCI35879
- Parker D, Planet PJ, Soong G, Narechania A, Prince A. Induction of type I interferon signaling determines the relative pathogenicity of *Staphylococcus aureus* strains. *PLoS Pathog*. (2014) 10:e1003951. doi: 10.1371/journal.ppat.1003951
- Parker D, Prince A. *Staphylococcus aureus* induces type I IFN signaling in dendritic cells via TLR9. *J Immunol*. (2012) 189:4040–6. doi: 10.4049/jimmunol.1201055
- Chow OA, von Kockritz-Blickwede M, Bright AT, Hensler ME, Zinkernagel AS, Cogen AL, et al. Statins enhance formation of phagocyte extracellular traps. *Cell Host Microbe*. (2010) 8:445–54. doi: 10.1016/j.chom.2010.10.005
- Morshed M, Hlushchuk R, Simon D, Walls AF, Obata-Ninomiya K, Karasuyama H, et al. NADPH oxidase-independent formation of extracellular DNA traps by basophils. *J Immunol*. (2014) 192:5314–23. doi: 10.4049/jimmunol.1303418
- Yousefi S, Gold JA, Andina N, Lee JJ, Kelly AM, Kozłowski E, et al. Catapult-like release of mitochondrial DNA by eosinophils contributes to antibacterial defense. *Nat Med*. (2008) 14:949–53. doi: 10.1038/nm.1855
- von Kockritz-Blickwede M, Goldmann O, Thulin P, Heinemann K, Norrby-Teglund A, Rohde M, et al. Phagocytosis-independent antimicrobial activity of mast cells by means of extracellular trap formation. *Blood*. (2008) 111:3070–80. doi: 10.1182/blood-2007-07-104018
- Clark SR, Ma AC, Tavenner SA, McDonald B, Goodarzi Z, Kelly MM, et al. Platelet TLR4 activates neutrophil extracellular traps to ensnare bacteria in septic blood. *Nat Med*. (2007) 13:463–9. doi: 10.1038/nm1565
- Yousefi S, Mihalache C, Kozłowski E, Schmid I, Simon HU. Viable neutrophils release mitochondrial DNA to form neutrophil extracellular traps. *Cell Death Differ*. (2009) 16:1438–44. doi: 10.1038/cdd.2009.96
- Wan T, Zhao Y, Fan F, Hu R, Jin X. Dexamethasone inhibits *S. aureus*-induced neutrophil extracellular pathogen-killing mechanism, possibly through toll-like receptor regulation. *Front Immunol*. (2017) 8:60. doi: 10.3389/fimmu.2017.00060
- Saitoh T, Komano J, Saitoh Y, Misawa T, Takahama M, Kozaki T, et al. Neutrophil extracellular traps mediate a host defense response to human immunodeficiency virus-1. *Cell Host Microbe*. (2012) 12:109–16. doi: 10.1016/j.chom.2012.05.015
- Lood C, Arve S, Ledbetter J, Elkon KB. TLR7/8 activation in neutrophils impairs immune complex phagocytosis through shedding of Fc γ RIIA. *J Exp Med*. (2017) 214:2103–19. doi: 10.1084/jem.20161512
- Yipp G, Petri B, Salina D, Jenne CN, Scott BN, Zbytniuk LD, et al. Infection-induced NETosis is a dynamic process involving neutrophil multitasking *in vivo*. *Nat Med*. (2012) 18:1386–93. doi: 10.1038/nm.2847
- Xu F, Zhang C, Zou Z, Fan EK Y, Chen L, Li Y, et al. Aging-related Atg5 defect impairs neutrophil extracellular traps formation. *Immunology*. (2017) 151:417–32. doi: 10.1111/imm.12740
- Awasthi D, Nagarkoti S, Kumar A, Dubey M, Singh AK, Pathak P, et al. Oxidized LDL induced extracellular trap formation in human neutrophils via TLR-PKC-IRAK-MAPK and NADPH-oxidase activation. *Free Radic Biol Med*. (2016) 93:190–203. doi: 10.1016/j.freeradbiomed.2016.01.004
- Itagaki K, Kaczmarek E, Lee YT, Tang IT, Isal B, Adibnia Y, et al. Mitochondrial DNA released by trauma induces neutrophil extracellular traps. *PLoS ONE*. (2015) 10:e0120549. doi: 10.1371/journal.pone.0120549
- Sharma A, Steichen AL, Jondle CN, Mishra BB, Sharma J. Protective role of Mincle in bacterial pneumonia by regulation of neutrophil mediated phagocytosis and extracellular trap formation. *J Infect Dis*. (2014) 209:1837–46. doi: 10.1093/infdis/jit820
- Sharma A, Simonson TJ, Jondle CN, Mishra BB, Sharma J. Mincle-mediated neutrophil extracellular trap formation by regulation of autophagy. *J Infect Dis*. (2017) 215:1040–8. doi: 10.1093/infdis/jix072
- Chen ST, Li FJ, Hsu TY, Liang SM, Yeh YC, Liao WY, et al. CLEC5A is a critical receptor in innate immunity against *Listeria* infection. *Nat Commun*. 8:299. doi: 10.1038/s41467-017-00356-3
- Aleyd E, van Hout MW, Ganzevles SH, Hoeben KA, Everts V, Bakema JE, et al. IgA enhances NETosis and release of neutrophil extracellular traps by polymorphonuclear cells via Fc α receptor. *J Immunol*. (2014) 192:2374–83. doi: 10.4049/jimmunol.1300261
- Aleman OR, Mora N, Cortes-Vieyra R, Uribe-Querol E, Rosales C. Differential use of human neutrophil f γ receptors for inducing neutrophil extracellular trap formation. *J Immunol Res*. (2016) 2016:2908034. doi: 10.1155/2016/2908034
- Malachowa N, Kobayashi SD, Freedman B, Dorward DW, DeLeo FR. *Staphylococcus aureus* leukotoxin GH promotes formation of neutrophil extracellular traps. *J Immunol*. (2013) 191:6022–9. doi: 10.4049/jimmunol.1301821
- Bhattacharya M, Berends ET, Chan R, Schwab E, Roy S, Sen CK, et al. *Staphylococcus aureus* biofilms release leukocidins to elicit extracellular trap

- formation and evade neutrophil-mediated killing. *Proc Natl Acad Sci USA*. (2018) 115:7416–21. doi: 10.1073/pnas.1721949115
37. Bjornsdottir H, Dahlstrand Rudin A, Klose FP, Elmwall J, Welin A, Stylianou M, et al. Phenol-soluble modulins alpha peptide toxins from aggressive *Staphylococcus aureus* induce rapid formation of neutrophil extracellular traps through a reactive oxygen species-independent pathway. *Front Immunol*. (2017) 8:257. doi: 10.3389/fimmu.2017.00257
 38. Hoppenbrouwers T, Sultan AR, Abraham TE, Lemmens-den Toom NA, Hansenova Manaskova S, van Cappellen WA, et al. Staphylococcal protein A is a key factor in neutrophil extracellular traps formation. *Front Immunol*. 9:165. (2018) doi: 10.3389/fimmu.2018.00165

Conflict of Interest Statement: The authors declare that the research was conducted in the absence of any commercial or financial relationships that could be construed as a potential conflict of interest.

Copyright © 2019 Chen, Yu, Zhou, Zhang, Gao, Li, Liu, Han and Yang. This is an open-access article distributed under the terms of the Creative Commons Attribution License (CC BY). The use, distribution or reproduction in other forums is permitted, provided the original author(s) and the copyright owner(s) are credited and that the original publication in this journal is cited, in accordance with accepted academic practice. No use, distribution or reproduction is permitted which does not comply with these terms.



TonEBP Suppresses the HO-1 Gene by Blocking Recruitment of Nrf2 to Its Promoter

Eun Jin Yoo¹, Hwan Hee Lee¹, Byeong Jin Ye¹, Jun Ho Lee¹, Chae Young Lee¹, Hyun Je Kang¹, Gyu Won Jeong¹, Hyun Park¹, Sun Woo Lim², Whaseon Lee-Kwon¹, Hyug Moo Kwon^{1*} and Soo Youn Choi^{1*}

¹ School of Life Sciences, Ulsan National Institute of Science and Technology, Ulsan, South Korea, ² Transplantation Research Center, Catholic University of Korea, Seoul, South Korea

OPEN ACCESS

Edited by:

Catarina R. Almeida,
University of Aveiro, Portugal

Reviewed by:

Jianhui Rong,
The University of Hong Kong, Hong
Kong

Anna Grochot-Przeczek,
Jagiellonian University, Poland

*Correspondence:

Hyug Moo Kwon
hmkwon@unist.ac.kr
Soo Youn Choi
sychoi@unist.ac.kr

Specialty section:

This article was submitted to
Molecular Innate Immunity,
a section of the journal
Frontiers in Immunology

Received: 28 December 2018

Accepted: 02 April 2019

Published: 18 April 2019

Citation:

Yoo EJ, Lee HH, Ye BJ, Lee JH,
Lee CY, Kang HJ, Jeong GW, Park H,
Lim SW, Lee-Kwon W, Kwon HM and
Choi SY (2019) TonEBP Suppresses
the HO-1 Gene by Blocking
Recruitment of Nrf2 to Its Promoter.
Front. Immunol. 10:850.
doi: 10.3389/fimmu.2019.00850

TonEBP is a key transcriptional activator in macrophages with an M1 phenotype. High expression of TonEBP is associated with many inflammatory diseases. Heme oxygenase-1 (HO-1), a stress-inducible protein, is induced by various oxidative and inflammatory signals, and its expression is regarded as an adaptive cellular response to inflammation and oxidative injury. Here, we show that TonEBP suppresses expression of HO-1 by blocking Nrf2 binding to the HO-1 promoter, thereby inducing polarization of macrophages to the M1 phenotype. Inhibition of HO-1 expression or activity significantly reduced the inhibitory responses on M1 phenotype and stimulatory effects on M2 phenotype by TonEBP knockdown. Additional experiments showed that HO-1 plays a role in the paracrine anti-inflammatory effects of TonEBP knockdown in macrophages. Identification of HO-1 as a downstream effector of TonEBP provides new possibilities for improved therapeutic approaches to inflammatory diseases.

Keywords: NFAT5, M1 macrophages, M2 macrophages, inflammation, innate immunity

INTRODUCTION

Macrophages are a heterogeneous population of immune cells that is present in all tissues and plays a central role in initiation and resolution of inflammation induced by pathogens or tissue damage (1, 2). Macrophages can acquire two distinct functional phenotypes, classical (M1) and alternative (M2), depending on the activating (environmental) stimulus (3, 4). Whereas, the M1 phenotype plays a causal role in inflammatory diseases, the M2 phenotype functions to resolve pathologic inflammation and aid tissue repair during wound healing (5, 6). Plasticity and flexibility are key features of activated macrophages (5–7). Macrophages can undergo dynamic transition between the M1 and M2 states and promote differentiation of neighboring macrophages to their same activation state. Moreover, dynamic changes in macrophage phenotype frequently reveal divergent roles in health and disease. Thus, identification of molecules and mechanisms associated with phenotypic switching of macrophages provides a molecular basis for macrophage-centered diagnostic and therapeutic strategies.

Heme oxygenase (HO) is the rate-limiting enzyme during heme degradation (8), which leads to generation of carbon monoxide (CO), free iron, and biliverdin (9–11). These by-products of HO enzymatic activity are regarded as cytoprotective molecules because of their antioxidant activity [reviewed in (12, 13)]. Two mammalian HO isoforms, HO-1 and HO-2, have been identified (13). HO-1 is a stress-inducible protein induced by various oxidative and inflammatory signals,

while HO-2 is a constitutively expressed form. HO-1 has strong immunomodulatory and anti-inflammatory properties (14), which have been demonstrated in HO-1-deficient mice and human cases of genetic HO-1 deficiency (15–20). At present, evidence suggests that induction of HO-1 can drive the phenotypic shift from M1 to M2 in macrophages [(21), reviewed in (22, 23)] HO-1 modulates the immune system during homeostasis and disease by regulating the function and phenotype of macrophages (21, 24–26).

Tonicity-responsive enhancer binding protein (TonEBP), also known as nuclear factor of activated T cells 5 (NFAT5), belongs to the Rel family of transcriptional factors, which includes nuclear factor- κ B (NF- κ B) and NFAT1–4 (27, 28). TonEBP was initially identified as the central regulator of cellular responses to hypertonic stress (27, 29–31). Recent studies show that high expression of TonEBP in humans and mice is associated with inflammatory and autoimmune diseases (32–36). TonEBP induces M1 macrophages by stimulating expression of pro-inflammatory genes and by suppressing expression of anti-inflammatory genes (37–39). Consequently, downregulation of TonEBP reduces inflammation, thereby helping to prevent inflammatory and autoimmune diseases (32–36). Here, we explored the potential interplay between TonEBP and HO-1 in macrophages. We found that TonEBP is a potent suppressor of HO-1 in human and mouse macrophages. Double knockdown of TonEBP/HO-1 or co-treatment with a HO inhibitor reduced the inhibitory responses on M1 phenotype and stimulatory effects on M2 phenotype by TonEBP knockdown, thereby supporting a role of HO-1 in the anti-inflammatory effects of TonEBP knockdown in macrophages.

MATERIAL AND METHODS

Animals, Peritoneal Macrophages, and Bone Marrow-Derived Macrophages

The TonEBP^{+/-Δ} mice on C57BL/6 background (31) were crossed back to the C57BL/6 line (The Jackson Laboratory, Bar Harbor, ME) to produce TonEBP^{+/-Δ} animals and their TonEBP^{+/+} littermates. Mice were kept on a 12-h light/dark cycle with free access to standard chow and water. Peritoneal macrophages (PMs) were isolated from our previously developed mouse model of type 1 diabetes (35). Briefly, males were selected and made diabetic by daily intraperitoneal injections of freshly prepared streptozotocin (STZ) (50 mg/kg body weight; Sigma-Aldrich, St. Louis, MO) in 0.1 M citrate buffer (pH 4.5) for 4 days. Animals displaying fasting blood glucose levels above 250 mg/dl after 2 weeks of STZ injections were considered diabetic. Control, non-diabetic animals were injected with the buffer. Six weeks post the STZ injections the animals were analyzed for PMs. PMs were isolated from non-diabetic and diabetic mice as described (40). In short, 1 ml thioglycollate (30 mg/ml) was injected intraperitoneally and the peritoneal cells were collected 4 days later. The macrophages were adhesion-purified for 1 h followed by a wash with PBS to remove non-adherent cells and analyzed. Bone marrow cells obtained from femurs were

differentiated for 7 days using 20% L929-conditioned medium, as a source of M-CSF, to obtain bone marrow-derived macrophages (BMDMs) (41). The cells were treated as indicated in the figure legends and analyzed. All experimental protocols were approved by the Institutional Animal Care and Use Committee of the Ulsan National Institute of Science and Technology (UNISTACUC-12-15-A).

Isolation of the Human Primary Monocytes and Differentiation of Monocyte-Derived Macrophages

Human monocyte-derived macrophages were prepared as described previously (39). The study was approved by the Institutional Review Board of the Ulsan National Institute of Science and Technology (UNISTIRB-15-25-A). Briefly, human peripheral blood mononuclear cells (PBMCs) were isolated by centrifugation of whole blood (donated by healthy volunteers) on Histopaque-1077 (Sigma-Aldrich, St. Louis, MO, USA). Monocytes were enriched from freshly isolated PBMCs by positive selection on CD14 microbeads followed by separation on MACS columns (Miltenyi Biotec, Bergisch, Germany). Macrophages were obtained from human monocytes after 7 days of culture in RPMI-1640 medium supplemented with 10% fetal bovine serum (FBS), 1% sodium pyruvate, 0.1% β -mercaptoethanol, and human M-CSF (20 ng/ml; Miltenyi Biotec) (42).

Cell Culture, Transfection, and Adenoviral Infection

Human monocyte-like THP-1 (ATCC TIB-202) cells were cultured in Dulbecco's Modified Eagle's Medium (DMEM) containing 10% FBS (ThermoFisher Scientific Inc., Waltham, MA, USA) and penicillin/streptomycin (100 U/ml and 100 μ g/ml, respectively; GE Healthcare Life Sciences, UT, USA) and then differentiated into macrophages by exposure to 5 ng/ml phorbol 12-myristate 13-acetate (PMA; Sigma-Aldrich) for 2 days. The murine macrophage cell line RAW264.7 (ATCC TIB-71) was cultured in DMEM containing 10% FBS and penicillin/streptomycin (100 U/ml and 100 μ g/ml, respectively). All siRNA duplexes were purchased from Integrated DNA Technologies (Coralville, IA, USA). Human monocyte-derived macrophages and PMA-differentiated THP-1 and RAW264.7 cells were transfected with concentration-matched pairs of scrambled (Scr) siRNA or with siRNAs specific for target genes at concentration of 2 nM using HiPerFect transfectant (Qiagen, Valencia, CA, USA) as previously described (42) or using lipofectamine 2000 (Invitrogen, Carlsbad, CA, USA) according to the manufacturer's instructions, respectively, for 24 h. The transfected cells were then cultured in fresh complete medium, treated with vehicle or chemicals and analyzed as indicated in the figure legends. For overexpression, RAW264.7 cells were infected with an empty control virus (Ad-EV) or an adenovirus carrying the human TonEBP gene (Ad-TonEBP) at a multiplicities of infection (MOI) of 50 for 24 h followed by treatment with LPS (100 ng/ml) for 6 h. The 4 kb fragment of the mouse HO-1 promoter (−4,045/+74 pGL2), a gift from Dr.

S.W. Chung (University of Ulsan, Ulsan, South Korea) (43), was subcloned into pGL3B (Promega, Madison, WI, USA). AREs or TonE sites in the promoter were mutated using a two-step PCR procedure and overlapping internal primers. All plasmids were purified using an endotoxin-free purification system (Qiagen) and transfected into cells using lipofectamine 2000 (Invitrogen).

Immunoblot Assay

Western blotting was performed using standard methods. Briefly, cells were washed with cold PBS and lysed in RIPA buffer [10 mM Tris (pH 7.5), 150 mM NaCl, 1 mM EDTA, 1 mM EGTA, 1% Triton X-100] containing 1 mM sodium orthovanadate, phosphatase inhibitor cocktail, and protease inhibitor cocktail. Lysates were centrifuged at $16,000 \times g$ for 15 min at 4°C. The protein concentration was measured in a BCA protein assay system (Pierce, Rockford, IL, USA). Proteins were resolved by SDS-PAGE, transferred to nitrocellulose membranes (Whatman, Clifton, NJ, USA), and probed with anti-TonEBP (26), anti-HO-1, anti-HO-2, anti-p65, anti-lamin B (all from Santa Cruz Biotechnology, Santa Cruz, CA, USA), anti-Nrf2 (Abcam, Cambridge, UK), and anti-Hsc70 (Rockland, Gilbertsville, PA, USA) antibodies.

RNA Isolation and qPCR

Total RNA was isolated from human monocyte-derived macrophages and cultured cells using TRIzol reagent (Invitrogen). First-strand cDNA was synthesized with 2 µg of total RNA and subjected to quantitative real-time PCR (qPCR) using SYBR Green mastermix in a LightCycler 480 system (Roche, Rotkreuz, Switzerland). Relative amount of mRNA was determined by using the comparative CT ($\Delta\Delta CT$) method, normalized to cyclophilin A gene as the internal control and expressed as arbitrary units. Primers used are described in **Supplementary Table 1**.

Immunocytochemistry

The cells were grown on glass coverslips and fixed with 4% paraformaldehyde in PBS (pH 7.4) for 20 min at 4°C. Cells were permeabilized with 0.25% Triton-X 100 in PBS for 30 min and blocked with PBS containing 5% FBS and 5% bovine serum albumin for 1 h at room temperature. After incubation with rabbit anti-Nrf2 overnight at 4°C, the cells were washed with PBS and treated with goat anti-rabbit Alexa Fluor 488-conjugated secondary antibodies for 1 h. Cells were washed with PBS and incubated in 0.1 µg/ml Hoechst (DAPI) for 30 min. After wash with PBS, coverslips were mounted onto microscope slides. Images were recorded using an Olympus FV1000 confocal fluorescence microscope.

ROS Assay

Cells transfected with Scr siRNA or siRNA targeting TonEBP were pre-treated for 30 min with vehicle or NAC (10 mM) and then cultured in the presence of LPS (100 ng/ml). Then, cells were trypsinized and resuspended in PBS. Intracellular accumulation of ROS was measured using a flow cytometer (Becton-Dickinson, Franklin Lakes, NJ, USA) and the fluorescent probe 2',7'-dichlorodihydrofluorescein diacetate (Sigma-Aldrich).

Luciferase Reporter Assay

Cells were transfected for 48 h with Scr siRNA or siRNA targeting TonEBP, followed by transfection with the HO-1 promoter-driven luciferase reporter vector. The Renilla luciferase reporter plasmid was used as a control for transfection efficiency. At 24 h post-transfection, cells were treated with LPS (100 ng/ml). After 8 h, cells were lysed in passive lysis buffer and a luciferase assay was performed using the dual-luciferase reporter system (Promega).

ChIP Assay

Chromatin immunoprecipitation (ChIP) was performed using a commercial kit (Millipore, Bedford, MA, USA). In brief, cells were crosslinked with formaldehyde (1% final concentration; Sigma-Aldrich) followed by addition of 125 mM glycine. After washing, chromatin fragmentation was performed by sonication on ice to yield an average fragment length <500 bp. Supernatants containing fragmented lysates were diluted 10-fold with chromatin dilution buffer. Samples were pre-cleared for 1 h at 4°C with protein A Sepharose beads (Millipore, MA, USA) that were pre-adsorbed with salmon sperm DNA. Specific antibodies (anti-Nrf2 IgG, anti-Pol II IgG, normal rabbit IgG (Abcam), anti-TonEBP serum, and normal rabbit serum (Merck Millipore, Darmstadt, Germany) were added after removing the pre-clearing beads. After adding the antibodies, the lysates were incubated overnight at 4°C. After elution and reverse crosslinking the antibody/DNA complexes, DNA was purified using a DNA purification kit (Qiagen) and analyzed by qPCR using primer pairs covering AREs, TonE, or TSS regions of the HO-1 promoter and exon 3 of the HO-1 gene. Primers used for qPCR are described in **Supplementary Table 1**. Immunoprecipitated DNA from each sample was normalized to its respective chromatin input.

Transwell Co-culture Assay

BMDMs were plated in 6-well plates (Corning Incorporated, Corning, NY, USA). RAW264.7 cells were plated on transwell permeable supports with 0.4 µm pore size (Corning Incorporated), transfected with Scr siRNA or siRNA specific for target genes for 24 h, and treated with LPS (100 ng/ml) for 12 h. The cells were then added to 6-well companion plates containing the BMDMs and co-cultured for 3 or 12 h. At the end point of the experiment, BMDMs were collected for use in a gene expression assay to assess the paracrine effects of macrophages.

Statistical Analysis

Data are expressed as the mean + SD or SEM. Statistical significance was estimated using two-way ANOVA with Tukey's *post-hoc* test for multiple comparisons. All statistical analyses were performed using GraphPad Prism 5.0 software (GraphPad, CA, USA).

RESULTS

TonEBP Suppresses Expression of HO-1 in Macrophages

We previously reported that TonEBP in macrophages promotes hyperglycemia-mediated proinflammatory activation and

chronic renal inflammation leading to diabetic nephropathy (DN) (35). Given the protective role of HO-1 on diabetic complications including DN (24, 44, 45), we asked whether TonEBP affected HO-1 expression in macrophages. To address the question, we examined peritoneal macrophages (PMs) obtained from our previously developed mouse model of type 1 diabetes (35). In macrophages from both diabetic and non-diabetic animals, TonEBP haplo-deficiency (TonEBP^{+/-}) was associated with elevated HO-1 mRNA expression (**Figure 1A**). In order to characterize the regulation of HO-1 by TonEBP further, we examined PMs and bone marrow derived macrophages (BMDMs) obtained from non-diabetic TonEBP^{+/+} and TonEBP^{+/-} mice. PMs and BMDMs were cultured with medium containing normal (5.5 mM) or high (25 mM) glucose in the presence or absence of lipopolysaccharide (LPS), a potent trigger of hyperglycemia-induced inflammation and diabetic complications (23, 46, 47), to mimic a diabetic condition. PMs and BMDMs from the TonEBP^{+/-} mice cultured in normal glucose (5.5 mM) showed reduced TonEBP expression and enhanced HO-1 expression compared to those from TonEBP^{+/+} littermates in both resting and LPS-stimulated cells (**Supplementary Figure 1A**). Raising glucose concentration to 25 mM in the presence of LPS resulted in a higher expression of TonEBP and HO-1 mRNA in PMs (**Figure 1B**) and BMDMs (**Figure 1C**) while addition of mannitol to the same osmolality did not. Importantly, the cells from the TonEBP^{+/-} mice showed enhanced HO-1 expression compared to those from TonEBP^{+/+} littermates. These data suggest that elevated levels of TonEBP may limit hyperglycemia-mediated induction of HO-1 in macrophages.

Next, we asked whether knocking down TonEBP by siRNA-mediated gene silencing would affect expression of HO-1. RAW264.7 cells were transiently transfected with two siRNAs (mTon #1 and mTon #2) targeting different regions of the mouse TonEBP mRNA. Both siRNAs efficiently reduced protein levels of TonEBP and increased expression of HO-1 protein after 24 h of transfection (**Figure 1D**). Targeting TonEBP by siRNA mTon #1 resulted in a dose-dependent knockdown (**Figure 1E**). This led to increased expression of HO-1 protein for up to 96 h (**Figure 1E**). For the following experiments, we used the siRNA mTon #1 at 2 nM, because siRNA mTon #1 was more effective in silencing TonEBP than mTon #2 (**Figure 1D**). LPS increased expression of HO-1 (43) and TonEBP (37, 39) proteins (**Figure 1F**), as previously reported. Notably, TonEBP knockdown increased expression of HO-1 protein and mRNA in resting and LPS-stimulated RAW264.7 cells (**Figures 1E,G**). Neither LPS nor TonEBP knockdown affected expression of the HO-2 protein, a constitutive isoform (**Figure 1F**). High glucose (25 mM) enhanced the expression of both TonEBP and HO-1 mRNA in response to LPS in RAW264.7 cells, and TonEBP knockdown increased the expression of HO-1 mRNA both under normal and high glucose conditions (**Supplementary Figure 1B**). We found that adenoviral vectors can be used to transduce RAW264.7 cells without toxicity up to MOI of 100 without cytotoxicity (**Supplementary Figure 1C**). Overexpression of TonEBP using the adenoviral vector at an MOI of 50 resulted in a reduced expression of HO-1 mRNA in resting and LPS-stimulated cells

(**Figure 1H**), further confirming that TonEBP suppresses HO-1 expression in murine macrophages.

We asked whether the suppression of HO-1 by TonEBP occurred in human macrophages. For this we used human monocyte-derived macrophages obtained from three donors as described previously (39) and macrophages differentiated from the human monocyte cell line THP-1. LPS induced expression of HO-1 mRNA in human monocyte-derived macrophages, and TonEBP knockdown increased the expression of HO-1 mRNA under unstimulated and LPS-stimulated conditions (**Figure 1I**). Similar results were observed for macrophage-differentiated THP-1 cells. Expression of HO-1 in response to LPS was induced at 1 h, and increased further up to 6 h (**Figure 1J**). This response was dose-dependent (**Figure 1K**). TonEBP knockdown increased expression of HO-1 in THP-1 cells under unstimulated and LPS-stimulated conditions (**Figures 1J,K**). The elevated HO-1 mRNA levels were associated with increased expression of HO-1 protein (**Figure 1L**). These data demonstrate that TonEBP suppresses HO-1 expression in human and murine macrophages.

TonEBP Induces the Macrophage M1 Phenotype via Downregulation of HO-1

Here we asked whether M1 genes tumor necrosis factor α (TNF α), cyclooxygenase-2 (COX-2), chemokine (C-X-C motif) ligand 10 (IP-10), and chemokine (C-C motif) ligand 5 (RANTES), that are associated with diabetic complications (48–50), were affected by the increased expression of HO-1 in response to TonEBP knockdown. First, we examined the effects of siRNA-mediated silencing of TonEBP and HO-1 in PMA-differentiated THP-1 and RAW264.7 cells. Both siRNAs (hTon #1 and hTon #2) targeting different regions of the human TonEBP mRNA efficiently reduced protein levels of TonEBP and increased expression of HO-1 protein after 24 h of transfection in THP-1 cells (**Supplementary Figure 1D**). For the following studies we used the siRNA hTon #1 at concentration of 2 nM. TonEBP targeting siRNA TonEBP reduced expression of TonEBP mRNA while increasing HO-1 mRNA in THP-1 (**Supplementary Figure 2A**) and RAW264.7 cells (**Supplementary Figure 2B**), whereas siRNA targeting of HO-1 reduced HO-1 mRNA without affecting TonEBP mRNA expression. LPS induces rapid expression of the pro-inflammatory M1 genes (51). LPS-induced expression of mRNA encoding TNF α , COX-2, IP-10, and RANTES in THP-1 cells fell after TonEBP knockdown. Notably, TonEBP/HO-1 double knockdown reduced the suppressive effects of TonEBP knockdown on expression of these genes (**Figure 2A**). Same pattern of changes was observed in RAW264.7 cells (**Figure 2B**), demonstrating that TonEBP induces M1 genes in human and murine macrophages (at least in part) by downregulating HO-1.

Next, we examined the effects of zinc protoporphyrin (ZnPP), which inhibits HO-1 activity and cobalt protoporphyrin (CoPP), an inducer of HO-1. Both ZnPP and CoPP increased HO-1 mRNA expression, a finding in line with previous reports (52, 53) while not affecting TonEBP mRNA expression (**Supplementary Figures 2C,D**). TonEBP knockdown significantly increased CoPP or ZnPP-mediated

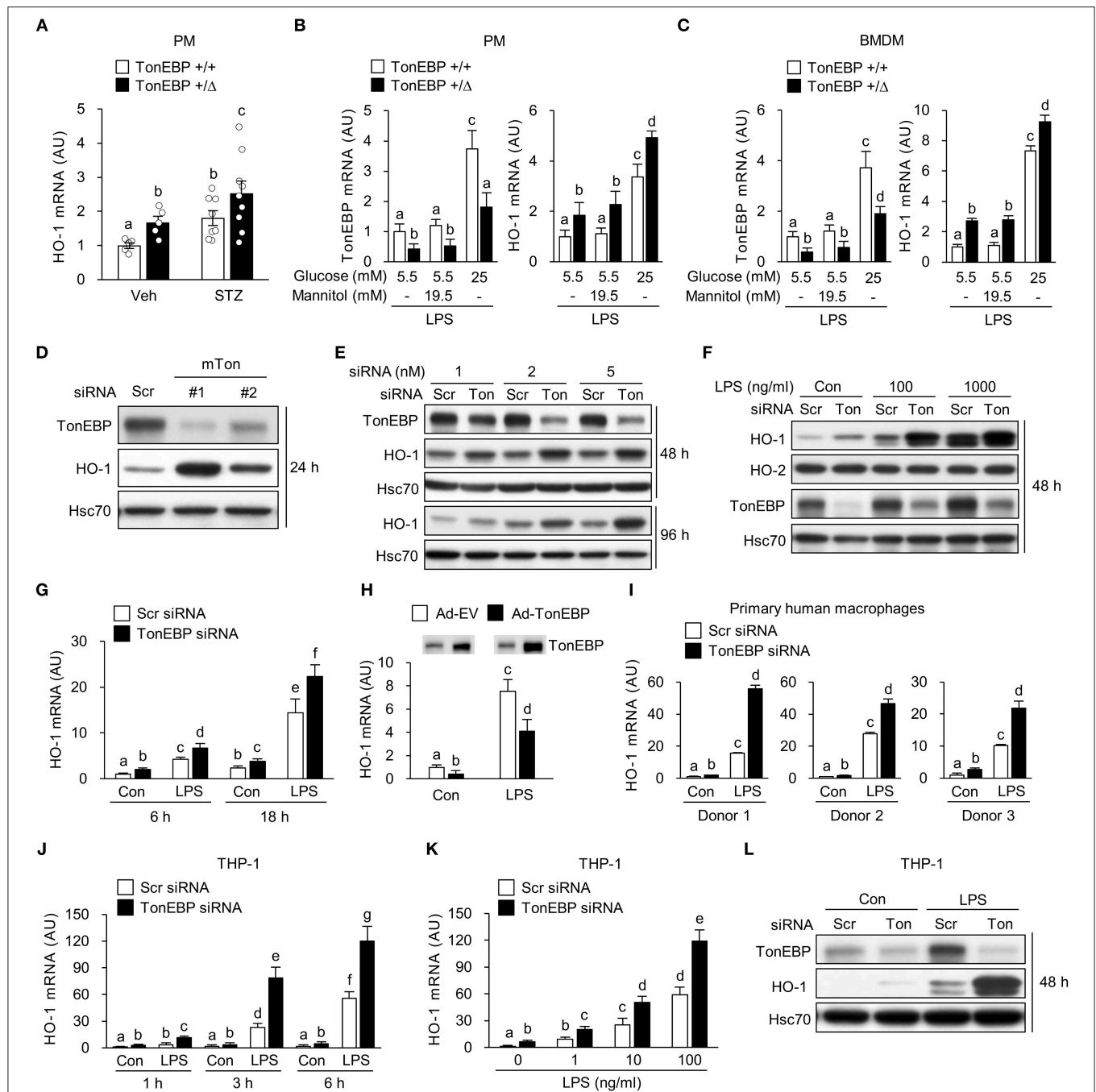


FIGURE 1 | TonEBP reduces expression of HO-1 both in human and murine macrophages. **(A)** Peritoneal macrophages (PM) were obtained from non-diabetic (Veh, $n = 5$) and streptozotocin-induced diabetic (STZ, $n = 8-9$) TonEBP $+/+$ and TonEBP $+/\Delta$ mice (34). The abundance of HO-1 mRNA was measured by quantitative RT-PCR. Mean \pm SEM. **(B,C)** PM **(B)** and bone marrow-derived macrophages (BMDM) **(C)** obtained from TonEBP $+/+$ or TonEBP $+/\Delta$ mice were cultured in normal glucose (5.5 mM), high glucose (25 mM), or 5.5 mM glucose + 19.5 mM mannitol (osmotic control for high glucose) for 24 h and then treated with LPS (100 ng/ml) for 6 h. Quantitative RT-PCR was performed to measure expression of mRNA encoding TonEBP and HO-1. **(D)** RAW264.7 cells were transfected with scrambled [Scr (-)] or two siRNAs (Ton #1 or Ton #2) targeting different regions of mouse TonEBP mRNA for 24 h. Immunoblotting to detect TonEBP, HO-1 and Hsc70 was performed. **(E-G)** RAW264.7 cells transfected with scrambled (Scr) siRNA or siRNA targeting TonEBP (Ton) for 24 h. **(E)** Transfected cells were further cultured for 24 or 72 h, followed by immunoblotting to detect TonEBP, HO-1, and Hsc70. **(F)** Transfected cells were treated with vehicle (Con) or LPS (100 or 1,000 ng/ml) for 24 h and immunoblotted with antibodies specific for TonEBP, HO-1, HO-2, and Hsc70. **(G)** Transfected cells were treated with LPS (100 ng/ml) for 6 or 18 h, and abundance of HO-1 mRNA was measured by quantitative RT-PCR. **(H)** RAW264.7 cells infected with adenovirus expressing TonEBP (Ad-TonEBP) or with empty vector (Ad-EV) at an MOI of 50 for 24 h and then treated with LPS for 6 h, followed by immunoblotting to detect TonEBP and quantitative RT-PCR to detect HO-1 mRNA. **(I)** Human peripheral blood monocyte-derived macrophages were transfected for 48 h with Scr siRNA or siRNA targeting TonEBP and then treated with LPS (100 ng/ml) for 6 h. (Continued)

FIGURE 1 | Quantitative RT-PCR to measure HO-1 mRNA was performed. **(J,L)** Human PMA-differentiated THP-1 cells transfected for 24 h with Scr siRNA or siRNA targeting TonEBP. **(J,K)** Transfected cells were treated with vehicle (Con) or LPS as indicated. The abundance of mRNA encoding HO-1 was measured by quantitative RT-PCR. **(L)** Transfected cells were treated with vehicle (Con) or LPS (100 ng/ml) for 24 h, followed by immunoblotting to detect TonEBP, HO-1, and Hsc70. **(A–C,G–K)** Two-way ANOVA with Tukey's *post-hoc* test was used for multiple comparisons. Different letters indicate statistical differences at $P < 0.05$. **(B,C,G–K)** Data (mean + SD) were from three independent experiments ($n = 3$) each with more than three replicates. **(D–F,L)** Data are representative of three independent experiments. AU, arbitrary units.

expression of HO-1 mRNA (**Supplementary Figures 2C,D**). ZnPP increased expression of TNF α , COX-2, IP-10, and RANTES in LPS-stimulated RAW264.7 cells (**Figure 2C**). In addition, inhibition of these genes' expression upon TonEBP knockdown was attenuated by treatment with ZnPP (**Figure 2C**). CoPP increased expression of HO-1 protein in resting and LPS-stimulated RAW264.7 cells and TonEBP knockdown increased CoPP-mediated protein expression of HO-1 (**Supplementary Figure 2E**). CoPP reduced expression of TNF α , COX-2, IP-10 and RANTES in LPS-stimulated RAW264.7 cells (**Figure 2D**). Furthermore, treatment of TonEBP knockdown cells with CoPP exacerbated the reduction in these genes' mRNA expression induced by TonEBP knockdown (**Figure 2D**). The opposite actions of ZnPP and CoPP provide further support that M1 induction by TonEBP is mediated by downregulation of HO-1.

TonEBP Suppresses the Macrophage M2 Phenotype via Downregulation of HO-1

LPS-stimulated inflammatory responses lead to expression of the anti-inflammatory cytokine interleukin-10 (IL-10) (54, 55), and M2 genes, such as arginase-1 (Arg-1) and CD206 (56); this acts as a feedback mechanism that curtails inflammatory responses. Because induction of HO-1 in macrophages promotes expression of IL-10 (57), we examined whether TonEBP knockdown-mediated induction of HO-1 played a role in the expression of IL-10. As reported previously (39), TonEBP knockdown increased expression of IL-10 mRNA in THP-1 and RAW264.7 cells under unstimulated and LPS-stimulated conditions, whereas HO-1 knockdown reduced IL10 expression (**Figure 3A**). The TonEBP knockdown-mediated increase in IL-10 expression in both cell types was attenuated by TonEBP/HO-1 double knockdown under unstimulated and LPS-stimulated conditions (**Figure 3A**). In addition, LPS-induced expression of mRNA encoding Arg-1 and CD206 increased upon TonEBP knockdown in both cell types, and TonEBP/HO-1 double knockdown attenuated the TonEBP knockdown-mediated increase in expression of Arg-1 and CD206 (**Figure 3B**). Furthermore, treatment of TonEBP knockdown cells with ZnPP almost completely abolished the TonEBP knockdown-mediated increase in expression of IL-10, Arg-1, and CD206 by LPS-stimulated RAW264.7 cells (**Figure 3C**). Reversely, treatment with CoPP promoted the TonEBP knockdown-mediated increase in expression of IL-10, Arg-1, and CD206 by LPS-stimulated RAW264.7 cells (**Figure 3D**). These data suggest that HO-1 mediates the stimulation of M2 genes in response to TonEBP knockdown.

In macrophages, HO-1 and IL-10 form a positive feedback loop that amplifies the anti-inflammatory response. Briefly, HO-1 promotes expression of IL-10 (58), which then feeds back

to induce expression of HO-1 (59, 60). Given the finding that TonEBP knockdown increases expression of HO-1, and the results of our previous report showing that TonEBP knockdown induces the M2 phenotype by upregulating IL-10 (39), we next used siRNA to elucidate the relationship between HO-1 and IL-10. Expression of HO-1 mRNA was not affected by siRNA-mediated knockdown of IL-10 in resting and LPS-stimulated RAW264.7 cells (**Supplementary Figure 3A**). However, knockdown of HO-1 reduced IL-10 expression in both cell types (**Supplementary Figure 3B**), demonstrating that HO-1 contributes to expression of IL-10 both in resting and LPS-stimulated RAW264.7 cells.

Next, we asked whether increased expression of HO-1 in response to TonEBP knockdown played a role in induction of the M2 phenotype in IL-4-stimulated macrophages. As previously reported (39), IL-4 induced expression of mRNA encoding IL-10, Arg-1, and CD206 in RAW264.7 cells (**Figure 4A**). TonEBP knockdown promoted IL-4-induced expression of mRNA encoding IL-10, Arg-1, and CD206, whereas HO-1 knockdown reduced expression of these genes in response to IL-4 (**Figure 4B**). The TonEBP knockdown-mediated increase in expression of mRNA encoding IL-10, Arg-1, and CD206 was suppressed by TonEBP/HO-1 double knockdown (**Figure 4B**). Taken together, the data in **Figures 3, 4** demonstrate that suppression of M2 phenotype by TonEBP is mediated by reduced expression of HO-1.

TonEBP Blocks Recruitment of Nrf2 to the Enhancer Region of the HO-1 Gene

Next, we investigated molecular mechanism underlying TonEBP-mediated regulation of the HO-1 gene. First, we examined generation of reactive oxygen species (ROS), which induce expression of the HO-1 gene (61). TonEBP knockdown did not affect ROS levels in resting macrophages for up to 48 h (**Supplementary Figure 4A**). Furthermore, TonEBP knockdown reduced LPS-mediated ROS generation and acted synergistically with NAC, a ROS scavenger, to reduce ROS levels further (**Figure 5A**). Pre-treatment of resting and LPS-stimulated cells with NAC reduced expression of HO-1 (**Figure 5B**) as expected. TonEBP knockdown increased expression of HO-1 in control and NAC-exposed cells, despite the lower levels of ROS accumulation (**Figure 5B**). These data demonstrate that depleting TonEBP induces HO-1 expression independently of ROS.

Next, we asked whether TonEBP knockdown increased transcription of HO-1. For this, we constructed a pGL3 luciferase reporter using a ~4 kb HO-1 promoter fragment containing the enhancer E1 region which is a key regulator of the HO-1 gene transcription [reviewed in Ref. (62)]. TonEBP knockdown

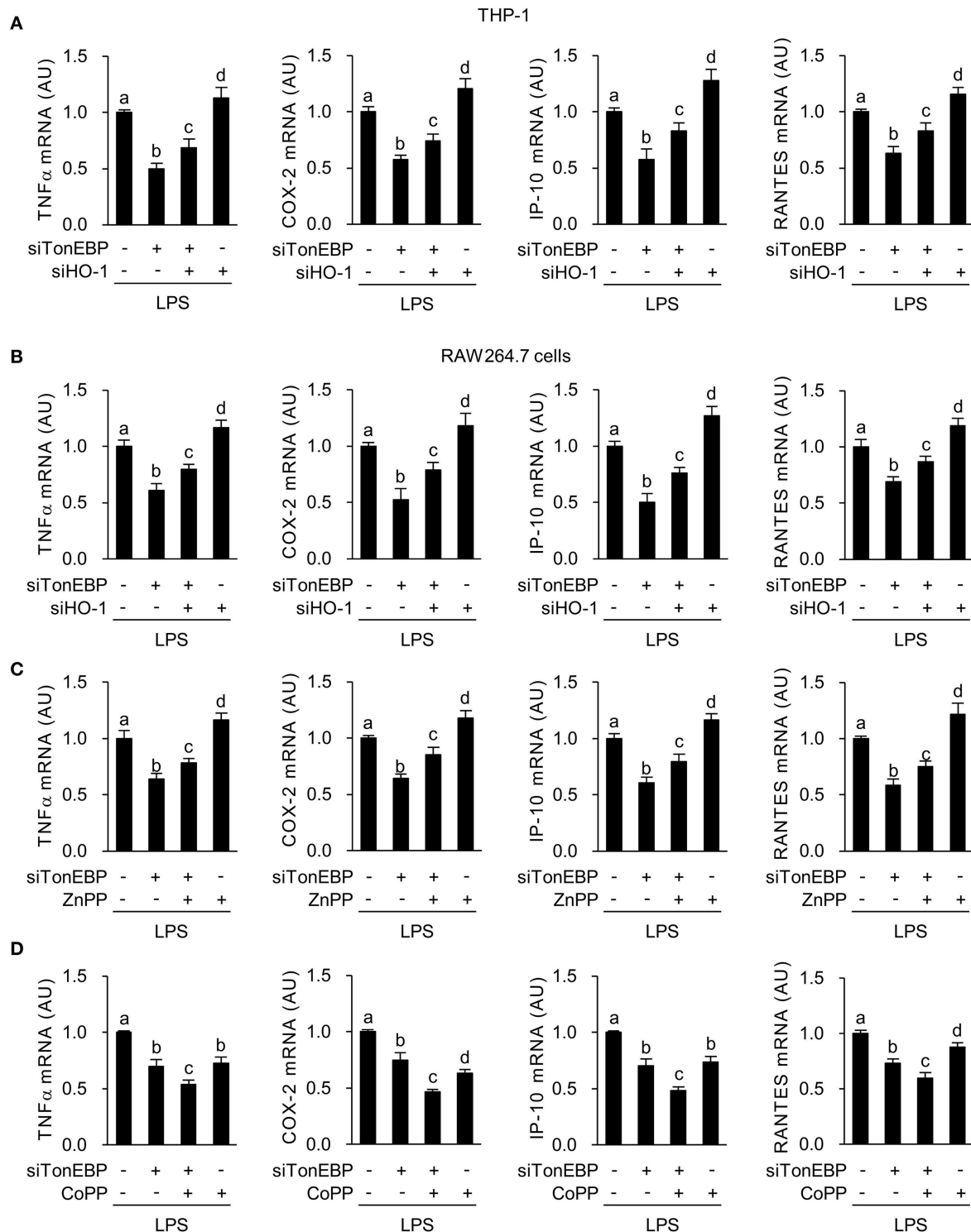


FIGURE 2 | TonEBP induces the macrophage M1 phenotype by downregulating HO-1. **(A,B)** Differentiated THP-1 **(A)** and RAW264.7 **(B)** cells were transfected with scrambled [Scr (-)], TonEBP-targeting, and HO-targeting siRNA in the combinations indicated at the bottom of the panels for 24 h. The concentration of total siRNA was equalized by adjusting the concentration of Scr (-) siRNA. Transfected cells were then treated with LPS (100 ng/ml) for 3 h (for TNFα) or 6 h (for COX-2, IP-10 and RANTES). Expression of mRNA was measured by quantitative RT-PCR. **(C,D)** RAW264.7 cells transfected with Scr (-) or TonEBP-targeting siRNA were treated for 3 h (for TNFα) or 6 h (COX-2, IP-10, and RANTES) with LPS in the presence of ZnPP (20 μM), CoPP (5 μM), or vehicle (-). Expression of mRNA was measured by quantitative RT-PCR. Two-way ANOVA with Tukey's *post-hoc* test was used for multiple comparisons. Different letters indicate statistical differences at $P < 0.05$. Data (mean + SD) were from three independent experiments ($n = 3$) each with more than three replicates. AU, arbitrary units.

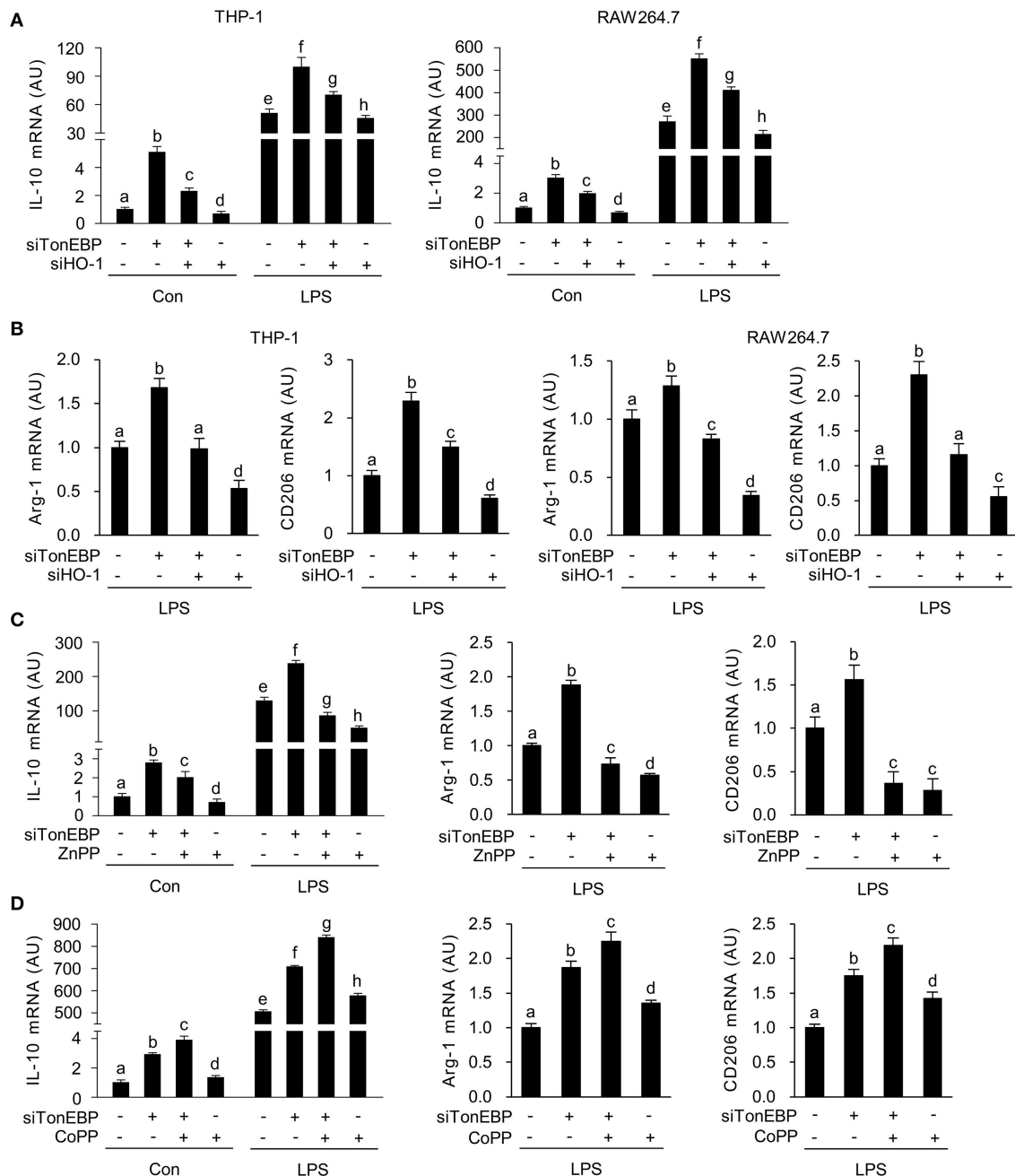


FIGURE 3 | TonEBP suppresses the macrophage M2 phenotype by downregulating HO-1. **(A,B)** Differentiated THP-1 **(A)** and RAW264.7 **(B)** cells were transfected with scrambled [Scr (-)], TonEBP-targeting, or HO-targeting siRNA in the combinations indicated at the bottom of the panels for 24 h. The concentration of total siRNA was equalized by adjusting the concentration of Scr (-) siRNA. Transfected cells were then treated with LPS (100 ng/ml) for 12 h, and expression of mRNA encoding IL-10, Arg-1, and CD206 was measured by quantitative RT-PCR. **(C,D)** RAW264.7 cells transfected with Scr (-) or TonEBP-targeting siRNA were treated for 12 h with LPS in the presence of ZnPP (20 μ M), CoPP (5 μ M), or vehicle (-). The abundance of mRNA encoding IL-10, Arg-1, and CD206 was measured by quantitative RT-PCR. Two-way ANOVA with Tukey's *post-hoc* test was used for multiple comparisons. Different letters indicate statistical differences at $P < 0.05$. Data (mean + SD) were from three independent experiments ($n = 3$) each with more than three replicates. AU, arbitrary units.

stimulated the HO-1 promoter-driven luciferase expression in resting and LPS-stimulated RAW264.7 cells (**Figure 5C**). The 4 kb fragment contains one TonE sequence (a TonEBP binding sequence) near the three antioxidant response elements (AREs) that bind to nuclear factor erythroid-derived 2-like 2 (NFE2L2,

Nrf2), a critical regulator of HO-1 (**Figure 5D**). Therefore, we asked whether TonEBP binds to the TonE site. Because TonEBP knockdown activated basal expression of HO-1 even in the absence of LPS (**Figure 1**), we performed a ChIP assay using resting RAW264.7 cells. Fragments of the region containing

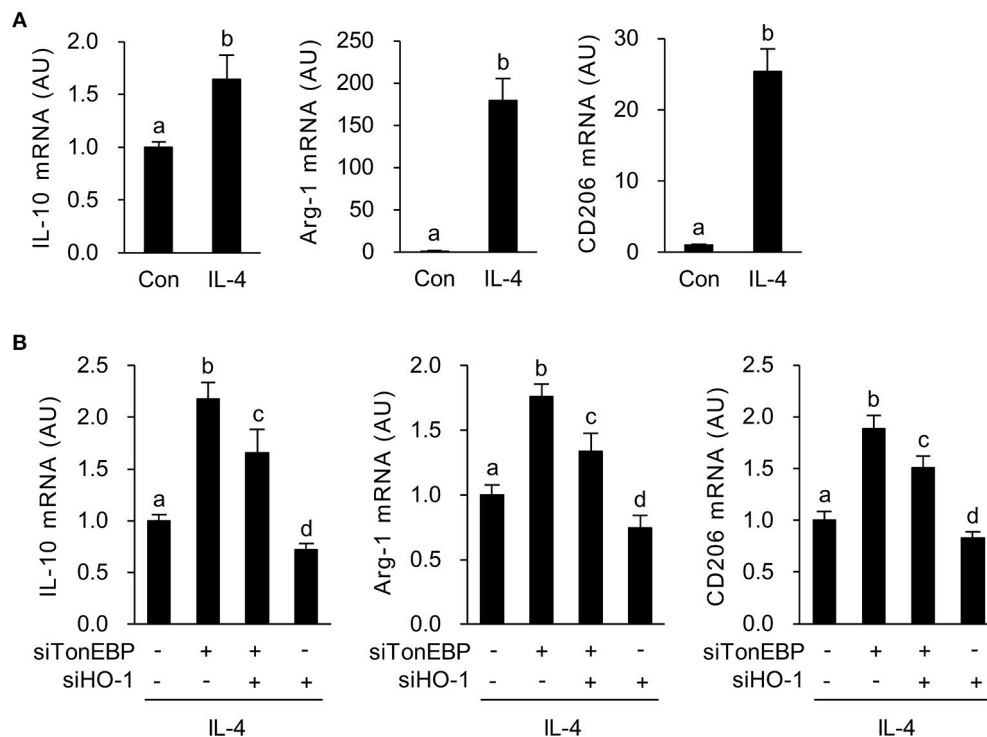


FIGURE 4 | HO-1 mediates the stimulatory effects of TonEBP knockdown on the M2 phenotype. **(A)** RAW264.7 cells were treated with IL-4 (10 ng/ml) for 12 h. Expression of mRNA encoding IL-10, Arg-1, and CD206 was measured by quantitative RT-PCR. **(B)** Cells were transfected with scrambled [Scr (-)], TonEBP-targeting, or HO-1-targeting siRNA in the combinations indicated at the bottom of the panel for 24 h. The concentration of total siRNA was equalized by adjusting the concentration of Scr (-) siRNA. Transfected cells were then treated with IL-4 (10 ng/ml) for 12 h, and expression of mRNA encoding IL-10, Arg-1, and CD206 was measured by quantitative RT-PCR. Two-way ANOVA with Tukey's *post-hoc* test was used for multiple comparisons. Different letters indicate statistical differences at $P < 0.05$. Data (mean + SD) were from three independent experiments ($n = 3$) each with more than three replicates. AU, arbitrary units.

TonE were precipitated by an antibody specific for TonEBP; this precipitation was abrogated by TonEBP deficiency (**Figure 5E**), demonstrating that TonEBP binds to this region on chromatin. To investigate whether stimulation of the HO-1 promoter in response to TonEBP knockdown was dependent on the TonE sequence within the promoter, we constructed a mutant construct (mTonE) in which TonE was inactivated by site-directed mutagenesis. mTonE showed enhanced transcriptional activity, which was not affected by TonEBP knockdown (**Figure 5F**), confirming the functionality of TonE on the HO-1 promoter activity. Next, we asked whether binding of TonEBP to the TonE site affected binding of Nrf2 to the neighboring AREs. Recruitment of Nrf2 to the AREs in the enhancer E1 region was stimulated by TonEBP knockdown (**Figure 5G**). On the other hand, TonEBP knockdown did not affect protein expression (**Supplementary Figure 4B**) or nuclear translocation of Nrf2 (**Figure 5H** and **Supplementary Figure 4C**), suggesting that TonEBP directly prevents recruitment of Nrf2 to the enhancer E1 region of the HO-1 gene. Anti-Nrf2 antibody specificity was confirmed in cells transfected with Nrf2-targeting siRNA (**Supplementary Figure 4D**). Because recruitment of Nrf2 to the HO-1 enhancer E1 region facilitates binding of RNA polymerase II (RNA Pol II) to the human HO-1 promoter region (63), we examined RNA Pol II enrichment at the transcription start site (TSS). Recruitment of Pol II to the TSS region of the HO-1

promoter was detected in resting cells, and its binding increased in response to TonEBP knockdown (**Figure 5J**), consistent with elevated Nrf2 binding to the AREs. These data demonstrate that TonEBP binding reduces Nrf2 recruitment to the AREs leading to reduced Pol II binding to the promoter.

Finally, we asked whether increased expression of HO-1 upon TonEBP knockdown required Nrf2 binding to AREs. To answer the question, we deleted the three AREs from the HO-1 promoter reporter construct (**Figure 5D**). Deletion of AREs (Δ AREs) markedly reduced HO-1 promoter activity, which is consistent with the function of Nrf2 as a major transcriptional regulator of HO-1 [reviewed in Ref. (62)] (**Figure 5K**). Importantly, while wild-type HO-1 promoter-driven luciferase activity increased after TonEBP knockdown, TonEBP knockdown did not alter HO-1 promoter activity in the construct lacking AREs, demonstrating Nrf2-dependent suppression of HO-1 transcription by TonEBP.

TonEBP-deficient M1 Macrophages Exert Paracrine Anti-inflammatory Effects

To examine whether TonEBP deficiency in M1-primed macrophages affects activation of resting macrophages, we conducted indirect co-culture experiments using the Transwell system. Control and TonEBP knockdown RAW264.7 cells were

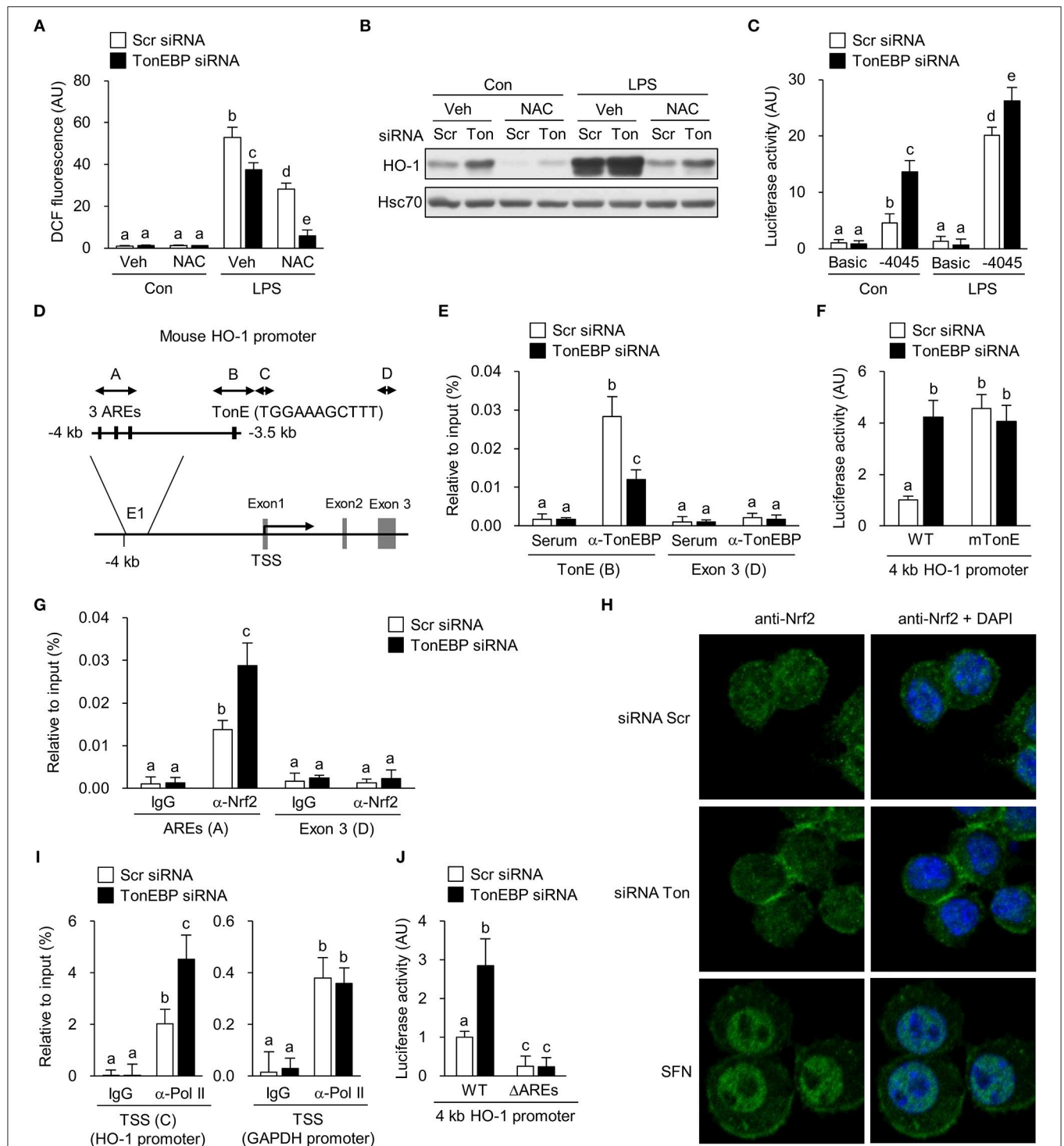


FIGURE 5 | TonEBP regulates recruitment of Nrf2 to the enhancer region of the HO-1 gene. **(A–C)** RAW264.7 cells were transfected with scrambled (Scr) or TonEBP-targeting siRNA (Ton) for 24 h. Cells were pre-treated with vehicle (Veh) or NAC (10 mM) for 30 min and cultured in the presence of LPS (100 ng/ml) for 24 h. **(A)** Intracellular ROS levels were measured by DCF oxidation. **(B)** Immunoblotting to detect HO-1 and Hsc70 was performed. **(C)** The siRNA-transfected cells were transfected a second time with plasmid constructs containing a -4,045/+74 kb fragment of the mouse HO-1 promoter (-4,045/+74 pGL3) for 24 h. Luciferase activity was measured 8 h after treatment with vehicle (Con) or 100 ng/ml LPS. **(D)** Schematic representation of the mouse HO-1 gene promoter region (E1), including the AREs and TonE. **(A–D)** Indicate regions targeted by ChIP-quantitative RT-PCR. **(E)** RAW264.7 cells were transfected with Scr or TonEBP-targeting siRNA for 24 h. Immunoprecipitation was performed using an anti-TonEBP antibody or serum. Precipitated DNA, along with input DNA, was analyzed by quantitative RT-PCR using (Continued)

FIGURE 5 | primer pairs specific for two regions of the HO-1 promoter: a proximal region covering the TonEBP binding site and exon 3 region (as a control). **(F)** The siRNA-transfected cells were transfected a second time with the $-4,045/+74$ promoter construct (WT) or with a mutant $-4,045/+74$ construct [in which the TonE site was mutated (mTonE)] and luciferase activity was measured ($n = 4$). **(G)** RAW264.7 cells were transfected with Scr or TonEBP-targeting siRNA for 24 h. ChIP assay was performed using an anti-Nrf2 antibody or IgG to detect AREs **(A)** ($n = 3$) and the exon 3 (E3) region on the HO-1 gene of RAW264.7 cells. **(H)** Confocal immunofluorescence images of Nrf2 protein. RAW264.7 cells were transfected with scrambled (Scr) or TonEBP-targeting siRNA (Ton) for 24 h. Sulforaphane (SFN) was used as a positive control of Nrf2 nuclear localization. The signals of Nrf2 protein (green) were detected using anti-Nrf2 antibody. Nuclei were counterstained with DAPI (blue). Data are representative of three independent experiments. **(I)** A ChIP assay was performed using an anti-Pol II antibody or IgG to detect the TSS **(C)** of the HO-1 promoter and the TSS region of the GAPDH promoter (as a control). **(J)** The siRNA-transfected cells were transfected a second time with the $-4,045/+74$ promoter construct (WT) or a mutant $-4,045/+74$ construct [in which the three AREs are mutated (Δ AREs)]. Luciferase activity was measured. **(A,C,E-G,I,J)** Two-way ANOVA with Tukey's *post-hoc* test was used for multiple comparisons. Different letters indicate statistical differences at $P < 0.05$. Data (mean + SD) were from three independent experiments ($n = 3$) each with more than three replicates. AU, arbitrary units.

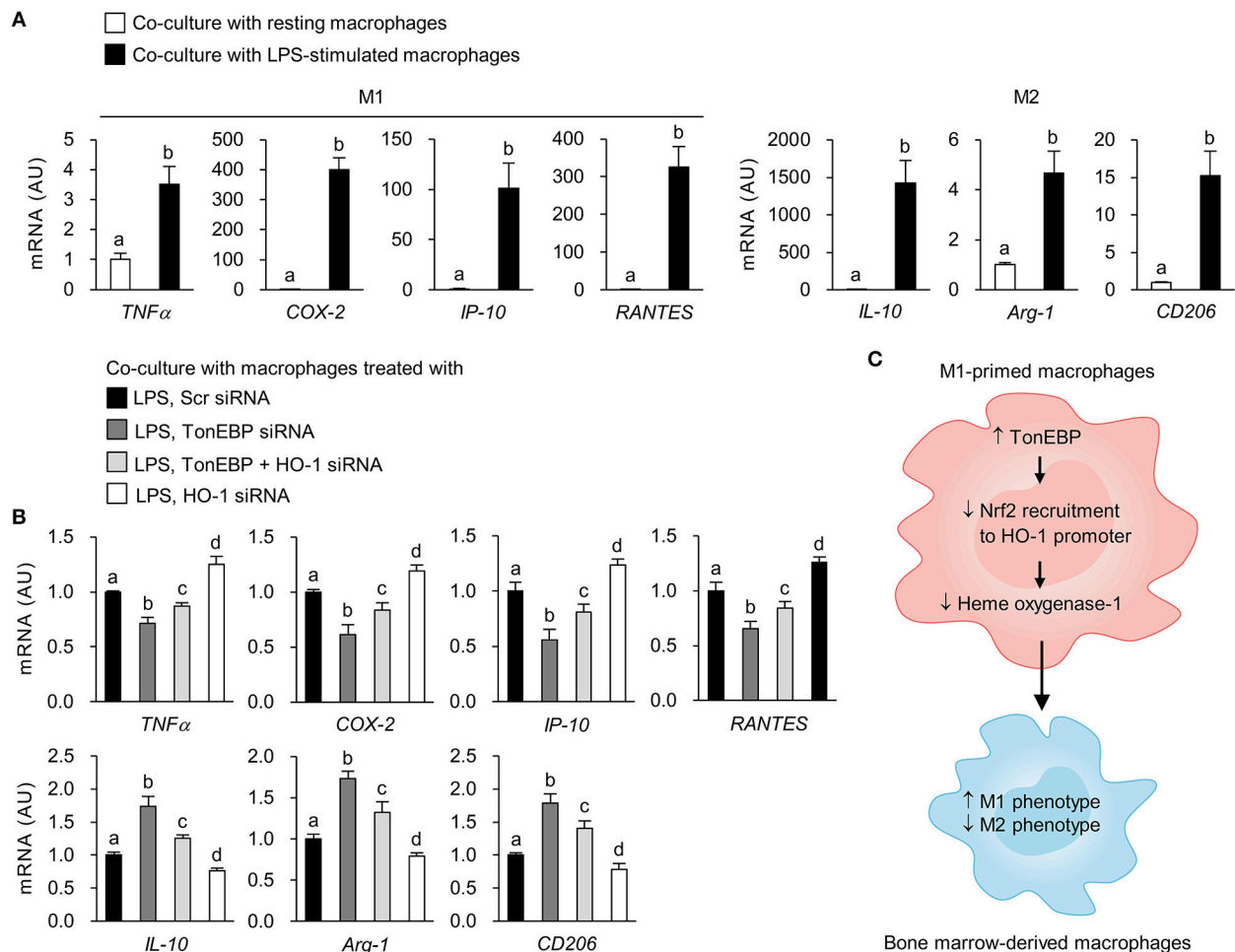


FIGURE 6 | Loss of TonEBP from M1 macrophages induces paracrine anti-inflammatory effects on bone marrow-derived macrophages. **(A,B)** RAW264.7 cells were plated in transwell permeable supports, transfected with scrambled siRNA or siRNA specific for target genes for 24 h, and then treated with LPS (100 ng/ml) for 12 h. RAW264.7 cells were then added to the 6-well companion plates and co-cultured with BMDMs for 3 h (for *TNF α*) or 12 h (for *COX-2*, *IP-10*, *RANTES*, *IL-10*, *Arg-1*, and *CD206*) (see **Supplementary Figure 5**). BMDMs were collected, and expression of mRNA encoding the genes indicated at the bottom of the panel was measured by quantitative RT-PCR. Two-way ANOVA with Tukey's *post-hoc* test was used for multiple comparisons. Different letters indicate statistical differences at $P < 0.05$. Data (mean + SD) were from three independent experiments ($n = 3$) each with more than three replicates. AU, arbitrary units. **(C)** Proposed mechanism for the role of TonEBP. Increased expression of TonEBP by M1-primed macrophages suppresses HO-1 expression, leading to increased expression of M1 genes and reduced expression of M2 genes.

stimulated with LPS to induce an M1 phenotype. Then, LPS was removed prior to co-culture of M1-primed macrophages with resting BMDMs (**Supplementary Figure 5**). Co-culture with M1-primed macrophages induced expression of M1

(*TNF α* , *COX-2*, *IP-10*, *RANTES*) and M2 genes (*IL-10*, *Arg-1*, *CD206*) in BMDMs (**Figure 6A**). Co-culture of BMDMs with TonEBP knockdown M1 macrophages resulted in lower expression of pro-inflammatory M1 genes and higher expression

of anti-inflammatory M2 genes (compared with control macrophages) (**Figure 6B**). However, co-culture of BMDMs with HO-1 knockdown M1 macrophages induced expression of M1 genes and attenuated expression of M2 genes (compared with controls) (**Figure 6B**). Moreover, double knockdown of TonEBP and HO-1 reduced the effects of TonEBP knockdown on activation of BMDMs (**Figure 6B**), confirming that M1 macrophages push surrounding resting macrophages into M1 phenotype, and that TonEBP-mediated priming toward M1 macrophages is driven by downregulation of HO-1 expression.

DISCUSSION

Dynamic changes in the functional phenotype of macrophages are associated with pathogenesis of inflammatory diseases (5–7). TonEBP primes macrophages toward an M1 phenotype, which has pro-inflammatory properties. TonEBP does this by promoting expression of pro-inflammatory genes via interaction with NF- κ B (36) and by binding directly to the promoter (37, 64). In addition, TonEBP suppresses expression of the anti-inflammatory cytokine IL-10 by limiting chromatin access to the promoter (37). The pro-inflammatory function of TonEBP suggests that inhibiting its expression or activation could suppress inflammatory responses. Indeed, TonEBP haplo-deficient and myeloid-specific TonEBP knockout mice are effectively protected from inflammatory diseases. TonEBP haplo-insufficiency in a mouse model of rheumatoid arthritis almost completely prevented pannus formation and cartilage destruction, which was related to the reduced survival of macrophages (16, 34). Also, formation of atherosclerotic lesions in *ApoE*^{−/−} mice fed a high fat diet is reduced when mice are TonEBP haplo-deficient; this reduction is dependent on TonEBP depletion from macrophages (32). In a mouse model of diabetic nephropathy (DN), TonEBP haplo-deficiency is associated with reduced activation of macrophages by hyperglycemia, with fewer macrophages in the kidney, with lower renal expression of pro-inflammatory genes, and with attenuated DN (35). Moreover, increased activity of TonEBP in monocytes is associated with early DN in humans (65). A recent study shows that TonEBP promotes hepatocellular carcinogenesis, recurrence, and metastasis in patients with hepatocellular carcinoma (HCC) and in mouse models of HCC (36).

Here, we identified a novel function of TonEBP as a potent suppressor of HO-1 expression both in human and murine macrophages. The role of TonEBP in suppressing expression of HO-1 is important given the well-established immunosuppressive activity of HO-1. HO-1-deficient mice show increased oxidative stress, a tendency toward pro-inflammatory responses (15, 21), and increased susceptibility to sepsis (17). Phenotypical alterations in human cases of genetic HO-1 deficiency are similar to those observed in HO-1 knockout mice (19, 20). Furthermore, increased HO-1 expression in macrophages leads to a reduced capacity for foam cell formation (a potent anti-inflammatory and tissue regenerative function) and thereby suppresses atherosclerosis (66). Activation of HO-1 ameliorates renal damage in STZ-induced DN in rats through anti-inflammatory and antioxidant mechanisms (44).

Genetic and pharmacological induction of HO-1 expression in synovial cells from RA patients reduces expression of pro-inflammatory genes (67). In this regard, TonEBP depletion-driven immunosuppression resembles the immunosuppressive effects of HO-1. Importantly, we show here that depleting TonEBP promotes expression of HO-1 even under basal conditions. This finding is of great interest because increasing of evidence suggests basal HO-1 levels are more important in the protection against inflammation and oxidative stress than the degree of upregulation of HO-1 following injury (21, 68, 69). Thus, this study provides an opportunity to further our understanding of the role of TonEBP during polarization, and on the functions, of macrophages. As such, it may facilitate design of new regimens that prevent inflammatory diseases.

Expression of HO-1 is regulated primarily at the transcriptional level, and distinct DNA sequence-dependent enhancer regions in the upstream regulatory regions of the HO-1 promoter mediate basal and inducible HO-1 gene expression in different species [reviewed in Refs. (14, 62)]. One major *cis*-acting DNA sequence element in the enhancers is called stress-responsive element which contains AREs. Cognate transcription factor for AREs is Nrf2, a Cap“n”collar/basic-leucine zipper transcription factor (70). Under basal conditions, Keap1 forms a complex with Nrf2 and limits its nuclear translocation (71). When cells are exposed to inducing stimuli, such as endotoxin, heme, and oxidants, Nrf2 dissociates from Keap1, translocates to the nucleus, and binds to the AREs (72). Here, we suggest a new regulatory mechanism for Nrf2-mediated HO-1 induction in macrophages: downregulation of TonEBP stimulates HO-1 expression by recruitment of Nrf2 to the enhancer region of the HO-1 gene without affecting nuclear translocation of Nrf2. The TonEBP depletion-mediated increase in HO-1 expression attenuates polarization of macrophages toward the pro-inflammatory M1 phenotype while enhancing M2 polarization (**Figure 6C**). Identification of HO-1 as a downstream target of TonEBP provides an exciting opportunity for the design and development of novel therapeutic approaches that resolve chronic inflammation associated with inflammatory diseases.

ETHICS STATEMENT

All experimental protocols were approved by the Institutional Animal Care and Use Committee of the Ulsan National Institute of Science and Technology (UNISTACUC-12-15-A).

AUTHOR CONTRIBUTIONS

EY, SC, and HMK designed the experiments and wrote the manuscript. EY, SC, HL, BY, JL, CL, HJK, GJ, HP, SL, and WL performed the experiments. EY, SC, and HMK analyzed data.

FUNDING

This work was supported by the National Research Foundation grants (NRF-2018R1A5A1024340, 2017R1E1A1A074673, and 2016R1D1A1B03932335) and Health Technology R&D Project

grant (HI16C1837) of Korea. This work was also supported by UNIST funds (1.180018.01 and 1.170085.01).

SUPPLEMENTARY MATERIAL

The Supplementary Material for this article can be found online at: <https://www.frontiersin.org/articles/10.3389/fimmu.2019.00850/full#supplementary-material>

Supplementary Figure 1 | TonEBP suppresses expression of HO-1 in macrophages. **(A)** PM and BMDM obtained from TonEBP^{+/+} or TonEBP^{Δ/Δ} mice were cultured in normal glucose (5.5 mM) and treated for 6 h with vehicle (Con) or LPS (100 ng/ml). Quantitative RT-PCR was performed for mRNA for TonEBP and HO-1. **(B)** RAW264.7 cells were transfected with scrambled siRNA or siRNA targeting TonEBP. The transfected cells were cultured in normal glucose (5.5 mM), high glucose (25 mM), or 5.5 mM glucose + 19.5 mM mannitol (osmotic control for high glucose) for 24 h and then treated with LPS (100 ng/ml) for 6 h. Quantitative RT-PCR was performed to measure expression of mRNA encoding TonEBP and HO-1. **(C)** RAW264.7 cells were infected with an empty control virus (Ad-EV) or an adenovirus carrying the human TonEBP gene (Ad-TonEBP) at an MOI of 20, 50, 100 or 200 for 24 h. Control cells were mock-infected with PBS. Cytotoxicity was assessed by release of LDH into the culture media after 24 h of infection. **(D)** Differentiated THP-1 cells were transfected with scrambled [Scr (-)] or two siRNAs (hTon #1 or hTon #2) targeting different regions of human TonEBP mRNA for 24 h. Immunoblotting to detect TonEBP, HO-1 and Hsc70 was performed. Data are representative of three independent experiments. **(A–C)** Two-way ANOVA with Tukey's *post-hoc* test was used for multiple comparisons. Different letters indicate statistical differences at $P < 0.05$. Data (mean + SD) were from three independent experiments ($n = 3$) each with more than three replicates. AU, arbitrary units.

Supplementary Figure 2 | The expression of TonEBP and HO-1 by gene-targeting siRNAs or modulators of HO-1 in THP-1 and RAW264.7 cells. **(A–D)** Differentiated THP-1 **(A)** and RAW264.7 **(B–D)** cells were transfected with scrambled [Scr (-)], TonEBP-targeting, and HO-targeting siRNA for 24 h in the combinations indicated at the bottom of the panels. The concentration of total siRNA was equalized by adjusting the concentration of Scr (-) siRNA. **(A,B)** Transfected cells were then treated with LPS (100 ng/ml) for 3 h. Expression of TonEBP and HO-1 mRNA was measured by quantitative RT-PCR. **(C,D)** RAW264.7 cells transfected with Scr (-) or TonEBP-targeting siRNA were treated for 3 h with LPS in the presence of ZnPP (20 μM), CoPP (5 μM), or vehicle (-). Expression of mRNA was measured by quantitative RT-PCR. **(E)** RAW264.7 cells transfected with scrambled [Scr (-)] or TonEBP-targeting siRNA (Ton) for 24 h were

treated for 18 h with LPS in the presence of vehicle (-) or CoPP (1 or 5 μM). Immunoblotting was performed to detect HO-1 and Hsc70. Data are representative of three independent experiments. **(A–D)** Two-way ANOVA with Tukey's *post-hoc* test was used for multiple comparisons. Different letters indicate statistical differences at $P < 0.05$. Data (mean + SD) were from three independent experiments ($n = 3$) each with more than three replicates. AU, arbitrary units.

Supplementary Figure 3 | HO-1 contributes to expression of IL-10 in macrophages. RAW264.7 cells were transfected with scrambled (Scr), or IL-10- or HO-1-targeting siRNA for 24 h, followed by treatment with vehicle (Con) or 100 ng/ml LPS for 6 h. Quantitative RT-PCR was performed to measure expression of mRNA encoding HO-1 **(A)** and IL-10 **(B)**. Two-way ANOVA with Tukey's *post-hoc* test was used for multiple comparisons. Different letters indicate statistical differences at $P < 0.05$. Data (mean + SD) were from three independent experiments ($n = 3$) each with more than three replicates. AU, arbitrary units.

Supplementary Figure 4 | TonEBP knockdown does not affect ROS levels and nuclear translocation of Nrf2. **(A–D)** RAW264.7 cells were transfected with scrambled (Scr) or TonEBP-targeting siRNA (Ton) for 24 h. **(A)** Cells were pre-treated with vehicle (Veh) or NAC (10 mM) for 30 min and then cultured for 24 or 48 h. Intracellular ROS levels were determined by DCF oxidation. Two-way ANOVA with Tukey's *post-hoc* test was used for multiple comparisons. Data (mean + SD) were from three independent experiments ($n = 3$) each with more than three replicates. AU: arbitrary units. **(B,D)** Cells were treated with vehicle (Veh) or LPS (100 ng/ml) for 1 h and harvested, and cell nuclei and cytoplasm were separated using a Nuclear and Cytoplasmic extraction kit (Pierce) according to the manufacturer's instructions. **(B)** Immunoblotting was performed to detect Nrf2, p65, TonEBP, and Hsc70 (control) in whole cell lysates derived from cells transfected with Scr or TonEBP-targeting siRNA. **(C)** Anti-Nrf2 antibody specificity was confirmed in cells transfected with Nrf2-targeting siRNA. **(D)** Immunoblotting was performed to detect Nrf2, p65, and TonEBP in the nuclear or cytosolic fractions. The nuclear fraction was confirmed by detection of Lamin B. Data are representative of three independent experiments.

Supplementary Figure 5 | A diagram of the system used to co-culture mouse RAW264.7 cells and bone marrow-derived macrophages (BMDMs). Progenitors in the bone marrow were differentiated into macrophages by exposure to M-CSF for 9 days and then plated into 6-well plates. RAW264.7 cells were plated into culture inserts, transfected with scrambled siRNA or siRNA specific for target genes for 24 h, and then treated with LPS (100 ng/ml) for 12 h. The cells were then added to the 6-well companion plates and co-cultured with BMDMs for 3 or 12 h. At the end point of the experiment, BMDMs were collected and used in a gene expression assay to assess the paracrine effects of macrophages.

REFERENCES

- Gordon S, Taylor PR. Monocyte and macrophage heterogeneity. *Nat Rev Immunol.* (2005) 5:953–64. doi: 10.1038/nri1733
- Laskin DL, Sunil VR, Gardner CR, Laskin JD. Macrophages and tissue injury: agents of defense or destruction? *Annu Rev Pharmacol Toxicol.* (2011) 51:267–88. doi: 10.1146/annurev.pharmtox.010909.105812
- Gordon S. Alternative activation of macrophages. *Nat Rev Immunol.* (2003) 3:23–35. doi: 10.1038/nri978
- Martinez FO, Helming L, Gordon S. Alternative activation of macrophages: an immunologic functional perspective. *Annu Rev Immunol.* (2009) 27:451–83. doi: 10.1146/annurev.immunol.021908.132532
- Mosser DM, Edwards JP. Exploring the full spectrum of macrophage activation. *Nat Rev Immunol.* (2008) 8:958–69. doi: 10.1038/nri2448
- Mantovani A, Sica A, Sozzani S, Allavena P, Vecchi A, Locati M. The chemokine system in diverse forms of macrophage activation and polarization. *Trends Immunol.* (2004) 25:677–86. doi: 10.1016/j.it.2004.09.015
- Sica A, Mantovani A. Macrophage plasticity and polarization: *in vivo* veritas. *J Clin Invest.* (2012) 122:787–95. doi: 10.1172/JCI59643
- Maines MD. The heme oxygenase system: a regulator of second messenger gases. *Annu Rev Pharmacol Toxicol.* (1997) 37:517–54. doi: 10.1146/annurev.pharmtox.37.1.517
- Maines MD. Heme oxygenase: function, multiplicity, regulatory mechanisms, and clinical applications. *FASEB J.* (1998) 2:2557–68. doi: 10.1096/fasebj.2.10.3290025
- Tenhunen R, Marver H, Pimstone NR, Trager WF, Cooper DY, Schmid R. Enzymatic degradation of heme. Oxygenative cleavage requiring cytochrome P-450. *Biochemistry.* (1972) 11:1716–20. doi: 10.1021/bi00759a029
- Tenhunen R, Marver HS, Schmid R. Microsomal heme oxygenase. Characterization of the enzyme. *J Biol Chem.* (1969) 244:6388–94.
- Abraham NG, Kappas A. Pharmacological and clinical aspects of heme oxygenase. *Pharmacol Rev.* (2008) 60:79–127. doi: 10.1124/pr.107.07104
- Gozzelino R1, Jeney V, Soares MP. Mechanisms of cell protection by heme oxygenase-1. *Annu Rev Pharmacol Toxicol.* (2010) 50:323–54. doi: 10.1146/annurev.pharmtox.010909.105600
- Ryter SW, Choi AM. Heme oxygenase-1/carbon monoxide: from metabolism to molecular therapy. *Am J Respir Cell Mol Biol.* (2009) 41:251–60. doi: 10.1165/rcmb.2009-0170TR
- Poss KD, Tonegawa S. Heme oxygenase 1 is required for mammalian iron reutilization. *Proc Natl Acad Sci USA.* (1997) 94:10919–24. doi: 10.1073/pnas.94.20.10919
- Yet SF, Perrella MA, Layne MD, Hsieh CM, Maemura K, Kobzik L, et al. Hypoxia induces severe right ventricular dilatation and infarction in heme oxygenase-1 null mice. *J Clin Invest.* (1999) 103:R23–9. doi: 10.1172/JCI6163

17. Wiesel P, Patel AP, DiFonzo N, Marria PB, Sim CU, Pellacani A, et al. Endotoxin-induced mortality is related to increased oxidative stress and end-organ dysfunction, not refractory hypotension, in heme oxygenase-1-deficient mice. *Circulation*. (2000) 102:3015–22. doi: 10.1161/01.CIR.102.24.3015
18. Yachie A, Niida Y, Wada T, Igarashi N, Kaneda H, Toma T, et al. Oxidative stress causes enhanced endothelial cell injury in human heme oxygenase-1 deficiency. *J Clin Invest*. (1999) 103:129–35. doi: 10.1172/JCI4165
19. Radhakrishnan N, Yadav SP, Sachdeva A, Pruthi PK, Sawhney S, Piplani T, et al. Human heme oxygenase-1 deficiency presenting with hemolysis, nephritis, and asplenia. *J Pediatr Hematol Oncol*. (2011) 33:74–8. doi: 10.1097/MPH.0b013e3181fd2aae
20. Kawashima A, Oda Y, Yachie A, Koizumi S, Nakanishi I. Heme oxygenase-1 deficiency: the first autopsy case. *Hum Pathol*. (2002) 33:125–30. doi: 10.1053/hupa.2002.30217
21. Zhang M, Nakamura K, Kageyama S, Lawal AO, Gong KW, Bhattacharaya M, et al. Myeloid HO-1 modulates macrophage polarization and protects against ischemia-reperfusion injury. *JCI Insight*. (2018) 3:e120596. doi: 10.1172/jci.insight.120596
22. Ryter SW, Choi AM. Targeting heme oxygenase-1 and carbon monoxide for therapeutic modulation of inflammation. *Transl Res*. (2016) 167:7–34. doi: 10.1016/j.trsl.2015.06.011
23. Vijayan V, Wagener FADTG, Immenschuh S. The macrophage heme-heme oxygenase-1 system and its role in inflammation. *Biochem Pharmacol*. (2018) 153:159–67. doi: 10.1016/j.bcp.2018.02.010
24. Choi KM, Kashyap PC, Dutta N, Stoltz GJ, Ordog T, Shea Donohue T, et al. CD206-positive M2 macrophages that express heme oxygenase-1 protect against diabetic gastroparesis in mice. *Gastroenterology*. (2010) 138:2399–409 e1. doi: 10.1053/j.gastro.2010.02.014
25. Harusato A, Naito Y, Takagi T, Uchiyama K, Mizushima K, Hirai Y, et al. BTB and CNC homolog 1 (Bach1) deficiency ameliorates TNBS colitis in mice: role of M2 macrophages and heme oxygenase-1. *Inflamm Bowel Dis*. (2013) 19:740–53. doi: 10.1097/MIB.0b013e3182802968
26. Ndisang JF, Mishra M. The heme oxygenase system selectively suppresses the proinflammatory macrophage m1 phenotype and potentiates insulin signaling in spontaneously hypertensive rats. *Am J Hypertens*. (2013) 26:1123–31. doi: 10.1093/ajh/hpt082
27. Miyakawa H, Woo SK, Dahl SC, Handler JS, Kwon HM. Tonicity-responsive enhancer binding protein, a rel-like protein that stimulates transcription in response to hypertonicity. *Proc Natl Acad Sci U S A*. (1999) 96:2538–42. doi: 10.1073/pnas.96.5.2538
28. Lopez-Rodriguez C, Aramburu J, Rakeman AS, Rao A. NFAT5, a constitutively nuclear NFAT protein that does not cooperate with Fos and Jun. *Proc Natl Acad Sci U S A*. (1999) 96:7214–9. doi: 10.1073/pnas.96.13.7214
29. Aramburu J, Drews-Elger K, Estrada-Geloch A, Minguillon J, Moranco B, Santiago V, et al. Regulation of the hypertonic stress response and other cellular functions by the Rel-like transcription factor NFAT5. *Biochem Pharmacol*. (2006) 72:1597–604. doi: 10.1016/j.bcp.2006.07.002
30. Lee SD, Choi SY, Lim SW, Lamitina ST, Ho SN, Go WY, et al. TonEBP stimulates multiple cellular pathways for adaptation to hypertonic stress: organic osmolyte-dependent and -independent pathways. *Am J Physiol Renal Physiol*. (2007) 300:F707–15. doi: 10.1152/ajprenal.00227.2010
31. Go WY, Liu X, Roti MA, Liu F, Ho SN. NFAT5/TonEBP mutant mice define osmotic stress as a critical feature of the lymphoid microenvironment. *Proc Natl Acad Sci U S A*. (2004) 101:10673–8. doi: 10.1073/pnas.0403139101
32. Halterman JA, Kwon HM, Leitinger N, Wamhoff BR. NFAT5 expression in bone marrow-derived cells enhances atherosclerosis and drives macrophage migration. *Front Physiol*. (2012) 3:1–7. doi: 10.3389/fphys.2012.00313
33. Kleinewietfeld M, Manzel A, Titze J, Kvakana H, Yosef N, Linker RA, et al. Sodium chloride drives autoimmune disease by the induction of pathogenic TH17 cells. *Nature*. (2013) 496:518–22. doi: 10.1038/nature11868
34. Choi S, You S, Kim D, Choi SY, Kwon HM, Kim HS, et al. Transcription factor NFAT5 promotes macrophage survival in rheumatoid arthritis. *J Clin Invest*. (2017) 127:954–69. doi: 10.1172/JCI87880
35. Choi SY, Lim SW, Salimi S, Yoo EJ, Lee-Kwon W, Lee HH, et al. Tonicity-responsive enhancer-binding protein mediates hyperglycemia-induced inflammation and vascular and renal injury. *J Am Soc Nephrol*. (2018) 29:492–504. doi: 10.1681/ASN.2017070718
36. Lee JH, Suh JH, Choi SY, Kang HJ, Lee HH, Ye BJ, et al. Tonicity-responsive enhancer-binding protein promotes hepatocellular carcinogenesis, recurrence and metastasis. *Gut*. (2018) 68:347–58. doi: 10.1136/gutjnl-2017-315348
37. Buxade M, Lunazzi G, Minguillon J, Iborra S, Berga-Bolanos R, Del Val M, et al. Gene expression induced by Toll-like receptors in macrophages requires the transcription factor NFAT5. *J Exp Med*. (2012) 209:379–93. doi: 10.1084/jem.20111569
38. Lee HH, Sanada S, An SM, Ye BJ, Lee JH, Seo YK, et al. LPS-induced NFκB enhanceosome requires TonEBP/NFAT5 without DNA binding. *Sci Rep*. (2016) 6:24921. doi: 10.1038/srep24921
39. Choi SY, Lee HH, Lee JH, Ye BJ, Yoo EJ, Kang HJ, et al. TonEBP suppresses IL-10-mediated immunomodulation. *Sci Rep*. (2016) 6:25726. doi: 10.1038/srep25726
40. Zhang X, Goncalves R, Mosser DM. The isolation and characterization of murine macrophages. *Curr Protoc Immunol*. (2008) 83:14.1: 14.1.1–14. doi: 10.1002/0471142735.im1401s83
41. Weischenfeldt J, Porse B. Bone marrow-derived macrophages (BMM): isolation and applications. *CSH Protoc*. (2008) 2008:pdb.prot5080. doi: 10.1101/pdb.prot5080
42. Troeger A, Lastrucci C, Duval C, Tanne A, Cougoule C, Maridonneau-Parini I, et al. An efficient siRNA-mediated gene silencing in primary human monocytes, dendritic cells and macrophages. *Immunol Cell Biol*. (2014) 92:699–708. doi: 10.1038/icb.2014.39
43. Chung SW, Chen YH, Perrella MA. Role of Ets-2 in the regulation of heme oxygenase-1 by endotoxin. *J Biol Chem*. (2005) 280:4578–84. doi: 10.1074/jbc.M409125200
44. Ali MAM, Heeba GH, El-Sheikh AAK. Modulation of heme oxygenase-1 expression and activity affects streptozotocin-induced diabetic nephropathy in rats. *Fundam Clin Pharmacol*. (2017) 31:546–57. doi: 10.1111/fcp.12296
45. Zhao Y, Zhang L, Qiao Y, Zhou X, Wu G, Wang L, et al. Heme oxygenase-1 prevents cardiac dysfunction in streptozotocin-diabetic mice by reducing inflammation, oxidative stress, apoptosis and enhancing autophagy. *PLoS ONE*. (2013) 8:e75927. doi: 10.1371/journal.pone.0075927
46. Pussinen PJ, Havulinna AS, Lehto M, Sundvall J, Salomaa V. Endotoxemia is associated with an increased risk of incident diabetes. *Diabetes Care*. (2011) 34:392–7. doi: 10.2337/dc10-1676
47. Naito Y, Takagi T, Higashimura Y. Heme oxygenase-1 and anti-inflammatory M2 macrophages. *Arch Biochem Biophys*. (2014) 564:83–8. doi: 10.1016/j.abb.2014.09.005
48. Donate-Correa J, Martín-Núñez E, Muros-de-Fuentes M, Mora-Fernández C, Navarro-González JF. Inflammatory cytokines in diabetic nephropathy. *J Diabetes Res*. (2015) 2015:948417. doi: 10.1155/2015/948417
49. Cosentino F, Eto M, De Paolis P, van der Loo B, Bachschmid M, Ullrich V, et al. High glucose causes upregulation of cyclooxygenase-2 and alters prostanoid profile in human endothelial cells: role of protein kinase C and reactive oxygen species. *Circulation*. (2003) 107:1017–23. doi: 10.1161/01.CIR.0000051367.92927.07
50. Ruster C, Wolf G. The role of chemokines and chemokine receptors in diabetic nephropathy. *Front Biosci*. (2008) 3:944–55. doi: 10.2741/2734
51. Takeuchi O, Akira S. Pattern recognition receptors and inflammation. *Cell*. (2010) 140:805–20. doi: 10.1016/j.cell.2010.01.022
52. Drechsler Y, Dolganiuc A, Norkina O, Romics L, Li W, Kodys K, et al. Heme oxygenase-1 mediates the anti-inflammatory effects of acute alcohol on IL-10 induction involving p38 MAPK activation in monocytes. *J Immunol*. (2006) 177:2592–600. doi: 10.4049/jimmunol.177.4.2592
53. Yang G, Nguyen X, Ou J, Rekulapelli P, Stevenson DK, Dennerly PA. Unique effects of zinc protoporphyrin on HO-1 induction and apoptosis. *Blood*. (2001) 97:1306–13. doi: 10.1182/blood.V97.5.1306
54. Pengal RA, Ganesan LP, Wei G, Fang H, Ostrowski MC, Tridandapani S. Lipopolysaccharide-induced production of interleukin-10 is promoted by the serine/threonine kinase Akt. *Mol Immunol*. (2006) 43:1557–64. doi: 10.1016/j.molimm.2005.09.022
55. Iyer SS, Ghaffari AA, Cheng. Lipopolysaccharide-mediated IL-10 transcriptional regulation requires sequential induction of type I IFNs and IL-27 in macrophages. *J Immunol*. (2010) 185:6599–607. doi: 10.4049/jimmunol.1002041
56. Makita N, Hizukuri Y, Yamashiro K, Murakawa M, Hayashi Y. IL-10 enhances the phenotype of M2 macrophages induced by IL-4 and confers the ability to increase eosinophil migration. *Int Immunol*. (2015) 27:131–41. doi: 10.1093/intimm/idx090

57. Piantadosi CA, Withers CM, Bartz RR, MacGarvey NC, Fu P, Sweeney TE, et al. Heme oxygenase-1 couples activation of mitochondrial biogenesis to anti-inflammatory cytokine expression. *J Biol Chem.* (2011) 286:16374–85. doi: 10.1074/jbc.M110.207738
58. Otterbein LE, Bach FH, Alam J, Soares M, Tao Lu H, Wysk M, et al. Carbon monoxide has anti-inflammatory effects involving the mitogen-activated protein kinase pathway. *Nat Med.* (2000) 6:422–8. doi: 10.1038/74680
59. Lee TS, Chau LY. Heme oxygenase-1 mediates the anti-inflammatory effect of interleukin-10 in mice. *Nat Med.* (2002) 8:240–6. doi: 10.1038/nm0302-240
60. Ricchetti GA, Williams LM, Foxwell BM. Heme oxygenase 1 expression induced by IL-10 requires STAT-3 and phosphoinositide-3 kinase and is inhibited by lipopolysaccharide. *J Leukoc Biol.* (2004) 76:719–26. doi: 10.1189/jlb.0104046
61. Alvarez-Maqueda M, El Bekay R, Alba G, Monteseirín J, Chacon P, Vega A, et al. 15-deoxy-delta 12,14-prostaglandin J2 induces heme oxygenase-1 gene expression in a reactive oxygen species-dependent manner in human lymphocytes. *J Biol Chem.* (2004) 279:21929–37. doi: 10.1074/jbc.M400492200
62. Ryter SW, Alam J, Choi AM. Heme oxygenase-1/carbon monoxide: from basic science to therapeutic applications. *Physiol Rev.* (2006) 86:583–650. doi: 10.1152/physrev.00011.2005
63. Zhang J, Ohta T, Maruyama A, Hosoya T, Nishikawa K, Maher JM, et al. BRG1 interacts with Nrf2 to selectively mediate HO-1 induction in response to oxidative stress. *Mol Cell Biol.* (2006) 26:7942–52. doi: 10.1128/MCB.00700-06
64. Roth I, Leroy V, Kwon HM, Martin PY, Feraille E, Hasler U, et al. Osmoprotective transcription factor NFAT5/TonEBP modulates nuclear factor-kappaB activity. *Mol Biol Cell.* (2010) 21:3459–74. doi: 10.1091/mbc.e10-02-0133
65. Yang B, Hodgkinson AD, Oates PJ, Kwon HM, Millward BA, Demaine AG. Elevated activity of transcription factor nuclear factor of activated T-cells 5 (NFAT5) and diabetic nephropathy. *Diabetes.* (2006) 55:1450–5. doi: 10.2337/db05-1260
66. Orozco LD, Kapturczak MH, Barajas B, Wang X, Weinstein MM, Wong J, et al. Heme oxygenase-1 expression in macrophages plays a beneficial role in atherosclerosis. *Circ Res.* (2007) 100:1703–11. doi: 10.1161/CIRCRESAHA.107.151720
67. Kobayashi H, Takeno M, Saito T, Takeda Y, Kirino Y, Noyori K, et al. Regulatory role of heme oxygenase 1 in inflammation of rheumatoid arthritis. *Arthritis Rheum.* (2006) 54:1132–42. doi: 10.1002/art.21754
68. Tsuchihashi S, Livhits M, Zhai Y, Busuttill RW, Araujo JA, Kupiec-Weglinski JW. Basal rather than induced heme oxygenase-1 levels are crucial in the antioxidant cytoprotection. *J Immunol.* (2006) 177:4749–57. doi: 10.4049/jimmunol.177.7.4749
69. Romanoski CE, Che N, Yin F, Mai N, Pouladar D, Civelek M, et al. Network for activation of human endothelial cells by oxidized phospholipids: a critical role of heme oxygenase 1. *Circ Res.* (2011) 109:E27–41. doi: 10.1161/CIRCRESAHA.111.241869
70. Alam J, Stewart D, Touchard C, Boinapally S, Choi AM, Cook JL. Nrf2, a Cap'n'Collar transcription factor, regulates induction of the heme oxygenase-1 gene. *J Biol Chem.* (1999) 274:26071–8.
71. Dinkova-Kostova AT, Holtzclaw WD, Cole RN, Itoh K, Wakabayashi N, Katoh Y, et al. Direct evidence that sulfhydryl groups of Keap1 are the sensors regulating induction of phase 2 enzymes that protect against carcinogens and oxidants. *Proc Natl Acad Sci U S A.* (2002) 99:11908–13. doi: 10.1073/pnas.172398899
72. Sun J, Hoshino H, Takaku K, Nakajima O, Muto A, Suzuki H, et al. Hemoprotein Bach1 regulates enhancer availability of heme oxygenase-1 gene. *EMBO J.* (2002) 21:5216–24. doi: 10.1093/emboj/cdf516

Conflict of Interest Statement: The authors declare that the research was conducted in the absence of any commercial or financial relationships that could be construed as a potential conflict of interest.

Copyright © 2019 Yoo, Lee, Ye, Lee, Kang, Jeong, Park, Lim, Lee-Kwon, Kwon and Choi. This is an open-access article distributed under the terms of the Creative Commons Attribution License (CC BY). The use, distribution or reproduction in other forums is permitted, provided the original author(s) and the copyright owner(s) are credited and that the original publication in this journal is cited, in accordance with accepted academic practice. No use, distribution or reproduction is permitted which does not comply with these terms.



Dendritic Cell-Derived TSLP Negatively Regulates HIF-1 α and IL-1 β During Dectin-1 Signaling

Matthew J. Elder^{1,2}, Steve J. Webster^{1,3}, Timothy J. Fitzmaurice¹, Aran S. D. Shaunak¹, Martin Steinmetz⁴, Ronnie Chee⁵, Ziad Mallat⁶, E. Suzanne Cohen⁷, David L. Williams⁸, J. S. Hill Gaston¹ and Jane C. Goodall^{1*}

¹ Department of Medicine, School of Clinical Medicine, Addenbrookes Hospital, University of Cambridge, Cambridge, United Kingdom, ² Early Oncology R&D Division, AstraZeneca, Cambridge, United Kingdom, ³ Department of Veterinary Medicine, University of Cambridge, Cambridge, United Kingdom, ⁴ Unit 970, INSERM, Paris Cardiovascular Research Center, Paris, France, ⁵ Department of Immunology, Royal Free Hospital, London, United Kingdom, ⁶ Division of Cardiovascular Medicine, Department of Medicine, University of Cambridge, Cambridge, United Kingdom, ⁷ Biopharmaceutical Research Division, AstraZeneca, Cambridge, United Kingdom, ⁸ Department of Surgery, Center for Inflammation, Infectious Disease and Immunity, James H. Quillen College of Medicine, East Tennessee State University, Johnson City, TN, United States

OPEN ACCESS

Edited by:

Catarina R. Almeida,
University of Aveiro, Portugal

Reviewed by:

Elisabetta Volpe,
Fondazione Santa Lucia (IRCCS), Italy
Kushagra Bansal,
Harvard Medical School,
United States

*Correspondence:

Jane C. Goodall
jcg23@medschl.cam.ac.uk

Specialty section:

This article was submitted to
Molecular Innate Immunity,
a section of the journal
Frontiers in Immunology

Received: 22 November 2018

Accepted: 10 April 2019

Published: 08 May 2019

Citation:

Elder MJ, Webster SJ, Fitzmaurice TJ,
Shaunak ASD, Steinmetz M, Chee R,
Mallat Z, Cohen ES, Williams DL,
Gaston JSH and Goodall JC (2019)
Dendritic Cell-Derived TSLP
Negatively Regulates HIF-1 α and
IL-1 β During Dectin-1 Signaling.
Front. Immunol. 10:921.
doi: 10.3389/fimmu.2019.00921

Thymic stromal lymphopoietin (TSLP) is a functionally pleiotropic cytokine important in immune regulation, and TSLP dysregulation is associated with numerous diseases. TSLP is produced by many cell types, but has predominantly been characterized as a secreted factor from epithelial cells which activates dendritic cells (DC) that subsequently prime T helper (T_H) 2 immunity. However, DC themselves make significant amounts of TSLP in response to microbial products, but the functional role of DC-derived TSLP remains unclear. We show that TSLPR signaling negatively regulates IL-1 β production during dectin-1 stimulation of human DC. This regulatory mechanism functions by dampening Syk phosphorylation and is mediated via NADPH oxidase-derived ROS, HIF-1 α and pro-IL-1 β expression. Considering the profound effect TSLPR signaling has on the metabolic status and the secretome of dectin-1 stimulated DC, these data suggest that autocrine TSLPR signaling could have a fundamental role in modulating immunological effector responses at sites removed from epithelial cell production of TSLP.

Keywords: TSLP, dectin-1, IL-1 β , hypoxia, ROS, HIF-1 α , Syk

INTRODUCTION

Thymic Stromal Lymphopoietin (TSLP) is a four-helix bundle cytokine belonging to the IL-2 family that was initially described as a lymphocyte growth factor (1). Since this initial report, it has been shown to be produced by a plethora of cell types (2–8). Functionally TSLP is pleiotropic; TSLP is described to have an important role in maintaining tolerance within the gut (9, 10) yet it is implicated in asthma (11) and in the skin in both the development of itch (12) and atopic inflammation (12–14). TSLP binds to its unique receptor, called the TSLP receptor (TSLPR) composed of a unique TSLPR chain and the IL-7 receptor alpha (15) which initiates JAK-STAT mediated activation of downstream target genes (16–18).

Dendritic cells (DC) are immunologically important TSLP responsive cells (19). DC activated with TSLP can induce naïve CD4⁺ T cell proliferation (20) and T helper (T_H) 2-cell differentiation (21) which requires the up-regulation of OX40L on the DC (22). DC can also produce TSLP in

response to pattern recognition receptor (PRR) engagement (3, 4, 8, 23). Therefore, DC are the only cell population known to both produce and respond to TSLP by altering their effector responses. However, the functional role of DC-derived TSLP remains unclear; this work addresses this issue.

Amongst PRRs, dectin-1 stimulation induces TSLP production by DC (8, 23). Dectin-1 recognizes exposed β -1,3 glucan residues on the cell surface of fungi and studies utilizing dectin-1 gene knockout ($^{-/-}$) mice emphasize the importance of this PRR to anti-fungal immunity (24). Activation of dectin-1 signaling induces immunological effector responses including phagocytosis (25), oxidative burst (26, 27) and the secretion of inflammatory cytokines including IL-1 β , IL-6, and IL-23 (27–32). IL-1 β production plays a critical role in the generation of protective anti-fungal immunity (33, 34). However, IL-1 β dysregulation is associated with numerous diseases including inflammatory bowel disease (IBD) and auto-inflammatory conditions such as the cryopyrin associated periodic syndromes (CAPS) (35, 36). Therefore, IL-1 β production is tightly regulated in DC, requiring two independent signals for its production. An initial priming signal (signal 1) is generated from ligation of PRRs, activating the inflammatory transcription factor NF- κ B required for the up-regulated transcription of pro-IL-1 β (36). A second activatory signal (signal 2) then causes inflammasome-mediated cleavage of pro-IL-1 β into its active form (26, 27, 30, 32, 36–39). Recent work has augmented the understanding of IL-1 β regulation, describing how changes to cellular metabolism after PRR stimulation regulate IL-1 β expression (40, 41).

We report here that autocrine TSLPR signaling in human DC negatively regulates IL-1 β production in response to dectin-1 stimulation. It likely does this through limiting a metabolic switch to glycolysis in DC which is required for IL-1 β expression.

RESULTS

Inhibition of TSLPR Signaling in mDC Modulates IL-1 β Production

DC secretion of TSLP can be readily induced following dectin-1 stimulation (4, 8, 23). We investigated the functional relevance of DC-derived TSLP by neutralizing TSLP signaling in human monocyte-derived dendritic cells (mDC) which had been stimulated with heat-killed *C. albicans* or β -glucan purified from either *S. cerevisiae* (SC glucan) or *C. albicans* (CA glucan). We blocked TSLP activity or TSLPR signaling using neutralizing antibodies, and evaluated IL-1 β , IL-6, IL-23, TSLP, and CCL22 secretion. Inhibition of either TSLP or TSLPR on mDC augmented the production of IL-1 β , IL-6, IL-23 (Figures 1A–C), and TSLPR inhibition augmented TSLP itself (Figure 1G) from mDC in response to dectin-1 stimulation. These effects were not observed using control antibodies. CCL22 is a known TSLP-responsive chemokine in epithelial cells (21), and as expected inhibition of TSLPR signaling also reduced DC CCL22 production in response to

dectin-1 stimulation (Figure 1H). Augmented IL-1 β , IL-6, and IL-23 were all dependent on signaling through dectin-1 via Syk (Supplemental Figures 1A–F). To ensure that this effect was not an artifact caused by antibody binding and subsequent mDC activation, we generated bone marrow-derived dendritic cells (BMDC) from wildtype TSLPR $^{+/+}$ and knockout TSLPR $^{-/-}$ BALB/c mice. In agreement with the results using TSLPR blocking antibodies, TSLPR $^{-/-}$ BMDC stimulated with either *C. albicans* or β -glucans produced more IL-1 β , IL-6, and IL-23 compared to TSLPR $^{+/+}$ BMDC (Figures 1D–F). Furthermore, inhibiting TSLPR signaling on human blood-derived CD1c $^{+}$ DC also increased IL-1 β secretion confirming that these findings were not an artifact of *in vitro* differentiation of monocytes (Figure 1I).

TSLPR Signaling Negatively Regulates IL-6 and IL-23 Secretion by Controlling IL-1 β

The importance of IL-1 β for generating effective anti-fungal immunity is well-established (31). Therefore, we wanted to determine whether the increase in IL-6 and IL-23 secretion from mDC was a direct effect of inhibiting TSLPR signaling on production of these cytokines or due to the effects of increased IL-1 β . We have showed that IL-1 β mRNA expression precedes that of IL-6 and IL-23p40 (Supplemental Figures 2A–D) and inhibition of IL-1 receptor signaling with IL-1 receptor antagonist (IL-1RA) significantly inhibits IL-6 and IL-23 secretion from SC glucan-stimulated mDC (Supplemental Figures 2E,F). However, to directly address this, we stimulated mDC with *C. albicans* or β -glucans and neutralized TSLPR signaling in the presence or absence of IL-1RA, or caspase-1 and caspase-8 inhibitors to prevent inflammasome-mediated processing of IL-1 β which our group has previously demonstrated (8). This showed that the increased IL-6 and IL-23 observed when TSLPR was blocked, was reduced in the presence of IL-1RA or caspase-1 and caspase-8 inhibitors (Figures 2A–F). Therefore, autocrine TSLPR signaling indirectly regulated IL-6 and IL-23 secretion by its effect on IL-1 β production.

Dectin-1-Induced TSLP Negatively Regulates Pro-IL-1 β and HIF-1 α

Recent work has described how LPS-treated macrophages and β -glucan-stimulated monocytes undergo a metabolic switch toward glycolysis and away from oxidative phosphorylation (40). This is a process which has many parallels with the Warburg effect observed in tumors. We observed that mDC culture media was more acidic when TSLPR signaling was neutralized during dectin-1 stimulation. Therefore, we measured lactate production to determine whether increased lactic acid production accounted for the pH change. Significantly higher concentrations of lactate were indeed detected in cell culture supernatants from mDC when TSLPR signaling was neutralized (Figure 3A) and from TSLPR $^{-/-}$ BMDC (Supplemental Figure 3A), suggesting that autocrine mDC-derived TSLP negatively regulates this metabolic shift to lactate production. Tannahill et al reported that this cellular metabolic switch was crucial for pro-IL-1 β expression via the induction

Abbreviations: TSLP, Thymic stromal lymphopoietin; mDC, monocyte-derived DC; BMDC, bone marrow-derived dendritic cell.

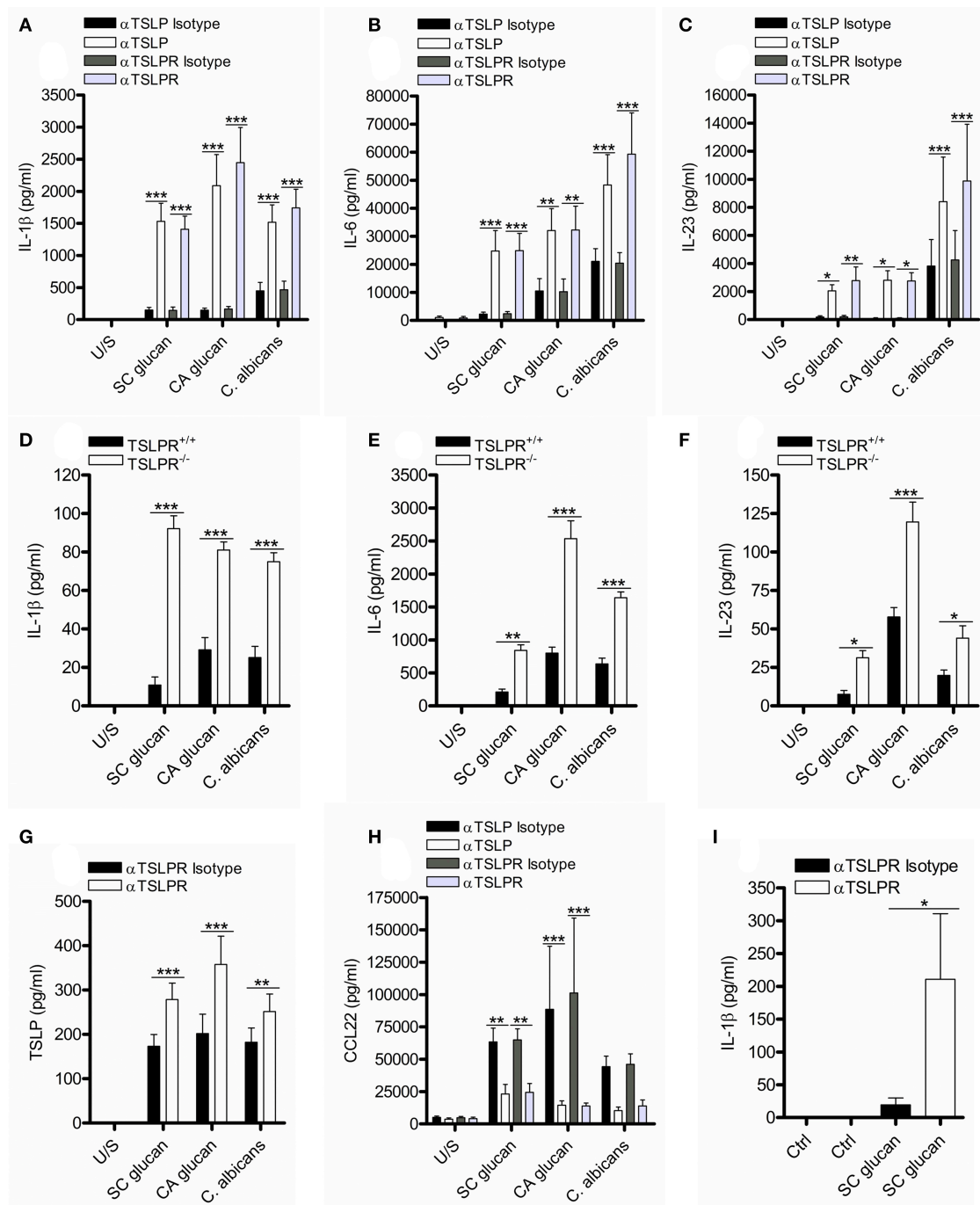
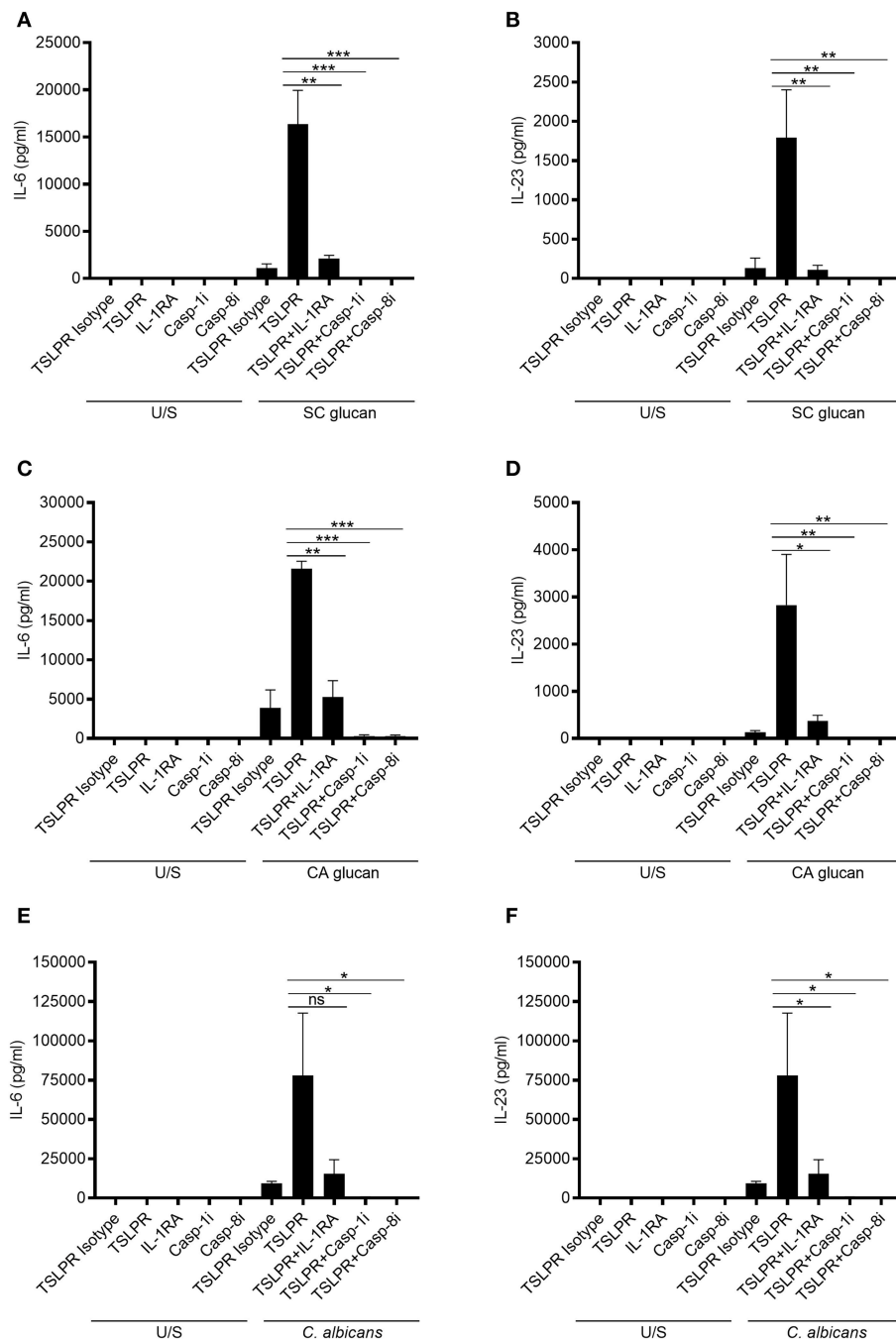


FIGURE 1 | Inhibition of TSLPR signaling in mDC modulates IL-1 β production. **(A–C,G,H)** Human mDC stimulated with SC glucan, CA glucan or heat killed *C. albicans* hyphae with anti-TSLP, anti-TSLPR or IgG isotype control antibodies for 24 h ($n = 14$ independent donors, presented as pooled data for SC glucan stimulated mDC), ($n = 6$ independent donors, presented as pooled data for CA glucan stimulated mDC) and ($n = 10$ independent donors, presented as pooled data for heat killed *C. albicans* hyphae stimulated mDC). **(D–F)** Wildtype TSLPR^{+/+} or TSLPR^{-/-} BMDC derived from BALB/c mice were stimulated with, SC glucan, CA glucan or *C. albicans* hyphae for 24 h ($n = 4$ independent animals from a representative experiment, presented as pooled data. Experiment was repeated four times). **(I)** Human ex vivo CD1c⁺ DC stimulated with SC glucan with anti-TSLPR or IgG isotype control antibodies for 24 h ($n = 3$ independent donors, presented as pooled data). IL-1 β , IL-6, IL-23, TSLP and CCL22 was measured in 24-h cell culture supernatants by ELISA. Cumulative data displayed as mean \pm SEM. Statistical analysis calculated using one-way ANOVA with Bonferroni post-tests (** $p = 0.001$, * $p = 0.01$, $p = 0.05$).



of the transcription factor, hypoxia-inducible factor 1- α (HIF-1 α), and in agreement with this report TSLP or TSLPR neutralization in mDC during dectin-1 signaling augmented both HIF-1 α and pro-IL-1 β protein expression (**Figures 3B–E**). An identical augmentation was observed in TSLPR^{-/-} BMDC

(**Supplemental Figure 3B**). The enhancement in HIF-1 α expression could not be explained by changes in gene expression since HIF-1 α mRNA expression was not significantly modulated by inhibition of TSLPR signaling. In contrast pro-IL-1 β mRNA expression was augmented in mDC when TSLPR activity was

neutralized (**Supplemental Figures 4A,B**). These effects were specific and not as a result of a general increase in expression of effector molecules downstream of dectin-1 signaling; for instance p38 mitogen-activated protein kinase (MAPK) activation (Thr 180/Tyr 182) was not modulated by TSLP or TSLPR neutralization (**Figures 3B,F**). It has previously been shown that chemicals which induce AMP-activated protein kinase (AMPK) activation can oppose the metabolic switch in DCs and macrophages which is induced by PRR stimulation (41). Accordingly, neutralization of TSLPR signaling reduced phosphorylation of Thr 172 on the catalytic subunit of AMPK, a key modification required for AMPK activation (**Figures 3B,G**). To determine whether the modulation of HIF-1 α expression and AMPK phosphorylation occurred as a result of the increased IL-1 β expression, IL-1 β activity was neutralized in combination with inhibition of TSLPR signaling. This showed that the modulation of AMPK activation by inhibition of TSLPR activity was dependent on IL-1 β signaling, but this did not apply to HIF-1 α expression (**Figures 4A–C**).

Dectin-1-Induced TSLP Limits IL-1 β , HIF-1 α Expression, Syk Phosphorylation and the Activation of NADPH Oxidase-Derived ROS

It has previously been shown that reactive oxygen species (ROS) are induced in macrophages during dectin-1 signaling and are important for IL-1 β production (26, 27). Chronic granulomatous disease (CGD) patients possess mutations in genes encoding proteins that form the nicotinamide adenine dinucleotide phosphate-oxidase (NADPH) complex; thus these patients are unable to generate NADPH oxidase-derived ROS (**Supplemental Figure 5**) and TSLP from mDC in response to dectin-1 agonists (23). mDC from CGD donors did not show induction of HIF-1 α and pro-IL-1 β in response to dectin-1 signaling, highlighting the critical role of ROS in the expression of HIF-1 α and pro-IL-1 β by DCs (**Figures 5A–D**). In contrast, induction of AMPK phosphorylation was unaffected by the absence of a functional NADPH oxidase (**Figures 5A,E**), indicating that AMPK activation has distinct signaling from that required for HIF-1 α expression. Given the important role of ROS in HIF-1 α protein expression, we investigated whether inhibition of TSLPR signaling in CGD patients modulated IL-1 β production. TSLPR neutralization during dectin-1 stimulation did not alter the minimal amount of IL-1 β secretion seen in CGD donors (**Figures 5F–H**). Our data suggest NADPH oxidase-derived ROS contributes to the enhancement of HIF-1 α and IL-1 β expression observed with the loss of TSLPR signaling.

Dectin-1-Induced TSLP Negatively Regulates Syk Activation

Dectin-1-mediated effector responses are controlled by the recruitment and activation of Syk (28), and we have previously shown that inhibition of Syk signaling in mDC stimulated with dectin-1 agonists substantially reduces TSLP and IL-1 β expression (8). Furthermore, inhibition of Syk activity in DCs

with the Syk inhibitor R406 reduced SC glucan-induced HIF-1 α and pro-IL-1 β expression (**Supplemental Figure 6A**). We hypothesized that TSLPR signaling may directly modulate Syk activation and therefore examined the phosphorylation status of critical Tyr residues in Syk which are associated with its activation and interaction with downstream signaling pathways. As expected, SC glucan-induced Syk phosphorylation (Tyr 525/526) was dectin-1 dependent (**Supplemental Figure 6B**). Neutralization of autocrine TSLPR signaling resulted in enhanced Syk phosphorylation at this residue (**Figures 6A–D**). Furthermore, analysis of the phosphorylation state of other Tyr residues associated with Syk activation was also enhanced (**Figures 6A,C**). These data suggest that autocrine mDC-derived TSLP limits Syk-mediated activation. This in turn may negatively regulate the metabolic shift to glycolysis, the production of HIF-1 α and hence expression of pro-IL-1 β .

DISCUSSION

We have previously demonstrated that human mDC and murine BMDC generate TSLP in response to *C. albicans* or β -glucans (8, 23). In this study, we showed that this TSLP acts in an mDC autocrine fashion to regulate IL-1 β , and hence IL-6 and IL-23 production. We propose that this increase in inflammatory cytokine expression which is seen when DC responses to TSLP are blocked is a result of enhanced HIF-1 α expression and a more marked glycolytic shift in the metabolism of the DC. Furthermore, we showed that TSLPR signaling dampens Syk phosphorylation likely acting to decrease HIF-1 α and pro-IL-1 β production.

TSLPR signaling negatively regulates IL-1 β production, which in turn modulates the expression of IL-6 and IL-23. It is well-established that IL-1 β production plays a critical role in the generation of protective anti-fungal immunity (31); however, IL-1 β dysregulation is associated with IBD and CAPS such as Muckle-Wells syndrome (35, 36). Given the importance of IL-1 β regulation, we speculate that DC-derived TSLP acts as an important molecular checkpoint to limit IL-1 β -mediated effector responses. Furthermore, the differentiation of naïve CD4⁺ T cells to T_H1- and T_H17-cells is important for protective anti-fungal immunity and the inflammatory cytokines IL-1 β , IL-6, and IL-23 are important in generating these T cell phenotypes (28, 31, 42–44). TSLPR^{−/−} mice have been shown to produce more IFN- γ in an experimental model of *Trypanosoma congolense* infection (45), more IFN- γ and IL-17 in an inducible model of colitis (46) compared to TSLPR^{+/+} mice and IL-1 β is crucial for the generation of inflammatory IFN- γ /IL-17 double producing T cells during *C. albicans* infection (31, 42). Given that autocrine TSLPR signaling negatively regulated IL-1 β production during *C. albicans* and β -glucan stimulation: TSLPR signaling might also function to regulate T_H1- and T_H17-cell differentiation.

Recent work has established that myeloid-derived cells stimulated with activators of PRRs switch from oxidative phosphorylation to aerobic glycolysis (40). Similarly, we observed that *C. albicans* and β -glucan stimulated mDC also induced HIF-1 α and increased the production of lactate. Furthermore, both

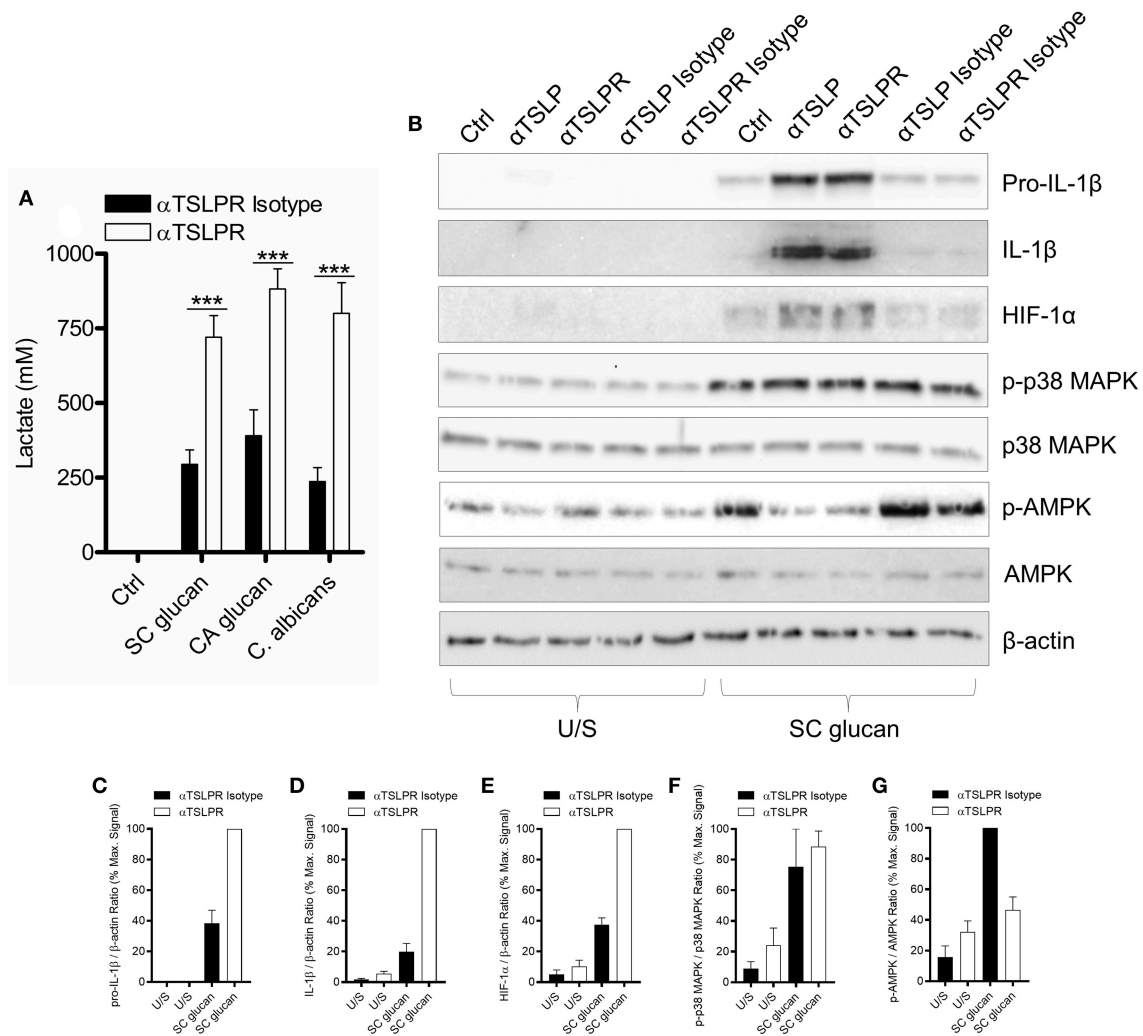


FIGURE 3 | Dectin-1-induced TSLP negatively regulates pro-IL-1 β and HIF-1 α . **(A)** Human mDC were stimulated with SC glucan, CA glucan or heat killed *C. albicans* hyphae with anti-TSLPR antibodies or IgG isotype control for 24 h ($n = 6$ independent donors, presented as pooled data). Lactate production was measured in cell-culture supernatants using colourimetric L-lactate detection kit. **(B)** Human mDC were stimulated SC glucan with either anti-TSLP, anti-TSLPR or IgG isotype control antibodies for 8 h ($n = 1$ representative donor presented, three separate experiments performed). Pro-IL-1 β , IL-1 β , HIF-1 α , phospho-p38 MAPK, p38 MAPK, phospho-AMPK, AMPK and β -actin were measured by immunoblot. **(C–G)** Densitometry of cumulative data was performed using Image Studio Lite software with pro-IL-1 β , IL-1 β and HIF-1 α normalized to β -actin and phospho-p38 MAPK and phospho-AMPK normalized to total p38 MAPK and AMPK respectively. Data is reported as percentage of maximal signal observed within each donor ($n = 3$ independent donors, presented as pooled data). Cumulative data displayed as mean \pm SEM. Statistical analysis calculated using one-way ANOVA with Bonferroni post-tests ($***p = 0.001$).

HIF-1 α and lactate production were further augmented when TSLPR signaling was neutralized on dectin-1-stimulated mDC. Given that Tannahill et al identified that HIF-1 α expression was crucial for pro-IL-1 β induction in LPS-treated macrophages (40) and β -glucan stimulated monocytes induce HIF-1 α expression required for this glycolytic switch (41): these data are compatible with the idea that autocrine TSLPR signaling controls pro-IL-1 β expression in mDC by regulating HIF-1 α . Further work will be required to confirm that HIF-1 α is a key factor that promotes increased IL-1 β expression when TSLPR signaling is inhibited.

IL-1 β has been shown to directly induce HIF-1 α expression (47–49), but despite an increase in IL-1 β when inhibiting TSLPR

signaling, our data provide evidence that the enhanced HIF-1 α expression induced by dectin-1 occurred independently of this cytokine. In contrast to the regulation of HIF-1 α , modulation of AMPK phosphorylation was shown to be dependent on the secretion of IL-1 β and to our knowledge this is the first report that suggests that IL-1 β may negatively regulate AMPK activation. Our data also highlighted the differences in the signaling requirements for ROS in AMPK activation and HIF-1 α expression. We showed that following dectin-1 stimulation, phosphorylation of the AMPK catalytic subunit was unaffected by the absence of ROS but in contrast, HIF-1 α expression was completely dependent on ROS production. Given that AMPK

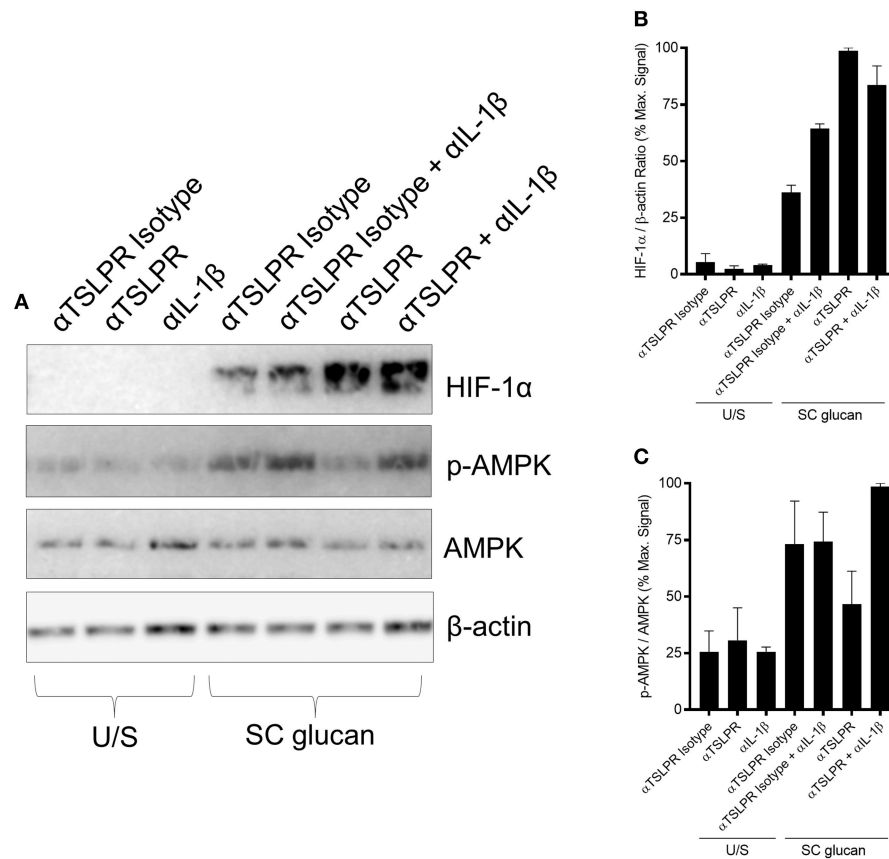


FIGURE 4 | Increased HIF-1 α expression is regulated by TSLPR inhibition and not IL-1 β secretion (A) Human mDC were stimulated with SC glucan with either anti-TSLPR or IgG isotype control antibodies for 8 h in the presence or absence of IL-1 β neutralization antibodies ($n = 1$ representative donor presented, three separate experiments performed). Pro-IL-1 β , IL-1 β , HIF-1 α , phospho-p38 MAPK, p38 MAPK, phospho-AMPK, AMPK and β -actin were measured by immunoblot. (B,C) Densitometry of cumulative data was performed using Image Studio Lite software with HIF-1 α normalized to β -actin and phospho-AMPK normalized to AMPK. Data is reported as percentage of maximal signal observed within each donor ($n = 3$ independent donors, presented as pooled data). Cumulative data displayed as mean \pm SEM.

activation has been shown to antagonize HIF-1 α expression, it may not be surprising that the signaling requirements for these factors have shared and distinct arms, highlighting the potential for independent regulation of these factors in the dectin-1 signaling pathway. Most importantly, the modulation of HIF-1 α and AMPK in the presence of TSLPR neutralizing antibodies, could be interpreted as complimentary responses, since enhanced HIF-1 α or a reduction in AMPK activation have been shown to contribute to a metabolic shift toward aerobic glycolysis and the increased production of inflammatory cytokines in monocytes and DC (41, 50).

Our data also showed that inhibition of TSLPR signaling on mDC enhanced Syk activation. We show that CGD patients cannot generate ROS, HIF-1 α or IL-1 β secretion; and unlike in healthy donors, mDC-derived from CGD patients do not augment HIF-1 α expression or IL-1 β secretion when autocrine TSLPR signaling is neutralized. These data are in agreement with published work showing that both Syk and ROS regulate IL-1 β cleavage during dectin-1 stimulation (27) and that ROS can activate HIF-1 α expression (51). Therefore, autocrine TSLP

production may directly regulate HIF-1 α and pro-IL-1 β , via Syk-mediated activation of NADPH oxidase-derived ROS: a regulatory mechanism that does not exist in CGD patients.

Therefore, dysregulation of TSLP production or TSLPR signaling might be a feature of diseases associated with Syk and IL-1 β overproduction. Opportunistic invasive fungal infections present serious clinical complications particularly in immunosuppressed individuals. Given the importance of IL-1 β to anti-fungal immunity these findings describe an important regulatory mechanism of IL-1 β that could ultimately lead to the development of approaches to boost resistance.

MATERIALS AND METHODS

Ethics Statement

Human blood was sourced from apheresis cones derived from healthy donors (HD) (Addenbrooke's Hospital, Cambridge) and age- and sex-matched CGD patients (Royal Free Hospital, London). Appropriate consent to use blood-derived cells for research was obtained. These studies were approved by the

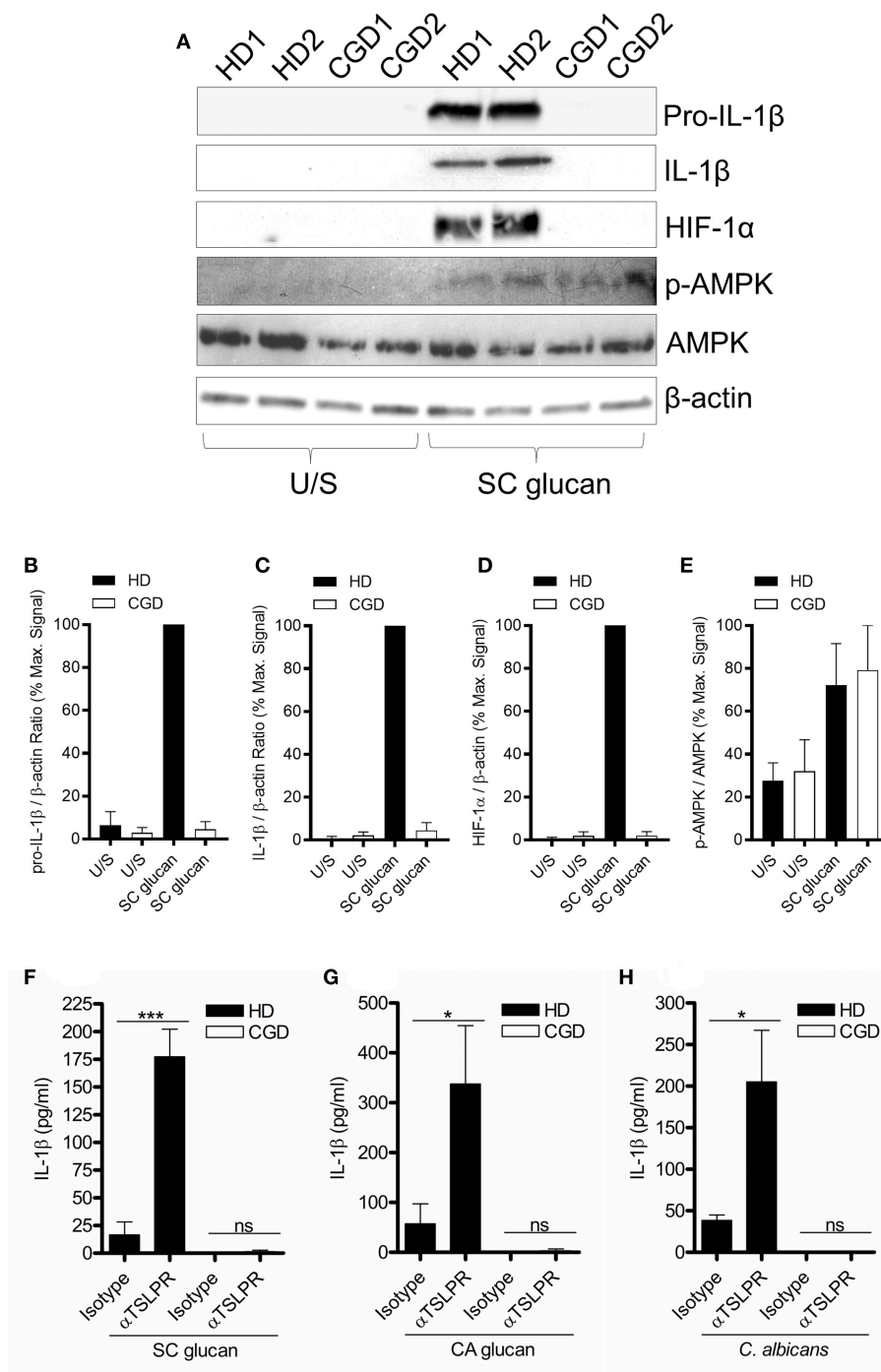


FIGURE 5 | Dectin-1-induced NADPH oxidase-derived ROS is required for augmented IL-1 β during TSLPR inhibition. **(A)** Human mDC derived from healthy donors (HD) or CGD patients were stimulated with SC glucan for 8 h ($n = 2$ representative donors presented, three separate experiments performed). Pro-IL-1 β , IL-1 β , HIF-1 α , phospho-AMPK, AMPK and β -actin were measured by immunoblot. **(B–E)** Densitometry of cumulative data was performed using Image Studio Lite software with pro-IL-1 β , IL-1 β and HIF-1 α normalized to β -actin and phospho-AMPK normalized to total AMPK. Data is reported as percentage of maximal signal observed within each donor ($n = 3$ independent donors, presented as pooled data). **(F–H)** Human mDC derived from HD or CGD patients were stimulated with SC glucan, CA glucan or heat killed *C. albicans* hyphae with anti-TSLPR or IgG isotype control antibodies for 24 h ($n = 3$ independent donors, presented as pooled data). IL-1 β was measured in 24-h cell culture supernatants by ELISA. Cumulative data displayed as mean \pm SEM. Statistical analysis calculated using one-way ANOVA with Bonferroni post-tests ($***p = 0.001$, $*p = 0.05$).

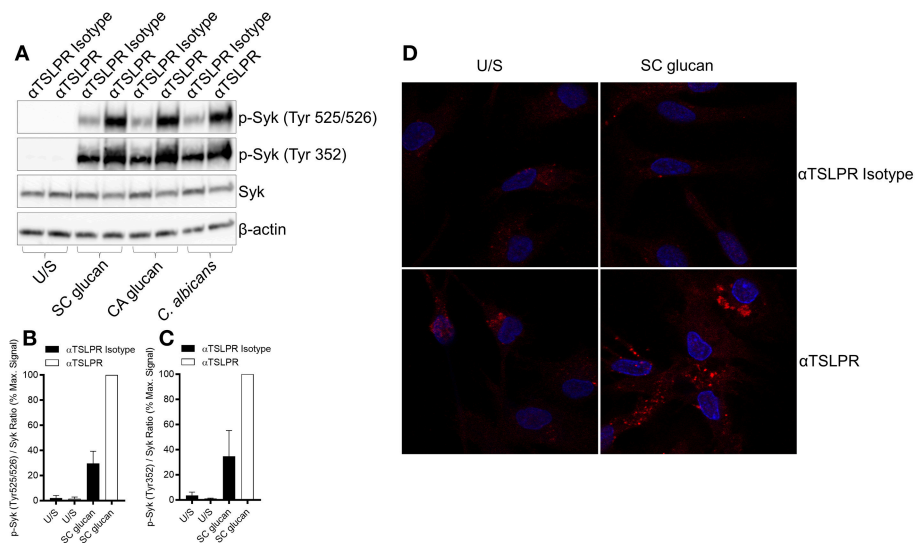


FIGURE 6 | Dectin-1-induced TSLP negatively regulates Syk activation. **(A–D)** Human mDC were stimulated with SC glucan with anti-TSLPR or IgG isotype control antibodies for 2 h ($n = 1$ representative donor presented, three separate experiments performed). **(B,C)** Densitometry of cumulative data was performed using Image Studio Lite software with phospho-Syk normalized to total Syk. Data is reported as percentage of maximal signal observed within each donor ($n = 3$ independent donors, presented as pooled data). Phospho-Syk measured by **(A)** immunoblot and **(D)** confocal microscopy (Red represents p-Syk and Blue represents nuclear DAPI staining).

Joint UCL/UCLH Committee for the Ethics of Human Research, project number 04/Q0501/119.

Cell Isolation and Generation of Dendritic Cells

Human monocyte-derived dendritic cells (mDC) were generated from CD14⁺ monocytes isolated from human PBMC by magnetic bead separation (Miltenyi) and were differentiated by culturing for 6-days in RPMI1640 (Lonza) 5% FCS (Biosera) supplemented with 20 ng/ml GM-CSF (Life Technologies) and 4 ng/ml IL-4 (BD Biosciences) as described previously (8). CGD donors were recruited at the Royal Free Hospital, London and age and sex matched to healthy donors recruited at the University of Cambridge, in accordance with ethical rules set out by each institution. Human CD1c⁺ DC were isolated from PBMC by magnetic bead separation (Miltenyi). Murine bone marrow-derived dendritic cells (BMDC) were generated by culturing cells isolated from bone marrow of wildtype (TSLPR^{+/+}) and TSLPR knockout (TSLPR^{-/-}) BALB/c mice for 7-days in RPMI1640 10% FCS supplemented with 5% X63 conditioned media and 10 ng/ml IL-4 (Peprotech).

Cell Stimulations

mDCs were stimulated with 50 μg/ml of either β-1,3 glucan (SC glucan) derived from *Saccharomyces cerevisiae* (*S. cerevisiae*) isolated by David. L. Williams, East Tennessee State University as previously described (52), β-1,3 glucan (CA glucan) derived from hyphal *Candida albicans* (*C. albicans*) isolated by David. L. Williams as previously described (53) or heat-killed hyphal *C. albicans* (MOI 2:1) gifted from John Trowsdale, University of Cambridge. *C. albicans* was grown in sabouraud dextrose broth

for 8 h at 37°C to an optical density of 0.2. *C. albicans* was killed by heating for 1 h at 70°C.

Reagents

10 μg/ml sheep anti-TSLP blocking antibody (R&D Systems), 10 μg/ml sheep IgG isotype control (R&D Systems), 10 μg/ml goat anti-TSLPR blocking antibody (R&D Systems), 10 μg/ml goat IgG isotype control (R&D Systems), 2 μg/ml IL-1β blocking antibody (R&D Systems), 10 μg/ml mouse IgG_{2B} dectin-1 blocking antibody (clone-259931 R&D Systems), 10 μg/ml mouse IgG_{2B} isotype control (clone-20116 R&D Systems), 1 μM Syk inhibitor, R406 (Selleckchem), 1 μg/ml IL-1 receptor antagonist (IL-1RA) (R&D Systems), 50 μM caspase-1 inhibitor (Z-YVAD-FMK) (Calbiochem), 50 μM caspase-8 inhibitor (Z-IE(OMe)TD(OMe)-FMK) (Calbiochem). Where inhibitors, blocking antibodies and modifiers were used, mDCs were pre-treated 1 h prior to cell stimulation. Repeated experiments were performed on independent donors unless otherwise stated.

Cytokine Production

IL-1β, IL-6, IL-23 (eBioscience), TSLP, and CCL22 (R&D) were measured in 24 h mDC, CD1c⁺ DC or BMDC culture supernatants by ELISA according to manufacturer's protocols.

Quantitative Real-Time PCR

mDC were stimulated for indicated time period and IL-1β, HIF-1α, IL-6, IL-23p19 and IL-23p40 mRNA expression was measured by quantitative real-time PCR from isolated RNA (Norgen) using TaqMan Gene Expression Assays (Applied Biosystems). Gene expression was normalized to HPRT and calculated as relative expression (2-dCT).

Immunoblot

mDC were stimulated for indicated time period and protein lysates were generated, quantified by Bradford assay (Thermo) and resolved using SDS-PAGE. IL-1 β (R&D, AB-201-AB), HIF-1 α (Novus, NB100-449), phospho-AMPK (Thr 172) (Cell Signaling, 2535), AMPK (Cell Signaling, 5831), phospho-Syk (Tyr 525/526) (Cell Signaling, 2710), phospho-Syk (Tyr 352) (Cell Signaling, 2701), Syk (Cell Signaling, 13198), phospho-p38 MAPK (Thr 180/ Tyr 182) (Cell Signaling, 4511), p38 MAPK (Cell Signaling, 8690) and β -actin (Abcam, 8226) protein expression were measured by immunoblot, by incubation with indicated primary antibodies followed by incubation with HRP-conjugated secondary antibodies, ECL detection (PerkinElmer) and visualized using GBox (Syngene). Densitometry of cumulative data was performed using Image Studio Lite software. Pro-IL-1 β , IL-1 β and HIF-1 α expression was normalized to β -actin and phospho-p38 MAPK, phospho-AMPK and phospho-Syk was normalized to total p38 MAPK, AMPK and Syk respectively. Cumulative data is reported as percentage of maximal signal observed within each donor.

Quantification of Reactive Oxygen Species (ROS) Production

mDC derived from HD or CGD patients were stimulated with SC glucan and ROS production was measured by fluorescence of the luminol-based chemiluminescent probe L-012 (WAKO) over 30 min using a luminometer (Centro LB960, Berthold).

Confocal Microscopy

mDC were stimulated for indicated time period on poly-D-lysine coated coverslips (BD), washed with cold PBS and stained for phospho-Syk (Tyr 525/526) (Cell Signaling, 2710). Coverslips were then mounted on slides with DAPI fluoromount G (Southern Biotech) and analyzed by confocal microscopy (Leica SP5).

Lactate Detection

mDC were stimulated and lactate production was measured instantly from 24 h cell-culture supernatants using colourimetric L-lactate detection kit (Abcam) according to manufacturer's protocols.

REFERENCES

1. Friend SL, Hosier S, Nelson A, Foxworthe D, Williams DE, Farr A. A thymic stromal cell line supports *in vitro* development of surface IgM+ B cells and produces a novel growth factor affecting B and T lineage cells. *Exp Hematol.* (1994) 22:321–8.
2. Lee HC, Ziegler SF. Inducible expression of the proallergic cytokine thymic stromal lymphopoietin in airway epithelial cells is controlled by NF κ B. *Proc Natl Acad Sci USA.* (2007) 104:914–9. doi: 10.1073/pnas.0607305104
3. Goodall JC, Wu C, Zhang Y, McNeill L, Ellis L, Saudek V, et al. Endoplasmic reticulum stress-induced transcription factor, CHOP, is crucial for dendritic cell IL-23 expression. *Proc Natl Acad Sci USA.* (2010) 107:17698–703. doi: 10.1073/pnas.1011736107
4. Kashyap M, Rochman Y, Spolski R, Samsel L, Leonard WJ. Thymic stromal lymphopoietin is produced by dendritic cells. *J Immunol.* (2011) 187:1207–11. doi: 10.4049/jimmunol.1100355
5. Urata Y, Osuga Y, Izumi G, Takamura M, Koga K, Nagai M, et al. Interleukin-1 β stimulates the secretion of thymic stromal lymphopoietin (TSLP) from endometrioma stromal cells: possible involvement of TSLP in endometriosis. *Hum Reprod.* (2012) 27:3028–35. doi: 10.1093/humrep/des291

Data Analysis

Data were analyzed using GraphPad Prism statistical package. Cumulative data are displayed as mean \pm SEM. Statistical analysis using either t test (*p*-values stated in figures legends) or one-way ANOVAs with Bonferroni post-tests ns = not significant, **p* < 0.05, ***p* < 0.01, ****p* < 0.001.

ETHICS STATEMENT

Human blood was sourced from apheresis cones derived from healthy donors (Addenbrooke's Hospital, Cambridge) and age and sex-matched CGD patients (Royal Free Hospital, London). Appropriate consent to use blood-derived cells for research was obtained. Ethics Reference Number: 04/Q0501/119.

AUTHOR CONTRIBUTIONS

ME designed, performed and analyzed all experimental data and drafted the manuscript. SW, ZM, EC, JSG, and JCG were key to experimental design, data interpretation, and reviewed manuscript. TF, AS, and MS performed and analyzed experimental data. RC facilitated access to patient blood and aided data interpretation and reviewed manuscript. DW facilitated access to β -glucan agonists and aided experimental design, data interpretation, and reviewed manuscript.

FUNDING

This research was supported by Arthritis Research UK 19962 to JSG and Arthritis Research UK RG61798 to JCG and in part, by NIH R01GM53522, R01GM119197, and R01GM083016 to DW and NIH C06RR0306551 to ES.

ACKNOWLEDGMENTS

We would like to thank Sarita Workman and Professor John Trowsdale for providing us with key reagents; Lou Ellis and Sarah Gibbs for some of the sample processing and Sam Strickson for some of the data analysis.

SUPPLEMENTARY MATERIAL

The Supplementary Material for this article can be found online at: <https://www.frontiersin.org/articles/10.3389/fimmu.2019.00921/full#supplementary-material>

6. Zhang Y, Zhou X, Zhou B. DC-derived TSLP promotes Th2 polarization in LPS-primed allergic airway inflammation. *Eur J Immunol.* (2012) 42:1735–43. doi: 10.1002/eji.201142123
7. Dewas C, Chen X, Honda T, Junttila I, Linton J, Udey MC, et al. TSLP expression: analysis with a ZsGreen TSLP reporter mouse. *J Immunol.* (2015) 194:1372–80. doi: 10.4049/jimmunol.1400519
8. Elder MJ, Webster SJ, Williams DL, Gaston JS, Goodall JC. TSLP production by dendritic cells is modulated by IL-1 β and components of the endoplasmic reticulum stress response. *Eur J Immunol.* (2016) 46:455–63. doi: 10.1002/eji.201545537
9. Iliev ID, Spadoni I, Mileti E, Matteoli G, Sonzogni A, Sampietro GM, et al. Human intestinal epithelial cells promote the differentiation of tolerogenic dendritic cells. *Gut.* (2009) 58:1481–9. doi: 10.1136/gut.2008.175166
10. Taylor BC, Zaph C, Troy AE, Du Y, Guild KJ, Comeau MR, et al. TSLP regulates intestinal immunity and inflammation in mouse models of helminth infection and colitis. *J Exp Med.* (2009) 206:655–67. doi: 10.1084/jem.20081499
11. Corren J, Parnes JR, Wang L, Mo M, Roseti SL, Griffiths JM, et al. Tezepelumab in adults with uncontrolled asthma. *N Engl J Med.* (2017) 377:936–46. doi: 10.1056/NEJMoa1704064
12. Wilson SR, The L, Batia LM, Beattie K, Katibah GE, McClain SP, et al. The epithelial cell-derived atopic dermatitis cytokine TSLP activates neurons to induce itch. *Cell.* (2013) 155:285–95. doi: 10.1016/j.cell.2013.08.057
13. Zhou B, Comeau MR, De Smedt T, Liggett HD, Dahl ME, Lewis DB, et al. Thymic stromal lymphopoietin as a key initiator of allergic airway inflammation in mice. *Nat Immunol.* (2005) 6:1047–53. doi: 10.1038/ni1247
14. Volpe E, Pattarini L, Martinez-Cingolani C, Meller S, Donnadiu MH, Bogiatzi SI, et al. Thymic stromal lymphopoietin links keratinocytes and dendritic cell-derived IL-23 in patients with psoriasis. *J Allergy Clin Immunol.* (2014) 134:373–81. doi: 10.1016/j.jaci.2014.04.022
15. Park LS, Martin U, Garka K, Gliniak B, Di Santo JP, Muller W, et al. Cloning of the murine thymic stromal lymphopoietin (TSLP) receptor: formation of a functional heteromeric complex requires interleukin 7 receptor. *J Exp Med.* (2000) 192:659–70. doi: 10.1084/jem.192.5.659
16. Arima K, Watanabe N, Hanabuchi S, Chang M, Sun SC, Liu YJ. Distinct signal codes generate dendritic cell functional plasticity. *Sci Signal.* (2010) 3:ra4. doi: 10.1126/scisignal.2000567
17. Rochman Y, Kashyap M, Robinson GW, Sakamoto K, Gomez-Rodriguez J, Wagner KU, et al. Thymic stromal lymphopoietin-mediated STAT5 phosphorylation via kinases JAK1 and JAK2 reveals a key difference from IL-7-induced signaling. *Proc Natl Acad Sci USA.* (2010) 107:19455–60. doi: 10.1073/pnas.1008271107
18. Bell BD, Kitajima M, Larson RP, Stoklasek TA, Dang K, Sakamoto K, et al. The transcription factor STAT5 is critical in dendritic cells for the development of TH2 but not TH1 responses. *Nat Immunol.* (2013) 14:364–71. doi: 10.1038/ni.2541
19. Ziegler SE, Artis D. Sensing the outside world: TSLP regulates barrier immunity. *Nat Immunol.* (2010) 11:289–93. doi: 10.1038/ni.1852
20. Watanabe N, Hanabuchi S, Soumelis V, Yuan W, Ho S, de Waal Malefyt R, et al. Human thymic stromal lymphopoietin promotes dendritic cell-mediated CD4⁺ T cell homeostatic expansion. *Nat Immunol.* (2004) 5:426–34. doi: 10.1038/ni1048
21. Soumelis V, Reche PA, Kanzler H, Yuan W, Edward G, Homey B, et al. Human epithelial cells trigger dendritic cell mediated allergic inflammation by producing TSLP. *Nat Immunol.* (2002) 3:673–80. doi: 10.1038/ni805
22. Ito T, Wang YH, Duramad O, Hori T, Delespesse GJ, Watanabe N, et al. TSLP-activated dendritic cells induce an inflammatory T helper type 2 cell response through OX40 ligand. *J Exp Med.* (2005) 202:1213–23. doi: 10.1084/jem.20051135
23. Elder MJ, Webster SJ, Chee R, Williams DL, Hill Gaston JS, Goodall JC. Beta-glucan size controls dectin-1-mediated immune responses in human dendritic cells by regulating IL-1 β production. *Front Immunol.* (2017) 8:791. doi: 10.3389/fimmu.2017.00791
24. Taylor PR, Tsoni SV, Willment JA, Dennehy KM, Rosas M, Findon H, et al. Dectin-1 is required for beta-glucan recognition and control of fungal infection. *Nat Immunol.* (2007) 8:31–8. doi: 10.1038/ni1408
25. Brown GD, Taylor PR, Reid DM, Willment JA, Williams DL, Martinez-Pomares L, et al. Dectin-1 is a major beta-glucan receptor on macrophages. *J Exp Med.* (2002) 196:407–12. doi: 10.1084/jem.20020470
26. Underhill DM, Rossnagle E, Lowell CA, Simmons RM. Dectin-1 activates Syk tyrosine kinase in a dynamic subset of macrophages for reactive oxygen production. *Blood.* (2005) 106:2543–50. doi: 10.1182/blood-2005-03-1239
27. Gross O, Poeck H, Bscheidt M, Dostert C, Hanneschlagger N, Endres S, et al. Syk kinase signalling couples to the Nlrp3 inflammasome for anti-fungal host defence. *Nature.* (2009) 459:433–6. doi: 10.1038/nature07965
28. Goodridge HS, Wolf AJ, Underhill DM. Beta-glucan recognition by the innate immune system. *Immunol Rev.* (2009) 230:38–50. doi: 10.1111/j.1600-065X.2009.00793.x
29. Hise AG, Tomalka J, Ganesan S, Patel K, Hall BA, Brown GD, et al. An essential role for the NLRP3 inflammasome in host defense against the human fungal pathogen *Candida albicans*. *Cell Host Microbe.* (2009) 5:487–97. doi: 10.1016/j.chom.2009.05.002
30. Gringhuis SI, Kaptein TM, Wevers BA, Theelen B, van der Vlist M, Boekhout T, et al. Dectin-1 is an extracellular pathogen sensor for the induction and processing of IL-1 β via a noncanonical caspase-8 inflammasome. *Nat Immunol.* (2012) 13:246–54. doi: 10.1038/ni.2222
31. Zielinski CE, Mele F, Aschenbrenner D, Jarrossay D, Ronchi F, Gattorno M, et al. Pathogen-induced human TH17 cells produce IFN- γ or IL-10 and are regulated by IL-1 β . *Nature.* (2012) 484:514–8. doi: 10.1038/nature10957
32. Ganesan S, Rathinam VA, Bossaller L, Army K, Kaiser WJ, Mocarski ES, et al. Caspase-8 modulates Dectin-1 and complement receptor 3-driven IL-1 β production in response to beta-glucans and the fungal pathogen, *Candida albicans*. *J Immunol.* (2014) 193:2519–30. doi: 10.4049/jimmunol.1400276
33. Van't Wout JW, Van der Meer JW, Barza M, Dinarello CA. Protection of neutropenic mice from lethal *Candida albicans* infection by recombinant interleukin 1. *Eur J Immunol.* (1988) 18:1143–6.
34. Vonk AG, Netea MG, van Krieken JH, Iwakura Y, van der Meer JW, Kullberg BJ. Endogenous interleukin (IL)-1 α and IL-1 β are crucial for host defense against disseminated candidiasis. *J Infect Dis.* (2006) 193:1419–26. doi: 10.1086/503363
35. Kuemmerle-Deschner JB, Wittkowski H, Tyrrell PN, Koetter I, Lohse P, Ummerhofer K, et al. Treatment of Muckle-Wells syndrome: analysis of two IL-1-blocking regimens. *Arthritis Res Ther.* (2013) 15:R64. doi: 10.1186/ar4237
36. Latz E, Xiao TS, Stutz A. Activation and regulation of the inflammasomes. *Nat Rev Immunol.* (2013) 13:397–411. doi: 10.1038/nri3452
37. Mariathasan S, Weiss DS, Newton K, McBride J, O'Rourke K, Roose-Girma M, et al. Cryopyrin activates the inflammasome in response to toxins and ATP. *Nature.* (2006) 440:228–32. doi: 10.1038/nature04515
38. Hornung V, Bauernfeind F, Halle A, Samstad EO, Kono H, Rock KL, et al. Silica crystals and aluminum salts activate the NALP3 inflammasome through phagosomal destabilization. *Nat Immunol.* (2008) 9:847–56. doi: 10.1038/ni.1631
39. Munoz-Planillo R, Kuffa P, Martinez-Colon G, Smith BL, Rajendiran TM, Nunez G. K(+) efflux is the common trigger of NLRP3 inflammasome activation by bacterial toxins and particulate matter. *Immunity.* (2013) 38:1142–53. doi: 10.1016/j.immuni.2013.05.016
40. Tannahill GM, Curtis AM, Adamik J, Palsson-McDermott EM, McGettrick AF, Goel G, et al. Succinate is an inflammatory signal that induces IL-1 β through HIF-1 α . *Nature.* (2013) 496:238–42. doi: 10.1038/nature11986
41. Cheng SC, Quintin J, Cramer RA, Shephardson KM, Saeed S, Kumar V, et al. mTOR- and HIF-1 α -mediated aerobic glycolysis as metabolic basis for trained immunity. *Science.* (2014) 345:1250684. doi: 10.1126/science.1250684
42. van de Veerdonk FL, Joosten LA, Shaw PJ, Smeekens SP, Malireddi RK, van der Meer JW, et al. The inflammasome drives protective Th1 and Th17 cellular responses in disseminated candidiasis. *Eur J Immunol.* (2011) 41:2260–8. doi: 10.1002/eji.201041226
43. Lemoine S, Jaron B, Tabka S, Ettreiki C, Deriaud E, Zhivaki D, et al. Dectin-1 activation unlocks IL12A expression and reveals the TH1 potency of neonatal dendritic cells. *J Allergy Clin Immunol.* (2015) 136:1355–68 e1315. doi: 10.1016/j.jaci.2015.02.030
44. Li J, Leyva-Castillo JM, Hener P, Eisenmann A, Zafouri S, Jonca N, et al. Counterregulation between thymic stromal lymphopoietin and IL-23-driven immune axes shapes skin inflammation in mice with

- epidermal barrier defects. *J Allergy Clin Immunol.* (2016) 138:150–61 e113. doi: 10.1016/j.jaci.2016.01.013
45. Onyilagha C, Singh R, Gounni AS, Uzonna JE. Thymic stromal lymphopoietin is critical for regulation of proinflammatory cytokine response and resistance to experimental trypanosoma congolense infection. *Front Immunol.* (2017) 8:803. doi: 10.3389/fimmu.2017.00803
 46. Spadoni I, Iliev ID, Rossi G, Rescigno M. Dendritic cells produce TSLP that limits the differentiation of Th17 cells, fosters Treg development, and protects against colitis. *Mucosal Immunol.* (2012) 5:184–93. doi: 10.1038/mi.2011.64
 47. Hellwig-Burgel T, Rutkowski K, Metzen E, Fandrey J, Jelkmann W. Interleukin-1beta and tumor necrosis factor-alpha stimulate DNA binding of hypoxia-inducible factor-1. *Blood.* (1999) 94: 1561–7.
 48. Thornton RD, Lane P, Borghaei RC, Pease EA, Caro J, Mochan E. Interleukin 1 induces hypoxia-inducible factor 1 in human gingival and synovial fibroblasts. *Biochem J.* (2000) 350 Pt 1:307–12. doi: 10.1042/bj3500307
 49. Jung YJ, Isaacs JS, Lee S, Trepel J, Neckers L. IL-1beta-mediated up-regulation of HIF-1alpha via an NFkappaB/COX-2 pathway identifies HIF-1 as a critical link between inflammation and oncogenesis. *FASEB J.* (2003) 17:2115–7. doi: 10.1096/fj.03-0329fje
 50. Krawczyk CM, Holowka T, Sun J, Blagih J, Amiel E, DeBerardinis RJ, et al. Toll-like receptor-induced changes in glycolytic metabolism regulate dendritic cell activation. *Blood.* (2010) 115:4742–9. doi: 10.1182/blood-2009-10-249540
 51. Qutub AA, Popel AS. Reactive oxygen species regulate hypoxia-inducible factor 1alpha differentially in cancer and ischemia. *Mol Cell Biol.* (2008) 28:5106–19. doi: 10.1128/MCB.00060-08
 52. Williams DL, McNamee RB, Jones EL, Pretus HA, Ensley HE, Browder IW, et al. A method for the solubilization of a (1→3)-beta-D-glucan isolated from *Saccharomyces cerevisiae*. *Carbohydr Res.* (1991) 219:203–13. doi: 10.1016/0008-6215(91)89052-H
 53. Lowman DW, Greene RR, Bearden DW, Kruppa MD, Pottier M, Monteiro MA, et al. Novel structural features in *Candida albicans* hyphal glucan provide a basis for differential innate immune recognition of hyphae versus yeast. *J Biol Chem.* (2014) 289:3432–43. doi: 10.1074/jbc.M113.529131

Conflict of Interest Statement: ME and EC are employed by AstraZeneca.

The remaining authors declare that the research was conducted in the absence of any commercial or financial relationships that could be construed as a potential conflict of interest.

Copyright © 2019 Elder, Webster, Fitzmaurice, Shaunak, Steinmetz, Chee, Mallat, Cohen, Williams, Gaston and Goodall. This is an open-access article distributed under the terms of the Creative Commons Attribution License (CC BY). The use, distribution or reproduction in other forums is permitted, provided the original author(s) and the copyright owner(s) are credited and that the original publication in this journal is cited, in accordance with accepted academic practice. No use, distribution or reproduction is permitted which does not comply with these terms.



Regulation of Innate Immune Responses by Platelets

Lucas Secchim Ribeiro^{1*}, Laura Migliari Branco² and Bernardo S. Franklin¹

¹ Institute of Innate Immunity, University Hospitals, University of Bonn, Bonn, Germany, ² Centro de Terapia Celular e Molecular (CTC-Mol), Universidade Federal de São Paulo, São Paulo, Brazil

The role of platelets has been extensively studied in the context of coagulation and vascular integrity. Their hemostatic imbalance can lead to known conditions as atherosclerotic plaques, thrombosis, and ischemia. Nevertheless, the knowledge regarding the regulation of different cell types by platelets has been growing exponentially in the past years. Among these biological systems, the innate immune response is remarkably affected by the crosstalk with platelets. This interaction can come from the formation of platelet-leukocyte aggregates, signaling by direct contact between membrane surface molecules or by the stimulation of immune cells by soluble factors and active microparticles secreted by platelets. These ubiquitous blood components are able to sense and react to danger signals, guiding leukocytes to an injury site and providing a scaffold for the formation of extracellular traps for efficient microbial killing and clearance. Using several different mechanisms, platelets have an important task as they regulate the release of different cytokines and chemokines upon sterile or infectious damage, the expression of cell markers and regulation of cell death and survival. Therefore, platelets are more than clotting agents, but critical players within the fine inflammatory equilibrium for the host. In this review, we present pointers to a better understanding about how platelets control and modulate innate immune cells, as well as a summary of the outcome of this interaction, providing an important step for therapeutic opportunities and guidance for future research on infectious and autoimmune diseases.

Keywords: innate immunity, platelets, inflammation, leukocyte migration, cytokine production, cell survival

INTRODUCTION

Platelets are small disc-shaped cells derived from the fragmentation of megakaryocytes (MKs), in a process regulated by the binding of thrombopoietin (TPO) to its receptor (1–3). The human body contains around 750 billion circulating platelets and it is able to generate 200 billion new cells per day from its precursors in the bone marrow (4, 5) and in the lungs, as recently described (6). These cells stay in circulation for up to 10 days and they are later captured in the liver and in the spleen for degradation. As they grow senile, platelets lose their membrane sialic acid residues and reduce the TPO incorporation, an indication for their clearance. The decay is sensed by Ashwell-Morell receptors and, in a JAK2/STAT3-dependent mechanism, stimulate hepatocytes for the production of TPO, in order to command the generation of new platelets (7, 8). Since they are basically organized pieces of cytoplasm, platelets carry over several MK-derived molecules and factors that can be released upon activation. They do not have a nucleus, but are rich in mitochondrial DNA and RNA, the latest being useful for *de novo* protein synthesis (9–13). Small molecules, nucleic acids, lipid mediators and proteins can be stored in different types of organelles: alpha-granules, dense

OPEN ACCESS

Edited by:

Catarina R. Almeida,
University of Aveiro, Portugal

Reviewed by:

Angelo A. Manfredi,
Vita-Salute San Raffaele
University, Italy
Raymond B. Birge,
Rutgers University, The State
University of New Jersey,
United States

*Correspondence:

Lucas Secchim Ribeiro
ribeiro@uni-bonn.de

Specialty section:

This article was submitted to
Molecular Innate Immunity,
a section of the journal
Frontiers in Immunology

Received: 15 March 2019

Accepted: 23 May 2019

Published: 11 June 2019

Citation:

Ribeiro LS, Migliari Branco L and
Franklin BS (2019) Regulation of
Innate Immune Responses by
Platelets. *Front. Immunol.* 10:1320.
doi: 10.3389/fimmu.2019.01320

granules and lysosomal vesicles (14–16). Once activated, platelets undergo drastic shape changes and can release these factors to the extracellular compartment in their soluble forms or enclosed within bioactive microvesicles (17–19). Most of these secreted components and the membrane-bound proteins present in the vesicles have an important role in the control of the immune system. Given the ubiquitous nature of this featured cell type and the growing interest in its part in the defense of the organism (20, 21), here we present a brief summary of some of the effects that platelets can exert over innate immune cells, especially neutrophils, monocytes and macrophages.

PLATELET ROLES IN IMMUNE CELL MIGRATION, PHAGOCYTOSIS AND PATHOGEN CLEARANCE

Besides their known functions in hemostasis, platelets can also play an important role in the body defense against invading pathogens. They have a plethora of membrane receptors able to detect pathogen- and danger-associated molecular patterns (PAMPs and DAMPs), such as Toll-like receptors (TLRs) (22–26). Hence, platelets represent a prompt source of immune mediators, secreting several factors that act both on the invading pathogen or on surrounding cells (27, 28) (**Figure 1**).

Beyond the active function as immune cells, platelets guide leukocytes to injury site, enhancing and facilitating their immune functions. In the liver, platelets transiently scan Kupffer cells through interactions between the von Willebrand factor (VWF) and its receptor on platelets (glycoprotein Ib alpha chain gpIbA, also known as CD42b). Upon signs of infection, platelets are triggered by the Kupffer cells via the integrin GPIIb (CD41) to promote stronger adhesion, and to enclose microbes, facilitating their clearance. Mice with inactive platelet receptors display increased inflammation markers and higher mortality upon infection (46). In the blood, platelets contribute to microbial clearance and priming of adaptive responses by redirecting blood-borne bacteria to splenic dendritic cells (DCs) in a manner dependent on GPIb and complement C3 (47).

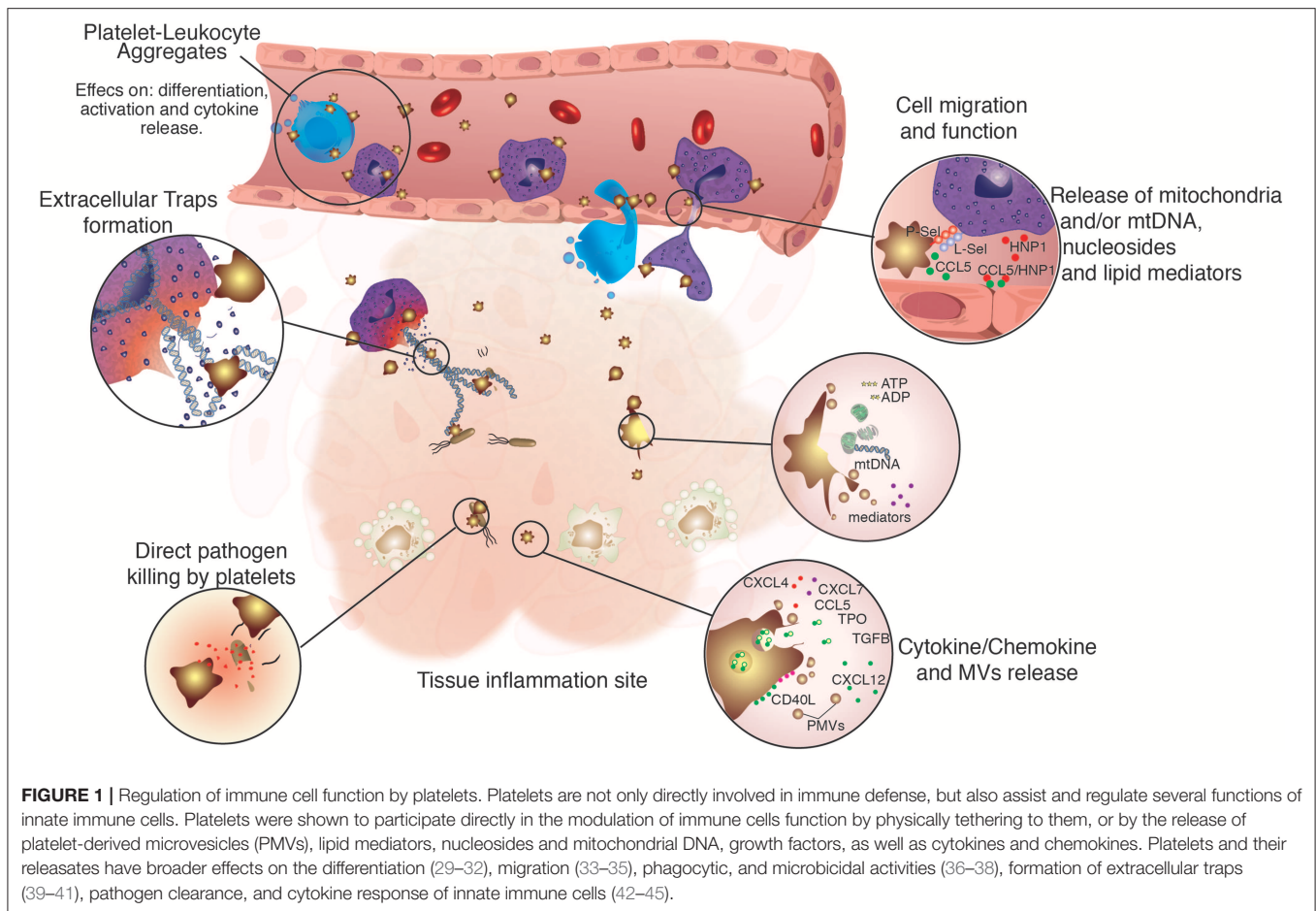
Apart from the direct clustering with microbes, platelets also contribute to pathogen clearance by coordinating the activity of immune cells such as neutrophils, which probe activated platelets via the P-selectin glycoprotein ligand-1 (PSGL-1, CD162) in order to trans-migrate to inflammatory sites. In platelet-depleted mice, or when the PSGL-1 interaction with its receptor on neutrophils was blocked, the neutrophil typical crawling was suppressed (42). These results were further validated by a novel *ex vivo* microfluidic system that allowed a better understanding of the interaction between these two cells types and the importance of the P-selectin and PSGL-1 (P-selectin glycoprotein ligand-1) in that context (48). Curiously, this same interaction also leads to the generation of neutrophil-derived vesicles filled with arachidonic acid, which are promptly internalized by platelets via Mac-1. Once inside, the arachidonic acid can be converted into thromboxane A₂ (TXA₂). Next, the platelet-derived TXA₂ acts on the neutrophil, increasing

the expression of ICAM-1 and consequent crawling and extravasation (43).

Depletion of platelets in a murine model of sepsis reduced the edema and neutrophil influx to the lungs and bronchoalveolar compartment, through the suppression of Mac-1 expression in the neutrophils (49). It has been also demonstrated that serotonin (5-HT) plays a major role in neutrophil adhesion and rolling. As platelets are the major source of peripheral serotonin, pharmacological and genetic inhibition of 5-HT signaling resulted in significant reduction in cell rolling and extravasation to lungs, peritoneum and skin wounds, as well as increased survival under LPS-induced shock, supporting the action of platelet-derived 5-HT on innate immune cells (50).

In case of breached endothelium, platelets can be recruited via CD41 and CD42b and cover a large area around the damage, proceeding to cover—but not occlude—the blood vessel. Migrating neutrophils then use the platelet scaffold to attach and crawl toward the inflammation site (33). It was also shown that this initial interaction between platelets and neutrophils can also bring inflammatory monocytes to the site of damage, in a CD40-CD40L-dependent mechanism. The blockage of this signaling cascade leads to inefficient migration, uncovering the critical role of platelets for diapedesis (34). Platelets also associate and synergize with neutrophils to promote monocyte recruitment through heteromers of platelet-derived CCL5 and neutrophil-derived HNP1 (alpha-defensin), which mediate monocyte adhesion through CCR5. Disruption of HNP1-CCL5 interactions attenuated monocyte and macrophage recruitment in a mouse model of myocardial infarction (35). Also, when platelets are activated, they release the content of their alpha granules, exposing important mediators such as adenosine diphosphate (ADP). The binding of this molecule to P2Y receptors (51) leads to quick translocation of P-selectin to the membrane, increasing the potential for recruitment of neutrophils, monocytes and lymphocytes to the injury site (52). Once they are recruited, the activity of leukocytes seems to be also dependent on ADP: the chemical blockage of the P2Y₁₂ receptor results in diminished production of reactive oxygen species (ROS) by mouse and human neutrophils (53). Platelet-released HMGB1—a critical protein for the onset of thrombosis (54)—has also been involved in the recruitment and survival of immune cells (55). Mice lacking this protein in platelets showed lower monocyte migration to the inflamed tissue in a mechanism dependent on the receptor for advanced glycation end products (RAGE) and TLR4-derived apoptosis (56). Recent *in vitro* data also point that CXCL4 (also known as PF4, platelet factor 4)—an important chemokine secreted by activated platelets—might be involved in monocyte migration upon binding to CCR1 receptor (57). The molecular pathway involving the platelets on leukocyte recruitment can range from adhesion, crawling, diapedesis and tissue invasion to injury clearance and inflammation resolution and the mechanisms observed should be further studied and explored (58). Those concepts are summarized in **Figure 1**.

Platelets can not only drive cells to an inflamed site, but also actively move in the direction of the injury.



Using a *in vivo* platelet-reporter model, it was shown that mobile platelets are capable of active adhesion and rolling by interacting with the endothelium, in a process dependent on ADP and TXA₂. Moreover, platelets can wrap and collect invading bacteria, acting as scavengers and enhancing the activity of phagocytes, such as neutrophils (5).

The formation of leukocyte-platelet aggregates also constitutes a hallmark in the modulation of innate immune cells by platelets. Bacteria can activate platelets by increasing the potential interaction with neutrophils, leading to enhanced phagocytosis, killing and clearance, in a mechanism dependent on TLR recognition (59). A cell-conditional model has shown that mice submitted to platelet depletion were prone to bacteremia to *Staphylococcus aureus* (60). It has also been reported that thrombin-activated platelets, as well as their releasates, can increase the engulfing and extermination of Gram-positive bacteria in bone marrow-derived dendritic cells, macrophages, and neutrophils. In the two first cell types, the effect was dependent on cytoskeleton remodeling. In DCs, the binding of CD40-CD40L was critical for the inflammatory

response. In macrophages, platelets also play an important role in the restriction of *S. aureus* infection (36, 37, 61). Besides blood-borne bacteria (47), platelets can also form aggregates with erythrocytes infected with *Plasmodium*, leading to the killing of the parasite. The platelet count, erythrocyte-platelet complexes and platelet-associated killing were inversely correlated with parasite loads, suggesting that platelets may contribute to the pathogenesis and control of the human malaria parasite (38, 62).

In addition to the platelets themselves, platelet-derived microvesicles (PMVs) play an important part in their communication with endothelium and innate immune cells. PMVs are the most abundant circulating particles in the body and can be loaded with nucleic acids, proteins, lipids, and small molecules originated from the platelets or MKs. Using a molecular approach to this system, it was shown that PMVs loaded with the microRNAs could modulate the transcription of different mRNA in macrophages, reprogramming them toward a phagocytic phenotype (63). Interestingly, besides stimulating more effective pathogen uptake by leukocytes, platelets also have phagocytic activity reported in several different models (64).

REGULATION OF IMMUNE CELLS FUNCTION

Cytokines and chemokines are fundamental pieces in the origin, growth, differentiation and function of immune cells. They compose a consistent and tunable communication channel that aims to keep the organism in a state of homeostasis. Injuries, infections, and autoimmune reactions interrupt this balance, leading to the production of massive amounts of such highly reactive components (65). Since platelets are so widely distributed in the body, it is reasonable to assume that they can sense these fluctuations and react properly in order to return to the homeostatic status, by direct contact or secretion of soluble factors, such as CCL5, CXCL4 and CD40L.

It is known that the adhesion of monocytes to platelets—a common event under inflammatory conditions—will result in the translocation of NF κ B to the nucleus, where it will trigger the enhance the expression of CCL2 and IL-8 by monocytes. A second signal from the platelet, CCL5, will activate the release of the monocyte pro-inflammatory chemokines and reinforce the interaction via P-selectin (66). Also the chemokine CXCL4 has an important role on systemic inflammation, such as in septic lung injury. Upon an inflammatory injury, platelets release CXCL4 via Rac-1, promoting neutrophil recruitment, edema, tissue damage, and high levels of CCL5, CXCL1, and CXCL2. The pharmacological neutralization of CXCL4 reduced the levels of pro-inflammatory factors and improved the overall condition of the animals (67, 68). Platelets are cellular sources of CD40L (CD154) and this protein has a strong effect on leukocytes. In systemic lupus erythematosus (SLE), platelets were found to be activated by immune complexes formed between autoantibodies via Fc γ RIIA and then driven to the formation of aggregates with monocytes and plasmacytoid DCs. The consequence of this interaction was an increased IFN- α release by the latter cells via CD40/CD40L. In the same study, an experimental murine model showed that the depletion or blocking of platelets in lupus-susceptible mice evoked better clinical parameters, while platelet transfusion aggravated the disease (44). The interaction of neutrophils and platelets via CD40 is also known to activate a positive feedback loop characterized by the increased release of superoxide and reactive oxygen species by the leukocytes, stimulating the secretion of CD40L by platelets (69). In the presence of autologous platelets, monocytes from older donors have greater capability for production of IL-8 and CCL2, when compared to young adults, in a mechanism initiated by granzyme A secreted from platelets. The inhibition of this factor restored the levels of IL-8 and CCL2 in a TLR-4/Caspase-1 dependent manner. However, the classical markers of platelet activation—P-selectin, CCL5, and CXCL4—were not correlated with this effect (70).

An important and tightly regulated cytokine deserves attention: IL-1 β is the product of a pre-protein cleaved by caspases, as one of the outcomes of inflammasome activation (71, 72). Leukocytes are a major source of this cytokine in the body and given the constant interaction among these cells, one can speculate how platelets can modulate the expression of this critical protein. In a cohort consisted of 500 healthy

individuals, a correlation was found between platelets and plasma levels of IL-1 β , in different scenarios: there is a positive association of platelet counts and the plasmatic concentration of the cytokine and the expression of P-selectin was linked to higher levels of IL-1 β and IL-6 after *ex vivo* stimulation (73). Looking deeper into mechanisms for such event, it was reported that, after a viral infection, platelets would release PMVs filled with the IL-1 β , as a result of to NLRP3 activation by reactive oxygen species (74). Next, healthy monocytes exposed to platelets from infected patients secreted more cytokines, such as IL-1 β , IL-8, IL-10, and the chemokine CCL2. This effect required the formation of platelet-monocyte aggregates (PMAs), but it was not present when healthy platelets were used (75). Other studies indicate that platelets themselves could be a source of inflammasome components, including IL-1 β itself and also IL-18, another inflammasome-related cytokine (76–81). Nevertheless, the presence of some IL-1 cytokines on platelets is disputed. Part of the discrepancies may be due to the process of platelet isolation from fresh whole blood, which is laborious and prone to contamination by leukocytes. Given the capacity of reaction by these nucleated cells, the smallest proportion (1:10⁵) of leukocytes within in a platelet suspension can lead to misleading interpretations (82). Therefore, further studies are necessary in order to establish the role of platelets as source of IL-1 cytokines and on their effects on the IL-1 β production by immune cells.

Despite abundant reports of pro-inflammatory effects of platelets on innate immune cells, platelets were also shown to dampen inflammation by direct interaction or release of different factors. A critical importance of platelets in the modulation of the immune response in sepsis was recently shown. Using a mouse model of platelet depletion, by chemical or genetic intervention, it was reported that platelets and their releasates can reduce the concentration of pro-inflammatory cytokines such as TNF- α and IL-6 after sterile or infectious stimuli. Platelet depletion led to greater mortality and organ failure in a mouse model of septic shock, while administration of platelets dampens the generalized and detrimental immune response. Platelets protected against septic shock through the activation of the COX-1-PGE₂-EP₄ pathway on macrophages (45). Other independent studies showed that the addition of platelets or their supernatants to a culture of mononuclear cells led to suppressed production of IL-6 and TNF- α and higher production of IL-10 after stimulation with PAMPs from different origins (83). The blockage of CD40-CD40L prevented the modulating effects, demonstrating the importance of the duo signaling for the platelet regulatory effect (84). Later, similar effects on TNF- α and IL-10 secretion by macrophages and monocytes were also found to be related to the release of PGE₂ by platelets and its binding to specific prostanoid receptors (85). Soluble factors secreted by platelets are also able to regulate the expression of mRNA of inflammatory markers, including reduced levels of NOS2 (iNOS) and consequent suppressed production of nitric oxide (NO), followed by inhibition of NF κ B signaling and higher arginase-1 expression (86, 87). A clinical approach was used to test whether platelet concentrates used in blood transfusion would have an effect on the response of dendritic cells. Upon mimicking of viral and bacterial infection, the myeloid cells

showed a reduction in co-stimulatory molecules and reduced production of IL-6, IL-8, IL-12, IP-10, and IFN- γ , suggesting that the patients undergoing platelet transfusion might not be able to assemble proper response against infectious threats (88).

INTERACTION WITH LEUKOCYTES FOR THE FORMATION OF EXTRACELLULAR TRAPS

Neutrophil extracellular traps (NETs) are physical barriers composed by cytoplasmatic proteins and nuclear content, expelled to the extracellular compartment in order to capture and eliminate pathogens, especially in systemic inflammation (89). Shortly after the original description, it was shown that platelets play a fundamental part in the formation of these structures in a septic model, by initially detecting TLR4 ligands and inducing adhesion to neutrophils (39). Circulating bacteria can be entangled by these structures, especially in the liver sinusoids and lungs capillaries, stopping them from disseminating through the bloodstream. Later, it was reported that the mechanism involving the bond between platelets and neutrophils was dependent on $\alpha_L\beta_2$ -integrin LFA-1 (CD11a/CD18) (40).

Besides the known activity in inflammation and other infectious diseases (90, 91), the role of platelets and NETs in systemic sclerosis was recently discovered. PMVs loaded with the protein HMGB1 are abundant in patients and in mouse disease models, were able to cause the formation of NETs, with higher proteolytic activity and degranulation (41, 55, 92). The interaction of platelet GPIb with neutrophil CD18 plus the release of VWF and CXCL4 are involved in the formation of NETs. This event is dependent on the production of thromboxane A2 and can be inhibited by aspirin and prostacyclin, showing the importance of platelet components for the NET formation (93, 94). On top of the formation of the extracellular traps, activated platelets can also trigger other inflammatory processes. In a model of venous thrombosis, platelets were shown to induce neutrophil death by necroptosis, via MLKL and RIPK1, leading to cell aggregation and final clot formation (95). Macrophages can also form extracellular traps as shown in a model of acute kidney injury. In the event of rhabdomyolysis derived from muscle damage, platelets are activated by the heme group released by the necrotic muscle and serve as scaffold for the formation of the macrophage extracellular traps (96).

CHANGES IN CELL MARKERS AND CONSEQUENCES TO INNATE IMMUNITY

Platelets are able to modulate other functions of innate immune cells through the release of inflammatory mediators or through cell-cell contact (97). This interaction can lead to changes in cell markers and phenotype, induce mutual cell activation and cytokine production that are implicated in the pathogenesis of inflammatory diseases and in the resolution of infections. Monocytes are central hubs of the innate immune system that present high plasticity and possess both pro-inflammatory and anti-inflammatory properties and can also mature into macrophages and dendritic cells. Human

monocytes can be divided in three different subsets accordingly to the expression of CD14 and CD16: classical monocytes (CD14^{high}CD16⁻), intermediate (CD14^{high}CD16^{high}) and non-classical monocytes (CD14^{low}CD16⁺) (98). Even though the functions of different subtypes of monocytes are still controversial and context-dependent, CD16⁺ monocyte subsets are related with inflammatory features, such as the release of IL-1 β and TNF- α , the differential expression of TLRs, scavenger receptors and the expression of the co-stimulatory molecules CD80 and CD86 (99).

The CD16⁺ monocyte subsets are also associated with the PMAs. These complexes are linked with various inflammatory diseases, such as acute thrombotic events, diabetes and auto-inflammatory disorders and are markers for both platelet and monocyte activation (97). The co-incubation of platelets with monocytes to induce PMAS formation lead to the shift of CD14^{high}CD16⁻ monocytes toward to the CD14^{high}CD16⁺ subtype. The physical interaction of activated platelets and monocytes is mainly mediated by P-selectin-PSGL-1 and induce up-regulation of COX-2, which induce an higher expression of both integrins CD11b and CD11c (97). Moreover, it was reported that PSGL-1 engagement also increased the expression of the integrin CD49d ($\alpha_4\beta_1$) and decreased CD62L expression. The phenotypic changes promoted by platelet interaction boosted monocyte adherence to the activated endothelium through a higher binding to fibronectin, vascular cell adhesion protein 1 (VCAM-1) and intercellular adhesion molecule 1 (ICAM-1) (100). It was also described that PMAS formation in rheumatoid arthritis drive the induction of the pro-inflammatory CD14^{high}CD16⁺ monocyte subset via the increased expression of CD147 on activated platelets (101).

In serum-free conditions cytosolic fractions of platelets were able to induce higher expression of CD16 and carboxypeptidases, reinforcing the importance of cell-cell contact to induce monocyte maturation (29). However, even though cell-cell contact might be critical to the regulation of monocytes, it was reported that the local release of TGF- β by activated platelets also leads to the expression of CD16 on infiltrating or resident monocytes, facilitating the lysis of murine anti-CD16 hybridomas (29). Platelets also contribute to the generation of CD14⁺CD16⁺ dendritic-like cells (DLCs) from peripheral blood monocytes. Cultivation of purified CD14⁺ monocytes with immobilized P-selectin in the presence of M-CSF and IL-4 induced the differentiation into CD14⁺CD16⁺ DLCs with increased expression of CD1a. The resulting DLCs presented reduced phagocytic activity and increased alloreactivity to naive T cells. Interestingly, P-selectin interaction with monocytes was also able to inhibit monocyte differentiation into macrophage in response to M-CSF (102).

Monocytes and platelets are fundamental parts in several inflammatory diseases and one of the most important conditions is atherosclerosis, a chronic inflammatory disease characterized by the formation of plaques in the arteries resulting from lipid accumulation and inflammation (103). Platelets are important players for the genesis and progression of the disorder due to their ability to interact with immune and endothelial cells and through the uptake of low-density lipoproteins (LDL). The release of soluble inflammatory mediators such as CCL5, CXCL4,

and CXCL7 by platelets induce the migration and activation of monocytes, dendritic cells and neutrophils to the damaged site, contributing to the progression of atherosclerosis (104). Platelets also secrete CXCL12 that mediate the chemotaxis of CD34⁺ progenitors to the sites of injury and promotes their differentiation into endothelial and macrophages/foam cell phenotype (30, 31). In mice, the dual engagement of CXCR4 and CXCR7 by platelet-derived CXCL12 induced the differentiation of monocytes into CD163⁺ macrophages, that contributes to hemoglobin clearance and thus it was associated with atheroprotection. However, it was described that CD163⁺ macrophages were associated with plaque progression, microvasculature, and up-regulation of hypoxia-inducible factor 1 α (HIF1 α) and vascular endothelial growth factor A (VEGF-A) in human atherosclerotic lesions samples, suggesting that these cells can also exert a pro-inflammatory role (32).

Monocytes that migrate to the atherosclerotic lesions can further differentiate into macrophages/foam cells that upregulate the scavenger receptor CD36. This receptor recognizes pathogens and apoptotic cells but also oxidized LDL (oxLDL) (105). The local release of CXCL4 promotes monocyte maturation into macrophages and support the retention of LDL on cell surfaces (106). Also, the uptake of oxLDL by macrophages is boosted by PF4, CXCL4, CXCL12, and platelet-derived growth factor (PDGF) (32). Moreover, platelet uptake of oxLDL induce platelet apoptosis and facilitates its phagocytosis by monocytes and macrophages, also contributing to foam cell formation (32). Even though monocytes and macrophages are the key players in atherogenesis, neutrophils, and platelet-neutrophil aggregates (PNA) also have an important role in this process (107). Similarly to what is observed in PMAs, P-selectin-PSGL1 interaction is crucial to the formation of PNAs and induce an higher expression of CD11b/CD18 on neutrophils, contributing to their activation and adherence to the activated endothelium (108).

ROLE ON CELL DEATH AND SURVIVAL

Apoptosis is a programmed cell death that contribute to terminate immune responses and control inflammation (109). Although the precise mechanism by which platelets can prevent human polymorphonuclear (PMN) leukocyte and monocyte cell death is still not established, there are evidence in the literature suggesting that platelets can increase cell survival.

Co-cultivation of neutrophils with thrombin-treated or untreated platelets was able to reduce neutrophil apoptosis in comparison with neutrophils cultured alone, in a mechanism that seems to be independent of P-selectin (110). In another study, TGF- β derived from thrombin-treated platelets or exogenous TGF- β was able to reduce neutrophil apoptosis in a dose-dependent manner (111). In atherosclerosis, the release of CXCL4 was reported to prevent neutrophil and monocyte apoptosis (104). Adenosine 5'-diphosphate-activated platelets co-cultivation with isolated neutrophils from patients with acute coronary syndromes was also able to reduce neutrophil cell death (112). Also, the uptake of platelets by monocytes downregulates caspase-9 and caspase-3, suppressing monocyte apoptosis (113).

Platelets can also favor cell survival through the induction of autophagy on neutrophils. Autophagy is a highly conserved biological process responsible for the degradation of organelles and cellular components. This pathway can be activated in response to starvation in order to replenish nutrient stores or to avoid the generation of toxic byproducts derived from unwanted organelles and proteins, contributing to maintain cellular homeostasis (114). HMGB1 released by activated platelets in coronary thrombi and its binding to RAGE receptors expressed on neutrophils was shown to promote the autophagic pathway on these cells. The induction of autophagy prevented apoptosis and enhanced cell survival, priming neutrophils for NET generation and contributing for venous thrombosis (92). Moreover, autophagy-dependent NET formation was also described to contribute to lung fibrosis (115). Since it was already described the role of platelets in this condition (116), these cells might also contribute to induce the autophagy-dependent NET in fibrosis.

The ability of platelets to induce pro-survival signaling can contribute to innate immune cell functions but also contribute to exacerbate the inflammation in different diseases. Since apoptosis induction is fundamental to ensure the resolution of the inflammatory response, the pharmacological modulation of cell death can have beneficial effects in inflammatory diseases (117).

PERSPECTIVES

Previously known as keepers of hemostasis, platelets gained importance over the last years due to exciting discoveries that place them as critical players of the innate immune system. Platelets can contribute to the resolution of infections and the genesis and progression of autoimmune and inflammatory diseases directly or through the regulation of immune cells. More recently, there is a growing interest and evidence in the literature suggesting that platelets can also be a target to treat inflammatory conditions with promising results. However, further studies are necessary to better understand how platelets modulate the immune response. The deep comprehension of platelet role in infections and diseases will permit the development of therapeutic strategies to treat conditions in which platelets have a detrimental role.

AUTHOR CONTRIBUTIONS

All authors have read and approved the publication of this manuscript. LSR and LM wrote the manuscript with input from BF.

FUNDING

This work is supported by grants from European Research Council (ERC, PLAT-IL-1 714175) and the Deutsche Forschungsgemeinschaft (DFG, German Research Foundation) under Germany's Excellence Strategy – EXC2151 – 390873048. LM is recipient of Ph.D. fellowship from BEPE/FAPESP (Fundação de Amparo à Pesquisa do Estado de São Paulo, Brazil).

REFERENCES

- Li R, Hoffmeister KM, Falet H. Glycans and the platelet life cycle. *Platelets*. (2016) 27:505–11. doi: 10.3109/09537104.2016.1171304
- Lebois M, Dowling MR, Gangatirkar P, Hodgkin PD, Kile BT, Alexander WS, et al. Regulation of platelet lifespan in the presence and absence of thrombopoietin signaling. *J Thromb Haemost*. (2016) 14:1882–7. doi: 10.1111/jth.13397
- Grozovsky R, Begonja AJ, Liu K, Visner G, Hartwig JH, Falet H, et al. The Ashwell-Morell receptor regulates hepatic thrombopoietin production via JAK2-STAT3 signaling. *Nat Med*. (2015) 21:47–54. doi: 10.1038/nm.3770
- Junt T, Schulze H, Chen Z, Massberg S, Goerge T, Krueger A, et al. Dynamic visualization of thrombopoiesis within bone marrow. *Science*. (2007) 317:1767–70. doi: 10.1126/science.1146304
- Gaertner F, Ahmad Z, Rosenberger G, Fan S, Nicolai L, Busch B, et al. Migrating platelets are mechano-scavengers that collect and bundle bacteria. *Cell*. (2017) 171:1368–82.e23. doi: 10.1016/j.cell.2017.11.001
- Lefrançois E, Ortiz-Muñoz G, Caudrillier A, Mallavia B, Liu F, Sayah DM, et al. The lung is a site of platelet biogenesis and a reservoir for haematopoietic progenitors. *Nature*. (2017) 544:105–9. doi: 10.1038/nature21706
- Li J, van der Wal DE, Zhu G, Xu M, Yougbare I, Ma L, et al. Desialylation is a mechanism of Fc-independent platelet clearance and a therapeutic target in immune thrombocytopenia. *Nat Commun*. (2015) 6:7737. doi: 10.1038/ncomms8737
- Li Y, Fu J, Ling Y, Yago T, McDaniel JM, Song J, et al. Sialylation on O-glycans protects platelets from clearance by liver Kupffer cells. *Proc Natl Acad Sci USA*. (2017) 114:8360–5. doi: 10.1073/pnas.1707662114
- McRedmond JP, Park SD, Shields DC, Maguire PB, Fitzgerald DJ, Coppinger JA. Integration of proteomics and genomics in platelets. *Mol Cell Proteomics*. (2003) 3:133–44. doi: 10.1074/mcp.m300063-mcp200
- Zimmerman GA, Weyrich AS. Signal-dependent protein synthesis by activated platelets. *Arterioscler Thromb Vasc Biol*. (2008) 28:S17–24. doi: 10.1161/ATVBAHA.107.160218
- Rowley JW, Oler AJ, Tolley ND, Hunter BN, Low EN, Nix DA, et al. Genome-wide RNA-seq analysis of human and mouse platelet transcriptomes. *Blood*. (2011) 118:e101–11. doi: 10.1182/blood-2011-03-339705
- Rowley JW, Weyrich AS. Coordinate expression of transcripts and proteins in platelets. *Blood*. (2013) 121:5255–6. doi: 10.1182/blood-2013-03-487991
- Garcia-Souza LF, Oliveira MF. Mitochondria: biological roles in platelet physiology and pathology. *Int J Biochem Cell Biol*. (2014) 50:156–60. doi: 10.1016/j.biocel.2014.02.015
- Chen CH, Lo RW, Urban D, Pluthero FG, Kahr WHA. α -granule biogenesis: from disease to discovery. *Platelets*. (2017) 28:147–54. doi: 10.1080/09537104.2017.1280599
- Pagel O, Walter E, Jurk K, Zahedi RP. Taking the stock of granule cargo: platelet releasate proteomics. *Platelets*. (2017) 28:119–28. doi: 10.1080/09537104.2016.1254762
- Sharda A, Flaumenhaft R. The life cycle of platelet granules. *F1000Research*. (2018) 7:236. doi: 10.12688/f1000research.13283.1
- Coppinger JA, Cagney G, Toomey S, Kislinger T, Belton O, McRedmond JP, et al. Characterization of the proteins released from activated platelets leads to localization of novel platelet proteins in human atherosclerotic lesions. *Blood*. (2004) 103:2096–104. doi: 10.1182/blood-2003-08-2804
- Melki I, Tessandier N, Zufferey A, Boilard E. Platelet microvesicles in health and disease. *Platelets*. (2017) 28:214–21. doi: 10.1080/09537104.2016.1265924
- Kuravi SJ, Harrison P, Rainger GE, Nash GB. Ability of platelet-derived extracellular vesicles to promote neutrophil-endothelial cell interactions. *Inflammation*. (2019) 42:290–305. doi: 10.1007/s10753-018-0893-5
- Semple JW, Italiano JE, Freedman J. Platelets and the immune continuum. *Nat Rev Immunol*. (2011) 11:264–74. doi: 10.1038/nri2956
- Yeaman MR. Platelets: at the nexus of antimicrobial defence. *Nat Rev Microbiol*. (2014) 12:426–37. doi: 10.1038/nrmicro3269
- Cognasse F, Hamzeh H, Chavarin P, Acquart S, Genin C, Garraud O. Evidence of Toll-like receptor molecules on human platelets. *Immunol Cell Biol*. (2005) 83:196–8. doi: 10.1111/j.1440-1711.2005.01314.x
- Andonegui G. Platelets express functional Toll-like receptor-4. *Blood*. (2005) 106:2417–23. doi: 10.1182/blood-2005-03-0916
- D'Atri LP, Schattner M. Platelet toll-like receptors in thromboinflammation. *Front Biosci*. (2017) 22:1867–83. doi: 10.2741/4576
- Hamzeh-Cognasse H, Berthelot P, Tardy B, Pozzetto B, Bourlet T, Laradi S, et al. Platelet toll-like receptors are crucial sensors of infectious danger moieties. *Platelets*. (2018) 29:533–40. doi: 10.1080/09537104.2018.1445842
- Thomas M, Storey R. The role of platelets in inflammation. *Thromb Haemost*. (2015) 114:449–58. doi: 10.1160/TH14-12-1067
- Lam FW, Vijayan KV, Rumbaut RE. Platelets and their interactions with other immune cells. *Compr Physiol*. (2015) 5:1265–80. doi: 10.1002/cphy.c140074
- Alonso AL, Cox D. Platelet interactions with viruses and parasites. *Platelets*. (2015) 26:317–23. doi: 10.3109/09537104.2015.1025376
- Ammon C, Kreutz M, Rehli M, Krause SW, Andreesen R. Platelets induce monocyte differentiation in serum-free coculture. *J Leukoc Biol*. (1998) 63:469–476. doi: 10.1002/jlb.63.4.469
- Stellos K, Langer H, Daub K, Schoenberger T, Gauss A, Geisler T, et al. Platelet-derived stromal cell–derived factor-1 regulates adhesion and promotes differentiation of human CD34+ cells to endothelial progenitor cells. *Circulation*. (2008) 117:206–15. doi: 10.1161/CIRCULATIONAHA.107.714691
- Langer H, May AE, Daub K, Heinzmann U, Lang P, Schumm M, et al. Adherent platelets recruit and induce differentiation of murine embryonic endothelial progenitor cells to mature endothelial cells *in vitro*. *Circ Res*. (2006) 98:e2–10. doi: 10.1161/01.RES.0000201285.87524.9e
- Chatterjee M, Von Ungern-Sternberg SNI, Seizer P, Schlegel F, Büttcher M, Sindhu NA, et al. Platelet-derived CXCL12 regulates monocyte function, survival, differentiation into macrophages and foam cells through differential involvement of CXCR4-CXCR7. *Cell Death Dis*. (2015) 6:e1989. doi: 10.1038/cddis.2015.233
- Slaba I, Wang J, Kolaczowska E, McDonald B, Lee W-Y, Kubers P. Imaging the dynamic platelet-neutrophil response in sterile liver injury and repair in mice. *Hepatology*. (2015) 62:1593–605. doi: 10.1002/hep.28003
- Zuchtriegel G, Uhl B, Pühr-Westerheide D, Pörnbacher M, Lauber K, Krombach F, et al. Platelets guide leukocytes to their sites of extravasation. *PLOS Biol*. (2016) 14:e1002459. doi: 10.1371/journal.pbio.1002459
- Alard J-E, Ortega-Gomez A, Wichapong K, Bongiovanni D, Horckmans M, Megens RTA, et al. Recruitment of classical monocytes can be inhibited by disturbing heteromers of neutrophil HNP1 and platelet CCL5. *Sci Transl Med*. (2015) 7:317ra196. doi: 10.1126/scitranslmed.aad5330
- Ali RA, Wuescher LM, Dona KR, Worth RG. Platelets mediate host defense against *Staphylococcus aureus* through direct bactericidal activity and by enhancing macrophage activities. *J Immunol*. (2017) 198:344–51. doi: 10.4049/jimmunol.1601178
- Nishat S, Wuescher LM, Worth RG. Platelets enhance dendritic cell responses against *Staphylococcus aureus* through CD40-CD40L. *Infect Immun*. (2018) 86:IAI.00186-18. doi: 10.1128/IAI.00186-18
- McMorran BJ, Marshall VM, de Graaf C, Drysdale KE, Shabbar M, Smyth GK, et al. Platelets kill intraerythrocytic malarial parasites and mediate survival to infection. *Science*. (2009) 323:797–800. doi: 10.1126/science.1166296
- Clark SR, Ma AC, Tavener SA, McDonald B, Goodarzi Z, Kelly MM, et al. Platelet TLR4 activates neutrophil extracellular traps to ensnare bacteria in septic blood. *Nat Med*. (2007) 13:463–9. doi: 10.1038/nm1565
- McDonald B, Urrutia R, Yipp BG, Jenne CN, Kubers P. Intravascular neutrophil extracellular traps capture bacteria from the bloodstream during sepsis. *Cell Host Microbe*. (2012) 12:324–33. doi: 10.1016/j.chom.2012.06.011
- Maugeri N, Capobianco A, Rovere-Querini P, Ramirez GA, Tombetti E, Della Valle P, et al. Platelet microparticles sustain autophagy-associated activation of neutrophils in systemic sclerosis. *Sci Transl Med*. (2018) 10:eaa03089. doi: 10.1126/scitranslmed.aao3089
- Sreeramkumar V, Adrover JM, Ballesteros I, Cuartero MI, Rossaint J, Bilbao I, et al. Neutrophils scan for activated platelets to initiate inflammation. *Science*. (2014) 346:1234–8. doi: 10.1126/science.1256478
- Rossaint J, Kühne K, Skupski J, Van Aken H, Looney MR, Hidalgo A, et al. Directed transport of neutrophil-derived extracellular vesicles

- enables platelet-mediated innate immune response. *Nat Commun.* (2016) 7:13464. doi: 10.1038/ncomms13464
44. Duffau P, Seneschal J, Nicco C, Richez C, Lazaro E, Douchet I, et al. Platelet CD154 potentiates interferon- α secretion by plasmacytoid dendritic cells in systemic lupus erythematosus. *Sci Transl Med.* (2010) 2:47ra63. doi: 10.1126/scitranslmed.3001001
 45. Xiang B, Zhang G, Guo L, Li X-A, Morris AJ, Daugherty A, et al. Platelets protect from septic shock by inhibiting macrophage-dependent inflammation via the cyclooxygenase 1 signalling pathway. *Nat Commun.* (2013) 4:2657. doi: 10.1038/ncomms3657
 46. Wong CHY, Jenne CN, Petri B, Chrobok NL, Kubes P. Nucleation of platelets with blood-borne pathogens on Kupffer cells precedes other innate immunity and contributes to bacterial clearance. *Nat Immunol.* (2013) 14:785–92. doi: 10.1038/ni.2631
 47. Verschoor A, Neuenhahn M, Navarini AA, Graef P, Plaumann A, Seidlmeier A, et al. A platelet-mediated system for shuttling blood-borne bacteria to CD8 α + dendritic cells depends on glycoprotein GPIb and complement C3. *Nat Immunol.* (2011) 12:1194–201. doi: 10.1038/ni.2140
 48. Frydman GH, Le A, Ellett F, Jorgensen J, Fox JG, Tompkins RG, et al. Technical Advance: changes in neutrophil migration patterns upon contact with platelets in a microfluidic assay. *J Leukoc Biol.* (2017) 101:797–806. doi: 10.1189/jlb.1TA1115-517RR
 49. Asaduzzaman M, Lavasani S, Rahman M, Zhang S, Braun OÖ, Jeppsson B, et al. Platelets support pulmonary recruitment of neutrophils in abdominal sepsis. *Crit Care Med.* (2009) 37:1389–96. doi: 10.1097/CCM.0b013e31819ceb71
 50. Duerschmied D, Suidan GL, Demers M, Herr N, Carbo C, Brill A, et al. Platelet serotonin promotes the recruitment of neutrophils to sites of acute inflammation in mice. *Blood.* (2013) 121:1008–15. doi: 10.1182/blood-2012-06-437392
 51. Léon C, Ravanat C, Freund M, Cazenave J-P, Gachet C. Differential Involvement of the P2Y₁ and P2Y₁₂ receptors in platelet procoagulant activity. *Arterioscler Thromb Vasc Biol.* (2003) 23:1941–7. doi: 10.1161/01.ATV.0000092127.16125.E6
 52. Liverani E, Rico MC, Yaratha L, Tsygankov AY, Kilpatrick LE, Kunapuli SP. LPS-induced systemic inflammation is more severe in P2Y₁₂ null mice. *J Leukoc Biol.* (2014) 95:313–23. doi: 10.1189/jlb.1012518
 53. Evangelista V, Manarini S, Dell'Elba G, Martelli N, Napoleone E, Santo A Di, et al. Clopidogrel inhibits platelet-leukocyte adhesion and platelet-dependent leukocyte activation. *Thromb Haemost.* (2005) 94:568–77. doi: 10.1160/TH05-01-0020
 54. Vogel S, Bodenstern R, Chen Q, Feil S, Feil R, Rheinlaender J, et al. Platelet-derived HMGB1 is a critical mediator of thrombosis. *J Clin Invest.* (2015) 125:4638–54. doi: 10.1172/JCI81660
 55. Zhou H, Deng M, Liu Y, Yang C, Hoffman R, Zhou J, et al. Platelet HMGB1 is required for efficient bacterial clearance in intra-abdominal bacterial sepsis in mice. *Blood Adv.* (2018) 2:638–48. doi: 10.1182/bloodadvances.2017011817
 56. Vogel S, Rath D, Borst O, Mack A, Loughran P, Lotze MT, et al. Platelet-derived high-mobility group box 1 promotes recruitment and suppresses apoptosis of monocytes. *Biochem Biophys Res Commun.* (2016) 478:143–8. doi: 10.1016/j.bbrc.2016.07.078
 57. Fox JM, Kausar F, Day A, Osborne M, Hussain K, Mueller A, et al. CXCL4/Platelet Factor 4 is an agonist of CCR1 and drives human monocyte migration. *Sci Rep.* (2018) 8:9466. doi: 10.1038/s41598-018-27710-9
 58. Rossaint J, Margraf A, Zarbock A. Role of platelets in leukocyte recruitment and resolution of inflammation. *Front Immunol.* (2018) 9:2712. doi: 10.3389/fimmu.2018.02712
 59. Assinger A, Laky M, Schabbauer G, Hirschl AM, Buchberger E, Binder BR, et al. Efficient phagocytosis of periodontopathogens by neutrophils requires plasma factors, platelets and TLR2. *J Thromb Haemost.* (2011) 9:799–809. doi: 10.1111/j.1538-7836.2011.04193.x
 60. Wuescher LM, Takashima A, Worth RG. A novel conditional platelet depletion mouse model reveals the importance of platelets in protection against *Staphylococcus aureus* bacteremia. *J Thromb Haemost.* (2015) 13:303–13. doi: 10.1111/jth.12795
 61. Hurley SM, Kahn F, Nordenfelt P, Mörgelin M, Sørensen OE, Shannon O. Platelet-Dependent neutrophil function is dysregulated by m protein from *Streptococcus pyogenes*. *Infect Immun.* (2015) 83:3515–25. doi: 10.1128/IAI.00508-15
 62. Kho S, Barber BE, Johar E, Andries B, Poesoprodjo JR, Kenangalem E, et al. Platelets kill circulating parasites of all major *Plasmodium* species in human malaria. *Blood.* (2018) 132:1332–44. doi: 10.1182/blood-2018-05-849307
 63. Laffont B, Corduan A, Rousseau M, Duchez AC, Lee CHC, Boilard E, et al. Platelet microparticles reprogram macrophage gene expression and function. *Thromb Haemost.* (2016) 115:311–23. doi: 10.1160/TH15-05-0389
 64. Nagasawa T, Nakayasu C, Rieger AM, Barreda DR, Somamoto T, Nakao M. Phagocytosis by thrombocytes is a conserved innate immune mechanism in lower vertebrates. *Front Immunol.* (2014) 5:445. doi: 10.3389/fimmu.2014.00445
 65. Nguyen TA, Pang KC, Masters SL. Intercellular communication for innate immunity. *Mol Immunol.* (2017) 86:16–22. doi: 10.1016/j.molimm.2016.10.002
 66. Weyrich AS, Elstad MR, McEver RP, McIntyre TM, Moore KL, Morrissey JH, et al. Activated platelets signal chemokine synthesis by human monocytes. *J Clin Invest.* (1996) 97:1525–34. doi: 10.1172/JCI118575
 67. Hwaiz R, Rahman M, Syk I, Zhang E, Thorlacius H. Rac1-dependent secretion of platelet-derived CCL5 regulates neutrophil recruitment via activation of alveolar macrophages in septic lung injury. *J Leukoc Biol.* (2015) 97:975–84. doi: 10.1189/jlb.4A1214-603R
 68. Hwaiz R, Rahman M, Zhang E, Thorlacius H. Platelet secretion of CXCL4 is Rac1-dependent and regulates neutrophil infiltration and tissue damage in septic lung damage. *Br J Pharmacol.* (2015) 172:5347–59. doi: 10.1111/bph.13325
 69. Vanichakarn P, Blair P, Wu C, Freedman JE, Chakrabarti S. Neutrophil CD40 enhances platelet-mediated inflammation. *Thromb Res.* (2008) 122:346–58. doi: 10.1016/j.thromres.2007.12.019
 70. Campbell RA, Franks Z, Bhatnagar A, Rowley JW, Manne BK, Supiano MA, et al. Granzyme A in human platelets regulates the synthesis of proinflammatory cytokines by monocytes in aging. *J Immunol.* (2018) 200:295–304. doi: 10.4049/jimmunol.1700885
 71. Latz E, Xiao TS, Stutz A. Activation and regulation of the inflammasomes. *Nat Rev Immunol.* (2013) 13:397–411. doi: 10.1038/nri3452
 72. Broz P, Dixit VM. Inflammasomes: mechanism of assembly, regulation and signalling. *Nat Rev Immunol.* (2016) 16:407–420. doi: 10.1038/nri.2016.58
 73. Tunjungputri R, Li Y, de Groot P, Dinarello C, Smeekens S, Jaeger M, et al. The inter-relationship of platelets with interleukin-1 β -mediated inflammation in humans. *Thromb Haemost.* (2018) 118:2112–25. doi: 10.1055/s-0038-1675603
 74. Hottz ED, Lopes JF, Freitas C, Valls-de-Souza R, Oliveira MF, Bozza MT, et al. Platelets mediate increased endothelium permeability in dengue through NLRP3-inflammasome activation. *Blood.* (2013) 122:3405–14. doi: 10.1182/blood-2013-05-504449
 75. Hottz ED, Medeiros-de-Moraes IM, Vieira-de-Abreu A, de Assis EF, Vals-de-Souza R, Castro-Faria-Neto HC, et al. Platelet activation and apoptosis modulate monocyte inflammatory responses in dengue. *J Immunol.* (2014) 193:1864–72. doi: 10.4049/jimmunol.1400091
 76. Loppnow H, Bil R, Hirt S, Schonbeck U, Herzberg M, Werdan K, et al. Platelet-derived interleukin-1 induces cytokine production, but not proliferation of human vascular smooth muscle cells. *Blood.* (1998) 91:134–41.
 77. Lindemann S, Tolley ND, Dixon DA, McIntyre TM, Prescott SM, Zimmerman GA, et al. Activated platelets mediate inflammatory signaling by regulated interleukin 1 β synthesis. *J Cell Biol.* (2001) 154:485–90. doi: 10.1083/jcb.200105058
 78. Brown GT, McIntyre TM. Lipopolysaccharide signaling without a nucleus: kinase cascades stimulate platelet shedding of proinflammatory IL-1-rich microparticles. *J Immunol.* (2011) 186:5489–96. doi: 10.4049/jimmunol.1001623
 79. Brown GT, Narayanan P, Li W, Silverstein RL, McIntyre TM. Lipopolysaccharide stimulates platelets through an IL-1 β autocrine loop. *J Immunol.* (2013) 191:5196–203. doi: 10.4049/jimmunol.1300354
 80. Allam O, Samarani S, Jenabian M-A, Routy J-P, Tremblay C, Amre D, et al. Differential synthesis and release of IL-18 and IL-18 binding protein from

- human platelets and their implications for HIV infection. *Cytokine*. (2017) 90:144–54. doi: 10.1016/j.cyt.2016.10.016
81. Murthy P, Durco F, Miller-Ocuin JL, Takedai T, Shankar S, Liang X, et al. The NLRP3 inflammasome and bruton's tyrosine kinase in platelets co-regulate platelet activation, aggregation, and in vitro thrombus formation. *Biochem Biophys Res Commun*. (2017) 483:230–6. doi: 10.1016/j.bbrc.2016.12.161
 82. Pillitteri D, Bassus S, Boller K, Mahnel R, Scholz T, Westrup D, et al. Thrombin-induced interleukin 1 β synthesis in platelet suspensions: Impact of contaminating leukocytes. *Platelets*. (2007) 18:119–27. doi: 10.1080/09537100600800792
 83. Hally KE, La Flamme AC, Harding SA, Larsen PD. Platelets regulate leukocyte responses to Toll-like receptor stimulation. *Clin Transl Immunol*. (2018) 7:e1036. doi: 10.1002/cti2.1036
 84. Gudbrandsdottir S, Hasselbalch HC, Nielsen CH. Activated platelets enhance IL-10 secretion and reduce TNF- α secretion by monocytes. *J Immunol*. (2013) 191:4059–67. doi: 10.4049/jimmunol.1201103
 85. Linke B, Schreiber Y, Picard-Willems B, Slatery P, Nüsing RM, Harder S, et al. Activated platelets induce an anti-inflammatory response of monocytes/macrophages through cross-regulation of PGE2 and cytokines. *Mediat Inflamm*. (2017) 2017:1463216. doi: 10.1155/2017/1463216
 86. Ando Y, Oku T, Tsuji T. Platelets attenuate production of cytokines and nitric oxide by macrophages in response to bacterial endotoxin. *Platelets*. (2016) 27:344–50. doi: 10.3109/09537104.2015.1103369
 87. Ando Y, Oku T, Tsuji T. Platelet supernatant suppresses LPS-induced nitric oxide production from macrophages accompanied by inhibition of NF- κ B signaling and increased arginase-1 expression. *PLoS ONE*. (2016) 11:e0162208. doi: 10.1371/journal.pone.0162208
 88. Ki KK, Faddy HM, Flower RL, Dean MM. Platelet concentrates modulate myeloid dendritic cell immune responses. *Platelets*. (2018) 29:373–82. doi: 10.1080/09537104.2017.1306045
 89. Brinkmann V, Reichard U, Goosmann C, Fauler B, Uhlemann Y, Weiss DS, et al. Neutrophil extracellular traps kill bacteria. *Science*. (2004) 303:1532–5. doi: 10.1126/science.1092385
 90. McDonald B, Davis RP, Kim S-J, Tse M, Esmon CT, Kolaczowska E, et al. Platelets and neutrophil extracellular traps collaborate to promote intravascular coagulation during sepsis in mice. *Blood*. (2017) 129:1357–67. doi: 10.1182/blood-2016-09-741298
 91. Deppermann C, Kubes P. Start a fire, kill the bug: the role of platelets in inflammation and infection. *Innate Immun*. (2018) 24:335–48. doi: 10.1177/1753425918789255
 92. Maugeri N, Campana L, Gavina M, Covino C, De Metrio M, Panciroli C, et al. Activated platelets present high mobility group box 1 to neutrophils, inducing autophagy and promoting the extrusion of neutrophil extracellular traps. *J Thromb Haemost*. (2014) 12:2074–88. doi: 10.1111/jth.12710
 93. Carestia A, Kaufman T, Rivadeneira L, Landoni VI, Pozner RG, Negrotto S, et al. Mediators and molecular pathways involved in the regulation of neutrophil extracellular trap formation mediated by activated platelets. *J Leukoc Biol*. (2016) 99:153–62. doi: 10.1189/jlb.3A0415-161R
 94. Carestia A, Kaufman T, Schattner M. Platelets: new bricks in the building of neutrophil extracellular traps. *Front Immunol*. (2016) 7:271. doi: 10.3389/fimmu.2016.00271
 95. Nakazawa D, Desai J, Steiger S, Müller S, Devarapu SK, Mulay SR, et al. Activated platelets induce MLKL-driven neutrophil necroptosis and release of neutrophil extracellular traps in venous thrombosis. *Cell Death Discov*. (2018) 4:71. doi: 10.1038/s41420-018-0073-2
 96. Okubo K, Kurosawa M, Kamiya M, Urano Y, Suzuki A, Yamamoto K, et al. Macrophage extracellular trap formation promoted by platelet activation is a key mediator of rhabdomyolysis-induced acute kidney injury. *Nat Med*. (2018) 24:232–8. doi: 10.1038/nm.4462
 97. Passacualle G, Vamadevan P, Pereira L, Hamid C, Corrigan V, Ferro A. Monocyte-platelet interaction induces a pro-inflammatory phenotype in circulating monocytes. *PLoS ONE*. (2011) 6:e25595. doi: 10.1371/journal.pone.0025595
 98. Ziegler-Heitbrock L. The CD14+ CD16+ blood monocytes: their role in infection and inflammation. *J Leukoc Biol*. (2006) 81:584–92. doi: 10.1189/jlb.0806510
 99. Mukherjee R, Kanti Barman P, Kumar Thatoi P, Tripathy R, Kumar Das B, Ravindran B. Non-classical monocytes display inflammatory features: validation in sepsis and systemic lupus erythematosus. *Sci Rep*. (2015) 5:13886. doi: 10.1038/srep13886
 100. Martins PA da C, van Gils JM, Mol A, Hordijk PL, Zwaginga JJ. Platelet binding to monocytes increases the adhesive properties of monocytes by up-regulating the expression and functionality of β 1 and β 2 integrins. *J Leukoc Biol*. (2006) 79:499–507. doi: 10.1189/jlb.0605318
 101. Rong M, Wang C, Wu Z, Zeng W, Zheng Z, Han Q, et al. Platelets induce a proinflammatory phenotype in monocytes via the CD147 pathway in rheumatoid arthritis. *Arthritis Res Ther*. (2014) 16:478. doi: 10.1186/s13075-014-0478-0
 102. Li G, Kim Y-J, Mantel C, Broxmeyer HE. P-selectin enhances generation of CD14+CD16+ dendritic-like cells and inhibits macrophage maturation from human peripheral blood monocytes. *J Immunol*. (2003) 171:669–77. doi: 10.4049/jimmunol.171.2.669
 103. Hansson GK, Libby P. The immune response in atherosclerosis: a double-edged sword. *Nat Rev Immunol*. (2006) 6:508–19. doi: 10.1038/nri1882
 104. von Hundelshausen P, Schmitt MMN. Platelets and their chemokines in atherosclerosis-clinical applications. *Front Physiol*. (2014) 5:294. doi: 10.3389/fphys.2014.00294
 105. Li AC, Glass CK. The macrophage foam cell as a target for therapeutic intervention. *Nat Med*. (2002) 8:1235–42. doi: 10.1038/nm1102-1235
 106. Gawaz M, Langer H, May AE. Platelets in inflammation and atherogenesis. *J Clin Invest*. (2005) 115:3378–84. doi: 10.1172/JCI27196
 107. Lisman T. Platelet-neutrophil interactions as drivers of inflammatory and thrombotic disease. *Cell Tissue Res*. (2018) 371:567–76. doi: 10.1007/s00441-017-2727-4
 108. Page C, Pitchford S. Neutrophil and platelet complexes and their relevance to neutrophil recruitment and activation. *Int Immunopharmacol*. (2013) 17:1176–84. doi: 10.1016/j.intimp.2013.06.004
 109. Kolb JB, Oguin TH, Oberst A, Martinez J. Programmed cell death and inflammation: winter is coming. *Trends Immunol*. (2017) 38:705–18. doi: 10.1016/j.it.2017.06.009
 110. Andonegui G, Trevani AS, López DH, Raiden S, Giordano M, Geffner JR. Inhibition of human neutrophil apoptosis by platelets. *J Immunol*. (1997) 158:3372–7.
 111. Brunetti M, Martelli N, Manarini S, Mascetra N, Musiani P, Cerletti C, et al. Polymorphonuclear leukocyte apoptosis is inhibited by platelet-released mediators, role of TGF β -1. *Thromb Haemost*. (2000) 84:478–83. doi: 10.1055/s-0037-1614048
 112. Garlachs CD, Eskafi S, Cicha I, Schmeisser A, Walzog B, Raaz D, et al. Delay of neutrophil apoptosis in acute coronary syndromes. *J Leukoc Biol*. (2004) 75:828–35. doi: 10.1189/jlb.0703358
 113. Lang D, Dohle F, Terstesse M, Bangen P, August C, Pauels H-G, et al. Down-regulation of monocyte apoptosis by phagocytosis of platelets: involvement of a caspase-9, caspase-3, and heat shock protein 70-dependent pathway. *J Immunol*. (2002) 168:6152–8. doi: 10.4049/jimmunol.16.8.6152
 114. Gatica D, Lahiri V, Klionsky DJ. Cargo recognition and degradation by selective autophagy. *Nat Cell Biol*. (2018) 20:233–42. doi: 10.1038/s41556-018-0037-z
 115. Chrysanthopoulou A, Mitroulis I, Apostolidou E, Arelaki S, Mikroulis D, Konstantinidis T, et al. Neutrophil extracellular traps promote differentiation and function of fibroblasts. *J Pathol*. (2014) 233:294–307. doi: 10.1002/path.4359
 116. Crooks MG, Fahim A, Naseem KM, Morice AH, Hart SP. Increased platelet reactivity in idiopathic pulmonary fibrosis is mediated by a plasma factor. *PLoS ONE*. (2014) 9:e111347. doi: 10.1371/journal.pone.0111347
 117. Lavrik IN. Caspases: pharmacological manipulation of cell death. *J Clin Invest*. (2005) 115:2665–72. doi: 10.1172/JCI26252

Conflict of Interest Statement: The authors declare that the research was conducted in the absence of any commercial or financial relationships that could be construed as a potential conflict of interest.

Copyright © 2019 Ribeiro, Migliari Branco and Franklin. This is an open-access article distributed under the terms of the Creative Commons Attribution License (CC BY). The use, distribution or reproduction in other forums is permitted, provided the original author(s) and the copyright owner(s) are credited and that the original publication in this journal is cited, in accordance with accepted academic practice. No use, distribution or reproduction is permitted which does not comply with these terms.



Macrophages Down-Regulate Gene Expression of Intervertebral Disc Degenerative Markers Under a Pro-inflammatory Microenvironment

Ana J. Silva^{1,2}, Joana R. Ferreira^{1,2,3}, Carla Cunha^{1,2}, João V. Corte-Real^{1,2,4}, Mafalda Bessa-Gonçalves^{1,2,3}, Mario A. Barbosa^{1,2,3}, Susana G. Santos^{1,2,3} and Raquel M. Gonçalves^{1,2,3*}

¹ I3S – Instituto de Investigação e Inovação em Saúde, Porto, Portugal, ² INEB – Instituto de Engenharia Biomédica, Porto, Portugal, ³ ICBAS – Instituto de Ciências Biomédicas Abel Salazar, Universidade do Porto, Porto, Portugal, ⁴ FCUP – Faculdade de Ciências da Universidade do Porto, Porto, Portugal

OPEN ACCESS

Edited by:

Barbara Bottazzi,
Milan University, Italy

Reviewed by:

Sibylle Grad,
AO Foundation, Switzerland
Cristina Sobacchi,
Italian National Research Council
(CNR), Italy

*Correspondence:

Raquel M. Gonçalves
raquelg@ineb.up.pt

Specialty section:

This article was submitted to
Molecular Innate Immunity,
a section of the journal
Frontiers in Immunology

Received: 03 April 2019

Accepted: 17 June 2019

Published: 03 July 2019

Citation:

Silva AJ, Ferreira JR, Cunha C, Corte-Real JV, Bessa-Gonçalves M, Barbosa MA, Santos SG and Gonçalves RM (2019) Macrophages Down-Regulate Gene Expression of Intervertebral Disc Degenerative Markers Under a Pro-inflammatory Microenvironment. *Front. Immunol.* 10:1508. doi: 10.3389/fimmu.2019.01508

Low back pain is a highly prevalent clinical problem and intervertebral disc (IVD) degeneration is now accepted as the major pathophysiological mechanism responsible for this condition. Accumulating evidence suggests that inflammation plays a crucial role in the progression of human IVD degeneration, with macrophages being pointed as the key immune cell players in this process since their infiltration in degenerated IVD samples has been extensively demonstrated. Since they are highly plastic, macrophages can play different roles depending on the microenvironmental cues. The study of inflammation associated with IVD degeneration has been somehow neglected and one of the reasons is related with lack of adequate models. To overcome this, we established and characterized a new model of IVD organ culture under pro-inflammatory conditions to further dissect the role of macrophages in IVD associated immune response. For that, human monocyte-derived macrophages were co-cultured either with bovine caudal IVD punches in the presence of the pro-inflammatory cytokine IL-1 β , or IVD-conditioned medium (CM), to investigate how IVD-produced factors influence macrophage phenotype. After 72 h, metabolic activity, gene expression and cytokine profile of macrophages and IVD cells were measured. Our results show that macrophages and IVDs remain metabolically active in the presence of IL-1 β , significantly upregulate CCR7 gene expression and increase production of IL-6 on macrophages. When treating macrophages with IL-1 β -IVD-CM, CCR7 upregulation follows the same trend, while for IL-6 an opposite effect was observed. On the other hand, macrophages interfere with IVD ECM remodeling, decreasing MMP3 expression and downregulating aggrecan and collagen II gene expression in the presence of IL-1 β . Overall, the co-culture model established in this study can be considered a suitable approach to address the cellular and molecular pathways that regulate macrophage-IVD crosstalk, suggesting that degenerated IVD tissue tends to polarize human macrophages toward a more pro-inflammatory profile, which seems to aggravate IVD degeneration. This model could be used to improve the knowledge of the mechanisms that link IVD degeneration and the immune response.

Keywords: intervertebral disc, inflammation, tissue regeneration, organ culture, ex vivo model

INTRODUCTION

Low back pain (LBP) is a common clinical problem affecting about 70–85% of the world population (1). The efficacy of the current clinical solutions is limited by our lack of understanding of the LBP pathomechanism, however it is accepted that the pain associated with intervertebral disc (IVD) degeneration, without evident signs of nerve compression, is the main cause of chronic LBP (40% of the cases) (2). Although IVD degeneration is a complex and multifactorial process, it is known to involve the loss of proteoglycans and water content in nucleus pulposus (NP), the central gelatinous tissue of IVD, with up-regulation of metalloproteinases (MMPs) and inflammatory mediators (3). These molecules can be produced by both IVD cells or immune cells, such as macrophages (4–6). Macrophages were identified in human herniated IVD samples in several studies, associated with increased disc degeneration (5, 7–9), but they are also suggested to have an important role in the spontaneous hernia regression, a rare event occurring in some LBP patients (10). These immune cells are also implicated in non-herniated IVD degeneration, although this topic remains poorly understood (5, 11–13). Recent studies demonstrated that macrophages are the only type of inflammatory cells infiltrated in the degenerated NP tissue and this is correlated with disease progression (12). These results are in accordance with the conclusions of Nakazawa et al. but specifically in non-herniated discs (13). Thus, on one side macrophages have been associated with a higher inflammatory response and increased levels of IVD degeneration, while on the other side, they have also been linked to the phenomenon of spontaneous hernia regression. These apparent controversial results can be explained by the high plasticity of macrophages, that can express different functional profiles in response to distinct environmental cues, from the classic pro-inflammatory M1 to a more pro-regenerative M2 phenotype.

It is clear that the inflammatory microenvironment created by macrophages and IVD cells plays an important role during IVD degeneration. However, there is a need to deepen the knowledge of the mechanisms that link degeneration of IVD and the immune response.

There is a lack of adequate models to study inflammation within IVD degeneration. Most of the *in vitro* studies conducted so far rely on 2D co-cultures of IVD or NP cells and macrophages. Most of the 2D culture systems do not mimic the harsh, hypoxic and degenerative IVD 3D microenvironment and impair IVD cells to produce native IVD extracellular matrix (ECM) (14). Additionally, the currently used *in vivo* models do not mimic the natural process of human IVD degeneration. Thus, *ex vivo* organ culture models not only allow the study of IVD degeneration in a more physiologically relevant environment than cell models, but also reduce the costs and ethical issues of *in vivo* experiments (15). For explant experiments IVDs can be isolated from different species. Although IVDs should ideally be isolated from human tissue, this material is difficult to obtain because of ethical and government regulatory restrictions and it is not very abundant. Alternatively, bovine IVD has been proposed as a suitable biological and biomechanical model for studying human disc disorders, since it is easily available

and shows high similarities with human samples in terms of size, mechanical loading, composition, cell phenotype and distribution (15, 16). Our group has previously established an *ex vivo* proinflammatory/degenerative IVD organ culture model to be used as a more physiological model for drug and cell therapies screening (17). This model was successfully used to study anti-inflammatory nanoparticles (18) and the regenerative and immunomodulatory role of mesenchymal stem cells in IVD (19).

The models of IVD degeneration used so far often lack the presence of macrophages and if present, they are usually derived from mouse or immortalized cell lines, which are not completely representative of human macrophages since they have different gene expression profiles (20). By using monocyte-derived macrophages from human peripheral blood in this study, we adopted a more accurate model to study macrophage polarization *in vitro*, but in a context that resembles the *in vivo* conditions.

In the current work, we propose to study the macrophage crosstalk with IVD in a 3D IVD organ culture with associated human macrophage/immune response in pro-inflammatory conditions.

MATERIALS AND METHODS

Human Primary Monocyte Isolation and Differentiation

Human primary monocytes were obtained from buffy coats of healthy blood donors, after informed consent and ethical approval of Centro Hospitalar S. João, as previously described by Oliveira et al. (21). Briefly, buffy coats were centrifuged at room temperature (RT) for 20 min at 1,200 g, without active acceleration or brake, for blood components separation. Peripheral blood mononuclear cell (PBMC) layer was collected and incubated with RosetteSep human monocyte enrichment isolation kit (StemCell Technologies) for 20 min, under gentle mixing, according to the manufacturer's instructions. The mixture was then diluted at a 1:1 ratio with 2% fetal bovine serum (FBS, Biowest) in phosphate buffered saline (PBS), gently layered over Histopaque-1077 (Sigma) and centrifuged as described above. The enriched monocyte layer was collected, and washed with PBS for platelet depletion, by centrifugation at 97 g for 17 min. Recovered monocytes were seeded on 6-well transwell cell culture inserts (Corning, Cat. No. 353102) at a density of 5×10^5 cells/transwell. For monocyte-macrophage differentiation, cells were cultured in RPMI1640 medium (with GlutaMax) (Invitrogen) supplemented with 10% FBS (Biowest), 1% penicillin-streptomycin (P/S, Invitrogen) (macrophage culture medium), in the presence of 50 ng/mL of macrophage colony-stimulating factor (M-CSF, Immunotools). Cells were maintained in a humidified incubator, at 37°C and 5% CO₂. After 7 days, cell culture medium was replaced without M-CSF renewal.

Bovine IVD Tissue Isolation and Culture

Bovine IVD tissue was isolated from tails of young animals (~12 months old) from a local slaughterhouse, immediately

after animals sacrifice, accordingly with ethical approval from the national veterinary authorities. Caudal discs were isolated and cultured as previously described (17). Briefly, standardized disc punches (with diameter of 9 mm) were collected with NP in the center and few surrounding annulus fibrosus (AF) and maintained for 4 days in 6-well tissue culture plates, with transwell cell culture inserts and 0.46 MPa static loading. The constraining effect on IVDs organ cultures has been previously described (17) and the weight used for simulation of static loading was optimized to corresponds to physiological loads during standing phase (22). IVDs were cultured in Dulbecco's Modified Eagle's Medium with low glucose (DMEM, Invitrogen), supplemented with 5% FBS (Biowest), 1% penicillin/streptomycin (Invitrogen), 0.5% fungizone (Invitrogen) and with the osmolarity adjusted to IVD-physiological 400 mOsm by addition of 1.5% of a 5 M NaCl/0.4 M KCl solution (IVD culture medium) (0.030 ± 0.007 ml/mg tissue). Samples were incubated at reduced oxygen atmosphere (37°C , 6% O_2 and 8.5% CO_2) and saturated humidity. Culture medium was replaced on the day after IVD isolation. In order to create a proinflammatory environment in some conditions, 4 days after IVD isolation, IVDs were needle-punctured (21G), medium was renewed (5 ml) and supplemented with 10 ng/mL of recombinant human IL-1 β (PeproTech), and 3 h later, the co-culture with macrophages was performed. After the proinflammatory stimuli some of the discs were left in culture for additional 2 days in order to produce IVD conditioned media (IVD-CM). IVD-CM were centrifuged at 900 g for 5 min at 4°C and stored at -20°C until use.

Establishment of Macrophage-IVD Co-cultures

Ten days after monocyte isolation and 4 days after IVD isolation the transwells containing macrophages were transferred to the plates where IVDs were previously cultured. The permeable PET membrane of 1 μm pore size avoided macrophages to cross from the top to the lower compartment, allowing however the exchange of soluble factors between macrophages and IVDs. The co-cultures were maintained for 3 days in 5 ml of culture medium in a 1:1 proportion of macrophage medium and IVD medium and incubated at reduced oxygen atmosphere (37°C , 6% O_2 and 8.5% CO_2) and saturated humidity. Some conditions were supplemented with 10 ng/mL IL-1 β . The experimental setup and respective conditions are schematically presented in Figure 1.

Macrophage Treatment With IVD-CM

Ten days after monocyte isolation macrophages were cultured in 5 ml of culture medium a 1:1 proportion of macrophage culture medium and IVD-CM, respecting the same volume/cells ratio that in macrophage-IVD co-cultures, and incubated at reduced oxygen atmosphere (37°C , 6% O_2 and 8.5% CO_2) and saturated humidity for additional 3 days.

Macrophage and IVD Metabolic Activity

The IVD and macrophage metabolic activity was determined through resazurin reduction assay. Briefly, after macrophage-IVD co-culture, the transwells containing macrophages were

transferred to another plate. Both, IVDs and macrophages were separately incubated with resazurin redox dye (0.01 mg/mL) (Sigma-Aldrich) for 4 h at reduced oxygen atmosphere (37°C , 6% O_2 and 8.5% CO_2) and saturated humidity. Fluorescence intensity was measured (530 nm Ex/590 nm Em) using the multi-mode microplate reader Synergy MX (BioTek). Data is presented in percentage relative to control macrophages or control IVD.

Macrophage Surface Marker Expression

Macrophages were incubated with PBS-EDTA at room temperature during 20 min and harvested by gently scrapping. Cells were washed and resuspended in FACS buffer (PBS, 2% FBS, 0.01% sodium azide) containing appropriate conjugated antibodies, and stained in the dark for 30 min at 4°C . Macrophages were immunostained with the following antibodies: anti-human CD14-APC (clone MEM-18), CD86-FITC (clone BU63) (both immunotools) and CD163-PE (clone GHI/61) (R&D Systems). To define background staining isotype matched antibodies were used as negative controls. After additional washing steps, cells were acquired on a FACS Canto Flow Cytometer (BD Biosciences) with BD FACSDiva software. Results were analyzed using FlowJo software version 10 (TreeStar, Inc.).

Total RNA Isolation and Reverse Transcription for qPCR

Total RNA was isolated from macrophages and IVD cells using TRIzol reagent (Invitrogen) following manufacturer's instructions. For obtaining IVD cells, the IVD tissue samples were previously dissected into 2–3 mm³ fragments and enzymatically digested for 1 h in 2 mg/mL pronase E (Sigma-Aldrich) in DMEM, under slow stirring, reduced oxygen atmosphere (37°C , 6% O_2 and 8.5% CO_2) and saturated humidity. Cells were collected by centrifugation at 400 g for 10 min and washed twice with cold PBS using the same centrifugation settings. For IVD cells only, for more efficient RNA recovery, after the addition of isopropanol, the RNA extraction was carried out using the ReliaPrep RNA Cell Miniprep System (Promega), according to manufacturer's instructions. Total RNA was quantified by Nanodrop (Thermo Fisher). Complementary DNA (cDNA) was obtained through the High-capacity cDNA reverse transcription kit (Applied Biosystems), according to the manufacturer's instructions.

Quantitative Real-Time Polymerase Chain Reaction (qPCR)

Macrophage gene expression was assessed using TaqMan Gene Expression Master Mix and TaqMan Gene Expression Assays (Applied Biosystems), namely: C-C chemokine receptor type 7 (CCR7): Hs1013469_m1; tumor necrosis factor alpha (TNF- α): Hs00174128_m1; cluster of differentiation 163 (CD163): Hs00174705_m1; matrix metalloproteinase 7 (MMP7): Hs01042796_m1; and glyceraldehyde 3-phosphate dehydrogenase (GAPDH): Hs99999905_m1, as a reference gene.

Regarding IVD gene expression, iQTM SYBR[®] Green Supermix (Bio-Rad) was used and the analysis was carried out as before (17). Briefly, specific primer pairs were designed for

bovine interleukin 6 (IL-6), IL-8, aggrecan (ACAN), collagen II (COLII), MMP3, and GAPDH and synthesized by Thermo Fisher Scientific.

Quantitative polymerase chain reaction (qPCR) was carried out in an iQ5 Real-Time PCR Detection System (Bio-Rad Laboratories).

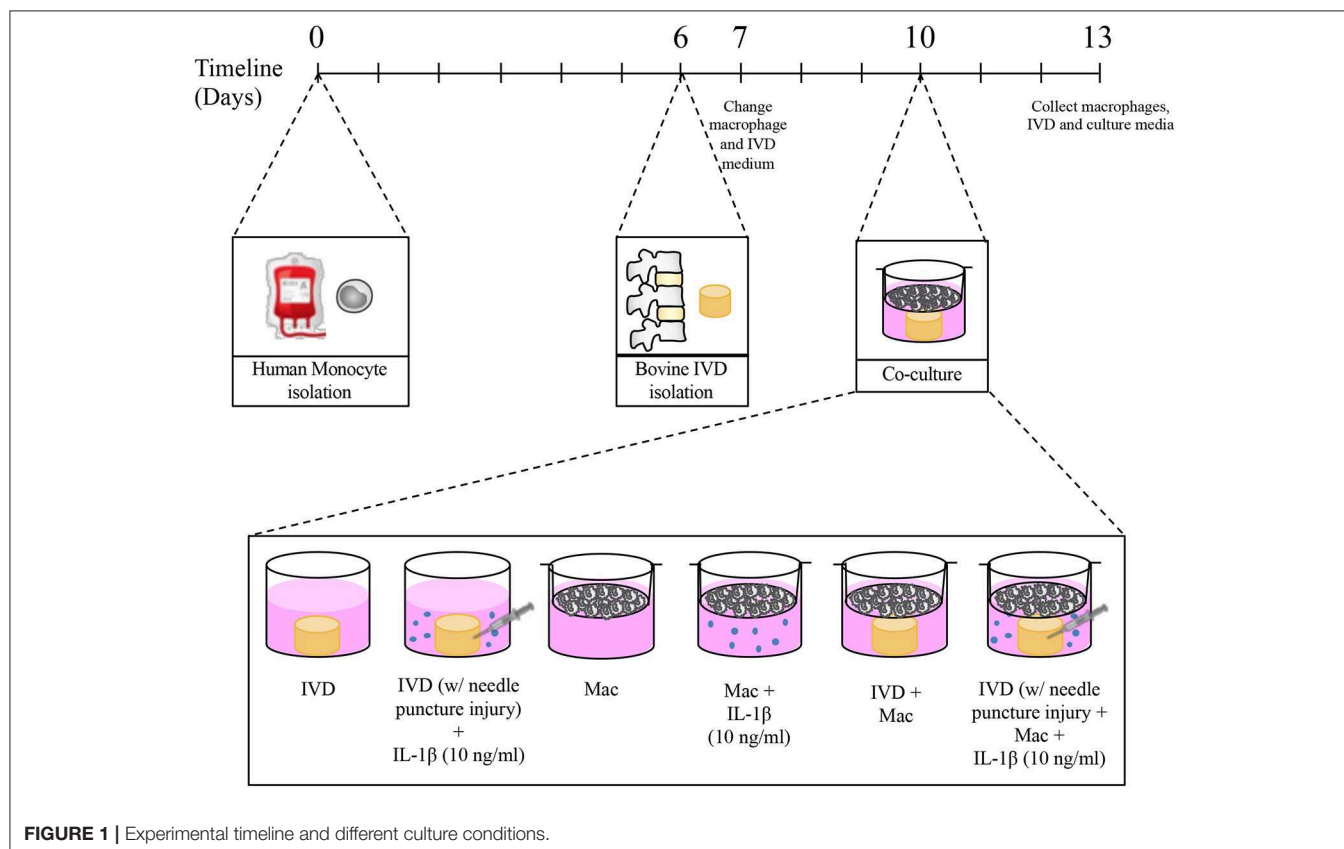
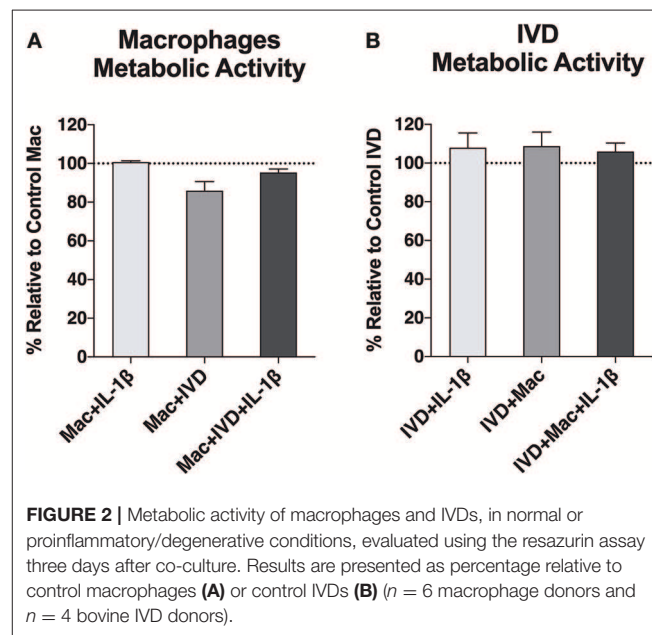
Relative gene expression levels were calculated using the quantification cycle (Cq) method, according to Livak and Schmittgen (23). Gene expression levels were presented as $2^{-\Delta C_t}$, where the average C_t value of each sample was normalized to the house-keeping gene GAPDH [$\Delta C_t = C_{t(\text{gene of interest})} - C_{t(\text{GAPDH})}$]. Normalized values of samples collected at the end of the experiments were compared with the control and between the different experimental groups.

Enzyme-Linked Immunosorbent Assay (ELISA)

Culture medium collected at day 13 was centrifuged (3,000 rpm, 5 min) and kept at -20°C for posterior analysis. Human IL-6, TNF- α , IL-8, monocyte chemoattractant protein 1 (MCP-1) and vascular endothelial growth factor (VEGF) were quantified by ELISA (Human Standard TMB ELISA Development Kits, PeproTech) according to manufacturer's instructions. Cytokine and VEGF concentrations (pg/mL) were determined using a standard calibration curve.

Statistical Analysis

Statistical analysis was performed using GraphPad Prism version 7 (GraphPad Software, Inc.) to evaluate significant differences



between the different samples. For macrophage data non-parametric Friedman Test was used, followed by Dunn's multiple comparison test. For IVD data, non-parametric unpaired Kruskal-Wallis test was used followed by Dunn's multiple comparison test. Statistical significance was considered for $p < 0.05$ (* $p < 0.05$, ** $p < 0.01$, *** $p < 0.001$).

RESULTS

Macrophages and IVD: Establishment of the Organ Culture

First, we investigated whether macrophage viability would be affected by the proinflammatory/degenerative IVD environment and whether IVDs viability would be compromised by the presence of macrophages. Macrophages differentiated from primary monocytes upon 10 days (7 days with M-CSF+3 days without M-CSF) were used. Macrophage differentiation was confirmed by the high level of CD14 expression (see **Supplementary Data**). Macrophage metabolic activity was assessed through resazurin assay (**Figure 2A**). The results showed that mitochondrial metabolic activity of macrophages was not affected when IL-1 β was added to the media, but slightly decreased when macrophages were co-cultured with IVD in the absence of pro-inflammatory stimuli. We did not observe the same effect in the presence of IVD and IL-1 β . IVDs metabolic activity was not altered by the presence of macrophages (**Figure 2B**).

Impact of IVD Organ Culture on Macrophage Gene Expression Profile

Macrophage profile in the presence of IVD organ cultures was evaluated by gene expression of two pro-inflammatory markers (hCCR7 and hTNF- α), one anti-inflammatory marker (hCD163) and one MMP (hMMP-7) after 3 days of co-culture with IVD (**Figure 3A**). In the presence of the proinflammatory/degenerated IVD organ culture, a significant ($p < 0.001$) upregulation of hCCR7 gene expression in macrophages was observed, that did not occur in basal conditions, in presence of IL-1 β or in presence of IVD by itself (**Figure 4A**). Regarding hTNF- α and hCD163 genes, no statistical difference was observed between the groups (**Figure 3A**). When macrophages were in the presence of (IVD+IL-1 β)-CM, the same tendency of hCCR7 upregulation was observed, however without reaching statistical significance ($p = 0.057$) (**Figure 3B**). Contrarily to what was observed in the presence of IVD, when macrophages were cultured with CM, hTNF- α gene expression was significantly up-regulated ($p < 0.01$) in presence of (IVD+IL-1 β)-CM, reinforcing the differentiation of macrophages toward a more proinflammatory phenotype (**Figure 3B**). Regarding hMMP-7 gene expression it was up-regulated in IL-1 β -treated macrophages compared with basal conditions (**Figure 4B**, $p = 0.052$) and was significantly down-regulated in presence of (IVD+IL-1 β)-CM ($p < 0.05$) compared with IL-1 β treatment of macrophages, suggesting that despite IL-1 β inducing this MMP gene expression in macrophages, the IVD produces molecules that can inhibit this upregulation (**Figure 3B**). In addition,

surface marker expression for M1 (CD86) and M2 (CD163) markers was evaluated by flow cytometry, however no significant differences were observed between the different conditions tested (see **Supplementary Data**).

Impact of IVD Organ Culture on Macrophage Cytokine Production Profile

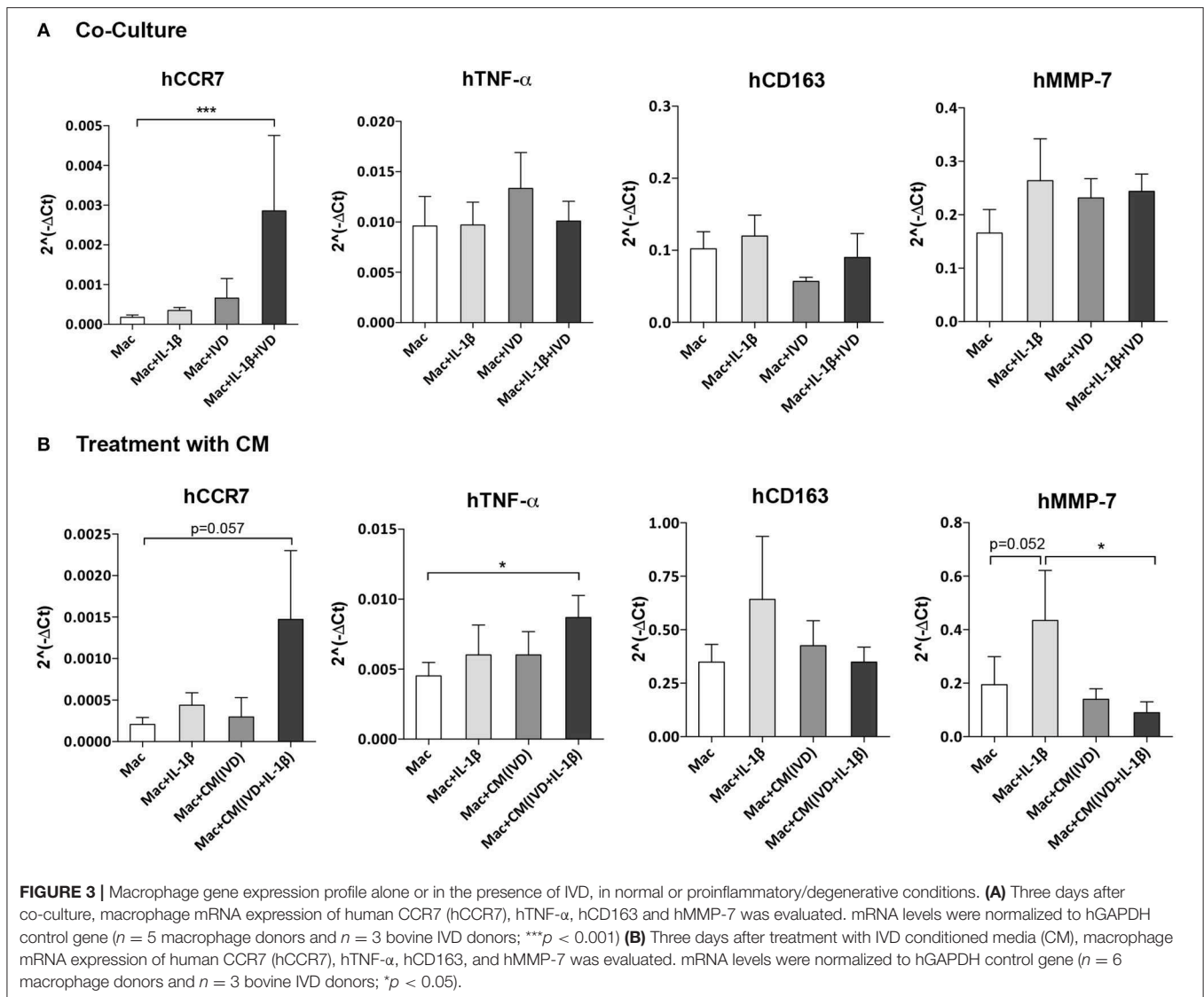
To further evaluate the modulation of macrophage phenotype by IVD, human cytokine production was analyzed by ELISA, in macrophage co-cultures with IVD (**Figure 4A**) and with IVD-CM (**Figure 4B**). As expected, macrophages produced higher levels of hIL-6 ($p = 0.062$), hTNF- α ($p < 0.01$) and hIL-8 ($p = 0.052$) when treated with IL-1 β (**Figures 4A,B**). Control groups with bovine IVD cultures were performed, demonstrating cytokines species specificity. However, when in presence of the proinflammatory/degenerated IVD, hIL-6 levels were significantly higher ($p < 0.05$) (**Figure 4A**), which was not observed when macrophages were treated with (IVD+IL-1 β)-CM, suggesting that the crosstalk between macrophages and IVD is crucial for the production of this pro-inflammatory cytokine (**Figure 4B**). Surprisingly, the trend observed for increased levels of hTNF- α gene expression in the presence of (IVD+IL-1 β)-CM (**Figure 3B**), was not confirmed at the protein level (**Figure 4B**), suggesting some post-transcription regulation affecting protein production. Regarding hIL-8 and hMCP-1 no differences were observed in the presence of the different groups or in the presence of IVD-CM (**Figures 4A,B**).

Influence of Macrophages on IVD Cells Gene Expression Profile

The crosstalk between IVD and macrophages was also evaluated by assessing how macrophages influence IVD cells gene expression (**Figure 5**). Selection of bovine genes was performed based on our previous work (17). Both bIL-6 ($p < 0.01$), bIL-8 ($p < 0.05$) and bMMP-3 ($p < 0.01$) were significantly upregulated in the proinflammatory/degenerated IVD model, while bACAN and bCOLII were reduced, comparatively to the normal IVD (**Figure 5**), confirming what was previously reported (17). However, when macrophages were added to the proinflammatory/degenerated IVD model, bIL-6, bIL-8, and bMMP-3 were reduced (**Figure 5**), suggesting that macrophages reduced the pro-inflammatory profile and ECM remodeling proteases by IVD cells in the presence of IL-1 β . Regarding the expression of ECM components by IVD cells, macrophages contribute to decrease bACAN ($p = 0.09$) and bCOLII ($p < 0.05$) in proinflammatory/degenerative conditions (**Figure 5**). bACAN was even down-regulated in IVD in the presence of macrophages in basal conditions ($p < 0.05$) (**Figure 5**).

Influence of Macrophages on IVD Production of Angiogenic Factors

Increased angiogenesis is one of the phenomena associated with IVD degeneration (24). To evaluate if macrophages can influence the angiogenesis in the IVD microenvironment, the supernatants of macrophages/IVD co-cultures were tested for



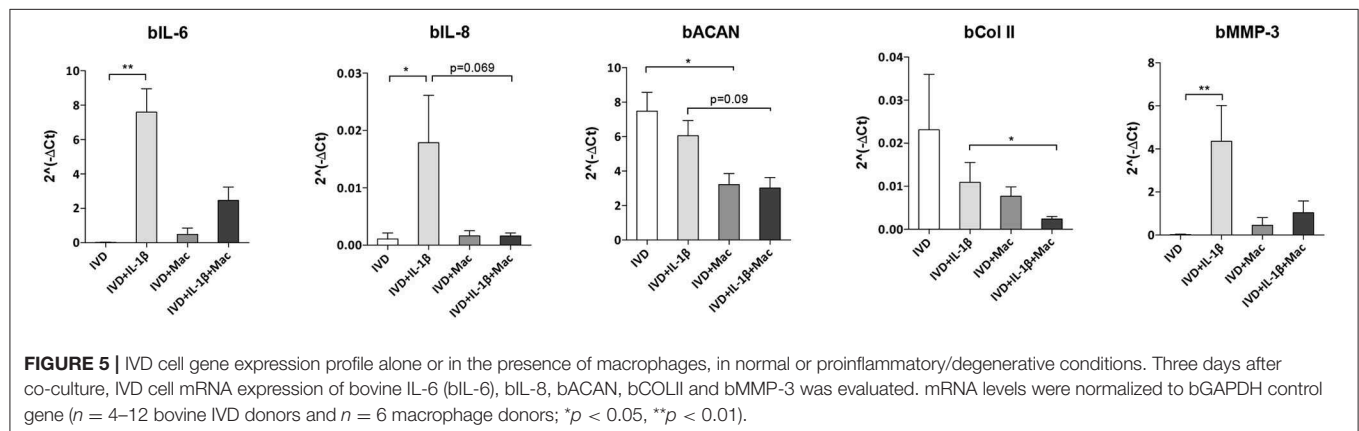
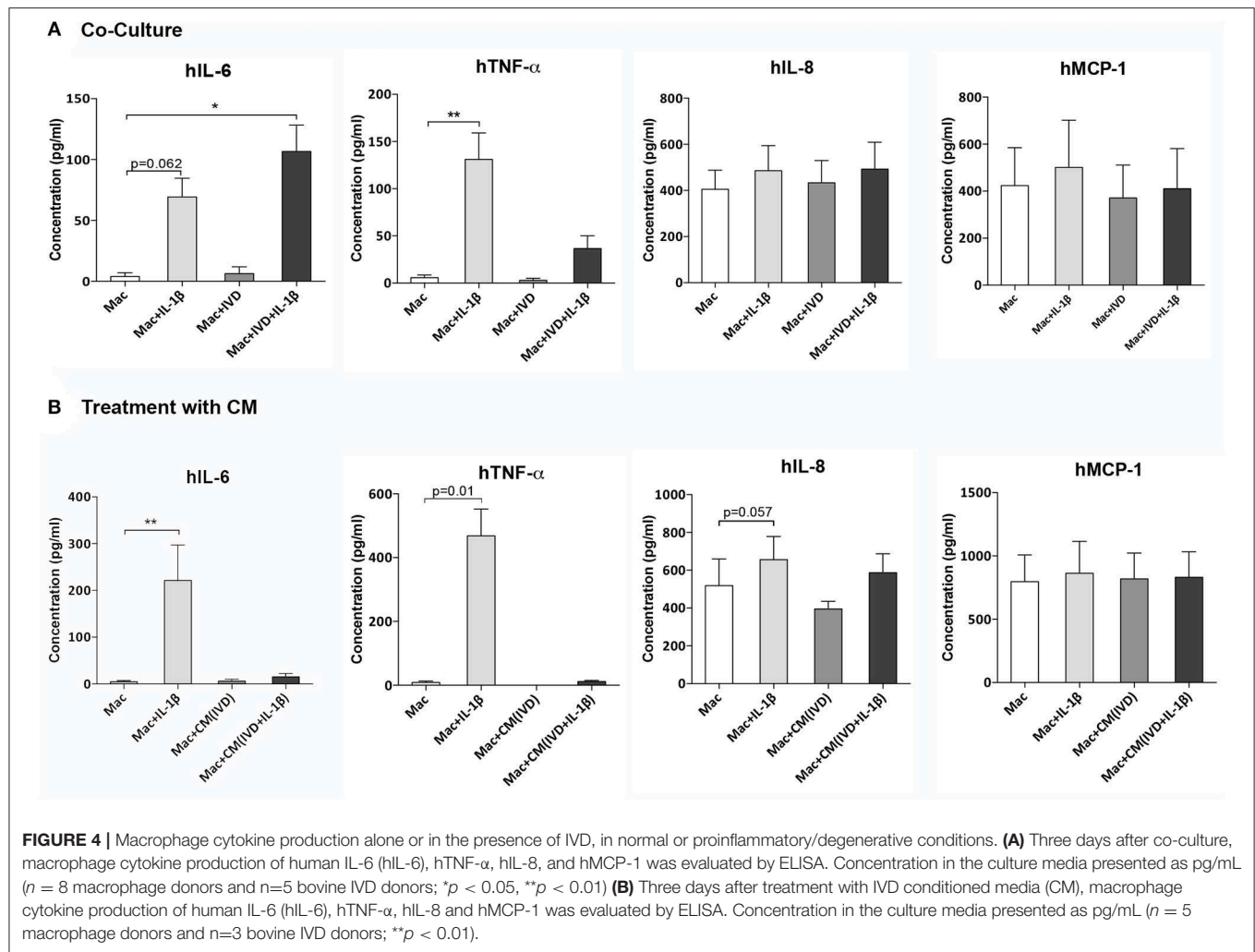
VEGF presence by ELISA (Figure 6). Our results show that macrophages did not produce VEGF either in basal conditions or in the presence of IL-1β. VEGF is mainly produced by IVD, both in normal or proinflammatory/degenerated conditions, with a slight tendency of increased VEGF production by IVD in the presence of IL-1β (Figure 6). When in co-culture, the presence of macrophages seems to increase VEGF production, however without statistical significance (Figure 6). When macrophages are treated with IVD-CM there is a decrease in VEGF levels, when compared to IVD alone ($p = 0.1$), which is not observed when they are treated with (IVD+IL-1β)-CM where the decrease in VEGF levels is not so accentuated (Figure 6). These observations suggest that macrophages consume more VEGF in normal vs. proinflammatory/degenerated cultured conditions or that in the presence of (IVD+IL-1β)-CM they are consuming VEGF but also producing it. This result indicates that macrophages may act as pro-vascularization mediators within IVD microenvironment.

DISCUSSION

This study investigates the crosstalk between IVD and macrophages during the process of IVD degeneration. This work is of pivotal importance given the need of adequate models to study the interaction between inflammation and IVD degeneration. Whilst the use of *ex vivo* animal models will not preclude the use of human tissue or *in vivo* models, they may be able to clarify some crucial questions, reducing study costs and ethical concerns (15).

For that purpose, we complexed a proinflammatory/degenerative bovine IVD *ex vivo* model, which had been formerly validated (17), to include human macrophages. These immune cells have been pointed as key players in the process of degeneration-associated pain and hernia resorption (8, 10, 12, 13).

Macrophage mitochondrial function was evaluated using the resazurin reduction assay. Our results evidenced that



macrophages and IVD are both metabolically active in co-culture. Metabolic activity slightly decreased when macrophages were in co-culture with IVD in the absence of pro-inflammatory stimuli. This could be a consequence of alterations in macrophage profile. For example, it has been reported that

M1 and M2 macrophages exhibit distinct metabolic profiles (25, 26). In M1 macrophages, aerobic glycolysis is induced upon activation, which involves an increase in glucose uptake as well as the conversion of pyruvate to lactate, while M2 macrophages obtained their energy from fatty acid oxidation and

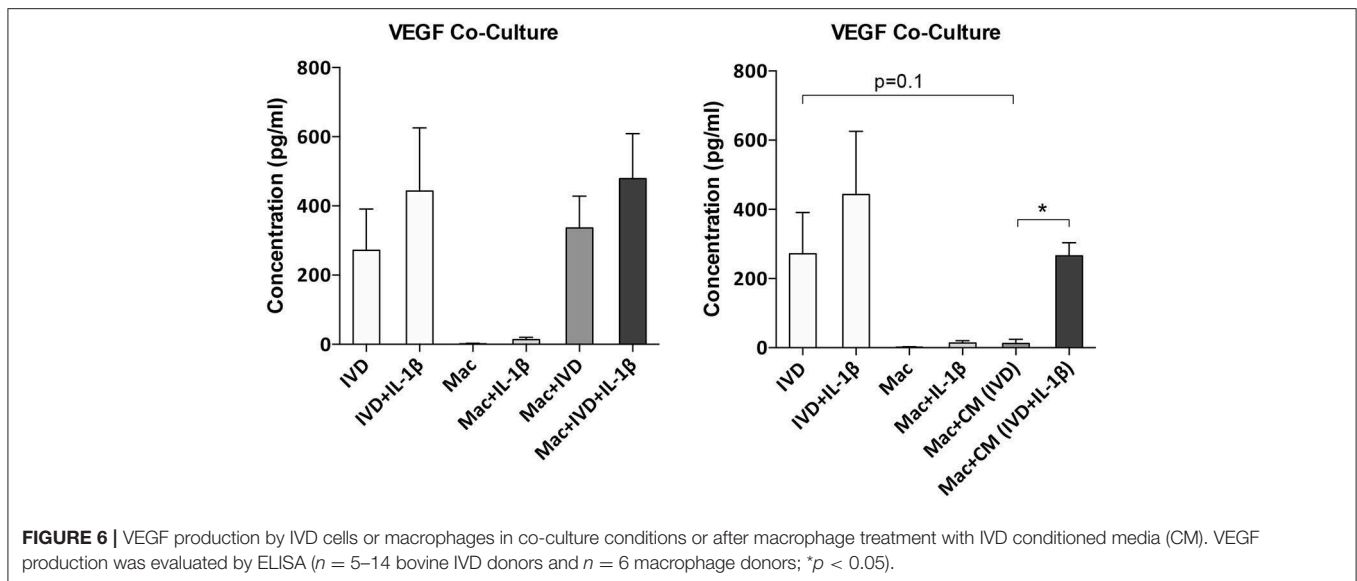


FIGURE 6 | VEGF production by IVD cells or macrophages in co-culture conditions or after macrophage treatment with IVD conditioned media (CM). VEGF production was evaluated by ELISA ($n = 5-14$ bovine IVD donors and $n = 6$ macrophage donors; $*p < 0.05$).

oxidative metabolism, which can be sustained for longer periods (25). Thus, M1 macrophages were demonstrated to display enhanced glycolytic metabolism and reduced mitochondrial activity and M2 macrophages show high mitochondrial oxidative phosphorylation (27). Although these metabolic differences between differentially activated macrophages are widely accepted, how the cell's metabolic status regulates polarization and which are the mechanisms responsible for switching the metabolic profile between different phenotypes remains to be understood.

Resazurin is internalized by cells and metabolically reduced to the highly fluorescent pink compound resorufin, that is freely released from cells in a process mediated by intracellular diaphorase enzymes. Resazurin conversion has been linked to mitochondrial activity, where oxidative phosphorylation occurs. Therefore, our resazurin results suggest slightly lower levels of oxidative phosphorylation in macrophages cultured with IVD, but not with IVD+IL1 β , suggesting a higher level of M2 macrophages in the presence of healthy IVD, which was not confirmed by CD163 expression.

Furthermore, in this proinflammatory/degenerative IVD model, macrophages seem to exhibit a more proinflammatory profile, expressing higher amounts of CCR7 and producing more IL-6. CCR7, a typical macrophage proinflammatory marker, was also upregulated in human samples of degenerated IVD in herniated samples, as reported by Nakazawa and colleagues in non-herniated IVD, in the NP region (13). This is also in accordance with another study showing that macrophages in degenerated IVD samples expressed high levels of iNOS and CD86, two pro-inflammatory markers (12). Macrophages treated with CM from NP cells of degenerated samples have also shown an upregulation of the levels of iNOS (12). Moreover, Takada et al. demonstrated that the levels of IL-6 were increased in a co-culture model of rat IVD and macrophages and that most IL-6 producing cells were macrophages (28). Using

the same co-culture model, they found that IVD-macrophage interaction induced an early upregulation of TNF- α , followed by upregulation of IL-6, IL-8, and PGE₂ (29). We did not observe this increase of TNF- α in our co-culture system and this might be due to the different time points used since they have also described that the levels of this cytokine decreased after 6 h of co-culture (29).

Concerning the influence of macrophages on IVD cell phenotype, our results showed that the levels of IL-6 and IL-8 were increased in IVD cells when they were treated with IL-1 β , as showed before (17). Indeed, the levels of these cytokines in disc tissue from patients with LBP were significantly higher than in tissue from patients undergoing discectomy for sciatica (4). Nonetheless, macrophages seem to contribute to a less proinflammatory profile of native IVD cells under proinflammatory/degenerative conditions since there is an apparent decrease, although not statistically significant, of IL-6 and IL-8 in IVD cells when macrophages are added to the system. Interestingly, this effect was observed before using the same system with MSCs. While MSCs demonstrated a more proinflammatory profile in co-culture with the proinflammatory/degenerative IVD model, they also contributed to a less proinflammatory profile of native IVD cells (19).

Concerning MMP-3 levels, they were significantly upregulated in IVD cells in the presence of IL-1 β , however this upregulation is not observed when macrophages are added to this system, suggesting that macrophages are impairing the expression of this matrix remodeling agent. Haro et al. observed a marked enhancement of MMP-3 protein and mRNA in chondrocytes after exposure to macrophages in a co-culture model (30). This divergence with our results may be due to the differences between study models (murine vs. bovine/human) and/or the culture stimulation with IL-1 β . In another study, Haro et al. concluded that the generation of soluble TNF- α by macrophages

was essential for the induction of MMP-3 in disc co-cultures (31). Interestingly, our protein levels of TNF- α produced by macrophages were decreased when they were in the presence of IVD + IL-1 β , comparatively to when they were treated with IL-1 β alone, which can be linked to the low expression of MMP-3 by IVD cells in the presence of macrophages in proinflammatory/degenerative conditions.

Regarding ECM production by IVD cells, we observed a decrease in the gene expression levels of both ACAN and COLII in the presence of macrophages, suggesting that macrophages in pro-inflammatory conditions contribute to aggravate the loss of native ECM components of healthy IVD.

We also evaluated the levels of VEGF in the supernatants of co-cultures and when macrophages were treated with CM to better understand if macrophages can influence angiogenesis in the IVD microenvironment. Our results demonstrated that this pro-angiogenic growth factor seems to be mainly produced by IVD cells. Nonetheless, the levels of VEGF decrease when macrophages were treated with IVD-CM comparatively to IVD alone, and this accentuated reduction was not observed when they were treated with (IVD+IL-1 β)-CM. This result suggests that VEGF can be consumed in higher amounts in healthy comparatively to proinflammatory/degenerative IVD or, that macrophages start to produce VEGF in these conditions, which overall demonstrates that these cells can contribute to a more pro-vascularization microenvironment. However, angiogenesis is a highly complex process, involving several factors. In the future, the evaluation of the expression of other angiogenesis-related factors and an angiogenesis functional assay will be conducted.

This model can be a new tool to address the role of macrophages in IVD degeneration, which is somehow neglected in the literature, although might be limited in the analysis of the immune cell response to a tissue from different species. Nevertheless, the analysis of human macrophage response to bovine IVD tissue in two different scenarios, healthy vs. pro-inflammatory/degenerative conditions, safeguards the conclusions obtained.

Taken together, our results demonstrate a more pro-inflammatory profile of macrophages when they were in presence of proinflammatory/degenerative IVD, which is in concordance with previous findings using human samples (12, 13).

CONCLUSIONS

Overall, the co-culture system established in this study seems to provide a simple and useful model to investigate *in vitro* the interaction between macrophages and IVD. This model can

be a valuable tool to characterize the mechanisms by which macrophages and IVD cells interact during IVD aging and degeneration. By constituting a more refined model of the study of inflammation in degenerated IVD, this model may be used for drug screening before animal experimentation and may provide new targets to LBP.

DATA AVAILABILITY

All datasets generated for this study are included in the manuscript and/or the **Supplementary Files**.

AUTHOR CONTRIBUTIONS

AS, SS, and RG contributed to the study conception and design. AS, JC-R, JF, CC, and MB-G contributed to the acquisition of data. AS and RG contributed to the analysis and interpretation of data and drafted the article. MB, SS, and RG provided the funding for the experiments. All authors have critically revised the article for important intellectual content, and all authors approved the final submitted version.

FUNDING

This work was financed by European Union funds through Bioengineered Therapies for infectious diseases and tissue regeneration (Norte-01-0145-FEDER-000012), Projetos Estruturados de I& D& I - Norte-01-0145-FEDER-000012, Portugal 2020 - FEDER, and through EUROSPINE TRF (2017_05) by the project Disc degeneration-, immune-, and neuro-modulation.

ACKNOWLEDGMENTS

The authors also acknowledge FCT – Fundação para a Ciência e a Tecnologia, in the framework of the FCT Investigator Grant of RMG (IF/00638/2014), CC Junior Research contract (DL 57/2016/CP1360/CT0004) and the Ph.D. grant of JF (PD/BI/128357/2017). The authors would like to thank Serviço de Imunohemoterapia of Centro Hospitalar Universitário de São João (CHUSJ), for kindly donating Buffy Coats.

SUPPLEMENTARY MATERIAL

The Supplementary Material for this article can be found online at: <https://www.frontiersin.org/articles/10.3389/fimmu.2019.01508/full#supplementary-material>

REFERENCES

- Andersson GB. Epidemiological features of chronic low-back pain. *Lancet*. (1999) 354:581–5. doi: 10.1016/S0140-6736(99)01312-4
- DePalma MJ, Ketchum JM, Saullo T. What is the source of chronic low back pain and does age play a role? *Pain Med*. (2011) 12:224–33. doi: 10.1111/j.1526-4637.2010.01045.x
- Sehgal N, Fortin JD. Internal disc disruption and low back pain. *Pain Physician*. (2000) 3:143–57.
- Burke JG, Watson RW, McCormack D, Dowling FE, Walsh MG, Fitzpatrick JM. Intervertebral discs which cause low back pain secrete high levels of proinflammatory mediators. *J Bone Joint Surg Br*. (2002) 84:196–201. doi: 10.1302/0301-620X.84B2.0840196
- Shamji MF, Setton LA, Jarvis W, So S, Chen J, Jing L, et al. Proinflammatory cytokine expression profile in degenerated and herniated human intervertebral disc tissues. *Arthritis Rheum*. (2010) 62:1974–82. doi: 10.1002/art.27444

6. Burke JG, Watson RW, McCormack D, Dowling FE, Walsh MG, Fitzpatrick JM. Spontaneous production of monocyte chemoattractant protein-1 and interleukin-8 by the human lumbar intervertebral disc. *Spine*. (2002) 27:1402–7.
7. Ikeda T, Nakamura T, Kikuchi T, Umeda S, Senda H, Takagi K. Pathomechanism of spontaneous regression of the herniated lumbar disc: histologic and immunohistochemical study. *J Spinal Disord*. (1996) 9:136–40.
8. Rothoerl R, Woertgen C, Holzschuh M, Brehme K, Ruschoff J, Brawanski A. Macrophage tissue infiltration, clinical symptoms, and signs in patients with lumbar disc herniation. A clinicopathological study on 179 patients. *Acta Neurochir*. (1998) 140:1245–8.
9. Koike Y, Uzuki M, Kokubun S, Sawai T. Angiogenesis and inflammatory cell infiltration in lumbar disc herniation. *Spine*. (2003) 28:1928–33. doi: 10.1097/01.BRS.0000083324.65405.AE
10. Cunha C, Silva AJ, Pereira P, Vaz R, Goncalves RM, Barbosa MA. The inflammatory response in the regression of lumbar disc herniation. *Arthritis Res Ther*. (2018) 20:251. doi: 10.1186/s13075-018-1743-4
11. Peng B, Hao J, Hou S, Wu W, Jiang D, Fu X, et al. Possible pathogenesis of painful intervertebral disc degeneration. *Spine*. (2006) 31:560–6. doi: 10.1097/01.brs.0000201324.45537.46
12. Yang C, Cao P, Gao Y, Wu M, Lin Y, Tian Y, et al. Differential expression of p38 MAPK alpha, beta, gamma, delta isoforms in nucleus pulposus modulates macrophage polarization in intervertebral disc degeneration. *Sci Rep*. (2016) 6:22182. doi: 10.1038/srep22182
13. Nakazawa KR, Walter BA, Laudier DM, Krishnamoorthy D, Mosley GE, Spiller KL, et al. Accumulation and localization of macrophage phenotypes with human intervertebral disc degeneration. *Spine J*. (2018) 18:343–56. doi: 10.1016/j.spinee.2017.09.018
14. Hwang PY, Chen J, Jing L, Hoffman BD, Setton LA. The role of extracellular matrix elasticity and composition in regulating the nucleus pulposus cell phenotype in the intervertebral disc: a narrative review. *J Biomech Eng*. (2014) 136:021010. doi: 10.1115/1.4026360
15. Alini M, Eisenstein SM, Ito K, Little C, Kettler AA, Masuda K, et al. Are animal models useful for studying human disc disorders/degeneration? *Eur Spine J*. (2008) 17:2–19. doi: 10.1007/s00586-007-0414-y
16. Roberts S, Menage J, Sivan S, Urban JP. Bovine explant model of degeneration of the intervertebral disc. *BMC Musculoskelet Disord*. (2008) 9:24. doi: 10.1186/1471-2474-9-24
17. Teixeira GQ, Boldt A, Nagl I, Pereira CL, Benz K, Wilke HJ, et al. A Degenerative/proinflammatory intervertebral disc organ culture: an *ex vivo* model for anti-inflammatory drug and cell therapy. *Tissue Eng Part C Methods*. (2016) 22:8–19. doi: 10.1089/ten.tec.2015.0195
18. Teixeira GQ, Leite Pereira C, Castro F, Ferreira JR, Gomez-Lazaro M, Aguiar P, et al. Anti-inflammatory Chitosan/Poly-gamma-glutamic acid nanoparticles control inflammation while remodeling extracellular matrix in degenerated intervertebral disc. *Acta Biomater*. (2016) 42:168–79. doi: 10.1016/j.actbio.2016.06.013
19. Teixeira GQ, Pereira CL, Ferreira JR, Maia AF, Gomez-Lazaro M, Barbosa MA, et al. Immunomodulation of human mesenchymal stem/stromal cells in intervertebral disc degeneration: insights from a proinflammatory/degenerative *ex vivo* model. *Spine*. (2018) 43:E673–82. doi: 10.1097/BRS.00000000000002494
20. Kohro T, Tanaka T, Murakami T, Wada Y, Aburatani H, Hamakubo T, et al. A comparison of differences in the gene expression profiles of phorbol 12-myristate 13-acetate differentiated THP-1 cells and human monocyte-derived macrophage. *J Atheroscler Thromb*. (2004) 11:88–97. doi: 10.5551/jat.11.88
21. Oliveira MI, Santos SG, Oliveira MJ, Torres AL, Barbosa MA. Chitosan drives anti-inflammatory macrophage polarisation and pro-inflammatory dendritic cell stimulation. *Eur Cell Mater*. (2012) 24:136–52. doi: 10.22203/eCM.v024a10
22. Malandrino A, Noailly J, Lacroix D. Numerical exploration of the combined effect of nutrient supply, tissue condition and deformation in the intervertebral disc. *J Biomech*. (2014) 47:1520. doi: 10.1016/j.jbiomech.2014.02.004
23. Livak KJ, Schmittgen TD. Analysis of relative gene expression data using real-time quantitative PCR and the 2^{(-Delta Delta C(T))} method. *Methods*. (2001) 25:402–8. doi: 10.1006/meth.2001.1262
24. David G, Ciurea AV, Iencean SM, Mohan A. Angiogenesis in the degeneration of the lumbar intervertebral disc. *J Med Life*. (2010) 3:154–61.
25. Galvan-Pena S, O'Neill LA. Metabolic reprogramming in macrophage polarization. *Front Immunol*. (2014) 5:420. doi: 10.3389/fimmu.2014.00420
26. O'Neill LA, Pearce EJ. Immunometabolism governs dendritic cell and macrophage function. *J Exp Med*. (2016) 213:15–23. doi: 10.1084/jem.20151570
27. Van den Bossche J, Baardman JPJ, de Winther M. Metabolic characterization of polarized M1 and M2 bone marrow-derived macrophages using real-time extracellular flux analysis. *J Vis Exp*. (2015) 28:53424. doi: 10.3791/53424
28. Takada T, Nishida K, Doita M, Miyamoto H, Kurosaka M. Interleukin-6 production is upregulated by interaction between disc tissue and macrophages. *Spine*. (2004) 29:1089–92.
29. Takada T, Nishida K, Maeno K, Kakutani K, Yurube T, Doita M, et al. Intervertebral disc and macrophage interaction induces mechanical hyperalgesia and cytokine production in a herniated disc model in rats. *Arthritis Rheum*. (2012) 64:2601–10. doi: 10.1002/art.34456
30. Haro H, Crawford HC, Fingleton B, MacDougall JR, Shinomiya K, Spengler DM, et al. Matrix metalloproteinase-3-dependent generation of a macrophage chemoattractant in a model of herniated disc resorption. *J Clin Invest*. (2000) 105:133–41. doi: 10.1172/JCI7090
31. Haro H, Crawford HC, Fingleton B, Shinomiya K, Spengler DM, Matrisian LM. Matrix metalloproteinase-7-dependent release of tumor necrosis factor-alpha in a model of herniated disc resorption. *J Clin Invest*. (2000) 105:143–50. doi: 10.1172/JCI7091

Conflict of Interest Statement: The authors declare that the research was conducted in the absence of any commercial or financial relationships that could be construed as a potential conflict of interest.

Copyright © 2019 Silva, Ferreira, Cunha, Corte-Real, Bessa-Gonçalves, Barbosa, Santos and Gonçalves. This is an open-access article distributed under the terms of the Creative Commons Attribution License (CC BY). The use, distribution or reproduction in other forums is permitted, provided the original author(s) and the copyright owner(s) are credited and that the original publication in this journal is cited, in accordance with accepted academic practice. No use, distribution or reproduction is permitted which does not comply with these terms.



Comparative Structure and Function Analysis of the RIG-I-Like Receptors: RIG-I and MDA5

Morgan Brisse^{1,2} and Hinh Ly^{2*}

¹ Biochemistry, Molecular Biology, and Biophysics Graduate Program, University of Minnesota, Twin Cities, St. Paul, MN, United States, ² Department of Veterinary & Biomedical Sciences, University of Minnesota, Twin Cities, St. Paul, MN, United States

OPEN ACCESS

Edited by:

Dominic De Nardo,
Monash University, Australia

Reviewed by:

Michaela Gack,
University of Chicago, United States
Surya Pandey,
University of Chicago, United States

*Correspondence:

Hinh Ly
hly@umn.edu

Specialty section:

This article was submitted to
Molecular Innate Immunity,
a section of the journal
Frontiers in Immunology

Received: 16 May 2019

Accepted: 25 June 2019

Published: 17 July 2019

Citation:

Brisse M and Ly H (2019) Comparative
Structure and Function Analysis of the
RIG-I-Like Receptors: RIG-I and
MDA5. *Front. Immunol.* 10:1586.
doi: 10.3389/fimmu.2019.01586

RIG-I (Retinoic acid-inducible gene I) and MDA5 (Melanoma Differentiation-Associated protein 5), collectively known as the RIG-I-like receptors (RLRs), are key protein sensors of the pathogen-associated molecular patterns (PAMPs) in the form of viral double-stranded RNA (dsRNA) motifs to induce expression of type 1 interferons (IFN1) (IFN α and IFN β) and other pro-inflammatory cytokines during the early stage of viral infection. While RIG-I and MDA5 share many genetic, structural and functional similarities, there is increasing evidence that they can have significantly different strategies to recognize different pathogens, PAMPs, and in different host species. This review article discusses the similarities and differences between RIG-I and MDA5 from multiple perspectives, including their structures, evolution and functional relationships with other cellular proteins, their differential mechanisms of distinguishing between host and viral dsRNAs and interactions with host and viral protein factors, and their immunogenic signaling. A comprehensive comparative analysis can help inform future studies of RIG-I and MDA5 in order to fully understand their functions in order to optimize potential therapeutic approaches targeting them.

Keywords: RIG-I, MDA5, PAMP, CARD, interferon, antiviral, inflammation, PRRs

INTRODUCTION

RIG-I (Retinoic acid-inducible gene I) encoded by the DDX58 gene in the human genome (1, 2) and MDA5 (Melanoma Differentiation-Associated protein 5) encoded by the IFIH1 gene (3, 4) are known as important protein initiators of earliest immune responses to viral infection. A relatively large body of work has focused on understanding their roles in triggering the same innate immune pathway as they indeed share many similarities at a structural and functional level. However, it is becoming increasingly clear that there are unique differences between RIG-I and MDA5, such as their activation mechanisms and contextual functionalities, that need to be considered in order to fully appreciate their individual function. A comprehensive analysis of multiple aspects of RIG-I and MDA5 from their evolutionary origins and behavior among different species to their structures and molecular signaling will allow for a more nuanced understanding of their functional purposes.

FUNCTIONAL SIMILARITIES AND DIFFERENCES BETWEEN RIG-I AND MDA5

The innate immune response is a combination of non-specific defense mechanisms by the host that are critical for early detection and inhibition of pathogen growth before the adaptive immune response has time to produce proper cell-mediated immunity, such as the development of antibodies and cytotoxic T-lymphocyte responses (CTL) against the invading pathogen and/or the pathogen-infected cells (5). Cells of the innate immune arm, such as leukocytes and epithelial cells, are able to recognize general components of the microbes (e.g., viruses) that are shared among related microbes. These microbial structures are called pathogen-associated molecular patterns (PAMPs) (e.g., viral dsRNA) that are specifically recognized by the cellular pattern recognition receptors (PRRs) (e.g., RIG-I, MDA5, or Toll-like receptors TLRs) which are then activated (**Figure 1**). The specific signaling mechanisms of RIG-I and MDA5 activation will be discussed in detail below. Here, the cascade of event leading to IFN1 production is briefly summarized. Upon binding to PAMP (e.g., dsRNA), the activated RIG-I and MDA5 interact with the mitochondrial antiviral signaling proteins (MAVS), which forms a multilayered protein complex contain several different proteins (6–9). The MAVS complex then catalyzes the interaction of inhibitor of nuclear factor kappa-B kinase subunit epsilon (IKK ϵ) and the serine/threonine-protein kinase 1 (TBK1) (10–12), which phosphorylate the transcription factors interferon regulatory factors 3 and 7 (IRF3 and IRF7) (13). Phosphorylated p-IRF7 (14) and -pIRF3 (15) factors then dimerize and translocate into the nucleus, where they activate the expression of the type 1 interferon genes (IFN1: IFN α and IFN β). IFN1 proteins are then exported out of the cell to activate IFN1 signaling cascade by binding to their receptor (the IFN α/β receptor or IFNAR) either on the same cells or neighboring cells in an autocrine or paracrine fashion. This results in the production of more IFN1 (in a positive feedback loop) and a variety of interferon-stimulated genes (ISGs), which mediate vasodilation near the site of the pathogen infection and uptake of fluid, recruitment of innate immune cells, such as macrophages, neutrophils, and dendritic cells to the site of the infection that is aided by chemokine gradients to mediate innate immune cell-mediated killing of the infected cells (16).

RIG-I and MDA5 appear to differentially induce IFN1 in response to different viral pathogens (17), with RIG-I generally responding most potently to negative-strand RNA viruses, such as influenza viruses (18, 19), bunyaviruses (20, 21), filoviruses (22), and rhabdoviruses (18, 23) as well as the positive-stranded Japanese encephalitis virus (18), while MDA5 is activated during infection by positive-strand picornaviruses (18, 24, 25) and arteriviruses (26, 27) as well as by hepatitis D virus (28), Kaposi's sarcoma-associated herpesvirus (KSHV) (29). RIG-I and MDA5 may also play a role in recognizing non-viral pathogens, as MDA5 has been found to respond to malaria (30) (**Figure 2**). Neither are individually critical in reovirus (24) and in dengue virus infection (24, 31) but the presence of either in combination with Toll-like receptor 3 (TLR3) is critical to have effective anti-viral responses (32). Each serves an additive role during West Nile

virus infection (33), which is likely mediated by the production of multiple PAMP species in the infected cells (34). Indeed, RIG-I and MDA5 have also been shown to recognize different sections of the same viral genome due to their differing preferences for RNA binding (35), illustrating how RIG-I and MDA5 can act both independently and synergistically. This has also been shown functionally in viruses where both RIG-I and MDA5 have been found to be essential to induce the necessary levels of IFN β signaling for antiviral control against paramyxovirus (18, 36–38) and rotavirus infections (39).

While RIG-I and MDA5 participate in the IFN1 signaling pathway (40), it is clear from animal modeling that they might be functionally distinct. While C57BL/6 MDA5 KO mice exhibit no obvious phenotypes (18), C57BL/6 RIG-I KO have high embryonic lethality as they don't live past 3 weeks of birth and experience growth retardation and liver degeneration (18, 41). Furthermore, when RIG-I KO mice are back crossed onto the more genetically flexible 129S1 strain (18), these mice can spontaneously develop colitis symptoms (42). Clinical cases with mutations in RIG-I and MDA5 have distinct autoimmune presentations, with RIG-I mutations being associated with atypical Singleton-Merten Syndrome, while MDA5 mutations have been linked to classical Singleton-Merten Syndrome, Aicardi-Goutières syndrome, Systemic Lupus Erythematosus, Type 1 Diabetes and Graves disease (43, 44) (**Figure 2**). There is growing evidence that overt innate-immune interferon signaling plays a critical role in the development of other forms of autoimmune conditions (45). Taken together, this suggests that RIG-I and MDA5 may differ significantly in their roles during development as well as in responding to different types of viral infection that is partially dependent on the PAMPs that are available in any given context.

There is also increasing evidence that RIG-I and MDA5 have additional distinct molecular functionalities in immune signaling (43). It is well-established that the interferon regulatory factor (IRF) and innate immune NF κ B cytokine signaling pathways have many areas of cross-regulation and expression (46). Accordingly, both RIG-I and MDA5 have been shown to activate NF κ B signaling during RSV infection, but only RIG-I appears to act upstream of the canonical I κ B α -NF κ B pathway (47, 48) (**Figure 1**). While both are known to activate NF κ B mediated expression of IL-6 and pro-IL-1 β through the interaction of CARD9 with BCL10 (49, 50), the independence of MDA5 from the I κ B α pathway suggests that it influences NF κ B signaling in other as yet uncharacterized ways (43). A possible explanation for MDA5's independence from the I κ B α pathway may be that MDA5-mediated NF κ B (but not IRF) signaling requires TRIM25, which activates RIG-I by ubiquitination (to be discussed in detail below). This potentially implicates TRIM25 in other mechanisms besides activating RIG-I (51, 52). RIG-I (but not MDA5) also induces inflammasome assembly-mediated cleavage and maturation of pro-IL-1 β by caspase 1 (24, 34, 53). Finally, RIG-I has been shown to inhibit RNAi complexes mediated by the endoribonuclease Dicer, which is encoded by the DICER1 gene and cleaves dsRNA and pre-micro RNA into short single-stranded RNA fragments known as small interfering RNA (siRNA) and microRNA

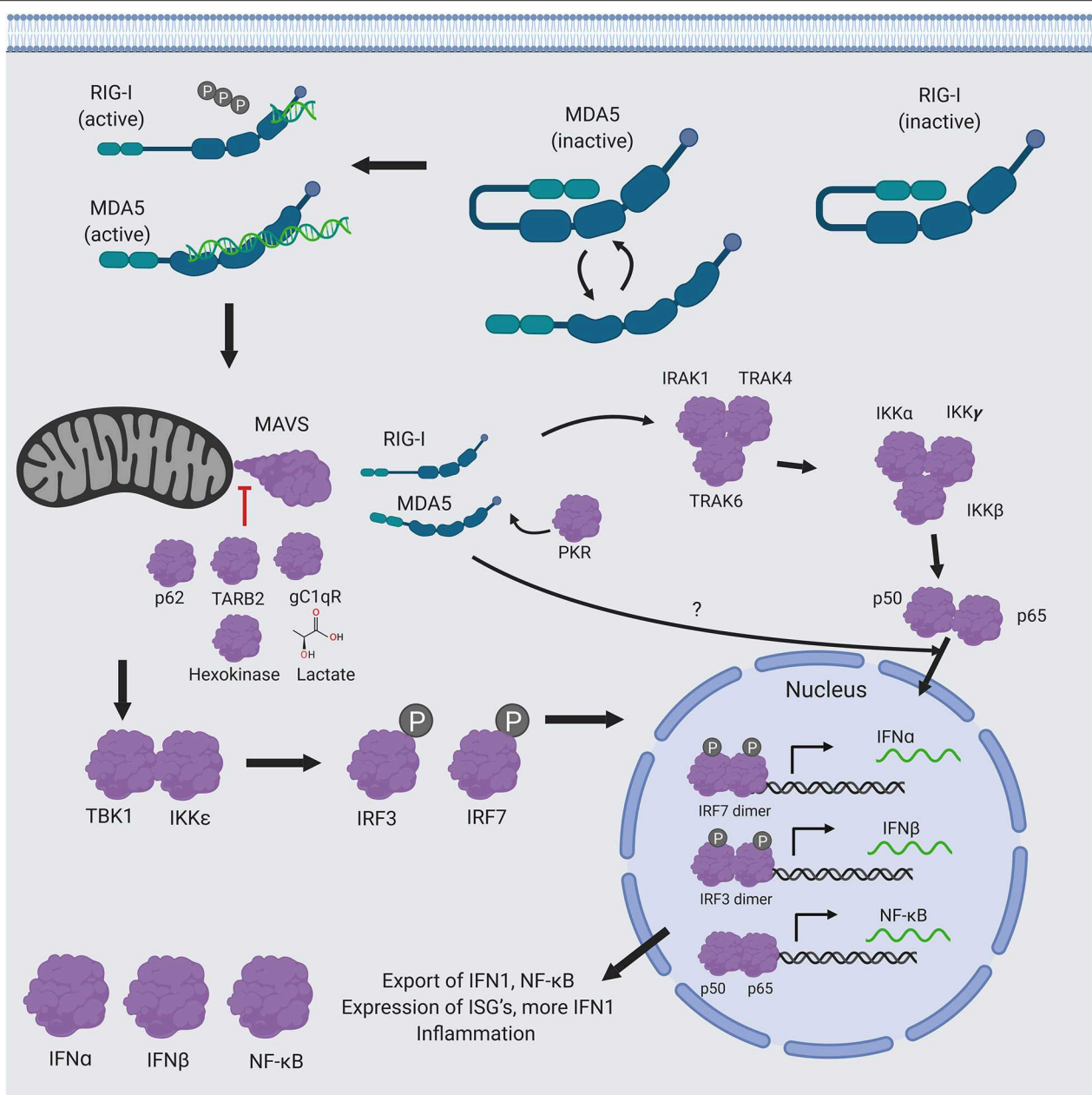
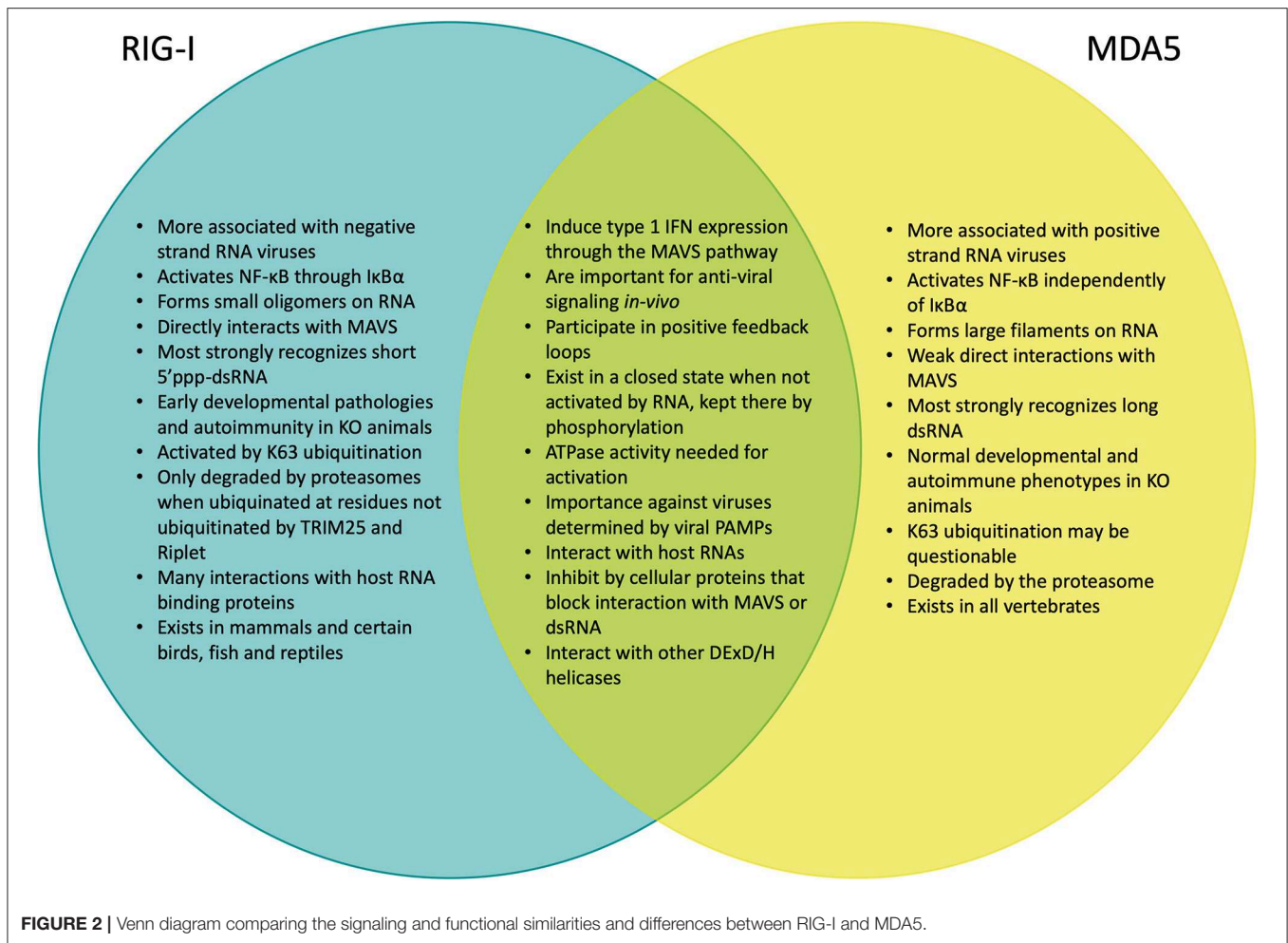


FIGURE 1 | RIG-I/MDA5 signaling pathway RIG-I and MDA5 are first activated by recognition of PAMP dsRNA, which causes them to interact with MAVS. Following the activation of MAVS by RIG-I/MDA5, a molecular cascade involves the interaction of IKKε and TBK1, which is followed by phosphorylation of the transcription factors IRF3 and IRF7, ensure to translocate the phosphorylated p-IRF3 and p-IRF7 into the nucleus, where they dimerize and bind to transcription factor binding sites of the IFNα and IFNβ genes to activate their transcriptions. Expression and exportation of these genes into the cellular milieu trigger the IFN1 signaling cascade in an autocrine or paracrine fashion to induce expression of hundreds of interferon stimulated genes (ISGs) and inflammatory genes to confer antiviral resistance. RIG-I and MDA5 also activate the NF-κB pathway. RIG-I appears to act upstream of the canonical pathway, which results in the translocation of the two functional NF-κB units (p50 and p65) into the nucleus, while MDA5 appears to affect NF-κB expression independently from this pathway. Figure created using BioRender software.

(54), by interacting with the probable ATP-dependent RNA helicase DHX58 (also known as the Laboratory of Genetics and Physiology 2 LGP2 protein), which inhibits Dicer (55) as well as the Dicer-complex protein TRBP (56). LGP2 has been shown to exhibit conflicting effects on RIG-I and MDA5 signaling (57–59), and future studies are needed in order to clarify these regulatory mechanisms.

STRUCTURES OF RIG-I AND MDA5

RIG-I and MDA5 are expressed in all cell types (60), but are most well-known for their functions inside innate immune cells, such as macrophages, neutrophils, and dendritic cells, as well as in other cells like mucosal epithelial cells. They are classified as ATP-dependent DExD/H box RNA helicases. Their structure



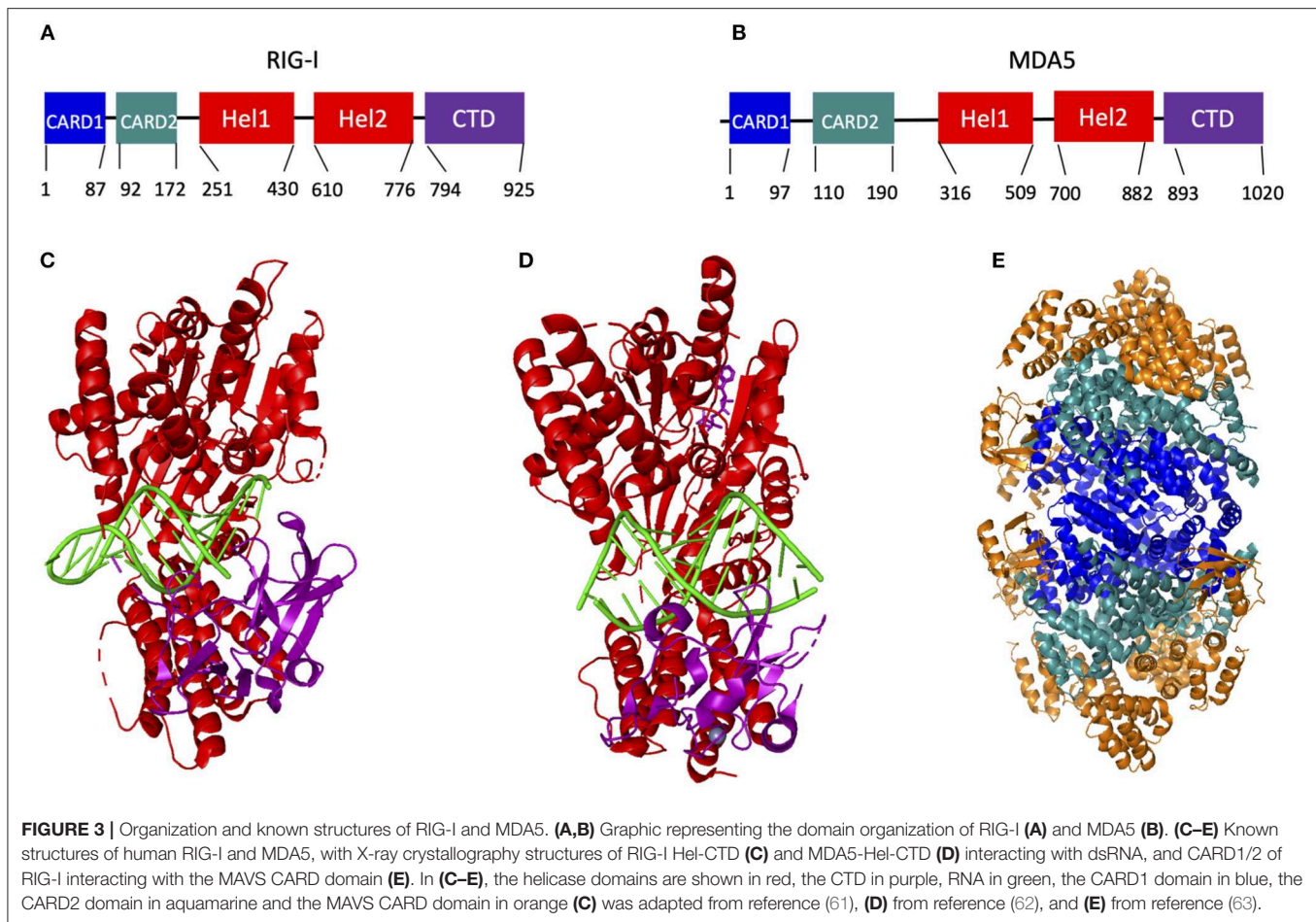
is highly helical and consists of two caspase activating and recruiting domains (CARD) at the N terminus of ~85 amino acids each, followed by a flexible hinge region and the helicase domain that consists of the RecA-like Hel1 and Hel2 domains with an ATP binding and hydrolyzing domain at their interface (**Figures 3A,B**). In particular, the structure of the ATP binding site distinguishes RIG-I and MDA5 from other helicase proteins, such as Dicer. Unlike other DExD/H box helicases where RNA binding catalyzes the ATP binding site to become structurally organized, the ATP binding site in RIG-I and MDA5 remains comparatively open and structurally dynamic following RNA binding. This is aided by the ATP binding site being formed by an interface between the two Hel domains, which are relatively far apart (64).

These structural features are connected by another flexible hinge region to the unique and predominantly β -sheet C terminal domain (CTD), which recognizes and binds to RNA (65). The CTD in RIG-I and MDA5 contains a zinc binding domain that is related to those of the GDP/GTP exchange factors (66). Each protein also contains a positively charged groove within this domain that recognizes dsRNA and this groove is structurally unique in each protein, potentially explaining their different

RNA binding preferences (66). RIG-I primarily recognizes short double-stranded RNA with 5' triphosphate groups (67–75), while MDA5 primarily recognizes long double-stranded RNA (76–79) (to be discussed in detail below.) It is notable in this regard that the Hel-CTD motifs adopt different orientations relative to dsRNA in RIG-I and MDA5. Specifically, the RIG-I Hel-CTD domain is tilted relative to dsRNA with the CTD interacting with the 5' and 3' ends of the dsRNA (61), whereas the MDA5 Hel-CTD domain runs parallel to the RNA strand (**Figures 3C,D**).

ACTIVATION OF RIG-I AND MDA5 BY POST-TRANSLATIONAL MODIFICATIONS

The series of steps required for RIG-I and MDA5 activation have been described in depth elsewhere (80–84). Briefly summarized, these proteins endogenously exist in the cytoplasm of the cell in a phosphorylated and inactivated conformation when they are not activated by PAMP (dsRNA) (85–87) (**Figures 4A,F**). Phosphorylation is mediated at the N terminal CARD domains (S8 and T170) of RIG-I by PKC- α/β (88, 89) and at the C terminal RNA interaction domain (S854, S855, and T770) by



CK β (90). On the other hand, MDA5 is phosphorylated at S828 by RIOK3 (91) as well as by other yet unknown kinases (92, 93). RIG-I is also acetylated at K909 in its C terminal domain that requires deacetylation by HDAC6 to be able to recognize RNA in its activated form (94). Upon recognition of PAMP (dsRNA), RIG-I unfolds into an open and activated state that is mediated by the flexible hinge regions between the CARD domains and the helicase domain, and between the helicase and the C terminal domain (64, 87, 95–98) (**Figure 4B**). On the contrary, there is evidence to suggest that MDA5 has a more dynamic structure (99). Unlike a model of RIG-I activation described above, MDA5 exists in a conformational equilibrium between close and open forms, with close forms favored in the dsRNA unliganded state. While not yet formally demonstrated, it is possible that MDA5 may be inhibited in the absence of the dsRNA ligand by its structural dynamics, which may prevent strong protein-protein interactions (**Figure 4F**). However, upon binding to dsRNA ligand, MDA5 adopts an open and activated form, which is perhaps more conducive for protein-protein interactions (**Figures 4G,H**).

Once the C terminal domains have been de-phosphorylated, the E3 ubiquitin ligase Riplet attaches ubiquitin peptides onto the C terminal domain of RIG-I at residues K849 and K851

(100, 101). It was previously shown that ubiquitination by Riplet was necessary for opening RIG-I and for ubiquitination of the CARD domain (102). However, *in-situ* studies found that dsRNA was sufficient to weaken the interaction between purified RIG-I C terminal domain and RIG-I CARD domains (86) and that dsRNA was necessary for Riplet ubiquitination (103), calling into question the sequential order for RIG-I activation (**Figure 4C**). Following de-phosphorylation of the CARD domain by the phosphatase PP1- α/γ (92), this domain is polyubiquitinated at K172 by the E3 TRIM25 ubiquitin ligase (104), which itself is activated by Caspase 12 (105) (**Figure 4D**). TRIM25 interacting with RIG-I may also be mediated by their mutual interactions with certain host long non-coding RNA (lncRNA), which occurs outside of the dsRNA recognizing domain in the CTD of RIG-I (106).

A recent study showed that Riplet rather than TRIM25 was primarily responsible for ubiquitinating and activating RIG-I (103). However, there are several factors to take into consideration with this study. These recent results were obtained using KO 293T and mouse embryonic fibroblast (MEF) cells and that it was not clear whether K63 ubiquitination occurred at other known lysine sites in RIG-I. The question remains whether Riplet can ubiquitinate other lysine residues

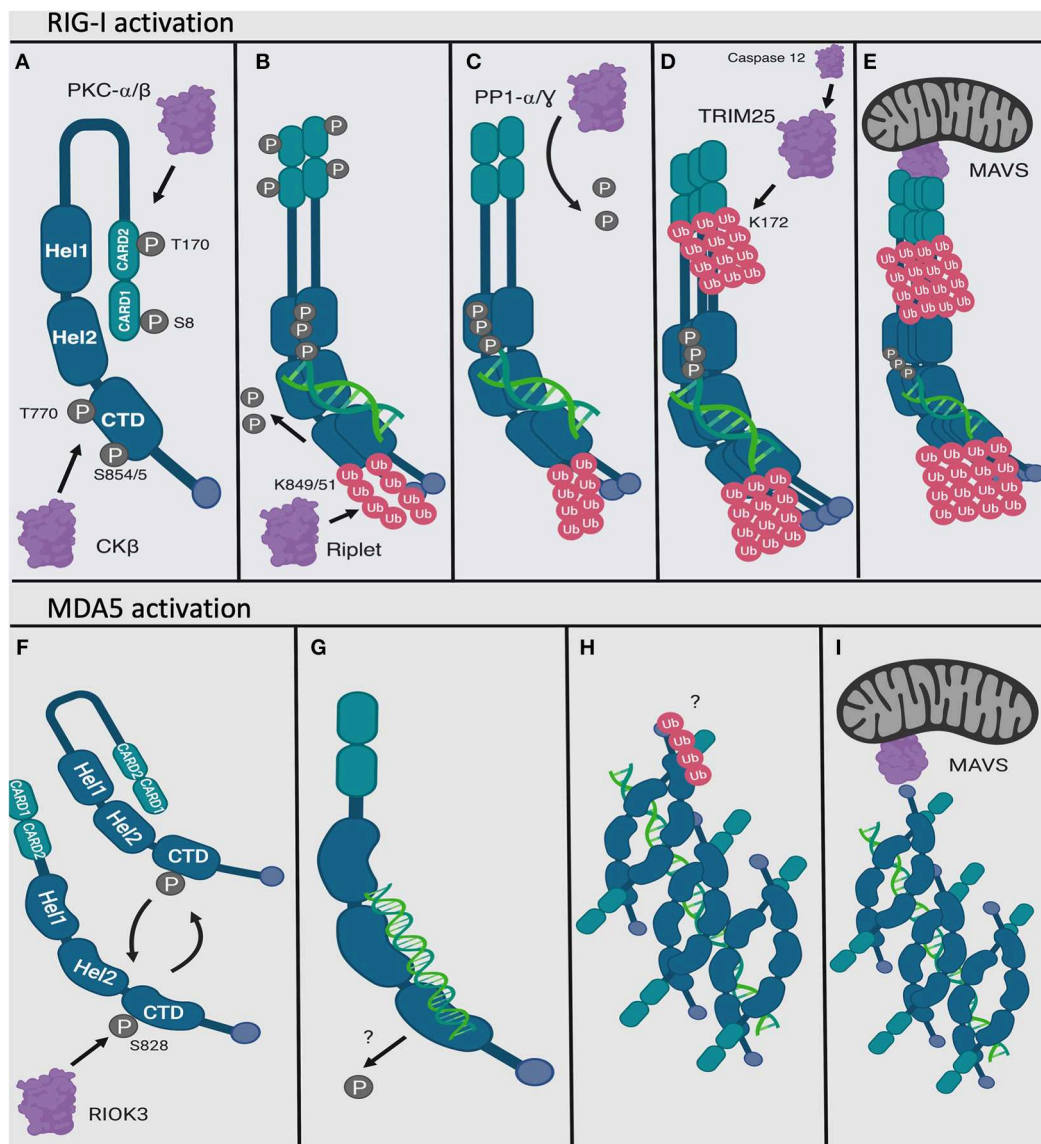


FIGURE 4 | Activation mechanisms of RIG-I and MDA5. RIG-I and MDA5 are activated by interacting with viral dsRNA at the C terminal domain. In their endogenous and inactivated state, RIG-I and MDA5 are phosphorylated at their N and C terminal domains (**A,F**). MDA5 may exist between open and close forms in its inactivated state (**F**). Upon recognizing PAMP dsRNA, the C terminal domain becomes dephosphorylated and ubiquitinated for RIG-I and dephosphorylated for MDA5 (**B,G**). RIG-I also dimerizes (**B**). Next, RIG-I oligomerizes (**D**) and MDA5 forms longer filaments on dsRNA (**H**), and the N terminal CARD domains of RIG-I becomes dephosphorylated (**C**) then ubiquitinated (**D**). Finally, the CARD domain of the RIG-I oligomers interacts with the mitochondrial protein MAVS (**E**), and the MDA5 dsRNA filaments also activate MDA5 (though it has a weaker CARD-CARD interaction with MAVS) (**I**). Figure created using BioRender software.

in the absence of TRIM25. Additionally, *in-situ* experiments comparing RIG-I ubiquitination by Riplet and TRIM25 utilized an E2 enzyme (103) that had been found to be specific for Riplet (107). While the E2 that utilizes TRIM25 has not yet been identified, TRIM25 has been shown to ubiquitinate RIG-I *in-situ* when a general mixture of E2 proteins was used (108). The protein levels of TRIM25 may also have to be at a certain level in order for it to productively ubiquitinate RIG-I, as the ubiquitin protease USP15 deubiquitinates TRIM25 at later time points in viral infection (109).

Finally, TRIM25 has been found to be essential for RIG-I activation and IFN signaling *in-vitro* and *in-vivo*. For the former, siRNA-mediated knock-down (110, 111), cellular knock-out (112) and inhibition by viral protein (109, 113–116) conditions for TRIM25 in multiple cell types have been shown to change RIG-I cellular localization (110) and to negatively affect RIG-I K63 ubiquitination, association with MAVS and IFN signaling [when the constitutively active RIG-I CARD domain was overexpressed (109, 112–116) or during viral infection (109, 111, 114)]. Viral inhibition of TRIM25 may even be a source of a positive selection during the evolution of certain viruses,

as NS1 IAV proteins have been found to interact with species specific TRIM25 (114). For the latter, MEFs from TRIM25 KO mice have significantly downregulated IFN1 production upon viral infection (113) and KO mice for NLRP12, which is a competitive interactor with TRIM25 to RIG-I, show increased interferon production and more resistance to viral infection (117). The known contributions of TRIM25 to innate immunity have recently been summarized elsewhere (52).

It is clear that both Riplet and TRIM25 can mediate K63-linked polyubiquitination. However, it has also been found that *in-situ* incubation of purified RIG-I CARD domains with ubiquitin can be activated by free and unlinked K63 polyubiquitin chains (118), calling into question whether TRIM25 only attaches K63-linked ubiquitin motifs to RIG-I-CARD or if it also catalyzes the formation of unlinked K63 polyubiquitination chains (119). A possible explanation for these differing results is that RIG-I has been shown to be covalently K63 ubiquitinated by TRIM25 when analyzed by mass spectrometry from cells (104), while experiments that demonstrate non-covalent K63 ubiquitination are those involve primarily interactions with purified proteins.

It has also been recently found that RIG-I is K63 ubiquitinated at K164 and that it may be functionally redundant to K172 (120, 121), with their ubiquitination possibly upregulating the K63 ubiquitination of the other 6 lysine residues in RIG-I (121). However, it is unknown whether TRIM25 ubiquitinates K164 or any of the other RIG-I lysine residues. Notably, these additional lysine residues in the CARD and C terminal domains of RIG-I and MDA5 are known to be K27 and K48 ubiquitinated [which are associated with degradation of RIG-I (122, 123) and MDA5 (123)], but the four listed above appear to be the essential residues for activation of RIG-I (122, 124).

The presence of K63 ubiquitin modifications on MDA5 is more controversial. Independent studies have found that MDA5 is (125, 126) or is not (126) K63 polyubiquitinated. It has also been independently found that TRIM25 does not affect ubiquitination of MDA5 (without distinguishing between K63 and K48 polyubiquitination) (104) and for TRIM25 to increase K63 ubiquitination (125), the only apparent difference in the experimental models being the usage of HEK293T (104, 126) vs. HEK293 (125) cells. TRIM65 has also been recently found to be essential for MDA5 activation by K63 polyubiquitination at K743 (127). It is clear that additional studies are needed in order to clarify the ubiquitination mechanisms of MDA5.

OLIGOMERIZATION AND FILAMENTATION TO ACTIVATE RIG-I AND MDA5 FUNCTIONS

Upon binding to PAMP (dsRNA), RIG-I oligomerizes with other RIG-I/dsRNA complexes to form helical oligomers (128) in a 2:2 complex using the purified RIG-I protein (87), where the activating ubiquitin motifs serve as a scaffold to link the oligomers together (118). These oligomers have been found to be necessary under normal conditions to activate RIG-I. This may be due to the helical structure of the RIG-I oligomers closely

matching those formed by MAVS (63), which is known to form filaments *in-vitro* (129, 130) mediated by its own CARD domains (131, 132). A structural model of MAVS activation by RIG-I has been proposed of stacking MAVS CARD domains on top of RIG-I CARD domains to extend the RIG-I helix (133).

The minimum length of dsRNA found to activate RIG-I is 13 base pairs, which is equivalent to the minimum length to facilitate the formation of a 2-RIG-I/dsRNA dimer (75). That being said, shorter (~10 bp) 5'ppp stem loop dsRNA complexes that have previously been used to obtain X-ray crystallographic structures of RIG-I interacting with dsRNA (61, 134, 135) (Figure 3C) can also activate IFN β signaling in cells (135, 136) and in mice (136). Furthermore, A549 cells that were transfected with RIG-I plasmid 6 h prior to RNA transfection had a minimum dsRNA length of only 8–10 bp required for activation (75). This indicates that RIG-I oligomerization may not be necessary for activation of the IFN β pathway under some experimental conditions, which need to be further investigated.

MDA5 has also been shown to oligomerize to form long RNA-associated filaments *in vitro* (62, 137, 138) (Figures 3D, 4H), which may be aided by chaperone proteins (139). Given that the K743 residue found to have been ubiquitinated by TRIM65 (127) is located on the surface of Hel2, it is possible that K63 ubiquitin residues may also help stabilize MDA5-dsRNA filaments (140). However, MDA5 also spontaneously forms filaments and induce MAVS to form filaments independently of ubiquitin *in-situ*. It is also thought that the formation of longer filaments by MDA5 may be mediated by a longer linkage region between CARD2 and Hel1 than in RIG-I by 50 amino acids (the length of which is well-conserved across species), allowing for the association of more CARD domains in an oligomer (133).

The formation of longer filaments by RIG-I has been more controversial, giving rise to two alternate models of RIG-I activation: formation of individual single unit of RIG-I with short dsRNA monomers (leaving a free dsRNA end, such as a hairpin loop), which then oligomerizes via CARD tetramerization that is linked by their ubiquitin chains, or filamentation on longer dsRNA. Like MDA5, RIG-I can form filaments *in-situ* independent of ubiquitin (141, 142) and induces MAVS to also form filaments (142), and MAVS is known to form filaments *in-vitro* (129, 130) mediated by its own CARD domains (131, 132). However, RIG-I filamentation on an RNA template (forming “beads on a string”) as opposed to smaller-scale oligomerization hasn't yet been shown to occur *in-vitro*. Part of the reasons for the suggestion that RIG-I was strongly activated by shorter dsRNA was based the comparison on mass equivalents of RNA species as there were less 5' triphosphorylated ends for longer dsRNAs with greater mass than shorter dsRNAs with more 5' triphosphorylated ends (76). However, when RNA species were normalized by molar equivalence, dsRNA length appeared to be positively correlated with RIG-I signaling (141–143), which became insignificant at around 500 bp (141, 143). It is significantly shorter than the length of dsRNA that activates MDA5, which forms filaments on 2,000 bp dsRNA (137). The kinetics of RIG-I and MDA5 interacting with dsRNA (which will be discussed in detail below) might possibly explain the decrease in dsRNA length efficiency to activate RIG-I as compared to

MDA5, as RIG-I seems to first recognize the 5'ppp end before sliding down the length of the dsRNA (144), whereas MDA5 dynamically associates and disassociates along the length of long dsRNA (137). Meanwhile, it is still unclear whether RIG-I can preferentially be activated by longer dsRNA independently of its unknown ability to form filaments *in-vitro* (145).

MODES OF RLR-MAVS INTERACTION AND RLR DOWNSTREAM SIGNALING

Once fully activated and oligomerized, the RIG-I CARD domain can then interact with MAVS (146–149) (**Figures 4E,I**), which is part of a protein complex containing a variety of other cellular proteins (6–9). While the MDA5 CARD domain has much weaker direct association with MAVS than the RIG-I CARD domain, it is sufficient to lead to its activation and potentiates activation of MAVS by RIG-I (146), the mechanisms of which have yet to be determined. The activated MAVS complex then initiates a molecular cascade which eventually results in expression of IFN1 (150) (**Figure 2**).

Interestingly, full length RIG-I, when overexpressed, has been found to associate with MAVS in the absence of activating dsRNA and the interaction can be ablated by phosphorylation at S8 and T170 (87), suggesting that the CARD phosphorylation sites function at least in part to prevent association of the inactive form of RIG-I with MAVS. Furthermore, the crystal structure of the interaction between the RIG-I CARD and MAVS CARD domains shows the RIG-I CARD2 domain (92–173) interacting with MAVS CARD domains on the outside of the tetramer and the RIG-I CARD1 (1–87) domain facing toward the center of the tetramer (63) (**Figure 3E**). NMR solution structures of RIG-I CARD2 also shows that T170 (which is required for dephosphorylation by PP1- α/γ) is largely buried within the CARD2 domain in a section that would be in closer contact with the helicase domains, suggesting that dephosphorylation of T170 affects an interaction domain between CARD2 and the C terminus (151). Furthermore, NMR of a C terminal construct of RIG-I with the CARD2 domain shows stable interactions of CARD2 and the C terminal domain (151). What all this may mean is that, while the CARD1 domain of RIG-I is somewhat exposed in its inactivated form and therefore can be shown to interact with MAVS, full exposure and engagement of both RIG-I CARD domains (CARD1 and CARD2) with the CARD domain of MAVS is necessary in order to induce IFN1 signaling. The CARD domains of RIG-I also appear to be generally structurally stable, as electron microscopic structures have been obtained of the full length RIG-I bound to blunt-ended dsRNA showing both CARD domains exposed (87). On the contrary, the CARD domains of MDA5 may be comparatively more flexible than those of RIG-I in order to mediate long MDA5-dsRNA filament formation (99).

The activated MAVS complex induces association of the inhibitor of nuclear factor kappa-B kinase subunit epsilon (IKK ϵ) and the serine/threonine-protein kinase 1 (TBK1) (10–12), which collectively phosphorylate the interferon regulatory factors 3 and 7 (IRF3 and IRF7) (13) (**Figure 1**). IKK ϵ and TBK1 also interact


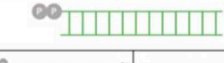
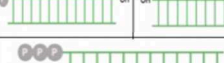
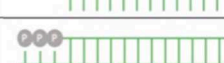


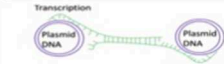
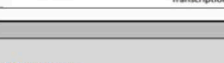




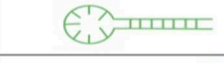


with a number of other co-factors (152, 153), such as the DEAD-box helicase 3 (DDX3) (154). The activated p-IRF3 (15) and p-IRF7 (14) then translocate into the nucleus and dimerize, where they then act as the primary transcription factors for IFN α and IFN β , respectively. Existing evidence suggests that IFN α is more primarily produced in the earliest time points following RIG-I/MDA5 activation, while IFN β is produced later and is responsible for more robust anti-viral control throughout the innate immune response period (155). There is also a distinction between innate immune cell types for IFN1 production, as cells like fibroblasts and conventional dendritic cells produce IFN α and IFN β (41, 156), while neutrophils only produce IFN β (157) and plasmacytoid dendritic cells only produce IFN α primarily through the TLR signaling pathways (41, 158). Signaling through RIG-I is also known to be essential for the process of TLR-mediated phagocytosis by macrophages (159).

Interferons are then secreted out of the cell, where they bind to their own receptor (IFNAR) and activate the Janus kinase/Signal Transducer and Activator of Transcription proteins (JAK/STAT) signaling pathways, which result in a positive feedback signaling loop to further increase RIG-I/MDA5 expression and activation (160) and IFN1 production (161, 162). Expression levels of RIG-I and MDA5 have consistently been found to be upregulated downstream of type I (163, 164) and type II (165, 166) IFN signals. MDA5 upregulation has additionally been found to occur independently of cytokine expression at least during picornavirus infection (167).

SPECIFIC RNA FEATURES RECOGNIZED BY RIG-I AND MDA5

One of the most obvious distinctions between RIG-I and MDA5 is in the RNA species to which they bind for activation (**Figures 1, 5**). RIG-I has the highest affinity for short dsRNA that is tri-phosphorylated at the 5' end (67–75), with RIG-I having been found to directly interact with the 5' tri-phosphate group of the dsRNA (71, 73). While RIG-I can bind to ss-5' tri-phosphorylated RNA (69), RIG-I cannot be activated by it (69, 168, 169), likely due to a conformational need to recognize double-stranded RNA. As a result, RIG-I is greatly attenuated by a 5' overhang as well as those with a 3' overhanging the 5' tri-phosphate end (170). In fact, a single unpaired 5' tri-phosphorylated nucleotide is sufficient to competitively inhibit RIG-I, which has been exploited by RNA viruses to evade RIG-I recognition and IFN1 signaling (171). The unique preference of RIG-I for 5' tri-phosphorylated RNA can be explained by the specific orientation that the RIG-I C terminus adopts when directly interacting with the 5' tri-phosphate group of the 5' tri-phosphorylated dsRNA (71, 73) as compared to unphosphorylated blunt-ended dsRNA (172).

The minimally required and exclusionary features of the 5' and 3' dsRNA ends for RIG-I activation have proven to be complex. Certain studies suggest that a 5' diphosphate group is the minimum feature required for RIG-I binding and activation, with 5' monophosphate dsRNA failing to productively activate RIG-I as compared to 5' di and tri-phosphate dsRNA (173).

RIG-I				
Viral and synthetic RNAs				
RNA structure	RNA name	Source of RNA used for experimental findings	ATPase activated?	Additional Notes
	5'ppp-dsRNA	Viral genomes (infectious and DI particles), RNA pol III and synthetic	Yes	Noted preferences for A/T and A/AG rich regions; DI particles especially known for activation; Minimum length of activation 13 bp, as low as 10 bp when IFN was previously induced
	5'pp-dsRNA	Viral genomes and synthetic	Yes	
	5' and 3' p-dsRNA	Short synthetic oligos, RNase III and RNase L digested RNA	Yes (under certain conditions)	Possibly need higher order stem loop structures for activation
	5'ppp-ssRNA	Synthetic	No	
	5'ppp-dsRNA with a 3' overhang	Synthetic	No	
	5'ppp-dsRNA with a single unpaired 5' nucleotide	Synthetic	Yes (at very low levels)	
	dsRNA-DNA hybrid with a RNP at spots 2 and 5 on the DNA strand	Synthetic	Yes, but IFN expression wasn't induced	
	RNA produced by rolling-circle transcription	Synthetic	Yes (at low levels)	
Host RNAs				
RNA structure	RNA name	Source of RNA used for experimental findings	ATPase activated?	Additional Notes
	circRNA	Host cell during viral infection and synthetic	No	Thought to directly compete with viral RNA
	SKIV2L products	Host cell	No	
	Hairpin structures in host mRNAs	Host cell	No	
	Small hairpin structures from RNaseL digestion	Host cell during viral infection	Yes	
	Vault RNAs	Host cell during viral infection	Yes	
	Pseudogene ribosomal RNAs	Host cell during viral infection	Yes	
	Retrotransposons	Host cell	Yes	

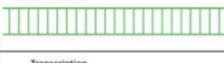
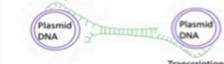

MDA5				
Viral and synthetic RNAs				
RNA structure	RNA name	Source of RNA used for experimental findings	ATPase activated?	Additional Notes
	long dsRNA	Viral genomes (Infectious and DI particles) and synthetic	Yes	Filaments formed for strands up to 2000 bp, notably activated by DI particle genomes in dendritic cells early in infection
	RNA produced by rolling-circle transcription	Synthetic	Yes (at low levels)	
Host RNAs				
RNA structure	RNA name	Source of RNA used for experimental findings	ATPase activated?	Additional Notes
	Retrotransposons	Host cell	Yes	

FIGURE 5 | RNA species that interact with RIG-I and MDA5. Table summarizes the general structural features of RNA species, their source during experimental studies and their ability to activate the ATPase functions of RIG-I and MDA5. RNA constructs are shown in green, and DNA constructs in purple.

Additionally, RIG-I poorly distinguishes between dsRNAs with either 5' tri-phosphate and 5' diphosphate group. When the free energies of each interaction are calculated, the affinity for 5' triphosphate being lowered by disassociation of magnesium from the RIG-I/dsRNA complex. Both are significantly more favorable for binding RIG-I monophosphate dsRNA (174). This similarity in affinity appears to be important in the context of infection with viruses that produce 5' diphosphate RNAs, such as reoviruses (173). Likewise, the difference of energetic binding between monophosphate dsRNA and bi- and tri-phosphate dsRNAs is likely important for distinction between self (host) and non-self (foreign) RNA, the mechanisms of which will be discussed in detail below. The ATP hydrolysis functions of RIG-I have been shown to drive rapid disassociation from certain RNA features, such as 5' monophosphate dsRNA (174, 175) and 5'OH RNA (144, 176), which is particularly important for 5' monophosphate dsRNA because it is found in mRNA after decapping during the mRNA degradation process (177).

On the other hand, other studies have shown that RIG-I can interact with monophosphate dsRNA to a certain degree, as has been found to be the case for short synthetic dsRNA with a 5' and 3' monophosphate group (69), poly(I:C) digested with RNase III (76) [which generates 5' mono-phosphate/3'-OH dsRNA (178)] and HCV RNA (179) and mitochondrial RNA [in the p53 deficient mice (180)] digested with RNase L [which produces 5' OH and 3' mono-phosphate dsRNA at subnanomolar levels (181), as has been found to be the case for HCV RNA (179).] It appears that the 5' monophosphate is the determinate feature for RIG-I activation independently of the 5' or 3' OH group in all these cases. A possible explanation for the discrepancy between the studies was that higher order RNA structures might compensate for the less optimal 5' and 3' ends, as monophosphate dsRNA that did not contain stem-loop structures did not activate RIG-I and RNA regions repetitive in certain nucleotides had been found to be critical for RIG-I activation (179). Future studies are required to further characterize the behavior of RIG-I with these RNA species.

As previously mentioned, MDA5 preferentially associates with long dsRNA (76–79). The crystal structure and molecular modeling of MDA5/dsRNA complex suggest that it can recognize the entire first turn of the blunt-ended dsRNA (182) in a similar way as LGP2 can (183). Like RIG-I and MDA5, LGP2 belongs to the ATP-dependent DExD/H box RNA helicases (184), which is structurally similar to RIG-I and MDA5 but lacks the CARD domains at the N terminus (185). MDA5 has also been found to be activated by the digested products of RNase L specifically from parainfluenza virus (186).

The presence of certain repetitive RNA elements appears to be another contributing factor in determining interaction of RNA with RIG-I and MDA5, which has recently been described in detail elsewhere (187). While RIG-I and MDA5 are mostly implicated in the immune response to RNA viruses, it has also been found to be activated by 5' tri-phosphorylated dsRNA intermediates generated by cellular RNA polymerase III from AT-rich DNA sequences (188) and during infection with Epstein-Barr virus (a DNA virus) (189). RIG-I has additional

binding preferences for certain nucleotide motifs, such as uridine-rich 5' tri-phosphorylated hairpin RNA (190), synthetic AU- rich hairpins (191) and those naturally found in the genomes of Sendai virus defective-interfering (DI) particles (192), measles (193), Influenza A virus (IAV) (194) and in KSHV RNA transcripts (195), and poly (U/UC) regions (196) and poly (A/AG) regions (197) in the antisense Hepatitis C virus (HCV) genome. It is of particular interest that the poly (A/AG) HCV regions are located significantly downstream of the 5'triphosphate group (197), thus potentially implicating other parts of RIG-I (e.g., helicase domain) as potential RNA interacting domains. Repetitive RNA elements may also be important in allowing for interaction of inhibitory RNAs that do not have 5' or 3' features needed for full activation of RIG-I, as has been shown to be the case with GA-rich regions in circular long-non-coding RNA lnc-Lsm3b (198). These specific interactions explain their primary role as anti-viral receptors, as these viral motifs are mostly not found in cellular RNAs (199).

RIG-I and MDA5 have been particularly implicated in their response to RNA genomes of viral defective interfering (DI) particles, as these defective viral genomes (DVGs) have originally been found to induce interferon signaling (150). DI particles are produced by many viruses during infection, and while they are similar in many regards to standard viral particles, such as in appearance and composition, they cannot productively infect cells (200). This is largely thought to be due to the presence of large and deleterious deletions in the DVG of DI particles (201). Some DVG RNAs have also been noted to have “copy-back” motifs in which one end of the genome can base pair with an inverted copy at the opposite end of the genome, which may be due to stalled and aberrant replication (202, 203).

Copy-back RNA motifs specifically seem to be important for RLR activation in that they tend to contain hairpin motifs and 5' tri-phosphate groups, as has been found for Sendai (204–206), measles (35, 207), and chikungunya (35) DVG RNAs in activating RIG-I. In the case of IAV, DVG RNAs might even be more potent activators of RIG-I than the full-length viral genome. Cells that were blocked from viral protein synthesis experienced RIG-I mediated IFN1 expression when infected with IAV stocks grown in chicken embryonic eggs (which produced higher relative quantities of DI particles with DVG RNAs) but not with IAV grown in cell culture, indicating that RIG-I activation by the genomes from primarily non-DI IAV particles may require active viral RNA synthesis (208). A potential explanation to this observation is that RIG-I appears to be activated by the full viral genome via its panhandle structure, the affinity of which is lowered by the presence of mismatched and unpaired nucleotides in this region of the viral genome that is conserved across influenza virus strains (209). However, the overall panhandle structure is conserved between DVGs (205) and the full length viral genome (209), and deletions within DVGs are monogenic and internal (210). The specific molecular mechanisms of enhanced RIG-I signaling by IAV DVGs have yet to be elucidated, although the level of exposure of the panhandle may play a role. While the full extent of MDA5 interacting with DI RNA is currently unknown, MDA5 appears to be more predominantly activated by DVG RNA than RIG-I specifically

in dendritic cells early in the viral infection cycle (211), which may be a contributor toward the phenomenon of DI particles enhancing dendritic cell maturation (212).

The comparative abilities for DI particles vs. infectious virions to activate RIG-I and MDA5 have important implications for understanding viral pathogenesis and for vaccine development. There is a burgeoning interest in this regard, especially in populations which are typically more challenging to achieve successful preventative vaccination, such as elderly populations with IAV vaccination (213). Elderly populations in general do not develop as strong of memory immune responses to vaccines as their younger counterparts (214–217) and have been found to have decreased RIG-I mediated IFN1 signaling (218). Correspondingly, the influenza vaccine has been shown to decrease in effectiveness in older populations as the influenza season progresses (219). A DI-vaccine that strongly activates innate immune cells and increases the adaptive immune response could therefore potentially boost the immune responses to vaccines in more vulnerable populations. Additionally, DI particles have shown to be an important contributor of viral persistence (200, 220, 221). This raises the question of whether a viral infection may alternate between producing primarily infectious virions which eventually activates the innate immune response and producing primarily DI particles which requires less cellular activity but may initiate an even stronger innate immune response (222–224). Taken altogether, DI particles provide yet another layer of distinction between RIG-I and MDA5 in terms of how each recognizes different species of dsRNA.

DISTINCTION OF SELF (HOST) AND NON-SELF (FOREIGN) RNAs BY RIG-I AND MDA5

The preference for specific RNA species by RIG-I and MDA5 allow for them to distinguish between viral RNA and host RNA in most circumstances (225), although the specific mechanisms of distinction are not as clear for MDA5 as for RIG-I. Studies from clinical cases of MDA5 mutations provide contradictory models, with certain mutations found in Aicardi-Goutières syndrome (AGS) increasing MDA5 avidity for self RNA (226) with Alu retroelements found to be significantly enriched for interaction with AGS MDA5 mutations (227). The modification of dsRNA by host cells may be a primary inhibitor of MDA5 activation by host RNA as knockout of adenosine deaminase (ADAR1), which weakens dsRNA structures, allows wild-type MDA5 to be activated by Alu retroelements (227). However, other MDA5 mutations decrease affinity for known MDA5 ligands and ATPase activity, yet still demonstrate increased IFN β expression (228, 229).

For RIG-I, a highly conserved residue in the C-terminal RNA binding pocket (H830) has been found to sterically exclude canonical self-RNA by the means of the N₁-2'-O-methyl self-RNA motif, also known as Cap1 RNA (61, 230). This results in a low binding affinity of RIG-I to cellular Cap1 RNA and decreased ATPase activity as compared to PAMP

(dsRNA) (61, 231). Flaviviruses take advantage of this precise discrimination by encoding a viral 2'-O-methyltransferase capable of N₁-2'-O-methylating its positive-strand RNA genome in order to evade RIG-I recognition and IFN1 activation (230). Conversely, the mutations E373A and C268F found in the RIG-I protein in patients with auto-immune disorder Singleton-Merten syndrome confer the ability of the protein to recognize Cap1 RNA and become activated by ATP dependent and independent mechanisms, respectively (232). Furthermore, the E373Q mutation of RIG-I, which was designed to constitutively bind ATP, was found to increase the affinity of RIG-I with ribosomal RNA (233). It is noteworthy that host RNA contains additional internal RNA modifications and non-Watson-Crick base pairing which can inhibit activation of the other known dsRNA-sensing protein, the interferon-induced double-stranded RNA-activated protein kinase (PKR) (234), and it is known that synthetic 5' triphosphorylated RNA containing pseudouridine, 2-thiouridine or 2'-O-methylated uridine has significantly decreased ability to activate RIG-I (67), which has been demonstrated to occur by preventing RIG-I filament formation *in-situ* (142). N-6-methyladenosine (m6A) nucleotides, which are well-known nucleotide modifications among viruses (235), have also been found to ablate dsRNA binding to RIG-I (236).

It has been demonstrated that certain RNA-DNA hybrid constructs with ribonucleotides at positions 2 and 5 of the DNA strand can bind to RIG-I and activate its ATPase activity (75). ATPase activity is necessary for full activation of RIG-I and expression of IFN β (75, 237), so the minimum requirement of a motif not found in host RNA for ATPase activity has significant implications for the distinction between self and non-self RNAs. Expanding on this observation, exogenous ATPase activity may also be sufficient to potentiate RIG-I and MDA5, as LGP2 ATPase mutant mice are significantly more susceptible to viral infection even in the presence of functional RIG-I and MDA5 (238). However, this model is further complicated by certain RNA-DNA hybrids that are able to bind RIG-I and activate ATPase activity, but don't induce IFN β expression (75). It is currently undetermined whether such hybrids can sterically inhibit RIG-I due to the presence of mostly dNTPs or whether they inhibit RIG-I in a yet undescribed way.

Recent kinetic studies of RIG-I and MDA5 activation by PAMP (dsRNA) help illustrate how ATPase activity is critical for their function and distinction between host (self) and foreign (non-self) RNA. RIG-I binding to ATP is sufficient for interaction with dsRNA (144, 176). RIG-I ATPase activity is inhibited in the absence of PAMP (dsRNA) by a helical arm that blocks the ATPase site (239). Upon interaction with PAMP (dsRNA), the helical arm shifts and the two helicase domains are brought together to form an active ATPase site (239). RIG-I then catalyzes ATP to break the 5'ppp dsRNA interactions within seconds. ATP is then rapidly hydrolyzed to facilitate translocation of RIG-I to the opposite dsRNA end, after which the RIG-I oligomers can form (144). On the other hand, ATP hydrolysis drives rapid disassociation of RIG-I from host RNA features. These features include dsRNA with a 5' monophosphate group (174, 175) that is

found in mRNA after decapping during the mRNA degradation process (177) and 3' overhang RNA (144, 170) found in miRNA (240) as well as other RNA motifs, such as 5'OH RNA (144, 176) found in bacteria (241). Furthermore, an impaired ATPase functionality increases the promiscuity of RIG-I binding these host RNA motifs (144, 176, 242).

Similar ATPase functions have been found during MDA5 filamentous formation. The C terminus of MDA5 is critical to form organized helical filaments (138) and ATP binding drives association and hydrolysis and disassociation from foreign dsRNA [with little coordination being observed between neighboring MDA5 proteins (137)] in a manner that involves MDA5 twisting along its flexible and hydrophobic interface domains (243). Taken together, ATPase activity may be directed toward rapid disassociation from host dsRNA and degradation of RNA-DNA hybrids, but primarily act on the translocation pathway upon interaction with PAMP (dsRNA). It is also possible that host and hybrid dsRNAs could inactivate RIG-I independently of their ability to bind the C-terminus and activate ATPase activity. This has been shown, for example, for a hybrid RNA that has one strand consists mostly of DNA except at positions 2 and 5, which appears to bind RIG-I and activate its ATPase activity but doesn't activate IFN1 signaling (75). Future studies are needed in order to determine these differential interaction mechanisms.

NOVEL MECHANISMS OF INHIBITION OR ACTIVATION OF RIG-I AND MDA5 BY CELLULAR RNAs

Contrary to the traditional paradigm, there is increasing evidence to suggest that RIG-I and MDA5 interact with certain host RNA motifs, resulting in auto-activation or auto-inhibition of the IRF pathway (Figure 5). One of the most strongly supported models is activation by host and viral circular RNAs (circRNA). Originally found in a variety of pathogen genomes, circRNAs in eukaryotic cells were first thought to be byproducts of the pre-mRNA splicing process. However, they have later been found to be produced by a non-canonical "backsplicing" process and there is increasing evidence to suggest that they play some important regulatory roles (244), suggesting that they may have specifically evolved for this purpose. RIG-I was first found to interact with circRNA produced *in situ* (245). Interestingly, the minimum component required for RIG-I activation is an intron of pathogenic origin to be spliced out during the circularization process. As human introns have been found to be associated with many RNA binding proteins, it is speculated that these proteins may have prevented circularization of this particular synthetic circRNA used in this study (245) and that host RNA binding proteins normally prevent endogenous circRNAs from being detected by the innate immune system. Nevertheless, some viral infections can potentially expose these endogenous circRNAs for immune detection, as has recently been found to be the case for a novel host-derived circRNA (lnc-Lsm3b) that is IFN-inducible and shows a down-regulation of its binding to host proteins during viral infection and therefore appears

to compete with viral dsRNA as an inhibitor of the RIG-I signaling feedback loop (198). Similar inhibitory mechanisms have also been noted for RNA products of the exonuclease SKIV2L (246). Finally, recent studies have found that hepatitis C virus (HCV) infection increases the expression of certain cellular RNAs that can inhibit RIG-I function. HCV infection increased the mRNA levels of hepatic selenoprotein, which was able to bind to RIG-I through a hairpin structure and inactivated it during viral infection (247). Infection by HCV, vesicular stomatitis virus (VSV), or Sendai virus, or direct exposure of cells to type 1 and 3 interferons increases expression of the cellular long non-coding RNA (lncRNA), namely lncATV, which similarly inhibits RIG-I function by directly interacting with it in order to promote virus replication (248). In addition to the greatly increased implications of RIG-I and MDA5 modulation, these findings also have significant implications in characterizing new biomarkers of disease, as increased serum selenoprotein level has been found to significantly associate with treatment failure of anti-viral drugs in HCV patients, and can possibly explain the increased prevalence of type 2 diabetes in HCV patients (247).

Cellular RNA has also been found to activate RLR signaling during viral infection. Vault RNAs, which are transcribed from four genes and are normally found in large ribonucleoprotein complexes in cytoplasmic "vaults," are significantly enriched for binding to RIG-I during infection with KSHV (29). This may be due partly to viral infection-induced reduction in the level of cellular triphosphatase DUSP11, which dephosphorylates the 5'ppp group on the vault RNAs, as they could only be immunogenic (in the absence of viral infection) by the addition of the 5'ppp group. RIG-I and MDA5 have also been found to be activated by RNA microparticles produced *in situ* by rolling circle transcription, generating tandem repeat RNA strands (249). Retrotransposons may also be able to activate both RIG-I and MDA5, as both can be activated by LINE1 RNA independently of DNA sensing mechanisms and retrotransposition (250).

Viral infections can also induce recognition of host RNAs. Herpes Simplex Virus 1 (HSV1) infection, for example, has been shown to induce translocation of the host pseudogene *RNA5SP141* ribosomal RNA into the cytosol to bind to RIG-I. Knockdown of *RNA5SP141* decreased cytokine signaling during infection with HSV and EBV as well as influenza A virus (IAV) (251). RIG-I has also been found to be activated by hairpin RNA structures generated by cleavage of RNA by RNase L, which has been demonstrated to occur during HCV infection (179) as well as from mitochondrial dsRNA produced in p53 deficient mice (180). The mitochondria, in particular, may be an important source of immunostimulatory host dsRNA. Viral infections are well-known to cause mitochondrial damage (252). Knockdown and hepatocyte-specific conditional KO of mitochondrial RNA degrading enzymes resulted in the increase of cytoplasmic mitochondrial dsRNA which was able to activate MDA5 (253). Additionally, extracellular vesicles (EV) secreted by apoptotic endothelial cells were found to contain long interspersed nuclear element (LINE) and short interspersed nuclear element (SINE) RNAs that are products

of RNA polymerase III and were able to activate RIG-I signaling (254). Collectively, these findings demonstrate the many unique ways by which cellular RNAs can modulate RIG-I and MDA5 functions as well as the potential implications of RIG-I activation by pharmaceuticals as an anti-viral or generalized immunotherapy, though much caution and studies would still be needed to determine the appropriate levels of RIG-I and MDA5 activation.

VIRAL MODULATIONS OF RIG-I AND MDA5 FUNCTIONS

Given that RIG-I and MDA5 are critical for activating expression of IFN1 during viral infection, there is much interest in studying the interactions of these cellular proteins with viral factors (RNAs or proteins), as the ability to modulate interferon expression is a major evolutionary driving force in viral evolution (255, 256). There are many mechanisms viruses have evolved to evade RIG-I and MDA5 signaling, which have been discussed at length elsewhere (257, 258). Such mechanisms are of particular importance to segmented RNA viruses, providing potentially more dsRNAs for RIG-I and MDA5 activation (259). IAV and the other orthomyxoviruses are unique in that they replicate in the nucleus of the cells (260), preventing the viral RNA from being detected by the PRRs. However, recent preliminary evidence seems to suggest that RIG-I may also endogenously be present in the nucleus and performs similar viral RNA binding and activation of the IFN1 pathway (261), yet this finding has yet to be replicated by other laboratories.

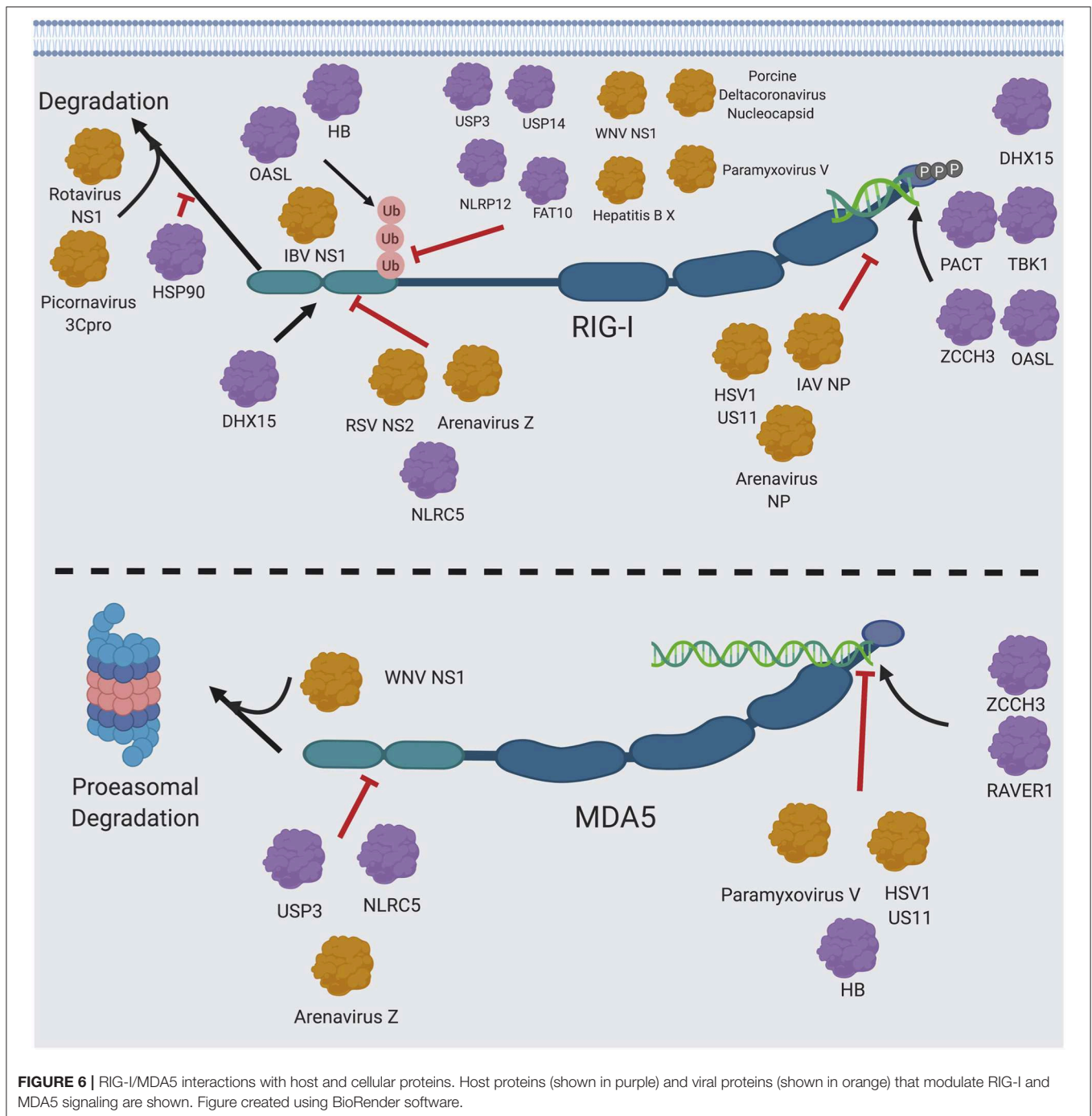
There is also increasing evidence to suggest that RNA processing is another mechanism of immune modulation. Certain bunyaviruses can cleave the 5' tri-phosphate group from their genomic RNA (262) in order to avoid immune detection. RIG-I has also been found to be subjected to negative modulation by RNAi during IAV infection (263). On the contrary, nucleoproteins from the Sendai virus (264) regulate the number of DI particles being produced, and IAV nucleoproteins also regulate the production of abortive replication RNA (208), mini viral RNAs (265) and DVG RNA (208), all of which are immunostimulatory. The Semliki Forest virus (SFV) polymerase has even been found to convert host RNA into 5'-ppp dsRNA to induce IFN1 expression (266). This raises an intriguing possibility that induction of IFN1 may actually benefit some viruses under certain circumstances despite IFN1 signaling negatively regulating viral replication.

The viral RNA levels and localization throughout the viral life cycle might also play an important role in immune evasion (267). Control of viral RNA levels by viral exoribonucleases in particular illustrates the complicated balance between viral production and immune evasion for optimal viral propagation, as has found to be the case for arenaviral nucleoproteins (NPs) (268, 269) and non-structural proteins found in coronaviruses (270, 271). Finally, viral infection has the capability to disrupt processes of the cell's basic functions, such as transcription and translation, thereby affecting viral replication and immune signaling in complicated ways (258).

One of the most significant ways viruses modulate RIG-I and MDA5 signaling is through their viral proteins (272) (**Figure 6**). The respiratory syncytial virus (RSV) non-structural protein (NS2) protein and the Z matrix proteins of pathogenic arenaviruses interact with the RIG-I CARD domains to block its interaction with MAVS (273, 274). The HSV1 deamidase UL37 specifically targets RIG-I through its helicase domain, abrogating its ability to bind to RNA (275). The IAV polymerase components also interact directly with RIG-I (276), though their biological significance has yet to be determined as they don't significantly affect IFN1 production. On the other hand, RNA binding appears to be an important bridge between the interaction of RIG-I with other viral proteins, as the nucleoproteins (NPs) of IAV (276) and arenaviruses (277, 278) both interact with RIG-I through viral RNA. The NS1 protein of rotaviruses targets RIG-I for degradation that is independent of proteasomes (279). The V protein of paramyxoviruses inhibits MDA5 (40) by targeting a unique feature of the ATP binding pocket in MDA5 (280) and by inhibiting MDA5 CARD dephosphorylation (93), but can also inhibit RIG-I by interacting with the CARD domain to prevent its ubiquitination by TRIM25 (281). Finally, the US11 protein of HSV1 (282) and the arenaviral Z matrix proteins (274) directly interact with and inhibit RIG-I and MDA5 in a similar fashion. There are also many other viral proteins that can regulate proteins in the RIG-I and MDA5 pathways, which have been discussed in detail elsewhere (44, 53, 59, 96, 257, 283).

MODULATIONS OF RIG-I AND MDA5 FUNCTIONS BY THEIR POST-TRANSLATIONAL MODIFICATIONS AND/OR BY OTHER VIRAL OR CELLULAR PROTEINS

It is important to consider the different regulatory mechanisms of RIG-I and MDA5 when considering their different functionalities (**Figures 4, 6**). One of the key differences between these proteins is in their post-translation modifications (96). Ubiquitination of RIG-I is necessary for its activation (118) and is a point of negative regulation by host proteins (117, 284, 285), viral proteins (281, 286, 287) and ubiquitin mimics (288) as well as positively regulated by influenza B NS1 protein (289) and another ubiquitin mimic (290). On the contrary, MDA5 is more well-known to be negatively regulated by ubiquitination (291), with positive regulation by K63 ubiquitination being more controversial. While the deubiquitinase USP3 inhibits MDA5 as well as RIG-I, it is thought that this may be due to USP3 directly binding the MDA5 CARD domain to prevent RNA filamentation (284). This raises the question of how RIG-I can maintain its stability outside of the proteasome, as ubiquitination at other lysine residues in RIG-I besides K172 induces proteasomal degradation (291–293). This proteasomal degradation may be mediated by a p62 autophagic complex that associates with LRRC25/ISG15 (294) and SQSTM1 (295) and also mediates mitophagy and downregulation of MAVS signaling during measles virus infection (296).



One key observation is that, while both RIG-I and MDA5 are cleaved during picornavirus infection, this cleavage is mediated by the viral proteinase 3C^{Pro} (297) and is independent of the proteasome (298) for RIG-I, whereas it is mediated by cellular caspases and the proteasome for MDA5 (299). MDA5 is also cleaved by caspases during apoptosis (4), though it hasn't been shown whether this is mediated by MDA5's ubiquitination sites. The ubiquitin linkage site may be a determinate of function, as the ubiquitin ligases RNF122 (300) and STUB1 (293, 301)

have been shown to negatively regulate RIG-I catalyzed K48-linked ubiquitination as opposed to the known K63-linked ubiquitination at the K172, K849 and K851 activating sites, and RNF125 has also been proposed to K48 ubiquitinate RIG-I (291) (though it hasn't been shown directly) (59). TRIM40 has also been shown to negatively regulate RIG-I and MDA5 by K27 and K48 ubiquitination (123).

Substantiating the possibility that K63 ubiquitination on RIG-I may be functionally distinct from its other ubiquitination

sites by protecting it from degradation is the finding that the NS1 protein of West Nile virus (WNV) targets both RIG-I and MDA5 for degradation by proteasomes. Additionally, NS1 inhibited K63 ubiquitination of RIG-I, but MDA5 was not found to be K63 ubiquitinated (126). Heat shock protein 90- α (HSP90) has been found to protect RIG-I from proteasomal degradation, but it is unknown which type of ubiquitination that is inhibited by HSP90 (302). Taken together, the experimental evidence suggests that RIG-I may be protected from proteasome degradation despite its activating ubiquitin moieties (52). This warrants further studies for mechanistic elucidation.

RIG-I and MDA5 additionally interact with different cellular co-factors, contributing to their differential regulations of function. RIG-I is well-known for being potentiated by proteins that also bind dsRNA, such as (PACT) (303, 304), which was first discovered as a protein activator of PKR, the serine/threonine-protein kinase 1 (TBK1) (305–309) and the oligoadenylate synthetase L (OASL) (310). PACT in particular has some functional similarities to RIG-I, as they each contain three distinct RNA binding domains (311) and interact with many of the same cellular co-factors, such as PKR (312) and Dicer (312, 313). Because of the important role of PACT in augmenting RIG-I function, it is a prime target for inhibition of RIG-I signaling by several viral proteins from diverse families of viruses (314–316), the molecular mechanisms of PACT inhibition by these viral proteins can vary and still need to be characterized in detail in future studies. Similarly, the host ribonucleoprotein RAVR1 can increase affinity of MDA5 for dsRNA (317), and the zinc-finger protein ZCCHC3 has recently been found to do so for both RIG-I and MDA5 (125) in similar mechanisms to the other known RNA-binding proteins. On the contrary, the human hemoglobin subunit beta (HB) has recently been suggested to decrease MDA5 signaling by competing for long dsRNA, while HB can enhance RIG-I signaling by increasing K63 ubiquitination on RIG-I (318).

Several host factors interacting with RIG-I and MDA5 do so by yet undescribed mechanisms. PKR [which is also activated by PACT (319, 320) and is sequestered by the cellular helicase DHX36 protein to form stress granules (321, 322) along with RIG-I (323, 324) and TRIM25 (324)] appears to have a novel and yet uncharacterized function in enhancing MDA5-dependent MAVS signaling that is dependent on the kinase activity of PKR (325). Additionally, the porcine Interferon-Inducible Oligoadenylate Synthetase-like protein (pOASL) has also been found to interact with and inhibit MDA5 by an unknown mechanism (326).

The RIG-I CARD domain interacts with MAVS to induce interferon signaling, so proteins that disrupt this interaction [as it has been proposed for the Atg5 and Atg12 autophagy proteins (59)] can specifically inhibit RIG-I signaling. However, other cellular proteins, such as the complement protein gC1qR (327) and TARBP2 (328) that interact directly with MAVS, inhibit both RIG-I and MDA5. Lactate and hexokinase have also recently been found to inhibit RIG-I and MDA5 by interacting with MAVS, which may be significant in explaining the interplay between metabolism and immune signaling as glycolysis was found to be greatly decreased upon RLR signaling (329). Likewise, cellular proteins, such as NLRC5 (330) that

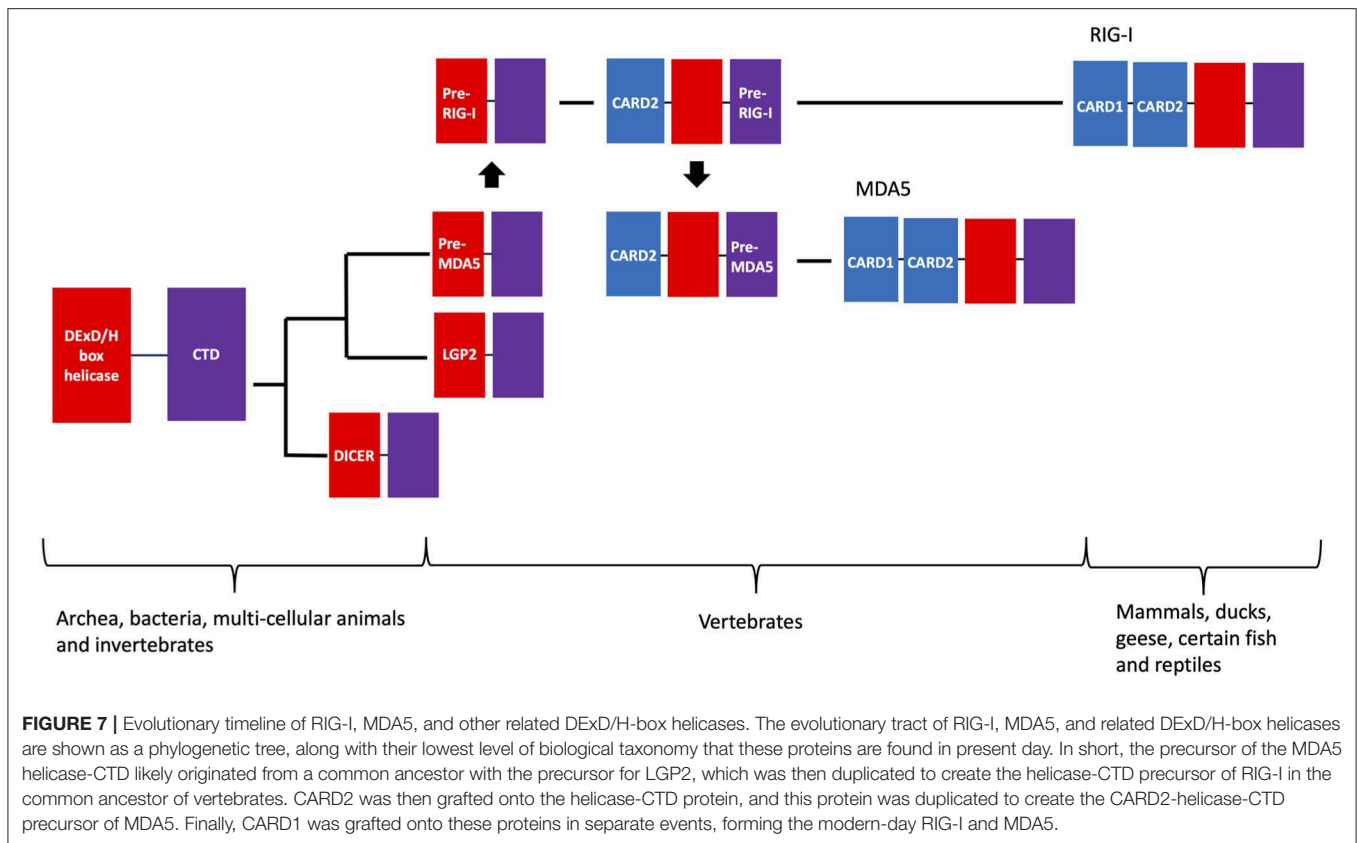
interacts with the RIG-I and MDA5 CARD domains have been shown to block interaction of both RIG-I and MDA5 with MAVS. Contrarily, DHX15 has been identified as a RIG-I cofactor that interacts with the RIG-I CARD domains and with PAMP (dsRNA), thereby increasing RIG-I ATPase activity (331). Additionally, ADP-ribosylation factor proteins can block RIG-I and MDA5 from interacting with PAMPs and thereby inhibit their activation (332, 333). Lastly, the green tea molecule EGCG has also been shown to inhibit the ATPase function of RIG-I (334). The similarities and differences between RIG-I and MDA5 modulations and signaling are complex and will need to be elucidated further in future studies.

EVOLUTION AND SPECIATION OF RIG-I/MDA5 AND RIG-I/MDA5-LIKE PROTEINS

Despite their structural and mechanistic differences, it is important to emphasize that existing phylogenetic analysis indicates that RIG-I and MDA5 come from a common origin that is also shared among several other protein families (Figure 7). The linkage of the helicase and DExD/H box protein appear to be ancient, as orthologs of these proteins are found in the Archaea kingdom (335, 336). MDA5 orthologs are found in most vertebrates (184), while RIG-I orthologs are only found in mammals, ducks, geese and some selected fish and reptiles (184, 337–343) (Figures 2, 7).

It is therefore likely that MDA5 evolved first, perhaps from a common ancestor with the closely related LGP2 helicase family (184), which is structural similar to RIG-I and MDA5 but lacks the CARD domains at its N terminus (185). LGP2 orthologs are also only found in vertebrates while the next closest related family of proteins (Dicer) are more ancient proteins. It has therefore been proposed that the RIG-I helicase-DExD/H complex may have been duplicated from MDA5 in the common ancestor of vertebrates (184). The association of the two CARD domains appears to have followed, as individual CARD domains are found in a variety of vertebrates that also encode caspases (344, 345), but only RIG-I, MDA5, and certain members of the Nact family of NTPases (346) have two CARD domains. Phylogenetic analysis has shown that the helicase-DExD/H and CARD2 have strong co-evolution history (347, 348), while CARD1 has evolved more independently (184). CARD2 appears to have been grafted onto the RIG-I helicase-DExD/H complex first, with the CARD2-MDA5 being duplicated from this event. Finally, CARD1 was grafted onto the CARD2-helicase-DExD/H complex in separate events for RIG-I and MDA5 (184). In mammals, positive selection can be seen in the flexible hinge region connecting the CARD domains to the helicase in RIG-I and MDA5. RIG-I contains an additional site of positive selection within the Hel1 structural motif (N421), while most of the unique positive selection sites for MDA5 are in regions specific to it, including a 29 amino acid insertion in Hel2 (349).

While RIG-I and MDA5 may both originate from common ancestors of vertebrates, there is increasing evidence to suggest



that proteins with similar functions may have evolved separately in other species from ancient helicase-DExD/H proteins, implicating RNA-mediated defense responses as a potentially universal biological function. A RIG-I homolog has recently been found in a planarian that is able to activate downstream inflammatory genes in the absence of the traditional CARD domains (350), and a similar homolog in *Caenorhabditis elegans* has been proposed to mediate anti-viral RNAi by complexing with Dicer and catalyzing their translocation on the viral genome (351). Additionally, insects have been found to primarily respond to RNA viruses by RNAi mediated by Dicer proteins (352). Dicer may potentially mediate dsRNA-activated anti-viral signaling pathways that is independent of RNAi pathways, as has been found to be the case for the expanded CAG-repeat dsRNA (353). Pattern recognition receptors (PRRs) that respond to viral RNA have not yet been found outside of the animal kingdom, as RLR-like proteins in prokaryotes do not have CARD domains and the PRRs in plants found so far are surface-receptor kinases that respond to external molecular elements of bacteria (354) [similar to the mammalian toll-like receptors (TLRs)]. However, RNA silencing has been demonstrated to be an important anti-viral strategy in plants (354, 355) and certain *Arabidopsis* mutants appear to be more susceptible to infection by RNA viruses (356).

RIG-I (357) and MDA5 (357, 358) are known to influence antiviral signaling in zebrafish (*Danio rerio*) and other fish species (357, 359–361) through the canonical MAVS signaling pathway. Fish RIG-I like receptors (RLRs) have been shown to

be regulated by the expression of alternate splicing isoforms (358, 362), which have also been found to occur with a dominant-negative splice variant of the human RIG-I (363). RIG-I and MDA5 have also been found to participate in anti-viral signaling in ducks (364–367) and geese (340, 368, 369), and MDA5 alone in chickens (370–372) and other birds (373). The observation across species of RLRs performing compensatory mechanisms when a function or a pathway protein is absent is reiterated in birds, as MDA5 has been found to sense short and long dsRNA in chickens (372) and in the Chinese shrew (374), both of which lack RIG-I. Additionally, TRIM25 activates RIG-I in ducks (364) and in the Chinese goose (375) in the absence of the K172 activating ubiquitin binding site that is conserved in primates and some rodents (364). Finally, the rainbow trout (*Oncorhynchus mykiss*) has been found to express a LGP2 variant in addition to the canonical LGP2 that contains an incomplete C-terminal domain of RIG-I (376). The differential presence of PRRs may also influence viral evolution. A mutation in the IAV polymerase subunit PB2 found in avian-adapted H1N1 strains decreases the inhibition of human RIG-I function by IAV nucleoproteins, which may indicate a differential selective pressure for viruses that propagate in species that don't contain RIG-I (377). The evolutionary pattern and compensatory mechanisms of RLRs across species implicate them as critical for anti-viral function, and that evolutionary forces drive the available pathway proteins to meet these functional needs. Future studies need to be done to further

differentiate RLR function among the different species, as this will provide critical information concerning the various methods of disease control by targeting the pathogen by these important host proteins.

There is also increasing evidence for other RNA-sensing DExD/H helicases serving important roles in anti-pathogen immune sensing, which have recently been reviewed elsewhere (187). Some RNA helicase (DDX) proteins appear to serve as complex proteins upon interacting with viral RNA. DDX3 is a well-known example, being suspected of being a transcription factor for IFN- β (378), associating with spliceosomes and the stress-induced p-bodies to influence mRNA splicing and decay, respectively (322, 378), and interacting with the MAVS complex during viral infection conditions (378, 379). In particular, DDX3 associating with MAVS has been found to be important for anti-viral control against several viruses (378–380), and since the two DDX3 homologs are found on the X and Y chromosomes, they may contribute to immunological differences between genders (381). This is a repeated theme, as DHX9 (382), DHX15 (383), and a complex consisting of DDX1/DDX21/DHX36 (384) have also been found to associate with the MAVS complex to enhance IFN1 signaling, while DHX33 interacts with MAVS independently of viral infection (385). DDX proteins can also activate other proteins in the IRF pathway. Multiple DDX proteins can interact with IKK ϵ , with DDX3 being phosphorylated by IKK ϵ to induce IRF3 interaction with the TBK1-IKK ϵ complex (378), and DDX19 blocking this interaction to inhibit IFN1 signaling (386). Similar control mechanisms have been demonstrated for DDX3 interacting with viral proteins. For example, DDX3 has recently been found to associate with arenaviral NPs to increase viral RNA synthesis and IFN1 expression (387). Additionally, the NP of the 1918 H1N1 IAV pandemic strain has been shown to target DDX3 for degradation as a potential mechanism of virulence (388). DHX15 (389) and DHX33 have also been found to activate NF κ B and

MAPK signaling pathways. Finally, DDX60 has been shown to act as a cofactor for RIG-I (390, 391) and DHX29 for MDA5 (392). Taken altogether, these cellular proteins have likely evolved to regulate RIG-I and MDA5 signaling from their common DExD/H helicase predecessors.

SUMMARY AND FUTURE OUTLOOKS

As our capacity to study the molecular mechanisms and to purposefully modulate immune responses increases in specificity, so will our needs to characterize the differences between related immune signaling proteins. The concept of personalized medicine derives from the idea that we can therapeutically intervene in a situation that is designed around the individual's unique characteristics. While this is an achievable realm of medicine in the future, an immediate step is to determine the functions of some critical proteins, such as the RIG-I and MDA5 of the innate immune arm. Examining their structural and functional similarities and differences at multiple levels will allow for a deeper level of appreciation of these proteins, which may be exploited therapeutically to differentially modulate RIG-I and MDA5 signalings by different RNA ligands (43, 191, 393, 394) or other pharmaceutical compounds (395) toward the goal of achieving personalized medicine.

AUTHOR CONTRIBUTIONS

MB and HL contributed to the literature review and writing of the manuscript. MB prepared all figures with inputs from HL.

FUNDING

This work was supported in part by NIH NIAID grant R01 AI131586 to HL and by a pre-doctoral NIH fellowship T32 DA007097 to MB.

REFERENCES

- Sun YW. RIG-I, a human homolog gene of RNA helicase, is induced by retinoic acid during the differentiation of acute promyelocytic leukemia cell. *Biochem Biophys Res Commun.* (1997) 292:274–9.
- Imaizumi T, Aratani S, Nakajima T, Carlson M, Matsumiya T, Tanji K, et al. Retinoic acid-inducible gene-I is induced in endothelial cells by LPS and regulates expression of COX-2. *Biochem Biophys Res Commun.* (2002) 292:274–9. doi: 10.1006/BBRC.2002.6650
- Kang D, Gopalakrishnan RV, Wu Q, Jankowsky E, Pyle AM, Fisher PB. mda-5: an interferon-inducible putative RNA helicase with double-stranded RNA-dependent ATPase activity and melanoma growth-suppressive properties. *Proc Natl Acad Sci USA.* (2002) 99:637–42. doi: 10.1073/PNAS.022637199
- Kovacsics M, Martinon F, Micheau O, Bodmer J-L, Hofmann K, Tschoep J. Overexpression of helicard, a CARD-containing helicase cleaved during apoptosis, accelerates DNA degradation. *Curr Biol.* (2002) 12:838–43. doi: 10.1016/S0960-9822(02)00842-4
- Randall RE, Goodbourn S. Interferons and viruses: an interplay between induction, signalling, antiviral responses and virus countermeasures. *J Gen Virol.* (2008) 89:1–47. doi: 10.1099/vir.0.83391-0
- Jacobs JL, Coyne CB. Mechanisms of MAVS regulation at the mitochondrial membrane. *J Mol Biol.* (2013) 425:5009–19. doi: 10.1016/j.jmb.2013.10.007
- Vazquez C, Horner SM. MAVS coordination of antiviral innate immunity. *J Virol.* (2015) 89:6974–7. doi: 10.1128/JVI.01918-14
- Tan P, He L, Cui J, Qian C, Cao X, Lin M, et al. Assembly of the WHIP-TRIM14-PPP6C mitochondrial complex promotes RIG-I-mediated antiviral signaling. *Mol Cell.* (2017) 68:293–307.e5. doi: 10.1016/j.molcel.2017.09.035
- Kouwaki T, Okamoto M, Tsukamoto H, Fukushima Y, Matsumoto M, Seya T, et al. Zyxin stabilizes RIG-I and MAVS interactions and promotes type I interferon response. *Sci Rep.* (2017) 7:11905. doi: 10.1038/s41598-017-12224-7
- Fitzgerald KA, McWhirter SM, Faia KL, Rowe DC, Latz E, Golenbock DT, et al. IKK ϵ and TBK1 are essential components of the IRF3 signaling pathway. *Nat Immunol.* (2003) 4:491–6. doi: 10.1038/ni921
- Sharma S, TenOever BR, Grandvaux N, Zhou G-P, Lin R, Hiscott J. Triggering the interferon antiviral response through an IKK-related pathway. *Science.* (2003) 300:1148–51. doi: 10.1126/science.1081315
- tenOever BR, Ng S-L, Chua MA, McWhirter SM, Garcia-Sastre A, Maniatis T. Multiple functions of the IKK-related kinase IKK ϵ in interferon-mediated antiviral immunity. *Science.* (2007) 315:1274–8. doi: 10.1126/science.1138527

13. Paz S, Sun Q, Nakhaei P, Romieu-Mourez R, Goubau D, Julkunen I, et al. Induction of IRF-3 and IRF-7 phosphorylation following activation of the RIG-I pathway. *Cell Mol Biol.* (2006) 52:17–28.
14. Ning S, Pagano JS, Barber GN. IRF7: activation, regulation, modification and function. *Genes Immun.* (2011) 12:399–414. doi: 10.1038/gene.2011.21
15. Mingzhu Zhu G, Fang T, Li S, Meng K. Activity of IFN regulatory factor 3 controls nuclear import and DNA-binding bipartite nuclear localization signal. *J Immunol.* (2015) 195:289–97. doi: 10.4049/jimmunol.1500232
16. Newton K, Dixit VM. Signaling in innate immunity and inflammation. *Cold Spring Harb Perspect Biol.* (2012) 4:a006049. doi: 10.1101/cshperspect.a006049
17. Kell AM, Gale M Jr. RIG-I in RNA virus recognition. *Virology.* (2015) 479–80:110–21. doi: 10.1016/j.virol.2015.02.017
18. Kato H, Takeuchi O, Sato S, Yoneyama M, Yamamoto M, Matsui K, et al. Differential roles of MDA5 and RIG-I helicases in the recognition of RNA viruses. *Nature.* (2006) 441:101–5. doi: 10.1038/nature04734
19. Weber-Gerlach M, Weber F. Standing on three legs: antiviral activities of RIG-I against influenza viruses. *Curr Opin Immunol.* (2016) 42:71–5. doi: 10.1016/J.COI.2016.05.016
20. Spengler JR, Patel JR, Chakrabarti AK, Zivcec M, García-Sastre A, Spiropoulou CF, et al. RIG-I mediates an antiviral response to crimean-congo hemorrhagic fever virus. *J Virol.* (2015) 89:10219–29. doi: 10.1128/JVI.01643-15
21. Yamada S, Shimojima M, Narita R, Tsukamoto Y, Kato H, Saijo M, et al. RIG-I-like receptor and toll-like receptor signaling pathways cause aberrant production of inflammatory cytokines/chemokines in a severe fever with thrombocytopenia syndrome virus infection mouse model. *J Virol.* (2018) 92:e02246-17. doi: 10.1128/JVI.02246-17
22. Spiropoulou CF, Ranjan P, Pearce MB, Sealy TK, Albariño CG, Gangappa S, et al. RIG-I activation inhibits ebolavirus replication. *Virology.* (2009) 392:11–5. doi: 10.1016/J.VIROL.2009.06.032
23. Furr SR, Moerdyk-Schauwecker M, Grdzelskshvili VZ, Marriott I. RIG-I mediates nonsegmented negative-sense RNA virus-induced inflammatory immune responses of primary human astrocytes. *Glia.* (2010) 58:1620–9. doi: 10.1002/glia.21034
24. Loo Y-M, Fornek J, Crochet N, Bajwa G, Perwitasari O, Martinez-Sobrido L, et al. Distinct RIG-I and MDA5 signaling by RNA viruses in innate immunity. *J Virol.* (2008) 82:335–45. doi: 10.1128/JVI.01080-07
25. Deddouche S, Goubau D, Rehwinkel J, Chakravarty P, Begum S, Maillard PV, et al. Identification of an LGP2-associated MDA5 agonist in picornavirus-infected cells. *Elife.* (2014) 3:e1535. doi: 10.7554/eLife.01535
26. Luo R, Xiao S, Jiang Y, Jin H, Wang D, Liu M, et al. Porcine reproductive and respiratory syndrome virus (PRRSV) suppresses interferon- β production by interfering with the RIG-I signaling pathway. *Mol Immunol.* (2008) 45:2839–46. doi: 10.1016/J.MOLIMM.2008.01.028
27. van Kasteren PB, Beugeling C, Ninaber DK, Frias-Staheli N, van Boheemen S, García-Sastre A, et al. Arterivirus and nairovirus ovarian tumor domain-containing deubiquitinases target activated RIG-I to control innate immune signaling. *J Virol.* (2012) 86:773–85. doi: 10.1128/JVI.06277-11
28. Zhang Z, Filzmayer C, Ni Y, Sülmann H, Mutz P, Hiet M-S, et al. Hepatitis D virus replication is sensed by MDA5 and induces IFN- β / λ responses in hepatocytes. *J Hepatol.* (2018) 69:25–35. doi: 10.1016/j.jhep.2018.02.021
29. Zhao Y, Ye X, Dunker W, Song Y, Karjohelch J. RIG-I like receptor sensing of host RNAs facilitates the cell-intrinsic immune response to KSHV infection. *Nat Commun.* (2018) 9:4841. doi: 10.1038/s41467-018-07314-7
30. Ye W, Chew M, Hou J, Lai F, Leopold SJ, Loo HL, et al. Microvesicles from malaria-infected red blood cells activate natural killer cells via MDA5 pathway. *PLoS Pathog.* (2018) 14:e1007298. doi: 10.1371/journal.ppat.1007298
31. Qin C-F, Zhao H, Liu Z-Y, Jiang T, Deng Y-Q, Yu X-D, et al. Retinoic acid inducible gene-I and melanoma differentiation-associated gene 5 are induced but not essential for dengue virus induced type I interferon response. *Mol Biol Rep.* (2011) 38:3867–73. doi: 10.1007/s11033-010-0502-7
32. Nasirudeen AMA, Wong HH, Thien P, Xu S, Lam K-P, Liu DX. RIG-I, MDA5 and TLR3 synergistically play an important role in restriction of dengue virus infection. *PLoS Negl Trop Dis.* (2011) 5:e926. doi: 10.1371/journal.pntd.0000926
33. Fredericksen BL, Keller BC, Fornek J, Katze MG, Gale M. Establishment and maintenance of the innate antiviral response to West Nile virus involves both RIG-I and MDA5 signaling through IPS-1[†]. *J Virol.* (2008) 82:609–16. doi: 10.1128/JVI.01305-07
34. Errett JS, Suthar MS, McMillan A, Diamond MS, Gale M. The essential, nonredundant roles of RIG-I and MDA5 in detecting and controlling West Nile virus infection. *J Virol.* (2013) 87:11416–25. doi: 10.1128/JVI.01488-13
35. Sanchez David RY, Combredet C, Sismeiro O, Dillies M-A, Jagla B, Coppée J-Y, et al. Comparative analysis of viral RNA signatures on different RIG-I-like receptors. *Elife.* (2016) 5:e11275. doi: 10.7554/eLife.11275
36. Gitlin L, Benoit L, Song C, Cella M, Gilfillan S, Holtzman MJ, et al. Melanoma Differentiation-Associated Gene 5 (MDA5) is involved in the innate immune response to paramyxoviridae infection *in vivo*. *PLoS Pathog.* (2010) 6:e1000734. doi: 10.1371/journal.ppat.1000734
37. Grandvaux N, Guan X, Yoboua F, Zucchini N, Fink K, Doyon P, et al. Sustained activation of interferon regulatory factor 3 during infection by paramyxoviruses requires MDA5. *J Innate Immun.* (2014) 6:650–62. doi: 10.1159/000360764
38. Kim W-K, Jain D, Sánchez MD, Koziol-White CJ, Matthews K, Ge MQ, et al. Deficiency of melanoma differentiation-associated protein 5 results in exacerbated chronic postviral lung inflammation. *Am J Respir Crit Care Med.* (2014) 189:437–48. doi: 10.1164/rccm.201307-1338OC
39. Broquet AH, Hirata Y, McAllister CS, Kagnoff MF. RIG-I/MDA5/MAVS are required to signal a protective IFN response in rotavirus-infected intestinal epithelium. *J Immunol.* (2011) 186:1618–26. doi: 10.4049/JIMMUNOL.1002862
40. Yoneyama M, Kikuchi M, Matsumoto K, Imaizumi T, Miyagishi M, Taira K, et al. Shared and unique functions of the DEXD/H-box helicases RIG-I, MDA5, and LGP2 in antiviral innate immunity. *J Immunol.* (2005) 175:2851–8. doi: 10.4049/JIMMUNOL.175.5.2851
41. Kato H, Sato S, Yoneyama M, Yamamoto M, Uematsu S, Matsui K, et al. Cell type-specific involvement of RIG-I in antiviral response. *Immunity.* (2005) 23:19–28. doi: 10.1016/J.IMMUNI.2005.04.010
42. Wang Y, Zhang H-X, Sun Y-P, Liu Z-X, Liu X-S, Wang L, et al. RIG-I $-/-$ mice develop colitis associated with downregulation of Gai2. *Cell Res.* (2007) 17:858–68. doi: 10.1038/cr.2007.81
43. Kasumba DM, Grandvaux N. Therapeutic targeting of RIG-I and MDA5 might not lead to the same Rome. *Trends Pharmacol Sci.* (2018) 40:116–27. doi: 10.1016/j.tips.2018.12.003
44. Ng CS, Kato H, Fujita T. Fueling type I interferonopathies: regulation and function of type I interferon antiviral responses. *J Interf Cytokine Res.* (2019). doi: 10.1089/jir.2019.0037. [Epub ahead of print].
45. Peckham D, Scambler T, Savic S, McDermott MF. The burgeoning field of innate immune-mediated disease and autoinflammation. *J Pathol.* (2017) 241:123–39. doi: 10.1002/path.4812
46. Czerkies M, Korwek Z, Prus W, Kochanczyk M, Jaruszewicz-Błonska J, Tudelska K, et al. Cell fate in antiviral response arises in the crosstalk of IRF, NF- κ B and JAK/STAT pathways. *Nat Commun.* (2018) 9:493. doi: 10.1038/s41467-017-02640-8
47. Yoboua F, Martel A, Duval A, Mukawera E, Grandvaux N. Respiratory syncytial virus-mediated NF- κ B p65 phosphorylation at serine 536 is dependent on RIG-I, TRAF6, and IKK β . *J Virol.* (2010) 84:7267–77. doi: 10.1128/JVI.00142-10
48. Rückle A, Haasbach E, Julkunen I, Planz O, Ehrhardt C, Ludwig S. The NS1 protein of influenza A virus blocks RIG-I-mediated activation of the noncanonical NF- κ B pathway and p52/RelB-dependent gene expression in lung epithelial cells. *J Virol.* (2012) 86:10211–7. doi: 10.1128/JVI.00323-12
49. Bertin J, Guo Y, Wang L, Srinivasula SM, Jacobson MD, Poyet JL, et al. CARD9 is a novel caspase recruitment domain-containing protein that interacts with BCL10/CLAP and activates NF- κ B. *J Biol Chem.* (2000) 275:41082–6. doi: 10.1074/jbc.C000726200
50. Poeck H, Bscheider M, Gross O, Finger K, Roth S, Rebsamen M, et al. Recognition of RNA virus by RIG-I results in activation of CARD9 and inflammasome signaling for interleukin 1 β production. *Nat Immunol.* (2010) 11:63–9. doi: 10.1038/ni.1824
51. Lee N-R, Kim H-I, Choi M-S, Yi C-M, Inn K-S. Regulation of MDA5-MAVS antiviral signaling axis by TRIM25 through TRAF6-mediated NF- κ B activation. *Mol Cells.* (2015) 38:759–64. doi: 10.14348/molcells.2015.0047

52. Martín-Vicente M, Medrano LM, Resino S, García-Sastre A, Martínez I. TRIM25 in the regulation of the antiviral innate immunity. *Front Immunol.* (2017) 8:1187. doi: 10.3389/fimmu.2017.01187
53. Loo Y-M, Gale M Jr. Immune signaling by RIG-I-like receptors. *Immunity.* (2011) 34:680–92. doi: 10.1016/j.immuni.2011.05.003
54. Song M-S, Rossi JJ. Molecular mechanisms of Dicer: endonuclease and enzymatic activity. *Biochem J.* (2017) 474:1603–18. doi: 10.1042/BCJ20160759
55. van der Veen AG, Maillard PV, Schmidt JM, Lee SA, Deddouche-Grass S, Borg A, et al. The RIG-I-like receptor LGP2 inhibits Dicer-dependent processing of long double-stranded RNA and blocks RNA interference in mammalian cells. *EMBO J.* (2018) 37:e97479. doi: 10.15252/embj.201797479
56. Takahashi T, Nakano Y, Onomoto K, Yoneyama M, Ui-Tei K. Virus sensor RIG-I represses RNA interference by interacting with TRBP through LGP2 in mammalian cells. *Genes.* (2018) 9:E511. doi: 10.3390/genes9100511
57. Moresco EMY, Beutler B. LGP2: positive about viral sensing. *Proc Natl Acad Sci USA.* (2010) 107:1261–2. doi: 10.1073/pnas.0914011107
58. Rodriguez KR, Bruns AM, Horvath CM. MDA5 and LGP2: accomplices and antagonists of antiviral signal transduction. *J Virol.* (2014) 88:8194–200. doi: 10.1128/JVI.00640-14
59. Quicke KM, Diamond MS, Suthar MS. Negative regulators of the RIG-I-like receptor signaling pathway. *Eur J Immunol.* (2017) 47:615–28. doi: 10.1002/eji.201646484
60. Uhlen M, Fagerberg L, Hallström BM, Lindskog C, Oksvold P, Mardinoglu A, et al. Tissue-based map of the human proteome. *Science.* (2015) 347:1260419. doi: 10.1126/science.1260419
61. Devarkar SC, Wang C, Miller MT, Ramanathan A, Jiang F, Khan AG, et al. Structural basis for m7G recognition and 2'-O-methyl discrimination in capped RNAs by the innate immune receptor RIG-I. *Proc Natl Acad Sci USA.* (2016) 113:596–601. doi: 10.1073/pnas.1515152113
62. Wu B, Peisley A, Richards C, Yao H, Zeng X, Lin C, et al. Structural basis for dsRNA recognition, filament formation, and antiviral signal activation by MDA5. *Cell.* (2013) 152:276–89. doi: 10.1016/j.cell.2012.11.048
63. Wu B, Peisley A, Tetrauld D, Li Z, Egelman EHH, Magor KEE, et al. Molecular imprinting as a signal-activation mechanism of the viral RNA sensor RIG-I. *Mol Cell.* (2014) 55:511–23. doi: 10.1016/j.molcel.2014.06.010
64. Rawling DC, Pyle AM. Parts, assembly and operation of the RIG-I family of motors. *Curr Opin Struct Biol.* (2014) 25:25–33. doi: 10.1016/j.SBI.2013.11.011
65. Yoneyama M, Kikuchi M, Natsukawa T, Shinobu N, Imaizumi T, Miyagishi M, et al. The RNA helicase RIG-I has an essential function in double-stranded RNA-induced innate antiviral responses. *Nat Immunol.* (2004) 5:730–7. doi: 10.1038/ni1087
66. Cui S, Eisenächer K, Kirchhofer A, Brzózka K, Lammens A, Lammens K, et al. The C-terminal regulatory domain is the RNA 5'-triphosphate sensor of RIG-I. *Mol Cell.* (2008) 29:169–79. doi: 10.1016/j.molcel.2007.10.032
67. Hornung V, Ellegast J, Kim S, Brzózka K, Jung A, Kato H, et al. 5'-Triphosphate RNA is the ligand for RIG-I. *Science.* (2006) 314:994–7. doi: 10.1126/science.1132505
68. Pichlmair A, Schulz O, Tan CP, Naslund TI, Liljestrom P, Weber F, et al. RIG-I-mediated antiviral responses to single-stranded RNA bearing 5'-Phosphates. *Science.* (2006) 314:997–1001. doi: 10.1126/science.1132998
69. Takahashi K, Yoneyama M, Nishihori T, Hirai R, Kumeta H, Narita R, et al. Nonself RNA-sensing mechanism of RIG-I helicase and activation of antiviral immune responses. *Mol Cell.* (2008) 29:428–40. doi: 10.1016/j.molcel.2007.11.028
70. Myong S, Cui S, Cornish PV, Kirchhofer A, Gack MU, Jung JU, et al. Cytosolic viral sensor RIG-I is a 5'-Triphosphate-dependent translocase on double-stranded RNA. *Science.* (2009) 323:1070–4. doi: 10.1126/science.1168352
71. Lu C, Xu H, Ranjith-Kumar CT, Brooks MT, Hou TY, Hu F, et al. The structural basis of 5' triphosphate double-stranded RNA recognition by RIG-I C-terminal domain. *Structure.* (2010) 18:1032–43. doi: 10.1016/j.str.2010.05.007
72. Rehwinkel J, Tan CP, Goubau D, Schulz O, Pichlmair A, Bier K, et al. RIG-I detects viral genomic RNA during negative-strand RNA virus infection. *Cell.* (2010) 140:397–408. doi: 10.1016/j.cell.2010.01.020
73. Wang Y, Ludwig J, Schuberth C, Goldeck M, Schlee M, Li H, et al. Structural and functional insights into 5'-ppp RNA pattern recognition by the innate immune receptor RIG-I. *Nat Struct Mol Biol.* (2010) 17:781–7. doi: 10.1038/nsmb.1863
74. Vela A, Fedorova O, Ding SC, Pyle AM. The thermodynamic basis for viral RNA detection by the RIG-I innate immune sensor. *J Biol Chem.* (2012) 287:42564–73. doi: 10.1074/jbc.M112.385146
75. Anchisi S, Guerra J, Garcin D. RIG-I ATPase activity and discrimination of self-RNA versus non-self-RNA. *MBio.* (2015) 6:e02349-14. doi: 10.1128/MBIO.02349-14
76. Kato H, Takeuchi O, Mikamo-Sato H, Hirai R, Kawai T, Matsushita K, et al. Length-dependent recognition of doublestranded ribonucleic acids by retinoic acid – inducible gene-I and melanoma differentiation – associated gene 5. *J Exp Med.* (2008) 205:1601–10. doi: 10.1084/jem.20080091
77. Pichlmair A, Schulz O, Tan C-P, Rehwinkel J, Kato H, Takeuchi O, et al. Activation of MDA5 requires higher-order RNA structures generated during virus infection. *J Virol.* (2009) 83:10761–9. doi: 10.1128/JVI.00770-09
78. Feng Q, Hato SV, Langereis MA, Zoll J, Virgen-Slane R, Peisley A, et al. MDA5 detects the double-stranded RNA replicative form in picornavirus-infected cells. *Cell Rep.* (2012) 2:1187–96. doi: 10.1016/j.celrep.2012.10.005
79. Triantafyllou K, Vakakis E, Kar S, Richer E, Evans GL, Triantafyllou M. Visualisation of direct interaction of MDA5 and the dsRNA replicative intermediate form of positive strand RNA viruses. *J Cell Sci.* (2012) 125:4761–9. doi: 10.1242/jcs.103887
80. Kolakofsky D, Kowalinski E, Cusack S. A structure-based model of RIG-I activation. *RNA.* (2012) 18:2118–27. doi: 10.1261/rna.035949.112
81. Luo D. Toward a crystal-clear view of the viral RNA sensing and response by RIG-I-like receptors. *RNA Biol.* (2014) 11:25–32. doi: 10.4161/rna.27717
82. Reikine S, Nguyen JB, Modis Y. Pattern recognition and signaling mechanisms of RIG-I and MDA5. *Front Immunol.* (2014) 5:342. doi: 10.3389/fimmu.2014.00342
83. Bruns AM, Horvath CM. Antiviral RNA recognition and assembly by RLR family innate immune sensors. *Cytokine Growth Factor Rev.* (2014) 25:507–12. doi: 10.1016/j.CYTOGRF.2014.07.006
84. Chiang C, Gack MU. Post-translational control of intracellular pathogen sensing pathways. *Trends Immunol.* (2017) 38:39–52. doi: 10.1016/j.IT.2016.10.008
85. Gee P, Chua PK, Gevorkyan J, Klumpp K, Najera I, Swinney DC, et al. Essential role of the N-terminal domain in the regulation of RIG-I ATPase activity. *J Biol Chem.* (2008) 283:9488–96. doi: 10.1074/jbc.M706777200
86. Kowalinski E, Lunardi T, McCarthy AA, Louber J, Brunel J, Grigorov B, et al. Structural basis for the activation of innate immune pattern-recognition receptor RIG-I by viral RNA. *Cell.* (2011) 147:423–35. doi: 10.1016/j.cell.2011.09.039
87. Feng M, Ding Z, Xu L, Kong L, Wang W, Jiao S, et al. Structural and biochemical studies of RIG-I antiviral signaling. *Protein Cell.* (2013) 4:142–54. doi: 10.1007/s13238-012-2088-4
88. Nistal-Villán E, Gack MU, Martínez-Delgado G, Maharaj NP, Inn K-S, Yang H, et al. Negative role of RIG-I serine 8 phosphorylation in the regulation of interferon-beta production. *J Biol Chem.* (2010) 285:20252–61. doi: 10.1074/jbc.M109.089912
89. Maharaj NP, Wies E, Stoll A, Gack MU. Conventional protein kinase C- α (PKC- α) and PKC- β negatively regulate RIG-I antiviral signal transduction. *J Virol.* (2012) 86:1358–71. doi: 10.1128/JVI.06543-11
90. Sun Z, Ren H, Liu Y, Teeling JL, Gu J. Phosphorylation of RIG-I by casein kinase II inhibits its antiviral response. *J Virol.* (2011) 85:1036–47. doi: 10.1128/JVI.01734-10
91. Takashima K, Oshiumi H, Takaki H, Matsumoto M, Seya T. RIG-I-mediated phosphorylation of MDA5 interferes with its assembly and attenuates the innate immune response. *Cell Rep.* (2015) 11:192–200. doi: 10.1016/j.celrep.2015.03.027
92. Wies E, Wang MK, Maharaj NP, Chen K, Zhou S, Finberg RW, et al. Dephosphorylation of the RNA sensors RIG-I and MDA5 by the phosphatase PP1 is essential for innate immune signaling. *Immunity.* (2013) 38:437–49. doi: 10.1016/j.immuni.2012.11.018
93. Davis ME, Wang MK, Rennick LJ, Full F, Gableske S, Mesman AW, et al. Antagonism of the phosphatase PP1 by the measles virus V protein is required for innate immune escape of MDA5. *Cell Host Microbe.* (2014) 16:19–30. doi: 10.1016/J.CHOM.2014.06.007

94. Choi SJ, Lee H-C, Kim J-H, Park SY, Kim T-H, Lee W-K, et al. HDAC6 regulates cellular viral RNA sensing by deacetylation of RIG-I. *EMBO J.* (2016) 35:429–42. doi: 10.15252/embj.201592586
95. Hilbert M, Karow AR, Klostermeier D. The mechanism of ATP-dependent RNA unwinding by DEAD box proteins. *Biol Chem.* (2009) 390:1237–50. doi: 10.1515/BC.2009.135
96. Gack MU. Mechanisms of RIG-I-like receptor activation and manipulation by viral pathogens. *J Virol.* (2014) 88:5213–6. doi: 10.1128/JVI.03370-13
97. Weber F. The catcher in the RIG-I. *Cytokine.* (2015) 76:38–41. doi: 10.1016/J.CYTO.2015.07.002
98. Yoneyama M, Onomoto K, Jogi M, Akaboshi T, Fujita T. Viral RNA detection by RIG-I-like receptors. *Curr Opin Immunol.* (2015) 32:48–53. doi: 10.1016/J.COI.2014.12.012
99. Berke IC, Modis Y. MDA5 cooperatively forms dimers and ATP-sensitive filaments upon binding double-stranded RNA. *EMBO J.* (2012) 31:1714–26. doi: 10.1038/emboj.2012.19
100. Oshiumi H, Matsumoto M, Hatakeyama S, Seya T. Riplet/RNF135, a RING finger protein, ubiquitinates RIG-I to promote interferon-beta induction during the early phase of viral infection. *J Biol Chem.* (2009) 284:807–17. doi: 10.1074/jbc.M804259200
101. Gao D, Yang Y-K, Wang R-P, Zhou X, Diao F-C, Li M-D, et al. REUL is a novel E3 ubiquitin ligase and stimulator of retinoic-acid-inducible gene-I. *PLoS ONE.* (2009) 4:e5760. doi: 10.1371/journal.pone.0005760
102. Oshiumi H, Miyashita M, Matsumoto M, Seya T. A distinct role of Riplet-mediated K63-linked polyubiquitination of the RIG-I repressor domain in human antiviral innate immune responses. *PLoS Pathog.* (2013) 9:e1003533. doi: 10.1371/journal.ppat.1003533
103. Cadena C, Ahmad S, Xavier A, Willemsen J, Park S, Park JW, et al. Ubiquitin-dependent and -independent roles of E3 ligase RIPLET in innate immunity. *Cell.* (2019) 0:1187–200.e16. doi: 10.1016/j.cell.2019.03.017
104. Gack MU, Shin YC, Joo C-H, Urano T, Liang C, Sun L, et al. TRIM25 RING-finger E3 ubiquitin ligase is essential for RIG-I-mediated antiviral activity. *Nature.* (2007) 446:916–20. doi: 10.1038/nature05732
105. Wang P, Arjona A, Zhang Y, Sultana H, Dai J, Yang L, et al. Caspase-12 controls West Nile virus infection via the viral RNA receptor RIG-I. *Nat Immunol.* (2010) 11:912–9. doi: 10.1038/ni.1933
106. Lin H, Jiang M, Liu L, Yang Z, Ma Z, Liu S, et al. The long noncoding RNA lnc3h7a promotes a TRIM25-mediated RIG-I antiviral innate immune response. *Nat Immunol.* (2019) 20:812–23. doi: 10.1038/s41590-019-0379-0
107. Shi Y, Yuan B, Zhu W, Zhang R, Li L, Hao X, et al. Ube2D3 and Ube2N are essential for RIG-I-mediated MAVS aggregation in antiviral innate immunity. *Nat Commun.* (2017) 8:15138. doi: 10.1038/ncomms15138
108. Liu Z, Wu C, Pan Y, Liu H, Wang X, Yang Y, et al. NDR2 promotes the antiviral immune response via facilitating TRIM25-mediated RIG-I activation in macrophages. *Sci Adv.* (2019) 5:eaav0163. doi: 10.1126/sciadv.aav0163
109. Pauli E-K, Chan YK, Davis ME, Gableske S, Wang MK, Feister KF, et al. The ubiquitin-specific protease USP15 promotes RIG-I-mediated antiviral signaling by deubiquitylating TRIM25. *Sci Signal.* (2014) 7:ra3. doi: 10.1126/scisignal.2004577
110. Liu HM, Loo Y-M, Horner SM, Zornetzer GA, Katze MG, Gale M. The mitochondrial targeting chaperone 14-3-3 ϵ regulates a RIG-I translocan that mediates membrane association and innate antiviral immunity. *Cell Host Microbe.* (2012) 11:528–37. doi: 10.1016/j.chom.2012.04.006
111. Yan J, Li Q, Mao A-P, Hu M-M, Shu H-B. TRIM4 modulates type I interferon induction and cellular antiviral response by targeting RIG-I for K63-linked ubiquitination. *J Mol Cell Biol.* (2014) 6:154–63. doi: 10.1093/jmcb/mju005
112. Sanchez JG, Chiang JJ, Sparrer KMJ, Alam SL, Chi M, Roganowicz MD, et al. Mechanism of TRIM25 catalytic activation in the antiviral RIG-I pathway. *Cell Rep.* (2016) 16:1315–25. doi: 10.1016/J.CELREP.2016.06.070
113. Gack MU, Albrecht RA, Urano T, Inn K-S, Huang I-C, Carnero E, et al. Influenza A virus NS1 targets the ubiquitin ligase TRIM25 to evade recognition by the host viral RNA sensor RIG-I. *Cell Host Microbe.* (2009) 5:439–49. doi: 10.1016/j.chom.2009.04.006
114. Rajsbaum R, Albrecht RA, Wang MK, Maharaj NP, Versteeg GA, Nistal-Villán E, et al. Species-specific inhibition of RIG-I ubiquitination and IFN induction by the influenza A virus NS1 protein. *PLoS Pathog.* (2012) 8:e1003059. doi: 10.1371/journal.ppat.1003059
115. Chiang C, Pauli E-K, Biryukov J, Feister KF, Meng M, White EA, et al. The human papillomavirus E6 oncoprotein targets USP15 and TRIM25 to suppress RIG-I-mediated innate immune signaling. *J Virol.* (2018) 92:e01737-17. doi: 10.1128/JVI.01737-17
116. Koliopoulos MG, Lethier M, van der Veen AG, Haubrich K, Hennig J, Kowalinski E, et al. Molecular mechanism of influenza A NS1-mediated TRIM25 recognition and inhibition. *Nat Commun.* (2018) 9:1820. doi: 10.1038/s41467-018-04214-8
117. Chen S-T, Chen L, Lin DS-C, Chen S-Y, Tsao Y-P, Guo H, et al. NLRP12 regulates anti-viral RIG-I activation via interaction with TRIM25. *Cell Host Microbe.* (2019) 25:602–16.e7. doi: 10.1016/j.chom.2019.02.013
118. Zeng W, Sun L, Jiang X, Chen X, Hou F, Adhikari A, et al. Reconstitution of the RIG-I pathway reveals a signaling role of unanchored polyubiquitin chains in innate immunity. *Cell.* (2010) 141:315–30. doi: 10.1016/j.cell.2010.03.029
119. Maelfait J, Beyaert R. Emerging role of ubiquitination in antiviral RIG-I signaling. *Microbiol Mol Biol Rev.* (2012) 76:33–45. doi: 10.1128/MMBR.05012-11
120. Sun X, Xian H, Tian S, Sun T, Qin Y, Zhang S, et al. A hierarchical mechanism of RIG-I ubiquitination provides sensitivity, robustness and synergy in antiviral immune responses. *Sci Rep.* (2016) 6:29263. doi: 10.1038/srep29263
121. Xian H, Xie W, Yang S, Liu Q, Xia X, Jin S, et al. Stratified ubiquitination of RIG-I creates robust immune response and induces selective gene expression. *Sci Adv.* (2017) 3:e1701764. doi: 10.1126/sciadv.1701764
122. Oshiumi H, Matsumoto M, Seya T. Ubiquitin-mediated modulation of the cytoplasmic viral RNA sensor RIG-I. *J Biochem.* (2012) 151:5–11. doi: 10.1093/jb/mvr111
123. Zhao C, Jia M, Song H, Yu Z, Wang W, Li Q, et al. The E3 ubiquitin ligase TRIM40 attenuates antiviral immune responses by targeting MDA5 and RIG-I. *Cell Rep.* (2017) 21:1613–23. doi: 10.1016/J.CELREP.2017.10.020
124. Okamoto M, Kouwaki T, Fukushima Y, Oshiumi H. Regulation of RIG-I activation by K63-linked polyubiquitination. *Front Immunol.* (2017) 8:1942. doi: 10.3389/fimmu.2017.01942
125. Lian H, Zang R, Wei J, Ye W, Hu M-M, Chen Y-D, et al. The zinc-finger protein ZCCHC3 binds RNA and facilitates viral RNA sensing and activation of the RIG-I-like receptors. *Immunity.* (2018) 49:438–48.e5. doi: 10.1016/j.immuni.2018.08.014
126. Zhang H-L, Ye H-Q, Liu S-Q, Deng C-L, Li X-D, Shi P-Y, et al. West Nile virus NS1 antagonizes interferon beta production by targeting RIG-I and MDA5. *J Virol.* (2017) 91:e02396-16. doi: 10.1128/JVI.02396-16
127. Lang X, Tang T, Jin T, Ding C, Zhou R, Jiang W. TRIM65-catalyzed ubiquitination is essential for MDA5-mediated antiviral innate immunity. *J Exp Med.* (2017) 214:459–73. doi: 10.1084/jem.20160592
128. Peisley A, Wu B, Xu H, Chen ZJ, Hur S. Structural basis for ubiquitin-mediated antiviral signal activation by RIG-I. *Nature.* (2014) 509:110–4. doi: 10.1038/NATURE13140
129. Tang ED, Wang C-Y. MAVS self-association mediates antiviral innate immune signaling. *J Virol.* (2009) 83:3420–8. doi: 10.1128/JVI.02623-08
130. Hou F, Sun L, Zheng H, Skaug B, Jiang QX, Chen ZJ. MAVS forms functional prion-like aggregates to activate and propagate antiviral innate immune response. *Cell.* (2011) 146:448–61. doi: 10.1016/j.cell.2011.06.041
131. Xu H, He X, Zheng H, Huang LJ, Hou F, Yu Z, et al. Structural basis for the prion-like MAVS filaments in antiviral innate immunity. *Elife.* (2014) 3:e1489. doi: 10.7554/eLife.01489
132. He L, Lührs T, Ritter C. Solid-state NMR resonance assignments of the filament-forming CARD domain of the innate immunity signaling protein MAVS. *Biomol NMR Assign.* (2015) 9:223–7. doi: 10.1007/s12104-014-9579-6
133. Wu B, Hur S. How RIG-I like receptors activate MAVS. *Curr Opin Virol.* (2015) 12:91–8. doi: 10.1016/j.coviro.2015.04.004
134. Luo D, Kohlway A, Vela A, Pyle AM. Visualizing the determinants of viral RNA recognition by innate immune sensor RIG-I. *Structure.* (2012) 20:1983–8. doi: 10.1016/j.str.2012.08.029
135. Kohlway A, Luo D, Rawling DC, Ding SC, Pyle AM. Defining the functional determinants for RNA surveillance by RIG-I. *EMBO Rep.* (2013) 14:772–9. doi: 10.1038/embor.2013.108
136. Linehan MM, Dickey TH, Molinari ES, Fitzgerald ME, Potapova O, Iwasaki A, et al. A minimal RNA ligand for potent RIG-I activation in living mice. *Sci Adv.* (2018) 4:e1701854. doi: 10.1126/sciadv.1701854

137. Peisley A, Lin C, Wu B, Orme-Johnson M, Liu M, Walz T, et al. Cooperative assembly and dynamic disassembly of MDA5 filaments for viral dsRNA recognition. *Proc Natl Acad Sci USA*. (2011) 108:21010–5. doi: 10.1073/pnas.1113651108
138. Berke IC, Yu X, Modis Y, Egelman EH. MDA5 assembles into a polar helical filament on dsRNA. *Proc Natl Acad Sci USA*. (2012) 109:18437–41. doi: 10.1073/pnas.1212186109
139. Lin J-P, Fan Y-K, Liu HM. The 14-3-3 η chaperone protein promotes antiviral innate immunity via facilitating MDA5 oligomerization and intracellular redistribution. *PLoS Pathog*. (2019) 15:e1007582. doi: 10.1371/journal.ppat.1007582
140. Zheng Y, Gao C. E3 ubiquitin ligases, the powerful modulator of innate antiviral immunity. *Cell Immunol*. (2019) 340:103915. doi: 10.1016/j.CELLIMM.2019.04.003
141. Patel JR, Jain A, Chou Y, Baum A, Ha T, García-Sastre A. ATPase-driven oligomerization of RIG-I on RNA allows optimal activation of type-I interferon. *EMBO Rep*. (2013) 14:780–7. doi: 10.1038/embor.2013.102
142. Peisley A, Wu B, Yao H, Walz T, Hur S. RIG-I forms signaling-competent filaments in an ATP-dependent, ubiquitin-independent manner. *Mol Cell*. (2013) 51:573–83. doi: 10.1016/j.MOLCEL.2013.07.024
143. Binder M, Eberle F, Seitz S, Mücke N, Hüber CM, Kiani N, et al. Molecular mechanism of signal perception and integration by the innate immune sensor retinoic acid-inducible gene-I (RIG-I). *J Biol Chem*. (2011) 286:27278–87. doi: 10.1074/jbc.M111.256974
144. Devarkar SC, Schweibenz B, Wang C, Marcotrigiano J, Patel SS. RIG-I uses an ATPase-powered translocation-throttling mechanism for kinetic proofreading of RNAs and oligomerization. *Mol Cell*. (2018) 72:355–68.e4. doi: 10.1016/j.molcel.2018.08.021
145. Sohn J, Hur S. Filament assemblies in foreign nucleic acid sensors. *Curr Opin Struct Biol*. (2016) 37:134–44. doi: 10.1016/j.sbi.2016.01.011
146. Kawai T, Takahashi K, Sato S, Coban C, Kumar H, Kato H, et al. IPS-1, an adaptor triggering RIG-I- and Mda5-mediated type I interferon induction. *Nat Immunol*. (2005) 6:981–8. doi: 10.1038/ni1243
147. Xu L-G, Wang Y-Y, Han K-J, Li L-Y, Zhai Z, Shu H-B. VISA is an adaptor protein required for virus-triggered IFN- β signaling. *Mol Cell*. (2005) 19:727–40. doi: 10.1016/j.MOLCEL.2005.08.014
148. Seth RB, Sun L, Ea C-K, Chen ZJ. Identification and characterization of MAVS, a mitochondrial antiviral signaling protein that activates NF- κ B and IRF3. *Cell*. (2005) 122:669–82. doi: 10.1016/j.CELL.2005.08.012
149. Hu J, Nistal-Villán E, Voho A, Ganee A, Kumar M, Ding Y, et al. A common polymorphism in the caspase recruitment domain of RIG-I modifies the innate immune response of human dendritic cells. *J Immunol*. (2010) 185:424–32. doi: 10.4049/jimmunol.0903291
150. Marcus PI, Sekellick MJ. Defective interfering particles with covalently linked (+/-)RNA induce interferon. *Nature*. (1977) 266:815–9. doi: 10.1038/266815a0
151. Ferrage F, Dutta K, Nistal-Villán E, Patel JR, Sánchez-Aparicio MT, De Ioannes P, et al. Structure and dynamics of the second CARD of human RIG-I provide mechanistic insights into regulation of RIG-I activation. *Structure*. (2012) 20:2048–61. doi: 10.1016/j.str.2012.09.003
152. Takeuchi O, Akira S. Pattern recognition receptors and inflammation. *Cell*. (2010) 140:805–20. doi: 10.1016/j.cell.2010.01.022
153. Arnoult D, Soares F, Tattoli I, Girardin SE. Mitochondria in innate immunity. *EMBO Rep*. (2011) 12:901–10. doi: 10.1038/EMBOR.2011.157
154. Schröder M, Baran M, Bowie AG. Viral targeting of DEAD box protein 3 reveals its role in TBK1/IKKepsilon-mediated IRF activation. *EMBO J*. (2008) 27:2147–57. doi: 10.1038/emboj.2008.143
155. Ng CT, Sullivan BM, Teijaro JR, Lee AM, Welch M, Rice S, et al. Blockade of interferon beta, but not interferon alpha, signaling controls persistent viral infection. *Cell Host Microbe*. (2015) 17:653–61. doi: 10.1016/j.chom.2015.04.005
156. Tsau JS, Huang X, Lai C-Y, Hedrick SM. The effects of dendritic cell hypersensitivity on persistent viral infection. *J Immunol*. (2018) 200:1335–46. doi: 10.4049/jimmunol.1601870
157. Camp JV, Jonsson CB. A role for neutrophils in viral respiratory disease. *Front Immunol*. (2017) 8:550. doi: 10.3389/fimmu.2017.00550
158. Gilliet M, Cao W, Liu Y-J. Plasmacytoid dendritic cells: sensing nucleic acids in viral infection and autoimmune diseases. *Nat Rev Immunol*. (2008) 8:594–606. doi: 10.1038/nri2358
159. Kong L, Sun L, Zhang H, Liu Q, Liu Y, Qin L, et al. An essential role for RIG-I in toll-like receptor-stimulated phagocytosis. *Cell Host Microbe*. (2009) 6:150–61. doi: 10.1016/j.chom.2009.06.008
160. Ma H, Han P, Ye W, Chen H, Zheng X, Cheng L, et al. The long noncoding RNA NEAT1 exerts antihantaviral effects by acting as positive feedback for RIG-I signaling. *J Virol*. (2017) 91:e02250-16. doi: 10.1128/JVI.02250-16
161. Marie I, Durbin JE, Levy D. Differential viral induction of distinct interferon-alpha genes by positive feedback through interferon regulatory factor-7. *EMBO J*. (1998) 17:6660–9. doi: 10.1093/emboj/17.22.6660
162. Haller O, Kochs G, Weber F. The interferon response circuit: Induction and suppression by pathogenic viruses. *Virology*. (2006) 344:119–30. doi: 10.1016/j.virol.2005.09.024
163. Hui KPY, Lee SMY, Cheung CY, Mao H, Lai AKW, Chan RWY, et al. H5N1 influenza virus-induced mediators upregulate RIG-I in uninfected cells by paracrine effects contributing to amplified cytokine cascades. *J Infect Dis*. (2011) 204:1866–78. doi: 10.1093/infdis/jir665
164. Shaw AE, Hughes J, Gu Q, Behdenna A, Singer JB, Dennis T, et al. Fundamental properties of the mammalian innate immune system revealed by multispecies comparison of type I interferon responses. *PLoS Biol*. (2017) 15:e2004086. doi: 10.1371/journal.pbio.2004086
165. Cui X-F, Imaizumi T, Yoshida H, Borden EC, Satoh K. Retinoic acid-inducible gene-I is induced by interferon- γ and regulates the expression of interferon- γ stimulated gene 15 in MCF-7 cells. *Biochem Cell Biol*. (2004) 82:401–5. doi: 10.1139/o04-041
166. Imaizumi T, Yagihashi N, Hatakeyama M, Yamashita K, Ishikawa A, Taima K, et al. Expression of retinoic acid-inducible gene-I in vascular smooth muscle cells stimulated with interferon- γ . *Life Sci*. (2004) 75:1171–80. doi: 10.1016/J.LFS.2004.01.030
167. Yount JS, Moran TM, López CB. Cytokine-independent upregulation of MDA5 in viral infection. *J Virol*. (2007) 81:7316–9. doi: 10.1128/JVI.00545-07
168. Schmidt A, Schwerd T, Hamm W, Hellmuth JC, Cui S, Wenzel M, et al. 5'-triphosphate RNA requires base-paired structures to activate antiviral signaling via RIG-I. *Proc Natl Acad Sci USA*. (2009) 106:12067–72. doi: 10.1073/pnas.0900971106
169. Marq J-B, Kolakofsky D, Garcin D. Unpaired 5' ppp-nucleotides, as found in arenavirus double-stranded RNA panhandles, are not recognized by RIG-I. *J Biol Chem*. (2010) 285:18208–16. doi: 10.1074/jbc.M109.089425
170. Schlee M, Roth A, Hornung V, Hagmann CA, Wimmenauer V, Barchet W, et al. Recognition of 5' triphosphate by RIG-I helicase requires short blunt double-stranded RNA as contained in panhandle of negative-strand virus. *Immunity*. (2009) 31:25–34. doi: 10.1016/j.immuni.2009.05.008
171. Marq J-B, Hausmann S, Veillard N, Kolakofsky D, Garcin D. Short double-stranded RNAs with an overhanging 5' ppp-nucleotide, as found in arenavirus genomes, act as RIG-I decoys. *J Biol Chem*. (2011) 286:6108–16. doi: 10.1074/jbc.M110.186262
172. Lu C, Ranjith-Kumar CT, Hao L, Kao CC, Li P. Crystal structure of RIG-I C-terminal domain bound to blunt-ended double-strand RNA without 5' triphosphate. *Nucleic Acids Res*. (2011) 39:1565–75. doi: 10.1093/nar/gkq974
173. Goubau D, Schlee M, Deddouch S, Pruijssers AJ, Zillinger T, Goldeck M, et al. Antiviral immunity via RIG-I-mediated recognition of RNA bearing 5'-diphosphates. *Nature*. (2014) 514:372–5. doi: 10.1038/nature13590
174. Kumar A, Satpati P. Energetics of preferential binding of retinoic acid-inducible gene-I to double-stranded viral RNAs with 5' Tri-/Diphosphate over 5' Monophosphate. *ACS Omega*. (2018) 3:3786–95. doi: 10.1021/acsomega.7b02019
175. Ren X, Linehan MM, Iwasaki A, Pyle AM. RIG-I selectively discriminates against 5'-monophosphate RNA. *Cell Rep*. (2019) 26:2019–27.e4. doi: 10.1016/j.celrep.2019.01.107
176. Rawling DC, Fitzgerald ME, Pyle AM. Establishing the role of ATP for the function of the RIG-I innate immune sensor. *Elife*. (2015) 4:e09391. doi: 10.7554/eLife.09391

177. Jiao X, Chang JH, Kilic T, Tong L, Kiledjian M. A mammalian pre-mRNA 5' end capping quality control mechanism and an unexpected link of capping to pre-mRNA processing. *Mol Cell*. (2013) 50:104–15. doi: 10.1016/j.molcel.2013.02.017
178. Court DL, Gan J, Liang Y-H, Shaw GX, Tropea JE, Costantino N, et al. RNase III: genetics and function; structure and mechanism. *Annu Rev Genet*. (2013) 47:405–31. doi: 10.1146/annurev-genet-110711-155618
179. Malathi K, Saito T, Crochet N, Barton DJ, Gale M, Silverman RH, et al. RNase L releases a small RNA from HCV RNA that refolds into a potent PAMP. *RNA*. (2010) 16:2108–19. doi: 10.1261/rna.2244210
180. Wiatrek DM, Candela ME, Sedmik J, Oppelt J, Keegan LP, O'Connell MA. Activation of innate immunity by mitochondrial dsRNA in mouse cells lacking p53 protein. *RNA*. (2019) 25:713–26. doi: 10.1261/rna.069625.118
181. Chakrabarti A, Jha BK, Silverman RH. New insights into the role of RNase L in innate immunity. *J Interferon Cytokine Res*. (2011) 31:49–57. doi: 10.1089/jir.2010.0120
182. Li X, Lu C, Stewart M, Xu H, Strong RK, Igumenova T, et al. Structural basis of double-stranded RNA recognition by the RIG-I like receptor MDA5. *Arch Biochem Biophys*. (2009) 488:23–33. doi: 10.1016/j.ABB.2009.06.008
183. Li X, Ranjith-Kumar CT, Brooks MT, Dharmiah S, Herr AB, Kao C, et al. The RIG-I-like receptor LGP2 recognizes the termini of double-stranded RNA. *J Biol Chem*. (2009) 284:13881–91. doi: 10.1074/jbc.M900818200
184. Sarkar D, Desalle R, Fisher PB, Goodman M. Evolution of MDA-5/RIG-I-dependent innate immunity: independent evolution by domain grafting. *Proc Natl Acad Sci USA*. (2008) 105:17040–5. doi: 10.1073/pnas.0804956105
185. Saito T, Hirai R, Loo Y-M, Owen D, Johnson CL, Sinha SC, et al. Regulation of innate antiviral defenses through a shared repressor domain in RIG-I and LGP2. *Proc Natl Acad Sci USA*. (2007) 104:582–7. doi: 10.1073/pnas.0606699104
186. Luthra P, Sun D, Silverman RH, He B. Activation of IFN- β expression by a viral mRNA through RNase L and MDA5. *Proc Natl Acad Sci USA*. (2011) 108:2118–23. doi: 10.1073/pnas.1012409108
187. Chow KT, Gale M, Loo Y-M. RIG-I and Other RNA Sensors in Antiviral Immunity. *Annu Rev Immunol*. (2018) 36:667–94. doi: 10.1146/annurev-immunol-042617-053309
188. Chiu Y-H, Macmillan JB, Chen ZJ. RNA polymerase III detects cytosolic DNA and induces type I interferons through the RIG-I pathway. *Cell*. (2009) 138:576–91. doi: 10.1016/j.cell.2009.06.015
189. Ablasser A, Bauernfeind F, Hartmann G, Latz E, Fitzgerald KA, Hornung V. RIG-I-dependent sensing of poly(dA:dT) through the induction of an RNA polymerase III-transcribed RNA intermediate. *Nat Immunol*. (2009) 10:1065–72. doi: 10.1038/ni.1779
190. Chiang C, Beljanski V, Yin K, Olganier D, Ben Yebdri F, Steel C, et al. Sequence-specific modifications enhance the broad-spectrum antiviral response activated by RIG-I agonists. *J Virol*. (2015) 89:8011–25. doi: 10.1128/JVI.00845-15
191. Ho V, Yong HY, Chevrier M, Narang V, Lum J, Toh Y-X, et al. RIG-I activation by a designer short RNA ligand protects human immune cells against dengue virus infection without causing cytotoxicity. *J Virol*. (2019) 93:e00102-19. doi: 10.1128/JVI.00102-19
192. Xu J, Mercado-López X, Grier JT, Kim W, Chun LF, Irvine EB, et al. Identification of a natural viral RNA motif that optimizes sensing of viral RNA by RIG-I. *MBio*. (2015) 6:e01265-15. doi: 10.1128/mBio.01265-15
193. Runge S, Sparrer KMJ, Lässig C, Hembach K, Baum A, García-Sastre A, et al. *In vivo* ligands of MDA5 and RIG-I in measles virus-infected cells. *PLoS Pathog*. (2014) 10:e1004081. doi: 10.1371/journal.ppat.1004081
194. Davis WG, Bowzard JB, Sharma SD, Wiens ME, Ranjan P, Gangappa S, et al. The 3' untranslated regions of influenza genomic sequences are 5'PPP-independent ligands for RIG-I. *PLoS ONE*. (2012) 7:e32661. doi: 10.1371/journal.pone.0032661
195. Zhang Y, Dittmer DP, Mieczkowski PA, Host KM, Fusco WG, Duncan JA, et al. RIG-I detects Kaposi's sarcoma-associated herpesvirus transcripts in a RNA polymerase III-independent manner. *MBio*. (2018) 9:e00823-18. doi: 10.1128/mBio.00823-18
196. Saito T, Owen DM, Jiang F, Marcotrigiano J, Gale M Jr. Innate immunity induced by composition-dependent RIG-I recognition of hepatitis C virus RNA. *Nature*. (2008) 454:523–7. doi: 10.1038/nature07106
197. Uzri D, Gehrke L. Nucleotide sequences and modifications that determine RIG-I/RNA binding and signaling activities. *J Virol*. (2009) 83:4174–84. doi: 10.1128/JVI.02449-08
198. Jiang M, Zhang S, Yang Z, Lin H, Zhu J, Liu L, et al. Self-recognition of an inducible host lncRNA by RIG-I feedback restricts innate immune response. *Cell*. (2018) 173:906–19.e13. doi: 10.1016/j.cell.2018.03.064
199. Gebhardt A, Laudenbach BT, Pichlmair A. Discrimination of self and non-self ribonucleic acids. *J Interf Cytokine Res*. (2017) 37:184–97. doi: 10.1089/jir.2016.0092
200. Huang AS, Baltimore D. Defective viral particles and viral disease processes. *Nature*. (1970) 226:325–7. doi: 10.1038/226325a0
201. Huang AS. Defective interfering viruses. *Annu Rev Microbiol*. (1973) 27:101–18. doi: 10.1146/annurev.mi.27.100173.000533
202. Leppert M, Kort L, Kolakofsky D. Further characterization of Sendai virus DI-RNAs: a model for their generation. *Cell*. (1977) 12:539–52. doi: 10.1016/0092-8674(77)90130-1
203. Nichol ST, O'Hara PJ, Holland JJ, Perrault J. Structure and origin of a novel class of defective interfering particle of vesicular stomatitis virus. *Nucleic Acids Res*. (1984) 12:2775–90. doi: 10.1093/nar/12.6.2775
204. Strahle L, Marq J-B, Brini A, Hausmann S, Kolakofsky D, Garcin D. Activation of the beta interferon promoter by unnatural sendai virus infection requires RIG-I and is inhibited by viral C proteins. *J Virol*. (2007) 81:12227–37. doi: 10.1128/jvi.01300-07
205. Baum A, Sachidanandam R, García-Sastre A. Preference of RIG-I for short viral RNA molecules in infected cells revealed by next-generation sequencing. *Proc Natl Acad Sci USA*. (2010) 107:16303–8. doi: 10.1073/pnas.1005077107
206. Baum A, García-Sastre A. Differential recognition of viral RNA by RIG-I. *Virulence*. (2011) 2:166–9. doi: 10.4161/viru.2.2.15481
207. Ho T-H, Kew C, Lui P-Y, Chan C-P, Satoh T, Akira S, et al. PACT- and RIG-I-dependent activation of type I interferon production by a defective interfering RNA derived from measles virus vaccine. *J Virol*. (2016) 90:1557–68. doi: 10.1128/JVI.02161-15
208. Liu G, Lu Y, Liu Q, Zhou Y. Inhibition of ongoing influenza A virus replication reveals different mechanisms of RIG-I activation. *J Virol*. (2019) 93:e02066-18. doi: 10.1128/JVI.02066-18
209. Liu G, Park H-S, Pyo H-M, Liu Q, Zhou Y. Influenza A virus panhandle structure is directly involved in RIG-I activation and interferon induction. *J Virol*. (2015) 89:6067–79. doi: 10.1128/JVI.00232-15
210. Nayak DP, Sivasubramanian N. The structure of influenza virus defective interfering (DI) RNAs and their progenitor genes. In: Palese P, Kingsbury DW editors. *Genetics of Influenza Viruses*. Vienna: Springer Vienna (1983). p. 255–79. doi: 10.1007/978-3-7091-8706-7_8
211. Yount JS, Gitlin L, Moran TM, López CB. MDA5 participates in the detection of paramyxovirus infection and is essential for the early activation of dendritic cells in response to sendai virus defective interfering particles. *J Immunol*. (2008) 180:4910–8. doi: 10.4049/JIMMUNOL.180.7.4910
212. Yount JS, Kraus TA, Horvath CM, Moran TM, López CB. A novel role for viral-defective interfering particles in enhancing dendritic cell maturation. *J Immunol*. (2006) 177:4503–13. doi: 10.4049/JIMMUNOL.177.7.4503
213. Dimmock NJ, Easton AJ. Defective interfering influenza virus RNAs: time to reevaluate their clinical potential as broad-spectrum antivirals? *J Virol*. (2014) 88:5217–27. doi: 10.1128/JVI.03193-13
214. Weinberger B, Herndler-Brandstetter D, Schwanninger A, Weiskopf D, Grubeck-Loebenstein B. Biology of immune responses to vaccines in elderly persons. *Clin Infect Dis*. (2008) 46:1078–84. doi: 10.1086/529197
215. Chen WH, Kozlovsky BF, Effros RB, Grubeck-Loebenstein B, Edelman R, Sztein MB. Vaccination in the elderly: an immunological perspective. *Trends Immunol*. (2009) 30:351–9. doi: 10.1016/j.it.2009.05.002
216. Derhovanessian E, Pawelec G. Vaccination in the elderly. *Microb Biotechnol*. (2012) 5:226–32. doi: 10.1111/j.1751-7915.2011.00283.x
217. Ciabattini A, Nardini C, Santoro F, Garagnani P, Medaglini D. Vaccination in the elderly: the challenge of immune changes with aging. *Semin Immunol*. (2018) 40:83–94. doi: 10.1016/J.SMIM.2018.10.010
218. Molony RD, Nguyen JT, Kong Y, Montgomery RR, Shaw AC, Iwasaki A. Aging impairs both primary and secondary RIG-I signaling for interferon induction in human monocytes. *Sci Signal*. (2017) 10:eaa2392. doi: 10.1126/scisignal.aan2392

219. Newall AT, Chen C, Wood JG, Stockwell MS. Within-season influenza vaccine waning suggests potential net benefits to delayed vaccination in older adults in the United States. *Vaccine*. (2018) 36:5910–5. doi: 10.1016/j.vaccine.2018.08.007
220. Oldstone MB. Viral persistence: mechanisms and consequences. *Curr Opin Microbiol*. (1998) 1:436–41. doi: 10.1016/S1369-5274(98)80062-3
221. Manzoni TB, López CB. Defective (interfering) viral genomes re-explored: impact on antiviral immunity and virus persistence. *Future Virol*. (2018) 13:493–503. doi: 10.2217/fvl-2018-0021
222. Stauffer Thompson KA, Rempala GA, Yin J. Multiple-hit inhibition of infection by defective interfering particles. *J Gen Virol*. (2009) 90:888–99. doi: 10.1099/vir.0.005249-0
223. Ziegler CM, Eisenhauer P, Bruce EA, Beganovic V, King BR, Weir ME, et al. A novel phosphoserine motif in the LCMV matrix protein Z regulates the release of infectious virus and defective interfering particles. *J Gen Virol*. (2016) 97:2084–9. doi: 10.1099/jgv.0.000550
224. Ziegler C, Eisenhauer P, Manuvelan I, Weir M, Bruce E, Ballif B, et al. Host-driven phosphorylation appears to regulate the budding activity of the lassa virus matrix protein. *Pathogens*. (2018) 7:97. doi: 10.3390/pathogens7040097
225. Rehwinkel J, Reis e Sousa C. RIGorous detection: exposing virus through RNA sensing. *Science*. (2010) 327:284–6. doi: 10.1126/science.1185068
226. Rice GI, Del Toro Duany Y, Jenkinson EM, Forte GM, Anderson BH, Ariaudo G, et al. Gain-of-function mutations in IFIH1 cause a spectrum of human disease phenotypes associated with upregulated type I interferon signaling. *Nat Genet*. (2014) 46:503–9. doi: 10.1038/ng.2933
227. Ahmad S, Mu X, Yang F, Greenwald E, Park JW, Jacob E, et al. Breaching self-tolerance to Alu duplex RNA underlies MDA5-mediated inflammation. *Cell*. (2018) 172:797. doi: 10.1016/j.cell.2017.12.016
228. Oda H, Nakagawa K, Abe J, Awaya T, Funabiki M, Hijikata A, et al. Aicardi-Goutières syndrome is caused by IFIH1 mutations. *Am J Hum Genet*. (2014) 95:121–5. doi: 10.1016/j.ajhg.2014.06.007
229. Funabiki M, Kato H, Miyachi Y, Toki H, Motegi H, Inoue M, et al. Autoimmune disorders associated with gain of function of the intracellular sensor MDA5. *Immunity*. (2014) 40:199–212. doi: 10.1016/j.immuni.2013.12.014
230. Schuberth-Wagner C, Ludwig J, Bruder AK, Herzner A-M, Zillinger T, Goldeck M, et al. A conserved histidine in the RNA sensor RIG-I controls immune tolerance to N1-2' O-methylated Self RNA. *Immunity*. (2015) 43:41–51. doi: 10.1016/j.immuni.2015.06.015
231. Zheng J, Yong HY, Panutdaporn N, Liu C, Tang K, Luo D. High-resolution HDX-MS reveals distinct mechanisms of RNA recognition and activation by RIG-I and MDA5. *Nucleic Acids Res*. (2015) 43:1216–30. doi: 10.1093/nar/gku1329
232. Zheng J, Wang C, Chang MR, Devarkar SC, Schweibenz B, Crynen GC, et al. HDX-MS reveals dysregulated checkpoints that compromise discrimination against self RNA during RIG-I mediated autoimmunity. *Nat Commun*. (2018) 9:5366. doi: 10.1038/s41467-018-07780-z
233. Lässig C, Matheisl S, Sparrer KJMM, de Oliveira Mann CC, Moldt M, Patel JR, et al. ATP hydrolysis by the viral RNA sensor RIG-I prevents unintentional recognition of self-RNA. *Elife*. (2015) 4:e10859. doi: 10.7554/eLife.10859
234. Nallagatla SR, Toroney R, Bevilacqua PC. A brilliant disguise for self RNA: 5'-end and internal modifications of primary transcripts suppress elements of innate immunity. *RNA Biol*. (2008) 5:140–4. doi: 10.4161/rna.5.3.6839
235. Gokhale NS, Horner SM. RNA modifications go viral. *PLoS Pathog*. (2017) 13:e1006188. doi: 10.1371/journal.ppat.1006188
236. Durbin AF, Wang C, Marcotrigiano J, Gehrke L. RNAs containing modified nucleotides fail to trigger RIG-I conformational changes for innate immune signaling. *MBio*. (2016) 7:e00833–16. doi: 10.1128/mBio.00833-16
237. Oshiumi H, Mifsud EJ, Daito T. Links between recognition and degradation of cytoplasmic viral RNA in innate immune response. *Rev Med Virol*. (2016) 26:90–101. doi: 10.1002/rmv.1865
238. Satoh T, Kato H, Kumagai Y, Yoneyama M, Sato S, Matsushita K, et al. LGP2 is a positive regulator of RIG-I- and MDA5-mediated antiviral responses. *Proc Natl Acad Sci USA*. (2010) 107:1512–7. doi: 10.1073/pnas.0912986107
239. Civril F, Bennett M, Moldt M, Deimling T, Witte G, Schiesser S, et al. The RIG-I ATPase domain structure reveals insights into ATP-dependent antiviral signalling. *EMBO Rep*. (2011) 12:1127–34. doi: 10.1038/embor.2011.190
240. Wilson RC, Doudna JA. Molecular mechanisms of RNA interference. *Annu Rev Biophys*. (2013) 42:217–39. doi: 10.1146/annurev-biophys-083012-130404
241. Peach SE, York K, Hesselberth JR. Global analysis of RNA cleavage by 5'-hydroxyl RNA sequencing. *Nucleic Acids Res*. (2015) 43:e108. doi: 10.1093/nar/gkv536
242. Louber J, Brunel J, Uchikawa E, Cusack S, Gerlier D. Kinetic discrimination of self/non-self RNA by the ATPase activity of RIG-I and MDA5. *BMC Biol*. (2015) 13:54. doi: 10.1186/s12915-015-0166-9
243. Yu Q, Qu K, Modis Y. Cryo-EM structures of MDA5-dsRNA filaments at different stages of ATP hydrolysis. *Mol Cell*. (2018) 72:999–1012.e6. doi: 10.1016/j.molcel.2018.10.012
244. Wang M, Yu F, Wu W, Zhang Y, Chang W, Ponnusamy M, et al. Circular RNAs: a novel type of non-coding RNA and their potential implications in antiviral immunity. *Int J Biol Sci*. (2017) 13:1497–506. doi: 10.7150/ijbs.22531
245. Chen YG, Kim MV, Chen X, Batista PJ, Aoyama S, Wilusz JE, et al. Sensing self and foreign circular RNAs by intron identity. *Mol Cell*. (2017) 67:228–38.e5. doi: 10.1016/j.molcel.2017.05.022
246. Eckard SC, Rice GI, Fabre A, Badens C, Gray EE, Hartley JL, et al. The SKIV2L RNA exosome limits activation of the RIG-I-like receptors. *Nat Immunol*. (2014) 15:839–45. doi: 10.1038/ni.2948
247. Murai K, Honda M, Shirasaki T, Shimakami T, Omura H, Misu H, et al. Induction of selenoprotein P mRNA during hepatitis C virus infection inhibits RIG-I-mediated antiviral immunity. *Cell Host Microbe*. (2019) 25:588–601.e7. doi: 10.1016/j.chom.2019.02.015
248. Fan J, Cheng M, Chi X, Liu X, Yang W. Human long non-coding RNA LncATV promotes viral replication by restricting RIG-I-mediated innate immunity. *Front Immunol*. (2019) 10:1711. doi: 10.3389/fimmu.2019.01711
249. Kim D, Kim H, Han S, Scatena M, Kim D-H, Lee JB. Immunostimulatory effects triggered by self-assembled microspheres with tandem repeats of polymerized RNA strands. *Adv Healthc Mater*. (2019) 8:1801395. doi: 10.1002/adhm.201801395
250. Zhao K, Du J, Peng Y, Li P, Wang S, Wang Y, et al. LINE1 contributes to autoimmunity through both RIG-I- and MDA5-mediated RNA sensing pathways. *J Autoimmun*. (2018) 90:105–15. doi: 10.1016/j.jaut.2018.02.007
251. Chiang JJ, Sparrer KMJ, van Gent M, Lässig C, Huang T, Osterrieder N, et al. Viral unmasking of cellular 5S rRNA pseudogene transcripts induces RIG-I-mediated immunity. *Nat Immunol*. (2018) 19:53–62. doi: 10.1038/s41590-017-0005-y
252. Khan M, Syed GH, Kim S-J, Siddiqui A. Mitochondrial dynamics and viral infections: a close nexus. *Biochim Biophys Acta*. (2015) 1853:2822–33. doi: 10.1016/j.bbamcr.2014.12.040
253. Dhir A, Dhir S, Borowski LS, Jimenez L, Teitell M, Rötig A, et al. Mitochondrial double-stranded RNA triggers antiviral signalling in humans. *Nature*. (2018) 560:238–42. doi: 10.1038/s41586-018-0363-0
254. Hardy M-P, Audemard E, Migneault F, Feghaly A, Brochu S, Gendron P, et al. Apoptotic endothelial cells release small extracellular vesicles loaded with immunostimulatory viral-like RNAs. *Sci Rep*. (2019) 9:7203. doi: 10.1038/s41598-019-43591-y
255. Hoffmann H-H, Schneider WM, Rice CM. Interferons and viruses: an evolutionary arms race of molecular interactions. *Trends Immunol*. (2015) 36:124–38. doi: 10.1016/j.it.2015.01.004
256. Schulz KS, Mossman KL. Viral evasion strategies in type I IFN signaling - a summary of recent developments. *Front Immunol*. (2016) 7:498. doi: 10.3389/fimmu.2016.00498
257. Chan YK, Gack MU. Viral evasion of intracellular DNA and RNA sensing. *Nat Rev Microbiol*. (2016) 14:360–73. doi: 10.1038/nrmicro.2016.45
258. Garcia-Sastre A. Ten strategies of interferon evasion by viruses. *Cell Host Microbe*. (2017) 22:176–84. doi: 10.1016/j.chom.2017.07.012
259. Weber M, Weber F. Segmented negative-strand RNA viruses and RIG-I: divide (your genome) and rule. *Curr Opin Microbiol*. (2014) 20:96–102. doi: 10.1016/j.mib.2014.05.002
260. Samji T. Influenza A: understanding the viral life cycle. *Yale J Biol Med*. (2009) 82:153–9.

261. Liu G, Lu Y, Thulasi Raman SN, Xu F, Wu Q, Li Z, et al. Nuclear-resident RIG-I senses viral replication inducing antiviral immunity. *Nat Commun.* (2018) 9:3199. doi: 10.1038/s41467-018-05745-w
262. Habjan M, Andersson I, Klingström J, Schumann M, Martin A, Zimmermann P, et al. Processing of genome 5' termini as a strategy of negative-strand RNA viruses to avoid RIG-I-dependent interferon induction. *PLoS ONE.* (2008) 3:e2032. doi: 10.1371/journal.pone.0002032
263. Ingle H, Kumar S, Raut AA, Mishra A, Kulkarni DD, Kameyama T, et al. The microRNA miR-485 targets host and influenza virus transcripts to regulate antiviral immunity and restrict viral replication. *Sci Signal.* (2015) 8:ra126. doi: 10.1126/scisignal.aab3183
264. Yoshida A, Kawabata R, Honda T, Sakai K, Ami Y, Sakaguchi T, et al. A single amino acid substitution within the paramyxovirus sendai virus nucleoprotein is a critical determinant for production of interferon-beta-inducing copyback-type defective interfering genomes. *J Virol.* (2018) 92:e02094–17. doi: 10.1128/JVI.02094-17
265. Te Velthuis AJW, Long JC, Bauer DLV, Fan RLY, Yen H-L, Sharps J, et al. Mini viral RNAs act as innate immune agonists during influenza virus infection. *Nat Microbiol.* (2018) 3:1234–42. doi: 10.1038/s41564-018-0240-5
266. Nikonov A, Mölder T, Sikut R, Kiiver K, Männik A, Toots U, et al. RIG-I and MDA-5 detection of viral RNA-dependent RNA polymerase activity restricts positive-strand RNA virus replication. *PLoS Pathog.* (2013) 9:e1003610. doi: 10.1371/journal.ppat.1003610
267. King BR, Samacots A, Eisenhauer PL, Ziegler CM, Bruce EA, Zenklusen D, et al. Visualization of arenavirus RNA species in individual cells by single-molecule fluorescence *in situ* hybridization (smFISH) suggests a model of cyclical infection and clearance during persistence. *J Virol.* (2018) 92:e02241–17. doi: 10.1128/JVI.02241-17
268. Hastie KM, Kimberlin CR, Zandonatti MA, MacRae IJ, Saphire EO. Structure of the Lassa virus nucleoprotein reveals a dsRNA-specific 3' to 5' exonuclease activity essential for immune suppression. *Proc Natl Acad Sci USA.* (2011) 108:2396–401. doi: 10.1073/pnas.1016404108
269. Huang Q, Shao J, Lan S, Zhou Y, Xing J, Dong C, et al. *In vitro* and *in vivo* characterizations of pichinde viral nucleoprotein exoribonuclease functions. *J Virol.* (2015) 89:6595–607. doi: 10.1128/JVI.00009-15
270. Ma Y, Wu L, Shaw N, Gao Y, Wang J, Sun Y, et al. Structural basis and functional analysis of the SARS coronavirus nsp14-nsp10 complex. *Proc Natl Acad Sci USA.* (2015) 112:9436–41. doi: 10.1073/pnas.1508686112
271. Durzynska I, Sauerwald M, Karl N, Madhugiri R, Ziebuhr J. Characterization of a bafinivirus exoribonuclease activity. *J Gen Virol.* (2018) 99:1253–60. doi: 10.1099/jgv.0.001120
272. Chiang JJ, Davis ME, Gack MU. Regulation of RIG-I-like receptor signaling by host and viral proteins. *Cytokine Growth Factor Rev.* (2014) 25:491–505. doi: 10.1016/j.cytogfr.2014.06.005
273. Ling Z, Tran KC, Teng MN. Human respiratory syncytial virus non-structural protein NS2 antagonizes the activation of beta interferon transcription by interacting with RIG-I. *J Virol.* (2009) 83:3734–42. doi: 10.1128/JVI.02434-08
274. Xing J, Ly H, Liang Y. The Z proteins of pathogenic but not non-pathogenic arenaviruses inhibit RIG-I-like receptor-dependent interferon production. *J Virol.* (2015) 89:2944–55. doi: 10.1128/JVI.03349-14
275. Zhao J, Zeng Y, Xu S, Chen J, Shen G, Yu C, et al. A viral deamidase targets the helicase domain of RIG-I to block RNA-induced activation. *Cell Host Microbe.* (2016) 20:770–84. doi: 10.1016/j.chom.2016.10.011
276. Li W, Chen H, Sutton T, Obadan A, Perez DR. Interactions between the Influenza A virus RNA polymerase components and retinoic acid-inducible gene I. *J Virol.* (2014) 88:10432–47. doi: 10.1128/JVI.01383-14
277. Reynard S, Russier M, Fizet A, Carnec X, Baize S. Exonuclease domain of the Lassa virus nucleoprotein is critical to avoid RIG-I signaling and to inhibit the innate immune response. *J Virol.* (2014) 88:13923–7. doi: 10.1128/JVI.01923-14
278. Shao J, Huang Q, Liu X, Di D, Liang Y, Ly H. Arenaviral nucleoproteins suppress PACT-induced augmentation of RIG-I function to inhibit type I interferon production. *J Virol.* (2018) 92:e02777. doi: 10.1128/JVI.00482-18
279. Qin L, Ren L, Zhou Z, Lei X, Chen L, Xue Q, et al. Rotavirus non-structural protein 1 antagonizes innate immune response by interacting with retinoic acid inducible gene I. *J Virol.* (2011) 85:526. doi: 10.1186/1743-422X-8-526
280. Motz C, Schuhmann KM, Kirchhofer A, Moldt M, Witte G, Conzelmann K-K, et al. Paramyxovirus V proteins disrupt the fold of the RNA sensor MDA5 to inhibit antiviral signaling. *Science.* (2013) 339:690–3. doi: 10.1126/science.1230949
281. Sánchez-Aparicio MT, Feinman LJ, García-Sastre A, Shaw ML. Paramyxovirus V proteins interact with the RIG-I/TRIM25 regulatory complex and inhibit RIG-I signaling. *J Virol.* (2018) 92:e01960–17. doi: 10.1128/JVI.01960-17
282. Xing J, Wang S, Lin R, Mossman KL, Zheng C. Herpes simplex virus 1 tegument protein US11 downmodulates the RLR signaling pathway via direct interaction with RIG-I and MDA-5. *J Virol.* (2012) 86:3528–40. doi: 10.1128/JVI.06713-11
283. Liu Y, Olganier D, Lin R. Host and viral modulation of RIG-I-mediated antiviral immunity. *Front Immunol.* (2017) 7:662. doi: 10.3389/fimmu.2016.00662
284. Cui J, Song Y, Li Y, Zhu Q, Tan P, Qin Y, et al. USP3 inhibits type I interferon signaling by deubiquitinating RIG-I-like receptors. *Cell Res.* (2014) 24:400–16. doi: 10.1038/cr.2013.170
285. Li H, Zhao Z, Ling J, Pan L, Zhao X, Zhu H, et al. USP14 promotes K63-linked RIG-I deubiquitination and suppresses antiviral immune responses. *Eur J Immunol.* (2018) 49:42–53. doi: 10.1002/eji.201847603
286. Jiang J, Tang H. Mechanism of inhibiting type I interferon induction by hepatitis B virus X protein. *Protein Cell.* (2010) 1:1106–17. doi: 10.1007/s13238-010-0141-8
287. Likai J, Shasha L, Wenxian Z, Jingjiao M, Jianhe S, Hengan W, et al. Porcine deltacoronavirus nucleocapsid protein suppressed IFN- β production by interfering porcine RIG-I dsRNA-binding and K63-linked polyubiquitination. *Front Immunol.* (2019) 10:1024. doi: 10.3389/fimmu.2019.01024
288. Nguyen NTH, Now H, Kim W-J, Kim N, Yoo J-Y. Ubiquitin-like modifier FAT10 attenuates RIG-I mediated antiviral signaling by segregating activated RIG-I from its signaling platform. *Sci Rep.* (2016) 6:23377. doi: 10.1038/srep23377
289. Jiang J, Li J, Fan W, Zheng W, Yu M, Chen C, et al. Robust Lys63-linked ubiquitination of RIG-I promotes cytokine eruption in early influenza B virus infection. *J Virol.* (2016) 90:6263–75. doi: 10.1128/JVI.00549-16
290. Zhu J, Zhang Y, Ghosh A, Cuevas RA, Forero A, Dhar J, et al. Antiviral activity of human OASL protein is mediated by enhancing signaling of the RIG-I RNA sensor. *Immunity.* (2014) 40:936–48. doi: 10.1016/j.immuni.2014.05.007
291. Arimoto K, Takahashi H, Hishiki T, Konishi H, Fujita T, Shimotohno K. Negative regulation of the RIG-I signaling by the ubiquitin ligase RNF125. *Proc Natl Acad Sci USA.* (2007) 104:7500–5. doi: 10.1073/PNAS.0611551104
292. Chen W, Han C, Xie B, Hu X, Yu Q, Shi L, et al. Induction of Siglec-G by RNA viruses inhibits the innate immune response by promoting RIG-I degradation. *Cell.* (2013) 152:467–78. doi: 10.1016/j.cell.2013.01.011
293. Zhao K, Zhang Q, Li X, Zhao D, Liu Y, Shen Q, et al. Cytoplasmic STAT4 promotes antiviral type I IFN production by blocking CHIP-mediated degradation of RIG-I. *J Immunol.* (2016) 196:1209–17. doi: 10.4049/jimmunol.1501224
294. Du Y, Duan T, Feng Y, Liu Q, Lin M, Cui J, et al. LRRC25 inhibits type I IFN signaling by targeting ISG15-associated RIG-I for autophagic degradation. *EMBO J.* (2018) 37:351–66. doi: 10.15252/emboj.201796781
295. Xian H, Yang S, Jin S, Zhang Y, Cui J. LRRC59 modulates type I interferon signaling by restraining the SQSTM1/p62-mediated autophagic degradation of pattern recognition receptor DDX58/RIG-I. *Autophagy.* (2019). doi: 10.1080/15548627.2019.1615303. [Epub ahead of print].
296. Xia M, Gonzalez P, Li C, Meng G, Jiang A, Wang H, et al. Mitophagy enhances oncolytic measles virus replication by mitigating DDX58/RIG-I-like receptor signaling. *J Virol.* (2014) 88:5152–64. doi: 10.1128/JVI.03851-13
297. Barral PM, Sarkar D, Fisher PB, Racaniello VR. RIG-I is cleaved during picornavirus infection. *Virology.* (2009) 391:171–6. doi: 10.1016/j.virol.2009.06.045
298. Zhu Z, Wang G, Yang F, Cao W, Mao R, Du X, et al. Foot-and-mouth disease virus viroporin 2B antagonizes RIG-I-mediated antiviral

- effects by inhibition of its protein expression. *J Virol.* (2016) 90:11106–21. doi: 10.1128/JVI.01310-16
299. Barral PM, Morrison JM, Drahos J, Gupta P, Sarkar D, Fisher PB, et al. MDA-5 is cleaved in poliovirus-infected cells. *J Virol.* (2007) 81:3677–84. doi: 10.1128/JVI.01360-06
 300. Wang W, Jiang M, Liu S, Zhang S, Liu W, Ma Y, et al. RNF122 suppresses antiviral type I interferon production by targeting RIG-I CARDs to mediate RIG-I degradation. *Proc Natl Acad Sci USA.* (2016) 113:9581–6. doi: 10.1073/pnas.1604277113
 301. Zhou P, Ding X, Wan X, Liu L, Yuan X, Zhang W, et al. MLL5 suppresses antiviral innate immune response by facilitating STUB1-mediated RIG-I degradation. *Nat Commun.* (2018) 9:1243. doi: 10.1038/s41467-018-03563-8
 302. Matsumiya T, Imaizumi T, Yoshida H, Satoh K, Topham MK, Stafforini DM. The levels of retinoic acid-inducible gene I are regulated by heat shock protein 90- α . *J Immunol.* (2009) 182:2717–25. doi: 10.4049/jimmunol.0802933
 303. Iwamura T, Yoneyama M, Koizumi N, Okabe Y, Namiki H, Samuel CE, et al. PACT, a double-stranded RNA binding protein acts as a positive regulator for type I interferon gene induced by Newcastle disease virus. *Biochem Biophys Res Commun.* (2001) 282:515–23. doi: 10.1006/BBRC.2001.4606
 304. Kok K-HH, Lui P-YY, Ng M-HJH, Siu K-LL, Au SWN, Jin D-YY. The double-stranded RNA-binding protein PACT functions as a cellular activator of RIG-I to facilitate innate antiviral response. *Cell Host Microbe.* (2011) 9:299–309. doi: 10.1016/j.chom.2011.03.007
 305. Chen K-R, Chang C-H, Huang C-Y, Lin C-Y, Lin W-Y, Lo Y-C, et al. TBK1-associated protein in endolysosomes (TAPE)/CC2D1A is a key regulator linking RIG-I-like receptors to antiviral immunity. *J Biol Chem.* (2012) 287:32216–21. doi: 10.1074/jbc.C112.394346
 306. Suzuki T, Oshiumi H, Miyashita M, Aly HH, Matsumoto M, Seya T. Cell type-specific subcellular localization of phospho-TBK1 in response to cytoplasmic viral DNA. *PLoS ONE.* (2013) 8:e83639. doi: 10.1371/journal.pone.0083639
 307. Onorati M, Li Z, Liu F, Sousa AMM, Nakagawa N, Li M, et al. Zika virus disrupts phospho-TBK1 localization and mitosis in human neuroepithelial stem cells and radial glia. *Cell Rep.* (2016) 16:2576–92. doi: 10.1016/j.celrep.2016.08.038
 308. Li S, Lu L-F, Li Z-C, Zhang C, Zhou X-Y, Zhou Y, et al. Zebrafish MVP recruits and degrades TBK1 to suppress IFN production. *J Immunol.* (2018) 202:559–66. doi: 10.4049/jimmunol.1801325
 309. Outlioua A, Pourcelot M, Arnoult D. The role of optineurin in antiviral type I interferon production. *Front Immunol.* (2018) 9:853. doi: 10.3389/fimmu.2018.00853
 310. Ibsen MS, Gad HH, Andersen LL, Hornung V, Julkunen I, Sarkar SN, et al. Structural and functional analysis reveals that human OASL binds dsRNA to enhance RIG-I signaling. *Nucleic Acids Res.* (2015) 43:5236–48. doi: 10.1093/nar/gkv389
 311. Beattie E, Denzler KL, Tartaglia J, Perkus ME, Paoletti E, Jacobs BL. Reversal of the interferon-sensitive phenotype of a vaccinia virus lacking E3L by expression of the reovirus S4 gene. *J Virol.* (1995) 69:499–505.
 312. Kok KH, Ng M-HJ, Ching Y-P, Jin D-Y. Human TRBP and PACT directly interact with each other and associate with dicer to facilitate the production of small interfering RNA. *J Biol Chem.* (2007) 282:17649–57. doi: 10.1074/jbc.M611768200
 313. Schlee M, Hartmann E, Coch C, Wimmenauer V, Janke M, Barchet W, et al. Approaching the RNA ligand for RIG-I? *Immunol Rev.* (2009) 227:66–74. doi: 10.1111/j.1600-065X.2008.00724.x
 314. Brisse M, Ly H, Brisse M, Ly H. Viral inhibitions of PACT-induced RIG-I activation. *Oncotarget.* (2017) 5: 60725–6. doi: 10.18632/oncotarget.18928
 315. Brisse ME, Ly H. Hemorrhagic fever-causing arenaviruses: lethal pathogens and potent immune suppressors. *Front Immunol.* (2019) 10:372. doi: 10.3389/fimmu.2019.00372
 316. Chen J, Fang P, Wang M, Peng Q, Ren J, Wang D, et al. Porcine deltacoronavirus nucleocapsid protein antagonizes IFN- β production by impairing dsRNA and PACT binding to RIG-I. *Virus Genes.* (2019). doi: 10.1007/s11262-019-01673-z. [Epub ahead of print].
 317. Chen H, Li Y, Zhang J, Ran Y, Wei J, Yang Y, et al. RAVR1 is a coactivator of MDA5-mediated cellular antiviral response. *J Mol Cell Biol.* (2013) 5:111–9. doi: 10.1093/jmcb/mjt006
 318. Yang Q, Bai S-Y, Li L-F, Li S, Zhang Y, Munir M, et al. Human hemoglobin subunit beta functions as a pleiotropic regulator of the RIG-I/MDA5-mediated antiviral innate immune responses. *J Virol.* (2019). doi: 10.1128/JVI.00718-19. [Epub ahead of print].
 319. Patel RC, Sen GC. PACT, a protein activator of the interferon-induced protein kinase, PKR. *EMBO J.* (1998) 17:4379–90. doi: 10.1093/emboj/17.15.4379
 320. Marques JT, White CL, Peters GA, Williams BRG, Sen GC. The role of PACT in mediating gene induction, PKR activation, and apoptosis in response to diverse stimuli. *J Interferon Cytokine Res.* (2008) 28:469–76. doi: 10.1089/jir.2007.0006
 321. Yoo J-S, Takahashi K, Ng CS, Ouda R, Onomoto K, Yoneyama M, et al. DHX36 enhances RIG-I signaling by facilitating PKR-mediated antiviral stress granule formation. *PLoS Pathog.* (2014) 10:e1004012. doi: 10.1371/journal.ppat.1004012
 322. Yoneyama M, Jogi M, Onomoto K. Regulation of antiviral innate immune signaling by stress-induced RNA granules. *J Biochem.* (2016) 159:mvv122. doi: 10.1093/jb/mvv122
 323. Onomoto K, Jogi M, Yoo J-S, Narita R, Morimoto S, Takemura A, et al. Critical role of an antiviral stress granule containing RIG-I and PKR in viral detection and innate immunity. *PLoS ONE.* (2012) 7:e43031. doi: 10.1371/journal.pone.0043031
 324. Sánchez-Aparicio MT, Ayllón J, Leo-Macias A, Wolff T, García-Sastre A. Subcellular localizations of RIG-I, TRIM25, and MAVS complexes. *J Virol.* (2017) 91:e01155-16. doi: 10.1128/JVI.01155-16
 325. Pham AM, Santa Maria FG, Lahiri T, Friedman E, Marié IJ, Levy DE. PKR transduces MDA5-dependent signals for type I IFN induction. *PLoS Pathog.* (2016) 12:e1005489. doi: 10.1371/journal.ppat.1005489
 326. Li L-F, Yu J, Zhang Y, Yang Q, Li Y, Zhang L, et al. Interferon-inducible oligoadenylate synthetase-like protein acts as an antiviral effector against classical swine fever virus via the MDA5-mediated type I interferon-signaling pathway. *J Virol.* (2017) 91:e01514-16. doi: 10.1128/JVI.01514-16
 327. Xu L, Xiao N, Liu F, Ren H, Gu J, Beutler BA. Inhibition of RIG-I and MDA5-dependent antiviral response by gC1qR at mitochondria. *PNAS.* (2009) 106:1530–5. doi: 10.1073/pnas.0811029106
 328. Ling T, Li S-N, Weng G-X, Wang W, Li C, Cao L, et al. TARBP2 negatively regulates IFN- β production and innate antiviral response by targeting MAVS. *Mol Immunol.* (2018) 104:1–10. doi: 10.1016/j.molimm.2018.10.017
 329. Zhang W, Wang G, Xu Z-G, Tu H, Hu F, Dai J, et al. Lactate is a natural suppressor of RLR signaling by targeting MAVS. *Cell.* (2019) 178:176–189.e15. doi: 10.1016/j.cell.2019.05.003
 330. Cui J, Zhu L, Xia X, Wang HY, Legras X, Hong J, et al. NLRC5 negatively regulates the NF- κ B and type I interferon signaling pathways. *Cell.* (2010) 141:483–96. doi: 10.1016/j.cell.2010.03.040
 331. Pattabhi S, Knoll ML, Gale M, Loo Y-M. DHX15 is a coreceptor for RLR signaling that promotes antiviral defense against RNA virus infection. *J Interf Cytokine Res.* (2019) 39:331–46. doi: 10.1089/jir.2018.0163
 332. Yang Y-K, Qu H, Gao D, Di W, Chen H-W, Guo X, et al. ARF-like protein 16 (ARL16) inhibits RIG-I by binding with its C-terminal domain in a GTP-dependent manner. *J Biol Chem.* (2011) 286:10568–80. doi: 10.1074/jbc.M110.206896
 333. Kitai Y, Takeuchi O, Kawasaki T, Ori D, Sueyoshi T, Murase M, et al. Negative regulation of melanoma differentiation-associated gene 5 (MDA5)-dependent antiviral innate immune responses by Arf-like protein 5B. *J Biol Chem.* (2015) 290:1269–80. doi: 10.1074/jbc.M114.611053
 334. Ranjith-Kumar CT, Lai Y, Sarisky RT, Kao CC. Green tea catechin, epigallocatechin gallate, suppresses signaling by the dsRNA innate immune receptor RIG-I. *PLoS ONE.* (2010) 5:1–11. doi: 10.1371/journal.pone.0012878
 335. Story RM, Li H, Abelson JN. Crystal structure of a DEAD box protein from the hyperthermophile *Methanococcus jannaschii*. *Proc Natl Acad Sci USA.* (2001) 98:1465–70. doi: 10.1073/pnas.98.4.1465
 336. Heung LJ, Del Poeta M. Unlocking the DEAD-box: a key to cryptococcal virulence? *J Clin Invest.* (2005) 115:593–5. doi: 10.1172/JCI24508

337. Poynter S, Lisser G, Monjo A, DeWitte-Orr S, Poynter S, Lisser G, et al. Sensors of infection: viral nucleic acid PRRs in fish. *Biology*. (2015) 4:460–93. doi: 10.3390/biology4030460
338. Barber MRW, Aldridge JR, Webster RG, Magor KE, Magor KE. Association of RIG-I with innate immunity of ducks to influenza. *Proc Natl Acad Sci USA*. (2010) 107:5913–8. doi: 10.1073/pnas.1001755107
339. Rajendran KV, Zhang J, Liu S, Peatman E, Kucuktas H, Wang X, et al. Pathogen recognition receptors in channel catfish: II. Identification, phylogeny and expression of retinoic acid-inducible gene I (RIG-I)-like receptors (RLRs). *Dev Comp Immunol*. (2012) 37:381–9. doi: 10.1016/J.DCI.2012.02.004
340. Sun Y, Ding N, Ding SS, Yu S, Meng C, Chen H, et al. Goose RIG-I functions in innate immunity against Newcastle disease virus infections. *Mol Immunol*. (2013) 53:321–7. doi: 10.1016/J.MOLIMM.2012.08.022
341. Aoki T, Hikima J, Hwang SD, Jung TS. Innate immunity of finfish: primordial conservation and function of viral RNA sensors in teleosts. *Fish Shellfish Immunol*. (2013) 35:1689–702. doi: 10.1016/J.FSI.2013.02.005
342. He Y, Pan H, Zhang G, He S. Comparative study on pattern recognition receptors in non-teleost ray-finned fishes and their evolutionary significance in primitive vertebrates. *Sci China Life Sci*. (2019) 62:566–78. doi: 10.1007/s11427-019-9481-8
343. Chen J, Shang S, Wu X, Zhong H, Zhao C, Wei Q, et al. Genomic analysis and adaptive evolution of the RIG-I-like and NOD-like receptors in reptiles. *Int J Biol Macromol*. (2019) 134:1045–51. doi: 10.1016/J.IJBIOMAC.2019.05.172
344. Inohara N, Chamaillard M, McDonald C, Nuñez G. NOD-LRR PROTEINS: role in host-microbial interactions and inflammatory disease. *Annu Rev Biochem*. (2005) 74:355–83. doi: 10.1146/annurev.biochem.74.082803.133347
345. Kersse K, Vanden Bergh T, Lamkanfi M, Vandenabeele P. A phylogenetic and functional overview of inflammatory caspases and caspase-1-related CARD-only proteins. *Biochem Soc Trans*. (2007) 35:1508–11. doi: 10.1042/BST0351508
346. Kufer TA, Fritz JH, Philpott DJ. NACHT-LRR proteins (NLRs) in bacterial infection and immunity. *Trends Microbiol*. (2005) 13:381–8. doi: 10.1016/j.tim.2005.06.004
347. Chiu J, DeSalle R, Lam HM, Meisel L, Coruzzi G. Molecular evolution of glutamate receptors: a primitive signaling mechanism that existed before plants and animals diverged. *Mol Biol Evol*. (1999) 16:826–38. doi: 10.1093/oxfordjournals.molbev.a026167
348. Leszczyniecka M, DeSalle R, Kang D, Fisher PB. The origin of polynucleotide phosphorylase domains. *Mol Phylogenet Evol*. (2004) 31:123–30. doi: 10.1016/J.YMPEV.2003.07.012
349. Cagliani R, Forni D, Tresoldi C, Pozzoli U, Filippi G, Rainone V, et al. RIG-I-like receptors evolved adaptively in mammals, with parallel evolution at LGP2 and RIG-I. *J Mol Biol*. (2014) 426:1351–65. doi: 10.1016/j.jmb.2013.10.040
350. Li N, Li A, Zheng K, Liu X, Gao L, Liu D, et al. Identification and characterization of an atypical RIG-I encoded by planarian *Dugesia japonica* and its essential role in the immune response. *Dev Comp Immunol*. (2019) 91:72–84. doi: 10.1016/J.DCI.2018.10.007
351. Coffman SR, Lu J, Guo X, Zhong J, Jiang H, Broitman-Maduro G, et al. *Caenorhabditis elegans* RIG-I homolog mediates antiviral RNA interference downstream of dicer-dependent biogenesis of viral small interfering RNAs. *MBio*. (2017) 8:e00264-17. doi: 10.1128/mBio.00264-17
352. Wang P-H, Weng S-P, He J-G. Nucleic acid-induced antiviral immunity in invertebrates: an evolutionary perspective. *Dev Comp Immunol*. (2015) 48:291–6. doi: 10.1016/J.DCI.2014.03.013
353. Eyk CL, Samaraweera SE, Scott A, Webber DL, Harvey DP, Mecinger O, et al. ‘Non-self’ mutation: double-stranded RNA elicits antiviral pathogenic response in a *Drosophila* model of expanded CAG repeat neurodegenerative diseases. *Hum Mol Genet*. (2019). doi: 10.1093/hmg/ddz096. [Epub ahead of print].
354. Zipfel C. Plant pattern-recognition receptors. *Trends Immunol*. (2014) 35:345–51. doi: 10.1016/j.it.2014.05.004
355. Incarbone M, Dunoyer P. RNA silencing and its suppression: novel insights from in planta analyses. *Trends Plant Sci*. (2013) 18:382–92. doi: 10.1016/j.tplants.2013.04.001
356. Körner CJ, Klauser D, Niehl A, Domínguez-Ferreras A, Chinchilla D, Boller T, et al. The immunity regulator BAK1 contributes to resistance against diverse RNA viruses. *Mol Plant-Microbe Interact*. (2013) 26:1271–80. doi: 10.1094/MPMI-06-13-0179-R
357. Gong X-Y, Zhang Q-M, Gui J-F, Zhang Y-B. SVCV infection triggers fish IFN response through RLR signaling pathway. *Fish Shellfish Immunol*. (2019) 86:1058–63. doi: 10.1016/J.FSI.2018.12.063
358. Zhang Q-M, Zhao X, Li Z, Wu M, Gui J-F, Zhang Y-B. Alternative splicing transcripts of zebrafish LGP2 gene differentially contribute to IFN antiviral response. *J Immunol*. (2018) 200:688–703. doi: 10.4049/jimmunol.1701388
359. Xu T, Chu Q, Cui J, Bi D. Inducible MicroRNA-3570 feedback inhibits the RIG-I-dependent innate immune response to rhabdovirus in teleost fish by targeting MAVS/IPS-1. *J Virol*. (2018) 92:e01594-17. doi: 10.1128/JVI.01594-17
360. Sun Y, Han J, Chu Q, Liu X, Xu T. microRNA-210 participates in regulating RIG-I signaling pathway via targeting DUBA in miuiy croaker after poly(I:C) stimulation. *Fish Shellfish Immunol*. (2018) 77:1–7. doi: 10.1016/J.FSI.2018.02.003
361. Gu T, Lu L, An C, Chen B, Wei W, Wu X, et al. MDA5 and LGP2 acts as a key regulator though activating NF- κ B and IRF3 in RLRs signaling of mandarinfinch. *Fish Shellfish Immunol*. (2019) 86:1114–22. doi: 10.1016/J.FSI.2018.12.054
362. Zou PF, Chang MX, Li Y, Huan Zhang S, Fu JP, Chen SN, et al. Higher antiviral response of RIG-I through enhancing RIG-I/MAVS-mediated signaling by its long insertion variant in zebrafish. *Fish Shellfish Immunol*. (2015) 43:13–24. doi: 10.1016/J.FSI.2014.12.001
363. Gack MU, Kirchhofer A, Shin YC, Inn K-S, Liang C, Cui S, et al. Roles of RIG-I N-terminal tandem CARD and splice variant in TRIM25-mediated antiviral signal transduction. *Proc Natl Acad Sci USA*. (2008) 105:16743–8. doi: 10.1073/pnas.0804947105
364. Miranzo-Navarro D, Magor KE. Activation of duck RIG-I by TRIM25 is independent of anchored ubiquitin. *PLoS ONE*. (2014) 9:e86968. doi: 10.1371/journal.pone.0086968
365. Helin AS, Wille M, Atterby C, Järhult J, Waldenström J, Chapman JR. Expression of immune genes RIG-I and Mx in mallard ducks infected with low pathogenic avian influenza (LPAI): a dataset. *Data Br*. (2018) 18:1562–6. doi: 10.1016/j.dib.2018.04.061
366. Huo H, Wang Y, Wang D, Wang Y, Chen X, Zhao L, et al. Duck RIG-I restricts duck enteritis virus infection. *Vet Microbiol*. (2019) 230:78–85. doi: 10.1016/J.VETMIC.2019.01.014
367. Sun X, Li W, Liu E, Huang H, Wang T, Wang X, et al. *In vivo* cellular and molecular study on duck spleen infected by duck Tembusu virus. *Vet Microbiol*. (2019) 230:32–44. doi: 10.1016/J.VETMIC.2018.12.003
368. Wei LM, Jiao PR, Song YF, Han F, Cao L, Yang F, et al. Identification and expression profiling analysis of goose melanoma differentiation associated gene 5 (MDA5) gene. *Poult Sci*. (2013) 92:2618–24. doi: 10.3382/ps.2013-03064
369. Sun Y, Mao X, Zheng H, Wu W, Rehman ZU, Liao Y, et al. Goose MAVS functions in RIG-I-mediated IFN- β signaling activation. *Dev Comp Immunol*. (2019) 93:58–65. doi: 10.1016/J.DCI.2018.12.006
370. Karpala AJ, Stewart C, McKay J, Lowenthal JW, Bean AGD. Characterization of chicken Mda5 activity: regulation of IFN- β in the absence of RIG-I functionality. *J Immunol*. (2011) 186:5397–405. doi: 10.4049/jimmunol.1003712
371. Liniger M, Summerfield A, Zimmer G, McCullough KC, Ruggli N. Chicken cells sense influenza A virus infection through MDA5 and CARDIF signaling involving LGP2. *J Virol*. (2012) 86:705. doi: 10.1128/JVI.00742-11
372. Hayashi T, Watanabe C, Suzuki Y, Tanikawa T, Uchida Y, Saito T. Chicken MDA5 senses short double-stranded RNA with implications for antiviral response against avian influenza viruses in chicken. *J Innate Immun*. (2014) 6:58–71. doi: 10.1159/000351583
373. Li G-Q, Tian Y, Chen L, Shen J-D, Tao Z-R, Zeng T, et al. Cloning, expression and bioinformatics analysis of a putative pigeon melanoma differentiation-associated gene 5. *Br Poult Sci*. (2018) 60:94–104. doi: 10.1080/00071668.2018.1564241

374. Xu L, Yu D, Fan Y, Peng L, Wu Y, Yao Y-G. Loss of RIG-I leads to a functional replacement with MDA5 in the Chinese tree shrew. *Proc Natl Acad Sci USA*. (2016) 113:10950–5. doi: 10.1073/pnas.1604939113
375. Wei Y, Zhou H, Wang A, Sun L, Wang M, Jia R, et al. TRIM25 identification in the Chinese goose: gene structure, tissue expression profiles, and antiviral immune responses *in vivo* and *in vitro*. *Biomed Res Int*. (2016) 2016:1403984. doi: 10.1155/2016/1403984
376. Chang M, Collet B, Nie P, Lester K, Campbell S, Secombes CJ, et al. Expression and functional characterization of the RIG-I-like receptors MDA5 and LGP2 in Rainbow trout (*Oncorhynchus mykiss*). *J Virol*. (2011) 85:8403–12. doi: 10.1128/JVI.00445-10
377. Weber M, Sediri H, Felgenhauer U, Binzen I, Bänfer S, Jacob R, et al. Influenza virus adaptation PB2-627K modulates nucleocapsid inhibition by the pathogen sensor RIG-I. *Cell Host Microbe*. (2015) 17:309–19. doi: 10.1016/j.CHOM.2015.01.005
378. Ariumi Y. Multiple functions of DDX3 RNA helicase in gene regulation, tumorigenesis, and viral infection. *Front Genet*. (2014) 5:423. doi: 10.3389/fgenet.2014.00423
379. Valiente-Echeverría F, Hermoso MA, Soto-Rifo R. RNA helicase DDX3: at the crossroad of viral replication and antiviral immunity. *Rev Med Virol*. (2015) 25:286–99. doi: 10.1002/rmv.1845
380. Gringhuis SI, Hertoghs N, Kaptein TM, Zijlstra-Willems EM, Sarrami-Fooroshani R, Sprockholt JK, et al. HIV-1 blocks the signaling adaptor MAVS to evade antiviral host defense after sensing of abortive HIV-1 RNA by the host helicase DDX3. *Nat Immunol*. (2016) 18:225–35. doi: 10.1038/ni.3647
381. Szappanos D, Tschismarov R, Perlot T, Westermayer S, Fischer K, Platanitis E, et al. The RNA helicase DDX3X is an essential mediator of innate antimicrobial immunity. *PLOS Pathog*. (2018) 14:e1007397. doi: 10.1371/journal.ppat.1007397
382. Zhang Z, Yuan B, Lu N, Facchinetti V, Liu Y-J. DHX9 pairs with IPS-1 to sense double-stranded RNA in myeloid dendritic cells. *J Immunol*. (2011) 187:4501–8. doi: 10.4049/jimmunol.1101307
383. Lu H, Lu N, Weng L, Yuan B, Liu Y-J, Zhang Z. DHX15 senses double-stranded RNA in myeloid dendritic cells. *J Immunol*. (2014) 193:1364–72. doi: 10.4049/jimmunol.1303322
384. Zhang Z, Kim T, Bao M, Facchinetti V, Jung SY, Ghaffari AA, et al. DDX1, DDX21, and DHX36 helicases form a complex with the adaptor molecule TRIF to sense dsRNA in dendritic cells. *Immunity*. (2011) 34:866–78. doi: 10.1016/j.immuni.2011.03.027
385. Liu Y, Lu N, Yuan B, Weng L, Wang F, Liu Y-J, et al. The interaction between the helicase DHX33 and IPS-1 as a novel pathway to sense double-stranded RNA and RNA viruses in myeloid dendritic cells. *Cell Mol Immunol*. (2014) 11:49–57. doi: 10.1038/cmi.2013.40
386. Zhang K, Zhang Y, Xue J, Meng Q, Liu H, Bi C, et al. DDX19 inhibits type I interferon production by disrupting TBK1-IKKe-IRF3 interactions and promoting TBK1 and IKKe degradation. *Cell Rep*. (2019) 26:1258–72.e4. doi: 10.1016/j.celrep.2019.01.029
387. Loureiro ME, Zorzetto-Fernandes AL, Radoshitzky S, Chi X, Dallari S, Marooki N, et al. DDX3 suppresses type I interferons and favors viral replication during Arenavirus infection. *PLOS Pathog*. (2018) 14:e1007125. doi: 10.1371/journal.ppat.1007125
388. Park E, Byun YH, Park S, Jang YH, Han W, Won J, et al. Co-degradation of interferon signaling factor DDX3 by PB1-F2 as a basis for high virulence of 1918 pandemic influenza. *EMBO J*. (2019) 38:e99475. doi: 10.15252/embj.201899475
389. Mosallanejad K, Sekine Y, Ishikura-Kinoshita S, Kumagai K, Nagano T, Matsuzawa A, et al. The DEAH-box RNA helicase DHX15 activates NF- κ B and MAPK signaling downstream of MAVS during antiviral responses. *Sci Signal*. (2014) 7:ra40. doi: 10.1126/scisignal.2004841
390. Miyashita M, Oshiumi H, Matsumoto M, Seya T. DDX60, a DEXD/H box helicase, is a novel antiviral factor promoting RIG-I-like receptor-mediated signaling. *Mol Cell Biol*. (2011) 31:3802–19. doi: 10.1128/MCB.01368-10
391. Oshiumi H, Miyashita M, Okamoto M, Morioka Y, Okabe M, Matsumoto M, et al. DDX60 is involved in RIG-I-dependent and independent antiviral responses, and its function is attenuated by virus-induced EGFR activation. *Cell Rep*. (2015) 11:1193–207. doi: 10.1016/j.celrep.2015.04.047
392. Zhu Q, Tan P, Li Y, Lin M, Li C, Mao J, et al. DHX29 functions as an RNA co-sensor for MDA5-mediated EMCV-specific antiviral immunity. *PLoS Pathog*. (2018) 14:e1006886. doi: 10.1371/journal.ppat.1006886
393. Elion DL, Cook RS. Activation of RIG-I signaling to increase the pro-inflammatory phenotype of a tumor. *Oncotarget*. (2019) 10:2338–9. doi: 10.18632/oncotarget.26729
394. Aznar MA, Planelles L, Perez-Olivares M, Molina C, Garasa S, Etxeberria I, et al. Immunotherapeutic effects of intratumoral nanoplexed poly I:C. *J Immunother Cancer*. (2019) 7:116. doi: 10.1186/s40425-019-0568-2
395. Yong HY, Luo D. RIG-I-like receptors as novel targets for pan-antivirals and vaccine adjuvants against emerging and re-emerging viral infections. *Front Immunol*. (2018) 9:1379. doi: 10.3389/fimmu.2018.01379

Conflict of Interest Statement: The authors declare that the research was conducted in the absence of any commercial or financial relationships that could be construed as a potential conflict of interest.

Copyright © 2019 Brisse and Ly. This is an open-access article distributed under the terms of the Creative Commons Attribution License (CC BY). The use, distribution or reproduction in other forums is permitted, provided the original author(s) and the copyright owner(s) are credited and that the original publication in this journal is cited, in accordance with accepted academic practice. No use, distribution or reproduction is permitted which does not comply with these terms.



Host Cell Death Responses to Non-typhoidal *Salmonella* Infection

Madeleine A. Wemyss^{1,2†} and Jaclyn S. Pearson^{1,2*†}

¹ Department of Molecular and Translational Research, Monash University, Clayton, VIC, Australia, ² Department of Microbiology, Monash University, Clayton, VIC, Australia

OPEN ACCESS

Edited by:

Barbara Bottazzi,
Milan University, Italy

Reviewed by:

Silvia Guglietta,
Medical University of South Carolina,
United States
Elsa Anes,
University of Lisbon, Portugal

*Correspondence:

Jaclyn S. Pearson
jaclyn.pearson@hudson.org.au

† Present address:

Madeleine A. Wemyss and
Jaclyn S. Pearson,
Centre for Innate Immunity and
Infectious Diseases, Hudson Institute
of Medical Research, Clayton, VIC,
Australia

Specialty section:

This article was submitted to
Microbial Immunology,
a section of the journal
Frontiers in Immunology

Received: 02 May 2019

Accepted: 11 July 2019

Published: 26 July 2019

Citation:

Wemyss MA and Pearson JS (2019)
Host Cell Death Responses to
Non-typhoidal *Salmonella* Infection.
Front. Immunol. 10:1758.
doi: 10.3389/fimmu.2019.01758

Salmonella enterica subsp. *enterica* serovar Typhimurium (*S. Typhimurium*) is a Gram-negative bacterium with a broad host range that causes non-typhoidal salmonellosis in humans. *S. Typhimurium* infects epithelial cells and macrophages in the small intestine where it replicates in a specialized intracellular niche called the *Salmonella*-containing vacuole (SCV) and promotes inflammation of the mucosa to induce typically self-limiting gastroenteritis. Virulence and spread of the bacterium is determined in part by the host individual's ability to limit the infection through innate immune responses at the gastrointestinal mucosa, including programmed cell death. *S. Typhimurium* however, has evolved a myriad of mechanisms to counteract or exploit host responses through the use of Type III Secretion Systems (T3SS), which allow the translocation of virulence (effector) proteins into the host cell for the benefit of optimal bacterial replication and dissemination. T3SS effectors have been found to interact with apoptotic, necroptotic, and pyroptotic cell death cascades, interfering with both efficient clearance of the bacteria and the recruitment of neutrophils or dendritic cells to the area of infection. The interplay of host inflammation, programmed cell death responses, and bacterial defenses in the context of non-typhoidal *Salmonella* (NTS) infection is a continuing area of interest within the field, and as such has been reviewed here.

Keywords: non-typhoidal *Salmonella*, programmed cell death, innate immunity, T3SS effector protein, immune evasion, host-pathogen interaction

PATHOGENICITY AND VIRULENCE OF *Salmonella enterica* SEROVAR TYPHIMURIUM

Infections caused by *Salmonella enterica* are a major challenge in both human and animal health. *Salmonella enterica* subsp. *enterica* serovars are categorized by their disease phenotypes into typhoidal (Typhi and Paratyphi) and non-typhoidal *Salmonella* (NTS) serovars (e.g., *S. Typhimurium*). Whereas, typhoidal serovars cause invasive disease and are human restricted, NTS serovars cause disease in a wide range of mammals and birds and typically cause self-limiting gastroenteritis (salmonellosis) in humans, with the bacteria restricted to the gastrointestinal mucosa (1, 2). *S. Typhimurium* is acquired via the fecal-oral route from consumption of raw or contaminated poultry products, and causes the majority of notified NTS infections in Australia (3, 4).

In immunocompromised individuals, *S. Typhimurium* can cause invasive disease that requires antibiotic treatment or hospitalization. Murine infections with *S. Typhimurium* result in invasive disease and bacteremia, and thus are a more representative model of invasive salmonellosis but are nevertheless used to great effect to study the pathogenesis of *S. Typhimurium in vivo*.

The interactions between NTS and host cell processes during host invasion and the initial establishment of infection have been reviewed previously by LaRock et al. and as such are only briefly described here (5). Once ingested, *S. Typhimurium* enters the gastrointestinal tract and uses flagella to access the epithelial layer of the terminal ileum. Inflammatory responses in the epithelium release key nutrients required by the bacteria, also causing diarrheal symptoms that promote transmission (6, 7). Following contact with the epithelium, *S. Typhimurium* utilizes a Type III Secretion System (T3SS) encoded on *Salmonella* pathogenicity island-1 (SPI-1) to translocate effector proteins (such as SopE2, SipA, and SopB) into the epithelial cell cytosol, inducing actin rearrangement, membrane ruffling, and non-phagocytic cellular uptake of the bacteria into the host cell (**Figure 1**) (8–10). Inside the intracellular space, flagella are no longer required for motility of the bacteria, and are typically downregulated in order to avoid host immune responses (11–14). Internalization of *S. Typhimurium* causes formation of an endosome termed the early *Salmonella*-containing vacuole (SCV). Here, a second T3SS (encoded by the SPI-2 locus) is used to translocate virulence proteins such as SifA, SopD2, and SseJ, acidifying the vacuole and maturing the SCV into the ideal replicative niche for the bacteria (15). The late stage SCV enables efficient bacterial replication, while interconnected networks of *Salmonella*-induced filaments (SIFs) allow enclosed bacteria to acquire nutrients (15, 16). Other SPI-2 effectors prevent lysosomal fusion with the SCV, inhibiting recruitment of lysosomal enzymes and trafficking markers that would promote degradation of the vacuole (15, 17). In epithelial cells, subpopulations of *S. Typhimurium* have been observed in the cytosol, resulting in bacterial hyper-replication and host cell extrusion (18). Host guanylate-binding

proteins (GBPs), expressed following Type I or II interferon (IFN) signaling, can also lyse the SCV, exposing *S. Typhimurium* to the cytosol (19–21).

Cytosolic *S. Typhimurium* enable the detection of pathogen-associated molecular patterns (PAMPs), such as lipopolysaccharide (LPS) and flagellin, by pattern recognition receptors (PRRs) or Nod-like receptors (NLRs). PRRs act to recruit immune cells to infected tissues and limit bacterial virulence through the activation of pro-inflammatory signaling. The ability of *Salmonella* infection to induce tumor necrosis factor (TNF) production in epithelial cells and macrophages is well-documented (22–24). TNF signaling typically reinforces the production of pro-survival cytokines and anti-apoptotic factors via nuclear factor kappa B (NF- κ B) or mitogen-activated protein kinase (MAPK) signaling cascades (25–27). However, effector proteins such as GtgA, SspH1, SptP, and potentially SseL can prevent the activation of these pathways, instead driving TNF signaling toward programmed cell death cascades (28–34). These include apoptosis, necroptosis, and pyroptosis, and are triggered by TNF and other death receptor ligands, or inflammasome activation (**Figure 1**). Death of the host cell allows escape of *S. Typhimurium* into the extracellular space, and uptake of the bacteria by professional phagocytes. Neutrophils play a key role in the overall clearance of *S. Typhimurium*, killing the phagocytosed bacteria through the activity of reactive oxygen species (ROS), while infected dendritic cells and macrophages can spread the bacteria to the mesenteric lymph nodes, spleen, and liver (12, 35–37).

APOPTOTIC CELL DEATH PATHWAYS DURING *SALMONELLA* INFECTION

Apoptosis is a caspase-dependent form of programmed cell death, induced in damaged or stressed cells in response to intrinsic or extrinsic signaling cascades (38). The apoptotic process results in DNA fragmentation, phosphatidylserine exposure, formation of apoptotic bodies, and the display of “eat me” signals to prompt phagocytic clearance of the dying cell. Intrinsic apoptosis is triggered by DNA damage, accumulation of ROS or endoplasmic reticulum (ER) stress, resulting in mitochondrial outer membrane permeabilization and activation of caspase-9. Caspase-9 catalyzes the activation of caspase-3 and caspase-7, which execute the biochemical and morphological changes characteristic of apoptosis (38). In contrast, extrinsic apoptosis responds to ligand or cytokine binding to transmembrane death receptors on the surface of the cell. Death receptors possess an apoptosis-activating death domain, and include receptors such as Fas, TNFR1, and TRAIL-R1. Upon TNF stimulation, TNFR1 recruits adaptor proteins such as TNFR1-associated death domain protein (TRADD), TNFR-associated factor 2 (TRAF2) and receptor-interacting serine/threonine-protein kinase 1 (RIPK1) (**Figure 1**). RIPK1 is subject to ubiquitylation and phosphorylation events that direct TNFR1 signaling toward pro-survival NF- κ B activation (39). In the absence of modifications, RIPK1 associates with pro-caspase-8, TRADD and Fas-associated protein with death

Abbreviations: A/E, attaching and effacing; AIM2, absent in melanoma 2; AP-1, activator protein 1; ASC, apoptosis-associated speck-like CARD-containing protein; AvrA, avirulence gene A; CARD, caspase activation and recruitment domain; cIAP, cellular inhibitor of apoptosis; EHEC, enterohemorrhagic *Escherichia coli*; EPEC, enteropathogenic *E. coli*; FADD, Fas-associated protein with death domain; GBP, guanylate-binding protein; GSDMD, gasdermin D; IFN, interferon; IFNAR1, interferon alpha/beta receptor alpha chain; IL-1 β , interleukin 1 β ; IKK, inhibitor of kappa kinase complex; JNK, c-Jun N-terminal kinase; LUBAC, linear ubiquitin chain assembly complex; MAPK, mitogen activated protein kinase; MLKL, mixed lineage kinase domain-like protein; MKK4, MAPK kinase 4; NF- κ B, nuclear factor kappa B; NLR, Nod-like receptor; NLR4, NLR family CARD domain-containing 4; NLRP3, NLR family pyrin domain-containing protein 3; PAMP, pathogen-associated molecular pattern; PipA, pathogenicity island-encoded protein A; PRR, pattern recognition receptor; RIPK, receptor interacting serine/threonine protein kinase; TAK1, transforming growth factor beta-activated kinase 1; TLR, Toll-like receptor; TNF, tumor necrosis factor; TNFR1, TNF receptor 1; TRADD, TNFR1-associated death domain protein; TRAF, TNFR associated factor; TRAIL, TNF-related apoptosis-inducing ligand; TRAIL-R1, TRAIL receptor 1; SIF, *Salmonella* induced filaments; SlrP, *Salmonella* leucine-rich repeat protein; SopB, *Salmonella* outer protein B; SpvB, *Salmonella* plasmid virulence gene B; SseL, *Salmonella* secreted effector L.

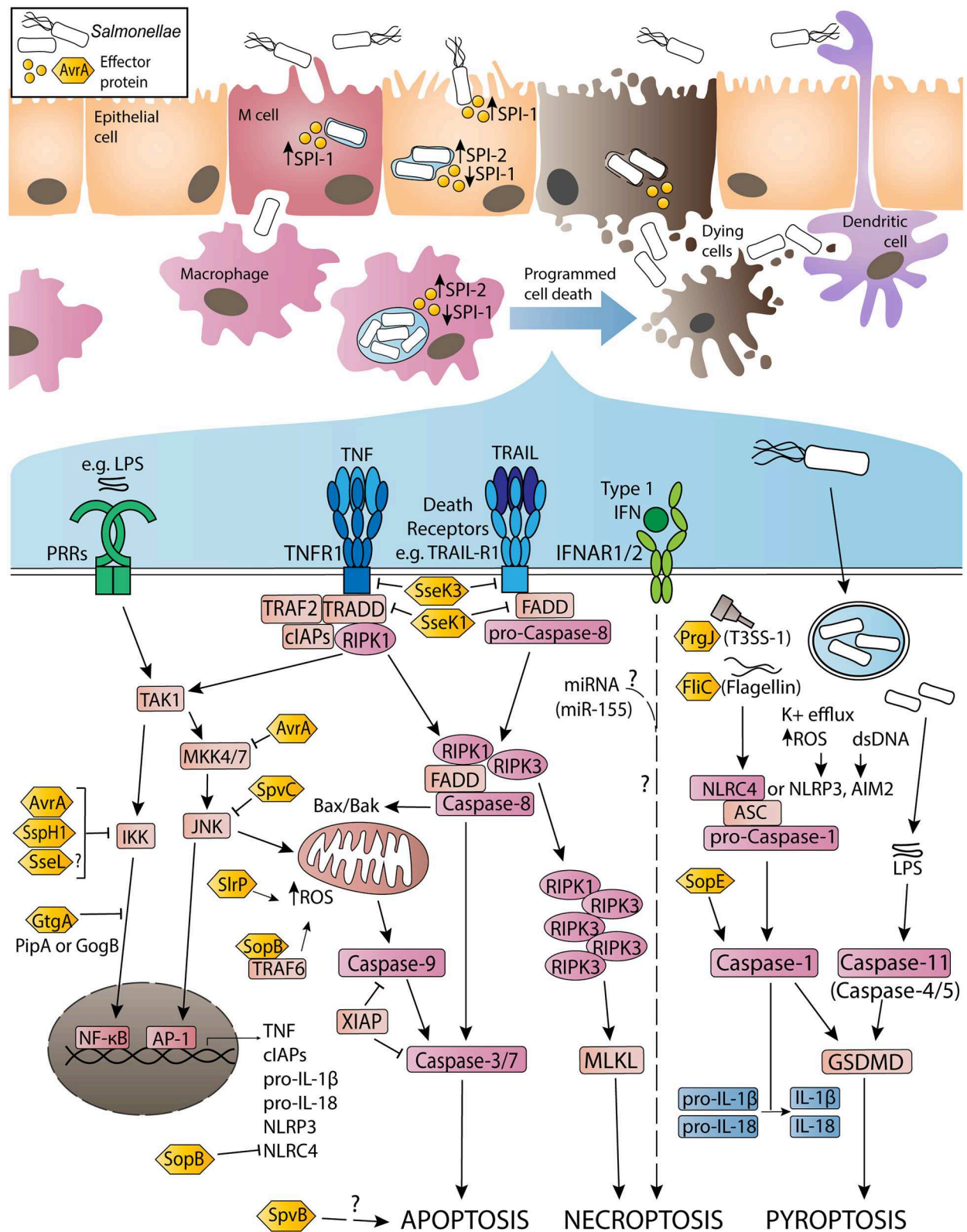


FIGURE 1 | Activation and inhibition of apoptosis, necroptosis and pyroptosis by non-typhoidal *Salmonella* virulence (effector) proteins and other stimuli during *Salmonella enterica* serovar Typhimurium infection. Non-typhoidal *Salmonella* species invade intestinal epithelial cells through the use of SPI-1 effectors to induce (Continued)

FIGURE 1 | membrane ruffling and actin rearrangement, resulting in non-phagocytic uptake of the bacteria. Alternatively, *Salmonella* uptake can occur due to M cell mediated transport across the epithelial barrier, or through sampling by phagocytic cells such as dendritic cells or macrophages. Once internalized, the SPI-1 T3SS and effectors are downregulated, while SPI-2 is upregulated to promote SCV formation and facilitate *Salmonella* replication. Throughout the infection, both SPI-1 and SPI-2 effector proteins interact with host innate immune pathways to either activate or inhibit inflammatory responses and programmed cell death. Signaling cascades have been simplified for clarity and are discussed in more detail in-text.

domain (FADD) to form a cytosolic secondary signaling complex (40, 41). Cellular FLICE-like inhibitory protein (cFLIP) also regulates complex assembly by inhibiting caspase-8 activation (42). Secondary complex activation allows caspase-8 to activate caspase-3/-7 and subsequent apoptosis.

During *S. Typhimurium* infection, autocrine or paracrine TNF signaling triggers cell death responses by initiating extrinsic apoptosis. *Salmonella* effector proteins also induce apoptosis via these signaling pathways. SlrP is an E3 ubiquitin ligase translocated by both SPI-1 and SPI-2 that interacts with thioredoxin-1 (Trx1) and the ER chaperone protein, ERdj3 (43–46). Expression of SlrP increased cytotoxicity in infected HeLa cells, suggesting a role for SlrP in inducing intrinsic apoptosis in infected epithelial cells (43, 44). Additionally, translocation of SPI-2 effector SpvB (an ADP-ribosylase) promotes apoptosis in human monocyte-derived macrophages (HMDMs), potentially due to loss of polymerized F-actin (47–50). SpvB may have a similar effect in *S. Dublin*-infected HT-29 cells, although apoptosis was markedly delayed in these cells (28 h post-infection *in vitro*) (51). However, the mechanism by which SpvB promotes apoptosis remains unclear.

Alternatively, effectors such as SopB may have a role in preventing intrinsic apoptosis. SopB (also known as SigD) is a phosphoinositide phosphatase translocated by SPI-1 that has multiple reported virulence functions (8, 52, 53). Infection of mouse embryonic fibroblasts revealed that SopB is ubiquitinated by TRAF6, potentially as a mechanism of directing SopB activity within the host cell (54, 55). SopB-TRAF6 interactions prevent the recruitment of TRAF6 to the mitochondria, inhibiting accumulation of ROS in the organelle, thus preventing intrinsic apoptosis (56). SopB phosphatase activity in epithelial cells also mediates the recruitment of Rho and Ras family GTPases to the site of infection, promoting pro-survival Akt signaling and inhibiting apoptotic responses downstream (57–59). Another SPI-1 translocated effector that alters apoptotic pathways is AvrA, which displays deubiquitinase and acetyltransferase activity. Studies of *S. Typhimurium*-infected HeLa or HCT116 cells demonstrated that AvrA deubiquitylates I κ B α to suppress pro-survival NF- κ B activation (60, 61). Interestingly, *in vivo* mouse infections, as well as transfection of AvrA into HEK293T cells, indicated that AvrA also prevents apoptotic responses by acetylating MAPK kinase 4 (MKK4) and inhibiting the c-Jun N-terminal-kinase (JNK) pathway (62–64). Similarly, SpvC (a phosphothreonine lyase) acts to both dampen inflammation and suppress apoptosis by inactivating members of the MAPK pathway (65, 66). While suppression of both pro-survival signaling and pro-apoptotic pathways may initially seem counterintuitive, it is likely that this duality allows *Salmonella* to prolong infection of epithelial cells, allowing greater opportunities for replication in this cell type.

SALMONELLA INFECTION AND NECROPTOTIC CELL DEATH

Necroptosis is a caspase-independent lytic form of programmed cell death that results in characteristic pore formation and the release of cellular contents and highly inflammatory damage-associated molecular patterns (DAMPs) into the extracellular space (67). Initially triggered by TNF binding to TNFR1, necroptosis occurs when caspase-8 is non-functional or inhibited. In the absence of active caspase-8, deubiquitinated RIPK1 is able to interact with RIPK3, subsequently forming an amyloid-like complex (called the necrosome), activating RIPK3 via autophosphorylation events (68). Active RIPK3 then mediates the phosphorylation of mixed lineage kinase domain-like protein (MLKL), enabling MLKL oligomerization and migration to the plasma membrane, triggering membrane permeabilization and lytic cell death (**Figure 1**) (68). Although RIPK3 and MLKL are critical for the induction of necroptosis, the precise mechanism by which active MLKL executes necroptosis remains unclear (38, 69, 70). Released DAMPs induce inflammatory responses in neighboring cells, promoting recruitment of innate immune cells and mediating tissue pathology in the immediate area (71).

Observations of necroptosis in response to *S. Typhimurium* infection have included studies comparing infected C57BL/6J wild type (WT) or type I IFN alpha/beta receptor 1 deficient (*Ifnar1*^{-/-}) mice (72). Type I IFNs act through heterodimeric IFNAR1/IFNAR2 complexes to activate Janus kinase (JAK)/signal transducer and activator of transcription (STAT) signaling cascades, resulting in the transcription of interferon-stimulated genes (ISGs) (73). Following intravenous *S. Typhimurium* infection, *Ifnar1*^{-/-} mice experienced improved survival compared to WT mice, while infected *Ifnar1*^{-/-} bone marrow derived macrophages (BMDMs) experienced reduced rates of cytotoxicity *in vitro*, with decreased activation of RIPK1 and RIPK3 (72). Immunoprecipitation of IFNAR1 in WT BMDMs indicated RIPK1 associates with IFNAR1 following Type I IFN stimulation, while *in vivo* infection of *Ripk3*^{-/-} mice induced similar cytotoxicity to *Ifnar1*^{-/-} mice (72). Robinson et al. thus proposed a role for Type I IFN signaling in inducing necroptosis in *S. Typhimurium*-infected macrophages (72). Later work found that signaling downstream of IFNAR1/RIPK1/RIPK3 interactions resulted in recruitment of phosphoglycerate mutase family member 5 (PGAM5) (74). PGAM5 recruitment by RIPK3 was suggested as a mechanism of promoting or executing necroptosis in *S. Typhimurium*-infected BMDMs via impaired production of antioxidants, resulting in ROS-mediated mitochondrial damage (74, 75). However, studies outside the *S. Typhimurium* infection context did not support PGAM5 as a mediator of necroptosis, instead proposing that PGAM5 counteracts necroptosis by promoting

autophagic degradation of mitochondria (inhibiting ROS production) (70, 76, 77).

Other explorations of necroptosis in the context of *S. Typhimurium* infection involved the use of qRT-PCR techniques to assess the expression of micro RNAs (miRNAs) induced by infection in RAW264.7 cells (78). A highly upregulated miRNA, miR-155, mediated cytotoxicity levels similar to *S. Typhimurium*-infected cells when transfected into RAW264.7s (78). Further *in vitro* transfections indicated that miR-155 induced RIPK1 and RIPK3 phosphorylation (indicative of necroptosis) by 18 h post-treatment, as well as cleavage of poly (ADP-ribose) polymerase-1 (PARP-1) in a similar manner to *S. Typhimurium* infection (78). Treatment with RIPK1 inhibitor necrostatin-1s partially rescued cell viability in miR-155 transfected cells, supporting a role for necroptosis in contributing to cytotoxicity (78). The authors suggested that PARP-1 activation occurs downstream of RIPK1/RIPK3 activation, however existing work in TNF-stimulated L929 cells instead proposes that PARP-1 contributes to a separate programmed necrosis pathway (78, 79).

Virulence proteins may also play a role in mediating host necroptotic responses during *S. Typhimurium* infection. *Salmonella* secreted effector K1 (SseK1), SseK2, and SseK3 are a family of related virulence proteins with glycosyltransferase activity that share high sequence homology with the Arg-GlcNAc transferase, NleB, found in attaching and effacing (A/E) pathogens (80–82). SseK effectors reportedly inhibit TNF-induced NF- κ B signaling and cell death in macrophages, through arginine glycosylation of FADD and TRADD by SseK1 and SseK3, respectively (83). *In vitro* infections of RAW264.7 cells with Δ sseK123 *S. Typhimurium* showed similar levels of caspase-3/-7 activation when compared to WT infection, but resulted in higher levels of MLKL phosphorylation, indicating that SseK1 and SseK3 may specifically inhibit necroptotic cell death (83). Reports of SseK binding targets remain inconclusive, with suggested glycosylation targets for SseK1 including GAPDH, FADD, and TRADD, while SseK2 may glycosylate FADD (83–85). Recently, mass spectrometry-based screens have identified TNFR1 and TRAIL-R as novel glycosylation targets of SseK3, and demonstrated that TRADD is the preferred binding target of SseK1 (85). Although the specific actions of SseK effectors have yet to be confirmed, collectively these results suggest that SseK1 and SseK3 modify TNFR superfamily members as well as TRADD or FADD, thus inhibiting both TNF-mediated NF- κ B signaling and cell death via apoptosis or necroptosis.

INFLAMMASOME ACTIVATION AND PYROPTOTIC CELL DEATH DURING *SALMONELLA* INFECTION

Pyroptosis is a highly inflammatory, caspase-dependent form of lytic cell death characterized by pore formation and release of active IL-1 β and IL-18 (86). Originally thought to be a caspase-1 dependent form of apoptosis or necrosis, pyroptosis is an important host defense mechanism against *S. Typhimurium* (87–89). Typically, pyroptosis in *S. Typhimurium*-infected cells

is triggered by the sensing of flagellin (FlhC and FlhB) or PrgJ (a SPI-1 rod protein) by NLR family apoptosis inhibitory proteins (NAIPs), which then interact with NLR family caspase activation and recruitment domain (CARD)-containing protein 4 (NLRC4) to trigger assembly of a multiprotein complex called the NLRC4 inflammasome (90–92). NLRC4 recruits pro-caspase-1 via shared CARD domains, and can also recruit apoptosis-associated speck-like protein containing a CARD domain (ASC), to assemble the inflammasome and induce the proteolytic activation of caspase-1 (**Figure 1**) (92). Active caspase-1 mediates pyroptosis by cleaving gasdermin-D (GSDMD), producing an N-terminal segment that forms multimeric pores in the cell membrane and releases cellular contents into the extracellular space (93, 94). Caspase-1 also cleaves IL-1 β and IL-18 into their active forms, allowing their release through the GSDMD-N pores, or following the process of necrosis or others [as reviewed by Eder et al. (95)] (93, 95–98).

Other sensors capable of inducing pyroptosis via ASC-caspase-1 inflammasomes include NLRP3 (senses K⁺ efflux or increased ROS), AIM2 (detects cytosolic dsDNA) and pyrin (senses inhibition of RhoA GTPase activity) (99–103). Both NLRP3 and NLRC4 contribute to IL-1 β and IL-18 maturation and pyroptosis in *S. Typhimurium*-infected macrophages (104). Activated NLRC4 amplifies caspase-1 activation in infected macrophages by recruiting NLRP3, forming a single inflammasome complex with ASC that mediates pyroptotic responses downstream (104–106). Alternatively, non-canonical inflammasome pathways can induce pyroptosis through the sensing of cytosolic LPS by murine caspase-11 (or human caspase-4/-5) which cleaves GSDMD independent of caspase-1 activation, however caspase-11 does not cleave IL-1 β or IL-18, thus reducing pro-inflammatory cytokine release (**Figure 1**) (107–112). Both NLRC4 and non-canonical inflammasome activation play a role in epithelial cell responses to infection, and may help reduce bacterial dissemination throughout the intestinal mucosa (108, 113–116).

Crosstalk with caspase-8 and apoptotic pathways can also promote inflammasome activation in *S. Typhimurium*-infected cells. Studies of NLRP3 and NLRC4 interactions during *S. Typhimurium* infection detected IL-1 β maturation mediated by ASC-caspase-8 specks, suggesting a role for caspase-8 as an inflammasome effector (105, 117). Other studies have proposed roles for caspase-8 in priming inflammasome activation, or coordinating cleavage of caspase-1 in the absence of NLRP3 or NLRC4 (118). Although not yet demonstrated, effectors such as SlrP, which induce downstream ROS accumulation, could contribute to inflammasome activation and pyroptotic responses due to NLRP3 detection of ROS. However, a study of IL-1 β release in a murine *S. Typhimurium* *in vivo* infection context found that SlrP signaling inhibited IL-1 β activation, contradicting this idea (119). Aside from SlrP, effectors such as SipB, SopE, or SopB may influence pyroptosis in *S. Typhimurium*-infected macrophage. Following secretion, SipB interacts with SipC to form a translocon pore, facilitating SPI-1 effector translocation into the host cell (120). SipB is reportedly sufficient to induce caspase-1-mediated “apoptosis” and IL-18 maturation in SipB transfected or *S. Typhimurium*-infected

dendritic cells and peritoneal macrophages, potentially via direct interactions with caspase-1 (121–123). These results likely indicate pyroptosis, however the mechanisms by which SipB interact with caspase-1 or the inflammasome remain unclear.

S. Typhimurium SPI-1 effector SopE is a guanine nucleotide exchange factor that catalyzes the activation of host cell Rho GTPases such as Cdc42 and Rac1 (124). Activation of Rac1 by SopE has been reported to induce caspase-1 activation and IL-1 β secretion during *S. Typhimurium* infection of HeLa or RAW264.7 cells, and *in vivo* infection of murine enterocytes (125). SopE-induced caspase-1 activation in macrophages was not due to NLRC4 sensing of flagellin, suggesting an alternative sensor mechanism (126). Other Gram-negative bacteria possess effectors that modify Rho GTPase activity, for instance *Yersinia* spp. effector YopT, which inhibits the activity of RhoA (102, 127). This RhoA inactivation allows assembly of the pyrin inflammasome, resulting in downstream caspase-1 activity and pyroptosis in infected cells (102). This suggests interesting avenues of research for SopE-induced caspase-1 activation; however, pyrin activation has not been observed in response to changes in Rac1 or Cdc42 activity (127). In contrast to SopE, SPI-1 effector SopB plays a role in dampening inflammasome activation. SopB has been associated with the downregulation of NLRC4 in *S. Typhimurium*-infected macrophages and B cells (128–130). NLRC4 depletion was associated with reductions in both IL-1 β maturation and cytotoxicity in *S. Typhimurium*-infected B cells, and was determined to be the result of Akt/YAP pathway activation (128, 130). Loss of NLRC4 inhibits the dominant inflammasome involved in the pyroptotic response to *S. Typhimurium* infection, thus allowing the bacteria better opportunities for replication before escaping the host cell.

Lastly, although *S. Typhimurium* effectors both activate and inhibit inflammasome activation, current understandings of these effectors suggest that their translocation is under temporal and spatial control by the bacteria due to their translocating T3SS type. A recent study demonstrated that mutation of the SPI-1 T3SS resulted in decreased HMDM cytotoxicity and IL-1 β release, while infection with Δ SPI-2 *S. Typhimurium* induced rapid cell death and IL-1 β production in these cells (131). SPI-2 mutation also resulted in increased expression of SPI-1 effectors detectable by NLRC4 (FljB, PrgI, and PrgJ), suggesting that SPI-2 activity helps suppress the translocation of SPI-1 effectors later in infection (131).

CONCLUDING REMARKS

Investigating cell death in the context of *S. Typhimurium* infection has revealed highly complex interactions between host signaling cascades and bacterial virulence effectors. Tightly regulated control of T3SS effector translocation supports bacterial requirements at different infection stages, allowing *S. Typhimurium* to evade or promote cell death responses. Our understanding of *Salmonella*-host interactions is continually evolving, with virulence mechanisms and effector proteins still to be characterized and improved *in vitro* and *in vivo* models for testing hypotheses frequently emerging. While the current literature does not describe immediate applications for exploiting programmed cell death in treatment of salmonellosis, further exploration of NTS virulence factors could help characterize clinical isolates, leading to personalized therapies and improved patient outcomes. Additionally, the high specificity of *Salmonella* effector proteins could prove crucial to the development of novel genome or proteome editing tools (such as the recently described use of effectors from *Shigella flexneri*) (132). Overall, exploration of pathogen-mediated cell death provides crucial insights into how bacteria can mediate survival and dissemination between host cells and can further improve our general understanding of the importance of cell death in counteracting bacterial pathogenesis.

AUTHOR CONTRIBUTIONS

MW wrote the initial manuscript and designed the figure. JP and MW edited and revised the manuscript. Both authors read and approved the final manuscript.

FUNDING

MW was supported by an Australian Government Research Training Program (RTP) Scholarship at Monash University, Melbourne, Australia. JP was supported by a National Health and Medical Research Council (NHMRC) Career Development Fellowship (APP1159230).

ACKNOWLEDGMENTS

The authors would like to thank Dr. Deborah Williamson and Dr. Rebecca Ambrose for critical reading of the manuscript.

REFERENCES

1. Broz P, Ohlson MB, Monack DM. Innate immune response to *Salmonella* Typhimurium, a model enteric pathogen. *Gut Microbes*. (2012) 3:62–70. doi: 10.4161/gmic.19141
2. Gal-Mor O, Boyle EC, Grassl GA. Same species, different diseases: how and why typhoidal and non-typhoidal *Salmonella enterica* serovars differ. *Front Microbiol*. (2014) 5:391. doi: 10.3389/fmicb.2014.00391
3. Moffatt CR, Musto J, Pingault N, Miller M, Stafford R, Gregory J, et al. *Salmonella* Typhimurium and outbreaks of egg-associated disease in Australia, 2001 to 2011. *Foodborne Pathog Dis*. (2016) 13:379–85. doi: 10.1089/fpd.2015.2110
4. Wilson HL, Kennedy KJ, Moffatt CRM. Epidemiology of non-typhoid *Salmonella* infection in the Australian Capital Territory over a 10-year period. *Intern Med J*. (2018) 48:316–23. doi: 10.1111/imj.13625
5. LaRock DL, Chaudhary A, Miller SI. *Salmonellae* interactions with host processes. *Nat Rev Microbiol*. (2015) 13:191–205. doi: 10.1038/nrmicro3420
6. Winter SE, Thiennimitr P, Winter MG, Butler BP, Huseby DL, Crawford RW, et al. Gut inflammation provides a respiratory electron acceptor for *Salmonella*. *Nature*. (2010) 467:426–9. doi: 10.1038/nature09415
7. Byndloss MX, Rivera-Chavez F, Tsois RM, Baumler AJ. How bacterial pathogens use type III and type IV secretion systems to facilitate their transmission. *Curr Opin Microbiol*. (2017) 35:1–7. doi: 10.1016/j.mib.2016.08.007

8. Raffatellu M, Wilson RP, Chessa D, Andrews-Polymenis H, Tran QT, Lawhon S, et al. SipA, SopA, SopB, SopD, and SopE2 contribute to *Salmonella enterica* serotype Typhimurium invasion of epithelial cells. *Infect Immun.* (2005) 73:146–54. doi: 10.1128/IAI.73.1.146-154.2005
9. Tahoun A, Mahajan S, Paxton E, Malterer G, Donaldson DS, Wang D, et al. *Salmonella* transforms follicle-associated epithelial cells into M cells to promote intestinal invasion. *Cell Host Microbe.* (2012) 12:645–56. doi: 10.1016/j.chom.2012.10.009
10. Zhang K, Riba A, Nietschke M, Torow N, Repnik U, Putz A, et al. Minimal SPI1-T3SS effector requirement for *Salmonella* enterocyte invasion and intracellular proliferation *in vivo*. *PLoS Pathog.* (2018) 14:e1006925. doi: 10.1371/journal.ppat.1006925
11. Cummings LA, Wilkerson WD, Bergsbaken T, Cookson BT. *In vivo*, *fliC* expression by *Salmonella enterica* serovar Typhimurium is heterogeneous, regulated by ClpX, and anatomically restricted. *Mol Microbiol.* (2006) 61:795–809. doi: 10.1111/j.1365-2958.2006.05271.x
12. Miao EA, Leaf IA, Treuting PM, Mao DP, Dors M, Sarkar A, et al. Caspase-1-induced pyroptosis is an innate immune effector mechanism against intracellular bacteria. *Nat Immunol.* (2010) 11:1136–42. doi: 10.1038/ni.1960
13. Lai MA, Quarles EK, Lopez-Yglesias AH, Zhao X, Hajjar AM, Smith KD. Innate immune detection of flagellin positively and negatively regulates *Salmonella* infection. *PLoS ONE.* (2013) 8:e72047. doi: 10.1371/journal.pone.0072047
14. Sporing I, Felgner S, Preusse M, Eckweiler D, Rohde M, Haussler S, et al. Regulation of flagellum biosynthesis in response to cell envelope stress in *Salmonella enterica* serovar Typhimurium. *MBio.* (2018) 9:e00736-17. doi: 10.1128/mBio.00736-17
15. Knuff K, Finlay BB. What the SIF is happening—the role of intracellular *Salmonella*-induced filaments. *Front Cell Infect Microbiol.* (2017) 7:335. doi: 10.3389/fcimb.2017.00335
16. Liss V, Swart AL, Kehl A, Hermanns N, Zhang Y, Chikkaballi D, et al. *Salmonella enterica* remodels the host cell endosomal system for efficient intravacuolar nutrition. *Cell Host Microbe.* (2017) 21:390–402. doi: 10.1016/j.chom.2017.02.005
17. Jennings E, Thurston TLM, Holden DW. *Salmonella* SPI-2 type III secretion system effectors: molecular mechanisms and physiological consequences. *Cell Host Microbe.* (2017) 22:217–31. doi: 10.1016/j.chom.2017.07.009
18. Castanheira S, Garcia-Del Portillo F. *Salmonella* populations inside host cells. *Front Cell Infect Microbiol.* (2017) 7:432. doi: 10.3389/fcimb.2017.00432
19. Meunier E, Dick MS, Dreier RF, Schurmann N, Kenzelmann Broz D, Warming S, et al. Caspase-11 activation requires lysis of pathogen-containing vacuoles by IFN- γ -induced GTPases. *Nature.* (2014) 509:366–70. doi: 10.1038/nature13157
20. Ingram JP, Brodsky IE, Balachandran S. Interferon-gamma in *Salmonella* pathogenesis: new tricks for an old dog. *Cytokine.* (2017) 98:27–32. doi: 10.1016/j.cyt.2016.10.009
21. Man SM, Place DE, Kuriakose T, Kanneganti TD. Interferon-inducible guanylate-binding proteins at the interface of cell-autonomous immunity and inflammasome activation. *J Leukoc Biol.* (2017) 101:143–50. doi: 10.1189/jlb.4MR0516-223R
22. Jung HC, Eckmann L, Yang SK, Panja A, Fierer J, Morzycka-Wroblewska E, et al. A distinct array of proinflammatory cytokines is expressed in human colon epithelial cells in response to bacterial invasion. *J Clin Invest.* (1995) 95:55–65. doi: 10.1172/JCI117676
23. Ciacci-Woolwine F, Blomfield IC, Richardson SH, Mizel SB. *Salmonella* flagellin induces tumor necrosis factor alpha in a human promonocytic cell line. *Infect Immun.* (1998) 66:1127–34.
24. Pietilä TE, Veckman V, Kyllönen P, Lähdenmäki K, Korhonen TK, Julkunen I. Activation, cytokine production, and intracellular survival of bacteria in *Salmonella*-infected human monocyte-derived macrophages and dendritic cells. *J Leukoc Biol.* (2005) 78:909–20. doi: 10.1189/jlb.1204721
25. Arthur JS, Ley SC. Mitogen-activated protein kinases in innate immunity. *Nat Rev Immunol.* (2013) 13:679–92. doi: 10.1038/nri3495
26. Liu T, Zhang L, Joo D, Sun SC. NF- κ B signaling in inflammation. *Signal Transduct Target Ther.* (2017) 2:17023. doi: 10.1038/sigtrans.2017.23
27. Sun SC. The non-canonical NF- κ B pathway in immunity and inflammation. *Nat Rev Immunol.* (2017) 17:545–58. doi: 10.1038/nri.2017.52
28. Lin SL, Le TX, Cowen DS. SptP, a *Salmonella* typhimurium type III-secreted protein, inhibits the mitogen-activated protein kinase pathway by inhibiting Raf activation. *Cell Microbiol.* (2003) 5:267–75. doi: 10.1046/j.1462-5822.2003.t01-1-00274.x
29. Haraga A, Miller SI. A *Salmonella* type III secretion effector interacts with the mammalian serine/threonine protein kinase PKN1. *Cell Microbiol.* (2006) 8:837–46. doi: 10.1111/j.1462-5822.2005.00670.x
30. Rytönen A, Poh J, Garmendia J, Boyle C, Thompson A, Liu M, et al. SseL, a *Salmonella* deubiquitinase required for macrophage killing and virulence. *Proc Natl Acad Sci USA.* (2007) 104:3502–7. doi: 10.1073/pnas.0610095104
31. Le Negrate G, Faustin B, Welsh K, Loeffler M, Krajewska M, Hasegawa P, et al. *Salmonella* secreted factor L deubiquitinase of *Salmonella* Typhimurium inhibits NF- κ B, suppresses I κ B α ubiquitination and modulates innate immune responses. *J Immunol.* (2008) 180:5045–56. doi: 10.4049/jimmunol.180.7.5045
32. Mesquita FS, Holden DW, Rolhion N. Lack of effect of the *Salmonella* deubiquitinase SseL on the NF-kappaB pathway. *PLoS ONE.* (2013) 8:e53064. doi: 10.1371/journal.pone.0053064
33. Sun H, Kamanova J, Lara-Tejero M, Galan JE. A family of *Salmonella* type III secretion effector proteins selectively targets the NF-kappaB signaling pathway to preserve host homeostasis. *PLoS Pathog.* (2016) 12:e1005484. doi: 10.1371/journal.ppat.1005484
34. Wu M, El Qaidi S, Hardwidge PR. SseL deubiquitinates RPS3 to inhibit its nuclear translocation. *Pathogens.* (2018) 7:86. doi: 10.3390/pathogens7040086
35. Pietro M. Immunity to systemic *Salmonella* infections. *Curr Mol Med.* (2002) 2:393–406. doi: 10.2174/1566524023362492
36. Morgan MJ, Liu ZG. Crosstalk of reactive oxygen species and NF-kappaB signaling. *Cell Res.* (2011) 21:103–15. doi: 10.1038/cr.2010.178
37. Voedisch S, Koenecke C, David S, Herbrand H, Forster R, Rhen M, et al. Mesenteric lymph nodes confine dendritic cell-mediated dissemination of *Salmonella enterica* serovar Typhimurium and limit systemic disease in mice. *Infect Immun.* (2009) 77:3170–80. doi: 10.1128/IAI.00272-09
38. Galluzzi L, Vitale I, Aaronson SA, Abrams JM, Adam D, Agostinis P, et al. Molecular mechanisms of cell death: recommendations of the Nomenclature Committee on Cell Death 2018. *Cell Death Differ.* (2018) 25:486–541. doi: 10.1038/s41418-017-0012-4
39. Silke J, Meier P. Inhibitor of apoptosis (IAP) proteins—modulators of cell death and inflammation. *Cold Spring Harb Perspect Biol.* (2013) 5:a008730. doi: 10.1101/cshperspect.a008730
40. Moquin DM, McQuade T, Chan FK. CYLD deubiquitinates RIP1 in the TNF α -induced necrosome to facilitate kinase activation and programmed necrosis. *PLoS ONE.* (2013) 8:e76841. doi: 10.1371/journal.pone.0076841
41. Annibaldi A, Meier P. Checkpoints in TNF-induced cell death: implications in inflammation and cancer. *Trends Mol Med.* (2018) 24:49–65. doi: 10.1016/j.molmed.2017.11.002
42. Tsuchiya Y, Nakabayashi O, Nakano H. FLIP the switch: regulation of apoptosis and necroptosis by cFLIP. *Int J Mol Sci.* (2015) 16:30321–41. doi: 10.3390/ijms161226232
43. Bernal-Bayard J, Ramos-Morales F. *Salmonella* type III secretion effector SlrP is an E3 ubiquitin ligase for mammalian thioredoxin. *J Biol Chem.* (2009) 284:27587–95. doi: 10.1074/jbc.M109.010363
44. Bernal-Bayard J, Cardenal-Munoz E, Ramos-Morales F. The *Salmonella* type III secretion effector, *Salmonella* leucine-rich repeat protein (SlrP), targets the human chaperone ERdj3. *J Biol Chem.* (2010) 285:16360–8. doi: 10.1074/jbc.M110.100669
45. Zouhir S, Bernal-Bayard J, Cordero-Alba M, Cardenal-Munoz E, Guimaraes B, Lazar N, et al. The structure of the SlrP-Trx1 complex sheds light on the autoinhibition mechanism of the type III secretion system effectors of the NEL family. *Biochem J.* (2014) 464:135–44. doi: 10.1042/BJ20140587
46. Cordero-Alba M, Garcia-Gomez JJ, Aguilera-Herce J, Ramos-Morales F. Proteomic insight into the effects of the *Salmonella* ubiquitin ligase SlrP on host cells. *Biochem Biophys Res Commun.* (2016) 472:539–44. doi: 10.1016/j.bbrc.2016.03.014
47. Libby SJ, Lesnick M, Hasegawa P, Weidenhammer E, Guiney DG. The *Salmonella* virulence plasmid *spv* genes are required for cytopathology

- in human monocyte-derived macrophages. *Cell Microbiol.* (2000) 2:49–58. doi: 10.1046/j.1462-5822.2000.00030.x
48. Lesnick ML, Reiner NE, Fierer J, Guiney DG. The *Salmonella* spvB virulence gene encodes an enzyme that ADP-ribosylates actin and destabilizes the cytoskeleton of eukaryotic cells. *Mol Microbiol.* (2001) 39:1464–70. doi: 10.1046/j.1365-2958.2001.02360.x
 49. Browne SH, Lesnick ML, Guiney DG. Genetic requirements for *Salmonella*-induced cytopathology in human monocyte-derived macrophages. *Infect Immun.* (2002) 70:7126. doi: 10.1128/IAI.70.12.7126-7135.2002
 50. Mesa-Pereira B, Medina C, Camacho EM, Flores A, Santero E. Novel tools to analyze the function of *Salmonella* effectors show that SvpB ectopic expression induces cell cycle arrest in tumor cells. *PLoS ONE.* (2013) 8:e78458. doi: 10.1371/journal.pone.0078458
 51. Paesold G, Guiney DG, Eckmann L, Kagnoff MF. Genes in the *Salmonella* pathogenicity island 2 and the *Salmonella* virulence plasmid are essential for *Salmonella*-induced apoptosis in intestinal epithelial cells. *Cell Microbiol.* (2002) 4:771–81. doi: 10.1046/j.1462-5822.2002.00233.x
 52. Bakowski MA, Cirulis JT, Brown NF, Finlay BB, Brumell JH. SopD acts cooperatively with SopB during *Salmonella enterica* serovar Typhimurium invasion. *Cell Microbiol.* (2007) 9:2839–55. doi: 10.1111/j.1462-5822.2007.01000.x
 53. Bakowski MA, Braun V, Brumell JH. *Salmonella*-containing vacuoles: directing traffic and nesting to grow. *Traffic.* (2008) 9:2022–31. doi: 10.1111/j.1600-0854.2008.00827.x
 54. Ruan HH, Li Y, Zhang XX, Liu Q, Ren H, Zhang KS, et al. Identification of TRAF6 as a ubiquitin ligase engaged in the ubiquitination of SopB, a virulence effector protein secreted by *Salmonella* Typhimurium. *Biochem Biophys Res Commun.* (2014) 447:172–7. doi: 10.1016/j.bbrc.2014.03.126
 55. Ruan HH, Zhang Z, Wang SY, Nickels LM, Tian L, Qiao JJ, et al. Tumor necrosis factor receptor-associated factor 6 (TRAF6) mediates ubiquitination-dependent STAT3 activation upon *Salmonella enterica* serovar Typhimurium infection. *Infect Immun.* (2017) 85:e00081-17. doi: 10.1128/IAI.00081-17
 56. Ruan H, Zhang Z, Tian L, Wang S, Hu S, Qiao JJ. The *Salmonella* effector SopB prevents ROS-induced apoptosis of epithelial cells by retarding TRAF6 recruitment to mitochondria. *Biochem Biophys Res Commun.* (2016) 478:618–23. doi: 10.1016/j.bbrc.2016.07.116
 57. Chang F, Lee JT, Navolanic PM, Steelman LS, Shelton JG, Blalock WL, et al. Involvement of PI3K/Akt pathway in cell cycle progression, apoptosis, and neoplastic transformation: a target for cancer chemotherapy. *Leukemia.* (2003) 17:590–603. doi: 10.1038/sj.leu.2402824
 58. Knodler LA, Finlay BB, Steele-Mortimer O. The *Salmonella* effector protein SopB protects epithelial cells from apoptosis by sustained activation of Akt. *J Biol Chem.* (2005) 280:9058–64. doi: 10.1074/jbc.M412588200
 59. Truong D, Boddy KC, Canadien V, Brabant D, Fairn GD, D'Costa VM, et al. *Salmonella* exploits host Rho GTPase signalling pathways through the phosphatase activity of SopB. *Cell Microbiol.* (2018) 20:e12938. doi: 10.1111/cmi.12938
 60. Collier-Hyams LS, Zeng H, Sun J, Tomlinson AD, Bao ZQ, Chen H, et al. Cutting edge: *Salmonella* AvrA effector inhibits the key proinflammatory, anti-apoptotic NF- κ B pathway. *J Immunol.* (2002) 169:2846–50. doi: 10.4049/jimmunol.169.6.2846
 61. Ye Z, Petrof EO, Boone D, Claud EC, Sun J. *Salmonella* effector AvrA regulation of colonic epithelial cell inflammation by deubiquitination. *Am J Pathol.* (2007) 171:882–92. doi: 10.2353/ajpath.2007.070220
 62. Jones RM, Wu H, Wentworth C, Luo L, Collier-Hyams L, Neish AS. *Salmonella* AvrA coordinates suppression of host immune and apoptotic defenses via JNK pathway blockade. *Cell Host Microbe.* (2008) 3:233–44. doi: 10.1016/j.chom.2008.02.016
 63. Du F, Galan JE. Selective inhibition of type III secretion activated signaling by the *Salmonella* effector AvrA. *PLoS Pathog.* (2009) 5:e1000595. doi: 10.1371/journal.ppat.1000595
 64. Wu H, Jones RM, Neish AS. The *Salmonella* effector AvrA mediates bacterial intracellular survival during infection *in vivo*. *Cell Microbiol.* (2012) 14:28–39. doi: 10.1111/j.1462-5822.2011.01694.x
 65. Mazurkiewicz P, Thomas J, Thompson JA, Liu M, Arbibe L, Sansonetti P, et al. SpvC is a *Salmonella* effector with phosphothreonine lyase activity on host mitogen-activated protein kinases. *Mol Microbiol.* (2008) 67:1371–83. doi: 10.1111/j.1365-2958.2008.06134.x
 66. Haneda T, Ishii Y, Shimizu H, Ohshima K, Iida N, Danbara H, et al. *Salmonella* type III effector SpvC, a phosphothreonine lyase, contributes to reduction in inflammatory response during intestinal phase of infection. *Cell Microbiol.* (2012) 14:485–99. doi: 10.1111/j.1462-5822.2011.01733.x
 67. Frank D, Vince JE. Pyroptosis versus necroptosis: similarities, differences, and crosstalk. *Cell Death Differ.* (2019) 26:99–114. doi: 10.1038/s41418-018-0212-6
 68. He S, Wang X. RIP kinases as modulators of inflammation and immunity. *Nat Immunol.* (2018) 19:912–22. doi: 10.1038/s41590-018-0188-x
 69. Murphy JM, Czabotar PE, Hildebrand JM, Lucet IS, Zhang JG, Alvarez-Diaz S, et al. The pseudokinase MLKL mediates necroptosis via a molecular switch mechanism. *Immunity.* (2013) 39:443–53. doi: 10.1016/j.immuni.2013.06.018
 70. Remijsen Q, Goossens V, Grootjans S, Van den Haute C, Vanlangenakker N, Dondelinger Y, et al. Depletion of RIPK3 or MLKL blocks TNF-driven necroptosis and switches towards a delayed RIPK1 kinase-dependent apoptosis. *Cell Death Dis.* (2014) 5:e1004. doi: 10.1038/cddis.2013.531
 71. Kaczmarek A, Vandenabeele P, Krysko DV. Necroptosis: the release of damage-associated molecular patterns and its physiological relevance. *Immunity.* (2013) 38:209–23. doi: 10.1016/j.immuni.2013.02.003
 72. Robinson N, McComb S, Mulligan R, Dudani R, Krishnan L, Sad S. Type I interferon induces necroptosis in macrophages during infection with *Salmonella enterica* serovar Typhimurium. *Nat Immunol.* (2012) 13:954–62. doi: 10.1038/ni.2397
 73. de Weerd NA, Nguyen T. The interferons and their receptors—distribution and regulation. *Immunol Cell Biol.* (2012) 90:483–91. doi: 10.1038/icb.2012.9
 74. Hos NJ, Ganesan R, Gutierrez S, Hos D, Klimek J, Abdullah Z, et al. Type I interferon enhances necroptosis of *Salmonella* Typhimurium-infected macrophages by impairing antioxidative stress responses. *J Cell Biol.* (2017) 216:4107–21. doi: 10.1083/jcb.201701107
 75. Wang Z, Jiang H, Chen S, Du F, Wang X. The mitochondrial phosphatase PGAM5 functions at the convergence point of multiple necrotic death pathways. *Cell.* (2012) 148:228–43. doi: 10.1016/j.cell.2011.11.030
 76. Lu W, Sun J, Yoon JS, Zhang Y, Zheng L, Murphy E, et al. Mitochondrial protein PGAM5 regulates mitophagic protection against cell necroptosis. *PLoS ONE.* (2016) 11:e0147792. doi: 10.1371/journal.pone.0147792
 77. Moriwaki K, Farias Luz N, Balaji S, De Rosa MJ, O'Donnell CL, Gough PJ, et al. The mitochondrial phosphatase PGAM5 is dispensable for necroptosis but promotes inflammasome activation in macrophages. *J Immunol.* (2016) 196:407–15. doi: 10.4049/jimmunol.1501662
 78. Ro YT, Jo GH, Jung SA, Lee EH, Shin J, Lee JH. *Salmonella* induced miR155 enhances necroptotic death in macrophage cells via targeting RIP1/3. *Mol Med Rep.* (2018) 18:5133–40. doi: 10.3892/mmr.2018.9525
 79. Sosna J, Voigt S, Mathieu S, Lange A, Thon L, Davarnia P, et al. TNF-induced necroptosis and PARP-1-mediated necrosis represent distinct routes to programmed necrotic cell death. *Cell Mol Life Sci.* (2014) 71:331–48. doi: 10.1007/s00018-013-1381-6
 80. Kujat Choy SL, Boyle EC, Gal-Mor O, Goode DL, Valdez Y, Vallance BA, et al. SseK1 and SseK2 are novel translocated proteins of *Salmonella enterica* serovar Typhimurium. *Infect Immun.* (2004) 72:5115–25. doi: 10.1128/IAI.72.9.5115-5125.2004
 81. Yang Z, Soderholm A, Lung TW, Giogha C, Hill MM, Brown NF, et al. SseK3 is a *Salmonella* effector that binds TRIM32 and modulates the host's NF- κ B signalling activity. *PLoS ONE.* (2015) 10:e0138529. doi: 10.1371/journal.pone.0138529
 82. Pearson JS, Giogha C, Ong SY, Kennedy CL, Kelly M, Robinson KS, et al. A type III effector antagonizes death receptor signalling during bacterial gut infection. *Nature.* (2013) 501:247–51. doi: 10.1038/nature12524
 83. Gunster RA, Matthews SA, Holden DW, Thurston TL. SseK1 and SseK3 type III secretion system effectors inhibit NF- κ B signaling and necroptotic cell death in *Salmonella*-infected macrophages. *Infect Immun.* (2017) 85:e00010–17. doi: 10.1128/IAI.00242-17
 84. El Qaidi S, Chen K, Halim A, Siukstaite L, Rueter C, Hurtado-Guerrero R, et al. NleB/SseK effectors from *Citrobacter rodentium*, *Escherichia coli*, and *Salmonella enterica* display distinct differences in host substrate specificity. *J Biol Chem.* (2017) 292:11423–30. doi: 10.1074/jbc.M117.790675

85. Newson JP, Scott NE, Yeuk Wah Chung I, Wong Fok Lung T, Giogha C, Gan J, et al. *Salmonella* effectors SseK1 and SseK3 target death domain proteins in the TNF and TRAIL signaling pathways. *Mol Cell Proteomics*. (2019) 18:1138–56. doi: 10.1101/359117
86. Shi J, Gao W, Shao F. Pyroptosis: gasdermin-mediated programmed necrotic cell death. *Trends Biochem Sci*. (2017) 42:245–54. doi: 10.1016/j.tibs.2016.10.004
87. Brennan MA, Cookson BT. *Salmonella* induces macrophage death by caspase-1-dependent necrosis. *Mol Microbiol*. (2000) 38:31–40. doi: 10.1046/j.1365-2958.2000.02103.x
88. Cookson BT, Brennan MA. Pro-inflammatory programmed cell death. *Trends Microbiol*. (2001) 9:113–4. doi: 10.1016/S0966-842X(00)01936-3
89. Monack DM, Navarre WW, Falkow S. *Salmonella*-induced macrophage death: the role of caspase-1 in death and inflammation. *Microbes Infect*. (2001) 3:1201–12. doi: 10.1016/S1286-4579(01)01480-0
90. Rayamajhi M, Zak DE, Chavarria-Smith J, Vance RE, Miao EA. Cutting edge: mouse NAIP1 detects the type III secretion system needle protein. *J Immunol*. (2013) 191:3986–9. doi: 10.4049/jimmunol.1301549
91. Yang J, Zhao Y, Shi J, Shao F. Human NAIP and mouse NAIP1 recognize bacterial type III secretion needle protein for inflammasome activation. *Proc Natl Acad Sci USA*. (2013) 110:14408–13. doi: 10.1073/pnas.1306376110
92. Vance RE. The NAIP/NLRC4 inflammasomes. *Curr Opin Immunol*. (2015) 32:84–9. doi: 10.1016/j.coi.2015.01.010
93. Shi J, Zhao Y, Wang K, Shi X, Wang Y, Huang H, et al. Cleavage of GSDMD by inflammatory caspases determines pyroptotic cell death. *Nature*. (2015) 526:660–5. doi: 10.1038/nature15514
94. Kovacs SB, Miao EA. Gasdermins: effectors of pyroptosis. *Trends Cell Biol*. (2017) 27:673–84. doi: 10.1016/j.tcb.2017.05.005
95. Eder C. Mechanisms of interleukin-1 β release. *Immunobiology*. (2009) 214:543–53. doi: 10.1016/j.imbio.2008.11.007
96. He WT, Wan H, Hu L, Chen P, Wang X, Huang Z, et al. Gasdermin D is an executor of pyroptosis and required for interleukin-1 β secretion. *Cell Res*. (2015) 25:1285–98. doi: 10.1038/cr.2015.139
97. Liu X, Zhang Z, Ruan J, Pan Y, Magupalli VG, Wu H, et al. Inflammasome-activated gasdermin D causes pyroptosis by forming membrane pores. *Nature*. (2016) 535:153–8. doi: 10.1038/nature18629
98. Cullen SP, Kearney CJ, Clancy DM, Martin SJ. Diverse activators of the NLRP3 inflammasome promote IL-1 β secretion by triggering necrosis. *Cell Rep*. (2015) 11:1535–48. doi: 10.1016/j.celrep.2015.05.003
99. Sagulenko V, Thygesen SJ, Sester DP, Idris A, Cridland JA, Vajjhala PR, et al. AIM2 and NLRP3 inflammasomes activate both apoptotic and pyroptotic death pathways via ASC. *Cell Death Differ*. (2013) 20:1149–60. doi: 10.1038/cdd.2013.37
100. Gross CJ, Mishra R, Schneider KS, Medard G, Wettmarshausen J, Dittlein DC, et al. K(+) Efflux-independent NLRP3 inflammasome activation by small molecules targeting mitochondria. *Immunity*. (2016) 45:761–73. doi: 10.1016/j.immuni.2016.08.010
101. He Y, Zeng MY, Yang D, Motro B, Nunez G. NEK7 is an essential mediator of NLRP3 activation downstream of potassium efflux. *Nature*. (2016) 530:354–7. doi: 10.1038/nature16959
102. Heilig R, Broz P. Function and mechanism of the pyrin inflammasome. *Eur J Immunol*. (2018) 48:230–8. doi: 10.1002/eji.201746947
103. Munoz-Planillo R, Kuffa P, Martinez-Colon G, Smith BL, Rajendiran TM, Nunez G. K(+) efflux is the common trigger of NLRP3 inflammasome activation by bacterial toxins and particulate matter. *Immunity*. (2013) 38:1142–53. doi: 10.1016/j.immuni.2013.05.016
104. Broz P, Newton K, Lamkanfi M, Mariathasan S, Dixit VM, Monack DM. Redundant roles for inflammasome receptors NLRP3 and NLRC4 in host defense against *Salmonella*. *J Exp Med*. (2010) 207:1745–55. doi: 10.1084/jem.20100257
105. Man SM, Hopkins LJ, Nugent E, Cox S, Gluck IM, Tourlomousis P, et al. Inflammasome activation causes dual recruitment of NLRC4 and NLRP3 to the same macromolecular complex. *Proc Natl Acad Sci USA*. (2014) 111:7403–8. doi: 10.1073/pnas.1402911111
106. Qu Y, Misaghi S, Newton K, Maltzman A, Izrael-Tomasevic A, Arnott D, et al. NLRP3 recruitment by NLRC4 during *Salmonella* infection. *J Exp Med*. (2016) 213:877–85. doi: 10.1084/jem.20132234
107. Kayagaki N, Wong MT, Stowe IB, Ramani SR, Gonzalez LC, Akashi-Takamura S, et al. Noncanonical inflammasome activation by intracellular LPS independent of TLR4. *Science*. (2013) 341:1246–9. doi: 10.1126/science.1240248
108. Knodler LA, Crowley SM, Sham HP, Yang H, Wrande M, Ma C, et al. Noncanonical inflammasome activation of caspase-4/caspase-11 mediates epithelial defenses against enteric bacterial pathogens. *Cell Host Microbe*. (2014) 16:249–56. doi: 10.1016/j.chom.2014.07.002
109. Kayagaki N, Stowe IB, Lee BL, O'Rourke K, Anderson K, Warming S, et al. Caspase-11 cleaves gasdermin D for non-canonical inflammasome signalling. *Nature*. (2015) 526:666–71. doi: 10.1038/nature15541
110. Yang J, Zhao Y, Shao F. Non-canonical activation of inflammatory caspases by cytosolic LPS in innate immunity. *Curr Opin Immunol*. (2015) 32:78–83. doi: 10.1016/j.coi.2015.01.007
111. Broz P, Ruby T, Belhocine K, Bouley DM, Kayagaki N, Dixit VM, et al. Caspase-11 increases susceptibility to *Salmonella* infection in the absence of caspase-1. *Nature*. (2012) 490:288–91. doi: 10.1038/nature11419
112. Man SM, Karki R, Briard B, Burton A, Gingras S, Pelletier S, et al. Differential roles of caspase-1 and caspase-11 in infection and inflammation. *Sci Rep*. (2017) 7:45126. doi: 10.1038/srep45126
113. Knodler LA, Vallance BA, Celli J, Winfree S, Hansen B, Montero M, et al. Dissemination of invasive *Salmonella* via bacterial-induced extrusion of mucosal epithelia. *Proc Natl Acad Sci USA*. (2010) 107:17733–8. doi: 10.1073/pnas.1006098107
114. Sellin ME, Muller AA, Felmy B, Dolowschiak T, Diard M, Tardivel A, et al. Epithelium-intrinsic NAIP/NLRC4 inflammasome drives infected enterocyte expulsion to restrict *Salmonella* replication in the intestinal mucosa. *Cell Host Microbe*. (2014) 16:237–48. doi: 10.1016/j.chom.2014.07.001
115. Rauch I, Deets KA, Ji DX, von Moltke J, Tenthorey JL, Lee AY, et al. NAIP-NLRC4 inflammasomes coordinate intestinal epithelial cell expulsion with eicosanoid and IL-18 release via activation of caspase-1 and –8. *Immunity*. (2017) 46:649–59. doi: 10.1016/j.immuni.2017.03.016
116. Lei-Leston AC, Murphy AG, Maloy KJ. Epithelial cell inflammasomes in intestinal immunity and inflammation. *Front Immunol*. (2017) 8:1168. doi: 10.3389/fimmu.2017.01168
117. Man SM, Tourlomousis P, Hopkins L, Monie TP, Fitzgerald KA, Bryant CE. *Salmonella* infection induces recruitment of Caspase-8 to the inflammasome to modulate IL-1 β production. *J Immunol*. (2013) 191:5239–46. doi: 10.4049/jimmunol.1301581
118. Feltham R, Vince JE, Lawlor KE. Caspase-8: not so silently deadly. *Clin Transl Immunology*. (2017) 6:e124. doi: 10.1038/cti.2016.83
119. Rao S, Schieber AMP, O'Connor CP, Leblanc M, Michel D, Ayres JS. Pathogen-mediated inhibition of anorexia promotes host survival and transmission. *Cell*. (2017) 168:503–16.e12. doi: 10.1016/j.cell.2017.01.006
120. Ly KT, Casanova JE. Mechanisms of *Salmonella* entry into host cells. *Cell Microbiol*. (2007) 9:2103–11. doi: 10.1111/j.1462-5822.2007.00992.x
121. Hersh D, Monack DM, Smith MR, Ghorri N, Falkow S, Zychlinsky A. The *Salmonella* invasin SipB induces macrophage apoptosis by binding to caspase-1. *Proc Natl Acad Sci USA*. (1999) 96:2396. doi: 10.1073/pnas.96.5.2396
122. Dreher D, Kok M, Obregon C, Kiama SG, Gehr P, Nicod LP. *Salmonella* virulence factor SipB induces activation and release of IL-18 in human dendritic cells. *J Leukoc Biol*. (2002) 72:743–51. Available online at: <https://jlb.onlinelibrary.wiley.com/doi/full/10.1189/jlb.72.4.743>
123. van der Velden AWM, Velasquez M, Starnbach MN. *Salmonella* rapidly kill dendritic cells via a caspase-1-dependent mechanism. *J Immunol*. (2003) 171:6742–9. doi: 10.4049/jimmunol.171.12.6742
124. Friebe A, Ilchmann H, Aepfelbacher M, Ehrbar K, Machleidt W, Hardt WD. SopE and SopE2 from *Salmonella* Typhimurium activate different sets of RhoGTPases of the host cell. *J Biol Chem*. (2001) 276:34035–40. doi: 10.1074/jbc.M100609200
125. Muller AJ, Hoffmann C, Galle M, Van Den Broeke A, Heikenwalder M, Falter L, et al. The *S. Typhimurium* effector SopE induces caspase-1 activation in stromal cells to initiate gut inflammation. *Cell Host Microbe*. (2009) 6:125–36. doi: 10.1016/j.chom.2009.07.007
126. Hoffmann C, Galle M, Dilling S, Kappeli R, Muller AJ, Songhet P, et al. In macrophages, caspase-1 activation by SopE and the type III secretion

- system-1 of *S. Typhimurium* can proceed in the absence of flagellin. *PLoS ONE*. (2010) 5:e12477. doi: 10.1371/journal.pone.0012477
127. Xu H, Yang J, Gao W, Li L, Li P, Zhang L, et al. Innate immune sensing of bacterial modifications of Rho GTPases by the Pyrin inflammasome. *Nature*. (2014) 513:237–41. doi: 10.1038/nature13449
 128. Perez-Lopez A, Rosales-Reyes R, Alpuche-Aranda CM, Ortiz-Navarrete V. *Salmonella* downregulates Nod-like receptor family CARD domain containing protein 4 expression to promote its survival in B cells by preventing inflammasome activation and cell death. *J Immunol*. (2013) 190:1201–9. doi: 10.4049/jimmunol.1200415
 129. Hu GQ, Song PX, Chen W, Qi S, Yu SX, Du CT, et al. Critical role for *Salmonella* effector SopB in regulating inflammasome activation. *Mol Immunol*. (2017) 90:280–6. doi: 10.1016/j.molimm.2017.07.011
 130. Garcia-Gil A, Galan-Enriquez CS, Perez-Lopez A, Nava P, Alpuche-Aranda C, Ortiz-Navarrete V. SopB activates the Akt-YAP pathway to promote *Salmonella* survival within B cells. *Virulence*. (2018) 9:1390–402. doi: 10.1080/21505594.2018.1509664
 131. Bierschenk D, Monteleone M, Moghaddas F, Baker PJ, Masters SL, Boucher D, et al. The *Salmonella* pathogenicity island-2 subverts human NLRP3 and NLRC4 inflammasome responses. *J Leukoc Biol*. (2019) 105:401–10. doi: 10.1002/JLB.MA0318-112RR
 132. Ludwicki MB, Li J, Stephens EA, Roberts RW, Koide S, Hammond PT, et al. Broad-spectrum proteome editing with an engineered bacterial ubiquitin ligase mimic. *ACS Cent Sci*. (2019) 5:852–66. doi: 10.1021/acscentsci.9b00127

Conflict of Interest Statement: The authors declare that the research was conducted in the absence of any commercial or financial relationships that could be construed as a potential conflict of interest.

Copyright © 2019 Wemyss and Pearson. This is an open-access article distributed under the terms of the Creative Commons Attribution License (CC BY). The use, distribution or reproduction in other forums is permitted, provided the original author(s) and the copyright owner(s) are credited and that the original publication in this journal is cited, in accordance with accepted academic practice. No use, distribution or reproduction is permitted which does not comply with these terms.



Pellino-1 Regulates Immune Responses to *Haemophilus influenzae* in Models of Inflammatory Lung Disease

OPEN ACCESS

Edited by:

Catarina R. Almeida,
University of Aveiro, Portugal

Reviewed by:

Eswari Dodagatta-Marri,
University of California, San Francisco,
United States
Joachim L. Schultze,
University of Bonn, Germany

*Correspondence:

Lynne R. Prince
L.r.prince@sheffield.ac.uk

† Joint first authors

‡ Present address:

Maisha F. Jabeen,
Respiratory Medicine Unit, Nuffield
Department of Medicine, University of
Oxford, Oxford, United Kingdom
Elizabeth K. Marsh,
Human Science Research Centre,
University of Derby, Derby,
United Kingdom

Specialty section:

This article was submitted to
Molecular Innate Immunity,
a section of the journal
Frontiers in Immunology

Received: 13 March 2019

Accepted: 09 July 2019

Published: 31 July 2019

Citation:

Hughes BM, Burton CS, Reese A,
Jabeen MF, Wright C, Willis J,
Khoshaein N, Marsh EK, Peachell P,
Sun SC, Dockrell DH, Marriott HM,
Sabroe I, Condliffe AM and Prince LR
(2019) Pellino-1 Regulates Immune
Responses to *Haemophilus influenzae*
in Models of Inflammatory Lung
Disease. *Front. Immunol.* 10:1721.
doi: 10.3389/fimmu.2019.01721

Bethany M. Hughes^{††}, Charlotte S. Burton^{††}, Abigail Reese¹, Maisha F. Jabeen^{†‡}, Carl Wright¹, Jessica Willis¹, Nika Khoshaein¹, Elizabeth K. Marsh^{†‡}, Peter Peachell¹, Shao C. Sun², David H. Dockrell^{1,3}, Helen M. Marriott¹, Ian Sabroe¹, Alison M. Condliffe¹ and Lynne R. Prince^{1*}

¹ Department of Infection, Immunity and Cardiovascular Disease, University of Sheffield, Sheffield, United Kingdom,

² Department of Immunology, The University of Texas MD Anderson Cancer Center, Houston, TX, United States, ³ MRC Centre for Inflammation Research, University of Edinburgh, Edinburgh, United Kingdom

Non-typeable *Haemophilus influenzae* (NTHi) is a frequent cause of lower respiratory tract infection in people with chronic obstructive pulmonary disease (COPD). Pellino proteins are a family of E3 ubiquitin ligases that are critical regulators of TLR signaling and inflammation. The aim of this study was to identify a role for Pellino-1 in airway defense against NTHi in the context of COPD. Pellino-1 is rapidly upregulated by LPS and NTHi in monocyte-derived macrophages (MDMs) isolated from individuals with COPD and healthy control subjects, in a TLR4 dependent manner. C57BL/6 *Peli1*^{-/-} and wild-type (WT) mice were subjected to acute (single LPS challenge) or chronic (repeated LPS and elastase challenge) airway inflammation followed by NTHi infection. Both WT and *Peli1*^{-/-} mice develop airway inflammation in acute and chronic airway inflammation models. *Peli1*^{-/-} animals recruit significantly more neutrophils to the airway following NTHi infection which is associated with an increase in the neutrophil chemokine, KC, in bronchoalveolar lavage fluid as well as enhanced clearance of NTHi from the lung. These data suggest that therapeutic inhibition of Pellino-1 may augment immune responses in the airway and enhance bacterial clearance in individuals with COPD.

Keywords: *Haemophilus influenzae*, Pellino-1, immunity, lung, inflammation

INTRODUCTION

COPD will be the third-leading cause of death worldwide by 2030 (1). Recurrent bacterial and viral infections are a significant cause of comorbidity in COPD, resulting in accelerated decline in lung function and posing a major economic and personal burden (2). The most common colonizing microorganism is NTHi, found in the lower respiratory tract of 30% of individuals with COPD (3). This, as well as the acquisition of new strains of NTHi, are important causes of acute exacerbations and NTHi directly contributes to airway inflammation in disease (4–6). The primary cellular immune response to NTHi is the alveolar macrophage (AM), but in COPD, they often fail to clear bacteria from the airway (7). NTHi infection leads to a Toll-like receptor (TLR)-dependent immune response in AMs, including the release of proinflammatory cytokines such as CXCL8 (8), which

recruits neutrophils to the lung. Neutrophils are an early and prominent component of the immune response in the lung to NTHi infection, as exemplified in murine models (9) and TLR-mediated neutrophil recruitment is likely to be an integral part of the airway response to NTHi.

Pellino proteins are a family of E3 ubiquitin ligases that play important roles in TLR signaling and human immunity (10). Increased Pellino-1 expression is associated with persistent bacterial infection of the airways (11). Pellino-1 knockout mice develop normally but are protected from the adverse effects of systemic administration of TLR3 and TLR4 agonists, and Pellino-1 is shown to mediate endotoxin tolerance, further supporting its importance in infection-related inflammation (12, 13). The aim of this study was to identify a role for Pellino-1 in airway defense against NTHi in the context of COPD. Here we show that induction of Pellino-1 is part of the cellular response to NTHi *in vitro* and negatively regulates bacterial clearance *in vivo*. Our work suggests that Pellino-1 is a key component of the immune response to NTHi in the airway and that therapeutically targeting Pellino-1 may enhance immunity in patients with COPD who are at risk of infection induced exacerbations.

MATERIALS AND METHODS

Animals

All work involving animals was performed in accordance with the Animal (Scientific procedures) Act 1986 and has been approved by the Animal welfare and ethical review body at University of Sheffield. Work was carried out under procedure project license 40/3726 (David Dockrell). C57BL/6 *Peli1*^{-/-} mice and WT littermates (13) were maintained via het/het breeding in a pathogen-free environment and were housed in shared cages. For full details of maintenance and experimental procedures see online **Supplementary Methods File**. COPD model: Mice were intranasally exposed to 7μg LPS (*E. coli* O26:B6, Sigma-Aldrich (St. Louis, MO) and 1.2 units elastase (Merck Millipore, Burlington, MA) each week for four consecutive weeks as previously described (14). Selected mice were treated with PBS as controls. All mice were randomized into treatment groups. On day 28 mice were subjected to bronchoalveolar lavage (BAL). Cell-free BAL fluid (BALF) was prepared and cell pellets were resuspended, counted using a haemocytometer and cytocentrifuge slides generated. Neutrophils and macrophages were identified based on cell morphology. COPD NTHi infection model: Mice were treated with weekly LPS/elastase as described above. On day 28 mice were infected with NTHi375 (15) (10⁷ CFU i.n.) for 24h. Following this, mice were subjected to BAL as above and lungs homogenized to measure bacterial viability by Miles and Misra viability counts. Acute lung injury LPS model: *Peli1*^{-/-} and WT mice were exposed to 7μg LPS i.n. After 24h mice were infected with NTHi375 (10⁷ CFU i.n.) for a further 24h. Mice were subjected to BAL, lung homogenisation and estimation of NTHi CFU counts as above. Bone marrow derived macrophages (BMDMs) were prepared as previously described (16). Bone marrow derived neutrophils (BMDNs) were isolated by negative magnetic selection (EasySep Mouse neutrophil enrichment kit, Stemcell Technologies) as per

TABLE 1 | Demographics of individuals with COPD and AMHC subjects.

Demographic	COPD (n = 3)	AMHC (n = 3)
Age (mean years)	61	63
Gender (m/f)	3/0	2/1
FEV ₁ % mean (range)	50.7 (30–71)	103 (87–113)
GOLD stage	2-3	NA
ICS	No (3)	No (3)
Smoking status	Current (1), ex (2)	Never (3)

FEV₁, forced expiratory volume in 1 second; ICS, inhaled corticosteroids.

manufacturer's recommendation. Following negative selection neutrophil purity was typically >95%.

Human Subjects

Peripheral blood was taken from healthy volunteers, people with a diagnosis of COPD, or age-matched healthy control (AMHC) subjects with written informed consent as per the declaration of Helsinki, and ethical approval in accordance with the recommendations of the South Sheffield Research Ethics Committee and the National Research Ethics Service Committee Yorkshire and the Humber (17). See **Table 1** for demographics of individuals with COPD and AMHC subjects.

Monocyte-Derived Macrophage (MDM)

Isolation and Culture

Neutrophils and mononuclear cells were isolated by plasma-Percoll gradient centrifugation from whole blood. MDMs were differentiated over 7 days as previously described (18). *Peli1* was knocked down in MDMs using Dharmacon ON-TARGET plus SMARTpoolTM siRNA and Lipofectamine 2000 (ThermoFisher Scientific), according to manufacturer's instructions. Knockdown of Pellino-1 protein was verified in each experiment by Western Blotting.

Isolation and Culture of AMs From Human Lung

The use of lung tissue was approved by the National Research Ethics' Service (REC ref:15/NW/0657) and informed written consent was obtained. Macrophages were isolated from resected non-lesional tissue by discontinuous Percoll gradient sedimentation as previously described (19). Macrophages were seeded and cultured overnight in media (RPMI 1640+10% FCS) before LPS challenge.

Western Blotting

Proteins in whole cell lysates were separated by SDS-polyacrylamide gel electrophoresis and transferred onto PVDF membranes. Membranes were probed against antibodies to Pellino-1, actin (Santa Cruz, Santa Cruz, CA), pStat-1 or Stat-6 (Cell-Signaling Technology, Leiden, The Netherlands).

Measurement of KC

Cell free BALF and cell culture supernatant were subjected to KC ELISA (Duoset, R&D Systems) as per manufacturer's

instructions. Formalin fixed lung sections from LPS/elastase treated mice were subjected to immunohistochemistry for KC.

NTHi Intracellular Viability Assays

Cells were infected with NTHi375 (MOI 10) for either 1 h (BMDNs) or 2 h (MDMs, BMDMs). Cells were lysed and viable NTHi measured by Miles and Misra assay. In separate wells, gentamicin [40 μ g/ml] was added for 30 min to kill extracellular bacteria following which lysates were made after a further 1 h

(neutrophils) or 2 h (MDMs, BMDMs) and viable intracellular NTHi was assessed as above.

Data Analysis and Statistics

Data were analyzed by One-way ANOVA (with post-test) or Students' *t*-test as appropriate using GraphPad Prism 7 (GraphPad Software, San Diego, CA). Data are expressed as mean \pm SEM or mean \pm SD, and significance was accepted at $p < 0.05$.

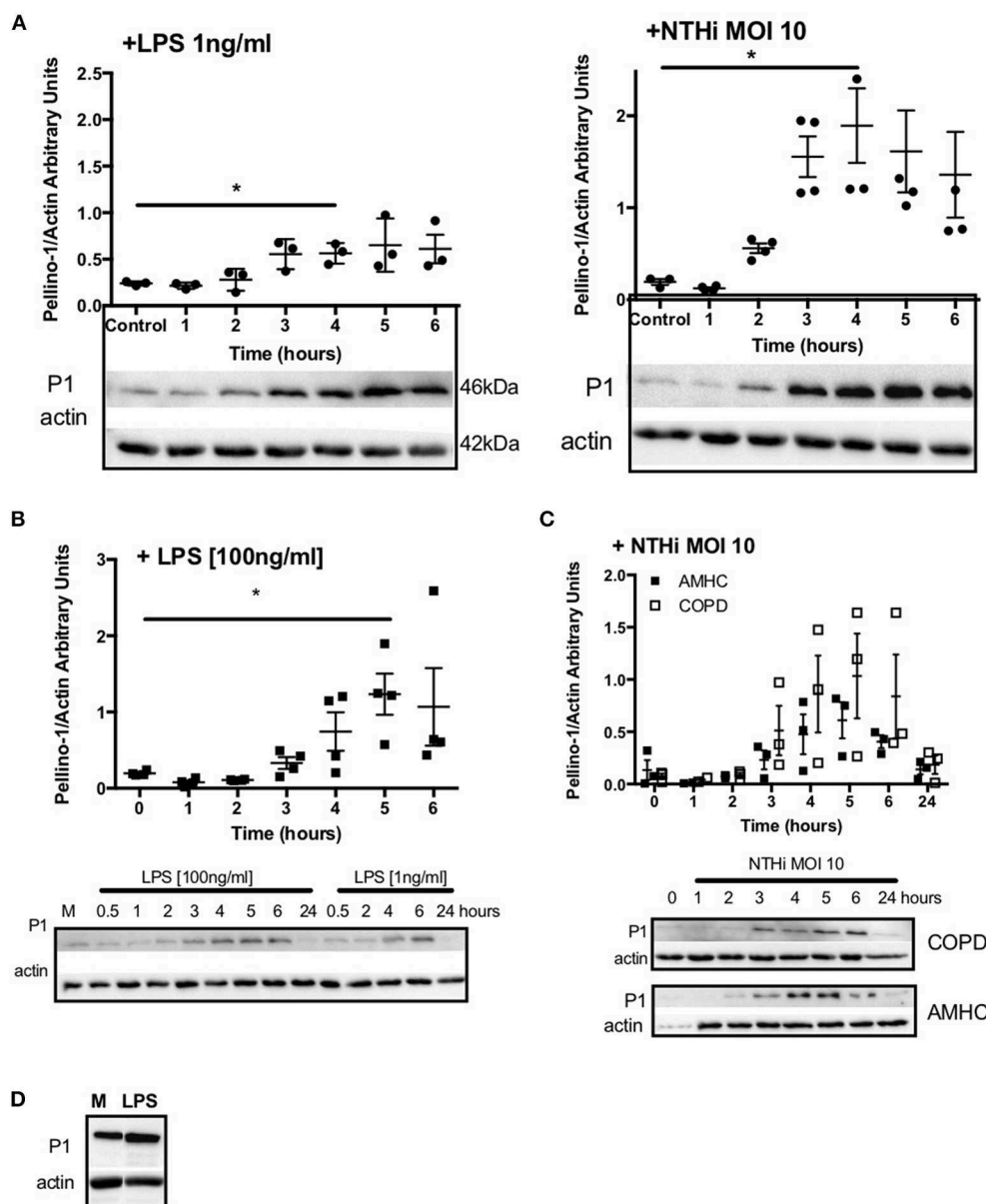
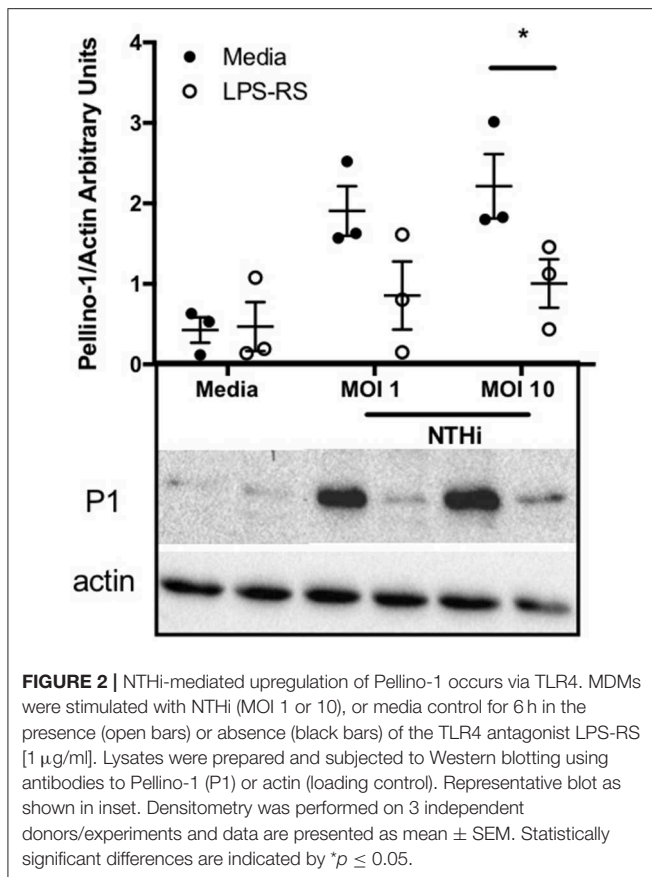


FIGURE 1 | Macrophages upregulate Pellino-1 in response to LPS and NTHi. MDMs were stimulated with LPS [1ng/ml] or NTHi (MOI 10) (A) for 1–6 h. Cells were also cultured in media for 6 h (control, A). MDMs differentiated from monocytes isolated from a COPD patient were treated with LPS at 1 or 100 ng/ml (B), or NTHi MOI 10 (C) over a time course of 24 h. MDMs from age-matched healthy control subjects (AMHC) were challenged with NTHi in matched experiments (C). Primary human neutrophils were treated with LPS [1ng/ml] for 6 h (D). Lysates for all cells were prepared and subjected to Western blotting using antibodies to Pellino-1 (P1) or actin (loading control). Densitometry was performed on independent donors/experiments and data are presented as mean \pm SEM. Panel d is representative of 3 experiments. Statistically significant differences are indicated by * $p \leq 0.05$.



RESULTS

Macrophages Upregulate Pellino-1 in Response to LPS and NTHi via TLR4

Since Pellino-1 has known roles in TLR4 signaling in monocytes (12), we explored Pellino-1 regulation in response to LPS and NTHi. In MDMs from healthy subjects, Pellino-1 protein is profoundly upregulated by LPS and NTHi (Figure 1A). This was confirmed in MDMs prepared from people with COPD and age-matched healthy control subjects (Figures 1B,C). Since macrophage phenotype can be sensitive to *in vitro* differentiation programmes, we also confirmed an LPS-dependent upregulation of Pellino-1 in preliminary work in primary AMs isolated from human lung (Supplemental Figure 1A). Primary human neutrophils also express Pellino-1 (Figure 1D). In contrast, Pellino-1 protein is not regulated by the Gram-positive bacteria, *Staphylococcus aureus* and *Streptococcus pneumoniae*, nor the TIR agonist IL-1β (Supplemental Figures 1B–D) although MDMs released CXCL8 in response to these stimuli (data not shown). Although LPS signals exclusively via TLR4, NTHi can also activate TLR2 in macrophages. Figure 2 shows that the TLR4 antagonist LPS-RS (20) significantly reduces NTHi-induced upregulation of Pellino-1, suggesting NTHi signals, at least in part, via TLR4 to induce Pellino-1 expression.

Peli1^{−/−} Mice Develop Airway Inflammation in Models of COPD

To establish a role for Pellino-1 in lung inflammation and infection, we adopted a murine model of COPD in Pellino-1 (*Peli1*^{−/−}) knockout mice and WT littermates (13, 14). *Peli1*^{−/−} and WT mice were treated with LPS and elastase (or PBS as control) once per week for 4 weeks. As expected, there was an increase in inflammatory cells in the WT LPS/elastase BALF compared to WT PBS treated mice (Figure 3A). The proportion and absolute number of neutrophils (Figures 3B,C) and macrophages (Figures 3D,E) in BALF was increased in WT LPS/elastase mice compared to WT PBS animals. No significant difference was observed between WT and *Peli1*^{−/−} LPS/elastase treated animals for either absolute number or proportion of cells by type (Figures 3A–E). WT and *Peli1*^{−/−} mice treated with PBS were comparable for all cell counts (data not shown). Lung histology from PBS-treated WT and *Peli1*^{−/−} mice shows no evidence of inflammation (Figure 3F, upper panels). Both WT and *Peli1*^{−/−} LPS/elastase-treated mice developed airway inflammation, illustrated by an increase in cellularity and loss of alveolar architecture consistent with emphysema (Figure 3F, lower panels). These findings show that loss of Pellino-1 does not impact on the development of airway inflammation in this model at the timepoint studied.

Peli1^{−/−} Mice Recruit More Neutrophils to the Airway in Response to NTHi and Clear the Infection More Effectively in Murine Models of COPD

WT and *Peli1*^{−/−} mice pre-treated with LPS/elastase were infected with NTHi (or PBS as control). Both WT and *Peli1*^{−/−} mice mounted an immune response to NTHi, as demonstrated by an increase in absolute cell number in BALF (Figure 4A). There was no significant difference in absolute cell number between WT and *Peli1*^{−/−} NTHi infected animals (Figure 4A). NTHi infected *Peli1*^{−/−} mice have proportionally more neutrophils in BALF compared with WT (Figure 4B, lower panels and Figures 4C,D). This was concomitant with a decrease in the number of macrophages (Figures 4E,F). Neutrophil apoptosis was assessed on BALF cytocentrifuge slides and there was no difference between WT and *Peli1*^{−/−} mice (Figure 4G). The principal neutrophil chemokine, KC, was significantly increased in BALF from *Peli1*^{−/−} mice (Figure 4H). CFU counts from homogenized lungs show fewer viable bacteria from *Peli1*^{−/−} mice compared to WT mice (Figure 4I). No viable bacteria were grown from blood cultures (data not shown).

Increased Airway Neutrophilia in *Peli1*^{−/−} Mice Following Acute Lung Injury and NTHi Infection

These findings were recapitulated in an LPS acute lung injury model, which typically results in a more marked neutrophilic inflammation (21). As before, the overall cell number in BALF was not different between WT and *Peli1*^{−/−} mice (Figures 5A,B). Both the number and proportion of neutrophils were significantly increased in *Peli1*^{−/−} mice (Figures 5C,D) and

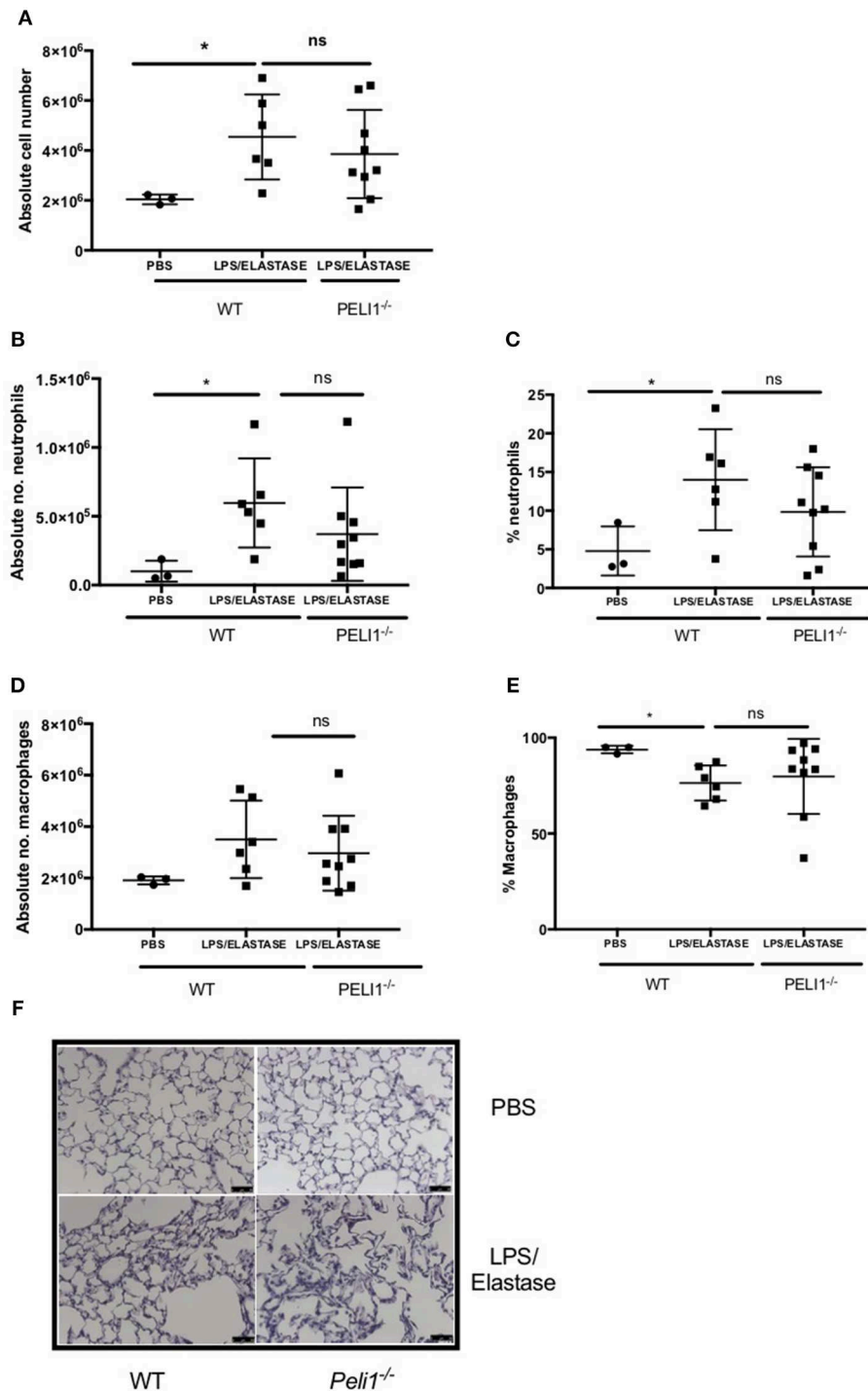


FIGURE 3 | WT and *Pel1*^{-/-} mice develop airway inflammation in response to repeated LPS and elastase. *Pel1*^{-/-} transgenic mice and WT littermates were given i.n. PBS (black circles) or LPS (7 μg) and porcine neutrophil elastase (1.2 units, black squares) every 7 days for 4 weeks. Mice were subjected to bronchoalveolar lavage (BAL) on day 28 and inflammation assessed by enumerating total cell number in BALF by haemocytometer (**A**) and number/proportion of neutrophils (**B,C**) and macrophages (**D,E**) by light microscopy. Lungs were removed and stained for histological analysis. Representative images are shown (**F**, scale bar = 50 μm). Individual data points represent a single mouse and panels show mean ± SD. Statistically significant differences are indicated by **p* < 0.05 (*n* = 3–5 **A**, *n* = 3–9 **B–E**).

concomitantly, the number and proportion of macrophages were significantly decreased (**Figures 5E,F**). There was no difference in the rate of neutrophil apoptosis in BALF between WT and

Pel1^{-/-} mice (**Figure 5G**). A trend toward fewer viable NTHi was observed in lungs of *Pel1*^{-/-} mice compared to WT mice, although this did not reach statistical significance, potentially

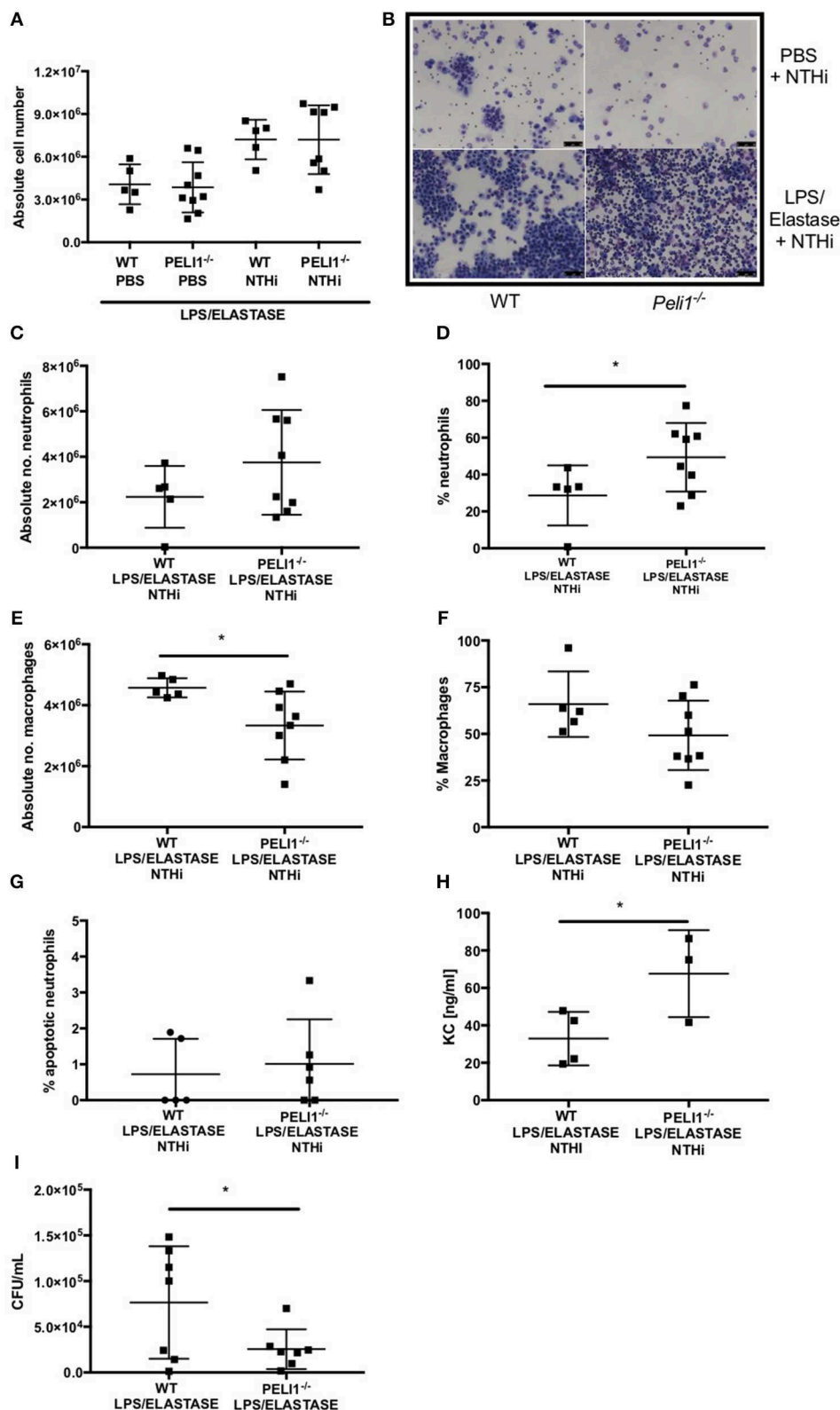


FIGURE 4 | *Peli1*^{-/-} COPD mice recruit more neutrophils following NTHi infection and clear NTHi more effectively compared to WT. *Peli1*^{-/-} transgenic mice and WT littermates were given i.n. LPS [7 μg] and 1.2 units porcine neutrophil elastase every 7 days for 4 weeks. On day 28, mice were infected with 1 × 10⁷ CFU NTHi. (Continued)

FIGURE 4 | After 24 h (day 29) lungs were lavaged and removed for homogenisation. Total cell number in BALF was enumerated by haemocytometer (**A**) and cell differential determined by light microscopy of cytocentrifuge slides, scale bar = 50 μ m (**B**). Number/proportion of neutrophils (**C,D**) and macrophages (**E,F**) were determined. Percentage of apoptotic neutrophils were scored on BALF cytocentrifuges by morphology (**G**). KC levels in BALF were measured by ELISA (**H**) and NTHi CFU in homogenized lungs was determined by Miles Misra (**I**). Individual data points represent a single mouse and panels show mean \pm SD. Statistically significant differences are indicated by * $p < 0.05$ ($n = 4$ –8 **A**, $n = 5$ –8 **C–F**, $n = 5$ –6 **G** (apoptosis), $n = 3$ –4 h (KC), $n = 7$ **I** (NTHi)).

due to sample size ($P = 0.056$, **Figure 5H**). Overall, these data suggest that suppression of Pellino-1 leads to improved bacterial clearance.

Loss of Pellino-1 Does Not Impact on Killing or Internalization of NTHi by Neutrophils and Macrophages

Based on known roles for Pellino-1 in macrophage polarization we next studied whether the enhanced clearance of NTHi in *Peli1*^{−/−} mice was due to promotion of a particular macrophage phenotype (22). To do this we used an *in vitro* siRNA approach in MDMs. STAT-1 and STAT-6 transcription factors facilitate distinct macrophage phenotypes and are activated by LPS/IFN γ and IL-4/IL-10, respectively (22, 23). IFN γ , but surprisingly not LPS, upregulated phosphorylated STAT-1 (pSTAT-1) (**Figure 6A**), which was significantly reduced in cells transfected with *Peli1* siRNA (**Figure 6B**). STAT1 is phosphorylated following TLR2 and TLR4 activation in macrophages (24) and here we show that NTHi induces pSTAT-1, which is reduced in *Peli1* siRNA transfected cells (**Figure 6C**). IL-4 failed to upregulate STAT-6 (**Figure 6A**) therefore we measured CD206 expression, which is regulated by STAT-6, and show it is upregulated by IL-4, but unaffected by *Peli1* knockdown (**Figure 6D**).

These data suggest that loss of Pellino-1 does not promote an anti-microbial macrophage phenotype. This was confirmed in NTHi killing assays where both scrambled and *Peli1* siRNA transfected MDMs were able to internalize (assayed at 2 h) and entirely eradicate (assayed at 4 h) NTHi to a comparable degree (**Figure 7A**). This was supported in BMDMs prepared from WT and *Peli1*^{−/−} mice (**Figure 7B**). Murine macrophages are a source of KC and synthesis of this chemokine occurs via TLR-mediated pathways. Histology on lung sections from LPS/elastase treated WT and *Peli1*^{−/−} mice show individual cells staining for KC (**Figure 7C**). Since these cells were of a macrophage like appearance and since we measured increased KC in BALF from *Peli1*^{−/−} mice (**Figure 4D**), we investigated KC production from BMDMs from WT and *Peli1*^{−/−} mice. **Figure 7D** shows no difference in NTHi-induced KC production by *Peli1*^{−/−} BMDMs compared to WT.

Since *Peli1*^{−/−} macrophages were no more effective at killing NTHi *in vitro*, we hypothesized that it is the increased neutrophil number in the lung of *Peli1*^{−/−} mice that results in enhanced bacterial clearance. Neutrophils can phagocytose and destroy NTHi (8) and we examined whether Pellino-1 knockout impacted on this neutrophil function. No viable bacteria were recovered from either WT nor *Peli1*^{−/−} bone marrow-derived neutrophils at any timepoint studied, despite being able to visualize NTHi inside these cells (**Figure 7E**).

These data demonstrate that despite loss of Pellino-1, neutrophils rapidly and completely kill internalized NTHi, and suggest it is feasible that increased neutrophil number in *Peli1*^{−/−} mice leads to better clearance of NTHi.

DISCUSSION

We show that human macrophages rapidly and profoundly upregulate Pellino-1 in response to LPS and NTHi, suggesting a potential role for this protein in the initial cellular immune response to NTHi. In *in vivo* models of acute and chronic inflammation, *Peli1*^{−/−} mice recruit more neutrophils to the airway following NTHi challenge, compared to WT animals. This is accompanied by an increase in the neutrophil chemoattractant KC in BALF. *Peli1*^{−/−} mice clear NTHi more effectively from the lung than WT littermates, which may be as a result of the increased neutrophilic immune response in the airway. Our work suggests that Pellino-1 is a key component of the airway immune response to NTHi and that therapeutically targeting Pellino-1 may enhance clearance of NTHi in patients with chronic inflammatory disease who are at risk of infection induced exacerbations.

Pellino-1 interacts with TIR signaling pathways at various points due to its ability to both mark proteins for degradation (via K48-linked ubiquitination) and initiate downstream signaling (via K63-linked ubiquitination) (25, 26). It has both negative and positive regulatory roles on signaling, depending on the cell type and stimulus (27, 28). Our previous work identifies a role for Pellino-1 in epithelial cell responses to rhinoviral infection (29) and this along with a growing literature on roles for Pellino-1 in infection (30), led us to hypothesize that loss of Pellino-1 would impact on responses to the airway pathogen, NTHi. The initial cellular immune response to NTHi is predominantly mediated by AMs, followed by recruitment of neutrophils, which primarily function during acute infective exacerbations (8, 31). Studies have shown that macrophages from people with COPD are defective in phagocytosing NTHi (32). Since healthy lungs are mostly resistant to NTHi infection and murine models also show rapid clearance, we adopted a murine model of COPD, which better mimics host-pathogen interactions in patients with this disease (33). LPS/elastase-induced lung inflammation occurred irrespective of genotype. This suggested that although Pellino-1 is a component of the TLR4 pathway it was not essential for mediating inflammatory signals via LPS in this context, perhaps indicating some functional redundancy in this pathway. NTHi infection resulted in additional neutrophil recruitment to the lung, confirming findings from similar studies (33), and which is observed in people with COPD colonized with NTHi (34). *Peli1*^{−/−} mice had more neutrophils and fewer macrophages

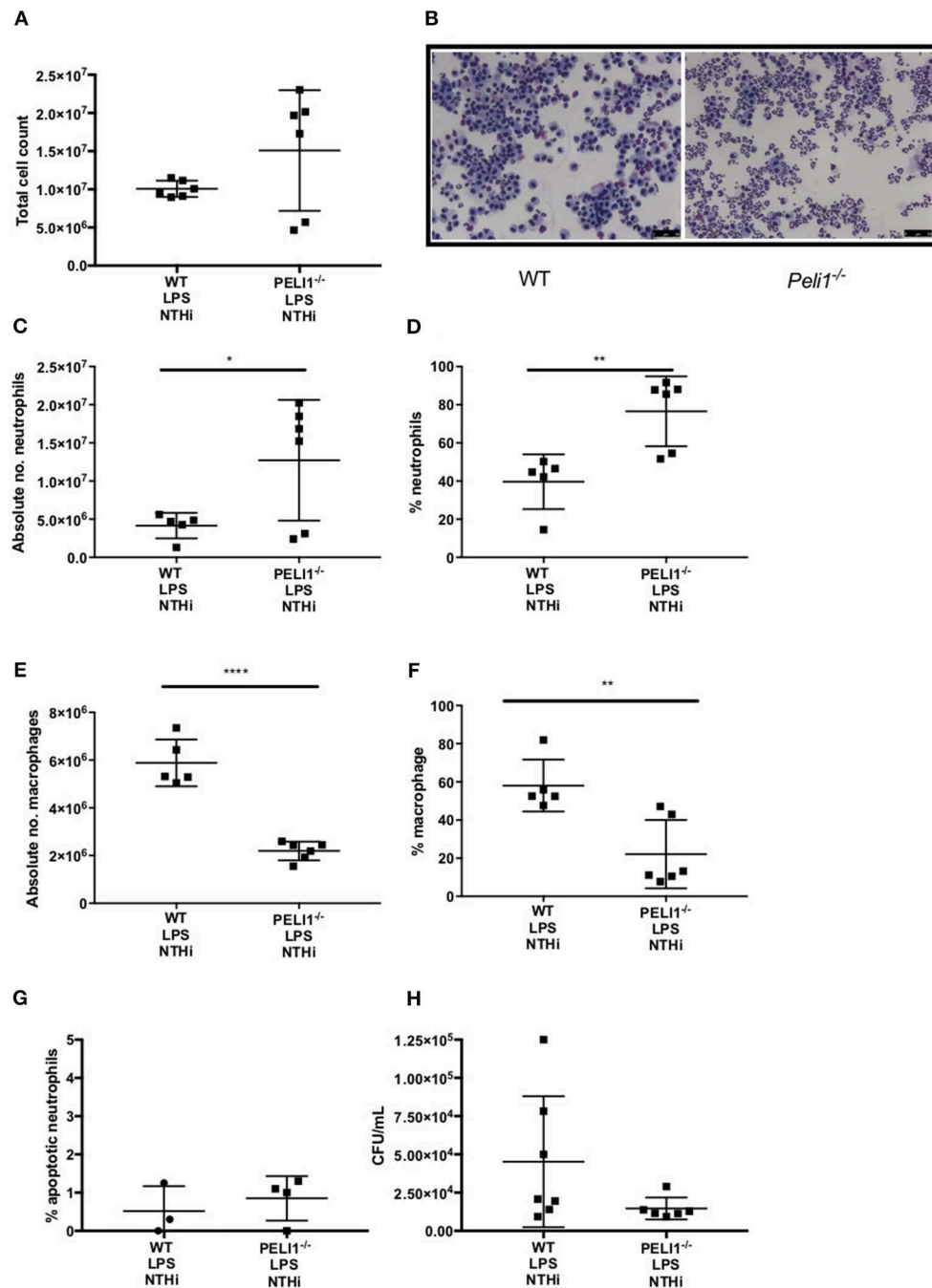


FIGURE 5 | *Pel1*^{-/-} acute lung injury mice recruit more neutrophils following NTHi infection and clear NTHi more effectively compared to WT. *Pel1*^{-/-} transgenic mice and WT littermates were given a single treatment of i.n. LPS [7 μg] (day 1). After 24h mice were infected with 1 × 10⁷ CFU NTHi (day 2). After 24h (day 3) lungs were lavaged and subsequently removed for homogenisation. Total cell number in BALF was enumerated by haemocytometer (A) and cell differential determined by light microscopy of cytocentrifuge slides, scale bar = 50 μm (B). The number/proportion of neutrophils (C,D) and macrophages (E,F) were determined. Percentage of apoptotic neutrophils were scored on BALF cytocentrifuges by morphology (G). NTHi CFU in homogenized lungs was determined by Miles and Misra method (H). Individual data points represent a single mouse and panels show mean ± SEM. Statistically significant differences are indicated by **p* < 0.05, ***p* < 0.01, *****p* < 0.0001 *n* = 6 A, *n* = 5–6 C–F, *n* = 3–4 G (apoptosis) *n* = 6–7 D (NTHi).

in BALF, which may in part be accounted for by an increase in KC. The source of the KC is not clear, and while resident tissue macrophages are thought to be a principal source of KC

in the murine lung, epithelial cells also produce this chemokine in concert with airway myeloid cells following infection (35). Lung histology images suggest cells with a macrophage-like

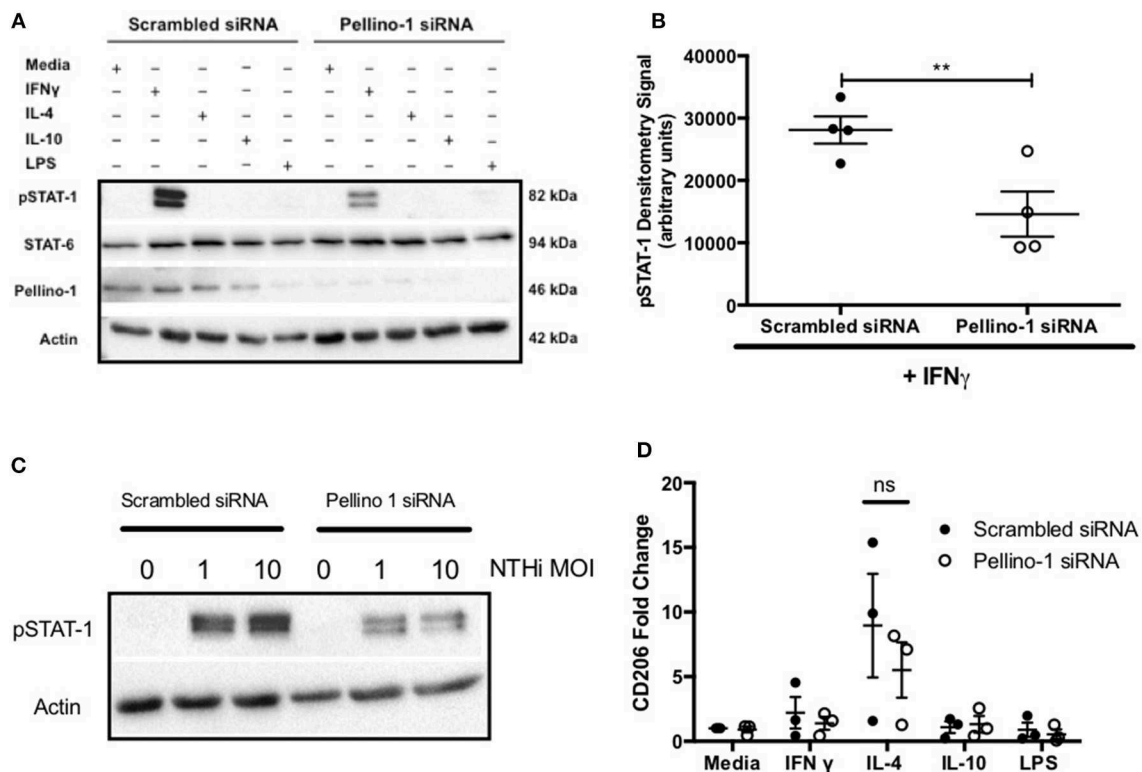


FIGURE 6 | Pellino-1 regulates macrophage STAT-1 signaling. MDMs were transfected with siRNA targeting Pellino-1 or scrambled siRNA (control). **(A,B,D)** 48 h following transfection, cells were stimulated with IFN- γ [20 ng/ml], IL-4 [20 ng/ml], IL-10 [20 ng/ml] or LPS [1 ng/ml] for 24 h. Whole cell lysates were analyzed by Western blot using antibodies specific to STAT-1, pSTAT-6, Pellino-1 or actin for 4 independent donors **(A)**. pSTAT-1 bands for IFN- γ -treated cells were analyzed by densitometry **(B)**. In separate experiments cells were challenged with NTHi (MOI 1 and 10) for 24 h and lysates probed for Pellino-1 and actin **(C)**. RNA was purified from cell lysates and transcribed to cDNA. *CD206* gene product was measured by qPCR **(D)**. Fold changes are shown relative to media treated MDMs transfected with scrambled siRNA (first open bar). Data are presented as mean \pm SEM of $n = 4$ independent experiments. Significant differences are indicated by ** $P < 0.01$.

morphology rather than epithelial cells appear to be more intensely stained for KC. *Peli1*^{-/-} BMDMs show a trend for increased KC production in response to NTHi *in vitro*, although this is not statistically significant, but may indicate a negative regulatory role for Pellino-1. Although Pellino-1 has previously been identified as a positive regulator of macrophage TLR signaling (27), it negatively regulates T cell activation (28). Th17 cells play an important role in neutrophil recruitment to the airway following NTHi infection (31), and heightened T cell activation in *Peli1*^{-/-} mice may be the cause of the airway neutrophilia we see in our model. Pellino also negatively regulates immunity in *Drosophila* and ablation of Pellino in adult flies promotes clearance of *Micrococcus luteus* (36). A similar role has been described for Pellino-3, where knockdown results in increased inflammatory cytokine production following bacterial infection of macrophages (12). Evidence for Pellino-1 in the negative regulation of inflammation is found in a murine ischemic skin flap study, where Pellino-1 overexpression leads to reduced infiltration of inflammatory lymphocytes to the dermis and faster resolution of inflammation (37). Moreover, the Smad-6 interacting peptide, Smaducin-6, disrupts Pellino-1 signaling and has been shown in murine models of sepsis to improve bacterial

clearance via increased neutrophil recruitment, supporting a role for Pellino-1 in negatively regulating immunity in the context of bacterial infections (38). Our findings may suggest a way to improve immunity in patients with COPD, which may be made possible by development of tools such as Smaducin-6. These observations are also interesting in that reducing neutrophilic inflammation because of its lung damaging potential in COPD is often considered to be a plausible therapeutic target: our data indicate that in people with chronic infection, reduction in lung neutrophil numbers may not always be a desirable aim. Whether inducing an airway neutrophilia is detrimental for patients with inflammatory disease in this way would need further study.

In our models, it is most likely that increased bacterial clearance is consequent upon neutrophil recruitment, since we did not show increased monocyte recruitment. Furthermore, although we showed some decrease in polarization markers in Pellino-1 knockout macrophages, macrophage killing of NTHi was unimpaired. Others have shown that Pellino1 promotes macrophage polarization *in vitro*, which is in support of the STAT-1 downregulation we observed in Pellino1 siRNA transfected MDMs (39). We would therefore expect loss of Pellino1 to result in impaired killing of NTHi, but we

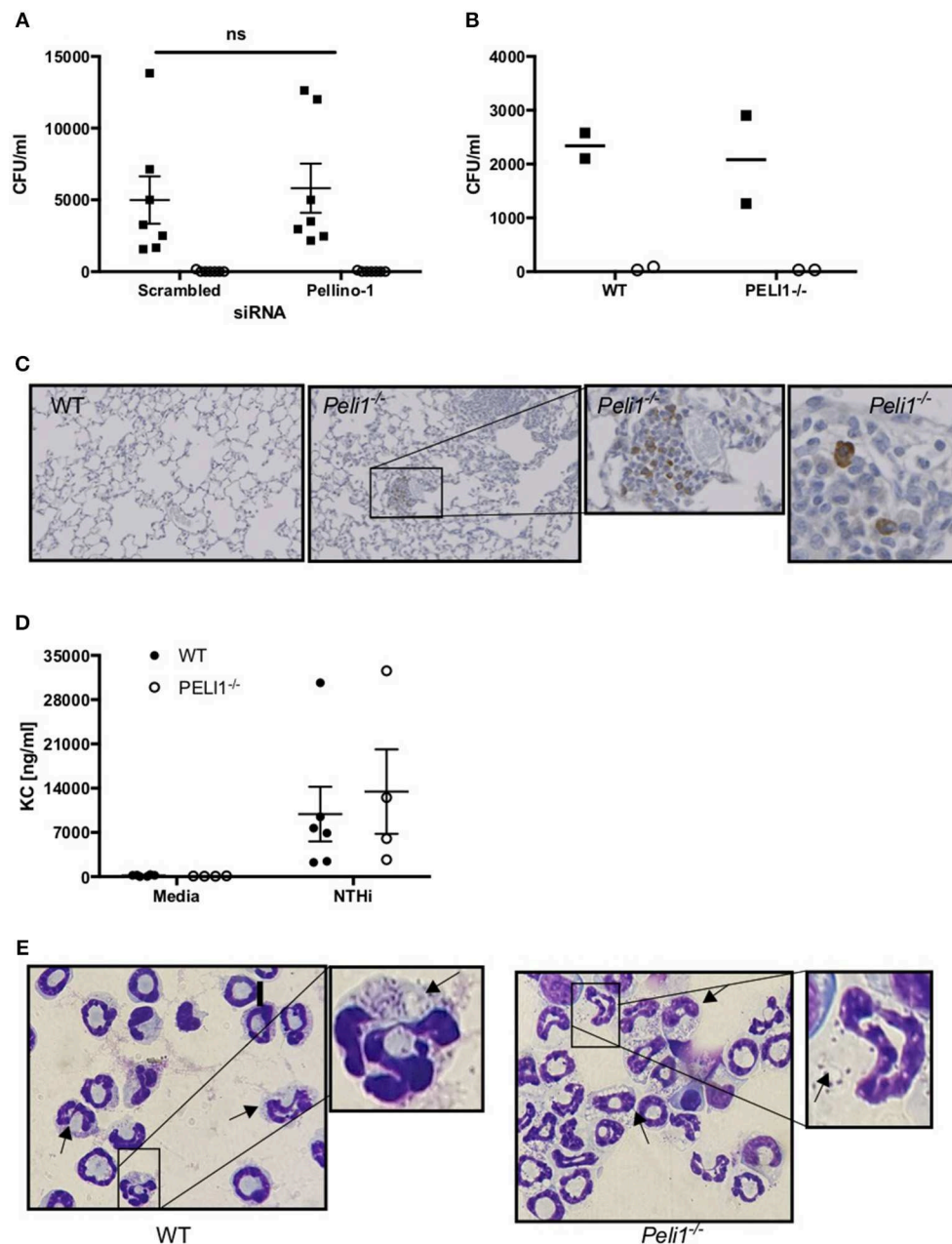


FIGURE 7 | Internalization and killing of NTHi is not impaired by loss of Pellino-1. **(A)** MDMs were transfected with siRNA targeting Pellino-1 or scrambled siRNA (control). 48 h following transfection, MDMs were infected with NTHi (MOI 10) for 2 h after which cells were lysed and viable intracellular bacteria enumerated by Miles Misra (2 h, black squares). In parallel wells, MDMs were treated with gentamycin to kill extracellular bacteria for a further 2 h, after which intracellular NTHi were enumerated by Miles Misra (4 h, open circles). **(B)** WT and *Peli1*^{-/-} BMDM were infected with NTHi (MOI 5) and viable bacteria enumerated at 2 and 4 h as above. **(C)** Lung sections from WT and *Peli1*^{-/-} mice treated with LPS/Elastase were subjected to histology and immunostained for KC. Zoomed inset shows individual cells staining for KC in brown. **(D)** Day 14 WT and *Peli1*^{-/-} BMDM were infected with NTHi (MOI 5) for 24 h and cell free supernatants subjected to KC ELISA. **(E)** neutrophils were isolated from WT and *Peli1*^{-/-} BMDM and infected with NTHi (MOI 10) for 1 h. Cytoentrifuge slides were prepared and arrows point to neutrophils containing NTHi. Zoomed inset highlights NTHi within intracellular vacuoles. Data are expressed as individual points with mean±SEM (**A**, $n = 7$) or mean (**B**, $n = 2$) or as bars (**C**, mean±SEM, $n = 3-5$).

could not find a difference in the internalization or killing capacity of Pellino1 deficient human or murine macrophages, which may indicate eradication of NTHi occurs irrespective of polarization state.

We show Pellino-1 expression is linked to TLR4 signaling and our data support previous studies showing Pellino-1 is regulated in response to LPS (12). TLR4 knockout mice have reduced inflammation and impaired bacterial clearance during

NTHi infection, further supporting a role for neutrophils in the eradication NTHi (40, 41). In *Drosophila*, ablation of Pellino in adult flies promotes clearance of bacteria (36), in comparison with Toll mutant flies who are profoundly vulnerable to infection (42). Taken together, these studies and our work indicate that Pellino-1 knockdown in a whole organism is associated with increased bacterial clearance, preserved antimicrobial signaling, and better induction of effective innate immunity. In conclusion, we demonstrate a role for Pellino-1 in mediating immune responses in the airway and suggest that therapeutic inhibition of Pellino-1 may enhance bacterial clearance in people with COPD.

DATA AVAILABILITY

All datasets generated for this study are included in the manuscript and/or the **Supplementary Files**.

ETHICS STATEMENT

All work involving animals was performed in accordance with the Animal (Scientific procedures) Act 1986 and has been approved by the Animal welfare and ethical review body at University of Sheffield. Work was carried out under procedure project license 40/3726 (DD). C57BL/6 *Peli1*^{-/-} mice and WT littermates (12) were maintained via het/het breeding in a pathogen-free environment and were housed in shared cages. Peripheral blood was taken from healthy volunteers, people with a diagnosis of COPD, or age-matched healthy control (AMHC) subjects with written informed consent as per the declaration of Helsinki, and ethical approval in accordance with the recommendations of the South Sheffield Research Ethics Committee and the National Research Ethics Service Committee Yorkshire and the Humber (16).

AUTHOR CONTRIBUTIONS

LP, IS, DD, and AC wrote the manuscript. All authors reviewed and edited drafts of the manuscript. LP, BH, CB, AR, MJ, CW,

JW, NK, and EM performed the experiments. BH, CB, AR, MJ, NK, EM, HM, LP, DD, IS, and AC contributed to experimental design and data analysis. PP provided human lung tissue samples, SS provided mice, and both contributed intellectual input to the study.

FUNDING

This work was supported by British Lung Foundation awards (RG14-4 and PPRG16-11 both to LP) and Medical Research Council award (MR/L009374/1 to IS and MRNO2995X/1 to DD). The University of Sheffield funds (where annual budgets allow) APCs for open access charges.

ACKNOWLEDGMENTS

We thank Lynne Williams for assistance with animal studies, Yvonne Stephenson, and Laura West for histology, Simon Cross (Professor of Diagnostic Histopathology) for reviewing lung sections, David Sammut for obtaining blood samples, and all subjects who contributed to this study. This majority of this work was supported by British Lung Foundation awards (RG14-4 and PPRG16-11 both to LP) and also in part by Medical Research Council awards (MR/L009374/1 to IS and MRNO2995X/1 to DD).

SUPPLEMENTARY MATERIAL

The Supplementary Material for this article can be found online at: <https://www.frontiersin.org/articles/10.3389/fimmu.2019.01721/full#supplementary-material>

Supplemental Figure 1 | Pellino-1 is not regulated by *S. aureus*, *S. pneumoniae* or IL-1 β . AMs isolated from a single lung tissue resection were treated with LPS [0.01–10 ng/ml] for 24h (A). MDMs were stimulated with media, *S. aureus* (B), *S. pneumoniae* (C) or IL-1 β (D) for 6h. Lysates were prepared and subjected to Western blotting using antibodies to Pellino-1 (P1) or actin (loading control). Densitometry was performed on 3 independent donors/experiments and data are presented as mean \pm SEM. No statistically significant differences were found.

REFERENCES

1. WHO. *World Health Statistics*. (2008). Available online at: http://www.who.int/whosis/whostat/EN_WHS08_Full.pdf?ua=1 (accessed October 20, 2011).
2. Papi A, Bellettato CM, Braccioni F, Romagnoli M, Casolari P, Caramori G, et al. Infections and airway inflammation in chronic obstructive pulmonary disease severe exacerbations. *Am J Respir Crit Care Med*. (2006) 173:1114–21. doi: 10.1164/rccm.200506-859OC
3. Eldika N, Sethi S. Role of nontypeable *Haemophilus influenzae* in exacerbations and progression of chronic obstructive pulmonary disease. *Curr Opin Pulm Med*. (2006) 12:118–24. doi: 10.1097/01.mcp.0000208451.50231.8f
4. Murphy TF. *Haemophilus influenzae* in chronic bronchitis. *Semin Respir Infect*. (2000) 15:41–51. doi: 10.1053/srin.2000.0150041
5. Hill AT, Bayley DL, Campbell EJ, Hill SL, and R.A. Stockley. Airways inflammation in chronic bronchitis: the effects of smoking and alpha1-antitrypsin deficiency. *Eur Respir J*. (2000) 15:886–90. doi: 10.1034/j.1399-3003.2000.15e12.x
6. Su YC, Jalalvand F, Thegerstrom J, Riesbeck K. The interplay between immune response and bacterial infection in COPD: focus upon non-typeable *haemophilus influenzae*. *Front Immunol*. (2018) 9:2530. doi: 10.3389/fimmu.2018.02530
7. Berenson CS, Kruzel RL, Eberhardt E, Sethi S. Phagocytic dysfunction of human alveolar macrophages and severity of chronic obstructive pulmonary disease. *J Infect Dis*. (2013) 208:2036–45. doi: 10.1093/infdis/jit400
8. King PT, Sharma R. The lung immune response to nontypeable *haemophilus influenzae* (lung immunity to NTHi). *J Immunol Res*. (2015) 2015:706376. doi: 10.1155/2015/706376
9. Toews GB, Vial WC, Hansen EJ. Role of C5 and recruited neutrophils in early clearance of nontypable *Haemophilus influenzae* from murine lungs. *Infect Immun*. (1985) 50:207–12.
10. Moynagh PN. The roles of Pellino E3 ubiquitin ligases in immunity. *Nat Rev Immunol*. (2014) 14:122–31. doi: 10.1038/nri3599
11. Baines KJ, Simpson JL, Wood LG, Scott RJ, Gibson PG. Transcriptional phenotypes of asthma defined by gene expression profiling of induced sputum samples. *J Allergy Clin Immunol*. (2011) 127:153–60. doi: 10.1016/j.jaci.2010.10.024
12. Murphy M, Xiong Y, Pattabiraman G, Qiu F, Medvedev AE. Pellino-1 positively regulates toll-like receptor (TLR) 2 and TLR4 signaling and is

- suppressed upon induction of endotoxin tolerance. *J Biol Chem.* (2015) 290:19218–32. doi: 10.1074/jbc.M115.640128
13. Chang M, Jin W, Sun SC. Peli1 facilitates TRIF-dependent Toll-like receptor signaling and proinflammatory cytokine production. *Nat Immunol.* (2009) 10:1089–95. doi: 10.1038/ni.1777
 14. Sajjan U, Ganesan S, Comstock AT, Shim J, Wang Q, Nagarkar DR, et al. Elastase- and LPS-exposed mice display altered responses to rhinovirus infection. *Am J Physiol.* (2009) 297:L931–44. doi: 10.1152/ajplung.00150.2009
 15. Cody AJ, Field D, Feil EJ, Stringer S, Deadman ME, Tsolaki AG, et al. High rates of recombination in otitis media isolates of nontypeable *Haemophilus influenzae*. *Infect Genet Evol.* (2003) 3:57–66. doi: 10.1016/S1567-1348(02)00152-1
 16. Bewley MA, Marriott HM, Tulone C, Francis SE, Mitchell TJ, Read RC, et al. A cardinal role for cathepsin d in co-ordinating the host-mediated apoptosis of macrophages and killing of pneumococci. *PLoS Pathog.* (2011) 7:e1001262. doi: 10.1371/journal.ppat.1001262
 17. Haslett C, Guthrie LA, Kopaniak MM, Johnston RB Jr, Henson PM. Modulation of multiple neutrophil functions by preparative methods or trace concentrations of bacterial lipopolysaccharide. *Am J Pathol.* (1985) 119:101–10.
 18. Bianchi SM, Prince LR, McPhillips K, Allen L, Marriott HM, Taylor GW, et al. Impairment of apoptotic cell engulfment by pyocyanin, a toxic metabolite of *Pseudomonas aeruginosa*. *Am J Respir Crit Care Med.* (2008) 177:35–43. doi: 10.1164/rccm.200612-1804OC
 19. Gill SK, Yao Y, Kay LJ, Bewley MA, Marriott HM, Peachell PT. The anti-inflammatory effects of PGE2 on human lung macrophages are mediated by the EP4 receptor. *Br J Pharmacol.* (2016) 173:3099–109. doi: 10.1111/bph.13565
 20. Baker PJ, Taylor CE, Stashak PW, Fauntleroy MB, Haslov K, Qureshi N, et al. Inactivation of suppressor T cell activity by the nontoxic lipopolysaccharide of *Rhodospseudomonas sphaeroides*. *Infect Immun.* (1990) 58:2862–8.
 21. Rowe SJ, Allen L, Ridger VC, Hellewell PG, Whyte MK. Caspase-1-deficient mice have delayed neutrophil apoptosis and a prolonged inflammatory response to lipopolysaccharide-induced acute lung injury. *J Immunol.* (2002) 169:6401–7. doi: 10.4049/jimmunol.169.11.6401
 22. Murray PJ, Wynn TA. Protective and pathogenic functions of macrophage subsets. *Nat Rev Immunol.* (2011) 11:723–37. doi: 10.1038/nri3073
 23. Wang N, Liang H, Zen K. Molecular mechanisms that influence the macrophage m1-m2 polarization balance. *Front Immunol.* (2014) 5:614. doi: 10.3389/fimmu.2014.00614
 24. Shoenfelt JL, Fenton MJ. TLR2- and TLR4-dependent activation of STAT1 serine phosphorylation in murine macrophages is protein kinase C-delta-independent. *J Endotoxin Res.* (2006) 12:231–40. doi: 10.1179/096805106X102219
 25. Choi SW, Park HH, Kim S, Chung JM, Noh HJ, Kim SK, et al. PELI1 selectively targets kinase-active RIP3 for ubiquitylation-dependent proteasomal degradation. *Mol Cell.* (2018) 70:920–935 e7. doi: 10.1016/j.molcel.2018.05.016
 26. Humphries F, Moynagh PN. Molecular and physiological roles of Pellino E3 ubiquitin ligases in immunity. *Immunol Rev.* (2015) 266:93–108. doi: 10.1111/imr.12306
 27. Medvedev AE, Murphy M, Zhou H, Li X. E3 ubiquitin ligases Pellinos as regulators of pattern recognition receptor signaling and immune responses. *Immunol Rev.* (2015) 266:109–22. doi: 10.1111/imr.12298
 28. Chang M, Jin W, Chang JH, Xiao Y, Brittain GC, Yu J, et al. The ubiquitin ligase Peli1 negatively regulates T cell activation and prevents autoimmunity. *Nat Immunol.* (2011) 12:1002–9. doi: 10.1038/ni.2090
 29. Bennett JA, Prince LR, Parker LC, Stokes CA, de Bruin HG, van den Berge M, et al. Pellino-1 selectively regulates epithelial cell responses to rhinovirus. *J Virol.* (2012) 86:6595–604. doi: 10.1128/JVI.06755-11
 30. Luo H, Winkelmann ER, Zhu S, Ru W, Mays E, Silvas JA, et al. Peli1 facilitates virus replication and promotes neuroinflammation during West Nile virus infection. *J Clin Invest.* (2018) 128:4980–91. doi: 10.1172/JCI99902
 31. Essilfie AT, Simpson JL, Horvat JC, Preston JA, Dunkley ML, Foster PS, et al. *Haemophilus influenzae* infection drives IL-17-mediated neutrophilic allergic airways disease. *PLoS Pathog.* (2011) 7:e1002244. doi: 10.1371/journal.ppat.1002244
 32. Berenson CS, Garlipp MA, Grove LJ, Maloney J, Sethi S. Impaired phagocytosis of nontypeable *Haemophilus influenzae* by human alveolar macrophages in chronic obstructive pulmonary disease. *J Infect Dis.* (2006) 194:1375–84. doi: 10.1086/508428
 33. Ganesan S, Faris AN, Comstock AT, Sonstein J, Curtis JL, Sajjan US. Elastase/LPS-exposed mice exhibit impaired innate immune responses to bacterial challenge: role of scavenger receptor A. *Am J Pathol.* (2012) 180:61–72. doi: 10.1016/j.ajpath.2011.09.029
 34. Sethi S, Maloney J, Grove L, Wrona C, Berenson CS. Airway inflammation and bronchial bacterial colonization in chronic obstructive pulmonary disease. *Am J Respir Crit Care Med.* (2006) 173:991–8. doi: 10.1164/rccm.200509-1525OC
 35. Dudek M, Puttur F, Arnold-Schrauf C, Kuhl AA, Holzmann B, Henriques-Normark B, et al. Lung epithelium and myeloid cells cooperate to clear acute pneumococcal infection. *Mucosal Immunol.* (2016) 9:1288–302. doi: 10.1038/mi.2015.128
 36. Ji S, Sun M, Zheng X, Li L, Sun L, Chen D, et al. Cell-surface localization of Pellino antagonizes Toll-mediated innate immune signalling by controlling MyD88 turnover in *Drosophila*. *Nat Commun.* (2014) 5:3458. doi: 10.1038/ncomms4458
 37. Rednam CK, Wilson RL, Selvaraju V, Rishi MT, Thirunavukkarasu M, Coca-Soliz V, et al. Increased survivability of ischemic skin flap tissue in Flk-1(+/-) mice by Pellino-1 intervention. *Microcirculation.* (2017) 24:e12362. doi: 10.1111/micc.12362 Available online at: <https://onlinelibrary.wiley.com/doi/epdf/10.1111/micc.12362>
 38. Lee YS, Park JS, Jung SM, Kim SD, Kim JH, Lee JY, et al. Park. Inhibition of lethal inflammatory responses through the targeting of membrane-associated Toll-like receptor 4 signaling complexes with a Smad6-derived peptide. *EMBO Mol Med.* (2015) 7:577–92. doi: 10.15252/emmm.201404653
 39. Kim D, Lee H, Koh J, Ko JS, Yoon BR, Jeon YK, et al. Cytosolic pellino-1-mediated K63-linked ubiquitination of IRF5 in M1 macrophages regulates glucose intolerance in obesity. *Cell Rep.* (2017) 20:832–45. doi: 10.1016/j.celrep.2017.06.088
 40. Wieland CW, Florquin S, Maris NA, Hoebe K, Beutler B, Takeda K, et al. The MyD88-dependent, but not the MyD88-independent, pathway of TLR4 signaling is important in clearing nontypeable *haemophilus influenzae* from the mouse lung. *J Immunol.* (2005) 175:6042–9. doi: 10.4049/jimmunol.175.9.6042
 41. Wang X, Moser C, Louboutin JP, Lysenko ES, Weiner DJ, Weiser JN, et al. Toll-like receptor 4 mediates innate immune responses to *Haemophilus influenzae* infection in mouse lung. *J Immunol.* (2002) 168:810–5. doi: 10.4049/jimmunol.168.2.810
 42. Lemaitre B, Nicolas E, Michaut L, Reichhart JM, Hoffmann JA. The dorsoventral regulatory gene cassette spatzle/Toll/cactus controls the potent antifungal response in *Drosophila* adults. *Cell.* (1996) 86:973–83. doi: 10.1016/S0092-8674(00)80172-5

Conflict of Interest Statement: The authors declare that the research was conducted in the absence of any commercial or financial relationships that could be construed as a potential conflict of interest.

Copyright © 2019 Hughes, Burton, Reese, Jabeen, Wright, Willis, Khoshaein, Marsh, Peachell, Sun, Dockrell, Marriott, Sabroe, Condliffe and Prince. This is an open-access article distributed under the terms of the Creative Commons Attribution License (CC BY). The use, distribution or reproduction in other forums is permitted, provided the original author(s) and the copyright owner(s) are credited and that the original publication in this journal is cited, in accordance with accepted academic practice. No use, distribution or reproduction is permitted which does not comply with these terms.



Exclusive Temporal Stimulation of IL-10 Expression in LPS-Stimulated Mouse Macrophages by cAMP Inducers and Type I Interferons

Orna Ernst^{1†}, Yifat Glucksam-Galnoy^{1†}, Bibek Bhatta¹, Muhammad Athamna^{1,2}, Iris Ben-Dror¹, Yair Glick³, Doron Gerber³ and Tsaffir Zor^{1*}

¹ Department of Biochemistry & Molecular Biology, School of Neurobiology, Biochemistry & Biophysics, Tel Aviv University, Tel Aviv, Israel, ² Triangle Regional Research and Development Center, Kafr Qara, Israel, ³ The Nanotechnology Institute, Bar-Ilan University, Ramat Gan, Israel

OPEN ACCESS

Edited by:

Catarina R. Almeida,
University of Aveiro, Portugal

Reviewed by:

Charles E. McCall,
Wake Forest Baptist Medical Center,
United States
Zsuzsa Szondy,
University of Debrecen, Hungary

*Correspondence:

Tsaffir Zor
tsaffyz@tauex.tau.ac.il

[†]These authors have contributed
equally to this work

Specialty section:

This article was submitted to
Molecular Innate Immunity,
a section of the journal
Frontiers in Immunology

Received: 15 May 2019

Accepted: 16 July 2019

Published: 06 August 2019

Citation:

Ernst O, Glucksam-Galnoy Y, Bhatta B, Athamna M, Ben-Dror I, Glick Y, Gerber D and Zor T (2019) Exclusive Temporal Stimulation of IL-10 Expression in LPS-Stimulated Mouse Macrophages by cAMP Inducers and Type I Interferons. *Front. Immunol.* 10:1788. doi: 10.3389/fimmu.2019.01788

Expression of the key anti-inflammatory cytokine IL-10 in lipopolysaccharide (LPS)-stimulated macrophages is mediated by a delayed autocrine/paracrine loop of type I interferons (IFN) to ensure timely attenuation of inflammation. We have previously shown that cAMP synergizes with early IL-10 expression by LPS, but is unable to amplify the late type I IFN-dependent activity. We now examined the mechanism of this synergistic transcription in mouse macrophages at the promoter level, and explored the crosstalk between type I IFN signaling and cAMP, using the β -adrenergic receptor agonist, isoproterenol, as a cAMP inducer. We show that silencing of the type I IFN receptor enables isoproterenol to synergize with LPS also at the late phase, implying that autocrine type I IFN activity hinders synergistic augmentation of LPS-stimulated IL-10 expression by cAMP at the late phase. Furthermore, IL-10 expression in LPS-stimulated macrophages is exclusively stimulated by either IFN α or isoproterenol. We identified a set of two proximate and inter-dependent cAMP response element (CRE) sites that cooperatively regulate early IL-10 transcription in response to isoproterenol-stimulated CREB and that further synergize with a constitutive Sp1 site. At the late phase, up-regulation of Sp1 activity by LPS-stimulated type I IFN is correlated with loss of function of the CRE sites, suggesting a mechanism for the loss of synergism when LPS-stimulated macrophages switch to type I IFN-dependent IL-10 expression. This report delineates the molecular mechanism of cAMP-accelerated IL-10 transcription in LPS-stimulated murine macrophages that can limit inflammation at its onset.

Keywords: IL-10 promoter, cAMP, type I interferons, IL-10 expression, lipopolysaccharide, cAMP response element, CREB, toll-like receptor 4

INTRODUCTION

The TLR4 ligand, LPS, stimulates macrophages to produce and secrete multiple pro-inflammatory mediators (1). Expression of the anti-inflammatory cytokine IL-10 peaks with a delay that is due to the essential involvement of LPS-stimulated type I interferons (IFN) that act in an autocrine and paracrine manner (2–7). For example, in LPS-stimulated RAW264.7 macrophages,

there is an approximately 10 h time gap between the TNF α and IL-10 expression peaks (8). Yet, anti-inflammatory macrophages, characterized by enhanced IL-10 expression, can be also generated by a combination of LPS and a second signal, such as an IgG immune complex, apoptotic cell remnants, or a cAMP inducer (1). We have previously shown that short co-stimulation of macrophages with LPS and a cAMP inducer results in synergistic IL-10 transcription, while either stimulus alone is largely ineffective (9). Synergistic IL-10 expression has also been demonstrated in macrophages stimulated by a cAMP inducer and agonists of other TLRs (9, 10). Recently, we further demonstrated that the enhancement of LPS-stimulated IL-10 expression by cAMP and by autocrine type I IFN is temporally distinct (11). Exogenous agents that elevate cAMP, such as the β -adrenergic receptor (β -AR) agonist isoproterenol or the phosphodiesterase (PDE)-4 inhibitor rolipram, synergize with early type I IFN-independent IL-10 expression by LPS, but in contrast, are unable to amplify the late type I IFN-dependent activity (11). In the current study we explored the mechanism of IL-10 expression temporal regulation at the promoter level.

LPS-stimulated IL-10 induction strictly depends on the p38 pathway, which inhibits IL-10 mRNA decay (12, 13). Additionally, p38 activates several transcription factors (TFs), among them Sp1 which has been shown to be involved in IL-10 expression (14). It has also been suggested that LPS-stimulated p38 activates CREB by MSK1/2-mediated phosphorylation on S133 (15), an event considered to be requisite for CREB function (16). However, we have shown that cAMP-stimulated PKA phosphorylates and activates CREB, whereas LPS-stimulated p38-MSK1/2 phosphorylates CREB but fails to activate CRE-dependent transcription (17), indicating that phosphorylation of CREB is required but not sufficient for its transcriptional activity (18). Indeed, the CREB-regulated transcription coactivator 3 (CRTC3) translocates to the nucleus following cAMP-dependent PKA activation, but not in response to LPS, where it cooperates with CREB in amplification of LPS-induced IL-10 expression (19). A cross-talk between LPS and cAMP signaling might occur also at the level of p38 activation, as cAMP induction in LPS-stimulated BMDM increased expression of the MAPK phosphatase DUSP1, leading to reduced MAPK activity (20). As expected, IL-10 expression is elevated in DUSP1-deficient macrophages in a p38-dependent manner (21). As the cAMP-DUSP1 axis down-regulates p38 activity and IL-10 expression in LPS-stimulated macrophages (20), whereas overall cAMP strongly amplifies IL-10 expression (11), we hypothesized that cAMP magnifies LPS-induced IL-10 via a p38-independent mechanism.

The repertoire of signaling pathways which are employed to induce IL-10 depends on the studied species and cell type (22–24). The TFs shown to be involved in LPS-stimulated IL-10 induction in murine macrophages, and whose respective response elements were mapped on the mouse IL-10 promoter, are: C/EBP (25), Sp1 and Sp3 (26, 27), STAT1 and STAT3

(3), KLF4 (28), and NF κ B p50 (29). Brightbill et al. (26) used a series of 5'-deletion mutants and point mutations of the mouse IL-10 promoter reporter to show that the Sp1 site, located at -89/-78 bp relative to the transcription start site (TSS), is primarily responsible for IL-10 reporter transcription in RAW264.7 macrophages stimulated by LPS (alone) for a long period of 24 h (26). The synergistic IL-10 transcription displayed by LPS and cAMP inducers (9, 11), together with the suppressive effect of CREB deficiency on IL-10 expression in mouse macrophages (19, 30), led us to hypothesize that LPS-stimulated Sp1 cooperates with cAMP-stimulated CREB at the mouse IL-10 promoter. While the location of CRE at the mouse IL-10 promoter remains elusive, Platzer et al. (31) stimulated human THP-1 monocytes for 24 h with cell-permeable cAMP (alone) and identified two functional and two non-functional CREs in the human IL-10 promoter. However, only one of these CRE sites is conserved in the mouse promoter, and importantly—their relevance to IL-10 expression in LPS-stimulated cells has not been explored. Binding of phosphorylated CREB to the proximal region of the mouse IL-10 promoter has been demonstrated, but the precise location of CRE has not been revealed (32, 33).

The above reports examined transcriptional regulation of the IL-10 promoter in cells stimulated for a prolonged period with either LPS or a cAMP inducer alone. The objective of the present study was to identify the mouse IL-10 promoter elements that mediate synergistic induction by cAMP at the early phase in co-stimulated macrophages, and to assess why up-regulation by cAMP is lost upon switch of LPS-stimulated macrophages to type I IFN-dependent IL-10 expression. We found that type I IFN receptor silencing enabled synergism between LPS and cAMP also at the late phase, suggesting that type I IFN stimulate IL-10 expression at the late phase via a mechanism which is not amenable for up-regulation by the cAMP pathway. We then identified a novel set of two functionally-dependent CREs at the mouse IL-10 promoter that is activated by the cAMP pathway and drives IL-10 reporter transcription in a cooperative manner with the Sp1 site, which is mainly constitutive at the early phase and then further activated by LPS via type I IFN at a later stage. Our results suggest that accelerated IL-10 transcription achieved by synergism between cAMP inducers and type I IFN-independent LPS signaling can limit inflammation at its onset in specific contexts.

MATERIALS AND METHODS

Reagents and Plasmids

Lipopolysaccharide (LPS; *Escherichia coli* serotype 055:B5) and isoproterenol were purchased from Sigma-Aldrich (St. Louis, MO). L-glutamine and penicillin-streptomycin-nystatin were purchased from Biological Industries (Beit Haemek, Israel). DMEM, OptiMEM and FBS were purchased from Gibco. BSA was purchased from Amresco (Solon, OH). The ELISA reagents set for IL-10 was purchased from R&D Systems (Minneapolis, MN). The rabbit anti-mouse CREB and monoclonal anti-mouse tubulin antibodies were from Cell Signaling Technology (Danvers, MA) and Santa Cruz Biotechnology (Santa Cruz,

Abbreviations: β -AR, β -adrenergic receptor; CRE, cAMP response element; interferon, IFN; Iso, isoproterenol; TF, transcription factor; TSS, transcription start site.

CA), respectively. Infrared dye-labeled secondary antibodies and blocking buffer were from Li-Cor Biosciences (Lincoln, NE). Immobilon-FL polyvinylidene fluoride (PVDF) membranes were from Millipore (Billerica, MA). The full-length (−1,538/+64) mouse IL-10 promoter luciferase reporter gene construct and the set of 5′-deletion mutants were a kind gift from Dr. S. Smale (26) and the dominant negative construct named A-CREB was generously given by Dr. C. Vinson (34). All vectors were amplified using DH10B bacteria (Invitrogen, Carlsbad, CA), and purified using Endofree Plasmid Maxi Kit (Qiagen, Hamburg, Germany). HD-fugene, Lipofectamine2000 and TransIT2020 transfection reagents were purchased from Roche (Mannheim, Germany), Invitrogen (Carlsbad, CA) and Mirus Bio (Madison, WI), respectively. Dual-luciferase reporter assay kit was from Promega (Fitchburg, WI). The siRNA against CREB (5′-GCAAGAGAAUGUCGUAGAA-3′) and a scrambled control sequence were purchased from Bioneer (Daejeon, Korea). Mouse IFN α was from Miltenyi Biotec (Bergisch Gladbach, Germany). PCERA-1 was kindly supplied by Dr. Nathanael Gray.

Cell Culture

Mouse RAW264.7 macrophage cells were obtained from American Type Culture Collection (ATCC, Rockville, MD). A RAW264.7 cell line stably expressing shRNA against CREB1a was generously given by Dr. I.D.C. Fraser (30). The cells were grown to 80–90% confluence in DMEM medium supplemented with 8 mM L-glutamine, 100 U/ml penicillin, 100 μ g/ml streptomycin and 1,250 U/ml nystatin (hereafter culture medium), and with 10% FBS, at 37°C in a humidified incubator with 5% CO₂.

IL-10 Release Assay

RAW264.7 macrophages were maintained for 48 h prior to the experiment in 96-well plates, at 1.0·10⁵ cells per well, in culture medium supplemented with 5% FBS, up to a confluence of 90%. The culture medium was replaced 2 h before treatment in order to avoid the artifact of medium replacement on signaling (35). The cells were stimulated with LPS (10 ng/ml) and/or isoproterenol (1 μ M) at 37°C for 3–24 h. IL-10 secretion to the medium were measured with commercially available ELISA reagents sets, according to the manufacturer's instructions, using a microplate reader (Bio-Tek, Winooski, Vermont). The samples were stored at −80°C until used.

Transfection and Reporter Gene Assay

RAW264.7 macrophages were grown for 24 h in 12-well plates, at 3·10⁵ cells per well, in culture medium supplemented with 10% FBS. The cells were then transfected for 24 h with 0.6 μ g of reporter plasmid and 0.2 μ g of Herpes Simplex Virus TK-renilla luciferase (for normalization), and where indicated—also with a dominant negative (A-CREB), silencing (sh-IFN α R1) or control construct. The plasmids were initially incubated with HD-fugene or TransIT2020 transfection reagent in OptiMEM for 15 min at room temperature. Following transfection, the cells were washed and stimulated with LPS (10 ng/ml) and/or isoproterenol at 37°C for 3–24 h, after which luciferase activity in cell extracts was determined following the manufacturer's instructions. Data

were expressed as a ratio of IL-10 promoter-driven luciferase activity divided by the renilla luciferase activity. Transfection with the empty reporter vector (pGL2B or pTAL) yielded no detectable activity.

CREB Silencing Using siRNA

RAW264.7 macrophages were grown for 24 h in 6-well plates, at 6·10⁵ cells per well, in culture medium supplemented with 10% FBS. Transfection with siRNA against CREB (or a scrambled control sequence) was performed as described by Fraser et al. (36). A mixture of each siRNA with Lipofectamine2000 transfection reagent, initially incubated in OptiMEM medium for 20 min at room temperature, was added to the cells at 100 nM for the first 4 h, after which the volume was increased so the siRNA was at a concentration of 62.5 nM for the following 20 h. The cells were washed and the transfection process was repeated the next day for another 24 h. The siRNA-containing medium was removed and the cells were seeded in a 48-wells plate for a recovery period of 24 h. LPS (100 ng/ml) \pm isoproterenol (1 μ M) were then added for 4 h at 37°C. CREB expression was analyzed by western blotting and IL-10 production by ELISA.

Construction of Plasmids

The full IL-10 promoter (−1,538/+64) luciferase reporter plasmid was mutated at the CREs and/or Sp1 sites according to the QuickchangeTM standard protocol (37). The sense primers for mutagenesis are listed below:

```

CRE1 - 5'-TAGCCCATTTATCCACaaaATTATGACCTG
      GGAGTGCg-3',
CRE2 - 5'-CGTCATTATGACCTGGGAGTaaTGAATGGA
      ATCCAC-3',
Sp1 - 5'-GGTTTAGAAGAGGGAGGAaaAGCCTGAAT
      AAC-3'.
  
```

The heterologous reporter constructs: CRE1x4 (TTTATCCAC GTCATTATG), CRE2x4 (GGGAGTGCgTGAATGGA), CRE consensus x4 (GGGAGTGACGTCAATGGA), IL-10 promoter Sp1 site x4 (GGAGGAGGAGCC) carrying four copies of the respective cis element upstream to a luciferase reporter gene, and the CRE1+CRE2 heterologous reporter carrying two copies of the IL-10 promoter region encompassing both CRE1 and CRE2 (−362/−323 relative to TSS), were generated using double stranded pre-synthesized oligonucleotides (Hylabs, Israel) cloned into the pTAL vector (Clontech, CA). The shRNA vector against IFN α R1 was constructed by cloning the shRNA oligonucleotide sequence (GATCGGAATGAGGTTGATCCGTTTATCTCGAGA TAAACGGATCAACCTCATTCTTTT) into the pGFP-RS shRNA vector (Origene, Rockville, MD). Sequence verification was performed using the ABI PRISM 3100 Genetic Analyzer sequencer. Plasmid production was done using Endofree Plasmid Maxi Kit.

Transcription Factor-DNA Interaction Assay

We used QPID to measure TFs affinity to a library of DNA sequences derived from the mouse IL-10 promoter (38). A

TABLE 1 | K_d values for binding of CREB and AP-1 heterodimers to CRE sequences.

Oligo	Position ^a		Sequence		Kd (μM) for various TF dimers				
	Site	Context			CREB/ ATF1	CREB	ATF1	c-Jun/ c-Fos	c-Jun/ ATF2
CRE ^b	–	–349/–315	consensus	TGACGTCA	0.06	0.07	0.03	0.15	0.05
CRE1	–357/–350	–368/–336	wt	CCACGTCA	0.06	0.56	0.05	3	2
			mutant	CC ^A aaaat	84	47	32		
CRE2	–335/–329	–349/–315	wt	TG-CGTGA	13	66	16	n.d. ^c	n.d. ^c
			mutant	Ta-aaTGA	n.d. ^c	109	48		
CRE1+ CRE2	As above	–366/–298	wt	As above	0.05	1.6	0.08		
			mut CRE1	As above	10	61	10		
TRE ^b	–	–349/–315	consensus	TGA-GTCA	12	53	17	0.5	9

^aPosition in the mouse IL-10 promoter, relative to TSS. Site = cis element, context = promoter region present in the oligonucleotide used for the binding assay.

^bThe depicted consensus sequence (40) was inserted in the context of the IL-10 promoter –349/–315 oligonucleotide, replacing the CRE2 sequence. Similar results were obtained when it was inserted in the context of the TNFα promoter CRE region.

^cn.d., no binding detected.

microfluidic device was designed and fabricated as described by Maerkl and Quake (39). The device was aligned to a dilution series microarray of Cy5-labeled dsDNA sequences (see Table 1) and its surface was derivatized as previously described (41–43). A construct of CREB tagged with both His₆ and c-Myc, and a construct of ATF1 tagged with both HA and V5, were prepared and proteins expressed *in-vitro* as previously described (41). Homo- and hetero-dimers of CREB and ATF1 were introduced into the microfluidic device, and spotted DNA was solubilized, allowing interaction with the transcription factors. Mechanically induced trapping of molecular interactions (MITOMI) was performed after 1 h incubation (39) to enable quantification of each interacting component (41). Data were fitted and K_d values determined using non-linear least squares minimization. Binding experiments for some sequences were repeated with AP-1 dimers, composed of doubly tagged c-Fos, c-Jun, and ATF2.

Protein Determination

Protein was determined by a modification of the Bradford procedure, which yields linear and thus more accurate results, increased sensitivity, and reduced detergent interference, as previously described by Zor and Selinger (44) and Ernst and Zor (45). BSA served as standard.

Western Blot Analysis

Whole cell lysates were prepared and used for western blot assays of CREB as previously described (17). Two-color imaging and quantitative analysis of western blots was performed using the Odyssey infrared imaging system (Li-Cor Biosciences), according to the manufacturer's instructions. Signal intensity was verified to be linear with protein quantity. An antibody against α-tubulin served for normalization.

Statistical Analysis

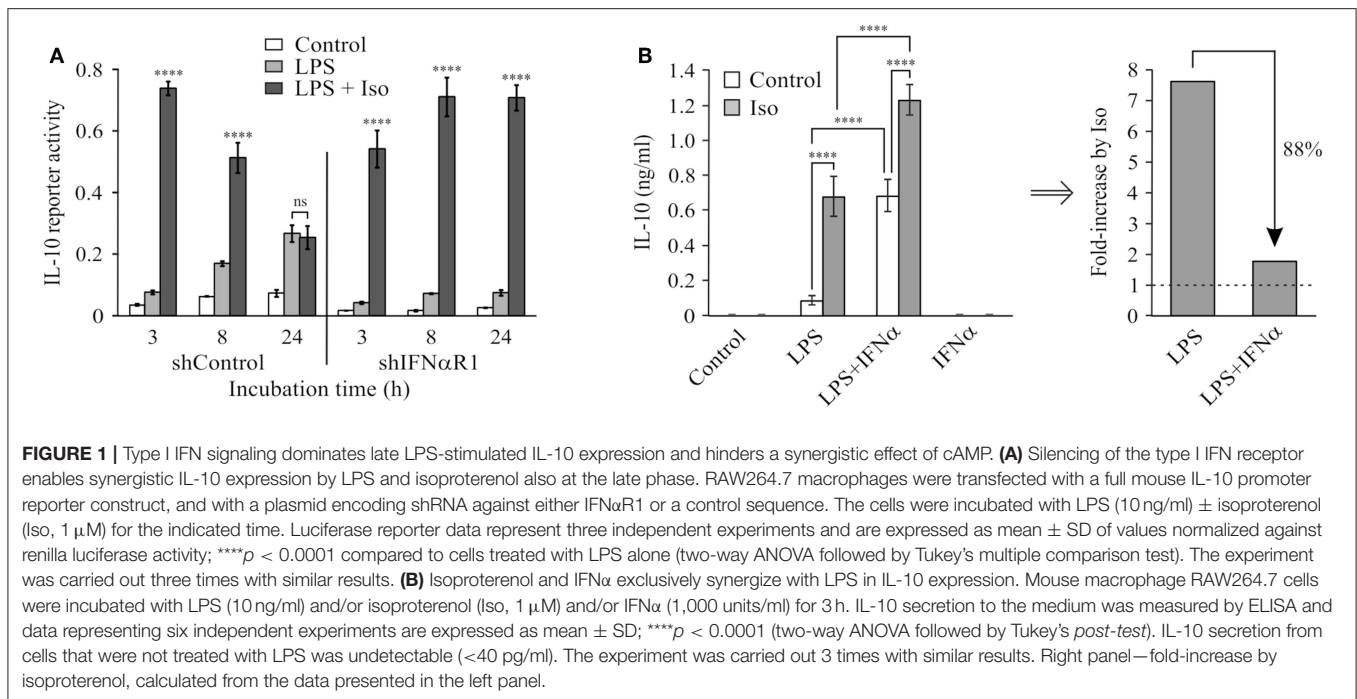
Data were analyzed using one- or two-ways ANOVA with the appropriate multiple comparison test wherever applicable, as

indicated in the figure legend. In all cases, differences of $p < 0.05$ were considered to be significant. All experiments were repeated at least twice.

RESULTS

The Autocrine Type I IFN Loop Confers cAMP-Insensitive LPS-Stimulated IL-10 Expression at the Late Phase

We recently demonstrated that elevated intra-cellular cAMP synergizes with LPS at IL-10 expression and secretion in LPS-stimulated RAW264.7 macrophages only at the early (3 h), but not late (24 h), phase (11). The temporal regulation trend of IL-10 protein expression was recapitulated in primary macrophages (BMDM), as well as *in-vivo* and was demonstrated also at the mRNA expression level in macrophages (11). We further showed that the loss of cAMP effect at the late phase was specific to IL-10 expression, while general cAMP-dependent transcriptional activity was retained (11). In contrast, autocrine/paracrine type I IFN activity is required for LPS-stimulated IL-10 expression at the late phase (2–7). We showed that neither recombinant IFNα nor secreted type I IFNs (conditioned medium from LPS-stimulated macrophages) can synergize with cAMP in IL-10 promoter activation (11). In the present study we further examined the interplay between type I IFN and cAMP in time-dependent IL-10 expression by silencing the common type I IFN receptor subunit, IFNαR1. To this end, RAW264.7 macrophages were co-transfected with a shIFNαR1 plasmid together with the IL-10 promoter reporter plasmid. Consistently with our previous report (11), the β-AR agonist isoproterenol, which stimulates intra-cellular cAMP formation (17), synergistically elevated LPS-stimulated IL-10 promoter reporter activity in control cells at the early phase, but not at the late phase (Figure 1A). Silencing the type I IFN receptor significantly reduced LPS-stimulated and basal IL-10 promoter reporter activity in a time-dependent manner, and strikingly—enabled synergism between LPS and

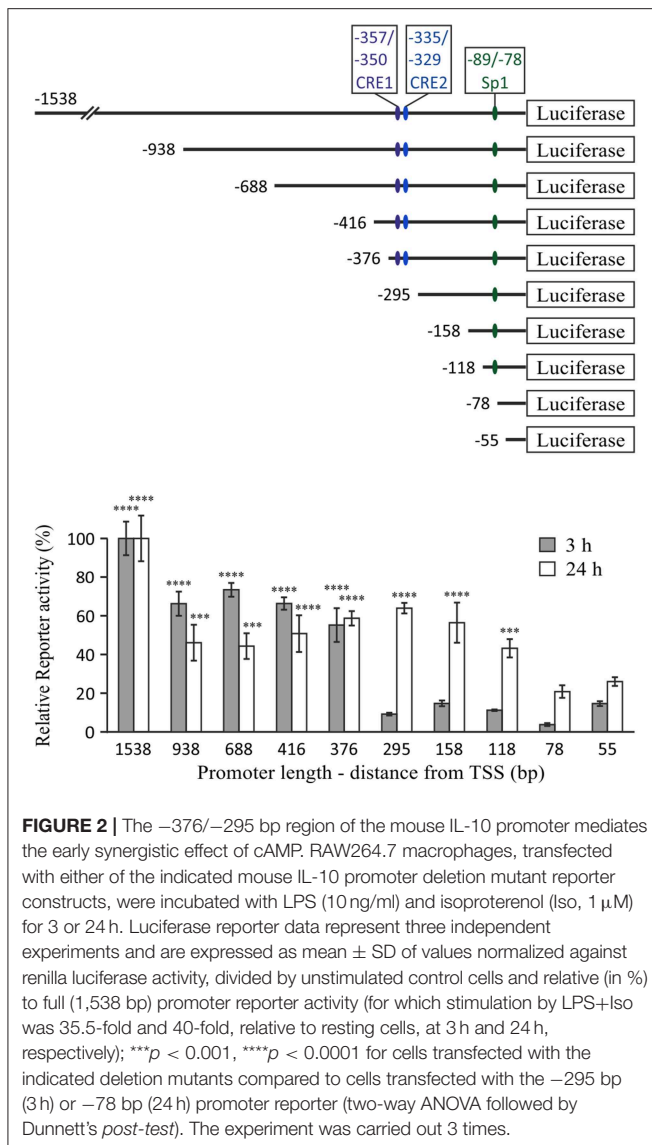


isoproterenol during the entire 24 h time-course (Figure 1A). This dramatic effect of IFN α R1 silencing, taken together with the inability of exogenous IFN α to synergize with isoproterenol (11), suggests that normally the cAMP pathway can amplify only the low-direct IL-10 inducing effect of LPS at the early phase, whereas an autocrine IFN α R1-dependent activity which cannot cooperate with the cAMP pathway dominates late IL-10 induction in LPS-stimulated macrophages.

We further examined how LPS-dependent IL-10 expression is stimulated by isoproterenol vs. type I IFN by incubating RAW264.7 macrophages with various combinations of LPS, isoproterenol and IFN α for 3 h. LPS alone only slightly stimulated IL-10 expression and secretion at this early time frame, while isoproterenol alone and IFN α alone had no detectable effect. Yet, either isoproterenol or IFN α synergistically amplified LPS-dependent IL-10 secretion by nearly 8-fold (Figure 1B). Importantly, the effect of isoproterenol on LPS-induced IL-10 expression was reduced in the presence of IFN α by 88%—from 7.7-fold in cells treated by LPS, to 1.8-fold in cells co-treated by LPS and IFN α together (Figure 1B). The usage of IFN β rather than IFN α similarly resulted in synergism with LPS and diminished amplification by cAMP (not shown). These findings indicate that LPS-dependent IL-10 expression can be synergistically amplified by either the cAMP pathway or type I IFN signaling, but in a largely exclusive manner. Both stimuli act permissively, i.e., inducing IL-10 expression only in macrophages co-treated with LPS. Moreover, even the combination of isoproterenol and IFN α (Figure 1B) or IFN β (not shown) was incapable of inducing IL-10 expression in the absence of LPS. Together with the lack of additivity of their synergistic potentials, this suggests that cAMP signaling and type I IFN signaling affect a common step in IL-10 expression.

CREB Is Required for Transcriptional Activation by cAMP at the $-376/-295$ bp Region of the Mouse IL-10 Promoter

IL-10 mRNA and protein expression regulation by cAMP in LPS-stimulated cells was most sensitively reflected in direct up-regulation of transcription, as measured using an IL-10 promoter reporter (11). Induction of IL-10 promoter activity by cAMP elevation was minimal, unless the macrophages were co-stimulated by LPS (11). Thus, in the current study we set a goal to identify the promoter region accountable for the synergistic IL-10 inducing effect of the cAMP elevating agent isoproterenol in LPS-stimulated macrophages, using a series of 5' deletion mutants of the mouse IL-10 promoter reporter (26). We reasoned that cAMP sensitivity will be manifested by identifying a promoter region critical for IL-10 reporter induction by a co-stimulus of LPS and isoproterenol only at the early phase. We indeed found that the promoter region at $-376/-295$ bp is most critical only during the early phase (3 h) of LPS and isoproterenol co-treatment (Figure 2). In contrast, at the late stage (24 h) of co-stimulation, the $-376/-295$ bp region was irrelevant while the $-118/-78$ bp region was important (Figure 2), as previously reported for 24 h of stimulation by LPS alone (26). The $-1,538/-938$ bp region was found to contribute to IL-10 expression at both early and late stages (Figure 2). These results suggest that early IL-10 transcription critically depends on a cAMP-regulated TF binding site located between 295 and 376 bp upstream of the TSS, and that LPS-regulated response elements located at the $-118/-78$ and $-1,538/-938$ bp regions are the dominant regulatory sites of IL-10 transcription at the late phase. We further focused on the $-376/-295$ bp region, as it was the only region demonstrating time-dependent relevance that fully matched the time course



of regulation by cAMP on IL-10 promoter reporter activation (Figure 1A) and endogenous IL-10 expression (11).

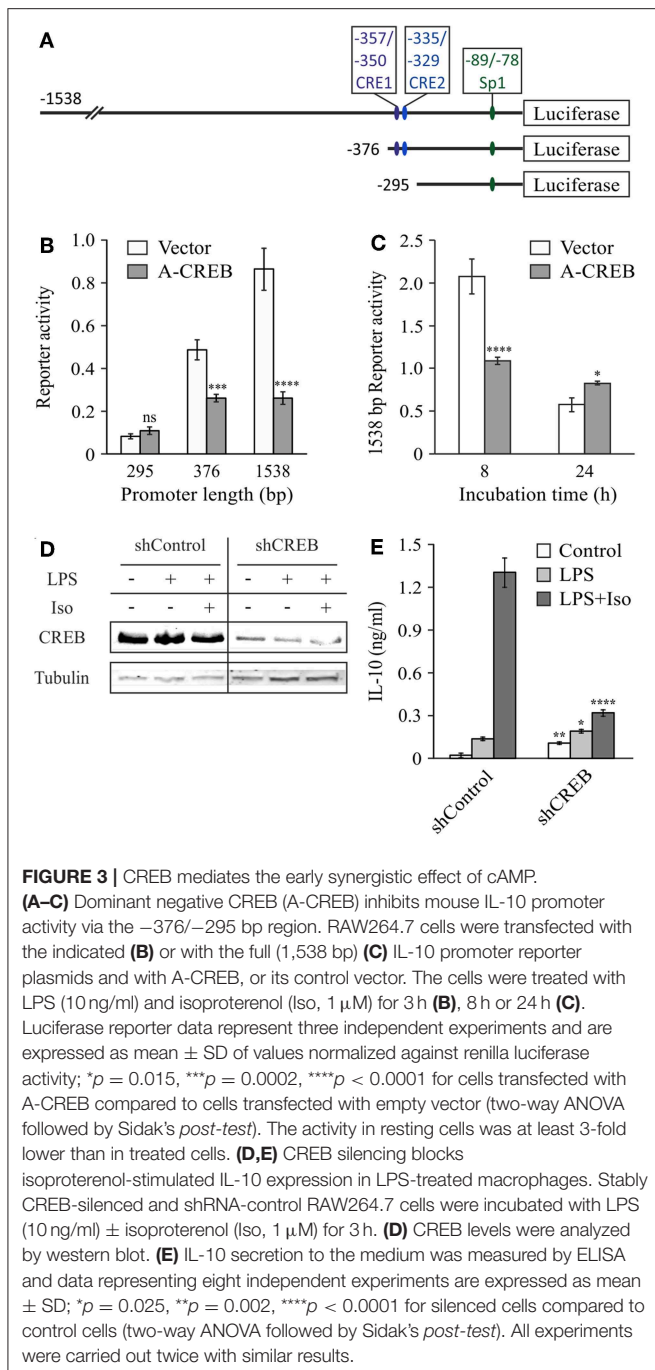
To explore the role of CREB in IL-10 promoter activation and to confirm the location of the cAMP-sensitive region (Figure 3A), we co-stimulated the cells with LPS and isoproterenol and used the dominant negative construct A-CREB, which sequesters native CREB by dimer formation and is unable to bind the DNA (34). Figure 3B shows that at 3 h, A-CREB inhibits reporter activity of the full 1,538 bp IL-10 promoter as well as of the shorter 376 bp construct, but has no effect on transcriptional activation of the further-shortened 295 bp IL-10 promoter. A-CREB also inhibits co-stimulation of the full (1,538 bp) IL-10 promoter reporter at 8 h but has no negative effect at 24 h (Figure 3C). These results support the finding above regarding the location of the cAMP-regulated site at the -376/-295 bp region of the mouse IL-10 promoter, and suggest that CREB mediates the enhancing effect of isoproterenol on

IL-10 reporter activity at the early (and mid-) phase whereas late IL-10 expression in LPS-stimulated cells is CREB-independent. Next, we validated the involvement of CREB in the regulation of endogenous IL-10 expression by the cAMP pathway, using a previously described RAW264.7 cell line (30) that stably expresses shRNA against CREB1a (hereafter shCREB), resulting in 80% CREB silencing efficiency (compared to shControl cells, Figure 3D). As observed with the dominant negative approach, isoproterenol was unable to significantly stimulate LPS-induced IL-10 secretion at the early phase in shCREB cells, unlike control cells (Figure 3E). Furthermore, transient siRNA-mediated CREB silencing (95% efficiency at the protein level) diminished the synergistic effect of isoproterenol (data not shown). These results indicate that CREB mediates the synergistic effect of cAMP on IL-10 expression in LPS-stimulated macrophages, and is consistent with a previous report, in which IL-10 mRNA levels in shCREB cells stimulated with LPS for 2 h were not further increased by cell-permeable cAMP (30).

Cooperative Tandem CRE Sites at the Mouse IL-10 Promoter

The human IL-10 promoter contains a single CRE which was demonstrated to be functional upon stimulation with exogenous cAMP for 24 h and is also conserved in the mouse IL-10 promoter (31). This site resides at -357/-350 bp relative to the TSS (hereafter CRE1, Table 1), within the region identified in Figure 2. Mutation of that conserved cis element at the human promoter only partially reduced the response to a cAMP stimulus (31), and thus we decided to perform a bioinformatics search to identify additional putative CREs within the -376/-295 bp region. A putative CRE-like 7 bp sequence was indeed found 21 bp apart from CRE1 (3' to 3'), at -335/-329 bp relative to the TSS (hereafter CRE2, Table 1).

To assess the binding of these sequences to CREB and its closely-related family member ATF1, we used a microfluidics approach named Quantitative Protein Interactions with DNA (QPID) (38, 39). We spotted increasing concentrations of Cy5-labeled oligonucleotides on a microfluidic array device; CREB and ATF1 homo- and hetero-dimers were allowed to bind and reach equilibrium, and we then quantified the protein-DNA interaction via fluorescence of the tags present on the DNA and the TF-bound antibodies. As shown in Table 1, the CREB homodimer bound to a CRE1 oligonucleotide with an affinity that was one order of magnitude lower than to a consensus CRE sequence, but two orders of magnitude higher than to a CRE2 oligonucleotide. CREB binding to an oligonucleotide containing both CRE1 and CRE2 was comparable to CRE1 alone. The binding affinities of the CREB homodimer to CRE1 and CRE2 were an order of magnitude lower than those of a ATF1 homodimer or CREB-ATF1 heterodimer. Compared to the CREB family members, AP-1 heterodimers displayed comparable high affinity to consensus CRE, low affinity to CRE1 and non-detected binding to CRE2. Based on these results, we predicted that CRE1 would be activated by cAMP-stimulated CREB/ATF-1, but not by LPS which stimulates AP-1 activity (40).



To examine the potential of the CRE1 and CRE2 sequences to mediate CREB-dependent transcription, we constructed reporter plasmids carrying four repeats of either sequence and compared their activity to that of the consensus CRE. **Figure 4A** shows that the CRE1 construct was activated 6-fold by isoproterenol in a 3 h assay, whereas the CRE2 construct was not activated, and the CRE consensus sequence was activated 43-fold by isoproterenol. Notably, CRE1 contains one consensus position in addition to a consensus CRE half-site (5 bp) which is known to be weakly activated by CREB relative to the full 8 bp palindrome CRE

(46). In contrast to isoproterenol, LPS neither activated these sequences by itself nor affected the activity of isoproterenol (**Figure 4A**). Next, we created reporter plasmids regulated by two repeats of the entire –362/–324 bp region of the IL-10 promoter containing both CRE1 and CRE2, wild-type (wt) or mutated in either sequence. Surprisingly, the 16-fold reporter activation induced by isoproterenol was not only completely abolished by mutation of CRE1 but also completely abolished by mutation of CRE2, indicating tight cooperativity between the two CRE sequences (**Figure 4B**). Finally, we created CRE mutants of the full IL-10 promoter reporter. These mutations only modestly affected the low LPS-induced activity at 3 h, and thus, in order to focus on the relevance of each CRE sequence to IL-10 transcription induction by cAMP, the Y axis in **Figure 4C** depicts IL-10 reporter activities in cells stimulated by LPS and isoproterenol, relative to LPS alone. Mutation of either CRE1 or CRE2 sharply reduced isoproterenol's effect on LPS-induced IL-10 reporter activity at the early and mid- phases (**Figure 4C**). Importantly, mutation of both CRE1 and CRE2 in the context of the full IL-10 promoter was just as detrimental as mutation of only a single CRE (**Figure 4C**). Consistent with the previous experiments, isoproterenol's effect on LPS-induced IL-10 reporter activity was time-dependent (**Figure 4C**). Thus, these results indicate complete synergism between CRE1 and CRE2 in mediating amplification of early LPS-induced IL-10 transcription in response to a cAMP stimulus.

Sp1 Critically Regulates IL-10 Transcription in Cooperativity With CRE

The Sp1 site located at –89/–78 bp was shown to mediate transcriptional induction of the mouse IL-10 promoter in macrophages stimulated with LPS for 24 h (26). However, its role at shorter LPS stimulation periods and its relevance regarding synergistic IL-10 expression have not been reported. Therefore, we initially compared the LPS-inducible activities of 5'-deletion constructs containing (–118 bp) or not containing (–78 bp) the reported Sp1 binding site (**Figure 5A**). As shown above (**Figure 2**), the activity of the –118 bp reporter in stimulated cells relative to resting cells was surprisingly similar to that of the shorter reporters at 3 h and only modestly higher (~2-fold) for the Sp1-containing construct at 24 h. However, separate analysis of the activities in resting cells, LPS-stimulated cells and cells co-stimulated by LPS and isoproterenol, indicated that deletion of the region that includes the Sp1 loci greatly reduces IL-10 promoter activity in all cellular activation states at both 3 h and 24 h (**Figure 5B**). These results imply that Sp1 has a critical role in both basal and inducible transcription of IL-10. Importantly, while LPS only slightly elevated the activities of the –78 and –118 bp reporters at the early phase (**Figure 5B**, left panel), it greatly stimulated the late phase activity of both reporters, and in particular that of the promoter construct that contains the Sp1 response element (–118 bp)—by an order of magnitude (**Figure 5B**, right panel). The modest positive effect of isoproterenol on LPS-stimulated activity of the –118 bp promoter was significantly less pronounced than that of LPS (**Figure 5B**, right panel), and isoproterenol had no effect on

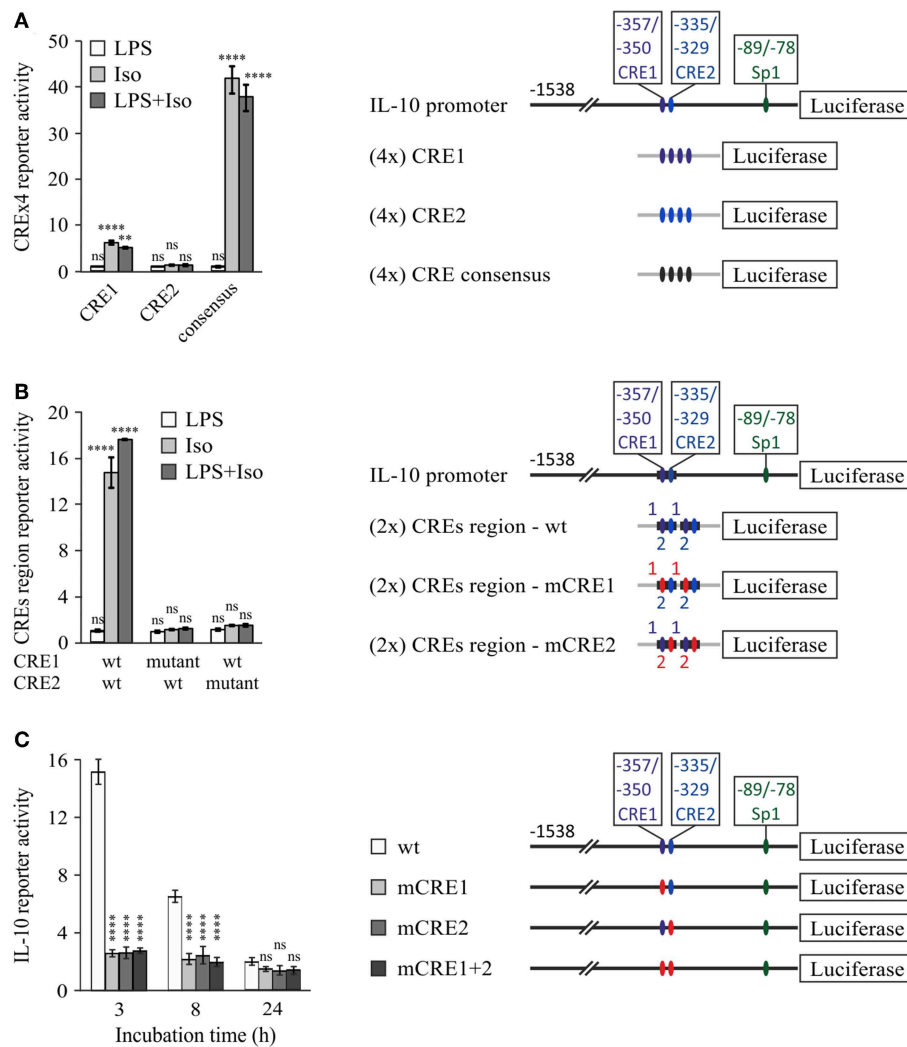


FIGURE 4 | Cooperativity between tandem CRE sites is essential for cAMP-stimulated IL-10 promoter activity. RAW264.7 macrophages were transfected with a luciferase reporter regulated by four repeats of either CRE1 or CRE2 or a consensus CRE (**A**), two repeats of the $-362/-324$ bp region with either the WT sequence, CRE1 mutant, or CRE2 mutant (**B**), or the full $(-1,538)$ bp IL-10 promoter, either wt, mutant in CRE1 (mCRE1), mutant in CRE2 (mCRE2) or a double mutant (mCRE1+2) (**C**). Site mutation is shown by red color. The cells were incubated with isoproterenol (Iso, $1 \mu\text{M}$) and/or LPS (10 ng/ml) for 3 h (**A,B**) or with both stimuli for the indicated time (**C**). Luciferase reporter data represent three independent experiments and are expressed as mean \pm SD of values normalized against renilla luciferase activity, relative to unstimulated (**A,B**) or LPS-stimulated (**C**) control cells; (**A,B**) $^{**}p < 0.001$, $^{****}p < 0.0001$ for cells treated with isoproterenol (\pm LPS) compared to control cells (two-way ANOVA followed by Dunnett's *post-test*). (**C**) Error bars represent the sum of SD (%) of both values in the ratio. $^{****}p < 0.0001$ for mutants compared to wt (two-way ANOVA followed by Dunnett's *post-test*). The experiments were carried out 3 times with similar results.

the basal activity of the 5'-deletion constructs or the full IL-10 promoter reporter in resting cells (not shown). These results suggest that at long incubations LPS up-regulates the activities of Sp1 and of another TF binding downstream to -78 bp, likely to be NF κ B p50 homodimer, as we (47) and others (29) have reported.

To further examine the ability of LPS to activate IL-10 transcription via the Sp1 site, we prepared a reporter plasmid regulated by four repeats of the IL-10 promoter Sp1 site. Consistent with the above findings, LPS was unable to induce reporter activity at the early phase (not shown), but stimulated its activity 3-fold at the late phase (24 h) (**Figure 5C**). In

contrast, isoproterenol was unable to increase, and even partially decreased, both the basal activity and the LPS-stimulated activity of the reporter (**Figure 5C**). The relatively modest effect of LPS on the Sp1 reporter suggests that in the full IL-10 promoter the Sp1 site cooperates with additional cis elements. Alternatively, different spacing between the four Sp1 sites in the reporter may enable a higher response to LPS. Nevertheless, our results indicate that LPS, but not isoproterenol, stimulates Sp1 activity at the late phase.

The opposite time-dependency of CREs activation by cAMP and Sp1 activation by LPS (early vs. late, respectively), echo the time-dependencies of IL-10 expression stimulation by cAMP and

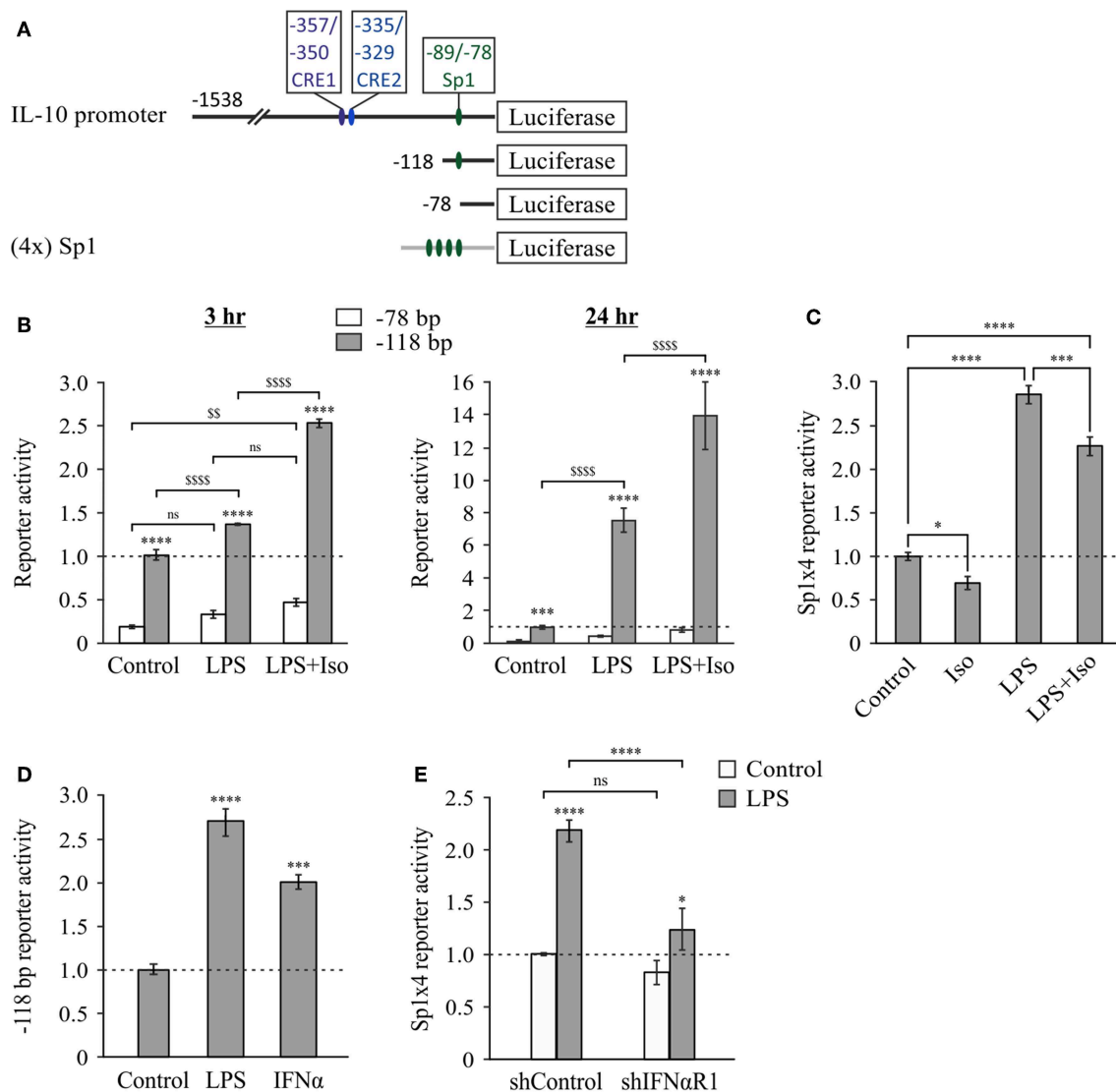


FIGURE 5 | The Sp1 response element at $-89/-78$ bp is constitutive at the early phase and further activated by LPS via type I IFN at the late phase. **(A)** Plasmid constructs used in the following panels. RAW264.7 cells were transfected with either the -78 bp **(B)** or the -118 bp **(B,D)** 5'-deletion IL-10 promoter reporter plasmid, or with a reporter construct regulated by four repeats of the putative IL-10 promoter Sp1 sequence ($-89/-78$ bp) **(C,E)**. **(E)** The cells were co-transfected with a plasmid encoding shRNA against either IFN α R1 or a control sequence. **(B–E)** The cells were incubated with vehicle, LPS (10 ng/ml) and/or isoproterenol (Iso, 1 μ M) or with mouse IFN α (1,000 units/ml), for 3 h **(B—left panel)** or 24 h **(B—right panel, and C–E)**. Luciferase Reporter data represent three independent experiments and are expressed as mean \pm SD of values normalized against renilla luciferase activity and relative to unstimulated control cells. **(B)** **** $p < 0.0001$ for cells transfected with -118 bp mutant compared to the -78 bp mutant (two-way ANOVA followed by Sidak's *post-test*); *** $p = 0.0004$ for resting cells transfected with -118 bp mutant compared to the -78 bp mutant (Student's *t-test*); \$\$\$ $p = 0.008$, \$\$\$\$ $p < 0.0001$ for cells transfected with the same plasmid and treated with different stimuli (two-way ANOVA followed by Sidak's *post-test*). All values were above the detection limit, except for resting control cells transfected with the -78 bp mutant. **(C)** * $p = 0.01$, *** $p = 0.001$, **** $p < 0.0001$ (one-way ANOVA followed by Sidak's *post-test*). **(D)** *** $p = 0.001$, **** $p < 0.0001$ (one-way ANOVA followed by Dunnett's *post-test*). **(E)** * $p = 0.025$, **** $p < 0.0001$ (two-way ANOVA followed by Sidak's *post-test*). The experiments were carried out 3 times **(B)**, 6 times **(C)** or twice **(D,E)** with similar results.

autocrine type I IFN (11) (**Figure 1A**). We therefore examined whether type I IFNs are involved in LPS-stimulated activation of the Sp1 response element of the IL-10 promoter. This indeed was demonstrated by the following two experiments. First, the minimal IL-10 promoter reporter that includes the Sp1 site (-118 bp) was activated by a 24 h treatment with either LPS or IFN α (**Figure 5D**). The lower reporter stimulation by IFN α , relative

to LPS, suggests that the autocrine type I IFN loop is required, but not sufficient for maximal Sp1 activation in response to LPS, as we showed also for the reporter of the full IL-10 promoter (11). Second, silencing the common type I IFN receptor subunit, IFN α R1, almost completely abolished LPS-stimulated activity (at 24 h) of the reporter for the Sp1 response element from the IL-10 promoter (**Figure 5E**). Taken together, our results suggest that

LPS up-regulates IL-10 transcription at the late phase, at least in part via autocrine type I IFN stimulating Sp1 activity at the -89/-78 bp cis element.

To examine the role of the Sp1 response element in the context of the full IL-10 promoter and in relation to the CRE sites, we mutated the Sp1 sequence in the full mouse IL-10 promoter reporter, alone or together with mutation of the CRE2 sequence. **Figure 6** shows WT and mutant IL-10 promoter reporter activities at 3, 8, and 24 h, in resting cells (left panel) and in cells stimulated with LPS in the absence or presence of isoproterenol (middle and right panels, respectively). Note that the Y axis has a logarithmic scale. Mutation of the Sp1 site resulted in a loss of activity by at least an order of magnitude at all incubation periods in resting and stimulated conditions. The detrimental effect of substitution mutation (**Figure 6**) or deletion (**Figure 5B**) of the Sp1 response element implies a critical role for that TF in IL-10 expression. Mutation at the CRE2 site reduced IL-10 reporter activity in cells co-stimulated with LPS and isoproterenol by an order of magnitude at 3 h, but had a more modest effect at 8 h and no effect at 24 h. The CRE2 mutation only moderately affected IL-10 reporter activity in both resting cells and cells stimulated with LPS alone for 3 h, and had no effect on IL-10 reporter activity during the longer LPS incubations of 8 and 24 h. This may represent a modest contribution of basal cAMP levels to early LPS-stimulated IL-10 expression, or a modest role for autocrine LPS-induced factors which elevate cAMP, such as eicosanoids (48), or a small medium replacement artifact (35). In any case, the effect of Sp1 mutation is considerably more pronounced than that of CRE2 mutation in all cellular states and time points, except for 3 h of co-stimulation with LPS and isoproterenol. Finally, while mutation of either CRE2 or Sp1 reduces IL-10 reporter activity in response to 3 h of co-stimulation (LPS and isoproterenol) to 8.5 and 18.1%, respectively, of WT IL-10 reporter activity, mutation of both CRE2 and Sp1 together reduces the respective IL-10 reporter activity to only 0.7% of WT activity (**Figure 6**, right panel). This synergism between the two cis elements is also evident at 8 h. Taken together, our results suggest (see cartoon in **Figure 7**) that cAMP-elevating agents up-regulate early (3 h) LPS-induced IL-10 expression by transcriptional activation at the CRE sites, which cooperate with the constitutive Sp1 site. At 24 h, the role of the Sp1 site is strengthened due to its activation by the LPS pathway via an autocrine type I IFN loop, whereas the CRE sites become largely irrelevant.

DISCUSSION

Crosstalk Between the cAMP Pathway and Type I IFN Signaling Regarding IL-10 Expression in Macrophages

Anti-inflammatory macrophages, characterized by reduced production of pro-inflammatory cytokines and increased levels of IL-10, mediate inflammation resolution and homeostasis. While these macrophages usually appear at a late stage of LPS stimulation, such macrophage sub-populations can also be generated following co-stimulation by a TLR ligand and a second

stimulus, including an IgG immune complex, apoptotic cell remnants, or a cAMP inducer (1).

We have previously shown that elevation of cAMP stimulates IL-10 expression in mouse macrophages in synergism with LPS (9), which occurs only at the early, but not late, phase of LPS stimulation (11). Mechanistically, we ruled out receptor desensitization as a possible explanation for the loss of synergism (11), and instead suggested that autocrine type I IFN signaling which is required for IL-10 expression at the late phase of LPS stimulation (2–7) interferes with cAMP effect at late IL-10 expression. Indeed we demonstrate that type I IFN and cAMP amplify LPS-dependent IL-10 expression by exclusive, non-additive and time-distinctive transcriptional mechanisms. This is concluded from a combination of evidences: (i) The inability of cAMP to synergistically elevate IL-10 expression with IFN α or with autocrine type I IFN present in conditioned medium from cells pre-treated with LPS for a prolonged time (11); (ii) The regained ability of cAMP to synergize with LPS even in late IL-10 reporter expression upon type I IFN receptor silencing; (iii) The diminished ability of cAMP to synergistically elevate early IL-10 secretion in cells treated with a combination of LPS and IFN α ; (iv) The opposing time-dependencies of the different IL-10 promoter sites activated by cAMP and type I IFN.

We show that an autocrine/paracrine type I IFN loop is essential for efficient activation of the IL-10 promoter in LPS-stimulated macrophages at the late stage, in accordance with previous reports (2–7). Yet, IFN α , similarly to cAMP inducers, can induce IL-10 expression only in the presence of LPS as a co-stimulator. This permissive property insinuates that in order to induce IL-10, both the LPS-driven autocrine type I IFN loop and the cAMP pathway must cooperate with a LPS-activated pathway(s) which is type I IFN-independent. Notably, LPS rapidly induces IL-10 mRNA expression without a concomitant activation of the IL-10 promoter reporter, pointing to IL-10 mRNA stabilization (11), which indeed was shown to occur via p38 (12, 13). Additionally, the ability of LPS to synergize with the cAMP pathway at the early phase, not only in endogenous IL-10 expression but also in IL-10 promoter reporter activation, suggests that LPS further augments cAMP-stimulated IL-10 transcription in a type I IFN-independent manner.

Regulation of the Mouse IL-10 Promoter by the cAMP Pathway

In the current study we explored the molecular mechanism of the time-dependent synergism between cAMP and LPS using a set of mouse IL-10 promoter deletion mutants previously used by Brightbill et al. (26). In that study the reporter series was used to locate the Sp1 binding site at the mouse IL-10 promoter and to demonstrate its critical role in IL-10 expression in RAW264.7 macrophages stimulated for 24 h by LPS alone (26). We found that synergistic IL-10 promoter activation in the early response to LPS and cAMP requires, in addition to the Sp1 site, two proximate CRE sites located at -357/-350 and -335/-329 bp relative to the TSS. The CREs-dependent synergism is most pronounced at short (3 h) duration of co-stimulation by LPS and a cAMP-elevating agent and it is later reduced (8 h) and even

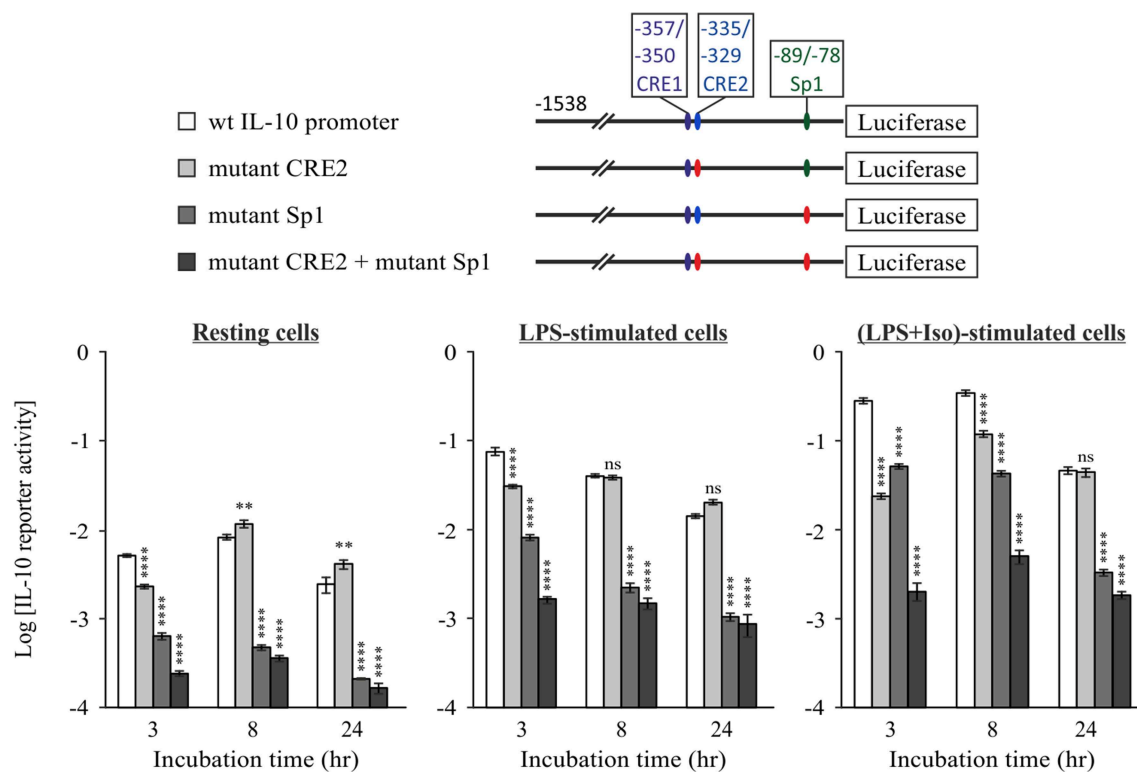


FIGURE 6 | The constitutive Sp1 response element cooperates with cAMP-stimulated CRE at the early phase, but not at the late cAMP-insensitive phase. RAW264.7 cells were transfected with the indicated WT or mutant full IL-10 promoter reporter plasmids. Site mutation is shown by red color. Reporter activities were measured following 3–24 h (as indicated) of treatment with vehicle (**left panel**) or with LPS (10 ng/ml) in the absence (**middle panel**) or presence (**right panel**) of isoproterenol (Iso, 1 μ M). Luciferase Reporter data represent three independent experiments and are expressed as mean \pm SD of values normalized against renilla luciferase activity. ** $p < 0.01$, **** $p < 0.0001$ for cells transfected with a mutant reporter compared to WT IL-10 promoter reporter (two-way ANOVA followed by Dunnett's *post-test*). The experiment was carried out twice with similar results.

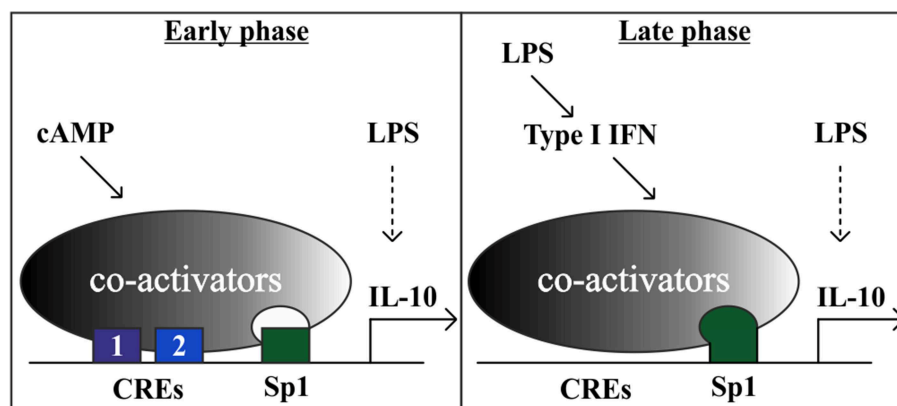


FIGURE 7 | A model showing that the cAMP pathway accelerates IL-10 transcription in LPS-stimulated macrophages at the early phase via a tandem set of CREs that synergize with a constitutive Sp1 site. At the late phase, the strong LPS-induced IL-10 transcription is mediated in part by an autocrine type I IFN loop, which relies on hyper-activation of the Sp1 site and obviates the requirement for the cAMP pathway. Additional LPS-regulated TFs, that are not depicted, include for example p50 NF κ B homodimer (47) and STAT1/3 (3).

abolished at the late phase (24 h). In contrast, Sp1 activity is constitutive at 3–8 h of LPS stimulation and is up-regulated only at 24 h. Basal activity at the CRE sites modestly contributes to the

low LPS-stimulated IL-10 production in the absence of a cAMP inducer at the early phase (3 h). These results are consistent with studies done on IL-10 mRNA expression in BMDM derived

from mice bearing a CREB S133A knock-in mutation, preventing phosphorylation (19, 32). The mutation reduced early (1 h), but not late (4 h) IL-10 mRNA expression in response to either LPS alone or to LPS and a cAMP elevating agent (19). Early IL-10 expression in the CREB S133A knock-in macrophages was reduced but still synergistic, likely due to ATF1 activation (19).

We confirmed the location of the cAMP-regulated region by using a dominant negative version of CREB that specifically inhibited the activity of only promoter constructs that include that region, but not of a shorter construct. A bioinformatics approach identified two putative CRE sites at that region, CRE1 and CRE2, whose critical role in mediating cAMP-dependent synergistic IL-10 transcription was established by point mutations. Surprisingly, the function of these adjacent CRE sites is completely inter-dependent. CRE1 and CRE2 have high and low affinities to CREB/ATF1 dimers, respectively, corresponding to their differential ability to mediate cAMP-dependent transcription from a heterologous promoter containing four copies of a single cis element. Interestingly, binding of the TF dimer to the weak CRE2 site does not increase the affinity of binding to the strong CRE1 site. It should be noted that the methodology used cannot exclude the opposite possibility that binding to the strong CRE1 site increases the affinity of binding to the weak CRE2 site. While our dominant negative approach blocks activity of both CREB and ATF1, the RNAi approaches specifically interfere with CREB and therefore suggest that CREB is more dominant than ATF1 in IL-10 induction, in line with a previous report (19). Consistently, there is a correlation between the magnitude of CRE1 and consensus CRE reporter activities in cells and their *in-vitro* binding affinities for CREB homodimers; yet, there is no such correlation with binding of ATF1-containing dimers. Taken together, these findings suggest that simultaneous binding of CREB dimers to the two adjacent CRE sites is required for synergistic IL-10 promoter activation at the early phase of co-stimulation by LPS and a cAMP-elevating agent.

As LPS activates the AP-1 transcription factor, which can potentially bind and activate CRE sites (40), it is important to note that the affinities of the two IL-10 promoter CRE sites for CREB/ATF1 are orders of magnitude higher than for AP-1 dimers and that these CREs were activated only by the cAMP pathway and not by LPS.

The two inter-dependent CRE sites are located within a 21 bp spacing (3' to 3' distance), which corresponds to two DNA helical turns. Therefore, the two CREB dimers are expected to be positioned closely and in parallel to each other, possibly interacting. This unique dual CRE arrangement also exists in the promoter of CREB itself, where two CRE half sites (TGACG) are distanced 21 bp apart from each other (3' to 3') and exhibit complete synergism (49), as we have shown for the IL-10 promoter CREs. Interestingly, in both the IL-10 and CREB promoters, the CRE sequences are imperfect, suggesting that the synergism between two 21 bp-spaced CRE sites results from or depends on relatively weak TF binding affinity to at least one of the sites. In contrast, the promoter of the human chorionic gonadotropin α -subunit is activated by cAMP via either of two perfect CRE consensus sequences that are distanced only 18 bp apart (3' to 3') and therefore the two CREB

dimers are non-parallel, have high affinity to both sites, and act independently (50). Cooperative interactions with additional proteins may be the mechanism of synergism between the two CRE sites at the IL-10 promoter. The coactivators CBP/p300 (51) and CRTC/TORC (52, 53) are recruited by CREB and act in concert at promoters of CREB target genes (54). Thus, one can envision that the concurrent binding of two CREB dimers to the proximate CRE1 and CRE2 sites at the IL-10 promoter facilitates recruitment of the multiple coactivators required for subsequent promoter activation.

While CRE1 is conserved in sequence and location between mouse and human, the mouse IL-10 promoter CRE2, discovered in this study, is not conserved (31). Interestingly, the mouse CRE2 is positioned equivalently to an AP-2 response element at the human IL-10 promoter (31). AP-2 activation is achieved by integration of cAMP-PKA and PKC signaling (55). As LPS activates PKC (56) it can be inferred that a co-stimulus of LPS and a cAMP inducer activates the AP-2 response element at the human promoter. Thus, it is intriguing that although CRE2 is not conserved, a location similarly distanced from a conserved CRE has been conserved for a TF that relays cAMP signaling, either by itself (mouse, -335/-329 bp) or in combination with LPS signaling (human, -337/-328 bp).

Regulation of the Mouse IL-10 Promoter by LPS

Brightbill et al. (26) showed that Sp1 is the major TF that mediates LPS-induced IL-10 transcription at 24 h and that it binds to a response element located at -89/-78 bp. We found that site to be regulated also in cells co-stimulated for 24 h with both LPS and a cAMP-elevating agent. Importantly, deletion of the -118/-78 bp region or site-directed mutagenesis markedly reduced IL-10 promoter reporter activities in both resting cells and stimulated cells. These results imply that Sp1 plays a critical role in both the basal transcription of IL-10 and in the inducible transcription caused by LPS and by LPS + isoproterenol, in line with a previous report (57). Consistently, Iyer et al. (3) found that the Sp1 site was critical for IL-10 reporter induction in LPS-stimulated RAW264.7 macrophages, but they showed that Sp1 is constitutively bound to the -89/-78 site at the chromosomal IL-10 promoter. Yet, we found that at 24 h LPS stimulated the activity of the promoter construct that contains the Sp1 response element (-118 bp) by an order of magnitude compared to resting cells, whereas a much smaller effect was observed for LPS at 3 h. This suggests that LPS significantly up-regulates Sp1 activity mainly at long incubations. Consistently, we showed that LPS stimulated expression of a reporter regulated by four copies of the IL-10 promoter Sp1 response element at 24 h, but not earlier. Furthermore, we show that IFN α also activates the minimal (-118 bp) promoter construct containing the Sp1 response element, and that autocrine type I IFN signaling mediates Sp1 reporter activation by LPS at the late phase. Taken together, the temporal correlation we found between Sp1 hyper-activation by LPS/type I IFN and loss of synergistic IL-10 induction by LPS and a cAMP-elevating agent insinuates that late Sp1 hyper-activation

by LPS via type I IFN obviates the requirement for cAMP signaling to achieve maximal IL-10 transcription and expression.

The Sp1-mutant IL-10 promoter reporter was still induced at least 5-fold by LPS, suggesting that additional cis elements are involved in LPS-induced IL-10 transcription. Indeed, the short -78 bp reporter that lacks the Sp1 site was positively regulated by LPS at 24 h. Accordingly, over-expression of the NF κ B p50 subunit in LPS-stimulated mouse macrophages amplified the activity of a short IL-10 promoter reporter that contains a specific p50-binding cis element located at -55/-46 bp in a CBP-dependent (29) and I κ B ζ -dependent (58) manner, while NF κ B p50 knockout in mice diminished IL-10 secretion (29). Consistently, we have previously reported that selective inhibitors of NF κ B p50 (but not p65) nuclear translocation blocked IL-10 secretion and reduced the activity of the short -78 bp IL-10 promoter reporter construct which contains the NF κ B p50 homodimer response element, but does not contain the upstream Sp1 and CRE sites (47).

In the current study we also found that the -938 bp 5'-deletion mutant of the IL-10 promoter reporter has reduced LPS-dependent activity relative to the full -1,538 bp construct both at 3 h and 24 h, suggesting that the -938/-1,538 region includes a site regulated by LPS at both early and late phases. Indeed, Iyer et al. (3) showed that STAT3 and STAT1 mediate type-I IFN-dependent LPS-stimulated IL-10 expression via a cis element located at -1,324/-1,319.

While the reporter gene assay, and in particular the 5'-deletion approach, is useful for the study of gene regulation as demonstrated here, some regulatory sites may be overlooked. Examples include when a given cis element functions only in concert with another cis element (and so deletion of the distal site may prevent identification of the proximal site), when two cis elements are partially redundant, or when proximate cis elements are included in a single deletion. Furthermore, epigenetic regulation is also overlooked when using reporter constructs, as shown for immune complexes which synergize with LPS to induce chromosomal IL-10 expression but not IL-10 reporter (59). Nevertheless, we recently showed that the direct regulation of LPS-stimulated IL-10 promoter reporter activity by cAMP adequately reflects regulation of IL-10 mRNA and protein expression by this pathway (11).

Mechanistic Basis for the Time-Dependency of Synergistic IL-10 Expression Amplification by cAMP

Both CRE and Sp1 mutations are detrimental for synergistic IL-10 reporter transcription at 3 h. The effect of Sp1 mutation is more pronounced in all other cellular states and time points. Early IL-10 expression by LPS alone depends mainly on Sp1 and to a lower extent on CRE, whereas during longer LPS stimulation, Sp1 activity becomes even more critical but CRE is irrelevant. Double mutation of the CRE and Sp1 sites reinforces the observations made by single mutations and highlights the synergism displayed between these two sites under all conditions

where CRE is relevant. Together, these results imply that cAMP-elevating agents up-regulate LPS-induced IL-10 transcription at short (3 h) and medium (8 h) periods in a synergistic manner, via cooperativity of the cAMP-regulated CRE sites with the constitutive Sp1 site which is only later up-regulated by LPS via type I IFN. In support, CREB and Sp1 were reported to synergistically drive transcription at the Na,K-ATPase β 1 promoter and to co-immunoprecipitate together with CBP (60). The interaction between CREB and Sp1 is likely to be indirect, as no direct binding was observed with recombinant proteins (61) and as both TFs independently bind CBP and TFIID (62). Moreover, the glutamine-rich domain of Sp1 can substitute for the equivalent Q2 domain of CREB in order to increase the DNA retention time governed by CREB's bZIP domain (63). Indeed, Zhang et al. (64) showed that cAMP induces activation of only a small and selective subset of the promoters which are occupied with phosphorylated CREB, and that this is reflected at the level of CBP recruitment which presumably depends on additional TFs to cooperate with CREB. We therefore propose that CREB and Sp1 synergize on the IL-10 promoter by stabilization of a complex involving these two TFs and co-activators (**Figure 7**). Notably, the Sp1 site appears to be mainly constitutive at the early phase, and therefore it is likely that additional LPS-regulated sites (such as those for p50 NF κ B homodimer and STAT1/3) are involved in the synergistic expression of IL-10.

We showed here that the cAMP pathway specifically amplifies only the low type I IFN-independent IL-10 promoter activation by LPS that occurs at the early phase, while the strong IL-10 induction by LPS at the late phase is largely indirect (type I IFN-dependent) and not amenable for up-regulation by the cAMP pathway. In this study we also explored the mechanism of LPS-stimulated IL-10 expression via autocrine type I IFN, and showed that IFN α can partially mimic LPS in late Sp1 activation, and that type I IFN receptor silencing blocks activation of the IL-10 promoter region containing Sp1. Taken together with the findings of time-dependent cooperativity at the promoter level discussed above, our data suggest a model (**Figure 7**) where the cAMP pathway can synergize at the IL-10 promoter, via novel tandem CREs, with Sp1 acting at a constitutive level and with the TFs directly activated by LPS (e.g., p50 NF κ B homodimer and STAT1/3), whereas the autocrine type I IFN loop dominates late LPS-stimulated IL-10 induction and prevents or obviates synergism with the cAMP pathway. Sp1 transcriptional activation by the autocrine type I IFN loop may explain, at least in part, the switch from synergistic IL-10 expression at the early phase to cAMP-insensitive IL-10 expression at the late phase. The time lag in IL-10 induction by LPS, resulting from the requirement for autocrine type I IFN, ensures a proportional inflammatory response to pathogen detection or tissue damage. However, certain pathogens manipulate the immune system to elevate IL-10 expression and reduce pro-inflammatory cytokine expression as a persistence mechanism (24). The accelerated induction of IL-10 when LPS-stimulated macrophages are exposed to a ligand of a GPCR upstream to the cAMP pathway prematurely diverts macrophages to

become anti-inflammatory and thus to diminish the innate immune response early at its inception. We recently evaluated the physiological effect of cAMP induction on IL-10 expression in a mouse septic shock model. We demonstrated that *in-vivo* administration of a macrophage-specific cAMP-elevating agent amplified early (but not late) LPS-induced IL-10 secretion to the serum, in accordance with the cell culture results (11). Selective knockout of β 2-AR in innate immune cells in mice promotes death from sepsis in response to administration of an otherwise sub-lethal LPS dose, while co-administration of IL-10 rescues the mice (10). A rapid and synergistic induction of IL-10 serum levels was also demonstrated in a controlled human study, where subjects were administered LPS and epinephrine (65). These studies imply that the cAMP-inducing drug epinephrine, routinely used in the clinic for the treatment of sepsis (66), may have a protective effect in part via acceleration of IL-10 expression by macrophages in synergism with LPS. However, this treatment might exacerbate sepsis-induced immunoparalysis, a term describing an acquired anti-inflammatory state preventing the clearance of the primary infection and increasing the vulnerability to a secondary infection (66). Thus, timely and proportional IL-10 expression is critical to achieve a balance between inflammation and resolution.

DATA AVAILABILITY

The datasets generated for this study are available on request to the corresponding author.

REFERENCES

1. Mosser DM, Edwards JP. Exploring the full spectrum of macrophage activation. *Nat Rev Immunol.* (2008) 8:958–69. doi: 10.1038/nri2448
2. Chang EY, Guo B, Doyle SE, Cheng G. Cutting edge: involvement of the type I IFN production and signaling pathway in lipopolysaccharide-induced IL-10 production. *J Immunol.* (2007) 178:6705–9. doi: 10.4049/jimmunol.178.11.6705
3. Iyer SS, Ghaffari AA, Cheng G. Lipopolysaccharide-mediated IL-10 transcriptional regulation requires sequential induction of type I IFNs and IL-27 in macrophages. *J Immunol.* (2010) 185:6599–607. doi: 10.4049/jimmunol.1002041
4. Bode JG, Ehrling C, Haussinger D. The macrophage response towards LPS and its control through the p38(MAPK)-STAT3 axis. *Cell Signal.* (2012) 24:1185–94. doi: 10.1016/j.cellsig.2012.01.018
5. Pattison MJ, Mackenzie KF, Arthur JS. Inhibition of JAKs in macrophages increases lipopolysaccharide-induced cytokine production by blocking IL-10-mediated feedback. *J Immunol.* (2012) 189:2784–92. doi: 10.4049/jimmunol.1200310
6. Baliu-Pique M, Jusek G, Holzmann B. Neuroimmunological communication via CGRP promotes the development of a regulatory phenotype in TLR4-stimulated macrophages. *Eur J Immunol.* (2014) 44:3708–16. doi: 10.1002/eji.201444553
7. Howes A, Taubert C, Blankley S, Spink N, Wu X, Graham CM, et al. Differential production of type I IFN determines the reciprocal levels of IL-10 and proinflammatory cytokines produced by C57BL/6 and BALB/c macrophages. *J Immunol.* (2016) 197:2838–53. doi: 10.4049/jimmunol.1501923

AUTHOR CONTRIBUTIONS

TZ conceived and coordinated the study and wrote the paper. OE and YG-G designed, performed, and analyzed most experiments, and OE also participated in writing the paper. BB and MA performed the experiment shown in **Figure 1B**. IB-D participated in several experiments. DG coordinated and YG designed, performed, and analyzed the experiments shown in **Table 1**. All authors reviewed the results and approved the final version of the manuscript.

FUNDING

This work was supported by grants from the United States – Israel Binational Science Foundation (BSF #2011360) and the European Commission (IRG #021862) to TZ and from the Israel Science Foundation (ISF #715/11) to DG.

ACKNOWLEDGMENTS

We are grateful to Dr. I.D.C. Fraser for the stable CREB-silenced cells, to Dr. S.T. Smale (UCLA, CA) for IL-10 promoter luciferase plasmids, to Dr. C. Vinson (NIH/CCR, MD) for a dominant negative A-CREB construct, and to Drs. G. Schreiber and A. Ariel for recombinant mouse IFN α . We thank A. Lilja, M. Avitan and Drs. I.D.C. Fraser, R. Margalit, P.E. Wright and M.R. Montminy for helpful discussions, and N. Silberstein and Dr. S. Katz for excellent technical help.

8. Hobbs S, Reynoso M, Geddis AV, Mitrophanov AY, and Matheny RW Jr. LPS-stimulated NF-kappaB p65 dynamic response marks the initiation of TNF expression and transition to IL-10 expression in RAW 264.7 macrophages. *Physiol Rep.* (2018) 6:e13914. doi: 10.14814/phy2.13914
9. Goldsmith M, Avni D, Ernst O, Glucksam Y, Levy-Rimler G, Meijler MM, et al. Synergistic IL-10 induction by LPS and the ceramide-1-phosphate analog PCERA-1 is mediated by the cAMP and p38 MAP kinase pathways. *Mol Immunol.* (2009) 46:1979–87. doi: 10.1016/j.molimm.2009.03.009
10. Agac D, Estrada LD, Maples R, Hooper LV, Farrar JD. The beta2-adrenergic receptor controls inflammation by driving rapid IL-10 secretion. *Brain Behav Immun.* (2018) 74:176–85. doi: 10.1016/j.bbi.2018.09.004
11. Ernst O, Glucksam-Galnoy Y, Athamna M, Ben-Dror I, Ben-Arosh H, Levy-Rimler G, et al. The cAMP pathway amplifies early MyD88-dependent and type I interferon-independent LPS-induced interleukin-10 expression in mouse macrophages. *Mediators Inflamm.* (2019) 2019:3451461. doi: 10.1155/2019/3451461
12. Tudor C, Marchese FP, Hitti E, Aubareda A, Rawlinson L, Gaestel M, et al. The p38 MAPK pathway inhibits tristetraprolin-directed decay of interleukin-10 and pro-inflammatory mediator mRNAs in murine macrophages. *FEBS Lett.* (2009) 583:1933–8. doi: 10.1016/j.febslet.2009.04.039
13. Teixeira-Coelho M, Guedes J, Ferreira P, Howes A, Pedrosa J, Rodrigues F, et al. Differential post-transcriptional regulation of IL-10 by TLR2 and TLR4-activated macrophages. *Eur J Immunol.* (2014) 44:856–66. doi: 10.1002/eji.201343734
14. Ma W, Lim W, Gee K, Aucoin S, Nandan D, Kozlowski M, et al. The p38 mitogen-activated kinase pathway regulates the human interleukin-10 promoter via the activation of Sp1 transcription factor in lipopolysaccharide-stimulated human macrophages. *J Biol Chem.* (2001) 276:13664–74. doi: 10.1074/jbc.M011157200

15. Caivano M, Cohen P. Role of mitogen-activated protein kinase cascades in mediating lipopolysaccharide-stimulated induction of cyclooxygenase-2 and IL-1 beta in RAW264 macrophages. *J Immunol.* (2000) 164:3018–25. doi: 10.4049/jimmunol.164.6.3018
16. Gonzalez GA, Montminy MR. Cyclic AMP stimulates somatostatin gene transcription by phosphorylation of CREB at serine 133. *Cell.* (1989) 59:675–80. doi: 10.1016/0092-8674(89)90013-5
17. Avni D, Ernst O, Philosoph A, Zor T. Role of CREB in modulation of TNFalpha and IL-10 expression in LPS-stimulated RAW264.7 macrophages. *Mol Immunol.* (2010) 47:1396–403. doi: 10.1016/j.molimm.2010.02.015
18. Mayr BM, Canetti G, Montminy MR. Distinct effects of cAMP and mitogenic signals on CREB-binding protein recruitment impart specificity to target gene activation via CREB. *Proc Natl Acad Sci USA.* (2001) 98:10936–41. doi: 10.1073/pnas.191152098
19. MacKenzie KE, Clark K, Naqvi S, McGuire VA, Noehren G, Kristariyanto Y, et al. PGE(2) induces macrophage IL-10 production and a regulatory-like phenotype via a protein kinase A-SIK-CRTC3 pathway. *J Immunol.* (2013) 190:565–77. doi: 10.4049/jimmunol.1202462
20. Koroskenyi K, Kiss B, Szondy Z. Adenosine A2A receptor signaling attenuates LPS-induced pro-inflammatory cytokine formation of mouse macrophages by inducing the expression of DUSP1. *Biochim Biophys Acta.* (2016) 1863 (7 Pt A):1461–71. doi: 10.1016/j.bbamcr.2016.04.003
21. Chi H, Barry SP, Roth RJ, Wu JJ, Jones EA, Bennett AM, et al. Dynamic regulation of pro- and anti-inflammatory cytokines by MAPK phosphatase 1 (MKP-1) in innate immune responses. *Proc Natl Acad Sci USA.* (2006) 103:2274–9. doi: 10.1073/pnas.0510965103
22. Mosser DM, Zhang X. Interleukin-10: new perspectives on an old cytokine. *Immunol Rev.* (2008) 226:205–18. doi: 10.1111/j.1600-065X.2008.00706.x
23. Saraiva M, O'Garra A. The regulation of IL-10 production by immune cells. *Nat Rev Immunol.* (2010) 10:170–81. doi: 10.1038/nri2711
24. Iyer SS, Cheng G. Role of interleukin 10 transcriptional regulation in inflammation and autoimmune disease. *Crit Rev Immunol.* (2012) 32:23–63. doi: 10.1615/CritRevImmunol.v32.i1.30
25. Chiang BT, Liu YW, Chen BK, Wang JM, Chang WC. Direct interaction of C/EBPdelta and Sp1 at the GC-enriched promoter region synergizes the IL-10 gene transcription in mouse macrophage. *J Biomed Sci.* (2006) 13:621–35. doi: 10.1007/s11373-006-9101-y
26. Brightbill HD, Plevy SE, Modlin RL, Smale ST. A prominent role for Sp1 during lipopolysaccharide-mediated induction of the IL-10 promoter in macrophages. *J Immunol.* (2000) 164:1940–51. doi: 10.4049/jimmunol.164.4.1940
27. Tone M, Powell MJ, Tone Y, Thompson SA, Waldmann H. IL-10 gene expression is controlled by the transcription factors Sp1 and Sp3. *J Immunol.* (2000) 165:286–91. doi: 10.4049/jimmunol.165.1.286
28. Liu J, Zhang H, Liu Y, Wang K, Feng Y, Liu M, et al. KLF4 regulates the expression of interleukin-10 in RAW264.7 macrophages. *Biochem Biophys Res Commun.* (2007) 362:575–81. doi: 10.1016/j.bbrc.2007.07.157
29. Cao S, Zhang X, Edwards JP, Mosser DM. NF-kappaB1 (p50) homodimers differentially regulate pro- and anti-inflammatory cytokines in macrophages. *J Biol Chem.* (2006) 281:26041–50. doi: 10.1074/jbc.M602222200
30. Wall EA, Zavzavadjian JR, Chang MS, Randhawa B, Zhu X, Hsueh RC, et al. Suppression of LPS-induced TNF-alpha production in macrophages by cAMP is mediated by PKA-AKAP95-p105. *Sci Signal.* (2009) 2:ra28. doi: 10.1126/scisignal.2000202
31. Platzer C, Fritsch E, Elsner T, Lehmann MH, Volk HD, Prosch S. Cyclic adenosine monophosphate-responsive elements are involved in the transcriptional activation of the human IL-10 gene in monocytic cells. *Eur J Immunol.* (1999) 29:3098–104.
32. Ananieva O, Darragh J, Johansen C, Carr JM, McIlrath J, Park JM, et al. The kinases MSK1 and MSK2 act as negative regulators of Toll-like receptor signaling. *Nat Immunol.* (2008) 9:1028–36. doi: 10.1038/ni.1644
33. Mellett M, Atzei P, Jackson R, O'Neill LA, Moynagh PN. Mal mediates TLR-induced activation of CREB and expression of IL-10. *J Immunol.* (2011) 186:4925–35. doi: 10.4049/jimmunol.1002739
34. Ahn S, Olive M, Aggarwal S, Krylov D, Ginty DD, Vinson C. A dominant-negative inhibitor of CREB reveals that it is a general mediator of stimulus-dependent transcription of c-fos. *Mol Cell Biol.* (1998) 18:967–77. doi: 10.1128/MCB.18.2.967
35. Smith ER, Jones PL, Boss JM, Merrill AH Jr. Changing J774A.1 cells to new medium perturbs multiple signaling pathways, including the modulation of protein kinase C by endogenous sphingoid bases. *J Biol Chem.* (1997) 272:5640–6. doi: 10.1074/jbc.272.9.5640
36. Fraser I, Liu W, Rebres R, Roach T, Zavzavadjian J, Santat L, et al. The use of RNA interference to analyze protein phosphatase function in mammalian cells. *Methods Mol Biol.* (2007) 365:261–86. doi: 10.1385/1-59745-267-X:261
37. Smith C. Cloning and mutagenesis: tinkering with the order of things. *Nat Meth.* (2007) 4:455–61. doi: 10.1038/nmeth0507-455
38. Glick Y, Orenstein Y, Avrahami D, Zor T, Shamir R, Gerber D. Integrated microfluidic approach for quantitative high-throughput measurements of transcription factor binding affinities. *Nucleic Acids Res.* (2016) 44:e51. doi: 10.1093/nar/gkv1327
39. Maerkl SJ, Quake SR. A systems approach to measuring the binding energy landscapes of transcription factors. *Science.* (2007) 315:233–7. doi: 10.1126/science.1131007
40. Manna PR, Stocco DM. Crosstalk of CREB and Fos/Jun on a single cis-element: transcriptional repression of the steroidogenic acute regulatory protein gene. *J Mol Endocrinol.* (2007) 39:261–77. doi: 10.1677/JME-07-0065
41. Fordyce PM, Gerber D, Tran D, Zheng J, Li H, DeRisi JL, et al. De novo identification and biophysical characterization of transcription-factor binding sites with microfluidic affinity analysis. *Nat Biotechnol.* (2010) 28:970–5. doi: 10.1038/nbt.1675
42. Glick Y, Avrahami D, Michaely E, Gerber D. High-throughput protein expression generator using a microfluidic platform. *J Vis Exp.* (2012) 66:e3849. doi: 10.3791/3849
43. Ben-Ari Y, Glick Y, Kipper S, Schwartz N, Avrahami D, Barbiro-Michaely E, et al. Microfluidic large scale integration of viral-host interaction analysis. *Lab Chip.* (2013) 13:2202–9. doi: 10.1039/c3lc00034f
44. Zor T, Selinger Z. Linearization of the Bradford protein assay increases its sensitivity: theoretical and experimental studies. *Anal Biochem.* (1996) 236:302–8. doi: 10.1006/abio.1996.0171
45. Ernst O, Zor T. Linearization of the Bradford protein assay. *J Vis Exp.* (2010) 38:e1918. doi: 10.3791/1918
46. Konkright MD, Guzman E, Flechner L, Su AI, Hogenesch JB, Montminy M. Genome-wide analysis of CREB target genes reveals a core promoter requirement for cAMP responsiveness. *Mol Cell.* (2003) 11:1101–8. doi: 10.1016/S1097-2765(03)00134-5
47. Avni D, Glucksam Y, Zor T. The phosphatidylinositol 3-kinase (PI3K) inhibitor LY294002 modulates cytokine expression in macrophages via p50 nuclear factor kappaB inhibition, in a PI3K-independent mechanism. *Biochem Pharmacol.* (2012) 83:106–14. doi: 10.1016/j.bcp.2011.09.025
48. Grainger JR, Wohlfert EA, Fuss IJ, Bouladoux N, Askenase MH, Legrand F, et al. Inflammatory monocytes regulate pathologic responses to commensals during acute gastrointestinal infection. *Nat Med.* (2013) 19:713–21. doi: 10.1038/nm.3189
49. Coven E, Ni Y, Widnell KL, Chen J, Walker WH, Habener JF, et al. Cell type-specific regulation of CREB gene expression: mutational analysis of CREB promoter activity. *J Neurochem.* (1998) 71:1865–74. doi: 10.1046/j.1471-4159.1998.71051865.x
50. Silver BJ, Bokar JA, Virgin JB, Vallen EA, Milsted A, Nilson JH. Cyclic AMP regulation of the human glycoprotein hormone alpha-subunit gene is mediated by an 18-base-pair element. *Proc Natl Acad Sci USA.* (1987) 84:2198–202. doi: 10.1073/pnas.84.8.2198
51. Chakravarti D, LaMorte VJ, Nelson MC, Nakajima T, Schulman IG, Juguilon H, et al. Role of CBP/P300 in nuclear receptor signalling. *Nature.* (1996) 383:99–103. doi: 10.1038/383099a0
52. Konkright MD, Canetti G, Screaton R, Guzman E, Miraglia L, Hogenesch JB, et al. TORCs: transducers of regulated CREB activity. *Mol Cell.* (2003) 12:413–23. doi: 10.1016/j.molcel.2003.08.013
53. Altarejos JY, Montminy M. CREB and the CRTC co-activators: sensors for hormonal and metabolic signals. *Nat Rev Mol Cell Biol.* (2011) 12:141–51. doi: 10.1038/nrm3072
54. Ravnskjaer K, Kester H, Liu Y, Zhang X, Lee D, Yates JR III, et al. Cooperative interactions between CBP and TORC2 confer selectivity to CREB

- target gene expression. *EMBO J.* (2007) 26:2880–9. doi: 10.1038/sj.emboj.7601715
55. Imagawa M, Chiu R, Karin M. Transcription factor AP-2 mediates induction by two different signal-transduction pathways: protein kinase C and cAMP. *Cell.* (1987) 51:251–60. doi: 10.1016/0092-8674(87)90152-8
 56. Monick MM, Carter AB, Flaherty DM, Peterson MW, Hunninghake GW. Protein kinase C zeta plays a central role in activation of the p42/44 mitogen-activated protein kinase by endotoxin in alveolar macrophages. *J Immunol.* (2000) 165:4632–9. doi: 10.4049/jimmunol.165.8.4632
 57. Liu YW, Tseng HP, Chen LC, Chen BK, Chang WC. Functional cooperation of simian virus 40 promoter factor 1 and CCAAT/enhancer-binding protein beta and delta in lipopolysaccharide-induced gene activation of IL-10 in mouse macrophages. *J Immunol.* (2003) 171:821–8. doi: 10.4049/jimmunol.171.2.821
 58. Horber S, Hildebrand DG, Lieb WS, Lorscheid S, Hailfinger S, Schulze-Osthoff K, et al. The atypical inhibitor of NF-kappaB, IkappaBzeta, controls macrophage interleukin-10 expression. *J Biol Chem.* (2016) 291:12851–61. doi: 10.1074/jbc.M116.718825
 59. Lucas M, Zhang X, Prasanna V, Mosser DM. ERK activation following macrophage FcgammaR ligation leads to chromatin modifications at the IL-10 locus. *J Immunol.* (2005) 175:469–77. doi: 10.4049/jimmunol.175.1.469
 60. Matlhagela K, Borsick M, Rajkhowa T, Taub M. Identification of a prostaglandin-responsive element in the Na,K-ATPase beta 1 promoter that is regulated by cAMP and Ca²⁺. Evidence for an interactive role of cAMP regulatory element-binding protein and Sp1. *J Biol Chem.* (2005) 280:334–46. doi: 10.1074/jbc.M411415200
 61. Shell SA, Fix C, Olejniczak D, Gram-Humphrey N, Walker WH. Regulation of cyclic adenosine 3',5'-monophosphate response element binding protein (CREB) expression by Sp1 in the mammalian testis. *Biol Reprod.* (2002) 66:659–66. doi: 10.1095/biolreprod66.3.659
 62. Asahara H, Santoso B, Guzman E, Du K, Cole PA, Davidson I, et al. Chromatin-dependent cooperativity between constitutive and inducible activation domains in CREB. *Mol Cell Biol.* (2001) 21:7892–900. doi: 10.1128/MCB.21.23.7892-7900.2001
 63. Mayr BM, Guzman E, Montminy M. Glutamine rich and basic region/leucine zipper (bZIP) domains stabilize cAMP-response element-binding protein (CREB) binding to chromatin. *J Biol Chem.* (2005) 280:15103–10. doi: 10.1074/jbc.M414144200
 64. Zhang X, Odom DT, Koo SH, Conkright MD, Canettieri G, Best J, et al. Genome-wide analysis of cAMP-response element binding protein occupancy, phosphorylation, and target gene activation in human tissues. *Proc Natl Acad Sci USA.* (2005) 102:4459–64. doi: 10.1073/pnas.0501076102
 65. van der Poll T, Coyle SM, Barbosa K, Braxton CC, Lowry SF. Epinephrine inhibits tumor necrosis factor-alpha and potentiates interleukin 10 production during human endotoxemia. *J Clin Invest.* (1996) 97:713–9. doi: 10.1172/JCI118469
 66. Stolk RF, van der Poll T, Angus DC, van der Hoeven JG, Pickkers P, Kox M. Potentially Inadvertent Immunomodulation: norepinephrine Use in Sepsis. *Am J Respir Crit Care Med.* (2016) 194:550–8. doi: 10.1164/rccm.201604-0862CP

Conflict of Interest Statement: The authors declare that the research was conducted in the absence of any commercial or financial relationships that could be construed as a potential conflict of interest.

Copyright © 2019 Ernst, Glucksam-Galnoy, Bhatta, Athamna, Ben-Dror, Glick, Gerber and Zor. This is an open-access article distributed under the terms of the Creative Commons Attribution License (CC BY). The use, distribution or reproduction in other forums is permitted, provided the original author(s) and the copyright owner(s) are credited and that the original publication in this journal is cited, in accordance with accepted academic practice. No use, distribution or reproduction is permitted which does not comply with these terms.



The Two Faces of Tumor-Associated Macrophages and Their Clinical Significance in Colorectal Cancer

Marta L. Pinto^{1,2,3,4}, Elisabete Rios^{1,5,6,7}, Cecília Durães^{1,5}, Ricardo Ribeiro^{1,2,8,9}, José C. Machado^{1,5,6}, Alberto Mantovani^{10,11}, Mário A. Barbosa^{1,2,3}, Fatima Carneiro^{1,5,6,7} and Maria J. Oliveira^{1,2,6*}

¹ I3S-Instituto de Investigação e Inovação em Saúde, Universidade do Porto, Porto, Portugal, ² INEB-Institute of Biomedical Engineering, University of Porto, Porto, Portugal, ³ Institute of Biomedical Sciences Abel Salazar (ICBAS), University of Porto, Porto, Portugal, ⁴ CNC-Center for Neuroscience and Cell Biology, University of Coimbra, Coimbra, Portugal, ⁵ IPATIMUP-Institute of Molecular Pathology and Immunology of the University of Porto, Porto, Portugal, ⁶ Department of Pathology, Faculty of Medicine, University of Porto, Porto, Portugal, ⁷ Department of Pathology, Centro Hospitalar São João, Porto, Portugal, ⁸ Laboratory of Genetics and Environmental Health Institute, Faculty of Medicine, University of Lisbon, Lisbon, Portugal, ⁹ Department of Clinical Pathology, Centro Hospitalar e Universitário de Coimbra, Coimbra, Portugal, ¹⁰ Humanitas Clinical and Research Center, Milan, Italy, ¹¹ Humanitas University, Milan, Italy

OPEN ACCESS

Edited by:

Kate E. Lawlor,
Hudson Institute of Medical
Research, Australia

Reviewed by:

Tracy Putoczki,
Walter and Eliza Hall Institute of
Medical Research, Australia
Una Riekstina,
University of Latvia, Latvia

*Correspondence:

Maria J. Oliveira
mariajo@ineb.up.pt

Specialty section:

This article was submitted to
Cancer Immunity and Immunotherapy,
a section of the journal
Frontiers in Immunology

Received: 23 May 2019

Accepted: 24 July 2019

Published: 20 August 2019

Citation:

Pinto ML, Rios E, Durães C, Ribeiro R, Machado JC, Mantovani A, Barbosa MA, Carneiro F and Oliveira MJ (2019) The Two Faces of Tumor-Associated Macrophages and Their Clinical Significance in Colorectal Cancer. *Front. Immunol.* 10:1875. doi: 10.3389/fimmu.2019.01875

Macrophages are one of the immune populations frequently found in colorectal tumors and high macrophage infiltration has been associated with both better and worst prognosis. Importantly, according to microenvironment stimuli, macrophages may adopt different polarization profiles, specifically the pro-inflammatory or M1 and the anti-inflammatory or M2, which display distinct functions. Therefore, concomitantly with the number of tumor-associated macrophages (TAMs), their characterization is fundamental to unravel their relevance in cancer. Here, we profiled macrophages in a series of 150 colorectal cancer (CRC) cases by immunohistochemistry, using CD68 as a macrophage lineage marker, CD80 as a marker of pro-inflammatory macrophages, and CD163 as a marker of anti-inflammatory macrophages. Quantifications were performed by computer-assisted analysis in the intratumoral region, tumor invasive front, and matched tumor adjacent normal mucosa (ANM). Macrophages, specifically the CD163⁺ ones, were predominantly found at the tumor invasive front, whereas CD80⁺ macrophages were almost exclusively located in the ANM, which suggests a predominant anti-inflammatory polarization of TAMs. Stratification according to tumor stage revealed that macrophages, specifically the CD163⁺ ones, are more prevalent in stage II tumors, whereas CD80⁺ macrophages are predominant in less invasive T1 tumors. Specifically in stage III tumors, higher CD68, and lower CD80/CD163 ratio associated with decreased overall survival. Importantly, despite the low infiltration of CD80⁺ cells in colorectal tumors, multivariate logistic regression revealed a protective role of these cells regarding the risk for relapse. Overall, this work supports the involvement of distinct microenvironments, present at the intra-tumor, invasive front and ANM regions, on macrophage modulation, and uncovers their prognostic value, further supporting the relevance of including macrophage profiling in clinical settings.

Keywords: colorectal cancer, tumor immunomodulation, tumor-associated macrophages, human macrophage surface markers, macrophage polarization, prognostic and tumor relapse

INTRODUCTION

A variety of non-malignant stromal cells present at the complex tumor microenvironment are active players in cancer progression (1). Specifically in solid tumors, tumor associated macrophages (TAMs) are one of the most represented populations (2) and have important roles in the invasive, angiogenic, and metastatic processes (3, 4).

Macrophages are extremely plastic cells that are able to respond and adapt to external stimuli (5). Currently, the most accepted model of macrophage classification describes several polarization statuses between two extreme populations: the M1-like or pro-inflammatory, and the M2-like or anti-inflammatory. In the presence of factors such as lipopolysaccharide (LPS), interferon (IFN)- γ or tumor necrosis factor (TNF)- α (6), macrophages adopt a pro-inflammatory phenotype, with high antigen presenting capacity and production of cytokines such as interleukin (IL)-6, IL-12, TNF- α , IFN- γ , and reactive oxygen species (ROS). These cells are known for their bactericidal and pro-inflammatory functions (7). On the other extreme of the spectrum are the M2-macrophages, induced by factors such as IL-4, IL-13, IL-10 or glucocorticoids, which produce anti-inflammatory cytokines, specifically transforming growth factor (TGF)- β and IL-10 (8). They are characterized by their scavenger, angiogenic, and pro-invasive properties (3, 4). As a consequence of the immunosuppressive tumor microenvironment, namely due to high IL-10 and TGF- β levels (9, 10), TAMs are reported to adopt features common to M2-like macrophages. They generally produce growth factors, chemokines, and matrix metalloproteinases (MMPs), which act directly on cancer cells or in other stromal cells, ultimately leading to tumor growth, invasion, and metastasis (3).

Several clinical and epidemiological studies have described a strong association between TAMs infiltration, worst prognosis and shorter survival in melanoma, breast, and ovarian cancer (11–15). In the specific case of colorectal cancer (CRC), some studies conclude that higher macrophage infiltration correlates with more advanced tumor stages (16) and worst prognosis (17), while others report that TAMs are associated with improved survival, specifically in the colon (18), and with reduced liver metastasis (19). Taken together, these findings suggest lack of agreement on the role of TAMs on CRC clinical course. Importantly, the majority of these studies were solely based on CD68, a macrophage lineage marker, without taking into consideration differences amongst the distinct pro- or anti-inflammatory subpopulations. Recognizing the importance of macrophage polarization, some authors analyzed markers which discriminate between M1 and M2 subpopulations. In this sense, Algars et al. (20) recently proposed that the type and distribution of TAMs may influence the carcinogenic process, ultimately affecting survival. In less advanced tumor stages, macrophage infiltration was associated with improved disease free survival, whereas, in stage IV CRC, high number of CLEVER-1/Stabilin-11⁺ cells, used as an M2-marker, correlated with shorter disease-free survival (20). A recent meta-analysis performed in head and neck squamous cell carcinoma reinforced the need to evaluate macrophage subsets: CD68 did not present any prognostic association,

contrarily to what was observed for CD163 which correlated with decreased survival (21). Nevertheless, in both studies, anti-inflammatory macrophages were not evaluated. Reports using nitric oxide synthase 2 (NOS2) as a M1 macrophages marker and CD163 as a M2 macrophage marker, yielded controversial results (22, 23). Although NOS2 has been frequently used to identify pro-inflammatory macrophages in mice, many research groups argued that differences in human nitric oxide metabolism likely preclude using it as an appropriate marker to identify M1 macrophages (24–26). Other limitations of published studies are related to the use of tissue microarrays (which may not accurately represent the characteristics of the tumor), the evaluation of hotspots (an approach that already presents some bias in the analysis) and the use of a semiquantitative scoring (which results in more subjective and less sensitive method).

In this study we performed a quantitative evaluation of the distinct macrophage subpopulations present in CRC, using CD68, CD80 and CD163 lineage, pro- and anti-inflammatory surface markers, respectively, in consecutive histological slides. Quantifications were performed in the intratumoral region (IT), tumor invasive front (IF), and tumor adjacent normal mucosa (ANM) of the same patient, to elucidate how the distinct region microenvironments may modulate macrophages. Histological profiling was then combined with clinicopathological and follow-up data, in order to unravel the clinical impact of distinct macrophage subpopulations within colorectal tumors, and discriminate which patients may benefit from immunotherapies targeting macrophages.

MATERIALS AND METHODS

Clinical Samples

One hundred and fifty CRC primary tumors (83 males and 67 females, median age 70.5 years old, range 22–93 years), containing in the same histological section tumor and normal mucosa, were retrieved from the files of the Pathology Department from Centro Hospitalar Universitário São João (CHUSJ, Porto, Portugal). Samples were collected during primary tumor surgical resections between 2007 and 2012. Synchronous tumors were not included.

All clinicopathological evaluations, including stage, grade, tumor type and lymphocytic infiltrate, were performed by experienced pathologists from the CHUSJ Pathology Department and are included in **Table 1**. The existence of tumor relapses, the therapeutic scheme and patient overall survival is also included. In this retrospective cohort, only five patients received pre-operative chemotherapy, of which three also received pre-operative radiotherapy. From the initial cohort, clinical data for survival analyses was obtained for 136 patients. The study was approved by the CHUSJ Ethics Committee for Health (References 259 and 260/11), in agreement with the Helsinki declaration. Informed consent was obtained from all the participants.

Immunohistochemical Staining

Specimens were fixed in formalin and embedded in paraffin in accordance with the routine protocol implemented at the

TABLE 1 | Patients' clinicopathological information.

Characteristics	No. of patients (%)
Age, median (IQR)	70.5 (62.0–79.0)
Gender, M/F	83 (55.3)/67 (44.7)
ANATOMIC TUMOR REGION	
Cecum	11 (7.3)
Ascending colon	25 (16.7)
Transverse colon	21 (14.0)
Descending colon	11 (7.3)
Sigmoid	53 (35.3)
Rectum	29 (19.3)
PATHOLOGICAL STAGE, TNM	
Tumor	
T1	9 (6.0)
T2	25 (16.7)
T3	93 (62.0)
T4	23 (15.3)
Nodes	
N0	85 (56.7)
N+	65 (43.3)
Metastasis	
M0	121 (80.7)
M+	29 (19.3)
CLINICAL STAGE	
I	26 (17.4)
II	51 (34.0)
III	44 (29.3)
IV	29 (19.3)
LYMPHOCYTIC INFILTRATION	
Absent/mild	92 (61.3)
Moderate/strong	58 (38.7)
ADJUVANT RADIOTHERAPY	
No	135 (90)
Yes	14 (9.3)
Unknown	1 (0.7)
ADJUVANT CHEMOTHERAPY	
No	81 (54)
Yes	69 (46)
RELAPSE	
No	132 (88.0)
Yes	17 (11.3)
Missing	1 (0.7)
SURVIVAL	
Alive	76 (50.7)
Death	60 (40.0)
Unknown	14 (9.3)
CAUSE OF DEATH	
Cancer-related	29 (19.3)
Other causes	27 (18)
Missing	4 (2.7)

IQR, interquartile range; M, male; F, female; No, number.

Pathology Department from CHUSJ. Sequential 5 μ m sections, from the most representative tumor region and selected by a Pathologist, were stained with antibodies against CD68 (Dako, PG-M1), CD80 (R&D, MAB140), and CD163 (Novocastra,

MRQ-26). Briefly, tissues were deparaffinized, hydrated and endogenous peroxidase activity was blocked with 3% methanol in hydrogen peroxide for 10 min. Following antigen retrieval in a water bath at 98°C with Tris EDTA, pH9 (CD68, 20 min) or citrate buffer, pH6 (CD80, 20 min; CD163, 40 min), primary antibodies were incubated as follows: CD80 overnight (1:50) at 4°C, CD68 30 min (1:100) and CD163 30 min (1:100), both at room temperature. After washing, labeled polymer secondary antibody (Envision Detection System, Dako) was added to slides and peroxidase activity was detected using diaminobenzidine (DAB) –tetrahydrochloride liquid plus substrate Chromogen System (Dako). The reaction was stopped with distilled water and sections were counterstained with haematoxylin and mounted in Richard-Allan Scientific Mounting Medium (ThermoFisher).

Macrophage Quantification

Following immunohistochemistry, the slides were digitalized using a NanoZoomer 2.0HT Hamamatsu camera (Meyer Instruments). For each marker, ten random areas of the ANM, IT, and IF were photographed (20x magnification). Using FIJI/IMAGEJ software, the immunoreactive area (IRA) for each cell surface marker and each region was calculated on the basis of red, green and blue segmentation, and represented as a percentage of the immunoreactive area (IRA%). Afterwards, the mean of the 10 distinct microscopic fields was calculated for each marker in each region. Importantly, the images of the three markers were acquired in the same area from consecutive sections.

Statistical Analysis

Statistical analyses were conducted in STATA version 12.0 (StataCorp, College Station, Texas) or GraphPad Prism Software v5 (GraphPad-trial version). Departure from normality was determined using the Shapiro-Wilk test. Descriptive statistics included count and frequencies for categorical variables and median with interquartile range for continuous variables. Comparison of macrophage populations between and within locations in the tumor region was performed using Friedman's test followed by inter-group comparisons with Wilcoxon test. Comparisons between left and right colon side were performed with Mann-Whitney *U*-test while Kruskal-Wallis with Dunns multiple comparisons correction was applied in the analysis according to stage and primary tumor invasiveness. Kaplan-Meier plots with survival curves were compared with Log-rank test. The strength of associations between continuous variables was tested using Spearman's rank correlation. Association between macrophage populations and location with relapse followed a multistep statistical procedure: first, empirical analyses with unconditional logistic regression adjusting for age and gender, were carried out to uncover the relevant independent variables to be included in subsequent multivariate models (*p* for retention > 0.05); then, multivariate logistic regression was conducted to assess the independent strength of association of macrophage's characteristics in predicting risk for CRC progression. Lastly, in order to confirm the strength of association of the results emerging from multivariate

analysis, bootstrapping analysis was performed using Monte Carlo simulations ($n = 1,000$).

RESULTS

CD68⁺ and CD163⁺ Cells Are Predominantly Found Within the Tumor Invasive Front Whereas CD80⁺ Cells Are Mainly Located in the Tumor Adjacent Normal Mucosa

Given the difficulty in accurately assessing macrophage number using the classical approach of counting cells under the microscope, macrophage populations were evaluated by digitally quantifying the percentage of IRA%, similarly to what was carried out by other groups (**Supplementary Figure 1**) (27, 28). Three markers were used to characterize macrophages: CD68, a macrophage lineage marker broadly used to identify these immune cells (16, 18, 20), CD80, a co-stimulatory molecule expressed by pro-inflammatory macrophages (29), and CD163, a scavenger receptor associated with anti-inflammatory macrophages (30). Quantifications were performed in three regions: the ANM, the IT and the IF (**Figure 1**). Macrophages are mainly located at the IF of colorectal tumors comparing with the IT (5.23 vs. 2.59%) (18, 31), and the ANM (2.27%) (**Figure 2A** and **Table 2**). CD163⁺ cells are also predominantly found at the IF (1.65%), whereas the ANM exhibits a higher density of these anti-inflammatory cells than the IT region (1.04 vs. 0.63%) (**Figure 2A** and **Table 2**). Notably, CD80 is almost exclusively located in the ANM (1.31%). In the tumor regions, CD80 staining is very low and, similarly to the other markers evaluated, its expression is higher in the IF than in the IT (0.12 vs. 0.04%) (**Figure 2A** and **Table 2**). In the three regions analyzed, Spearman's rank correlation test revealed a moderate association between CD68 and CD163 staining ($r_s > 0.5$), suggesting that tumors with higher levels of CD68 also present higher infiltration of CD163⁺ cells (**Supplementary Table 1**).

Since the quantifications for each marker were performed in consecutive sections of the same area, the percentage of pro-inflammatory and anti-inflammatory cells among the

overall macrophage population was assessed calculating the ratio between CD80 and CD68 or CD163 and CD68 expression (**Figure 2B** and **Table 2**). Interestingly, at the ANM, CD80 staining represented almost 75% of the total CD68 staining. Of note, some of the cases studied had a higher CD80 IRA% compared with CD68, suggesting that CD80 is not exclusively expressed by macrophages. Within the IT and IF, the percentage of cells expressing CD80 relatively to CD68 decreased to ~ 2 and 3.45%, respectively. As for CD163, its expression represents about 50% of the total CD68 staining in ANM. Despite the increase of CD163⁺ cells at the IF, their percentage relatively to CD68 expression is still lower than what was observed in ANM (38.7%). Taken together, these observations demonstrate the presence of a significant number of macrophages at the IF and IT regions that do not express CD80 or CD163.

The ratio CD80/CD163 was also calculated to evaluate the proportion between pro- and anti-inflammatory macrophages (**Figure 2C** and **Table 2**). In the ANM, CD80 expression is 1.5 times higher compared to CD163. Conversely, both in IT and IF, CD163 expression is 10 times higher than CD80. Spearman's test revealed a positive association regarding CD80/CD163 ratio between IT and IF ($r_s = 0.57$) (**Supplementary Table 1**), suggesting that specimens with lower CD80/CD163 ratio at the IT region, are also the ones with a lower CD80/CD163 ratio at the IF.

Adjacent Normal Mucosa and Tumors in the Right-Sided Colon Exhibit Higher Macrophage Infiltration

Given the known differences between the right and left-sided colon, not only in terms of anatomy and genetic alterations but also considering the microbiota present (32), macrophage populations in both locations were compared (**Supplementary Table 2**). Interestingly, CD68, CD80, and CD163 infiltration was higher in the ANM of tumors in the right than in the left-sided colon. Increased infiltration was also observed for CD68 and CD163 in the IT. Nevertheless, at the IF, the previously described differences between left and right-sided colon are lost for the three macrophage markers analyzed.

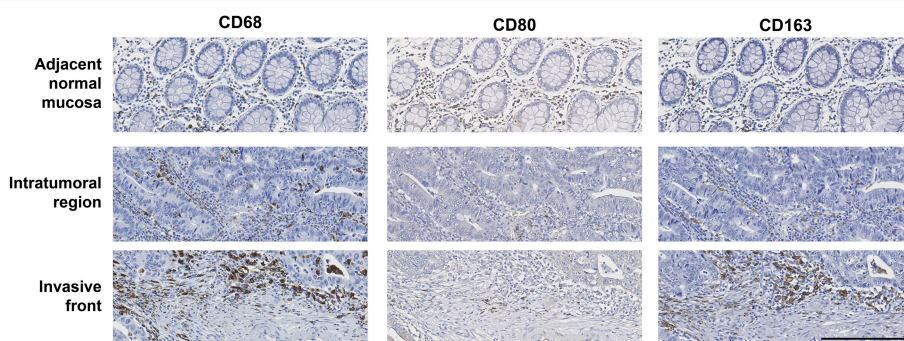


FIGURE 1 | Immunostaining of CD68, CD80, and CD163 in the tumor adjacent normal mucosa, intratumoral region and invasive front of a representative colorectal cancer case, in consecutive paraffin-embedded sections. Specifically, it belongs to a stage IIa colorectal tumor in the ascending colon. Scale bar = 200 μ m.

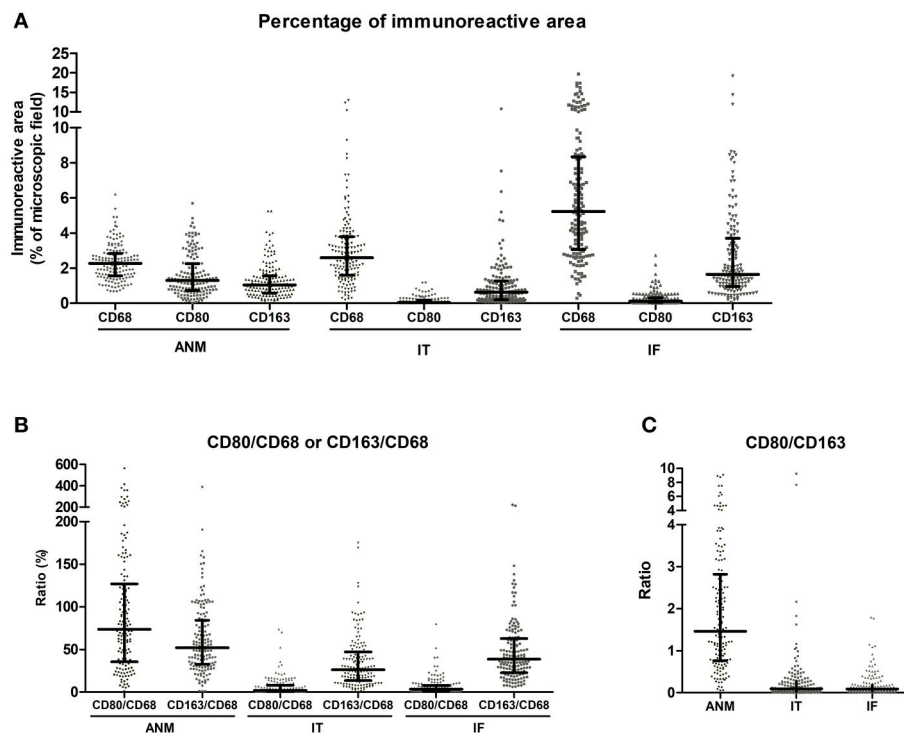


FIGURE 2 | Quantifications of CD68, CD80 and CD163 in the 150 colorectal cancer cases. **(A)** Percentage of immunoreactive area (IRA%) of CD68, CD80, and CD163 in the tumor adjacent normal mucosa (ANM), intratumoral region (IT) and invasive front (IF). **(B)** Percentage of CD80/CD68 and CD163/CD68 ratios in the ANM, IT, and IF calculated from the IRA%. **(C)** CD80/CD163 ratio in the ANM, IT and IF calculated from the IRA%. Each dot represents one patient, calculated by averaging the quantification of 10 areas. Median and inter-quartile range are also included.

TABLE 2 | Comparisons of percentage of immunoreactive area (IRA%) for CD68, CD80 and CD163, and CD80/CD68, CD163/CD68, and CD80/CD163 ratios in the adjacent normal mucosa, intratumoral region and invasive front.

	Adjacent normal mucosa	Intratumoral region	Invasive front	p value*
CD68	2.27	2.59	5.23	$p < 0.0001^a$
(IRA %)	(1.56–2.83)	(1.60–3.79)	(3.05–8.34)	
CD80	1.31	0.04	0.12	$p < 0.0001^b$
(IRA %)	(0.73–2.26)	(0.01–0.17)	(0.04–0.31)	
CD163	1.04	0.63	1.65	$p < 0.0001^c$
(IRA %)	(0.57–1.57)	(0.20–1.26)	(0.96–3.70)	
CD80/68	73.75	2.06	3.45	$p < 0.0001^d$
ratio (%)	(35.64–127.05)	(0.70–8.22)	(1.12–7.91)	
CD163/68	51.98	26.16	38.69	$p < 0.0001^e$
ratio (%)	(32.50–84.32)	(13.47–47.17)	(22.72–62.87)	
CD80/163	1.47	0.10	0.09	$p < 0.0001^f$
ratio	(0.76–2.82)	(0.03–0.28)	(0.04–0.19)	

Data presented as median and inter-quartile range.

*Friedman's test. Group comparisons using the Wilcoxon test.

^aANM vs. IT ($p = 4.70 \times 10^{-4}$), ANM vs. IF ($p = 3.65 \times 10^{-22}$), IT vs. IF ($p = 4.80 \times 10^{-19}$).

^bANM vs. IT ($p = 8.11 \times 10^{-26}$), ANM vs. IF ($p = 2.36 \times 10^{-25}$), IT vs. IF ($p = 2.22 \times 10^{-9}$).

^cANM vs. IT ($p = 5.36 \times 10^{-5}$), ANM vs. IF ($p = 1.55 \times 10^{-11}$), IT vs. IF ($p = 5.21 \times 10^{-21}$).

^dANM vs. IT ($p = 2.30 \times 10^{-26}$), ANM vs. IF ($p = 3.05 \times 10^{-26}$), IT vs. IF ($p = 0.089$).

^eANM vs. IT ($p = 1.97 \times 10^{-13}$), ANM vs. IF ($p = 1.46 \times 10^{-5}$), IT vs. IF ($p = 7.95 \times 10^{-9}$).

^fANM vs. IT ($p = 2.45 \times 10^{-24}$), ANM vs. IF ($p = 2.76 \times 10^{-26}$), IT vs. IF ($p = 0.155$).

IRA, immunoreactive area.

Stage II Tumors Have Higher Infiltration of CD68⁺ and CD163⁺ Cells Whereas CD80⁺ Cells Are More Abundant in T1 Tumors

Macrophage scores were then assessed according to tumor stage (Figure 3A). For the three markers analyzed, there were no differences in the ANM among the distinct CRC stages. Conversely, CD68⁺ and CD163⁺ macrophages were significantly more abundant at both IF and IT regions of stage II comparing with stage IV tumors. No differences were observed for CD80.

In a more profound analysis, macrophage populations were separately analyzed based on the primary tumor depth of invasion (Figure 3B). Interestingly, CD80⁺ cells were more frequent in the IT and IF of the less invasive T1 tumors. This was not observed in CD68⁺ or in CD163⁺ cells, which appear to predominantly infiltrate T3 tumors, although no statistical significant differences were detected.

Higher CD68 Expression in Stage III Colorectal Tumors Is Associated With Decreased Overall Survival

In CRC, the data regarding macrophage infiltration and patient survival is contradictory (17, 18). In order to perform this analysis, the IRA% for each marker was stratified into two

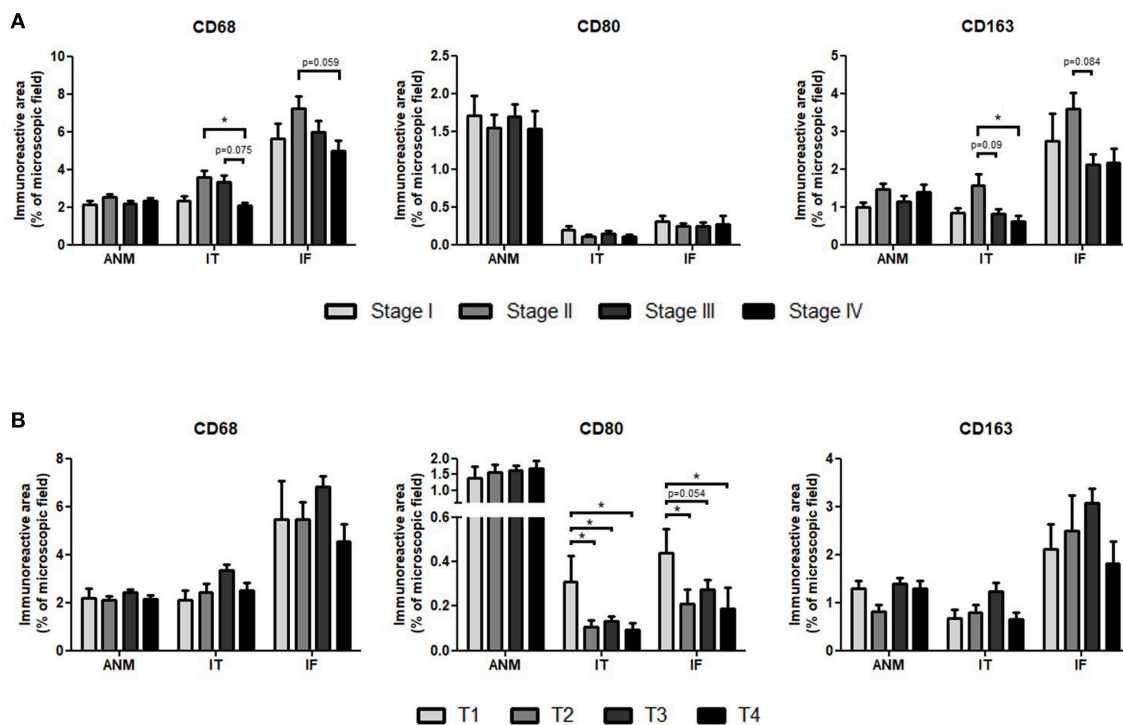


FIGURE 3 | Percentage of Immunoreactive area of CD68, CD80, and CD163 in the adjacent normal mucosa (ANM), intratumoral region (IT) and invasive front (IF) according to (A) tumor stage or (B) primary tumor invasive depth. Results are presented as mean and standard error of the mean (SEM). Stage I = 26 patients; Stage II = 51 patients; Stage III = 44 patients; Stage IV = 29 patients. T1 = 9 patients; T2 = 25 patients; T3 = 93 patients; T4 = 23 patients. * $p < 0.05$, Kruskal-Wallis with Dunn's multiple comparisons.

categories according to the median, as low and high-expressing. When all patients were included in survival analysis, no differences were observed regardless of the marker or region analyzed (data not shown). Moreover, analyses conducted in colon cancer patients, excluding rectum malignancy, also yielded no relationship of markers and survival (data not shown). Given that our retrospective cohort includes all tumor stages, with different prognosis, the association between macrophages and survival was evaluated considering stages I + II, stage III, and stage IV separately. Specifically in stage III tumors, higher infiltration of CD68⁺ cells in the IT was associated with decreased overall survival (Figure 4A). This was no longer observed in the IF (Figure 4B), nor regarding CD80 or CD163 expression (Figures 4C–F). The association between patients overall survival and the CD80/CD163 ratio was also assessed. In stage III tumors, although not statistically significant, there seems to be an association between higher CD80/CD163 ratio in the IF and improved overall survival (Figure 4H). This result suggests that, in stage III, a higher proportion between pro and anti-inflammatory cells, may represent a survival advantage. It would be interesting to perform the same analysis in a bigger cohort to validate these results.

Lower CD80 Infiltration Is Associated With Increased Relapse

Local recurrence is a frequent concern in CRC treatment (33) and efforts are being made to discover factors that might help predict such risk (34). Among the 150 cases of our series, 17 experienced relapse. No differences were detected in the percentage of CD68⁺ or CD163⁺ macrophage infiltration between patients with vs. without relapse, in the three regions analyzed. Conversely, specimens from patients without relapse, presented a significantly higher CD80 IRA% in both the IT ($p = 0.016$) and in the IF ($p = 1.16 \times 10^{-7}$). Univariate logistic regression revealed an association between higher CD80 staining at the IF and a decreased risk for relapse (Table 3). This finding was further confirmed on multivariate logistic regression that included only variables with significant risk and validated by bootstrap analysis (Supplementary Table 3). Overall, these results support a protective role of CD80⁺ cells at the IF of colorectal tumors for relapse.

Surprisingly, radiotherapy revealed a significant association with increased risk of relapse in multivariate analyses, further confirmed through bootstrapping. This may be related, not to the therapy itself, but to the specific characteristics of the colorectal tumors candidate for this therapeutic approach.

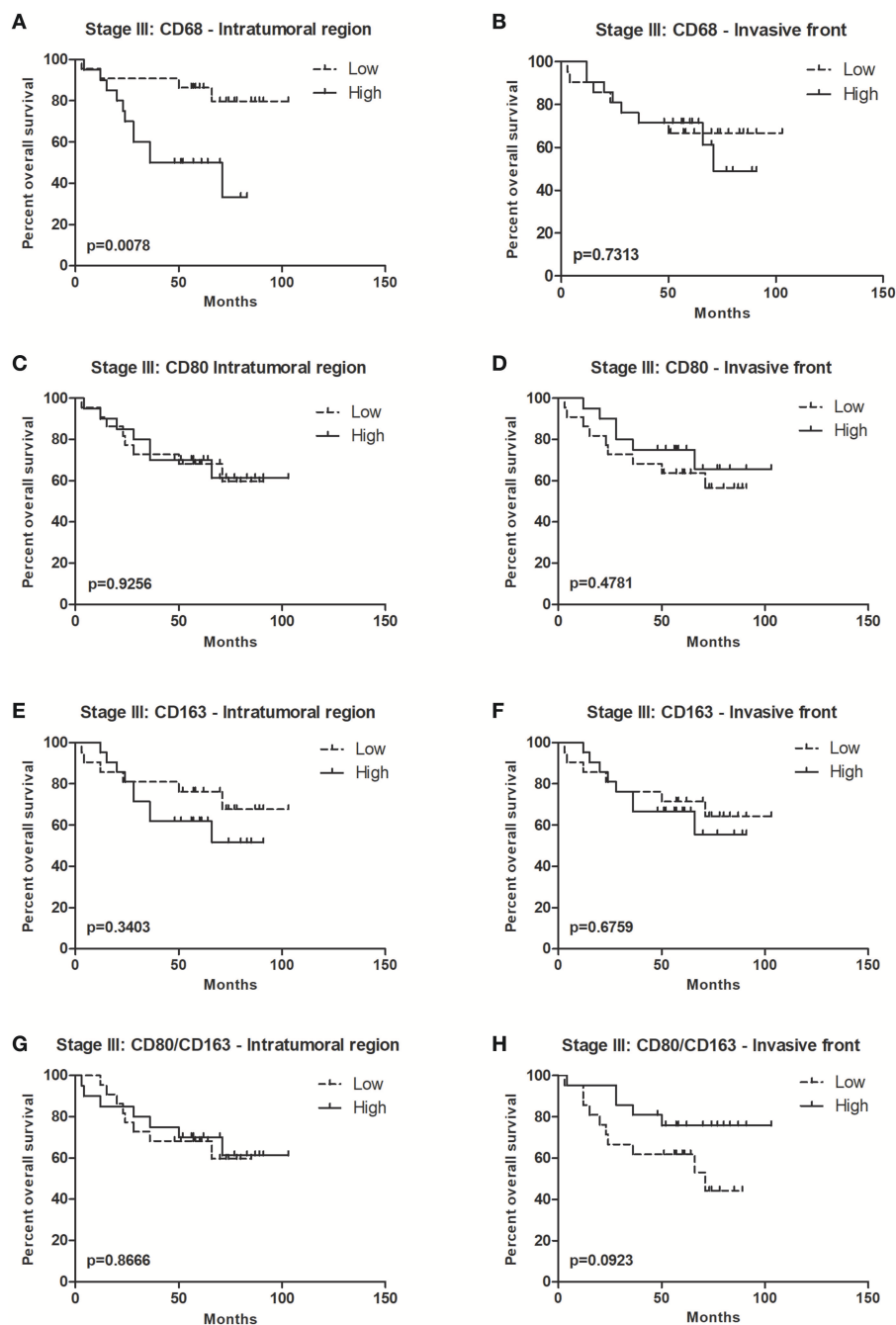


FIGURE 4 | Overall survival curves for stage III colorectal cancer patients. Forty-four stage III CRC patients were divided into two groups, low, and high, according to the median of immunoreactive area percentage for each marker: **(A)** CD68, **(C)** CD80, **(E)** CD163, and **(G)** CD80/CD163 ratio in the intratumoral region, and **(B)** CD68 **(D)** CD80, **(F)** CD163, and **(H)** CD80/CD163 ratio in the invasive front. Kaplan-Meier plots and curves were compared through Log-rank test.

DISCUSSION

Innate immune cells present at the tumor microenvironment may participate in several stages of cancer progression (28, 35, 36). In particular, TAMs play an important role in tumorigenesis (4) and, although controversy, high levels of macrophage

infiltration have been associated with poor prognosis and reduced therapy response, in distinct types of tumors.

In CRC, increased infiltration of lymphocytic cells correlates with improved clinical outcome. Higher infiltration of T cells (CD3⁺), cytotoxic T cells (CD8⁺), and memory T cells (CD45RO⁺) has been associated with longer disease-free and/or

TABLE 3 | Empirical univariate analysis of independent variables, clinicopathological and macrophage markers, in association with risk for disease relapse with adjustment for age and gender.

Variables	Risk for disease relapse	
	OR (95 CI)	p value
Tumor anatomic region	1.60 (1.04–2.40)	0.032
Clinical stage	0.68 (0.30–1.90)	0.461
Radiotherapy	18.2 (5.30–61.90)	<0.0001
Chemotherapy	3.00 (0.94–9.50)	0.062
ANM*		
CD68	0.92 (0.55–1.55)	0.757
CD80	0.85 (0.53–1.37)	0.502
CD163	0.91 (0.52–1.61)	0.757
IT*		
CD68	1.09 (0.87–1.36)	0.453
CD80	0.02 (0.00–4.40)	0.153
CD163	0.74 (0.40–1.38)	0.346
IF*		
CD68	0.93 (0.81–1.08)	0.365
CD80	0.001 (0.00–0.48)	0.030
CD163	0.82 (0.61–1.13)	0.191

OR, odds ratio; 95CI, 95% confidence interval; ANM, adjacent normal mucosa; IT, intratumoral region; IF, invasive front; *analyzed as continuous variables. Statistical significant associations are marked in bold.

overall survival (37). Moreover, the Immunoscore, based on the quantification of lymphocyte populations (CD3/CD8, CD3/CD45RO, or CD8/CD45RO), demonstrated higher robustness and prognostic value than the classical UICC's TNM classification for stages I–III. In agreement, this immune-based classification is currently being introduced into clinical settings (38–40). Despite being the most represented immune population in solid tumors, macrophages are not included in this classification, likely due to contradictory results in studies addressing their clinicopathologic significance in CRC.

In this study, macrophage profiling was assessed by quantitative evaluation of a macrophage lineage marker (CD68), a co-stimulatory receptor expressed by pro-inflammatory macrophages (CD80) and a scavenger receptor characteristic of their anti-inflammatory counterparts (CD163). The latter has been previously described in the literature, including in studies performed in CRC (23, 41–43). However, the identification of an ideal pro-inflammatory macrophage marker has been more challenging. Although several reports used NOS2 (22, 23, 44), it is becoming more evident that this is a specific marker of mice but not of human pro-inflammatory macrophages (25, 26). Our preliminary *in vitro* analysis revealed that CD80, referred in the literature as specifically expressed by M1 macrophages (45), and previously used to identify this specific subpopulation in tumors (46), is a suitable alternative (**Supplementary Figure 2**). Nevertheless, none of these markers is completely specific and it is possible that other immune cell populations, namely monocytes, dendritic cells, or activated B cells, are also recognized.

This study demonstrates that macrophage subpopulations are not uniformly distributed along the tumor, with distinct preferences for ANM, IT and IT regions. Our results showed increase CD68 staining in tumors compared to ANM, supporting the idea that these cells migrate towards the tumor site by chemotactic signals (47, 48). Although CD80 was highly expressed by macrophages at the tumor ANM (~74%), the majority of macrophages in intratumor regions lack the expression of this pro-inflammatory marker. This observation does not corroborate other studies performed in CRC using NOS2 as a marker, in which ~60% of the overall tumor macrophages were considered pro-inflammatory (23), but again we argue that this might not be an ideal pro-inflammatory marker of human macrophages. In accordance with the literature, we confirmed that the IF of colorectal tumors was densely infiltrated by macrophages and that, of these, <40% were CD163⁺ cells (23). We further demonstrated that only 3.5% of the IF macrophages stained positively for CD80. These results evidence an alteration of the macrophage inflammatory profile from the ANM to the neoplastic regions, with a major reduction of the CD80 expression, not counterbalanced by an increase of the CD163⁺ cells. Moreover, it also indicates that more than half of the TAMs are not expressing any of the polarization markers selected. Additionally, we cannot exclude that some macrophages might be expressing both M1 and M2 markers (22). Given the broad spectrum of M2-macrophages (5), these results highlight the heterogeneity in TAMs within CRC. A potential marker to include in future analysis is CD206. Work by Norton and colleagues describing TAMs subsets in CRC through flow cytometry showed distinct populations expressing CD163 and/or CD206 (49). More recently, Feng et al. also evidenced that, within stage II CRC patients which underwent radical resection, CD206/CD68 ratio can identify those with high risk of recurrence and poor prognosis and might benefit from adjuvant chemotherapy (50). In other models, namely esophageal squamous cell carcinoma, it was shown that there is a subpopulation of TAMs that does not express CD163 but is positive for CD204 (51). In fact, macrophage plasticity and ability to shift between polarization statuses represents a true challenge for their characterization. In the future, it will be of utmost importance to characterize macrophages not recognized by CD80 or CD163 antibodies, by isolating CD68⁺CD80[−]CD163[−] cells from formalin-fixed paraffin-embedded tissues and performing extensive gene expression analysis (52), to identify other subpopulations with putative relevant prognostic value or as novel targets for therapeutic modulation. As previously described by our group, one of the key players that might be determining these differential macrophage polarization within colorectal cancer is the extracellular matrix. By using decellularized human CRC and non-neoplastic mucosa, we demonstrated that, contrarily to what happens in normal tissues, tumor-ECM polarizes macrophages toward an anti-inflammatory, pro-invasive phenotype (53).

Interestingly, when macrophage populations were evaluated according to tumor stage, CD68 and CD163 expressing cells were more abundant in stage II tumors in comparison to stage IV, in agreement to findings from Sickert et al. (47). Conversely,

Bailey et al. reported a higher macrophage infiltration in stages III and IV, but this study included a small series of patients (54). Concerning CD80 staining, in our cohort, no differences were observed among tumor stages. It is generally hypothesized that during the initial steps of tumor development, macrophages recruited to the tumor site acquire pro-inflammatory and anti-tumor activities. Then, as a result of increased IL-10 and TGF- β levels, their polarization shifts toward a pro-tumor anti-inflammatory phenotype (45). For this reason, macrophage populations were separately analyzed according to the primary tumor invasiveness depth. Noteworthy, we observed that specifically CD80⁺ cells were predominant in T1 tumors, supporting, to some extent, the previously mentioned hypothesis.

Significant differences between ascending and descending colon might be partially explained by embryological origin: while ascending colon derives from the midgut, the descending colon is originated in the hindgut. Work by Glebov et al. reporting gene expression analysis of the ascending and descending normal colon mucosa from the same subject, revealed clear differences in the expression of genes involved in the control of many cellular functions, namely cell proliferation, adhesion, death, and signal transduction. Moreover, by including fetal samples in their study, they concluded that, although significant differences are indeed already established in the embryonic colon, additional alterations in gene expression arise in postnatal development (55). The gut microbiome has also been a subject of thorough investigation and it is now known that the amount and type of bacteria in the ascending and descending colon are distinct (56). These differences might be reflected in our findings, since CD68⁺, CD163⁺, and CD80⁺ macrophages were more prevalent in the tumor ANM on the ascending side of the colon. The same was observed in the IT region for both CD68 and CD163. Besides macrophages, other immune cells, namely some T lymphocytes subpopulations have also been reported as predominant in ascending colorectal tumors (57). Moreover, it is described that right-sided tumors have an higher mutational load which may be involved in the increased recruitment of immune cells (58). Interestingly, the differences disappeared at the tumor IF, suggesting that, in this specific region, the tumor can modulate the immune response regardless of the initial environment. This might be related with the different chemokines tumor cells release, which are known to have an impact in immune cell recruitment and differentiation (59). Our unexpected results suggesting that radiotherapy associates with increased risk of relapse are probably not related to the direct effect of ionizing radiation but, more likely, to the endogenous molecular characteristics of the tumors recommended for radiotherapy treatment. These results should be exploited in future studies.

In terms of prognosis, our results indicate that, within stage III tumors, higher CD68 infiltration in the IT is associated with decreased overall survival, contrarily to what was reported by Malesci et al. Using stage III CRC patients, they reported an association between high CD68 infiltration and increased overall survival, but only in patients undergoing 5-FU treatment (28). Our results further revealed an association between higher

CD80/CD163 ratio at the tumor IF and improved survival, similarly to what was reported in ovarian cancer (60). Recent work by Yank and colleagues describes an association between higher CD163⁺/CD68⁺ ratio at the IF of colorectal tumors and poor prognosis, which is not in accordance with our data. It would be important to clarify if the quantifications of CD68 and CD163 were performed in exactly the same tumor regions (61). This work strengthens the need to establish the inflammatory profile of existing macrophage populations and to perceive their distribution at the tumor microenvironment for an accurate prognostic prediction, and possible, therapeutic intervention. Different strategies targeting macrophages are currently under development (62), namely inhibition of monocyte recruitment (63), or of macrophage activation (64). More recently, the possibility of reprogramming M2 macrophages toward the M1-type has also been considered (65). In this sense, recent work by our group described the immunomodulatory capacity of polyelectrolyte multilayers containing IFN- γ and of nanoparticles composed of polyglutamic acid, specifically in reverting the pro-invasive capacity of IL-10-stimulated macrophages (66, 67). Accordingly, it is plausible to speculate that CRC patients might benefit from a therapeutic strategy aiming at reprogramming TAMs profile, which would result in an increase of M1 macrophages with a concomitant decrease of M2 subpopulations. The potential of this approach is further strengthened by the observation that lower infiltration of CD80⁺ cells strongly associated with increased risk of relapse. In hepatocellular carcinoma, an increase in M1 macrophages associated with increased time until recurrence (68), and a reduced CD163/CD68 ratio was correlated with a worse outcome (68), which corroborates, at least partially, our results. Specifically in CRC, a gene-expression based study published last year shows that tumors lacking M1 macrophages are associated with poor prognosis (69). Recent work revealed that CRC cells co-cultured with M1 macrophages exhibited increased cell death. Conversely, in the presence of naïve, unstimulated macrophages, cell death remained unchanged or even decreased, depending on the cell line (28). Nevertheless, since this is the first report describing the protective role of CD80⁺ cells in preventing CRC relapse, further studies should be performed to validate the current findings. Moreover, given the described reduced risk of relapse in colorectal tumors with higher immunoscore, it would be important to explore possible associations between the infiltration of CD80⁺ cells and cytotoxic or memory T cells.

Altogether, this work contributed to increase the knowledge regarding macrophage profile in CRC and further reinforced the complexity of macrophage polarization in tumors. Macrophage intrinsic plasticity and the capacity to adopt intermediate profiles between the two extreme populations, the M1 and the M2, require the use of multiple markers and a combination of strategies to accurately dissect the overall macrophage phenotype in tumors. The association of lower CD68 infiltration and higher CD80/CD163 ratio with increased overall survival within stage III CRC supports the need for further validations and reinforces the relevance of including such markers in the already established Immunoscore. Furthermore, the possible protective

role of CD80⁺ cells in preventing relapse might also open new perspectives in the immunotherapy field. Results presented here further support the need to foster research focusing on the development of novel therapeutic strategies to reprogram macrophages toward the pro-inflammatory and tumoricidal phenotype (70).

DATA AVAILABILITY

The datasets generated for this study are available on request to the corresponding author.

AUTHOR CONTRIBUTIONS

MP, FC, and MO conceived and designed the study. The experimental procedures, data analysis, and original draft writing were performed by MP. ER collected human colorectal samples, prepared histological sections, and contributed to pathological analysis. CD and RR assisted all statistical analysis and data interpretation. AM, MB, and JM contributed to data interpretation and discussion. FC supervised and monitored pathological data interpretation. MO supervised data analysis and discussion and obtained financial support. All authors discussed the results, contributed to the writing of the manuscript, and revised the final version.

REFERENCES

- Hanahan D, Weinberg RA. Hallmarks of cancer: the next generation. *Cell*. (2011) 144:646–74. doi: 10.1016/j.cell.2011.02.013
- van Ravenswaay Claassen HH, Kluin PM, Fleuren GJ. Tumor infiltrating cells in human cancer: on the possible role of CD16⁺ macrophages in antitumor cytotoxicity. *Lab Invest*. (1992) 67:166–74.
- Condeelis J, Pollard JW. Macrophages: obligate partners for tumor cell migration, invasion, and metastasis. *Cell*. (2006) 124:263–6. doi: 10.1016/j.cell.2006.01.007
- Quail DF, Joyce JA. Microenvironmental regulation of tumor progression and metastasis. *Nat Med*. (2013) 19:1423–37. doi: 10.1038/nm.3394
- Murray PJ, Allen JE, Biswas SK, Fisher EA, Gilroy DW, Goerdt S, et al. Macrophage activation and polarization: nomenclature and experimental guidelines. *Immunity*. (2014) 41:14–20. doi: 10.1016/j.immuni.2014.06.008
- Glass CK, Natoli G. Molecular control of activation and priming in macrophages. *Nat Immunol*. (2016) 17:26–33. doi: 10.1038/ni.3306
- Arango Duque G, Descoteaux A. Macrophage cytokines: involvement in immunity and infectious diseases. *Front Immunol*. (2014) 5:491. doi: 10.3389/fimmu.2014.00491
- Mantovani A, Sica A, Sozzani S, Allavena P, Vecchi A, Locati M. The chemokine system in diverse forms of macrophage activation and polarization. *Trends Immunol*. (2004) 25:677–86. doi: 10.1016/j.it.2004.09.015
- Mantovani A, Allavena P, Sica A. Tumour-associated macrophages as a prototypic type II polarised phagocyte population: role in tumour progression. *Eur J Cancer*. (2004) 40:1660–7. doi: 10.1016/j.ejca.2004.03.016
- Sica A, Schioppa T, Mantovani A, Allavena P. Tumour-associated macrophages are a distinct M2 polarised population promoting tumour progression: potential targets of anti-cancer therapy. *Eur J Cancer*. (2006) 42:717–27. doi: 10.1016/j.ejca.2006.01.003
- Zhang QW, Liu L, Gong CY, Shi HS, Zeng YH, Wang XZ, et al. Prognostic significance of tumor-associated macrophages in

FUNDING

This work was financed by FEDER—Fundo Europeu de Desenvolvimento Regional funds through the COMPETE 2020—Operacional Programme for Competitiveness and Internationalisation (POCI), Portugal 2020, and by Portuguese funds through FCT/MCTES in the framework of the project MAGICIAM: a MACrophage Immunomodulatory-delivery system to prevent Cancer Invasion and Metastasis (POCI-01-0145-FEDER-031859). FCT further supported this work under MP PhD grant (PD/BD/81103/2011), CD post-doctoral grant (SFRH/BPD/99442/2014), and MO FCT Investigator grant (IF/01066/2012).

ACKNOWLEDGMENTS

The authors acknowledge Dina Leitão for the help in the optimization of the immunohistochemistry protocols, Irene Gullo for her valuable opinion and Nuno Teixeira for his programming expertise.

SUPPLEMENTARY MATERIAL

The Supplementary Material for this article can be found online at: <https://www.frontiersin.org/articles/10.3389/fimmu.2019.01875/full#supplementary-material>

- solid tumor: a meta-analysis of the literature. *PLoS ONE*. (2012) 7:e50946. doi: 10.1371/journal.pone.0050946
- Leek RD, Lewis CE, Whitehouse R, Greenall M, Clarke J, Harris AL. Association of macrophage infiltration with angiogenesis and prognosis in invasive breast carcinoma. *Cancer Res*. (1996) 56:4625–9.
- Medrek C, Ponten F, Jirstrom K, Leandersson K. The presence of tumor associated macrophages in tumor stroma as a prognostic marker for breast cancer patients. *BMC Cancer*. (2012) 12:306. doi: 10.1186/1471-2407-12-306
- Hanada T, Nakagawa M, Emoto A, Nomura T, Nasu N, Nomura Y. Prognostic value of tumor-associated macrophage count in human bladder cancer. *Int J Urol*. (2000) 7:263–9. doi: 10.1046/j.1442-2042.2000.00190.x
- Falleni M, Savi F, Tosi D, Agape E, Cerri A, Moneghini L, et al. M1 and M2 macrophages' clinicopathological significance in cutaneous melanoma. *Melanoma Res*. (2017) 27:200–10. doi: 10.1097/CMR.0000000000000352
- Kang JC, Chen JS, Lee CH, Chang JJ, Shieh YS. Intratumoral macrophage counts correlate with tumor progression in colorectal cancer. *J Surg Oncol*. (2010) 102:242–8. doi: 10.1002/jso.21617
- Kwak Y, Koh J, Kim DW, Kang SB, Kim WH, Lee HS. Immunoscore encompassing CD3⁺ and CD8⁺ T cell densities in distant metastasis is a robust prognostic marker for advanced colorectal cancer. *Oncotarget*. (2016) 7:81778–90. doi: 10.18632/oncotarget.13207
- Forssell J, Oberg A, Henriksson ML, Stenling R, Jung A, Palmqvist R. High macrophage infiltration along the tumor front correlates with improved survival in colon cancer. *Clin Cancer Res*. (2007) 13:1472–9. doi: 10.1158/1078-0432.CCR-06-2073
- Zhou Q, Peng RQ, Wu XJ, Xia Q, Hou JH, Ding Y, et al. The density of macrophages in the invasive front is inversely correlated to liver metastasis in colon cancer. *J Transl Med*. (2010) 8:13. doi: 10.1186/1479-5876-8-13
- Algars A, Irjala H, Vaitinen S, Huhtinen H, Sundstrom J, Salmi M, et al. Type and location of tumor-infiltrating macrophages and lymphatic vessels predict survival of colorectal cancer patients. *Int J Cancer*. (2012) 131:864–73. doi: 10.1002/ijc.26457

21. Troiano G, Caponio VC A, Adipietro I, Tepedino M, Santoro R, Laino L, et al. Prognostic significance of CD68(+) and CD163(+) tumor associated macrophages in head and neck squamous cell carcinoma: a systematic review and meta-analysis. *Oral Oncol.* (2019) 93:66–75. doi: 10.1016/j.oraloncology.2019.04.019
22. Edin S, Wikberg ML, Dahlin AM, Rutegard J, Oberg A, Oldenborg P, et al. The distribution of macrophages with a M1 or M2 phenotype in relation to prognosis and the molecular characteristics of colorectal cancer. *PLoS ONE.* (2012) 7:e47045. doi: 10.1371/journal.pone.0047045
23. Koelzer VH, Canonica K, Dawson H, Sokol L, Karamitopoulou-Diamantis E, Lugli A, et al. Phenotyping of tumor-associated macrophages in colorectal cancer. Impact on single cell invasion (tumor budding) and clinicopathological outcome. *Oncoimmunology.* (2016) 5:e1106677. doi: 10.1080/2162402X.2015.1106677
24. Schneemann M, Schoeden G. Macrophage biology and immunology. man is not a mouse. *J Leukoc Biol.* (2007) 81:579. doi: 10.1189/jlb.1106702
25. Mestas J, Hughes CC. Of mice and not men. differences between mouse and human immunology. *J Immunol.* (2004) 172:2731–8. doi: 10.4049/jimmunol.172.5.2731
26. Schneemann M, Schoeden G. Species differences in macrophage NO production are important. *Nat Immunol.* (2002) 3:102. doi: 10.1038/ni0202-102a
27. Laghi L, Bianchi P, Miranda E, Balladore E, Pacetti V, Grizzi F, et al. CD3+ cells at the invasive margin of deeply invading (pT3-T4) colorectal cancer and risk of post-surgical metastasis: a longitudinal study. *Lancet Oncol.* (2009) 10:877–84. doi: 10.1016/S1470-2045(09)70186-X
28. Malesci A, Bianchi P, Celesti G, Basso G, Marchesi F, Grizzi F, et al. Tumor-associated macrophages and response to 5-fluorouracil adjuvant therapy in stage III colorectal cancer. *Oncoimmunology.* (2017) 6:e1342918. doi: 10.1080/2162402X.2017.1342918
29. Lim W, Gee K, Mishra S, Kumar A. Regulation of B7.1 costimulatory molecule is mediated by the IFN regulatory factor-7 through the activation of JNK in lipopolysaccharide-stimulated human monocytic cells. *J Immunol.* (2005) 175:5690–700. doi: 10.4049/jimmunol.175.9.5690
30. Buechler C, Ritter M, Orso E, Langmann T, Klucken J, Schmitz G. Regulation of scavenger receptor CD163 expression in human monocytes and macrophages by pro- and antiinflammatory stimuli. *J Leukoc Biol.* (2000) 67:97–103. doi: 10.1002/jlb.67.1.97
31. Gulubova M, Ananiev J, Yovchev Y, Julianov A, Karashmalakov A, Vlaykova T. The density of macrophages in colorectal cancer is inversely correlated to TGF-beta1 expression and patients' survival. *J Mol Histol.* (2013) 44:679–92. doi: 10.1007/s10735-013-9520-9
32. Merlano MC, Granetto C, Fea E, Ricci V, Garrone O. Heterogeneity of colon cancer. from bench to bedside. *ESMO Open.* (2017) 2:e000218. doi: 10.1136/esmoopen-2017-000218
33. Abulafi AM, Williams NS. Local recurrence of colorectal cancer: the problem, mechanisms, management and adjuvant therapy. *Br J Surg.* (1994) 81:7–19. doi: 10.1002/bjs.1800810106
34. Ryuk JP, Choi GS, Park JS, Kim HJ, Park SY, Yoon GS, et al. Predictive factors and the prognosis of recurrence of colorectal cancer within 2 years after curative resection. *Ann Surg Treat Res.* (2014) 86:143–51. doi: 10.4174/astr.2014.86.3.143
35. de Visser KE, Eichten A, Coussens LM. Paradoxical roles of the immune system during cancer development. *Nat Rev Cancer.* (2006) 6:24–37. doi: 10.1038/nrc1782
36. Van den Eynde M, Mlecnik B, Bindea G, Fredriksen T, Church SE, Lafontaine L, et al. The link between the multiverse of immune microenvironments in metastases and the survival of colorectal cancer patients. *Cancer Cell.* (2018) 34:1012–26.e3. doi: 10.1016/j.ccell.2018.11.003
37. Galon J, Costes A, Sanchez-Cabo F, Kirilovsky A, Mlecnik B, Lagorce-Pages C, et al. Type, density, and location of immune cells within human colorectal tumors predict clinical outcome. *Science.* (2006) 313:1960–4. doi: 10.1126/science.1129139
38. Galon J, Pages F, Marincola FM, Thurin M, Trinchieri G, Fox BA, et al. The immune score as a new possible approach for the classification of cancer. *J Transl Med.* (2012) 10:1. doi: 10.1186/1479-5876-10-1
39. Galon J, Pages F, Marincola FM, Angell HK, Thurin M, Lugli A, et al. Cancer classification using the Immunoscore: a worldwide task force. *J Transl Med.* (2012) 10:205. doi: 10.1186/1479-5876-10-205
40. Angell H, Galon J. From the immune contexture to the immunescore: the role of prognostic and predictive immune markers in cancer. *Curr Opin Immunol.* (2013) 25:261–7. doi: 10.1016/j.coi.2013.03.004
41. Nagorsen D, Voigt S, Berg E, Stein H, Thiel E, Loddenkemper C. Tumor-infiltrating macrophages and dendritic cells in human colorectal cancer. relation to local regulatory T cells, systemic T-cell response against tumor-associated antigens and survival. *J Transl Med.* (2007) 5:62. doi: 10.1186/1479-5876-5-62
42. Herrera M, Herrera A, Dominguez G, Silva J, Garcia V, Garcia JM, et al. Cancer-associated fibroblast and M2 macrophage markers together predict outcome in colorectal cancer patients. *Cancer Sci.* (2013) 104:437–44. doi: 10.1111/cas.12096
43. Shibutani M, Maeda K, Nagahara H, Fukuoka T, Nakao S, Matsutani S, et al. The peripheral monocyte count is associated with the density of tumor-associated macrophages in the tumor microenvironment of colorectal cancer. a retrospective study. *BMC Cancer.* (2017) 17:404. doi: 10.1186/s12885-017-3395-1
44. Waniczek D, Lorenc Z, Snietura M, Wesecki M, Kopec A, Muc-Wiergon M. Tumor-associated macrophages and regulatory T cells infiltration and the clinical outcome in colorectal cancer. *Arch Immunol Ther Exp.* (2017) 65:445–54. doi: 10.1007/s00005-017-0463-9
45. Mantovani A, Sozzani S, Locati M, Allavena P, Sica A. Macrophage polarization. tumor-associated macrophages as a paradigm for polarized M2 mononuclear phagocytes. *Trends Immunol.* (2002) 23:549–55. doi: 10.1016/S1471-4906(02)02302-5
46. Mori K, Hiroi M, Shimada J, Ohmori Y. Infiltration of m2 tumor-associated macrophages in oral squamous cell carcinoma correlates with tumor malignancy. *Cancers.* (2011) 3:3726–39. doi: 10.3390/cancers3043726
47. Sickert D, Aust DE, Langer S, Haupt I, Barrett GB, Dieter P. Characterization of macrophage subpopulations in colon cancer using tissue microarrays. *Histopathology.* (2005) 46:515–21. doi: 10.1111/j.1365-2559.2005.02129.x
48. Richards DM, Hettinger J, Feuerer M. Monocytes and macrophages in cancer. development and functions. *Cancer Microenviron.* (2013) 6:179–91. doi: 10.1007/s12307-012-0123-x
49. Norton SE, Dunn ET, McCall JL, Munro F, Kemp RA. Gut macrophage phenotype is dependent on the tumor microenvironment in colorectal cancer. *Clin Transl Immunology.* (2016) 5:e76. doi: 10.1038/cti.2016.21
50. Feng Q, Chang W, Mao Y, He G, Zheng P, Tang W, et al. Tumor-associated macrophages as prognostic and predictive biomarkers for postoperative adjuvant chemotherapy in patients with stage II colon cancer. *Clin Cancer Res.* (2019) 25:3896–907. doi: 10.1158/1078-0432.CCR-18-2076
51. Shigeoka M, Urakawa N, Nakamura T, Nishio M, Watajima T, Kuroda D, et al. Tumor associated macrophage expressing CD204 is associated with tumor aggressiveness of esophageal squamous cell carcinoma. *Cancer Sci.* (2013) 104:1112–9. doi: 10.1111/cas.12188
52. Jiang R, Scott RS, Hutt-Fletcher LM. Laser capture microdissection for analysis of gene expression in formalin-fixed paraffin-embedded tissue. *Methods Mol Biol.* (2011) 755:77–84. doi: 10.1007/978-1-61779-163-5_6
53. Pinto ML, Rios E, Silva AC, Neves SC, Caires HR, Pinto AT, et al. Decellularized human colorectal cancer matrices polarize macrophages towards an anti-inflammatory phenotype promoting cancer cell invasion via CCL18. *Biomaterials.* (2017) 124:211–24. doi: 10.1016/j.biomaterials.2017.02.004
54. Bailey C, Negus R, Morris A, Ziprin P, Goldin R, Allavena P, et al. Chemokine expression is associated with the accumulation of tumour associated macrophages (TAMs) and progression in human colorectal cancer. *Clin Exp Metastasis.* (2007) 24:121–30. doi: 10.1007/s10585-007-9060-3
55. Glebov OK, Rodriguez LM, Nakahara K, Jenkins J, Cliatt J, Humbyrd CJ, et al. Distinguishing right from left colon by the pattern of gene expression. *Cancer Epidemiol Biomarkers Prev.* (2003) 12:755–62.
56. Donaldson GP, Lee SM, Mazmanian SK. Gut biogeography of the bacterial microbiota. *Nat Rev Microbiol.* (2016) 14:20–32. doi: 10.1038/nrmicro3552
57. Zhang L, Zhao Y, Dai Y, Cheng JN, Gong Z, Feng Y, et al. Immune landscape of colorectal cancer tumor microenvironment from different primary tumor location. *Front Immunol.* (2018) 9:1578. doi: 10.3389/fimmu.2018.01578
58. Salem ME, Weinberg BA, Xiu J, El-Deiry WS, Hwang JJ, Gatalica Z, et al. Comparative molecular analyses of left-sided colon, right-sided colon, and rectal cancers. *Oncotarget.* (2017) 8:86356–68. doi: 10.18632/oncotarget.21169

59. Vilgelm AE, Richmond A. Chemokines modulate immune surveillance in tumorigenesis, metastasis, and response to immunotherapy. *Front Immunol.* (2019) 10:333. doi: 10.3389/fimmu.2019.00333
60. Zhang M, He Y, Sun X, Li Q, Wang W, Zhao A, et al. A high M1/M2 ratio of tumor-associated macrophages is associated with extended survival in ovarian cancer patients. *J Ovarian Res.* (2014) 7:19. doi: 10.1186/1757-2215-7-19
61. Yang C, Wei C, Wang S, Shi D, Zhang C, Lin X, et al. Elevated CD163(+)/CD68(+) ratio at tumor invasive front is closely associated with aggressive phenotype and poor prognosis in colorectal cancer. *Int J Biol Sci.* (2019) 15:984–98. doi: 10.7150/ijbs.29836
62. Mantovani A, Marchesi F, Malesci A, Laghi L, Allavena P. Tumour-associated macrophages as treatment targets in oncology. *Nat Rev Clin Oncol.* (2017) 14:399–416. doi: 10.1038/nrclinonc.2016.217
63. Pienta KJ, Machiels JP, Schrijvers D, Alekseev B, Shkolnik M, Crabb SJ, et al. Phase 2 study of carlumab (CNTO 888), a human monoclonal antibody against CC-chemokine ligand 2 (CCL2), in metastatic castration-resistant prostate cancer. *Invest New Drugs.* (2013) 31:760–8. doi: 10.1007/s10637-012-9869-8
64. Ries CH, Cannarile MA, Hoves S, Benz J, Wartha K, Runza V, et al. Targeting tumor-associated macrophages with anti-CSF-1R antibody reveals a strategy for cancer therapy. *Cancer Cell.* (2014) 25:846–59. doi: 10.1016/j.ccr.2014.05.016
65. Kloepper J, Riedemann L, Amoozgar Z, Seano G, Susek K, Yu V, et al. Ang-2/VEGF bispecific antibody reprograms macrophages and resident microglia to anti-tumor phenotype and prolongs glioblastoma survival. *Proc Natl Acad Sci USA.* (2016) 113:4476–81. doi: 10.1073/pnas.1525360113
66. Cardoso AP, Goncalves RM, Antunes JC, Pinto ML, Pinto AT, Castro F, et al. An interferon-gamma-delivery system based on chitosan/poly(gamma-glutamic acid) polyelectrolyte complexes modulates macrophage-derived stimulation of cancer cell invasion *in vitro*. *Acta Biomater.* (2015) 23:157–71. doi: 10.1016/j.actbio.2015.05.022
67. Castro F, Pinto ML, Silva AM, Pereira CL, Teixeira GQ, Gomez-Lazaro M, et al. Pro-inflammatory chitosan/poly(gamma-glutamic acid) nanoparticles modulate human antigen-presenting cells phenotype and revert their pro-invasive capacity. *Acta Biomater.* (2017) 63:96–109. doi: 10.1016/j.actbio.2017.09.016
68. Dong P, Ma L, Liu L, Zhao G, Zhang S, Dong L, et al. CD86(+)/CD206(+), diametrically polarized tumor-associated macrophages, predict hepatocellular carcinoma patient prognosis. *Int J Mol Sci.* (2016) 17:320. doi: 10.3390/ijms17030320
69. Xiong Y, Wang K, Zhou H, Peng L, You W, Fu Z. Profiles of immune infiltration in colorectal cancer and their clinical significant: a gene expression-based study. *Cancer Med.* (2018) 7:4496–508. doi: 10.1002/cam4.1745
70. Zheng X, Turkowski K, Mora J, Brune B, Seeger W, Weigert A, et al. Redirecting tumor-associated macrophages to become tumoricidal effectors as a novel strategy for cancer therapy. *Oncotarget.* (2017) 8:48436–52. doi: 10.18632/oncotarget.17061

Conflict of Interest Statement: The authors declare that the research was conducted in the absence of any commercial or financial relationships that could be construed as a potential conflict of interest.

Copyright © 2019 Pinto, Rios, Durães, Ribeiro, Machado, Mantovani, Barbosa, Carneiro and Oliveira. This is an open-access article distributed under the terms of the Creative Commons Attribution License (CC BY). The use, distribution or reproduction in other forums is permitted, provided the original author(s) and the copyright owner(s) are credited and that the original publication in this journal is cited, in accordance with accepted academic practice. No use, distribution or reproduction is permitted which does not comply with these terms.



Glycolysis Is Required for LPS-Induced Activation and Adhesion of Human CD14⁺CD16⁻ Monocytes

OPEN ACCESS

Edited by:

Kate E. Lawlor,
Hudson Institute of Medical
Research, Australia

Reviewed by:

Nicole K. Campbell,
Hudson Institute of Medical
Research, Australia
Evanna Mills,
Dana-Farber Cancer Institute,
United States
Kristiaan Wouters,
Maastricht University, Netherlands
Laurent Yvan-Charvet,
Institut National de la Santé et de la
Recherche Médicale
(INSERM), France

*Correspondence:

Man K. S. Lee
mankitsam.lee@baker.edu.au
Andrew J. Murphy
Andrew.murphy@baker.edu.au

[†]These authors have contributed
equally to this work

Specialty section:

This article was submitted to
Molecular Innate Immunity,
a section of the journal
Frontiers in Immunology

Received: 08 April 2019

Accepted: 14 August 2019

Published: 06 September 2019

Citation:

Lee MKS, Al-Sharea A, Shihata WA,
Bertuzzo Veiga C, Cooney OD,
Fleetwood AJ, Flynn MC, Claeson E,
Palmer CS, Lancaster GI,
Henstridge DC, Hamilton JA and
Murphy AJ (2019) Glycolysis Is
Required for LPS-Induced Activation
and Adhesion of Human
CD14⁺CD16⁻ Monocytes.
Front. Immunol. 10:2054.
doi: 10.3389/fimmu.2019.02054

Man K. S. Lee^{1,2*†}, Annas Al-Sharea^{1,2†}, Waled A. Shihata¹, Camilla Bertuzzo Veiga¹,
Olivia D. Cooney¹, Andrew J. Fleetwood^{3,4}, Michelle C. Flynn¹, Ellen Claeson⁵,
Clovis S. Palmer⁶, Graeme I. Lancaster¹, Darren C. Henstridge¹, John A. Hamilton^{3,4} and
Andrew J. Murphy^{1*}

¹ Division of Immunometabolism, Baker Heart and Diabetes Institute, Melbourne, VIC, Australia, ² Department of Diabetes, Monash University, Melbourne, VIC, Australia, ³ Department of Medicine, The Royal Melbourne Hospital, Parkville, VIC, Australia, ⁴ Australian Institute of Musculoskeletal Science, University of Melbourne and Western Health, St. Albans, VIC, Australia, ⁵ Faculty of Medicine and Health Sciences, Linköping University, Linköping, Sweden, ⁶ Department of Infectious Disease, Burnet Institute, Melbourne, VIC, Australia

Monocytes in humans consist of 3 subsets; CD14⁺CD16⁻ (classical), CD14⁺CD16⁺ (intermediate) and CD14^{dim}CD16⁺ (non-classical), which exhibit distinct and heterogeneous responses to activation. During acute inflammation CD14⁺CD16⁻ monocytes are significantly elevated and migrate to the sites of injury via the adhesion cascade. The field of immunometabolism has begun to elucidate the importance of the engagement of specific metabolic pathways in immune cell function. Yet, little is known about monocyte metabolism and the role of metabolism in mediating monocyte activation and adherence to vessels. Accordingly, we aimed to determine whether manipulating the metabolism of CD14⁺CD16⁻ monocytes alters their ability to become activated and adhere. We discovered that LPS stimulation increased the rate of glycolysis in human CD14⁺CD16⁻ monocytes. Inhibition of glycolysis with 2-deoxy-D-glucose blunted LPS-induced activation and adhesion of monocytes. Mechanistically, we found that increased glycolysis was regulated by mTOR-induced glucose transporter (GLUT)-1. Furthermore, enhanced glycolysis increased accumulation of reactive oxygen species (ROS) and activation of p38 MAPK, which lead to activation and adhesion of monocytes. These findings reveal that glycolytic metabolism is critical for the activation of CD14⁺CD16⁻ monocytes and contributes to our understanding of the interplay between metabolic substrate preference and immune cell function.

Keywords: glycolysis, monocytes, inflammation, metabolism, adhesion

INTRODUCTION

Innate immune cells such as monocytes play an essential role during inflammation. Monocytes emerge from the bone marrow or spleen into the blood when inflammatory cues are released from sites of injury and ultimately migrate from the blood into the inflamed tissue. This is commonly referred to as the leukocyte adhesion cascade (1). This is a stepwise process initially involving the activation of monocytes, allowing them to roll and tether and then

along the activated endothelium followed by firm adhesion and extravasation into inflamed sites. These events are necessary for the survival of the host, as inflammation is important for clearing invading pathogens and repairing damaged tissues (2). On the other hand, excessive inflammation can lead to detrimental effects, resulting in further damage to tissues, and the development of chronic inflammatory diseases such as atherosclerosis and other auto-inflammatory disorders (3–5). Therefore, understanding the underlying mechanisms that regulate monocyte adhesion can provide information on how to manipulate the cell's ability to adhere during acute or chronic inflammation.

It has become increasingly appreciated that the metabolic status of a cell can dictate its functional phenotype. We and others have shown that stimulating cells with inflammatory stimuli switches the energy profile of macrophages and T cells, i.e., from using mitochondrial oxidative phosphorylation (OXPHOS) to glycolysis (6–8). Changes in the cellular substrates and metabolic preferences under resting and activated states has sparked investigations into further understanding immune cell metabolism (i.e., immunometabolism) in relation to their function. It has become increasingly evident that manipulating metabolic pathways influences the development and function of cells. For example, inhibiting glycolysis in LPS-stimulated bone marrow-derived macrophages (BMDMs), prevents the release of the inflammatory cytokine interleukin (IL)-1 β (9).

In humans, blood monocytes consist of 3 functionally distinct subsets, CD14⁺CD16[−] (classical), CD14⁺CD16⁺ (intermediate), and CD14^{dim}CD16[−] (non-classical) (10). CD14⁺CD16[−] monocytes represent 85% of the circulating monocyte population whereas the other two subsets each make up ~5–8% of the population. In mice, however, monocytes consist of only two subsets, Ly6-C^{hi} and Ly6-C^{lo}. Ly6-C^{hi} monocytes are considered to be inflammatory and have been likened to the CD14⁺CD16[−] monocyte population in humans. During acute inflammation, such as a bacterial infection, these are the subsets that respond first. Therefore, in this study we aimed to investigate how human CD14⁺CD16[−] monocytes metabolically respond to inflammatory stimuli such as lipopolysaccharide (LPS) and how manipulating monocyte metabolism could alter their functional responses, particularly in relation to their activation and ability to undergo firm adhesion.

MATERIALS AND METHODS

Isolation of Peripheral Blood Mononuclear Cells From Human Buffy Coats

Peripheral blood mononuclear cells (PBMC) were isolated from buffy coats of healthy volunteers supplied by the Australian Red Cross Blood Service via density-centrifugation using Ficoll-Paque solution (density = 1.77). Ethics was obtained through the Alfred Hospital human ethics committee.

CD14⁺CD16[−] Monocyte Isolation From PBMCs

PBMCs were resuspended using PBS without Ca²⁺ and Mg²⁺ containing 2 mM EDTA and 5% FBS (FACS buffer) and labeled

with a cocktail of fluorescent markers (1:400) consisting of Lin (PE—CD2, PE—CD15, PE—CD56, PE—Nkp46, PE—19), APC—HLA-DR, PB—CD14, PE/Cy7—CD16. After 30 min of incubation on ice, they were then washed and Lin[−]HLA-DR⁺CD14⁺CD16[−] monocytes were collected via FACS using the BD Aria 1 (Biosciences) at the AMREP Flow cytometry core facility.

Stimulation/Inhibition of Cells

PBMCs (for flow cytometry assays) and isolated CD14⁺CD16[−] monocytes were stimulated with lipopolysaccharides (LPS) (100 ng/ml) for 1 h in the presence or absence of 1 h of metabolic inhibitor pre-treatment; glycolysis inhibitor: 2-Deoxy-D Glucose (2DG) (5 mM), mechanistic target of rapamycin (mTOR) inhibitor: rapamycin (20 nM), reactive oxygen species (ROS) inhibitor: NAC (1 mM), p38 MAPK inhibitor: SB-203580 (5 nM) and mitochondrial ROS scavenger: MitoQ (100 nM).

Flow Cytometry

PBMCs were resuspended in 200 μ l of FACS buffer. A cocktail of the fluorophores (1:400) were added to stain for the different monocyte subsets. These consisted of Lin (PE—CD2, PE—CD15, PE—CD56, PE—Nkp46, PE—19), APC—HLA-DR, PB—CD14, PE/Cy7—CD16. To measure CD11b levels or GLUT-1 expression, FITC-CD11b (1:400), and FITC—GLUT-1 was also added, respectively. After incubating on ice for 30 min, they were then washed and transferred into FACS tubes. In order to measure metabolism of cells via flow cytometry, 10 nM MitoTracker Deep Red, 4 μ M 2-NBDG, 5 μ M MitoSOX, and 10 μ M H2DCFDA were stained in RPMI 1640 and incubated in 37°C for 20 min before they were washed and transferred into FACS tubes. Cells were immediately run on the BD LSRII Fortessa (BD Biosciences). 100,000 cells were collected for analysis. Unstained and single stained controls were used to set up voltages to compensate for spectral overlap. Flow cytometry data were quantified using FlowJo vX0.7 (FlowJo LLC) software.

Seahorse Bioanalyser Assay

Monocytes were pre-treated with inhibitors and seeded at 100,000 cells/well in the XF^e 96 well cell culture microplate (Agilent Technologies). The microplate was spun at 1,000 RPM for 5 min at 4°C; acc = 5, dec = 0 to obtain a monolayer of monocytes in each well. The supernatant was discarded and 175 μ l of seahorse media [XF based minimal DMEM (Agilent Technologies) supplemented with 5.5 mM Glucose Solution (Gibco), 1 mM Sodium Pyruvate (Gibco) and 2 mM L-Glutamine (Gibco)], containing the same concentrations of inhibitors, were carefully added so as not to disturb the cell layer. The XF^e 96 well cell culture microplate was incubated at 37°C in a non-CO₂ incubator for at least 30 min. The assay cartridge was hydrated overnight with 200 μ l of XF Calibrant Media (Agilent Technologies) at 37°C (in non-CO₂ incubator) before LPS was suspended in 25 μ l of seahorse media and was added to Port A of the assay cartridge at a concentration of 100 ng/ml. Basal extracellular acidification rate (ECAR) was measured for 4 \times 6.5 min cycles. LPS was automatically injected into the XF^e cell culture plate after the 4th cycle and ECAR readings were recorded for 1 h post-LPS injection.

Vessel Chamber Adhesion Assay

Aortic vessels were isolated from C57BL/6 mice and stimulated in Krebs buffer with bovine serum albumin (BSA) (1:1,000 w/v) and TNF- α for 4 h at 37°C. TNF- α activated vessels were mounted onto the cannulas and Krebs solution warmed at 37°C was used to flood the vessel chamber to mimic *in-vivo* conditions. Monocytes were re-suspended in 6 ml of RPMI at the concentration of 1×10^6 cells/ml. 1 mM of Vybrant Dil (Invitrogen) was added for 10 min in dark conditions, to fluorescently label the cells. Cell solutions were transferred into a terafusion syringe pump (Teruma) which was used to direct the movement of the cells through the aortic vessel at a rate of 7.1 ml per hour. Images of adhered monocytes were taken using the Zeiss Discover V.20 Fluorescence Microscope (Carl Zeiss MicroImaging) mounted on a Hamamatsu HD Camera (Hamamatsu®) at 0, 2.5, 5, 7.5, and 10 min. Data was then quantified by calculating the number of stationary fluorescent dots per field of view (FOV).

F-Actin Assay

Eight well chamber slides (Lab-Tek) were pre-coated with 200 μ l/well of fibrinogen (100 μ g/ml) and incubated overnight at 4°C. The next day, each well was washed twice with PBS without Mg²⁺ and Ca²⁺ to get rid of non-adhered fibrinogen via aspiration. Two-hundred microliter of 3% BSA were then added and incubated at room temperature for 15 minutes before washing again with PBS twice. Two-hundred microliter of monocytes (at 1×10^6 /ml in RPMI 1640 media) were then added into each well and stimulated with 100 ng/ml LPS for 1 h at 37°C. Cells were then washed with PBS twice to remove unbound monocytes. Two-hundred microliter of 4% para-formaldehyde (PFA) was then added for 15 min at room temperature to fix adhered monocytes onto slides. Again, PBS was used to wash off the PFA before permeabilising cells with 0.1% Triton X-100 for 10 min at room temperature. After washing cells with PBS, 200 μ l of PBS containing 10% FBS was used to block any non-specific binding for 15 min at room temperature. Cells were washed again before staining with fluorescent markers of F-actin (33 nM phalloidin) and nucleus (1 ng/ml 4',6-diamidino-2-phenylindole (DAPI) for 20 min in the dark at room temperature. Cells were then washed twice with PBS and the gasket were removed. slides were finally allowed to completely dry before mounting on No. 2 glass coverslips (Menzel) using Dako fluorescence mounting media. Imaging was performed through the monash micro imaging core, on a Nikon A1r confocal microscope using NIS-elements software (Nikon) at 60X magnification. To quantify F-actin staining, the fluorescence intensity of phalloidin stain per cell, normalized to cell size, was measured using Image J. Moreover, cells were counted individually, using the Image J count function, to quantify the number of adherent monocytes.

Western Blot

Protein samples were isolated from lysed Monocytes. A 10% SDS-PAGE gel was used to separate the protein samples which were subsequently transferred onto a nitrocellulose membrane. Five percent fat-free skim milk in tris-buffered saline with

tween (TBST) was used to block the membrane for non-specific binding and washed with before the addition of various primary antibodies (1:1,000) consisting of p-mTOR (Santa Cruz), p-ERK1/2 (Cell Signaling Technologies), β -actin (Cell Signaling Technologies), p-p38 MAPK (Cell Signaling Technologies), p38 MAPK (Cell Signaling Technologies), and HSP90 (Cell Signaling Technologies). Membranes were then incubated overnight at 4°C. Appropriate secondary antibodies (1:2,000) were added for 1 h at room temperature and subsequently washed before visualization of the protein bands using enhanced chemiluminescence reagents (PerkinElmer) and quantified using Quantity One (Bio-Rad) software.

Statistical Analyses

Data are presented as mean \pm SEM where each individual donor was denoted by n. *P* values were calculated by using unpaired Student's *t*-test or one-way ANOVA followed by Tukey's *post-hoc* test using Graphpad Prism 7 (Graphpad Software). *P*-values of <0.05 were deemed to be statistically significant.

RESULTS

LPS Activation Increases Glycolysis in Human CD14⁺CD16[−] Monocytes

It is becoming increasingly appreciated that immune cells alter their metabolism when they become activated (11, 12). To determine the metabolic preference of human CD14⁺CD16[−] monocytes after activation with LPS, we isolated cells from buffy coats of healthy volunteers via fluorescence-activated cell sorting (FACS) before placing them in the seahorse XF^e 96 bioanalyser to characterize their metabolic preference. We noted a significant increase in extracellular acidification rate (ECAR) within 20 min of LPS stimulation (**Figures 1A,B**) indicating increased rate of glycolysis. This was also associated with enhanced glucose uptake, measured via flow cytometry using 2-NBDG (**Figure 1C**). Moreover, we found no significant change in oxygen consumption rate (OCR), which is a proxy of oxidative phosphorylation (OXPHOS), in CD14⁺CD16[−] monocytes after LPS stimulation (**Figures 1D,E**). We also used flow cytometry to quantify mitochondrial activity, which confirmed our findings from the seahorse bioanalyser (**Figure 1F**). These data suggest that stimulating monocytes with LPS causes an increase in glycolysis while not affecting OXPHOS.

Inhibiting Glycolysis Decreases Monocyte Activation and Adhesion

Given that we found CD14⁺CD16[−] monocytes increase glycolysis following LPS stimulation, we aimed to determine how important glucose utilization was to their ability to activate in response to LPS. To do this we used 2-Deoxy-D-glucose (2-DG), a glucose analog that enters into the cell like glucose but inhibits the first step of glycolysis via competitively blocking hexokinase, a rate limiting step of glycolysis (13). As expected, pre-treating cells with 2-DG reduced the increase in glycolysis caused by LPS (**Figures 2A,B**). Additionally, pre-treating cells with 2-DG significantly inhibited the activation of the CD14⁺CD16[−] monocytes as determined by the cell surface

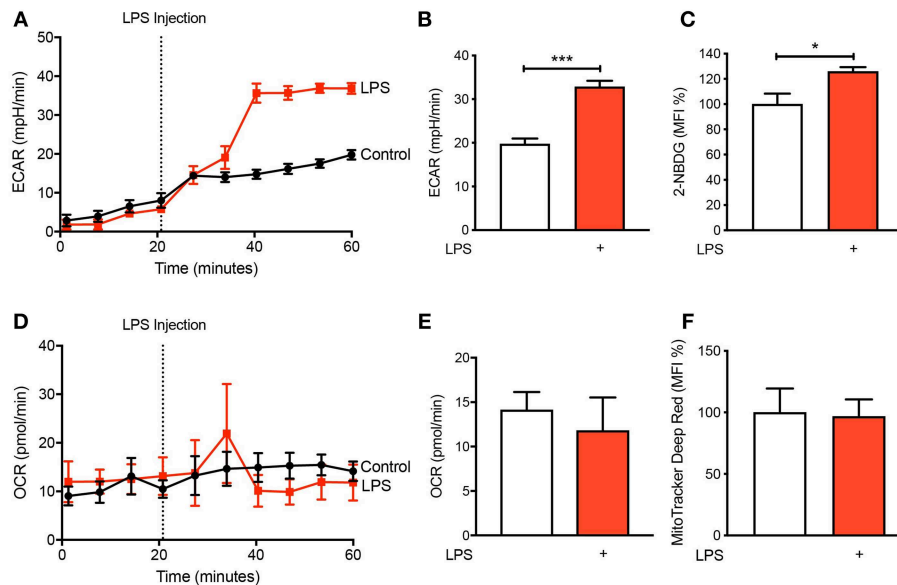


FIGURE 1 | LPS increases glycolysis in human CD14⁺CD16⁻ monocytes. Isolated human CD14⁺CD16⁻ monocytes were treated with or without 100 ng/ml LPS. A Seahorse bioanalyser was used to measure extracellular acidification rate (ECAR) (A,B); $n = 4$. Flow cytometry was used to measure glucose uptake using fluorescent analog 2-NBDG (C); $n = 6$. A Seahorse bioanalyser was used to measure oxygen consumption rate (OCR) (D,E); $n = 4$. Mitochondrial activity was measured using flow cytometry (F); $n = 7$. Data are mean \pm SEM (un-paired t -test: * $p < 0.05$, *** $p < 0.001$).

activation marker CD11b (Figure 2C). To functionally confirm the role of glycolysis in LPS-induced monocyte adhesion, we performed a static adhesion assay where we pre-coated wells with fibrinogen which allows activated monocytes to bind via CD11b. Monocyte adhesion was assessed using confocal microscopy where cells were also stained to quantify F-actin content as another measure of cell activation. As expected, following LPS stimulation, there was a significant increase in the number of monocytes adhering to fibrinogen as well as an increase in F-actin content. These effects were blunted when cells were pre-treated with 2-DG (Figures 2D–F). Furthermore, we performed a shear flow cell adhesion assay to monitor in real-time monocyte adhesion under shear stress in TNF- α activated mouse aorta *ex vivo*. We treated CD14⁺CD16⁻ human monocytes with LPS 1 h before flowing the cells through the endothelium and found that there was a significant increase in monocyte adhesion. This increase in monocyte adhesion was abolished when pre-treating with 2-DG (Figures 2G–I). This confirms our hypothesis that blocking glycolysis prevents LPS-induced monocyte activation and adhesion.

mTOR Is Involved in Regulating Glycolysis in LPS-Induced Monocytes

To understand the mechanisms by which LPS increases glycolysis, we explored the mTOR pathway as it has been known to be involved in regulating glycolysis (14). Following LPS treatment we found a significant increase in the phosphorylation of mTOR in the CD14⁺CD16⁻ monocytes and using rapamycin as a positive control for mTOR phosphorylation, phosphorylation of mTOR was significantly reduced as expected

(Figure 3A). The activation of mTOR is also known to further upregulate glucose transporter (GLUT)-1 to the cell surface in order to facilitate increased glucose uptake (15). When we measured GLUT-1 expression using flow cytometry, we found that LPS significantly increased cell surface GLUT-1 levels. When we inhibited mTOR activity using rapamycin, GLUT-1 expression was significantly blunted in LPS-induced monocytes (Figure 3B). This suggests that the increase in cell surface GLUT-1 is regulated by mTOR in monocytes. Furthermore, we also showed that inhibiting mTOR significantly prevented the increase in LPS-stimulated glycolysis (Figures 3C,D), suggesting mTOR is a master regulator of glycolysis in CD14⁺CD16⁻ monocytes. Next, we blocked mTOR to determine whether this affected the activation and adhesion of monocytes. When we pre-treated cells with rapamycin, we were able to prevent CD11b expression in LPS-induced monocytes (Figure 3E). The anti-inflammatory effects of mTOR blockade were also seen in the static adhesion assay where pre-treating cells with rapamycin prevented the number of monocytes adhered to fibrinogen. In addition, we found a decrease in F-actin content (Figures 3F–H). This suggests that the mTOR pathway is involved in LPS-induced activation and adhesion of CD14⁺CD16⁻ monocytes by controlling glucose uptake and glycolysis.

Blocking p-38 MAPK Signaling Prevents LPS-Induced Activation and Adhesion

To further understand the signaling pathways mediating the activation and adhesion of LPS-stimulated monocytes, we measured mitogen-activated protein kinases (MAPKs), extracellular signal-related kinases (ERKs) and p38 MAPK,

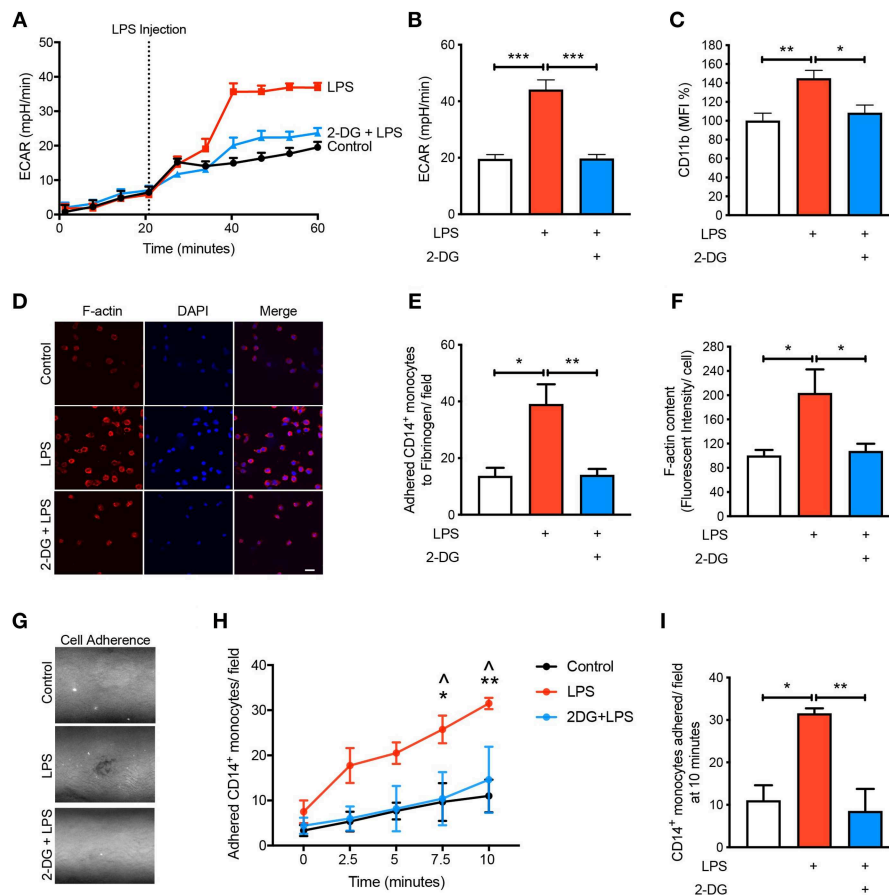


FIGURE 2 | Glycolysis is required for LPS-induced monocyte activation and adhesion. Isolated human CD14⁺CD16⁻ monocytes were pre-treated with or without 5 mM 2-DG for 1 h followed by 1 h of 100 ng/ml LPS stimulation. Seahorse bioanalyser was used to measure extracellular acidification rate (ECAR) (**A,B**); $n = 4$. Flow cytometry was used to measure CD11b expression (**C**); $n = 6-8$. Representative images (20 μ m scale bar) (**D**) of the number of adhered monocytes (**E**) and F-actin content measured via confocal microscopy (**F**); $n = 3-5$. Representative image of shear flow adhesion assay (white dots = adhered cells) (**G**). Quantification over 10 min time course (**H**) and at 10 min (**I**); $n = 3-5$. Data are mean \pm SEM (one-way ANOVA with Tukey's test: * $\&$ [^] $p < 0.05$, ** $\&$ [^] $p < 0.01$, *** $\&$ [^] $p < 0.0001$). In (**H**), [^] denotes comparison between LPS vs. 2DG-LPS.

which are known to be activated during inflammation (16–18). As expected, both MAPKs were significantly phosphorylated when monocytes were treated with LPS (**Figures 4A,B**). Interestingly, blocking glycolysis using 2-DG did not prevent the phosphorylation of ERK1/2 (**Figure 4A**). Moreover, when we pre-treated cells with rapamycin and 2-DG, p38 MAPK phosphorylation was significantly decreased (**Figure 4B**). Therefore, we decided to inhibit p38 MAPK to determine whether this affected LPS-induced monocyte activation and adhesion. We employed SB-203580, an inhibitor of p38 MAPK, which confirmed that this pathway was involved in monocyte activation as we noted LPS was no longer able to increase the cell surface expression of CD11b (**Figure 4C**). Consistent with the inability of LPS to induce CD11b, we also found a reduction in the number of monocytes adhering to fibrinogen when p38 MAPK was inhibited (**Figures 4D,E**). To further confirm p38 MAPK occurs downstream of mTOR and glycolysis, we measured mTOR phosphorylation via western blot and also GLUT-1 levels via flow cytometry with SB-203580 in the

presence of LPS and confirmed that phosphorylation of mTOR and GLUT-1 levels were unchanged (**Figures 4F,G**). These data suggest that LPS-mediated glycolysis and mTOR signaling induce p38 MAPK to promote CD14⁺CD16⁻ monocyte activation and adhesion.

Reactive Oxygen Species Are Involved in Glycolysis-Mediated Activation and Adhesion

Next, we aimed to mechanistically link glycolysis with the induction of p38 MAPK signaling in driving CD14⁺CD16⁻ monocyte activation and adhesion. Inflammatory signaling can trigger p38 MAPK activation by ROS and preventing ROS accumulation using anti-oxidants averts p38 MAPK activation (16, 19, 20). Since one of the by-products of glycolysis is ROS generation, we hypothesized that this may be the link between glycolysis and p38 MAPK activation. Indeed, we found that LPS increased ROS accumulation in monocytes via flow cytometry

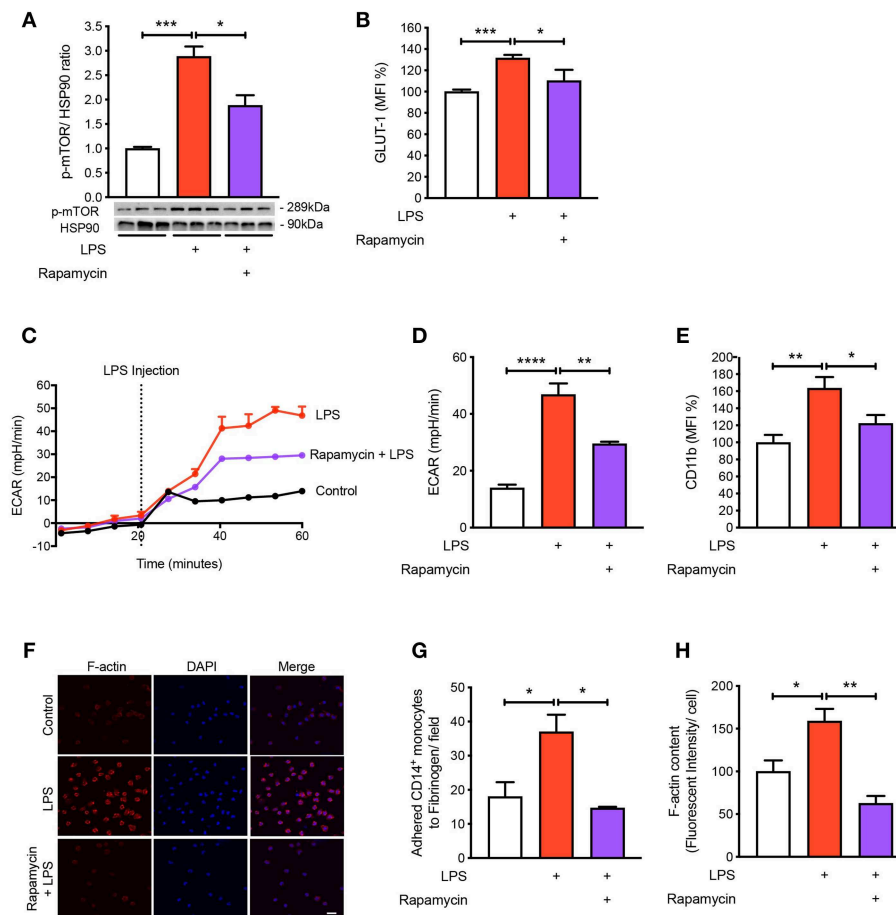


FIGURE 3 | mTOR pathway is involved in regulating glycolysis in LPS-induced monocytes. Isolated human CD14⁺CD16[−] monocytes were pre-treated with or without 20 nM rapamycin an hour before 1 h 100 ng/ml LPS stimulation. mTOR phosphorylation was quantified by western blot at 30 min after LPS stimulation (A); $n = 6-7$. Flow cytometry was used to measure GLUT-1 expression; $n = 3-5$ (B). Extracellular acidification rate (ECAR) was measured in real-time (C,D); $n = 3-4$. CD11b expression was measured by flow cytometry (E); $n = 6-7$. Static cell adhesion assay performed utilizing F-actin and DAPI stain via confocal microscopy (20 μ m scale bar) (F-H); $n = 3-4$. Data are mean \pm SEM (un-paired t -test and one-way ANOVA with Tukey's test: * $p < 0.05$, ** $p < 0.01$, *** $p < 0.001$, **** $p < 0.0001$).

(Figure 5A). Our data suggest that ROS generation was a consequence of increased glycolysis, as interventions upstream of glycolysis, rapamycin, and 2-DG, were able to block global ROS levels using the H₂DCFDA fluorescent indicator (Figure 5A). Moreover, to determine whether the increase in ROS production was generated from glycolysis and not glucose utilization via the mitochondria, we specifically stained for mitochondrial ROS using MitoSOX, which we found to be unchanged with LPS (Figure 5B). To confirm that mitochondrial ROS did not play a role during acute LPS activation, we treated cells with MitoQ that specifically reduces mitochondrial ROS and showed that global ROS levels (Figure 5C) and CD11b expression were unchanged (Figure 5D). We also measured ROS production in LPS-induced monocytes that were pre-treated with the p38 MAPK inhibitor SB-203580 and found no change in ROS, suggesting that p38 MAPK is downstream of ROS in LPS-activated monocytes (Figure 5E). Next, we inhibited ROS oxidation of cysteines using N-acetyl-L-cysteine (NAC) and measured phosphorylation of p38 MAPK to delineate whether ROS activated p38 MAPK.

Indeed, we found that pre-treating cells with NAC before incubating with LPS prevented p38 MAPK activation but not ERK1/2 phosphorylation, suggesting that the ROS driven pathway was specific to p38 MAPK signaling (Figures 5F,G). These results show that ROS production in LPS-induced monocytes occurs downstream of the mTOR and glycolytic pathway but upstream of p38 MAPK. More importantly, inhibiting ROS production using NAC, significantly prevented LPS-induced CD11b expression (Figure 5H). Furthermore, NAC was able to affect LPS-induced monocyte adhesion as well as reduce F-actin formation (Figures 5I-K). These results indicate that LPS stimulation of monocytes triggers mTOR regulated glycolysis, which drives ROS, causing downstream p38 MAPK activation, resulting in monocyte activation and adhesion.

DISCUSSION

During an acute inflammatory response, monocytes become activated, adhere to the endothelium, and transmigrate into

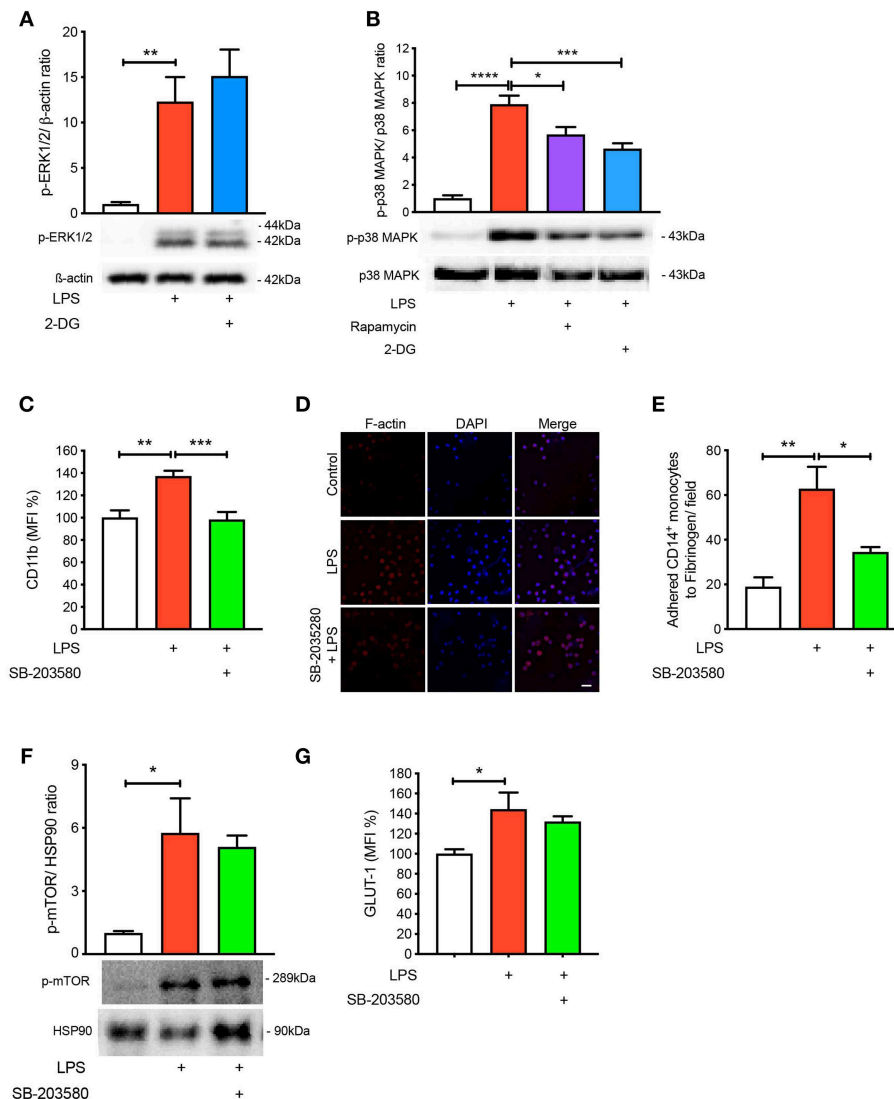


FIGURE 4 | p38 MAPK is involved in LPS-induced monocyte activation and adhesion. ERK1/2 phosphorylation were measured with or without 5 mM 2-DG followed by 1 h of 100 ng/ml LPS stimulation (A); $n = 4-5$. p38 MAPK phosphorylation was measured with or without 5 mM 2-DG or 20 nM rapamycin before 100 ng/ml LPS stimulation (B); $n = 6-7$. Cells were pre-treated with 5 nM SB-203580 followed by 1 h of 100 ng/ml LPS stimulation before measuring CD11b expression via flow cytometry (C); $n = 8$. Static cell adhesion assay was performed utilizing F-actin and DAPI stain via confocal microscopy (20 μm scale bar); $n = 3-4$ (D-E). mTOR phosphorylation was quantified by western blot at 30 min after LPS stimulation in the presence of 5 nM SB-203580 (F); $n = 3$. Flow cytometry was used to measure GLUT-1 expression; $n = 3-4$ (G). Data are mean \pm SEM (one-way ANOVA with Tukey's test: * $p < 0.05$, ** $p < 0.01$, *** $p < 0.001$, **** $p < 0.0001$).

the inflamed tissue. However, the mechanistic pathways by which human CD14⁺CD16⁻ monocytes activate and adhere, in particular the specific metabolic pathways are yet to be fully elucidated. In this study, we revealed that increased flux through glycolysis is critical to induce the signaling pathways that monocytes rely on for adherence. We found that LPS-stimulated human CD14⁺CD16⁻ monocytes increase CD11b expression and adhesion via the phosphorylation of mTOR which facilitates the uptake of glucose and glycolysis. When we further investigated the mechanistic link between glycolysis and adhesion, we found that an increase in glycolysis resulted in the production of ROS which activated

the p38 MAPK pathway, leading to monocyte activation and adhesion.

Glycolysis and oxidative phosphorylation (OXPHOS) via the mitochondria are the two main metabolic pathways, which can control the overall phenotype of the cell. A classic example of this are the metabolic status of inflammatory and anti-inflammatory macrophages. Inflammatory or M1-like macrophages are highly glycolytic, while anti-inflammatory or M2-like macrophages have been found to be mitochondrial dependent, using both glucose and fatty acids for OXPHOS (11, 12). More importantly, when glycolysis or OXPHOS are inhibited using specific metabolic inhibitors it reduces the ability

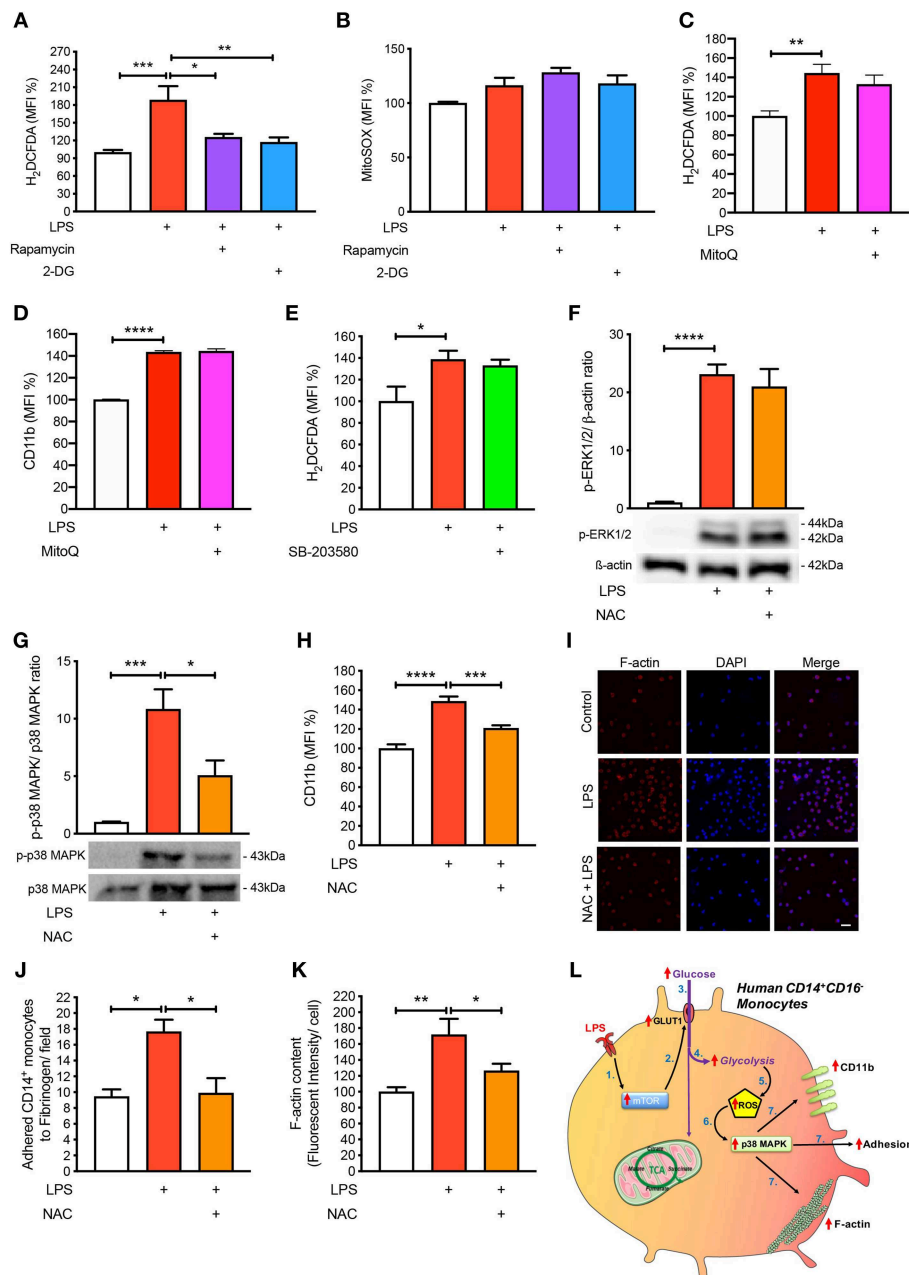


FIGURE 5 | ROS regulates p38 MAPK-induced monocyte activation and adhesion. Isolated human CD14⁺CD16[−] monocytes were pre-treated with or without 20 nM rapamycin or 5 mM 2-DG followed by 1 h of 100 ng/ml LPS stimulation before H₂DCFDA (A) and MitoSOX (B) levels were measured via flow cytometry; *n* = 4–8. Cells were pre-treated with 100 nM MitoQ followed by 1 h of 100 ng/ml LPS stimulation before H₂DCFDA (C) and CD11b (D) levels were measured via flow cytometry; *n* = 7–8. Cells were pre-treated with 5 nM SB-203580 followed by 1 h of 100 ng/ml LPS stimulation before measuring H₂DCFDA levels via flow cytometry (E); *n* = 4. Cells were pre-treated with or without 1 mM NAC before stimulating with 100 ng/ml LPS for 30 min before measuring ERK1/2 (F) and p38 MAPK (G) phosphorylation; *n* = 4–5. CD11b expression was measured via flow cytometry; *n* = 6–8 (H); *n* = 6–7. Static cell adhesion assay performed utilizing F-actin and DAPI stain via confocal microscopy (20 μm scale bar) (I–K); *n* = 3–6. Schematic diagram of proposed mechanistic pathway of acute LPS-induced CD14⁺CD16⁺ monocyte activation and adhesion (L). Data are mean ± SEM (one-way ANOVA with Tukey's test: **p* < 0.05, ***p* < 0.01, ****p* < 0.001, *****p* < 0.0001).

of macrophages to become inflammatory or anti-inflammatory, respectively. Here, we demonstrate a similar scenario in human CD14⁺CD16[−] monocytes where LPS increased glucose uptake and glycolysis. This is consistent with findings from Stienstra's

group who also show an increase in glycolysis with LPS (21). However, it was somewhat surprising OXPHOS or mitochondrial activity was not reduced in the presence of LPS. This could suggest that the mitochondria does not play an essential role

in providing the increase in energy metabolism for cellular activation in human CD14⁺CD16[−] monocytes during short (1h) exposure compared to 24h of LPS stimulation, where many other cellular changes are likely to be occurring (21). The non-reliance on the mitochondria in acute responses could be because CD14⁺CD16[−] monocytes do not require much energy as they are carried around the body by the circulatory system and require rapid activation upon an inflammatory stimulus and so have evolved to require little respirative metabolism. Thus, consistent with the hypothesis that CD14⁺CD16[−] monocytes use glycolytic metabolism, when this pathway was inhibited using 2-DG, we found a loss in the ability of these monocytes to increase cell surface CD11b and to adhere. This builds on a growing body of evidence that the cellular metabolic preference is a key determinate of cellular function.

Previously, it has been noted that mTOR is involved in regulating cell adhesion in cancer cells; however, the mechanistic pathway downstream of mTOR has not been explored. mTOR, the central regulator of cellular growth and proliferation, also governs glycolysis. Studies in BMDMs have shown that mTOR is responsible for upregulating glucose transporters, namely GLUT-1 (15). Glucose transporters are involved in facilitating the uptake of glucose which increases the rate of glycolysis. This pathway was also activated in our human CD14⁺CD16[−] monocytes as inhibition of mTOR with rapamycin prevented GLUT-1 movement to the surface as well as glycolysis, leading to a reduction in monocytic activation and adhesion.

Delving further into the mechanisms linking glycolysis to the activation and adhesion of LPS-induced monocytes, LPS has previously been known to stimulate many activation pathways including p38 MAPK and ERK1/2 in human CD14⁺CD16[−] monocytes. Additionally, p38 MAPK and ERK1/2 have been shown to regulate adhesion of tumor-associated macrophages, suggesting their involvement is important in cellular activation in order to cause adhesion to vessels or a matrix (16, 18). Interestingly, only p38 MAPK was found to be important in glycolysis-mediated cell adhesion in the CD14⁺CD16[−] monocytes, suggesting that glycolytic events are key in regulating the phosphorylation of p38 MAPK. One of the stressors that is capable of signaling via p38 MAPK is ROS. Within the glycolytic pathway, we found that non-mitochondrial generated ROS appeared to activate p38 MAPK in order to cause LPS-induced monocyte activation. The source of non-mitochondrial ROS is likely to be NADPH-oxidase (NOX)-dependent, which is induced via the glycolytic pathway (22). Additionally, studies have shown that NOX enzymes are increased in human monocytes and macrophages upon inflammatory conditions in addition with increased ROS levels (23).

Clinical trials testing the benefits of antioxidants in CVD-related clinical trials have been disappointing, with many larger clinical trials showing no beneficial effects when given antioxidants such as vitamin E, C or coenzyme Q. After careful reflection on these trials, the limitations of

these studies should be considered before closing the door to the therapeutic potential of antioxidants in CVD. These include dosage, efficacy, *in vivo* biological activity, specificity and statistical power (24–26). However, the importance of ROS in cellular metabolism in CVD is regaining traction. Importantly, we are now gaining a better understanding on the regulator of cellular ROS and how to harness the power of endogenous antioxidant pathways such as Nrf2 or restoring mitochondrial health (if the mitochondria is the driver) (27). Another important point to consider is the timing of intervention to therapeutic gain, perhaps antioxidants need to be administered earlier in life as opposed to testing this in middle to older aged participants in trial setting and formulating appropriate primary endpoints. How glycolysis regulates p38 MAPK is currently unknown, but given p38 MAPK is downstream of ROS, it is likely that MKK3/6, and potentially ASK1, are intermediary targets (19, 28). Nonetheless, LPS-induced glycolysis is required for the phosphorylation of p38 MAPK to cause monocyte activation.

In summary, we have found that the metabolism of glucose by human CD14⁺CD16[−] monocytes in response to LPS is critical for the activation of these cells (**Figure 5L**). These findings contribute to a larger body of evidence revealing that changes in cellular metabolism are central for the cell to respond to extrinsic stimuli (bacterial, viral, cytokines, etc). These metabolic changes assist the cell in performing effector functions and as such have become a key interest in disrupting unwanted processes, particularly in the immune system. Understanding these pathways and selectively inhibiting glycolysis may aid in chronic diseases where excessive monocyte recruitment is detrimental.

DATA AVAILABILITY

The datasets generated for this study are available on request to the corresponding author.

AUTHOR CONTRIBUTIONS

ML, AA-S, EC, WS, CB, OC, and MF conducted the experiments and analysis. ML, AA-S, AF, CP, GL, DH, JH, and AM contributed to the experimental design and intellectual input. ML, AA-S, and AM wrote and revised the manuscript. All authors contributed to editing the manuscript.

FUNDING

This work was supported by NHMRC grant (APP1142398) to AM, GL, and JH. AM was supported by a Centenary Award from CSL. ML was supported by a postdoctoral fellowship from the National Heart foundation (101951).

REFERENCES

- Ley K, Laudanna C, Cybulsky MI, Nourshargh S. Getting to the site of inflammation: the leukocyte adhesion cascade updated. *Nat Rev Immunol.* (2007) 7:678–89. doi: 10.1038/nri2156
- Liu L, Wei Y, Wei X. The immune function of Ly6Chi inflammatory monocytes during infection and inflammation. *Curr Mol Med.* (2017) 17:1–1. doi: 10.2174/1566524017666170220102732
- Al-Sharea A, Lee MK, Whillas A, Michell D, Shihata W, Nicholls AJ, et al. Chronic sympathetic driven hypertension promotes atherosclerosis by enhancing hematopoiesis. *Haematologica.* (2018) 104:456–67. doi: 10.3324/haematol.2018.192898
- Dragoljevic D, Kraakman MJ, Nagareddy PR, Ngo D, Shihata W, Kammoun HL, et al. Defective cholesterol metabolism in haematopoietic stem cells promotes monocyte-driven atherosclerosis in rheumatoid arthritis. *Eur Heart J.* (2018) 39:2158–67. doi: 10.1093/eurheartj/ehy119
- Al-Sharea A, Lee M, Whillas A, Flynn MC, Chin-Dusting J, Murphy AJ. Nicotinic acetylcholine receptor alpha 7 stimulation dampens splenic myelopoiesis and inhibits atherogenesis in ApoE ^{-/-} mice. *Atherosclerosis.* (2017) 265:47–53. doi: 10.1016/j.atherosclerosis.2017.08.010
- Fleetwood AJ, Lee M, Singleton W, Achuthan A, Lee M-C, O'Brien-Simpson NM, et al. Metabolic remodeling, inflammasome activation, and pyroptosis in macrophages stimulated by *Porphyromonas gingivalis* and its outer membrane vesicles. *Front Cell Infect Microbiol.* (2017) 7:351. doi: 10.3389/fcimb.2017.00351
- Shehata HM, Murphy AJ, Kit Lee M, Gardiner CM, Crowe SM, Sanjabi S, et al. Sugar or fat?—metabolic requirements for immunity to viral infections. *Front Immunol.* (2017) 8:1311. doi: 10.3389/fimmu.2017.01311
- Masson JJ, Murphy AJ, Lee MK, Ostrowski M, Crowe SM, Palmer CS. Assessment of metabolic and mitochondrial dynamics in CD4⁺ and CD8⁺ T cells in virologically suppressed HIV-positive individuals on combination antiretroviral therapy. *PLoS ONE.* (2017) 12:e0183931. doi: 10.1371/journal.pone.0183931
- Tannahill G, Curtis A, Adamik J, Palsson-rmott E, McGettrick A, Goel G, et al. Succinate is an inflammatory signal that induces IL-1 β through HIF-1 α . *Nature.* (2013) 496:238–42. doi: 10.1038/nature11986
- Cros J, Cagnard N, Woollard K, Patey N, Zhang S-Y, Senechal B, et al. Human CD14dim monocytes patrol and sense nucleic acids and viruses via TLR7 and TLR8 receptors. *Immunity.* (2010) 33:375–86. doi: 10.1016/j.immuni.2010.08.012
- Huang S, Smith AM, Everts B, Colonna M, Pearce EL, Schilling JD, et al. Metabolic reprogramming mediated by the mTORC2-IRF4 signaling axis is essential for macrophage alternative activation. *Immunity.* (2016) 45:817–30. doi: 10.1016/j.immuni.2016.09.016
- Huang S, Everts B, Ivanova Y, O'Sullivan D, Nascimento M, Smith A, et al. Cell-intrinsic lysosomal lipolysis is essential for alternative activation of macrophages. *Nat Immunol.* (2014) 15:846–55. doi: 10.1038/ni.2956
- Aft R, Zhang F, Gius D. Evaluation of 2-deoxy-D-glucose as a chemotherapeutic agent: mechanism of cell death. *Brit J Cancer.* (2002) 87:805–12. doi: 10.1038/sj.bjc.6600547
- Moon J-S, Hisata S, Park M-A, DeNicola GM, Ryter SW, Nakahira K, et al. mTORC1-induced HK1-dependent glycolysis regulates NLRP3 inflammasome activation. *Cell Rep.* (2015) 12:102–15. doi: 10.1016/j.celrep.2015.05.046
- Buller CL, Loberg RD, Fan M-H, Zhu Q, Park JL, Vesely E, et al. A GSK-3/TSC2/mTOR pathway regulates glucose uptake and GLUT1 glucose transporter expression. *Am J Physiol Cell Physiol.* (2008) 295:C836–43. doi: 10.1152/ajpcell.00554.2007
- Li L, Leung DY, Goleva E. Activated p38 MAPK in peripheral blood monocytes of steroid resistant asthmatics. *PLoS ONE.* (2015) 10:e0141909. doi: 10.1371/journal.pone.0141909
- Kim H, Ullevig SL, Zamora D, Lee C, Asmis R. Redox regulation of MAPK phosphatase 1 controls monocyte migration and macrophage recruitment. *Proc National Acad Sci USA.* (2012) 109:E2803–12. doi: 10.1073/pnas.1212596109
- Kurosawa M, Numazawa S, Tani Y, Yoshida T. ERK signaling mediates the induction of inflammatory cytokines by bufalin in human monocytic cells. *Am J Physiol Cell Physiol.* (2000) 278:C500–8. doi: 10.1152/ajpcell.2000.278.3.C500
- Noguchi T, Ishii K, Fukutomi H, Naguro I, Matsuzawa A, Takeda K, et al. Requirement of reactive oxygen species-dependent activation of ASK1-p38 MAPK pathway for extracellular ATP-induced apoptosis in macrophage. *J Biol Chem.* (2008) 283:7657–65. doi: 10.1074/jbc.M708402200
- Son Y, Kim S, Chung H-T, Pae H-O. Methods in enzymology. *Sect H2o2 Regul Cell Signal.* (2013) 528:27–48. doi: 10.1016/B978-0-12-405881-1.00002-1
- Lachmandas E, Boutens L, Ratter JM, Hijmans A, Hooiveld GJ, Joosten LA, et al. Microbial stimulation of different Toll-like receptor signalling pathways induces diverse metabolic programmes in human monocytes. *Nat Microbiol.* (2016) 2:16246. doi: 10.1038/nmicrobiol.2016.246
- Azevedo EP, Rochael NC, Gulmaras Costa AB, de Souza-Vieira TS, Ganilho J, Saraiva EM, et al. A metabolic shift toward pentose phosphate pathway is necessary for amyloid fibril- and phorbol 12-myristate 13-acetate-induce neutrophil extracellular trap (NET) formation. *J Biol Chem.* (2015) 36:22174–83. doi: 10.1074/jbc.M115.640094
- Manea A, Manea SA, Gan AM, Constantin A, Fenyo IM, Raicu M, et al. Human monocytes and macrophages express NADPH oxidase 5; a potential source of reactive oxygen species in atherosclerosis. *Biochem Biophys Res Commun.* (2015) 461:172–9. doi: 10.1016/j.bbrc.2015.04.021
- Manson JE, Gaziano JM, Spelsberg A, Ridker PM, Cook NR, Buring JE, et al. A secondary prevention trial of antioxidant vitamins and cardiovascular disease in women. Rationale, design, and methods. The WACS Research Group. *Ann Epidemiol.* (1995) 5:261–9. doi: 10.1016/1047-2797(94)00091-7
- Stephens NG, Parsons A, Schofield PM, Kelly F, Cheeseman K, Mitchinson MJ. Randomised controlled trial of vitamin E in patients with coronary disease: Cambridge Heart Antioxidant Study (CHAOS). *Lancet.* (1996) 347:781–6. doi: 10.1016/S0140-6736(96)90866-1
- Heart Protection Study Collaborative Group. MRC/BHF Heart protection study of antioxidant vitamin supplementation in 20,536 high-risk individuals: a randomised placebo-controlled trial. *Lancet.* (2002) 360:23–33. doi: 10.1016/S0140-6736(02)09328-5
- Mills EL, Ryan DG, Prag HA, Dikovskaya D, Menon D, Zasiana Z, et al. Accumulation of succinate controls activation of adipose tissue thermogenesis. *Nature.* (2018) 556:133–7. doi: 10.1039/nature25986
- Cuenda A, Rousseau S. p38 MAP-Kinases pathway regulation, function and role in human diseases. *Biochimica Biophysica Acta.* (2007) 1773:1358–75. doi: 10.1016/j.bbamcr.2007.03.010

Conflict of Interest Statement: The authors declare that the research was conducted in the absence of any commercial or financial relationships that could be construed as a potential conflict of interest.

The handling editor declared a past collaboration with the authors ML and AM.

Copyright © 2019 Lee, Al-Sharea, Shihata, Bertuzzo Veiga, Cooney, Fleetwood, Flynn, Claeson, Palmer, Lancaster, Henstridge, Hamilton and Murphy. This is an open-access article distributed under the terms of the Creative Commons Attribution License (CC BY). The use, distribution or reproduction in other forums is permitted, provided the original author(s) and the copyright owner(s) are credited and that the original publication in this journal is cited, in accordance with accepted academic practice. No use, distribution or reproduction is permitted which does not comply with these terms.



HECT E3 Ubiquitin Ligase-Regulated Txnip Degradation Facilitates TLR2-Mediated Inflammation During Group A Streptococcal Infection

Po-Chun Tseng^{1,2}, Chih-Feng Kuo^{3,4}, Miao-Huei Cheng⁵, Shu-Wen Wan⁵, Chiou-Feng Lin^{2,6}, Chih-Peng Chang^{7,8}, Yee-Shin Lin^{7,8}, Jiunn-Jong Wu⁹, Chi-Chen Huang¹⁰ and Chia-Ling Chen^{1,11*}

¹ School of Respiratory Therapy, College of Medicine, Taipei Medical University, Taipei, Taiwan, ² Department of Microbiology and Immunology, School of Medicine, College of Medicine, Taipei Medical University, Taipei, Taiwan, ³ School of Medicine, I-Shou University, Kaohsiung, Taiwan, ⁴ Department of Nursing, I-Shou University, Kaohsiung, Taiwan, ⁵ School of Medicine for International Students, College of Medicine, I-Shou University, Kaohsiung, Taiwan, ⁶ Graduate Institute of Medical Sciences, Taipei Medical University, Taipei, Taiwan, ⁷ Department of Microbiology and Immunology, College of Medicine, National Cheng Kung University, Tainan, Taiwan, ⁸ Center of Infectious Disease and Signaling Research, National Cheng Kung University, Tainan, Taiwan, ⁹ Department of Biotechnology and Laboratory Science in Medicine, School of Biomedical Science and Engineering, National Yang-Ming University, Taipei, Taiwan, ¹⁰ Graduate Institute of Neural Regenerative Medicine, College of Medical Science and Technology, Taipei Medical University, Taipei, Taiwan, ¹¹ Pulmonary Research Center, Wan Fang Hospital, Taipei Medical University, Taipei, Taiwan

OPEN ACCESS

Edited by:

Catarina R. Almeida,
University of Aveiro, Portugal

Reviewed by:

Inger Øynebråten,
Oslo University Hospital, Norway
Susanta Kar,
Central Drug Research Institute
(CSIR), India

*Correspondence:

Chia-Ling Chen
chialing66@tmu.edu.tw

Specialty section:

This article was submitted to
Molecular Innate Immunity,
a section of the journal
Frontiers in Immunology

Received: 09 February 2019

Accepted: 27 August 2019

Published: 18 September 2019

Citation:

Tseng P-C, Kuo C-F, Cheng M-H,
Wan S-W, Lin C-F, Chang C-P,
Lin Y-S, Wu J-J, Huang C-C and
Chen C-L (2019) HECT E3 Ubiquitin
Ligase-Regulated Txnip Degradation
Facilitates TLR2-Mediated
Inflammation During Group A
Streptococcal Infection.
Front. Immunol. 10:2147.
doi: 10.3389/fimmu.2019.02147

Thioredoxin-interacting protein (Txnip) inhibits the activity of thioredoxin (Trx) to modulate inflammatory responses. The burden of inflammation caused by microbial infection is strongly associated with disease severity; however, the role of Txnip in bacterial infection remains unclear. In Group A *Streptococcus* (GAS)-infected macrophages, Txnip was degraded independent of glucose consumption and streptococcal cysteine protease expression. Treatment with proteasome inhibitors reversed GAS-induced Txnip degradation. The activation of Toll-like receptor 2 (TLR2) initiated Txnip degradation, while no further Txnip degradation was observed in TLR2-deficient bone marrow-derived macrophages. NADPH oxidase-regulated NF- κ B activation and pro-inflammatory activation were induced and accompanied by Txnip degradation during GAS infection. Silencing Txnip prompted TLR2-mediated inducible nitric oxide synthase (iNOS)/NO, TNF- α , and IL-6 production whereas the blockage of Txnip degradation by pharmacologically inhibiting the HECT E3 ubiquitin ligase with heclin and AMP-dependent protein kinase with dorsomorphin effectively reduced such effects. Our findings reveal that TLR2/NADPH oxidase-mediated Txnip proteasomal degradation facilitates pro-inflammatory cytokine production during GAS infection.

Keywords: group A *Streptococcus*, Txnip, TLR2, itch, ubiquitination

INTRODUCTION

Recognition of Toll-like receptors (TLRs), the most important pathogen recognition receptors expressed on innate immune cells, with pathogen-associated molecular patterns can rapidly initiate the coordinated activation of transcriptional factors and result in the effective expression of pro-inflammatory mediators (1). In response to *Streptococcus pyogenes* infection, the production of

pro-inflammatory cytokines is mostly regulated by TLR-myeloid differentiation factor 88 (MyD88) signaling (2, 3). Group A *Streptococcus* (GAS) infection causes various diseases ranging from mild pharyngitis and impetigo to severe necrotizing fasciitis and streptococcal toxic shock syndrome (STSS) (4). In STSS, the excessive production of various cytokines is thought to be responsible for severe systemic effects, and serum levels of TNF- α and IL-6 show the highest correlation with disease severity (5, 6).

Thioredoxin-interacting protein (Txnip), a vitamin D₃-upregulated protein in 1 α ,25-dihydroxyvitamin D₃ (1,25[OH]₂D₃)-treated HL-60 cells (7), acts as an endogenous inhibitor of the antioxidant thioredoxin (Trx), which is involved in a wide variety of cellular processes including the response to oxidative stress, cancer development, metabolic diseases, and inflammatory processes (8–13). The reduction of Txnip protein facilitates tumor progression, whereas the overexpression of Txnip results in the inhibition of metastasis or further triggers cells undergoing apoptosis (9, 14, 15). In addition to the pro-apoptotic role of Txnip under stress, it also plays a crucial role in the induction of reactive oxygen species (ROS)-mediated NLRP3 inflammasomes whereby initiating inflammatory responses (12, 15, 16).

As a member of the alpha-arrestin protein family, Txnip comprises a PXXP sequence for the binding of SH3 domain-containing proteins such as Trx and a PPXY sequence for the recognition of WW domain-containing proteins such as the E3 ubiquitin ligase Itch (17, 18). Itch belongs to the Nedd4-like family of E3 ubiquitin ligases and has been reported to specifically mediate the transfer of ubiquitin from E2 ubiquitin-conjugating enzymes to Txnip followed by the triggering of proteasomal degradation (18). In addition, AMP-dependent protein kinase (AMPK) has been demonstrated to phosphorylate Txnip, causing its rapid degradation during energy stress (19). Reports indicate that the TNF- α -stimulated reduction of Txnip effectively causes Trx-mediated p65 denitrosylation, which results in the increased DNA binding activities of NF- κ B (20). Consistent with this, exacerbated endotoxic shock occurs along with overactivated NF- κ B and excessive nitric oxide (NO) induction in Txnip-deficient mice during lipopolysaccharide (LPS) stimulation (21). Therefore, the stability of Txnip has certain pathophysiological impacts on inflammatory diseases. Txnip is a vital regulator of NF- κ B activation; however, little is known about its stability in controlling inflammation during bacterial infection. In this study, we investigated TLR2/NADPH oxidase-initiated HECT E3 ubiquitin ligase-dependent Txnip degradation for cytokine induction during GAS infection.

MATERIALS AND METHODS

Bacteria

GAS strain NZ131 (type M49) was a gift from Dr. D. R. Martin (New Zealand Communicable Disease Center, Porirua). GAS strain A20 (type M1) and *speB*-deleted SW574 were kindly provided by Dr. Y. S. Lin (National Cheng Kung University Medical College, Taiwan). A clinically isolated strain of *Staphylococcus aureus* (S2-1790) was kindly provided by Dr. C. F. Lin (Taipei Medical University, Taiwan). A fresh colony was

inoculated into tryptic soy broth containing 0.5% yeast extract (TSBY) (Difco Laboratories, Detroit, MI, USA) for 16 h and then renewed with fresh TSBY broth for another 3 h incubation at 37°C. The bacterial density was determined by measuring the absorbance at 600 nm with a spectrophotometer (Beckman Instruments, Somerset, NJ, USA) and plating serial dilutions of the samples on TSBY agar for counting CFU after incubation overnight at 37°C. For the preparation of heat-killed GAS, suspended bacteria were treated at 100°C for 30 min.

Cell Cultures and Reagents

RAW264.7 macrophage cells and THP-1 monocytic cells kindly provided by Dr. C. F. Lin (Taipei Medical University, Taiwan) were obtained from American Type Culture Collection (ATCC) and cultured in Dulbecco's modified Eagle's medium (DMEM) and RPMI 1640 (Gibco, Grand Island, NY, USA) supplemented with 10% heat-inactivated fetal bovine serum (FBS), respectively. Murine BMDMs were isolated from wild-type, *Thr2*^{-/-}, or *Nox2*^{-/-} mice, which were kindly provided by Dr. C. P. Chang and Dr. C. C. Shieh (National Cheng Kung University Medical College, Taiwan) by flushing bone marrow cells from the femurs and tibias of 6- to 10-week-old C57BL/6 mice. Animal experiments were performed according to the guidelines of the Animal Protection Act of Taiwan and the experimental protocols according to guidelines established by the Ministry of Science and Technology, Taiwan were approved by the Laboratory Animal Care and Use Committee of National Cheng Kung University. Briefly, the femurs and tibias of both legs were sterilized by 75% ethanol, and cut at the end of bone. Bone marrow cells were flushed out using syringe and maintained in RPMI (Gibco) containing 10% FBS medium. After centrifuge, bone marrow cells (1 \times 10⁶) were cultured in 10 ml RPMI (Gibco) containing 10% FBS and 10 ng/ml recombinant mouse M-CSF (PeproTech, Rocky Hill, NJ, USA) for 4 days. On day 5, 5 ml of culture medium was replaced with the fresh differentiation medium (RPMI supplemented with 10% FBS and 10 ng/ml M-CSF) for additional 2 days incubation. Triplicate cultures were performed by seeding \sim 5 \times 10⁵ cells/ml in 12-wll plates or \sim 2 \times 10⁴ cells/ml in 96-wll plates for indicated experiments. Samples were then harvested from individual culture wells followed by the subsequent analysis. Lipoteichoic acid (LTA, catalog no. L2515) and peptidoglycans (PGNs, catalog no. 77140) from *S. aureus*, MG132, lactacystin (LAC), bafilomycin A1 (BafA1), chloroquine (CQ), N-acetylcysteine (NAC), heclin, and dorsomorphin were purchased from Sigma-Aldrich (St. Louis, MO, USA).

Bacterial Infection

Bacteria (GAS, HK-GAS, and *S. aureus*) were prepared at the indicated multiplicity of infection (MOI) and mixed with cells in antibiotic-free culture medium followed by 1,200 rpm centrifugation for 5 min. After 1 h incubation, all culture supernatants including controls and infected groups were replaced with fresh medium containing 10 μ g/ml penicillin and 50 μ g/ml gentamicin for further incubation at 37°C. The time point of replacing the antibiotics containing medium is defined as zero hour post-infection. At different hours post-infection (h.p.i), cells were harvested and analyzed. In LTA or PGN treatment, cells

were incubated in the culture medium containing no antibiotics and collected at indicated time points. The media glucose consumption during infection was measured using Breeze[®]2 blood glucose test strips and a Breeze[®]2 blood glucose meter (Bayer Health Care, Mishawaka, WI, USA) with a detection range of 20–600 mg/dL.

Western Blot Analysis and Immunoprecipitation Assay

Total cell lysates were extracted using a Triton X-100-based lysis buffer (1% Triton X-100, 150 mM NaCl, 10 mM Tris, pH 7.5, 5 mM EDTA, 5 mM NaN₃, 10 mM NaF, and 10 mM sodium pyrophosphate) with a protease inhibitor mix and phosphatase inhibitor cocktail I (Sigma) and centrifuged for 10 min at 13,300 rpm. Proteins were resolved using SDS-PAGE and then transferred to a PVDF membrane (Millipore Corporation, Billerica, MA, USA). After blocking, blots were developed with a series of antibodies against Txnip (MBL International Co, Woburn, MA, USA), Itch, ubiquitin and iNOS (Cell Signaling Technology, Beverly, MA, USA), and thioredoxin (Santa Cruz Biotechnology, Santa Cruz, CA, USA). GAPDH (Millipore Corporation) and β -actin (Santa Cruz Biotechnology) were used as internal controls. Finally, blots were hybridized with HRP-conjugated goat anti-rabbit IgG or anti-mouse IgG (Cell Signaling Technology) and developed using an ECL Western blot detection kit (Millipore Corporation) according to the manufacturer's instructions. The band intensity was measured using Image J software (NIH, Bethesda, MD, USA). For IP analysis, cell lysates were incubated with anti-Txnip Ab (5 μ g) and protein G-Sepharose beads for 16 h on a roller at 4°C. The beads were isolated and washed by centrifugation followed by Western blot analysis.

ROS Detection

ROS production was detected using a Cellular Reactive Oxygen Species Detection Assay Kit (Abcam, Cambridge, MA, USA) followed by flow cytometry (FACSCalibur; BD Biosciences, San Jose, CA, USA) analysis and fluorescence microscopic observation (Olympus BX51, Olympus, Center Valley, PA, USA). In brief, cells were infected with GAS and then coincubated with 20 μ M carboxymethyl-H2-dichlorofluorescein diacetate (CM-H₂DCFDA) fluorophore for 30 min at 37°C in the dark. After washing, cells were collected and analyzed using flow cytometry with the excitation at 488 nm. The emission was detected with the FL-1 channel followed by CellQuest Pro 4.0.2 software (BD Biosciences) analysis, and quantification was performed using WinMDI 2.8 software (The Scripps Institute, La Jolla, CA, USA). The percentages of ROS-positive cells each group were normalized to the mean of untreated control groups and shown.

Cell Transfection and RNA Interference

RAW 264.7 cells were transiently transfected with catalytically inactive mouse pCINeo-myc-Itch (C832A) or siRNA oligos for Txnip by Lipofectamine reagent (Invitrogen, Carlsbad, CA, USA) according to the manufacturer's instructions. The myc-Itch (C832A) was kindly provided by Dr. L. J. Hsu (National Cheng Kung University Medical College, Taiwan). The Stealth RNAi[™]

siRNA duplex oligoribonucleotides for Txnip (RNAi-1, 5'-UCC UCCUUGCUAU AUGGACAUC AUU-3'; RNAi-2, 5'-AAUGAU GUCCAUAUAGCAAGGAGGA-3'; RNAi-3, 5'-CCAGCCA ACUCAAGAGGCAAAGAAA-3'; RNAi-4, 5'-UUUCUUUGC CUCUUGAGUUGGCUGG-3'; RNAi-5, 5'-GAGAAGAAAG UUUCUGCAUGUUCA-3'; and RNAi-6, 5'-UGAACAUGC AGGAAACUUUCUUCUC-3') were purchased from Invitrogen. A non-specific scrambled siRNA kit (Stealth[™] RNAi Negative Control Duplexes; Invitrogen) was used as the negative control. To stably express a lentivirus-based short hairpin RNA (shRNA) targeting Itch, TRCN0000026908 (5'-CCCTACGAGTAAATT ATGTTT-3') obtained from the National RNAi Core Facility (Institute of Molecular Biology/Genomic Research Center, Academia Sinica, Taiwan) was used, and TRCN0000072247 (5'-GAATCGTCGTATGCAGTGAAA-3') was used as the control luciferase shRNA (shLuc). Lentiviral mouse Itch shRNA was obtained from the RNAi Core of Research Center of Clinical Medicine (National Cheng Kung University Hospital). Briefly, RAW 264.7 cells were infected with an appropriate MOI for 24 h followed by puromycin (Calbiochem) selection. The protein expression was then measured by Western blot analysis.

NO and Cytokine Determination

For NO detection, nitrite (NO₂⁻) accumulation in the cell culture medium was used as an indicator of NO production by the Griess reaction. Briefly, supernatants were mixed with an equal volume of Griess reagent (1% sulfanilamide, 0.1% naphthylethylenediamine dihydrochloride, and 2.5% H₃PO₄) and incubated for 10 min at room temperature. The relative optical density (OD) of nitrite was measured at 540 nm, and the concentration was evaluated by using sodium nitrite as a standard. TNF- α and IL-6 production were measured by enzyme-linked immunosorbent assay (ELISA) kits (R&D Systems, Minneapolis, MN, USA) according to the manufacturer's instructions.

NF- κ B Activation

RAW-Blue cells that stably express a secreted embryonic alkaline phosphatase (SEAP) reporter construct inducible by NF- κ B and AP-1 were kindly provided by Dr. K. F. Hua (Department of Biotechnology and Animal Science, National Ilan University, Taiwan) and originally purchased from InvivoGen Corp. (San Diego, CA, USA). SEAP activity was measured using QUANTI-Blue SEAP detection reagent (InvivoGen Corp.) according to the manufacturer's instructions. Briefly, RAW-Blue cells were cultured in 96-well plates and infected with GAS during cotreatment with NAC. Twenty microliters of culture supernatants were collected at 24 h post-infection and then incubated with 200 μ l of freshly prepared QUANTI-Blue reagent for 30 min, followed by measurement of the OD at 620–655 nm.

Thioredoxin Activity Assay

Thioredoxin (Trx) activity was measured by using the PROTEOSTAT[®] Thioredoxin-1 assay kit according to manufacturer's instructions (EnZo Life Science, Plymouth Meeting, PA, USA). Briefly, cells were harvested at the indicated time points followed by total protein extraction using a Triton

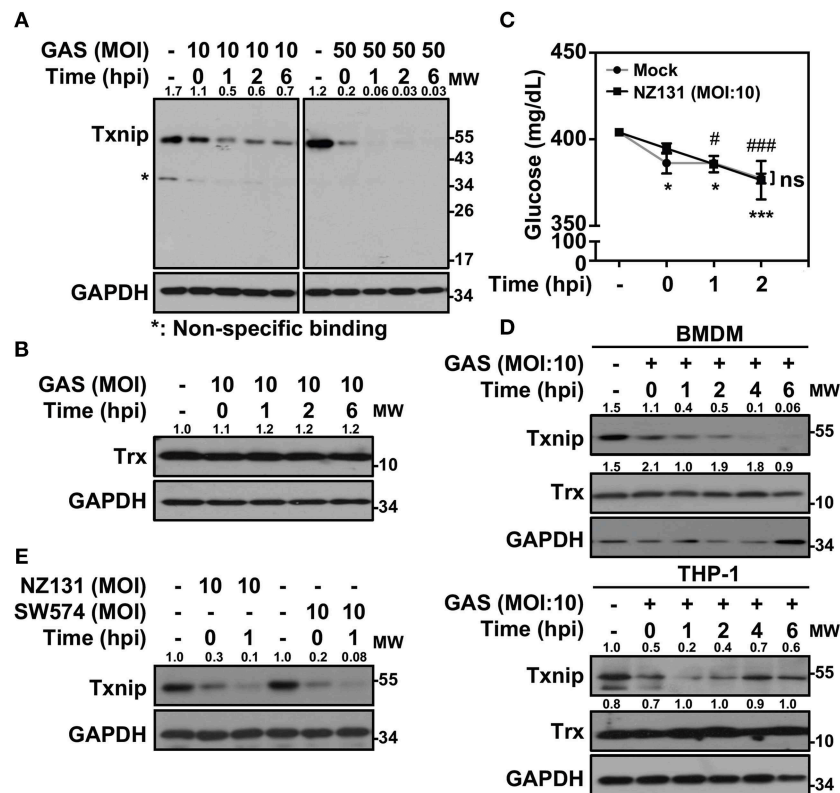


FIGURE 1 | Txnip is degraded in GAS-infected macrophages. **(A)** RAW264.7 cells were infected with the indicated MOI of GAS strain NZ131 (serotype M49) for 1 h. At different hours postinfection (hpi), Txnip expression was measured using Western blot analysis. GAPDH is used as an internal control. **(B)** Expression of Trx in GAS-infected RAW 264.7 cells at the indicated hpi is shown. **(C)** The concentrations of glucose in culture media with or without GAS infection were determined at the indicated hpi. Data are shown as the means \pm SD of triplicate cultures. * $p < 0.05$; *** $p < 0.001$; # $p < 0.05$; ### $p < 0.001$ compared with the culture medium alone. **(D)** Expression of Txnip and Trx in GAS-infected BMDMs and THP-1 cells at different hpi were detected. **(E)** Txnip expression in cells infected with the *speB* wild-type strain NZ131 and the *speB*-deleted strain SW574 at the indicated hpi was measured. GAPDH is used as an internal control. The expression ratios of Txnip and Trx to internal controls are shown. Protein molecular weights (MW) are indicated in kilodaltons. Western blot results represent at least two independent experiments.

X-100-based lysis buffer. Samples (20 μ g/10 μ l) were then incubated with 70 μ l of insulin containing Trx-1 Assay Master Mix and 10 μ l of dithiothreitol (DTT) at room temperature for 30 min in dark. After adding 10 μ l of Stop Reagent working solution, the fluorescence intensity was measured by a Varioskan Flash Multimode Reader at Ex500/Em603 nm (ThermoFisher Scientific Inc.). The fluorescence intensities of each group were then normalized to the mean of untreated control groups and shown.

Statistics

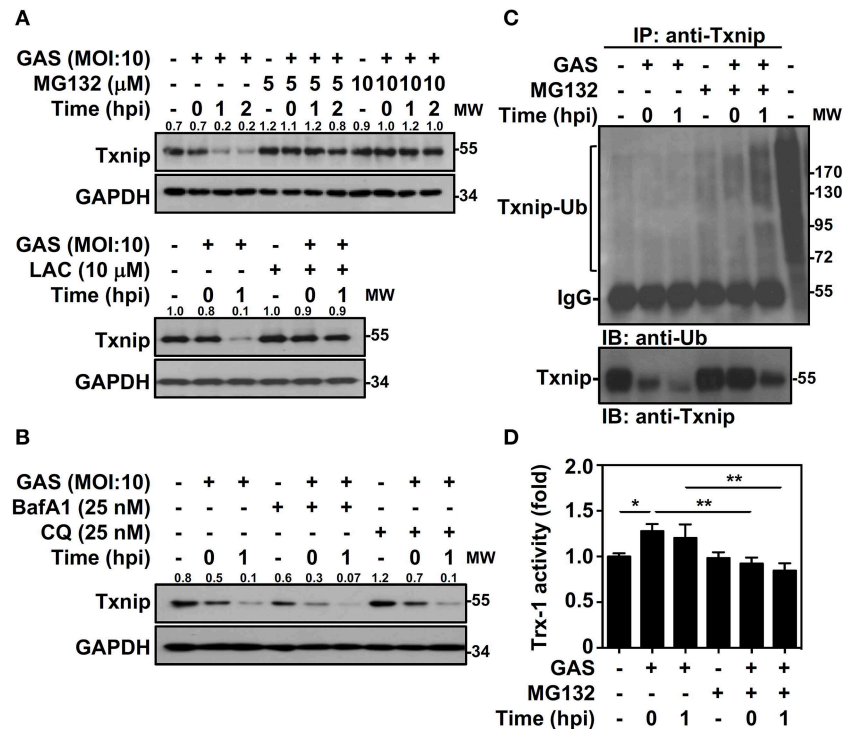
Comparisons between two treatments were performed by unpaired *t*-test, and comparisons between various groups were performed by one-way ANOVA with GraphPad Prism version 6.0 (La Jolla, CA). Statistical significance was set at $p < 0.05$.

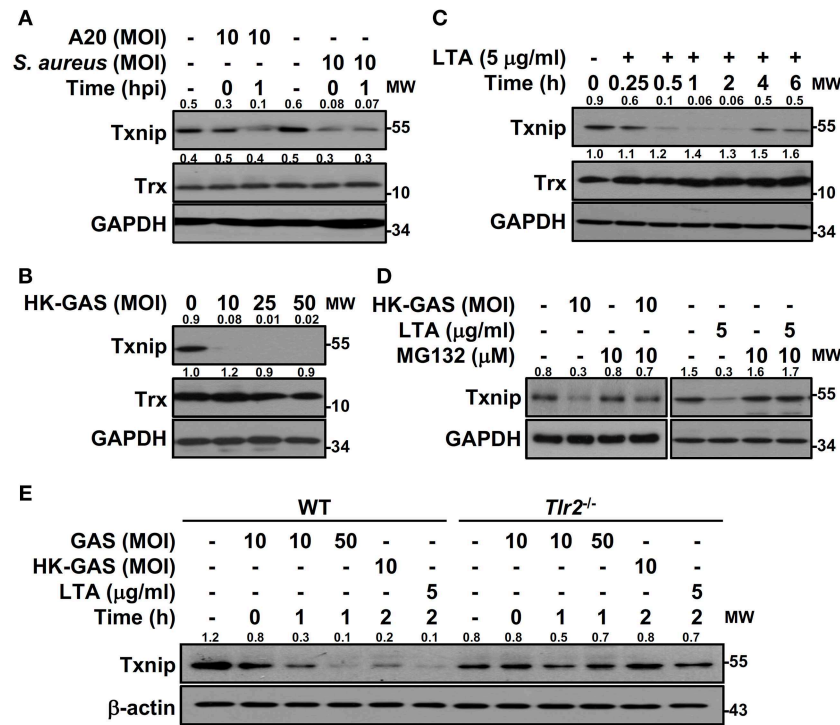
RESULTS

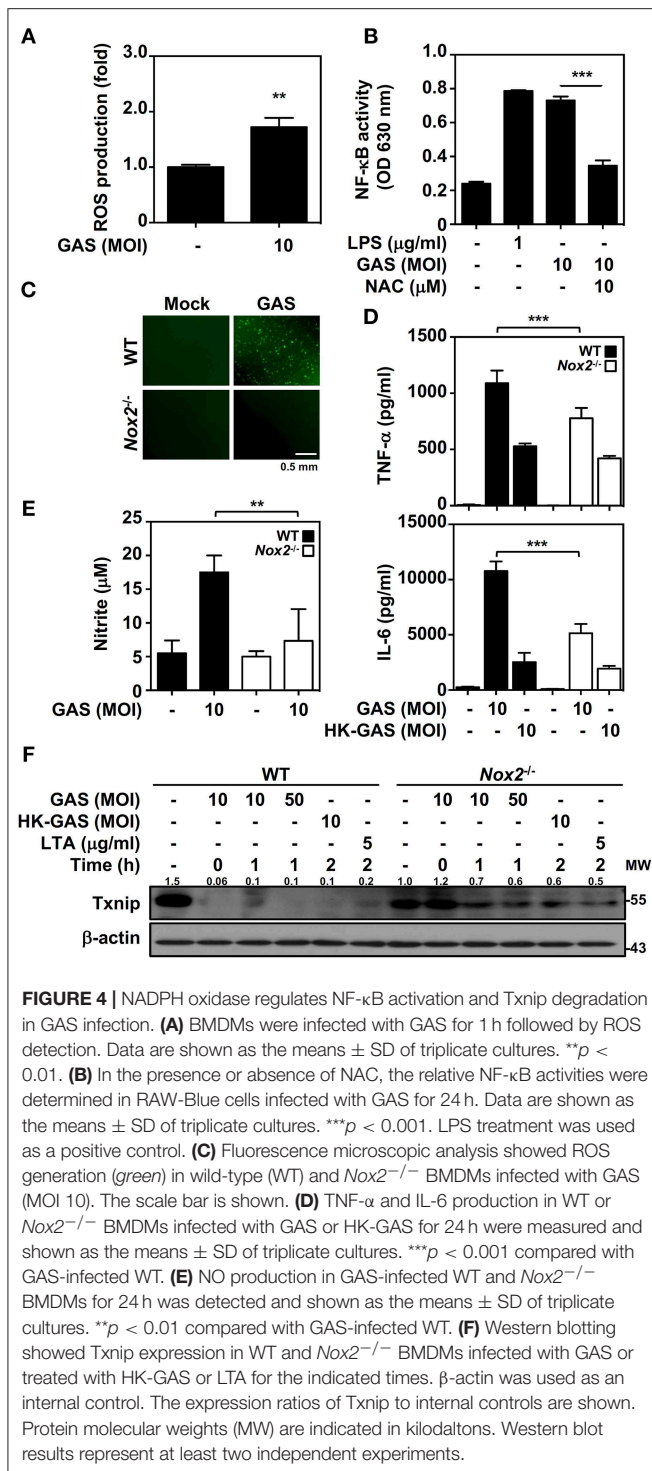
GAS Infection Triggers Txnip Degradation

Txnip^{-/-} mice were extremely susceptible to LPS-induced endotoxic shock via increasing NF- κ B activation and NO

production (21). In Gram-positive bacterial infection, the function of Txnip in regulating inflammatory induction remains unclear. Therefore, we sought to investigate the role of Txnip in GAS-infected macrophages. Murine macrophage RAW264.7 cells were infected with different multiplicities of infection (MOIs) of GAS for 1 h, and the protein expression of Txnip was determined at different times post-infection. Txnip protein exhibited time- and dose-dependent reductions in expression during GAS infection (Figure 1A), while the expression of Trx remained similar (Figure 1B). The expression of Txnip has been shown to be tightly correlated with the extracellular concentration of glucose (22); therefore, glucose consumption during GAS infection was determined. The results indicated that glucose consumption occurred both in non-infected and GAS-infected RAW 264.7 cells along with the incubation. However, there were no significant differences of glucose consumption between non-infected and infected cells within 2 h post-infection, while Txnip had already been degraded in GAS infection (Figure 1C). Further confirmation of the changes in Txnip expression in GAS-infected bone marrow-derived macrophages (BMDMs) and naïve human monocytic THP-1 cells revealed







with GAS or stimulated with HK-GAS and LTA. The degradation of Txnip was partly inhibited in *Nox2*^{-/-} BMDMs, which also corresponded to the lower production of TNF-α, IL-6, and NO (Figure 4F). In GAS infection or TLR2 activation, Txnip exhibits NADPH oxidase-dependent degradation accompanied by NF-κB-mediated pro-inflammation.

Txnip Degradation Prompts TLR2-mediated Inflammatory Mediator Production

Txnip^{-/-} mice were previously demonstrated to be capable of inducing abundant NF-κB activation in LPS stimulation (21). We further confirmed whether Txnip deficiency exerts similar effects on TLR2-mediated inflammatory induction. By the transient transfection of specific Txnip siRNAs into RAW264.7 cells, the expression of Txnip was suppressed (Figure 5A). HK-GAS- and LTA-mediated iNOS expression (Figure 5B), and HK-GAS-, LTA-, and PGN-initiated NO production (Figure 5C) were augmented in Txnip knockdown RAW264.7 cells. Likewise, inflammatory TNF-α and IL-6 production was profoundly enhanced in HK-GAS-, LTA-, and peptidoglycan (PGN)-stimulated Txnip knockdown cells (Figures 5D,E). Accordingly, Txnip deficiency certainly potentiates TLR2-mediated inflammatory cytokine induction.

Itch-independent Txnip Degradation in Response to TLR2 Signals

Itch E3 ubiquitin protein ligase has been demonstrated to directly interact with Txnip and act as a robust ubiquitin ligase for Txnip (18); the interaction between Txnip and Itch during GAS infection is therefore verified. Immunoprecipitation analysis revealed that there were very minimum amounts of Txnip interacting with Itch in GAS-infected RAW264.7 cells (data not shown). To further examine Itch-mediated Txnip degradation, Itch knockdown RAW264.7 cells were used (Figure 6A). Interestingly, Txnip protein remained degraded either in GAS-infected wild-type and control shLuc-cells or in GAS-infected shItch-cells (Figure 6B). Further stimulation of HK-GAS, LTA and PGN also revealed the similar degradation of Txnip in both control shLuc- and shItch-cells (Figure 6C). Itch is similar to other members of the E3 ligase family that utilize the critical cysteine residue in the HECT domain to mediate substrate ubiquitination (29); the mutation of this cysteine in Itch to alanine (C832A) was applied accordingly to validate Txnip degradation in response to TLR2 signals. Similarly, the overexpression of catalytically inactive Itch (C832A mutation) in RAW264.7 cells did not efficiently inhibit GAS-induced Txnip degradation (Figure 6D). Meanwhile, NO production remained similar in wild-type, Itch knockdown or Itch-mutated cells following HK-GAS, LTA, and PGN stimulation (Figure 6E). Moreover, JNK-regulated phosphorylation and activation of Itch is reported to initiate c-FLIP proteasomal degradation in TNF-α stimulation (30). In the presence of JNK and p38 inhibitor, Txnip remained being degraded during GAS infection (Supplemental Figure 3). Accordingly, we speculate that TLR2 activation could rapidly initiate the ubiquitination and proteasomal degradation of Txnip independent of Itch activation.

AMPK- and HECT E3 Ubiquitin Ligase-Regulated Txnip Degradation in TLR2 Activation

Itch belongs to the Nedd4-like family of E3 ubiquitin ligases, which also contains additional members including Nedd4,

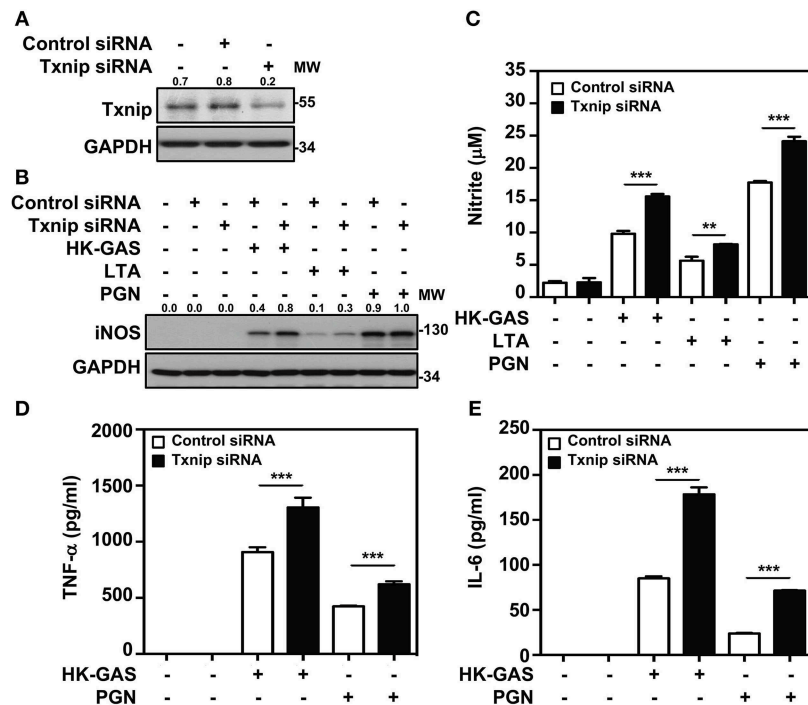


FIGURE 5 | Txnip silencing facilitates TLR2-mediated iNOS/NO, TNF- α , and IL-6 production. **(A)** Western blotting showed the expression levels of Txnip and GAPDH in RAW264.7 cells transfected with control siRNA or Txnip siRNA (5 nM) for 24 h. **(B)** iNOS expression and **(C)** NO production were detected in control siRNA- or Txnip siRNA-expressing cells stimulated with HK-GAS (MOI 10), LTA (5 μ g/ml), and PGN (5 μ g/ml) for 24 h. GAPDH was used as an internal control. The expression ratios of Txnip and iNOS to internal controls are shown. Nitrite concentrations are shown as the means \pm SD of triplicate cultures. ** p < 0.01; *** p < 0.001. The levels of **(D)** TNF- α and **(E)** IL-6 were measured in control siRNA- or Txnip siRNA-expressing cells that were treated with HK-GAS or PGN for 24 h and are shown as the means \pm SD of triplicate cultures. *** p < 0.001 compared with control siRNA-expressed cells. Protein molecular weights (MW) are indicated in kilodaltons. Western blot results represent at least two independent experiments.

Nedd4-2, Smurf1, WWP1, WWP2, NEDL1, and NEDL2 (31, 32). Because the blockage of Itch was insufficient to cease TLR2-mediated Txnip degradation, the involvement of other HECT E3 ubiquitin ligases (HECT E3s) was then investigated. A small molecular inhibitor, heclin, has been identified that specifically causes a conformational change of the HECT domain in Nedd4, Smurf2 and WWP1, resulting in the oxidation of the active site cysteine and inhibiting ligase activity (33). We found that the presence of heclin suppressed TLR2-induced Txnip degradation in RAW264.7 cells (Figure 7A). Similarly, HK-GAS-, LTA-, and PGN-mediated Txnip degradation could be partly reversed by heclin treatment in primary murine peritoneal macrophages as well (Supplemental Figure 4A). Consistent with the stabilization of Txnip, TLR2-activated IL-6 production in RAW264.7 cells was significantly reduced in the presence of heclin (Figure 7B). Nedd4, Smurf2, or WWP1 could be another essential E3 ubiquitin ligase that contributes to Txnip proteasomal degradation in TLR2 activation.

In addition, AMPK has been reported to phosphorylate Txnip, initiating its rapid degradation during energy stress (19). The phosphorylation of AMPK at threonine 172 (Thr172) in TLR2 activation was then measured. Results showed that HK-GAS, LTA, and PGN stimulation induced the rapid AMPK phosphorylation at Thr172 in RAW264.7 cells (Supplemental Figure 5). Interestingly, the

inhibition of AMPK by using its pharmaceutical inhibitor dorsomorphin in RAW264.7 cells distinctly obstructed TLR2-mediated Txnip degradation (Figure 7C) as well as TNF- α production (Figure 7D). TLR2-mediated Txnip degradation were likewise reversed by dorsomorphin treatment in murine peritoneal macrophages (Supplemental Figure 4B). Dorsomorphin is also used as an inhibitor for the bone morphogenetic protein (BMP) signaling (34). In HK-GAS-, LTA-, and PGN-stimulated RAW264.7 cells, the phosphorylation of BMP-mediated Smad1/5/8 was unaffected (Supplemental Figure 6A). Dorsomorphin treatment impeded TLR2-mediated Txnip degradation dose-dependently in RAW264.7 cells, while the phosphorylation of Smad1/5/8 remained unaffected (Supplemental Figure 6B). It suggests that AMPK activation regulates TLR2-mediated Txnip degradation. The present concentration of heclin and dorsomorphin treatment showed no significant cytotoxic effects on RAW264.7 cells (Supplemental Figure 1). Moreover, TLR2-activated NO production was significantly inhibited in the presence of heclin and dorsomorphin along with stable levels of Txnip (Figure 7E). Therefore, the decreased production of IL-6, TNF- α , and NO is consistent with the stabilization of Txnip, which indicates that TLR2-mediated inflammation is partly regulated by Txnip expression.

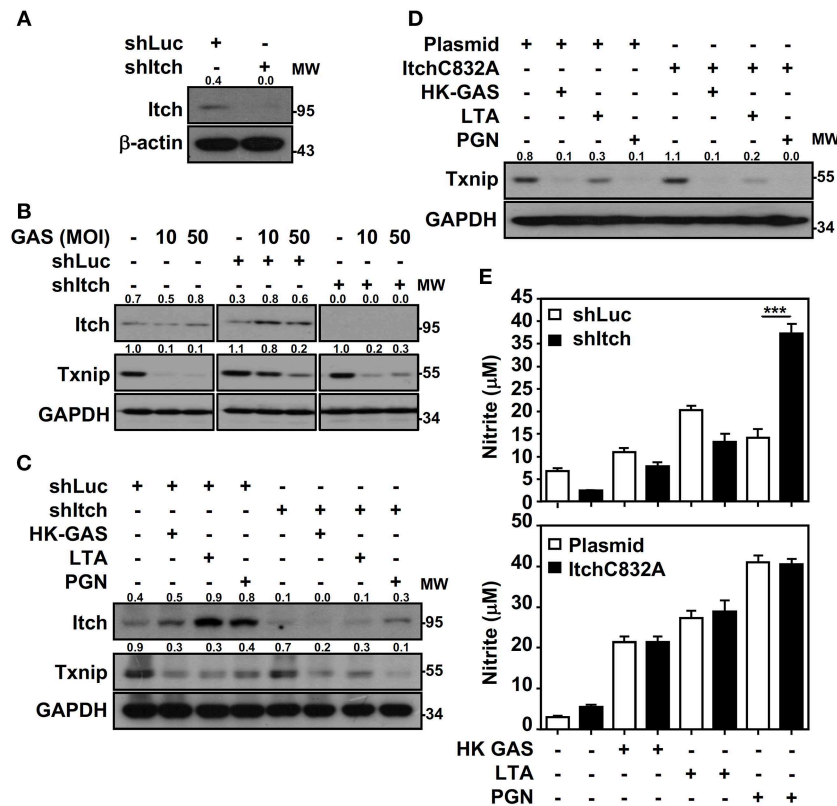


FIGURE 6 | Itch-independent Txnip degradation promotes TLR2-mediated NO production. **(A)** RAW264.7 cells stably expressed control luciferase shRNA (shLuc) and Itch shRNA (shItch). The expression of Itch and β -actin was measured. Western blotting showed Itch and Txnip expression in WT, shLuc-, and shItch-expressing RAW264.7 cells **(B)** infected with the indicated MOIs of GAS at 2 h postinfection or **(C)** stimulated with HK-GAS (MOI 10), LTA (5 μ g/ml), and PGN (5 μ g/ml) for 2 h. GAPDH was used as an internal control. **(D)** Txnip expression was detected in cells transiently transfected with a dominant-negative mutant of Itch (C832A) followed by HK-GAS, LTA, and PGN treatment for 2 h. GAPDH is shown as an internal control. The expression ratios of Txnip and Itch to internal controls are shown. **(E)** shLuc- or shItch-expressing (upper panel) and control plasmid- or ItchC832A-expressing (lower panel) RAW264.7 cells were treated with HK-GAS, LTA, and PGN for 24 h. NO production was measured and shown as the means \pm SD of triplicate cultures. *** $p < 0.001$ compared with shLuc-expressed cells. Protein molecular weights (MW) are indicated in kilodaltons. Western blot results represent at least two independent experiments.

DISCUSSION

In GAS infection, macrophages play a crucial role in the host innate defense against bacteria and in pro-inflammatory induction. The recognition of GAS with pattern recognition receptors (PRRs) such as TLRs can effectively trigger signaling cascades that elicit NF- κ B activation and inflammatory cytokine induction (35). The engagement of TLRs launches MyD88-dependent functional inflammatory responses, while MyD88 deficiency results in the distinct reduction in the levels of TNF- α , IL-6, IL-12 and interferons in GAS-infected phagocytes (2, 35). PRRs certainly mediate the fundamental immune responses for defense against bacterial infection; however, GAS-derived TLR activation and subsequent inflammatory mechanisms are not completely understood. Here, we first demonstrate that GAS initiated the rapid proteasomal degradation of Txnip, which is independent of glucose consumption or SPE B activation. GAS-mediated Txnip degradation exhibited TLR2- and NOX2-dependent regulation, which were also expressed in concert with the production of

inflammatory cytokines. Moreover, the blockage of HECT E3s and AMPK could stabilize Txnip expression whereby partly reducing TNF- α , IL-6, and NO generation in TLR2-activated macrophages. Accordingly, a represented model is provided and indicated that in response to GAS infection or LTA and PGN stimulation, the activation of TLR2 could sufficiently coordinate NOX2-producing ROS to potentiate AMPK- and HECT E3s-regulated Txnip degradation, resulting in inflammatory TNF- α , IL-6, and iNOS/NO production (Figure 7F).

As a stress-active protein, Txnip is involved in a wide variety of cellular processes. Txnip effectively interacts with Trx, resulting in the decreased ability of Trx to reduce downstream substrates (36). Trx acts as an oxidoreductase and denitrosylase to regulate NF- κ B activity through direct interaction with the p50/p65 heterodimer, reducing the redox-sensitive cysteine in the Rel domain and enhancing the ability of NF- κ B to bind DNA (37, 38). Txnip degradation has been demonstrated to contribute to Trx activation, which in turn facilitates TNF- α -stimulated NF- κ B activation in the respiratory epithelium (20). In addition, *Txnip*^{-/-} mice display

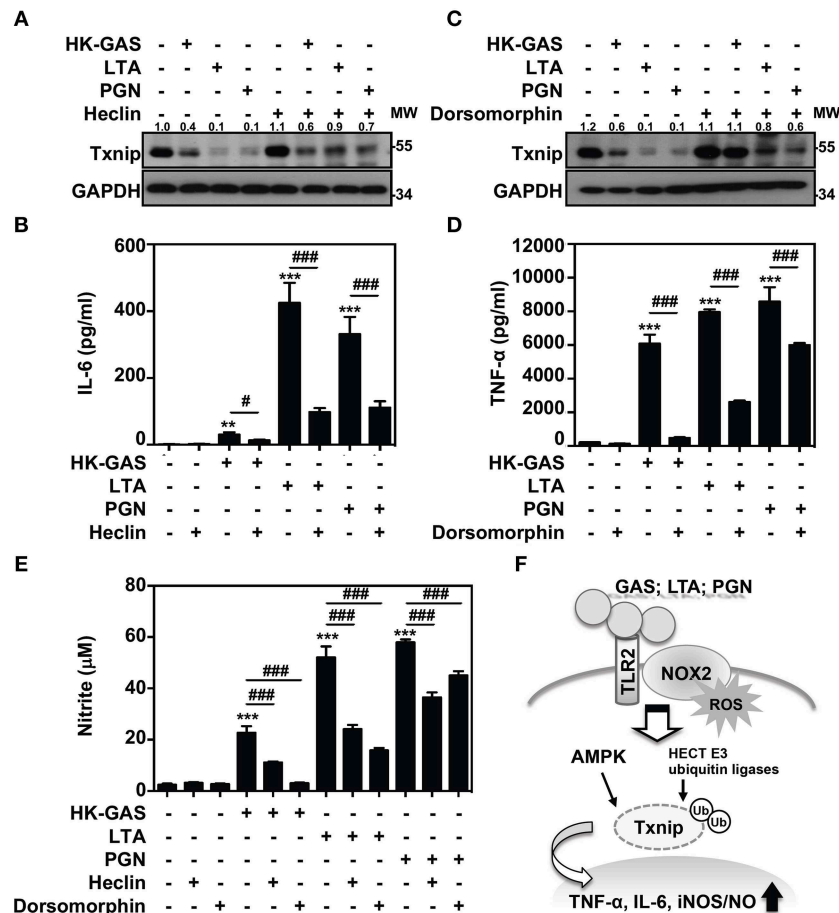


FIGURE 7 | AMPK and HECT E3 ligase are required for Txnip degradation in TLR2-mediated inflammation. RAW264.7 cells were pretreated with (A,B) heclin (25 μM) or (C,D) dorsomorphin (10 μM) for 1 h followed by stimulation with HK-GAS (MOI 10), LTA (5 μg/ml), and PGN (5 μg/ml). The expression of Txnip and GAPDH was detected at 2 h by Western blotting. The expression ratios of Txnip to GAPDH are shown. Protein molecular weights (MW) are indicated in kilodaltons. Western blot results represent at least two independent experiments. ELISA showed IL-6 and TNF-α production at 24 h in HK-GAS-, LTA-, and PGN-stimulated cells, and the concentrations were shown as the means ± SD of triplicate cultures. ** $p < 0.01$ and *** $p < 0.001$ compared to the untreated group; # $p < 0.05$ and ### $p < 0.001$ compared to each stimulated group. (E) In the presence of heclin and dorsomorphin, the Griess reaction showed NO generation in HK-GAS-, LTA-, and PGN-stimulated cells at 24 h. The measurements are shown as the means ± SD of triplicate cultures. *** $p < 0.001$ compared to the untreated group; ### $p < 0.001$ compared to each stimulated group. (F) A represented model of that GAS infection induces the TLR2/NOX2-dependent rapid degradation of Txnip via AMPK- and HECT E3-ligase-regulation, which subsequently potentiates downstream inflammatory TNF-α, IL-6, and iNOS/NO generation.

a higher susceptibility to NF-κB induction during TNF-α stimulation, which subsequently promotes diethylnitrosamine-induced hepatocarcinogenesis (39). Txnip deficiency aggravates LPS-induced endotoxic shock and *E. coli* infection-induced mortality through excessive NO production (21). However, in *P. aeruginosa*-induced bacteremic shock, Txnip inhibits macrophage phagocytosis by phosphatidylinositol 3-kinase inactivation and ROS degeneration, resulting in the inhibition of bacterial clearance (40). In GAS infection, Txnip degradation is involved in TLR2-mediated inflammatory induction, in which the suppression of Txnip causes magnified TNF-α, IL-6, and NO production. The potential role of Txnip in streptococcal toxic shock can be anticipated.

Txnip was previously shown to be rapidly degraded during cytokine and LPS stimulation, while the mechanisms regulating its proteasomal degradation remain unknown. Txnip normally

forms a stable complex with Itch and maintains a relatively rapid turnover in 293T and U2OS cells. The WW domain of Itch interacts with the PPXY region of Txnip, and the highly conserved cysteine residue in the HECT domain of Itch triggers the ubiquitination of Txnip (18). In GAS-infected macrophages, we found that Txnip could be polyubiquitinated and partially form a complex with Itch. However, both the specific silencing of Itch and the overexpression of inactive Itch ligase mutants (Itch-C832A) were insufficient to impede TLR2-initiated Txnip degradation, which suggests an additional E3 ubiquitin ligase that might manipulate TLR2-mediated Txnip degradation. Heclin is a broad inhibitor of a range of HECT E3s, particularly for the specific inhibition of Nedd4, Smurf2, WWP1, WWP2, and Nedd4L (33). The presence of heclin partly stabilized the expression of Txnip, while TLR2-activated inflammatory cytokines were reduced. This finding

indicates that HECT E3s play a crucial role in TLR2-initiated Txnip degradation and inflammation. In the present study, we confirmed an Itch-independent Txnip degradation in TLR2 and GAS stimulation; however, the specific HECT E3s in labeling Txnip for proteasomal degradation remains unclear. Therefore, further deciphering the detailed mechanisms of TLR2-mediated Txnip degradation by using specific siRNAs will be an urgent issue.

During GAS infection, M protein, the pore-forming toxin streptolysin O, and NAD-glycohydrolase have been shown to regulate the NLRP3 inflammasome, resulting in the maturation and release of the pro-inflammatory cytokine IL-1 β (41–43). Inflammasome induction represents an early warning sign in bacterial infection; however, hyperinflammation often aggravates tissue injury by causing systemic shock. Txnip has been revealed to dissociate from oxidized Trx that initiates the NLRP3 inflammasome in response to ROS activation (12, 36). So far, the role of Txnip in bacteria-incited inflammasomes has not been reported. In LPS or *E. coli* infection, Txnip-deficient macrophages manifest the partial decrease of active caspase-1 and IL-1 β production, which might result from increased S-nitrosylation of NLRP3 inflammasome components that hinder IL-1 β maturation (21). Because the TLR4-regulated inflammasome shows incomplete obstruction with Txnip deficiency, the Txnip/NLRP3-independent inflammasome may present in TLR signals. While TLR2 and GAS infection mediate the rapid degradation of Txnip, it increases exacerbated NO and inflammation by intensifying NF- κ B activation. Therefore, Txnip participates in GAS-mediated inflammasome induction which remains to be further investigated.

GAS infection initiates the assembly of NOX2 in macrophages, which often induces abundant ROS generation (28). NOX2-derived ROS not only exert bacterial killing but also transduce inflammatory signals and protein synthesis (28, 44). We previously demonstrate that GAS infection initiates NOX2-regulated glycogen synthase kinase-3 β activation whereby promoting the activation of NF- κ B in RAW264.7 cells (28, 45). In calcium oxalate crystal stimulation, NOX-mediated ROS are the crucial contributors that trigger Txnip dissociation from Trx and binding to NLRP3, which causes renal injury and inflammation (46). Here, we found that GAS increased ROS-associated Txnip degradation to potentially expedite NF- κ B activation, whereas NOX2 deficiency stabilized Txnip and reduced the generation of inflammatory cytokines. Moreover, *Nox2*^{-/-} BMDMs presented partial Txnip degradation during GAS infection or HK-GAS and LTA stimulation, while almost no obvious degradation occurred in *Tlr2*^{-/-} cells, suggesting that the stability of Txnip might be regulated through the TLR2/NOX2 axis. In addition to the ROS-regulated phosphorylation of I κ B α and MAPK phosphatases (47, 48), we speculate that Txnip may serve as an additional downstream responder following TLR2/NOX2 signaling to potentiate NF- κ B-mediated inflammation. In GAS-infected epithelial cells, the enriched transcription factor networks, including activator protein-1, activating transcription factor 2, and nuclear factor of activated T cells, are reported to play the crucial role in induction of proinflammation (49). Besides NF- κ B, the involvement of Txnip degradation in regulating other

transcription factors during GAS infection is worthwhile to study further. Moreover, the redox- and energy-responsive AMPK (50, 51) shows the part regulation on TLR2/NOX2-mediated Txnip degradation, whether ROS generation potentially initiates AMPK activation which needs to be further investigated.

In contrast to the anticipated role of Txnip in the induction of inflammasomes, GAS infection triggers the rapid degradation of Txnip that results primarily in abundant TNF- α , IL-6, and iNOS/NO production. Because the excessive generation of inflammatory cytokines is frequently associated with the severity of infectious disease, we speculate that the stabilization of Txnip could be a potential target to decelerate inflammation. Interestingly, two blockers, heclin and dorsomorphin, which are specialized to inhibit HECT E3s and AMPK, respectively, can prevent Txnip degradation and subsequent inflammatory cytokine production. Their application in the treatment of hyperinflammation and detailed mechanisms of their involvement in Txnip regulation during bacterial infection require further investigation.

ETHICS STATEMENT

The animal experiments were performed according to the guidelines of the Animal Protection Act of Taiwan and the experimental protocols according to guidelines established by the Ministry of Science and Technology, Taiwan were approved by the Laboratory Animal Care and Use Committee of National Cheng Kung University.

AUTHOR CONTRIBUTIONS

P-CT, C-FK, C-FL, Y-SL, and C-LC participated in the study design and data interpretation and drafted the manuscript. P-CT and C-LC performed the experiments. C-FK, M-HC, S-WW, C-PC, and J-JW assisted with experimental design and material preparation. C-LC wrote the first draft of the manuscript. C-FL, Y-SL, J-JW, and C-CH contributed to manuscript revision. All authors read and approved the final manuscript.

FUNDING

This work was supported by grants MOST 106-2320-B-038-029, MOST 107-2320-B-038-043-MY3, and MOST 108-2320-B-038-008 from the Ministry of Science and Technology in Taiwan.

ACKNOWLEDGMENTS

We thank Chi-Chang Shieh for supplying *Nox2*^{-/-} mice, and Tsung-Hao Chang, Yi-Lin Cheng, and Chi-Hsuan Yang for technical assistance.

SUPPLEMENTARY MATERIAL

The Supplementary Material for this article can be found online at: <https://www.frontiersin.org/articles/10.3389/fimmu.2019.02147/full#supplementary-material>

REFERENCES

- Akira S, Takeda K. Functions of toll-like receptors: lessons from KO mice. *C R Biol.* (2004) 327:581–9. doi: 10.1016/j.crv.2004.04.002
- Loof TG, Goldmann O, Gessner A, Herwald H, Medina E. Aberrant inflammatory response to *Streptococcus pyogenes* in mice lacking myeloid differentiation factor 88. *Am J Pathol.* (2010) 176:754–63. doi: 10.2353/ajpath.2010.090422
- Fieber C, Janos M, Koestler T, Gratz N, Li XD, Castiglia V, et al. Innate immune response to *Streptococcus pyogenes* depends on the combined activation of TLR13 and TLR2. *PLoS ONE.* (2015) 10:e0119727. doi: 10.1371/journal.pone.0119727
- Walker MJ, Barnett TC, McArthur JD, Cole JN, Gillen CM, Henningham A, et al. Disease manifestations and pathogenic mechanisms of Group A *Streptococcus*. *Clin Microbiol Rev.* (2014) 27:264–301. doi: 10.1128/CMR.00101-13
- Norrby-Teglund A, Pauksens K, Norgren M, Holm SE. Correlation between serum TNF alpha and IL6 levels and severity of group A streptococcal infections. *Scand J Infect Dis.* (1995) 27:125–30. doi: 10.3109/00365549509018991
- Saito M, Kajiura H, Iida K, Hoshina T, Kusuhara K, Hara T, et al. Systemic cytokine response in moribund mice of streptococcal toxic shock syndrome model. *Microb Pathog.* (2011) 50:109–13. doi: 10.1016/j.micpath.2010.12.001
- Chen KS, DeLuca HF. Isolation and characterization of a novel cDNA from HL-60 cells treated with 1,25-dihydroxyvitamin D-3. *Biochim Biophys Acta.* (1994) 1219:26–32. doi: 10.1016/0167-4781(94)90242-9
- Nishiyama A, Matsui M, Iwata S, Hirota K, Masutani H, Nakamura H, et al. Identification of thioredoxin-binding protein-2/vitamin D(3) up-regulated protein 1 as a negative regulator of thioredoxin function and expression. *J Biol Chem.* (1999) 274:21645–50. doi: 10.1074/jbc.274.31.21645
- Sheth SS, Bodnar JS, Ghazalpour A, Thipphavong CK, Tsutsumi S, Tward AD, et al. Hepatocellular carcinoma in Txnip-deficient mice. *Oncogene.* (2006) 25:3528–36. doi: 10.1038/sj.onc.1209394
- Chen CL, Lin CF, Chang WT, Huang WC, Teng CF, Lin YS. Ceramide induces p38 MAPK and JNK activation through a mechanism involving a thioredoxin-interacting protein-mediated pathway. *Blood.* (2008) 111:4365–74. doi: 10.1182/blood-2007-08-106336
- Watanabe R, Nakamura H, Masutani H, Yodoi J. Anti-oxidative, anti-cancer and anti-inflammatory actions by thioredoxin 1 and thioredoxin-binding protein-2. *Pharmacol Ther.* (2010) 127:261–70. doi: 10.1016/j.pharmthera.2010.04.004
- Zhou R, Tardivel A, Thorens B, Choi I, Tschopp J. Thioredoxin-interacting protein links oxidative stress to inflammasome activation. *Nat Immunol.* (2010) 11:136–40. doi: 10.1038/ni.1831
- Spindel ON, World C, Berk BC. Thioredoxin interacting protein: redox dependent and independent regulatory mechanisms. *Antioxid Redox Signal.* (2012) 16:587–96. doi: 10.1089/ars.2011.4137
- Dutta KK, Nishinaka Y, Masutani H, Akatsuka S, Aung TT, Shirase T, et al. Two distinct mechanisms for loss of thioredoxin-binding protein-2 in oxidative stress-induced renal carcinogenesis. *Lab Invest.* (2005) 85:798–807. doi: 10.1038/labinvest.3700280
- Osowski CM, Hara T, O'Sullivan-Murphy B, Kanekura K, Lu S, Hara M, et al. Thioredoxin-interacting protein mediates ER stress-induced beta cell death through initiation of the inflammasome. *Cell Metab.* (2012) 16:265–73. doi: 10.1016/j.cmet.2012.07.005
- Lerner AG, Upton JP, Praveen PV, Ghosh R, Nakagawa Y, Igbaria A, et al. IRE1alpha induces thioredoxin-interacting protein to activate the NLRP3 inflammasome and promote programmed cell death under irremediable ER stress. *Cell Metab.* (2012) 16:250–64. doi: 10.1016/j.cmet.2012.07.007
- Patwari P, Higgins LJ, Chutkow WA, Yoshioka J, Lee RT. The interaction of thioredoxin with Txnip. Evidence for formation of a mixed disulfide by disulfide exchange. *J Biol Chem.* (2006) 281:21884–91. doi: 10.1074/jbc.M600427200
- Zhang P, Wang C, Gao K, Wang D, Mao J, An J, et al. The ubiquitin ligase itch regulates apoptosis by targeting thioredoxin-interacting protein for ubiquitin-dependent degradation. *J Biol Chem.* (2010) 285:8869–79. doi: 10.1074/jbc.M109.063321
- Wu N, Zheng B, Shaywitz A, Dagon Y, Tower C, Bellinger G, et al. AMPK-dependent degradation of TXNIP upon energy stress leads to enhanced glucose uptake via GLUT1. *Mol Cell.* (2013) 49:1167–75. doi: 10.1016/j.molcel.2013.01.035
- Kelleher ZT, Sha Y, Foster MW, Foster WM, Forrester MT, Marshall HE. Thioredoxin-mediated denitrosylation regulates cytokine-induced nuclear factor κ B (NF- κ B) activation. *J Biol Chem.* (2014) 289:3066–72. doi: 10.1074/jbc.M113.503938
- Park YJ, Yoon SJ, Suh HW, Kim DO, Park JR, Jung H, et al. TXNIP deficiency exacerbates endotoxic shock via the induction of excessive nitric oxide synthesis. *PLoS Pathog.* (2013) 9:e1003646. doi: 10.1371/journal.ppat.1003646
- Schulze PC, Yoshioka J, Takahashi T, He Z, King GL, Lee RT. Hyperglycemia promotes oxidative stress through inhibition of thioredoxin function by thioredoxin-interacting protein. *J Biol Chem.* (2004) 279:30369–74. doi: 10.1074/jbc.M400549200
- Nelson DC, Garbe J, Collin M. Cysteine proteinase SpeB from *Streptococcus pyogenes* - a potent modifier of immunologically important host and bacterial proteins. *Biol Chem.* (2011) 392:1077–88. doi: 10.1515/BC.2011.208
- Chen CL, Wu YY, Lin CF, Kuo CF, Han CL, Wang S, et al. Streptococcal pyrogenic exotoxin B inhibits apoptotic cell clearance by macrophages through protein S cleavage. *Sci Rep.* (2016) 6:26026. doi: 10.1038/srep26026
- Hung CH, Tsao N, Zeng YF, Lu SL, Chuan CN, Lin YS, et al. Synergistic effects of streptolysin S and streptococcal pyrogenic exotoxin B on the mouse model of group A streptococcal infection. *Med Microbiol Immunol.* (2012) 201:357–69. doi: 10.1007/s00430-012-0241-6
- Underhill DM, Ozinsky A. Phagocytosis of microbes: complexity in action. *Annu Rev Immunol.* (2002) 20:825–52. doi: 10.1146/annurev.immunol.20.103001.114744
- West AP, Brodsky IE, Rahner C, Woo DK, Erdjument-Bromage H, Tempst P, et al. TLR signalling augments macrophage bactericidal activity through mitochondrial ROS. *Nature.* (2011) 472:476–80. doi: 10.1038/nature09973
- Chen CL, Cheng MH, Kuo CF, Cheng YL, Li MH, Chang CP, et al. Dexamethorphan attenuates NADPH oxidase-regulated glycogen synthase kinase β and NF- κ B activation and reduces nitric oxide production in Group A streptococcal infection. *Antimicrob Agents Chemother.* (2018) 62:e02045–17. doi: 10.1128/AAC.02045-17
- Riling C, Kamadurai H, Kumar S, O'Leary CE, Wu KP, Manion EE, et al. Itch WW domains inhibit its E3 ubiquitin ligase activity by blocking E2-E3 ligase trans-thiolation. *J Biol Chem.* (2015) 290:23875–87. doi: 10.1074/jbc.M115.649269
- Chang L, Kamata H, Solinas G, Luo JL, Maeda S, Venuprasad K, et al. The E3 ubiquitin ligase itch couples JNK activation to TNFalpha-induced cell death by inducing c-FLIP(L) turnover. *Cell.* (2006) 124:601–13. doi: 10.1016/j.cell.2006.01.021
- Yang B, Kumar S, Nedda4 and Nedda4-2: closely related ubiquitin-protein ligases with distinct physiological functions. *Cell Death Differ.* (2010) 17:68–77. doi: 10.1038/cdd.2009.84
- Scheffner M, Kumar S. Mammalian HECT ubiquitin-protein ligases: biological and pathophysiological aspects. *Biochim Biophys Acta.* (2014) 1843:61–74. doi: 10.1016/j.bbamcr.2013.03.024
- Mund T, Lewis MJ, Maslen S, Pelham HR. Peptide and small molecule inhibitors of HECT-type ubiquitin ligases. *Proc Natl Acad Sci USA.* (2014) 111:16736–41. doi: 10.1073/pnas.1412152111
- Yu PB, Hong CC, Sachidanandan C, Babbitt JL, Deng DY, Hoyng SA, et al. Dorsomorphin inhibits BMP signals required for embryogenesis and iron metabolism. *Nat Chem Biol.* (2008) 4:33–41. doi: 10.1038/nchembio.2007.54
- Fieber C, Kovarik P. Responses of innate immune cells to group A *Streptococcus*. *Front Cell Infect Microbiol.* (2014) 4:140. doi: 10.3389/fcimb.2014.00140
- Yoshihara E, Masaki S, Matsuo Y, Chen Z, Tian H, Yodoi J. Thioredoxin/Txnip: redoxosome, as a redox switch for the pathogenesis of diseases. *Front Immunol.* (2014) 4:514. doi: 10.3389/fimmu.2013.00514
- Matthews JR, Wakasugi N, Virelizier JL, Yodoi J, Hay RT. Thioredoxin regulates the DNA binding activity of NF-kappa B by reduction of a disulphide bond involving cysteine 62. *Nucleic Acids Res.* (1992) 20:3821–30. doi: 10.1093/nar/20.15.3821

38. Benhar M, Forrester MT, Hess DT, Stamler JS. Regulated protein denitrosylation by cytosolic and mitochondrial thioredoxins. *Science*. (2008) 320:1050–4. doi: 10.1126/science.1158265
39. Kwon HJ, Won YS, Suh HW, Jeon JH, Shao Y, Yoon SR, et al. Vitamin D3 upregulated protein 1 suppresses TNF- α -induced NF- κ B activation in hepatocarcinogenesis. *J Immunol*. (2010) 185:3980–9. doi: 10.4049/jimmunol.1000990
40. Piao ZH, Kim MS, Jeong M, Yun S, Lee SH, Sun HN, et al. VDUP1 exacerbates bacteremic shock in mice infected with *Pseudomonas aeruginosa*. *Cell Immunol*. (2012) 280:1–9. doi: 10.1016/j.cellimm.2012.11.003
41. Timmer AM, Timmer JC, Pence MA, Hsu LC, Ghochani M, Frey TG, et al. Streptolysin O promotes group A *Streptococcus* immune evasion by accelerated macrophage apoptosis. *J Biol Chem*. (2009) 284:862–71. doi: 10.1074/jbc.M804632200
42. Hancz D, Westerlund E, Bastiat-Sempe B, Sharma O, Valfridsson C, Meyer L, et al. Inhibition of Inflammasome-Dependent Interleukin 1 β Production by Streptococcal NAD $^{+}$ -Glycohydrolase: Evidence for Extracellular Activity. *MBio*. (2017) 8:e00756–17. doi: 10.1128/mBio.00756-17
43. Valderrama JA, Riestra AM, Gao NJ, LaRock CN, Gupta N, Ali SR, et al. Group A streptococcal M protein activates the NLRP3 inflammasome. *Nat Microbiol*. (2017) 2:1425–34. doi: 10.1038/s41564-017-0005-6
44. Dan DJ, Alvarez LA, Zhang X, Soldati T. Reactive oxygen species and mitochondria: A nexus of cellular homeostasis. *Redox Biol*. (2015) 6:472–85. doi: 10.1016/j.redox.2015.09.005
45. Chang YT, Chen CL, Lin CF, Lu SL, Cheng MH, Kuo CF, et al. Regulatory role of GSK-3 β on NF- κ B, nitric oxide, and TNF- α in group A streptococcal infection. *Mediators Inflamm*. (2013) 2013:720689. doi: 10.1155/2013/720689
46. Joshi S, Wang W, Peck AB, Khan SR. Activation of the NLRP3 inflammasome in association with calcium oxalate crystal induced reactive oxygen species in kidneys. *J Urol*. (2015) 193:1684–91. doi: 10.1016/j.juro.2014.11.093
47. Cheng Y, Marion TN, Cao X, Wang W, Cao Y. Park 7: A Novel Therapeutic Target for Macrophages in Sepsis-Induced Immunosuppression. *Front Immunol*. (2018) 9:2632. doi: 10.3389/fimmu.2018.02632
48. Zhang J, Wang X, Vikash V, Ye Q, Wu D, Liu Y, et al. ROS and ROS-mediated cellular signaling. *Oxid Med Cell Longev*. (2016) 2016:4350965. doi: 10.1155/2016/4350965
49. Soderholm AT, Barnett TC, Korn O, Rivera-Hernandez T, Seymour LM, Schulz BL, et al. Group A *Streptococcus* M1T1 intracellular infection of primary tonsil epithelial cells dampens levels of secreted IL-8 through the action of SpyCEP. *Front Cell Infect Microbiol*. (2018) 8:160. doi: 10.3389/fcimb.2018.00160
50. Cardaci S, Filomeni G, Ciriolo MR. Redox implications of AMPK-mediated signal transduction beyond energetic clues. *J Cell Sci*. (2012) 125:2115–25. doi: 10.1242/jcs.095216
51. Kim SY, Jeong S, Jung E, Baik KH, Chang MH, Kim SA, et al. AMP-activated protein kinase- α 1 as an activating kinase of TGF- β -activated kinase 1 has a key role in inflammatory signals. *Cell Death Dis*. (2012) 3:e357. doi: 10.1038/cddis.2012.95

Conflict of Interest Statement: The authors declare that the research was conducted in the absence of any commercial or financial relationships that could be construed as a potential conflict of interest.

Copyright © 2019 Tseng, Kuo, Cheng, Wan, Lin, Chang, Lin, Wu, Huang and Chen. This is an open-access article distributed under the terms of the Creative Commons Attribution License (CC BY). The use, distribution or reproduction in other forums is permitted, provided the original author(s) and the copyright owner(s) are credited and that the original publication in this journal is cited, in accordance with accepted academic practice. No use, distribution or reproduction is permitted which does not comply with these terms.



Profile of Histone H3 Lysine 4 Trimethylation and the Effect of Lipopolysaccharide/Immune Complex-Activated Macrophages on Endotoxemia

Vichaya Ruenjaiman¹, Patcharavadee Butta², Yu-Wei Leu³, Monnat Pongpanich⁴, Asada Leelahavanichkul¹, Patipark Kueanjinda⁵ and Tanapat Palaga^{1,2*}

¹ Interdisciplinary Graduate Program in Medical Microbiology, Graduate School, and Center of Excellence in Immunology and Immune-Mediated Diseases, Chulalongkorn University, Bangkok, Thailand, ² Department of Microbiology, Faculty of Science, Chulalongkorn University, Bangkok, Thailand, ³ Department of Life Science, National Chung Cheng University, Chiayi, Taiwan, ⁴ Department of Mathematics and Computer Science, Faculty of Science, Chulalongkorn University, Bangkok, Thailand, ⁵ Institute for Biomedical Sciences, Interdisciplinary Cluster for Cutting Edge Research, Shinshu University, Nagano, Japan

OPEN ACCESS

Edited by:

Dominic De Nardo,
Monash University, Australia

Reviewed by:

Panagiotis F. Christopoulos,
Oslo University Hospital, Norway
Tetsuro Yasui,
Teikyo University Mizonokuchi
Hospital, Japan

*Correspondence:

Tanapat Palaga
tanapat.p@chula.ac.th

Specialty section:

This article was submitted to
Molecular Innate Immunity,
a section of the journal
Frontiers in Immunology

Received: 15 April 2019

Accepted: 02 December 2019

Published: 10 January 2020

Citation:

Ruenjaiman V, Butta P, Leu Y-W,
Pongpanich M, Leelahavanichkul A,
Kueanjinda P and Palaga T (2020)
Profile of Histone H3 Lysine 4
Trimethylation and the Effect of
Lipopolysaccharide/Immune
Complex-Activated Macrophages on
Endotoxemia.
Front. Immunol. 10:2956.
doi: 10.3389/fimmu.2019.02956

Macrophage plasticity is a process that allows macrophages to switch between two opposing phenotypes based on differential stimuli. Interferon γ (IFN γ)-primed macrophages stimulated with lipopolysaccharide (LPS) [M(IFN γ +LPS)] produce high levels of pro-inflammatory cytokines such as IL-12, TNF α , and IL-6 and low levels of the anti-inflammatory cytokine IL-10, while those stimulated with LPS in the presence of the immune complex (IC) [M(IFN γ +LPS+IC)] produce high levels of IL-10 and low levels of IL-12. In this study, we investigated the plasticity between M(IFN γ +LPS) and M(IFN γ +LPS+IC) *in vitro* and compared one of the active histone marks [histone H3 lysine 4 trimethylation (H3K4me3)] between M(IFN γ +LPS) and M(IFN γ +LPS+IC) using murine bone marrow-derived macrophages. We found that in an *in vitro* system, macrophages exhibited functional plasticity from M(LPS) to M(LPS+IC) upon repolarization after 2 days of washout period while IFN γ priming before LPS stimulation prevented this repolarization. Phosphorylation of p38, SAPK/JNK, and NF- κ B p65 in M(LPS+IC) repolarized from M(LPS) was similar to that in M(LPS+IC) polarized from resting macrophages. To obtain the epigenetic profiles of M(IFN γ +LPS) and M(IFN γ +LPS+IC), the global enrichment of H3K4me3 was evaluated. M(IFN γ +LPS) and M(IFN γ +LPS+IC) displayed marked differences in genome-wide enrichment of H3K4me3. M(IFN γ +LPS+IC) showed increased global enrichment of H3K4me3, whereas M(IFN γ +LPS) showed decreased enrichment when compared to unstimulated macrophages. Furthermore, M(IFN γ +LPS+IC) exhibited high levels of H3K4me3 enrichment in all *cis*-regulatory elements. At the individual gene level, the results showed increased H3K4me3 enrichment in the promoters of known genes associated with M(IFN γ +LPS+IC), including *Il10*, *Cxcl1*, *Csf3*, and *Il33*, when compared with those of M(IFN γ +LPS). Finally, we investigated the impact of M(IFN γ +LPS+IC) on the systemic immune response by adoptive transfer of M(IFN γ +LPS+IC) in an LPS-induced endotoxemia model. The cytokine profile revealed that mice with adoptively transferred M(IFN γ +LPS+IC) had acutely reduced serum levels of the inflammatory

cytokines IL-1 β and IL-p12p70. This study highlights the importance of epigenetics in regulating macrophage activation and the functions of M(IFN γ +LPS+IC) that may influence macrophage plasticity and the potential therapeutic use of macrophage transfer *in vivo*.

Keywords: macrophage, LPS, immune complex, epigenetics, H3K4me3, endotoxemia

INTRODUCTION

Macrophages are cells of the innate immune system that are found in most tissues. They respond to infection as the first line of defense against pathogens (1). Macrophages play an important role in the immune response and homeostasis with functional diversity, such as inflammation, phagocytosis, metabolism, tissue remodeling, and immunoregulation. However, a key feature of macrophages is functional plasticity (2).

Macrophage plasticity is a process that allows macrophages to switch between two different phenotypes. The functional plasticity of macrophages contributes to the pathogenesis of various diseases, such as cancer, metabolic diseases, autoimmune diseases, and systemic infections (3). In this study, the common framework for macrophage activation nomenclature as proposed by Murray et al. is followed (4). Interferon γ (IFN γ) and lipopolysaccharide (LPS)-stimulated macrophages or classically activated macrophages [M(IFN γ +LPS)] exhibit pro-inflammatory activity, which is characterized by the production of high levels of pro-inflammatory cytokines (5). LPS and immune complex (IC)-stimulated macrophages [M(IFN γ +LPS+IC)] produce large amounts of the anti-inflammatory cytokine IL-10 and low levels of the pro-inflammatory cytokine IL-12 but produce high levels of tumor necrosis factor (TNF α), IL-6 and IL-1 β (6, 7). At least *in vitro*, optimal activation of M(LPS+IC) is reported in the presence of IFN γ (8). IL-10 is a key multifunction regulatory cytokine that regulates the immune response during infection and dampens immune hyperactivation (9, 10).

M(IFN γ +LPS+IC) are categorized as non-classically activated macrophages that show immunomodulatory activity due to the increased production of the anti-inflammatory cytokine IL-10 and reduced pro-inflammatory cytokine IL-12 production (6). Transcriptionally, M(IFN γ +LPS+IC) exhibit a distinctive gene expression profile that is unique and does not overlap with that of M(IFN γ +LPS) or M(IL-4) (11). Therefore, M(IFN γ +LPS+IC) have potential in dampening the overt immune response and can be used in cellular therapy. In one study, adoptive transfer of M(IFN γ +LPS+IC) reduced the severity in an animal model of multiple sclerosis (8). In another study, it was reported that mice with adoptively transferred M(IC) showed reducing disease severity in sepsis (11). To induce LPS-stimulated macrophages to produce higher amounts of IL-10, the signaling downstream of IC/FcR can be replaced with other stimuli, such as PGE2 (11). However, the stability of the M(IFN γ +LPS+IC) phenotype upon transfer *in vivo* remains unknown.

In macrophages, the expression of *Il10* is regulated by several transcription factors, including Sp1, ERK and NF- κ B (10, 12). We also reported that Notch signaling plays important roles in regulating IL-10 production in M(IFN γ +LPS+IC) (13). Fc γ R signaling activates Erk and p38 MAPK signaling in M(IFN γ +LPS+IC), resulting in the binding of Sp1 to the *Il10* promoter (14).

Regulation of cytokine production in macrophages is regulated at several levels, such as transcription factor activation, epigenetic regulation and post-transcriptional regulation (2). Epigenetic regulation plays a critical role in influencing long-term plasticity (15). Epigenetics regulate chromatin accessibility at the promoter and regulatory regions by several processes including histone modifications (16).

Histone methylation can be conducive or repressive to gene expression, depending on the locations of the modified amino acids and the type of methylation on the histone tails (17). Activation of Jmjd3, a demethylase that mediate trimethylation on lysine 27 of histone H3 (H3K27), results in increased chromatin accessibility leading to M(IL-4) signature gene expression and is crucial for regulating M(IL-4) polarization (18). Trimethylation on lysine 4 of histone H3 (H3K4me3) on genes encoding cell surface markers and chemokines correlates with the transcriptional activity in monocyte-derived macrophages (19). Together, these results strongly indicate that both H3K4me3 and H3K27me3 play an essential role in polarization and activation in macrophages (18, 19).

The regulation of IL-10 production in M(IFN γ +LPS+IC) by histone modification has been reported, where ERK activation leads to phosphorylation of serine 10 on histone H3 at the *Il10* promoter. This event increases the recruitment of the transcription factor SP-1 to the *Il10* promoter and increases *Il10* expression (20). However, the global profile of an active histone mark H3K4me3 in M(IFN γ +LPS+IC), in comparison to M(IFN γ +LPS), has not been characterized. In addition, whether M(IFN γ +LPS) can be repolarized to phenotypically become M(IFN γ +LPS+IC) has not been examined. This study, therefore, investigated the plasticity of M(LPS) and M(IC) *in vitro*. We next compared the profiles of H3K4me3 between M(IFN γ +LPS) and M(IFN γ +LPS+IC) to gain a comprehensive view of H3K4me3 involvement in the two distinctive macrophage phenotypes. Finally, the effect of M(IFN γ +LPS+IC) on systemic cytokine production was tested in an LPS-induced endotoxemia model by adoptive transfer approach. Gaining insight into the epigenetic involvement in M(IFN γ +LPS+IC) may shed light on the plasticity and stability of the M(IFN γ +LPS+IC) phenotype *in vivo*.

MATERIALS AND METHODS

Mice

Six to eight week-old female C57BL/6 mice were purchased from Nomura Siam International (Bangkok, Thailand). All procedures were reviewed and approved by the Chulalongkorn University animal care and use protocol committee (Approval No. 024/2558). All experiments involving laboratory animals were performed according to the regulations and recommendations of the Institute Animal Care and Use committee at Chulalongkorn University.

Murine Macrophages

Bone marrow-derived macrophages (BMDMs) were prepared as described elsewhere. Briefly, bone marrow cells were isolated from tibias and femurs by flushing with Dulbecco's Modified Eagle's Medium (DMEM) (HyClone, Logan, UT, USA) supplemented with 10% (v/v) fetal bovine serum (GIBCO, Grand Island, NY, USA), 1% (w/v) sodium pyruvate, 1% (w/v) HEPES, 100 U/ml penicillin, 0.25 mg/ml streptomycin, 20% L929 cell conditioned media and 5% horse serum (all reagents were purchased from HyClone). Cells were cultured for 1 week, and the medium was changed every 3 days. BMDMs were confirmed by detecting the cell surface markers CD11b and F4/80 by flow cytometry and plated in a tissue culture plate 24 h before use.

Generating M(IFN γ +LPS) and M(IFN γ +LPS+IC)

BMDMs were primed with recombinant mouse IFN- γ (10 ng/ml; BioLegend, San Diego, CA, USA) for 18 h before stimulation unless otherwise specified. M(IFN γ +LPS) and M(IFN γ +LPS+IC) were generated by adding *Salmonella* LPS (100 ng/ml; Sigma-Aldrich, St. Louis, MO, USA) or LPS in combination with IC. IC was prepared by adding a 10-fold molar excess of rabbit anti-OVA IgG to OVA (both from Sigma-Aldrich), and the complex was incubated for 30 min at room temperature (21). IC was used at a 1:100 volume ratio of IC to media for stimulation.

Repolarization of M(IFN γ +LPS) or M(LPS) to M(LPS+IC)

BMDMs were first polarized to M(IFN γ +LPS) or M(LPS) for 24 h. Cells were washed with warm media and rested in culture media for 2 h or 48 h before repolarization by adding LPS together with IC for M(LPS+IC). Culture media were harvested at 24 h after the secondary stimulation to measure IL-10 and IL-12p70 by ELISA. Resting BMDMs polarized to M(IFN γ +LPS) or M(LPS), M(IFN γ +LPS+IC) or M(LPS+IC) were used as controls, respectively. For Western blot analysis, BMDMs were polarized to M(LPS) for 24 h followed by a washout period of 2 or 48 h. The protein lysates were collected at 0, 5, 15, and 30 min after the secondary stimulation with LPS/IC. As a control, BMDMs were polarized to M(LPS+IC) and the lysates were collected at 0, 5, 15 min.

Enzyme-Linked Immunosorbent Assay (ELISA)

Culture supernatants from BMDMs treated as indicated were harvested to measure IL-10 and IL-12p70 by using an IL-10 ELISA (BioLegend) and an IL-12p70 ELISA (BD Biosciences, San Jose, CA, USA). ELISAs were performed following the manufacturer's protocol.

Western Blot Analysis

BMDMs were treated as indicated, and cell lysates were subjected to Western blot. The antibodies used in this study were rabbit anti-phospho-NF- κ B p65 (1:2000), rabbit anti-NF- κ B p65 (1:4000), rabbit anti-phospho-Akt (1:2000), rabbit anti-Akt (Ser473) (1:4000), rabbit anti-phospho-p38 (1:2000), rabbit anti-p38 (1:4000), rabbit anti-phospho-ERK1/2 (p42/44) (1:2000), rabbit anti-ERK1/2 (p42/44) (1:4000), rabbit anti-phospho-SAPK/JNK (1:2000), rabbit anti-SAPK/JNK (1:4000), and mouse anti- β -actin (1:10000), HRP-conjugated donkey anti-rabbit IgG and HRP-conjugated sheep anti-mouse IgG (1:4000) (all from Cell Signaling Technology, Danvers, MA, USA). The signals were detected by chemiluminescence. In order to quantify the band densities among different samples, Western blot images were subjected to analysis by ImageJ software.

ATP Luminescence Assay for Cell Viability

BMDMs were primed with IFN- γ followed by LPS stimulation for 24 h. Cell viability was measured using ATPlite 1-step Luminescence Assay (PerkinElmer, Waltham, MA, USA) according to the manufacturer's protocol. The signals were detected by Varioskan LUX Multimode Reader (ThermoFisher Scientific).

Endotoxemia and Adoptive Transfer of Macrophages

For the *in vivo* adoptive transfer study, 5×10^6 BMDMs were stimulated as described above for 4 h to generate M(IFN γ +LPS+IC) before transfer. Eight week-old female C57BL/6 mice ($n = 4$ per group) were adoptively transferred with 1×10^6 cells of M(IFN γ +LPS+IC) or control unstimulated macrophages per mouse by *i.p.* administration. Three hours later, mice were injected with *E. coli* LPS (Sigma-Aldrich) at a sublethal dose (1 mg/kg body weight, *i.p.* route) to induce endotoxemia. Blood was collected at 1 and 6 h after the LPS challenge and subjected to cytokine measurement by Bio-Plex assay.

Bio-Plex Assays

Blood serum of the endotoxemia model mice prepared as described above was subjected to multiple cytokine measurement (IL-1 β , IL-12p70, IL-6, TNF α , IL-17, IL-10, and IL-4) by using Bio-Plex ProTM Mouse Cytokine 7-plex Assay (Bio-Rad, Hercules, CA, USA). Assays were performed according to the manufacturer's instructions, and the data were analyzed using Bio-Plex ManagerTM software (Bio-Rad).

ChIP-seq and Data Analysis

BMDMs were polarized to M(IFN γ +LPS) and M(IFN γ +LPS+IC) for 4 h as described above. Cells were

fixed and subjected to the SimpleChIP® Enzymatic Chromatin IP Kit (Magnetic Beads) (Cell Signaling Technology) according to the manufacturer's protocol. The antibody used in the ChIP assay was rabbit anti-H3K4me3 or the isotype control (Cell Signaling Technology). ChIP DNA fragments were analyzed using 50 bp single-end sequencing by BGI (Beijing, China). The trimmed sequences were examined for quality by FastQC and aligned to the reference genome by Bowtie2 (more than 97% mapped) (22). Regions of enrichment were identified using MACS 1.4 and MACS2 (23). Circos and Venn diagrams were employed to visualize the designated ChIP enrichment globally. Epigenomic correlation was evaluated by TCOR in EpiMINE (24). CEAS was used to reveal enrichment in *cis*-regulatory regions. IGV and QIRI in EpiMINE were used to visualize and quantify the enrichment in target genes. The possible regulatory signaling pathways were analyzed by enriched KEGG pathway analysis using clusterProfiler (25) and DOSE (26) R packages. Statistical significance was reported as BH-adjusted *p*-value (27, 28).

RESULTS

IFN γ Priming and Resting Durations Determined the Plasticity of M(IFN γ +LPS)/M(LPS) for Repolarization to M(LPS+IC)

The plasticity between M1 and M2 macrophages has been reported (5). However, little is known about whether reverse polarization from M(IFN γ +LPS) to M(LPS+IC) is possible. Therefore, we first tested the repolarization plasticity of M(IFN γ +LPS) to become M(LPS+IC), as depicted in **Figure 1**. The washout periods of 2 or 48 h after the first LPS stimulation were examined. As shown in **Figures 1A,B**, upon LPS and IC stimulation, M(IFN γ +LPS) failed to increase the level of IL-10 and decrease the level of IL-12p70 as it was expected for M(LPS+IC), whether the washout period between the two stimulation was 2 or 48 h.

Next, to test whether IFN γ priming prevents the reverse polarization into M(LPS+IC), BMDMs were stimulated with LPS without IFN γ priming and subjected to reverse polarization to M(LPS+IC) with a washout period of 2 or 48 h as depicted in **Figure 2A**. The results showed that M(LPS+IC) polarized from resting macrophages and M(LPS) with a washout period of 48 h had increased IL-10 and decreased IL-12p70 to a comparable extent (**Figure 2B**), whereas the shorter washout durations (2, 6, and 24 h) between the primary LPS stimulation and secondary LPS/IC stimulation failed to yield M(LPS+IC) cytokine profiles (**Supplementary Figure 1A**). A slight decrease in the cell viability between unstimulated cells and M(IFN γ +LPS) was observed (**Supplementary Figure 1B**). Taken together, this result suggests that IFN γ priming during M(IFN γ +LPS) and a resting duration between the two rounds of stimulation are the key determinants of the plasticity of M(LPS) to be repolarized to M(LPS+IC) *in vitro*.

Successful Reverse Polarization of M(LPS) to M(LPS+IC) Correlated With the Activation of Early Signaling Pathways in Response to LPS and IC

From the previous results, we found that sufficient resting period between LPS and LPS with IC was important for the observed plasticity. Therefore, we next investigated the early signaling pathway downstream of TLR4. As depicted in **Figure 2C**, in the condition of 2 h resting between stimulations with LPS and LPS with IC, markedly decreased phosphorylation of MAPK p38, SAPK/JNK and NF- κ B p65 at 5, 15, and 30 min was observed in response to LPS with IC when compared to M(LPS+IC) polarized from naïve BMDMs (**Supplementary Figure 2**). The phosphorylation of Akt and p44/42 was comparable in this condition. In contrast, in the condition where the M(LPS+IC) phenotype was obtained with a resting time of 48 h between the two rounds of stimulation, the phosphorylation of MAPK p38, SAPK/JNK, and NF- κ B p65 was comparable with those of M(LPS+IC) from naïve BMDMs (**Supplementary Figure 2**). These results implied that the defects in early signaling pathways downstream of TLR4 are associated with the inability of M(LPS) to be repolarized to M(LPS+IC), and the increased duration between the two rounds of stimulation rescues this defect, which allows M(LPS) to respond to LPS and IC.

Increased Global H3K4me3 Enrichment in M(IFN γ +LPS+IC)

Because the priming with IFN γ and the resting durations between the two stimulation rounds are key determinants of the observed plasticity in the repolarization to M(LPS+IC), we wondered whether epigenetic changes occur during LPS or LPS+IC stimulation after the IFN γ priming. Therefore, epigenetic modifications by one of the active histone marks, H3K4me3, were investigated by ChIP-seq and the profiles were compared among unstimulated macrophages, M(IFN γ +LPS) and M(IFN γ +LPS+IC). A model-based analysis was used to identify significantly enriched H3K4me3 peaks with a *p* < 0.01. Circos plots were used to display global H3K4me3 enrichment among the three groups, and the results revealed clear differences among the samples (**Figure 3A**). As shown in **Figure 3B**, we found that the enrichment of H3K4me3 was higher in M(IFN γ +LPS+IC) than in unstimulated and M(IFN γ +LPS), and most H3K4me3 peaks that were enriched in M(IFN γ +LPS) overlapped with those in M(IFN γ +LPS+IC). Next, CEAS was used to identify the distribution of ChIP regions in M(IFN γ +LPS) and M(IFN γ +LPS+IC). M(IFN γ +LPS+IC) showed more distributed peaks in the distal intergenic regions of the promoter (1,000–2,000 bp), while M(IFN γ +LPS) had more peaks distributed in the promoter regions (<1,000 bp) and the coding exons. In both cases, the highest distributed peaks were enriched in the gene bodies, especially the promoter regions upstream <1,000 bp of the transcription start sites (TSSs) (**Figure 3C**). Taken together, these results reveal that M(IFN γ +LPS+IC) and M(IFN γ +LPS) display similar patterns of global H3K4me3

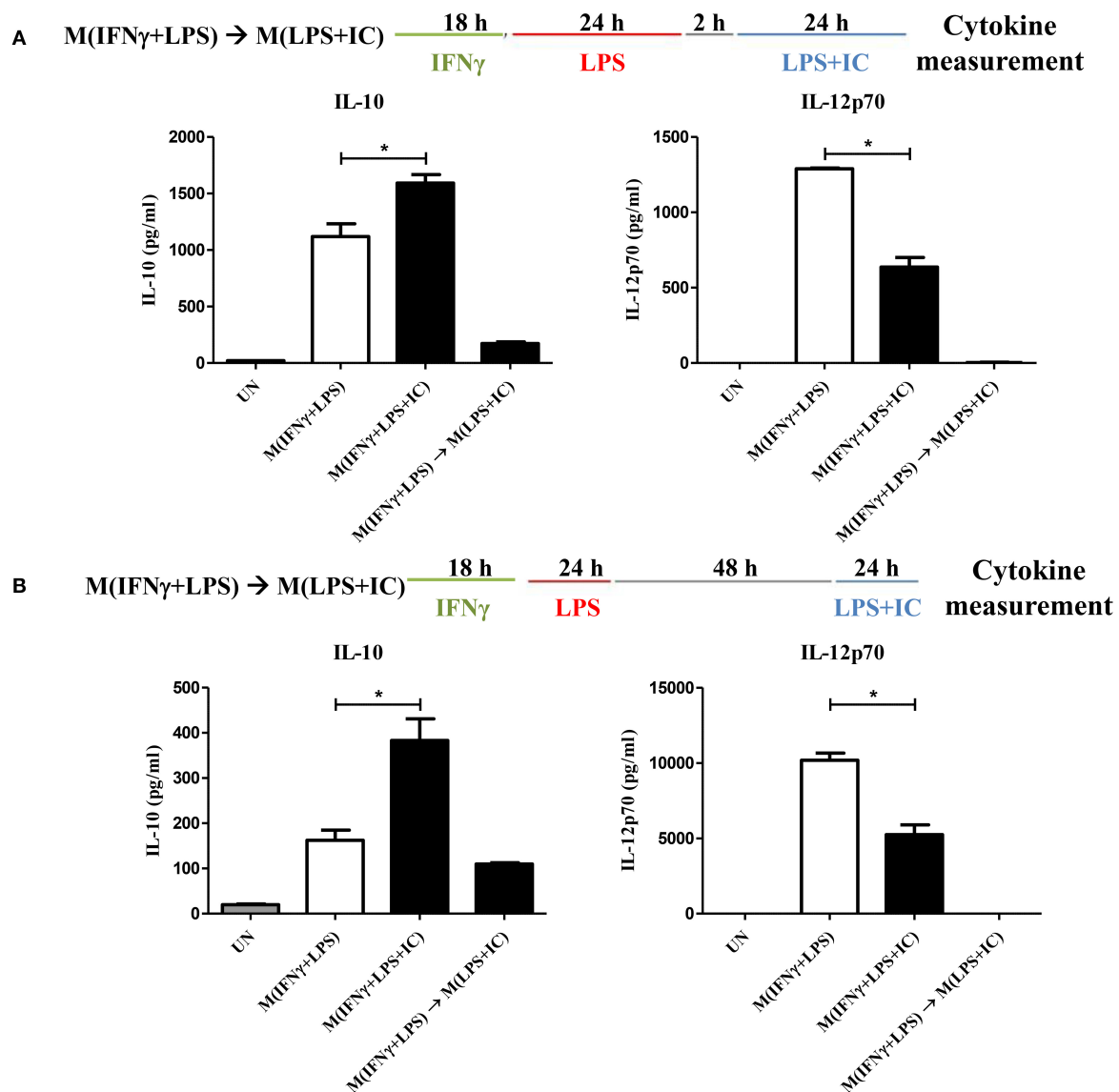


FIGURE 1 | Repolarization of M(IFN γ +LPS) to M(LPS+IC). **(A,B)** The protocol used for stimulation of IFN γ -primed macrophages with LPS and LPS with IC is shown with the washout period of 2 or 48 h. IL-10 and IL-12p70 in the culture supernatant harvested from cells treated as described were analyzed by ELISA. The results indicate the means \pm SD of triplicates determined from three independent experiments. *A significant difference at $p < 0.05$.

enrichment profiles, but M(IFN γ +LPS+IC) show increased H3K4me3 enrichment.

The Correlation of H3K4me3 Peaks Between M(IFN γ +LPS) and M(IFN γ +LPS+IC)

Next, we performed a correlation analysis at the genome-wide level using TCOR in EpiMINE. The datasets with two distinct correlation methods were analyzed using Pearson correlation and principal component analysis (PCA). The Pearson correlation represented by the scatter plot showed that the M(IFN γ +LPS) and M(IFN γ +LPS+IC) were highly correlated with a Pearson

score of more than 0.90, where the *cis*-regulatory elements include transcription factor binding sites (TFBS), CpG islands and promoter regions, and the non-*cis*-regulatory element regions are exons, 3'UTRs, 5'UTRs (Figure 4A) and introns (data not shown). However, the PCA plot revealed that the two top principal components between M(IFN γ +LPS) and M(IFN γ +LPS+IC) in all *cis*-regulatory regions, exons, 3'UTRs and 5'UTRs, are distinct (Figure 4B). These results demonstrated that M(IFN γ +LPS) and M(IFN γ +LPS+IC) are epigenetically highly correlated. More importantly, they show distinctive profiles in H3K4me3 enrichment that may result in differences in gene expression between these two phenotypically distinct effector macrophages.

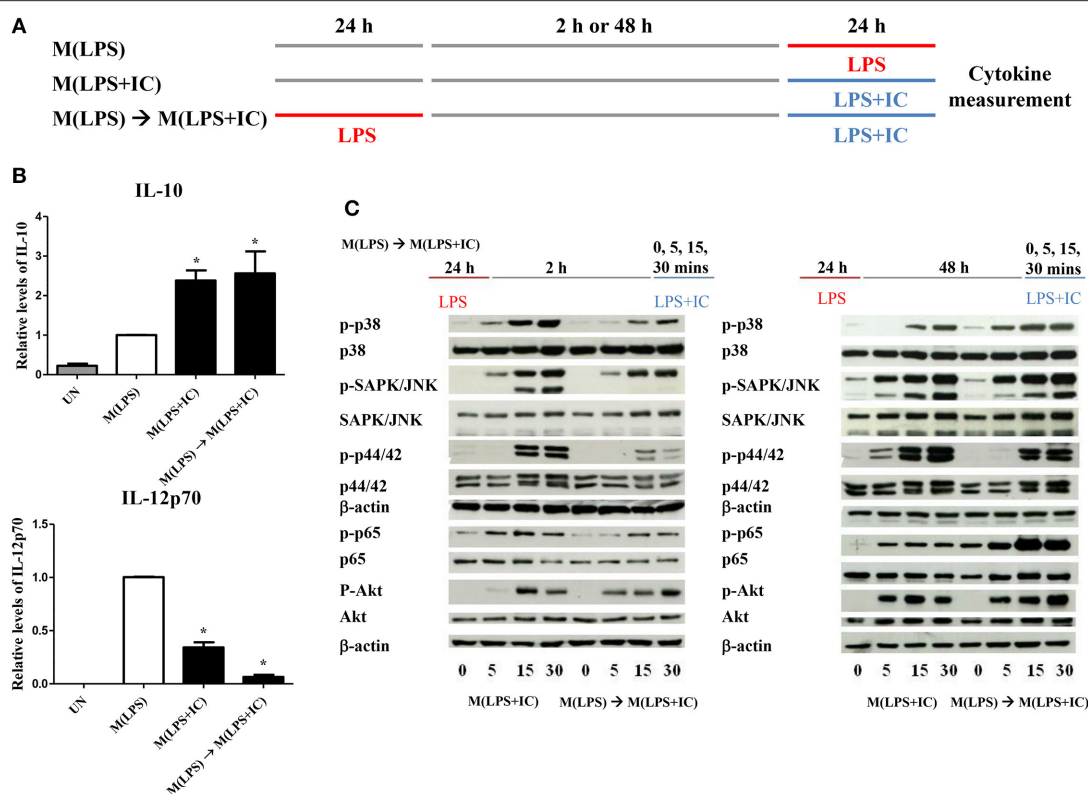


FIGURE 2 | Repolarization of M(LPS) to M(LPS+IC) and signaling downstream of TLR4. **(A)** The protocol used for macrophage stimulation with LPS and LPS with IC is shown. **(B)** IL-10 and IL-12p70 in the culture supernatant harvested from cells treated as described in **(A)** were analyzed by ELISA. The results indicate the means \pm SD of triplicates determined from three independent experiments. *A significant difference at $p < 0.05$. **(C)** BMDMs were polarized to M(LPS) and allowed to rest for 2 or 48 h. After re-stimulation with LPS and IC, phosphorylation of MAPKs, NF- κ B p65 and Akt was detected in cell lysates by Western blot. β -actin was used as a control. Representative data from one of three independent experiments are shown.

Higher H3K4me3 Enrichment in the *cis*-Regulatory Elements in M(IFN γ +LPS+IC) Than M(IFN γ +LPS)

We focused on specific genomic regions of the *cis*-regulatory elements, including the promoters and TFBS. A heatmap showed H3K4me3 enrichment within the TSSs and 1 kb near the TSSs (Figure 5A). M(IFN γ +LPS+IC) had increased global H3K4me3 enrichment signals when compared with those of M(IFN γ +LPS) (Figure 5A). H3K4me3 peaks at the promoter regions and the TFBS were observed (data not shown). The ChIP-seq peaks were analyzed by CEAS to obtain the average gene profiles of H3K4me3 within the TSSs and the nearby 5 kb. The average gene profiles of all three types of macrophages showed a similar pattern of H3K4me3 enrichment (Figure 5B). From previous results, M(IFN γ +LPS) showed higher percentages of H3K4me3 enrichment distribution in the promoter regions of <1,000 bp than M(IFN γ +LPS+IC) (Figure 3C). However, when QIRI was used to cluster H3K4me3 enrichment regions by k-mean, the results revealed twenty clusters (the presence to absence range was represented with values ranging from 0 to 1), and at the promoter regions, the enrichment of H3K4me3 was higher in M(IFN γ +LPS+IC) than in M(IFN γ +LPS) in all clusters (Figure 5C). These results suggest that H3K4me3

enrichment profiles of M(IFN γ +LPS+IC) in the promoter regions correlated with global H3K4me3 enrichment, and implies that M(IFN γ +LPS+IC) with increased enrichment of H3K4me3 in the promoter regions may have more active gene transcription than M(IFN γ +LPS).

H3K4me3 Enrichment in Regulatory Regions of Genes Uniquely Upregulated or Downregulated in M(IFN γ +LPS+IC)

To link the H3K4me3 profiles with the transcription of the genes, IGV was used to visualize the targeted loci. We investigated H3K4me3 enrichment of M(IFN γ +LPS+IC) in uniquely upregulated genes, including *Il10*, *Cxcl1*, *Csf3*, and *Il33*, and uniquely downregulated genes, including *Il12b* and *Il6*, as reported by RNA-seq (11). The results showed increased H3K4me3 enrichment in the uniquely upregulated genes *Il10*, *Cxcl1*, *Csf3*, and *Il33* in M(IFN γ +LPS+IC) when compared with that of M(IFN γ +LPS) (Figure 6A). In contrast, the H3K4me3 enrichment in uniquely downregulated genes in M(IFN γ +LPS+IC), *Il12b* and *Il6*, was not different between M(IFN γ +LPS+IC) and M(IFN γ +LPS) (Figure 6B). The quantification of H3K4me3 enrichment by QIRI showed that most of the genes induced during LPS and IC stimulation

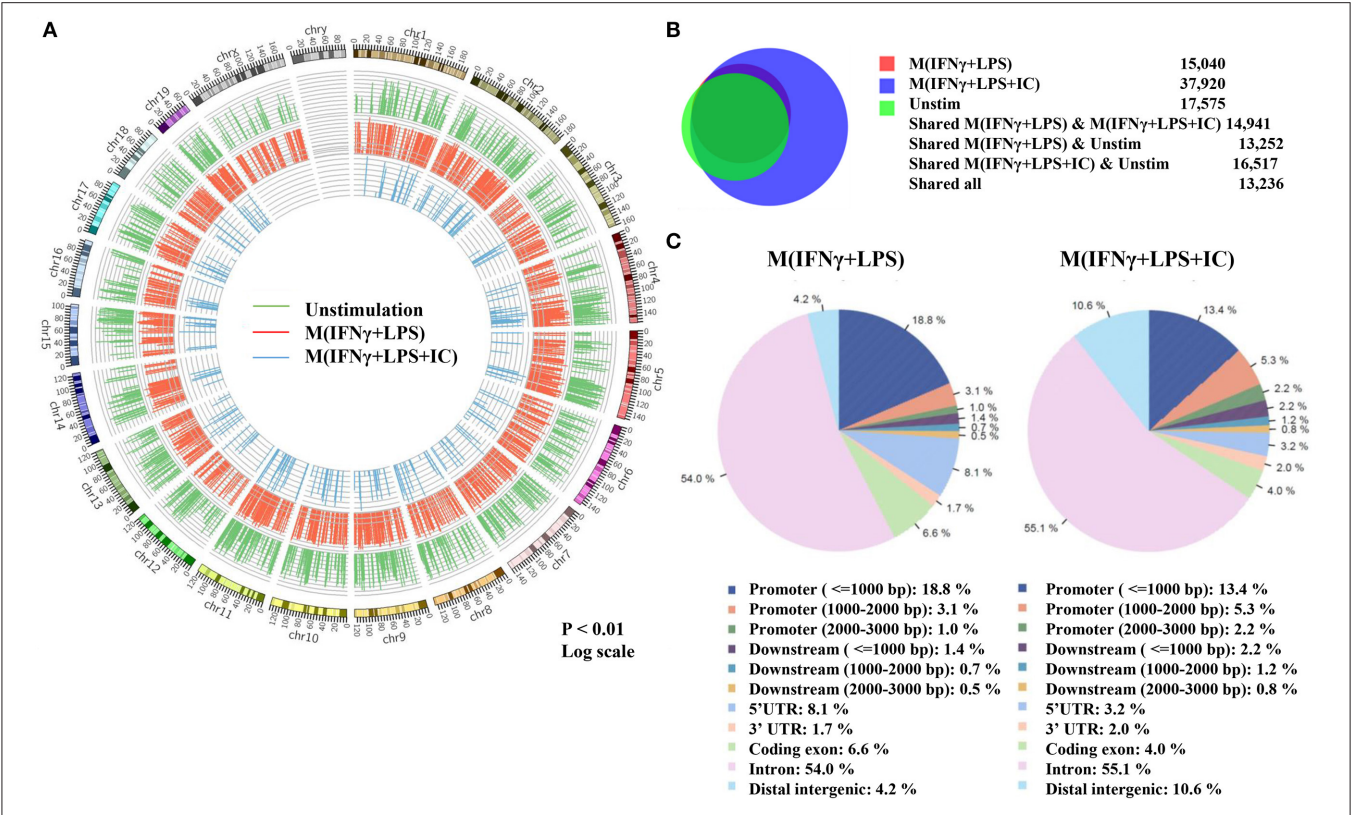
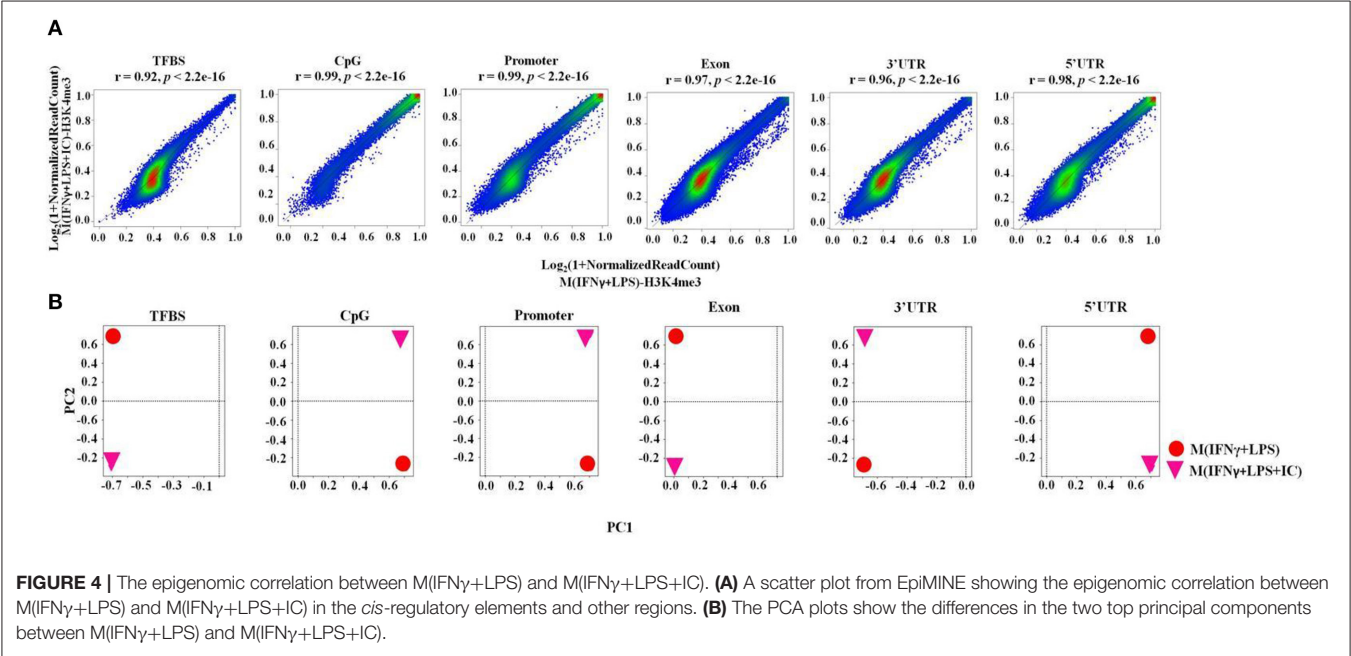


FIGURE 3 | Global enrichment of H3K4me3 in unstimulated macrophages, M(IFNγ+LPS) and M(IFNγ+LPS+IC). BMDMs were primed with IFNγ before stimulation with LPS with or without IC for 4 h. Cells were harvested for ChIP using an anti-H3K4me3 antibody. The ChIP samples were subjected to DNA sequencing. **(A)** Circos plot showing genome-wide H3K4me3 enrichment in unstimulated macrophages, M(IFNγ+LPS) and M(IFNγ+LPS+IC). The positions of log-transformed H3K4me3 enrichment in unstimulated macrophages (green circle), M(IFNγ+LPS) (red circle) and M(IFNγ+LPS+IC) (blue circle) were aligned according to chromosome position in the outer ring. **(B)** The total peaks after identification of H3K4me3 enrichment with MACS 1.4 were used to compare the overlap of H3K4me3 enrichment peaks, and the results are presented in a Venn diagram. **(C)** The *cis*-regulatory element annotation system (CEAS) showed the distribution pattern of H3K4me3 enrichment between M(IFNγ+LPS) and M(IFNγ+LPS+IC). All ChIP-seq results were analyzed from combined RAW files of two independent experiments.



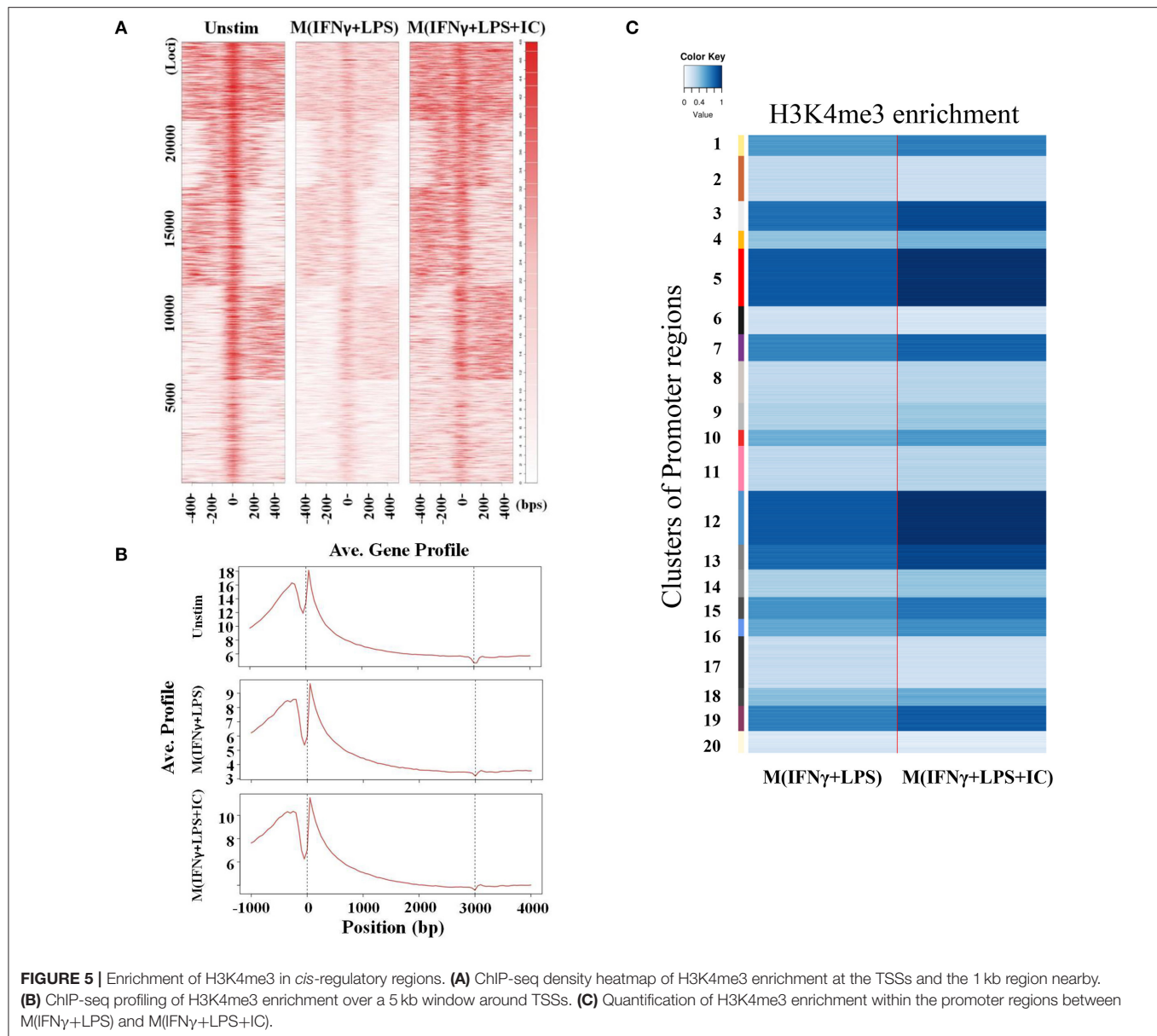


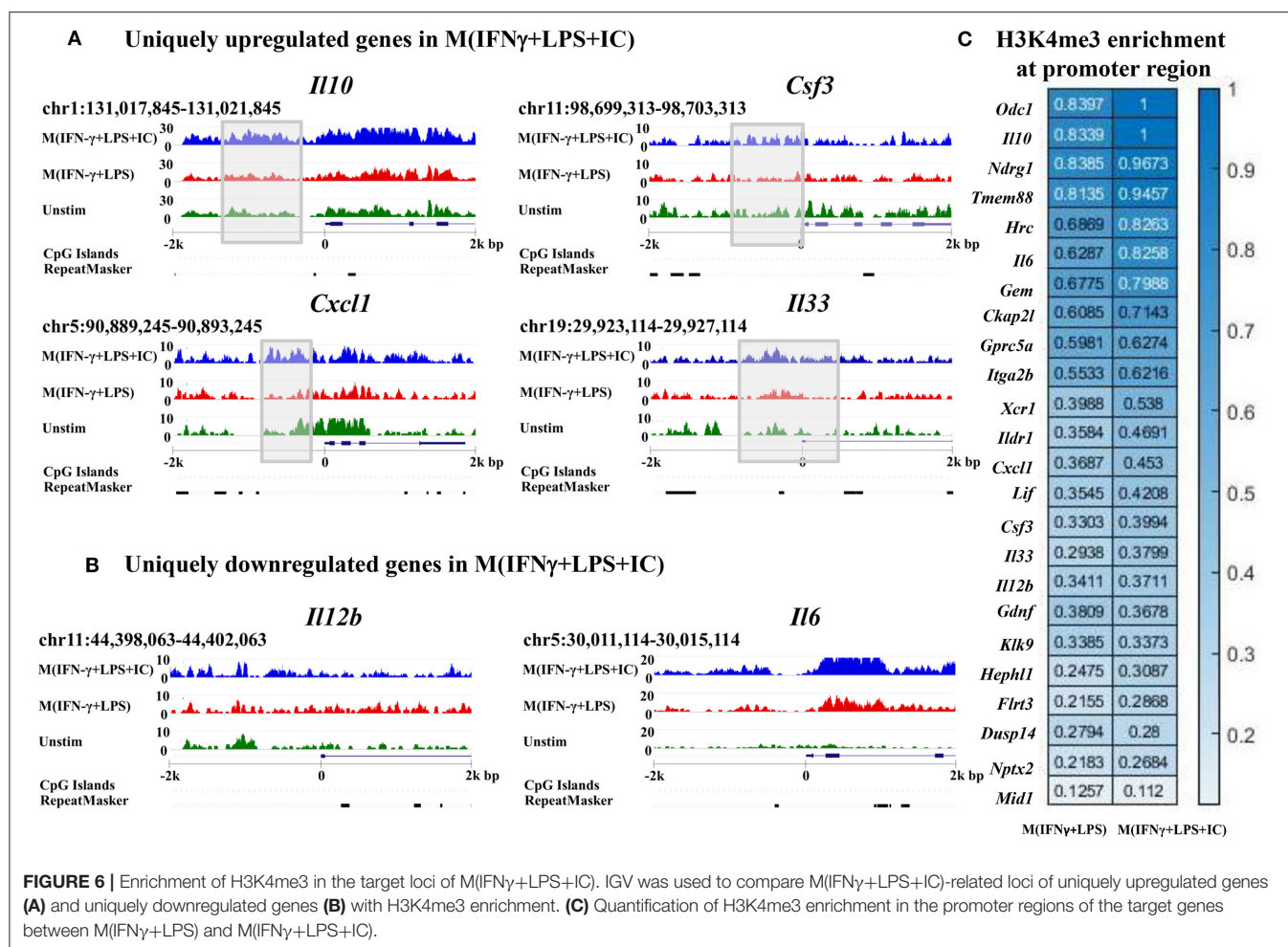
FIGURE 5 | Enrichment of H3K4me3 in *cis*-regulatory regions. **(A)** ChIP-seq density heatmap of H3K4me3 enrichment at the TSSs and the 1 kb region nearby. **(B)** ChIP-seq profiling of H3K4me3 enrichment over a 5 kb window around TSSs. **(C)** Quantification of H3K4me3 enrichment within the promoter regions between M(IFN γ +LPS) and M(IFN γ +LPS+IC).

described by Fleming et al. from RNA-seq data (11) had increased enrichment when compared to those of M(IFN γ +LPS) (Figure 6C). Overall, the H3K4me3 enrichment correlated well with the uniquely upregulated genes in M(IFN γ +LPS+IC), suggesting that the active histone mark H3K4me3 plays active roles in regulating the expression of genes in unique to M(IFN γ +LPS+IC).

KEGG Pathway Analysis of the Differentially Enriched H3K4me3 Genes in M(IFN γ +LPS+IC) Revealed Key Pathways in the Immune Responses

Gene ontology analysis using KEGG pathways was performed to investigate the possible regulatory molecules/signaling

pathways revealed by ChIP-seq data in M(IFN γ +LPS+IC). We used genes that showed unique H3K4me3 enrichment in M(IFN γ +LPS+IC) and filtered KEGG pathways for the immune system, signal transduction and signaling molecules to obtain the interaction profiling data. We found 10 significantly enriched pathways in M(IFN γ +LPS+IC) (Figure 7). Among these pathways, the cytokine-cytokine receptor interaction pathway was highly enriched. Cytokines are potent signaling molecules that can activate macrophages to change the phenotype and are crucial for intercellular regulation (29). From the enrichment quantification data, M(IFN γ +LPS+IC) exhibited increased H3K4me3 enrichment in most cytokine genes (Figures 5C, 6C) in the cytokine-cytokine receptor interaction pathway. M(IFN γ +LPS+IC) also showed significantly enriched cell adhesion molecules, RAP1 and cAMP signaling pathways.



This result suggests that increased H3K4me3 enrichment may regulate gene expression by inducing downstream signaling pathways that are crucial for functions, polarization and plasticity of M(IFN γ +LPS+IC).

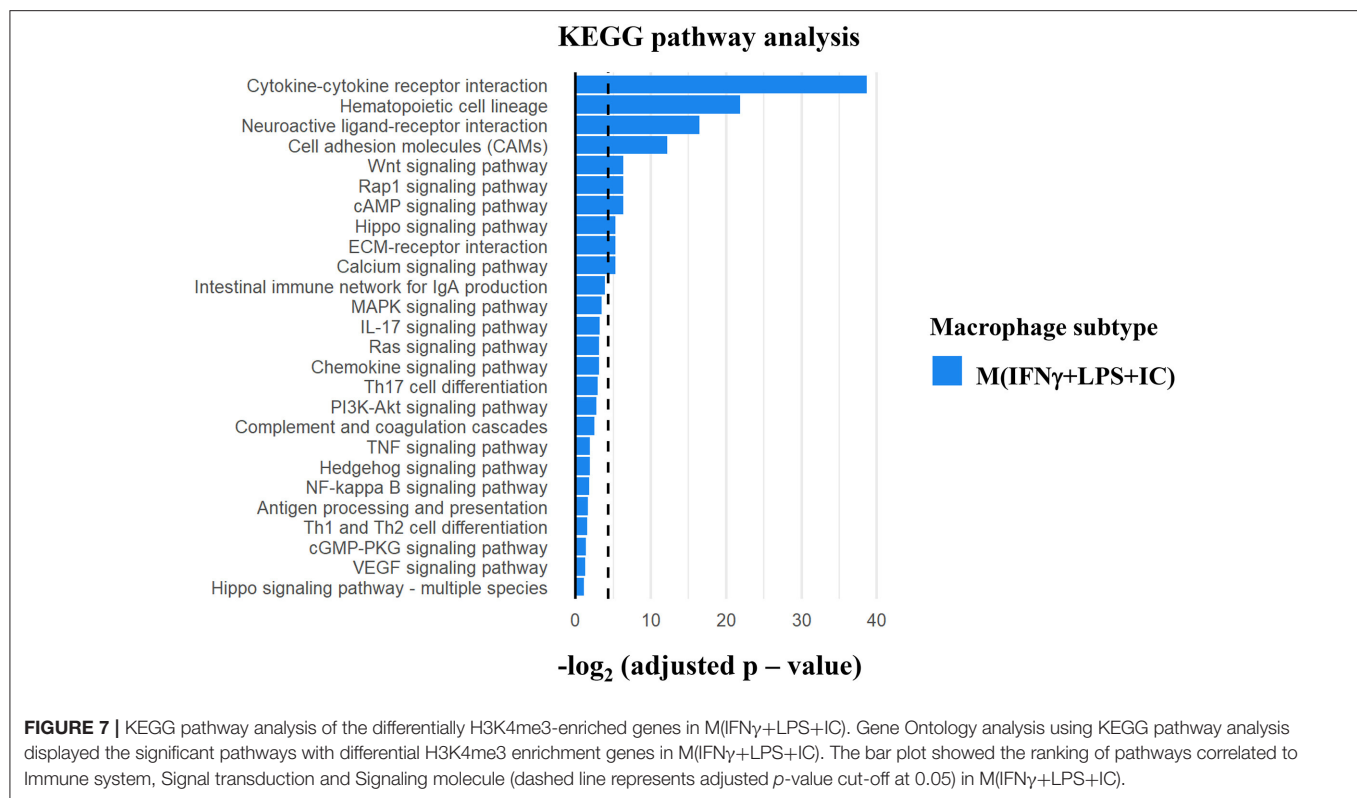
Adoptive Transfer of M(IFN γ +LPS+IC) Affected Cytokine Profiles in a Mouse LPS-Induced Endotoxemia Model

A previous study reported that mice receiving an adoptive transfer of M(IFN γ +LPS+IC) produced a high level of IL-10, resulting in decreased disease severity in autoimmune diseases such as experimental autoimmune encephalomyelitis (EAE) (8) and reduced mortality in sepsis (11). To evaluate the impact of M(IFN γ +LPS+IC) *in vivo*, we tested the effect of adoptive transfer of M(IFN γ +LPS+IC) on the systemic cytokine profiles in an LPS-induced endotoxemia model (Figure 8A). The production of the pro-inflammatory cytokines IL-1 β and IL-12p70 was significantly decreased at 6 h after LPS challenge in mice receiving adoptive transfer of M(IFN γ +LPS+IC) compared to those receiving unstimulated macrophages (Figure 8B). In contrast, the levels of other inflammatory cytokines, IL-6, TNF- α and IL-17, were not

significantly different between the two groups (Figure 8B). Furthermore, for the anti-inflammatory cytokine IL-10 and the Th2 cytokine IL-4, there was no difference between the two groups (Figure 8B). The cytokine profiles revealed that the adoptive transfer of M(IFN γ +LPS+IC) in mice with LPS-induced endotoxemia before LPS administration has a systemic impact on some pro-inflammatory cytokines but no detectable influence on IL-10.

DISCUSSION

The population diversity and functional plasticity of macrophages are important characteristics of macrophages that play an important role in several diseases (3, 30). LPS in the presence of immune complex stimulates macrophages to become regulatory effector macrophages that produce copious amounts of the anti-inflammatory cytokine IL-10 and reduced amounts of IL-12 (31). Extensive gene expression profiles of M(LPS+IC) have been reported, showing that they are a distinctive subset of activated macrophages (11). It is well-known that macrophages have functional plasticity and can switch phenotypes between M1 or M(LPS) and M2 or M(IL-4). However, no study has reported



whether M(LPS) can be reactivated to M(LPS+IC). This is an important question in light of the therapeutic implications of M(LPS+IC) in septicemia and autoimmune diseases such as EAE (8, 11).

To induce macrophages that produce high level of IL-10, IC was used in this study as a “reprogramming” stimulus but other stimuli such as prostaglandin E2 and adenosine were reported to yield similar phenotypes when applied to M(LPS) (11). Previously, we characterized in details whether IC alone can induce cytokine production in macrophages or M(IFN γ) and reported that IC alone was not sufficient to induce IL-10, IL-6, TNF α production in IFN γ -primed macrophages (13). This finding highlighted the importance of TLR-mediated stimulation in M(IFN γ +LPS+IC).

IFN γ is a key cytokine in activating macrophages. It has long been reported that stimulating macrophages with LPS together with IFN γ resulted in synergistic effect in inducing antimicrobial effector function of macrophages (32, 33). However, detailed transcriptomic analysis revealed that IFN γ priming of murine macrophages repressed subsets of pro-inflammatory genes and prevented the recruitment of neutrophils (34). When the optimal condition to induce IL-10 producing macrophages was examined, it was found that priming yielded better regulatory phenotypes, i.e., increased IL-10 production and decreased IL-12p70 production, of macrophages (8). In this study, it was found that IFN γ prevented the reverse polarization of M(IFN γ +LPS) to M(LPS+IC). Without the priming, it was possible to re-polarize M(LPS) to become M(LPS+IC). This

result led us to explore the involvement of epigenetic regulation in M(IFN γ +LPS) and M(IFN γ +LPS+IC).

Furthermore, we uncovered that at least *in vitro* re-stimulation of M(LPS) with LPS in the presence of IC requires a washout period of a minimum of 48 h between the two opposing stimuli. If the washout period was shorter (2–24 h), the ex-M(LPS) could not produce IL-10 at high level with reducing IL-12 upon re-stimulation with LPS and IC, as observed in M(LPS+IC). In contrast, the re-stimulated M(LPS) had decreased levels of most cytokines associated with M(LPS+IC). Some of the signaling pathways downstream of TLR4 and FcR (MAPK p38, SAPK/JNK, NF- κ B) were all reduced, which correlated with this unresponsive phenotype. IL-10 production in macrophages stimulated with TLR/LPS is regulated by the MAPK and NF- κ B signaling pathways (10). LPS tolerance of macrophages describes the phenomenon where macrophages become unresponsive to successive rounds of LPS stimulation (35). The shorter resting time that resulted in the failure of re-polarization may be partially explained by LPS tolerance. After 2 days of resting, re-stimulation of M(LPS) with LPS/IC rescued all early signal transduction and the production of high IL-10 and low IL-12.

A previous study demonstrated that ERK activation and histone modification by phosphorylation of serine 10 on H3 plays a key role in regulating IL-10 expression in M(LPS+IC) (20). In this study, we focused on H3K4me3 as a representative of active histone marks because it is the most dynamic epigenetic modification in activated macrophages found at gene

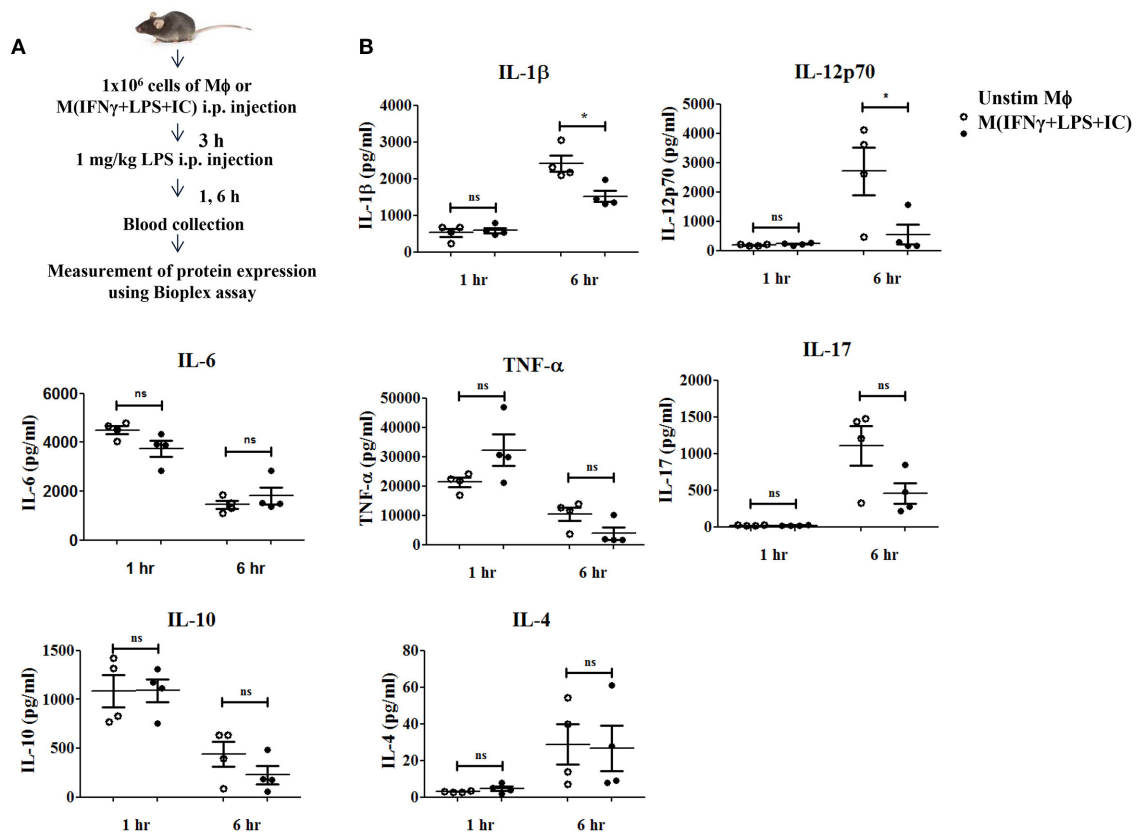


FIGURE 8 | The therapeutic application of M(IFNγ+LPS+IC) in a mouse endotoxemia model. **(A)** The protocol used for the adoptive transfer of M(IFNγ+LPS+IC) in the endotoxemia model. **(B)** Blood sera at 1 and 6 h after LPS challenge from mice with adoptive transfer of unstimulated macrophages or M(IFNγ+LPS+IC) were subjected to Bioplex cytokine assays for IL-6, IL-12p70, IL-1β, TNF-α, IL-17, IL-10, and IL-4. *Statistical significance at $p < 0.05$. The results represent the mean \pm SEM of each group ($n = 4$).

promoters (36). H3K4me3 are histone marks associated with actively transcribed genes (37). By ChIP-seq analysis, we found that compared to M(IFNγ+LPS), M(IFNγ+LPS+IC) had high H3K4me3 enrichment globally, especially in the *cis*-regulatory elements (**Figures 3A,B, 5A**). The quantification of enrichment in the promoter regions showed high H3K4me3 enrichment in M(IFNγ+LPS+IC) in all clusters and most of the genes that were found to be induced in M(LPS+IC) from RNA-seq (11).

Interestingly, the results also showed an increase in H3K4me3 enrichment in the promoter regions of most of the target loci that are uniquely upregulated in M(IFNγ+LPS+IC), i.e., *Il10*, *Cxcl1*, *Csf3*, and *Il33*. Our study revealed for the first time that H3K4me3 in M(IFNγ+LPS+IC) is another epigenetic modification that macrophages use to regulate IL-10 expression. In addition, the promoters of *Odc1* and *Ndgr1* showed a marked difference between M(IFNγ+LPS) and M(IFNγ+LPS+IC). *Odc1* encodes ornithine decarboxylase, a rate-limiting enzyme of the polyamine biosynthesis pathway. Ornithine decarboxylase is reported in macrophages to regulate M1, and specific deletion of this gene in macrophages results in hyperactivation of M1 and exacerbates colitis (38). Furthermore, ornithine decarboxylase modifies histones that impinge upon M1 gene expression (39). Our results imply that M(IC) may regulate *Odc1* expression by

increasing H3K4me3 in the promoter region. *Ndgr1* encodes N-myc downstream regulated 1, which is a member of the NDGR family. Interestingly, *Ndgr1* KO mice exhibit impaired M1/M2-type macrophage differentiation, and the expression of NDGR1 was found in tumor-infiltrating macrophages in renal cancer (40, 41).

For the downregulated genes in M(IFNγ+LPS+IC), *Il6* and *Il12b* showed no significant difference in H3K4me3 enrichment between M(IFNγ+LPS) and M(IFNγ+LPS+IC). This result suggests that other histone modifications that override H3K4me3 enrichment at promoter regions, may play dominant roles in transcriptional regulation.

For the epigenomic correlation, TCOR in EPIMINE were used to analyze the correlation between M(IFNγ+LPS) and M(IFNγ+LPS+IC). To our surprise, these two phenotypes of macrophages were highly correlated in all *cis*-regulatory elements and in other regions, even though the PCA plots showed a difference in the two top principal components between M(IFNγ+LPS) and M(IFNγ+LPS+IC).

We further investigated the possible regulatory molecules/signaling pathways using KEGG pathway analysis. H3K4me3 enrichment was found in regulatory regions of genes associated with cytokine-cytokine interactions, hematopoietic

cell lineage, cell adhesion molecules, the Wnt signaling pathway and the RAP1 signaling pathway. All of these pathways have been demonstrated to be involved in macrophage function and activation. RAP1 signaling regulates downstream signaling of MAPK and PI3K/Akt (42) that is crucial for M(LPS+IC) polarization and plasticity. The Wnt/ β -catenin pathway is linked to alternatively activated macrophages that contribute to kidney fibrosis (43, 44). Therefore, trimethylation of H3K4 may be a key epigenetic mechanism that regulates gene expression during macrophage activation.

Epigenetics includes a variety of regulatory mechanisms, including many types of histone modifications, both permissive and repressive, DNA methylation, and noncoding RNA-mediated regulation. In fact, many types of epigenetic modification have been reported during macrophage activation and function (45, 46). Therefore, we cannot rule out that other epigenetic regulations may also play important roles in M(IC) and their plasticity. How H3K4me3 is regulated in M(IFN γ +LPS) and M(IFN γ +LPS+IC) is currently not well-understood. Identification of H3K4 methyltransferase or demethylase in these subsets of macrophages will help us better understand this process and needs further investigation.

Finally, in the translational approach, we investigated the cytokine profiles in the blood serum of mice after adoptive transfer of M(IFN γ +LPS+IC) in a mouse sepsis model. Previously, it was reported that M(LPS+IC) reduce the lethality of LPS-induced endotoxemia, but the impact on the systemic cytokine profiles has not been explored (11). We found that mice with adoptively transferred M(IFN γ +LPS+IC) had specifically decreased IL-1 β and IL-12p70 levels in blood serum when compared to mice with adoptively transferred unstimulated macrophages (**Figure 8B**). Surprisingly, the IL-10 level was not significantly different between the two groups (**Figure 8B**). In the EAE model, adoptive transfer of M(IFN γ +LPS+IC) reduced the severity of Th1/Th17-mediated EAE, and the impact was seen in T cells that produce IL-10 and IL-4 upon re-stimulation (8). Currently, it is not known how adoptive transfer of M(IFN γ +LPS+IC) decreases IL-1 β and IL-12p70 levels in blood serum. It is possible that via IL-10, M(IFN γ +LPS+IC) directly dampen pro-inflammatory cytokine production. Alternatively, M(IFN γ +LPS+IC) may indirectly influence IL-1 β and IL-12p70 by other mechanisms.

In conclusion, our study demonstrated that M(LPS) and M(LPS+IC) have functional plasticity at least *in vitro*. The priming with IFN γ and the resting time between the two opposing stimuli are the keys for the recovery of the phosphorylation of important downstream signaling pathways.

We also showed that active histone H3K4me3 marks were increased to a greater extent in M(IFN γ +LPS+IC) than M(IFN γ +LPS). The significantly enriched pathways in M(IFN γ +LPS+IC) are associated with cytokines and gene expression in M(IFN γ +LPS+IC). Moreover, we investigated the therapeutic application of M(IFN γ +LPS+IC) that dampen the production of pro-inflammatory cytokines in a mouse sepsis model. Hence, the manipulation of the epigenetic regulation by H3K4me3 may help modulate M(IFN γ +LPS+IC) polarization and plasticity for future therapeutic applications.

DATA AVAILABILITY STATEMENT

The datasets generated for this study can be found in the NCBI Gene Expression Omnibus (GEO) and are accessible through GEO accession number GSE129284 (<https://www.ncbi.nlm.nih.gov/geo/query/acc.cgi?acc=GSE129284>).

ETHICS STATEMENT

All procedures were reviewed and approved by the Chulalongkorn University animal care and use protocol committee (CU-ACUP 024/2558).

AUTHOR CONTRIBUTIONS

VR designed and performed all experiments, analyzed all data and prepared all figures and the manuscripts. PB helped in performing ChIP-seq experiment. Y-WL, MP, and PK analyzed ChIP-seq data and the KEGG pathways. AL designed experiments and analyzed the sepsis data. TP designed all experiments, analyzed all data and prepared the manuscript.

FUNDING

This work was supported in part by the Thailand Research Fund (TRF Grant No. BRG5880007), and the Ratchadapisek Sompoch Endowment Fund from Chulalongkorn University (760001-HR) to TP and AL. VR was supported by the 100th Anniversary Chulalongkorn University Fund for Doctoral Scholarship, Chulalongkorn University, Bangkok, Thailand.

SUPPLEMENTARY MATERIAL

The Supplementary Material for this article can be found online at: <https://www.frontiersin.org/articles/10.3389/fimmu.2019.02956/full#supplementary-material>

REFERENCES

- Martinez FO, Gordon S. The M1 and M2 paradigm of macrophage activation: time for reassessment. *F1000Prime Rep.* (2014) 6:13. doi: 10.12703/P6-13
- Biswas SK, Chittethath M, Shalova IN, Lim JY. Macrophage polarization and plasticity in health and disease. *Immunol Res.* (2012) 53:11–24. doi: 10.1007/s12026-012-8291-9
- Sica A, Mantovani A. Macrophage plasticity and polarization: *in vivo* veritas. *J Clin Invest.* (2012) 122:787–95. doi: 10.1172/JCI59643
- Murray PJ, Allen JE, Biswas SK, Fisher EA, Gilroy DW, Goerdt S, et al. Macrophage activation and polarization: nomenclature and experimental guidelines. *Immunity.* (2014) 41:14–20. doi: 10.1016/j.immuni.2014.06.008
- Mantovani A, Biswas SK, Galdiero MR, Sica A, Locati M. Macrophage plasticity and polarization in tissue repair and remodelling. *J Pathol.* (2013) 229:176–85. doi: 10.1002/path.4133
- Grazia Cappiello M, Sutterwala FS, Trinchieri G, Mosser DM, Ma X. Suppression of IL-12 transcription in macrophages following

- Fc gamma receptor ligation. *J Immunol.* (2001) 166:4498–506. doi: 10.4049/jimmunol.166.7.4498
7. Mantovani A, Sica A, Sozzani S, Allavena P, Vecchi A, Locati M. The chemokine system in diverse forms of macrophage activation and polarization. *Trends Immunol.* (2004) 25:677–86. doi: 10.1016/j.it.2004.09.015
 8. Tierney JB, Kharkrang M, La Flamme AC. Type II-activated macrophages suppress the development of experimental autoimmune encephalomyelitis. *Immunol Cell Biol.* (2009) 87:235–40. doi: 10.1038/icb.2008.99
 9. Couper KN, Blount DG, Riley EM. IL-10: the master regulator of immunity to infection. *J Immunol.* (2008) 180:5771–7. doi: 10.4049/jimmunol.180.9.5771
 10. Saraiva M, O'garra A. The regulation of IL-10 production by immune cells. *Nat Rev Immunol.* (2010) 10:170–81. doi: 10.1038/nri2711
 11. Fleming BD, Chandrasekaran P, Dillon LA, Dalby E, Suresh R, Sarkar A, et al. The generation of macrophages with anti-inflammatory activity in the absence of STAT6 signaling. *J Leukoc Biol.* (2015) 98:395–407. doi: 10.1189/jlb.2A1114-560R
 12. Saraiva M, Christensen JR, Tsytyskova AV, Goldfeld AE, Ley SC, Kioussis D, et al. Identification of a macrophage-specific chromatin signature in the IL-10 locus. *J Immunol.* (2005) 175:1041–6. doi: 10.4049/jimmunol.175.2.1041
 13. Wongchana W, Kongkavitoon P, Tangtanatakul P, Sittplangkoon C, Butta P, Chawalitpong S, et al. Notch signaling regulates the responses of lipopolysaccharide-stimulated macrophages in the presence of immune complexes. *PLoS ONE.* (2018) 13:e0198609. doi: 10.1371/journal.pone.0198609
 14. Batten M, Kljavin NM, Li J, Walter MJ, De Sauvage FJ, Ghilardi N. Cutting edge: IL-27 is a potent inducer of IL-10 but not FoxP3 in murine T cells. *J Immunol.* (2008) 180:2752–6. doi: 10.4049/jimmunol.180.5.2752
 15. Carson WF, Cavassani KA, Dou Y, Kunkel SL. Epigenetic regulation of immune cell functions during post-septic immunosuppression. *Epigenetics.* (2011) 6:273–83. doi: 10.4161/epi.6.3.14017
 16. Egger G, Liang G, Aparicio A, Jones PA. Epigenetics in human disease and prospects for epigenetic therapy. *Nature.* (2004) 429:457–63. doi: 10.1038/nature02625
 17. He S, Tong Q, Bishop DK, Zhang Y. Histone methyltransferase and histone methylation in inflammatory T-cell responses. *Immunotherapy.* (2013) 5:989–1004. doi: 10.2217/imt.13.101
 18. Satoh T, Takeuchi O, Vandenbon A, Yasuda K, Tanaka Y, Kumagai Y, et al. The Jmjd3-Irf4 axis regulates M2 macrophage polarization and host responses against helminth infection. *Nat Immunol.* (2010) 11:936–44. doi: 10.1038/ni.1920
 19. Tserel L, Kolde R, Rebane A, Kisand K, Org T, Peterson H, et al. Genome-wide promoter analysis of histone modifications in human monocyte-derived antigen presenting cells. *BMC Genomics.* (2010) 11:642. doi: 10.1186/1471-2164-11-642
 20. Zhang X, Edwards JR, Mosser DM. Dynamic and transient remodeling of the macrophage IL-10 promoter during transcription. *J Immunol.* (2006) 177:1282–8. doi: 10.4049/jimmunol.177.2.1282
 21. Anderson CF, Mosser DM. Cutting edge: biasing immune responses by directing antigen to macrophage Fc gamma receptors. *J Immunol.* (2002) 168:3697–701. doi: 10.4049/jimmunol.168.8.3697
 22. Langmead B, Salzberg SL. Fast gapped-read alignment with Bowtie 2. *Nat Methods.* (2012) 9:357–9. doi: 10.1038/nmeth.1923
 23. Zhang Y, Liu T, Meyer CA, Eickhout J, Johnson DS, Bernstein BE, et al. Model-based analysis of ChIP-Seq (MACS). *Genome Biol.* (2008) 9:R137. doi: 10.1186/gb-2008-9-9-r137
 24. Jammula S, Pasini D. EpiMINE, a computational program for mining epigenomic data. *Epigenet. Chromatin.* (2016) 9:42. doi: 10.1186/s13072-016-0095-z
 25. Yu G, Wang LG, Han Y, He QY. clusterProfiler: an R package for comparing biological themes among gene clusters. *OMICS.* (2012) 16:284–7. doi: 10.1089/omi.2011.0118
 26. Yu G, Wang LG, Yan GR, He QY. DOSE: an R/Bioconductor package for disease ontology semantic and enrichment analysis. *Bioinformatics.* (2015) 31:608–9. doi: 10.1093/bioinformatics/btu684
 27. Benjamini Y, Hochberg Y. Controlling the false discovery rate: a practical and powerful approach to multiple testing. *J R Stat Soc Series B Stat Methodol.* (1995) 57:289–300. doi: 10.1111/j.2517-6161.1995.tb02031.x
 28. Dalmasso C, Broet P, Moreau T. A simple procedure for estimating the false discovery rate. *Bioinformatics.* (2005) 21:660–8. doi: 10.1093/bioinformatics/bti063
 29. Arango Duque G, Descoteaux A. Macrophage cytokines: involvement in immunity and infectious diseases. *Front Immunol.* (2014) 5:491. doi: 10.3389/fimmu.2014.00491
 30. Mosser DM, Edwards JP. Exploring the full spectrum of macrophage activation. *Nat Rev Immunol.* (2008) 8:958. doi: 10.1038/nri2448
 31. Sutterwala FS, Noel GJ, Salgame P, Mosser DM. Reversal of proinflammatory responses by ligating the macrophage Fc gamma receptor type I. *J Exp Med.* (1998) 188:217–22. doi: 10.1084/jem.188.1.217
 32. Sodhi A, Singh RK, Singh SM. Effect of interferon-gamma priming on the activation of murine peritoneal macrophages to tumouricidal state by cisplatin, IL-1, and tumour necrosis factor (TNF): production of IL-1 and TNF. *Clin Exp Immunol.* (1992) 88:350–5. doi: 10.1111/j.1365-2249.1992.tb03086.x
 33. Murray PJ, Wynn TA. Protective and pathogenic functions of macrophage subsets. *Nat Rev Immunol.* (2011) 11:723–37. doi: 10.1038/nri3073
 34. Hoeksema MA, Scicluna BP, Boshuizen MC, Van Der Velden S, Neele AE, Van Den Bossche J, et al. IFN-gamma priming of macrophages represses a part of the inflammatory program and attenuates neutrophil recruitment. *J Immunol.* (2015) 194:3909–16. doi: 10.4049/jimmunol.1402077
 35. Morris MC, Gilliam EA, Li L. Innate immune programming by endotoxin and its pathological consequences. *Front Immunol.* (2014) 5:680. doi: 10.3389/fimmu.2014.00680
 36. Logie C, Stunnenberg HG. Epigenetic memory: a macrophage perspective. *Semin Immunol.* (2016) 28:359–67. doi: 10.1016/j.smim.2016.06.003
 37. Lachner M, Sullivan RJ, Jenuwein T. An epigenetic road map for histone lysine methylation. *J Cell Sci.* (2003) 116:2117–24. doi: 10.1242/jcs.00493
 38. Singh K, Coburn LA, Asim M, Barry DP, Allaman MM, Shi C, et al. Ornithine decarboxylase in macrophages exacerbates colitis and promotes colitis-associated colon carcinogenesis by impairing M1 immune responses. *Cancer Res.* (2018) 78:4303–15. doi: 10.1158/0008-5472.CAN-18-0116
 39. Hardbower DM, Asim M, Luis PB, Singh K, Barry DP, Yang C, et al. Ornithine decarboxylase regulates M1 macrophage activation and mucosal inflammation via histone modifications. *Proc Natl Acad Sci USA.* (2017) 114:E751–60. doi: 10.1073/pnas.1614958114
 40. Nishie A, Masuda K, Otsubo M, Migita T, Tsuneyoshi M, Kohno K, et al. High expression of the Cap43 gene in infiltrating macrophages of human renal cell carcinomas. *Clin Cancer Res.* (2001) 7:2145–51. Available online at: <https://clincancerres.aacrjournals.org/content/7/7/2145.long>
 41. Watari K, Shibata T, Nabeshima H, Shinoda A, Fukunaga Y, Kawahara A, et al. Impaired differentiation of macrophage lineage cells attenuates bone remodeling and inflammatory angiogenesis in Ndr1 deficient mice. *Sci Rep.* (2016) 6:19470. doi: 10.1038/srep19470
 42. Sawada Y, Nakamura K, Doi K, Takeda K, Tobiume K, Saitoh M, et al. Rap1 is involved in cell stretching modulation of p38 but not ERK or JNK MAP kinase. *J Cell Sci.* (2001) 114:1221–7. Available online at: <https://jcs.biologists.org/content/114/6/1221.article-info>
 43. Feng Y, Liang Y, Ren J, Dai C. Canonical Wnt signaling promotes macrophage proliferation during kidney fibrosis. *Kidney Dis.* (2018) 4:95–103. doi: 10.1159/000488984
 44. Feng Y, Ren J, Gui Y, Wei W, Shu B, Lu Q, et al. Wnt/beta-catenin-promoted macrophage alternative activation contributes to kidney fibrosis. *J Am Soc Nephrol.* (2018) 29:182–93. doi: 10.1681/ASN.2017040391
 45. Ivashkiv LB. Epigenetic regulation of macrophage polarization and function. *Trends Immunol.* (2013) 34:216–23. doi: 10.1016/j.it.2012.11.001
 46. Zhou D, Yang K, Chen L, Zhang W, Xu Z, Zuo J, et al. Promising landscape for regulating macrophage polarization: epigenetic viewpoint. *Oncotarget.* (2017) 8:57693–706. doi: 10.18632/oncotarget.17027

Conflict of Interest: The authors declare that the research was conducted in the absence of any commercial or financial relationships that could be construed as a potential conflict of interest.

Copyright © 2020 Ruenjaiman, Butta, Leu, Pongpanich, Leelahavanichkul, Kueanjinda and Palaga. This is an open-access article distributed under the terms of the Creative Commons Attribution License (CC BY). The use, distribution or reproduction in other forums is permitted, provided the original author(s) and the copyright owner(s) are credited and that the original publication in this journal is cited, in accordance with accepted academic practice. No use, distribution or reproduction is permitted which does not comply with these terms.

Advantages of publishing in Frontiers



OPEN ACCESS

Articles are free to read
for greatest visibility
and readership



FAST PUBLICATION

Around 90 days
from submission
to decision



HIGH QUALITY PEER-REVIEW

Rigorous, collaborative,
and constructive
peer-review



TRANSPARENT PEER-REVIEW

Editors and reviewers
acknowledged by name
on published articles

Frontiers

Avenue du Tribunal-Fédéral 34
1005 Lausanne | Switzerland

Visit us: www.frontiersin.org

Contact us: info@frontiersin.org | +41 21 510 17 00



REPRODUCIBILITY OF RESEARCH

Support open data
and methods to enhance
research reproducibility



DIGITAL PUBLISHING

Articles designed
for optimal readership
across devices



FOLLOW US

@frontiersin



IMPACT METRICS

Advanced article metrics
track visibility across
digital media



EXTENSIVE PROMOTION

Marketing
and promotion
of impactful research



LOOP RESEARCH NETWORK

Our network
increases your
article's readership